

Mark Dallas  
Damian Bell *Editors*

# Patch Clamp Electro- physiology

Methods and Protocols

# METHODS IN MOLECULAR BIOLOGY

*Series Editor*

John M. Walker

School of Life and Medical Sciences

University of Hertfordshire

Hatfield, Hertfordshire, UK

For further volumes:  
<http://www.springer.com/series/7651>

For over 35 years, biological scientists have come to rely on the research protocols and methodologies in the critically acclaimed *Methods in Molecular Biology* series. The series was the first to introduce the step-by-step protocols approach that has become the standard in all biomedical protocol publishing. Each protocol is provided in readily-reproducible step-by-step fashion, opening with an introductory overview, a list of the materials and reagents needed to complete the experiment, and followed by a detailed procedure that is supported with a helpful notes section offering tips and tricks of the trade as well as troubleshooting advice. These hallmark features were introduced by series editor Dr. John Walker and constitute the key ingredient in each and every volume of the *Methods in Molecular Biology* series. Tested and trusted, comprehensive and reliable, all protocols from the series are indexed in PubMed.

# **Patch Clamp Electrophysiology**

## **Methods and Protocols**

Edited by

**Mark Dallas**

*University of Reading, Reading, UK*

**Damian Bell**

*Sophion Bioscience A/S, Ballerup, Denmark*

*Editors*

Mark Dallas  
University of Reading  
Reading, UK

Damian Bell  
Sophion Bioscience A/S  
Ballerup, Denmark

ISSN 1064-3745

ISSN 1940-6029 (electronic)

Methods in Molecular Biology

ISBN 978-1-0716-0817-3

ISBN 978-1-0716-0818-0 (eBook)

<https://doi.org/10.1007/978-1-0716-0818-0>

© Springer Science+Business Media, LLC, part of Springer Nature 2021

This work is subject to copyright. All rights are reserved by the Publisher, whether the whole or part of the material is concerned, specifically the rights of translation, reprinting, reuse of illustrations, recitation, broadcasting, reproduction on microfilms or in any other physical way, and transmission or information storage and retrieval, electronic adaptation, computer software, or by similar or dissimilar methodology now known or hereafter developed.

The use of general descriptive names, registered names, trademarks, service marks, etc. in this publication does not imply, even in the absence of a specific statement, that such names are exempt from the relevant protective laws and regulations and therefore free for general use.

The publisher, the authors, and the editors are safe to assume that the advice and information in this book are believed to be true and accurate at the date of publication. Neither the publisher nor the authors or the editors give a warranty, expressed or implied, with respect to the material contained herein or for any errors or omissions that may have been made. The publisher remains neutral with regard to jurisdictional claims in published maps and institutional affiliations.

This Humana imprint is published by the registered company Springer Science+Business Media, LLC, part of Springer Nature.

The registered company address is: 1 New York Plaza, New York, NY 10004, U.S.A.

---

## Preface

The flow of ions across cellular membranes has intrigued researchers for decades, and as such there has been a continual quest to develop and improve a methodology to understand the regulatory mechanisms underpinning ionic homeostasis. It is vital that we understand the role that ionic fluxes play in cellular physiology, given the pathological consequences of uncontrolled ionic flux. Central to this control are ion channels that present a large array of protein superfamilies that have been studied extensively to probe their structure and function. The development of the patch clamp technique in 1981 by Hamill and colleagues provided our first insight into the “real-time” functioning of these ion channels and with it the ability to define their biophysics and pharmacology. Indeed, the original single-channel work by Neher and Sakmann featured in [Nature’s 10 extraordinary papers](#). Since this seminal work, the ion channel field has grown exponentially with the addition of new technologies supporting our evolving ideas about “how ion channels work.”

This volume provides an invaluable update by describing a range of novel methodological approaches that have been developed to probe ion channel function across different modalities. These approaches have been applied to distinct channels or indeed distinct research areas, often transferable across the vast vistas of ion channel and transporter families. Here a global collection of experts share their substantial practical experience over a wide span of methods, from a basic introduction to patch clamp for the ion channel neophyte to more complex and bleeding-edge experimental protocols, including optogenetics. Naturally, the field of ion channel methodology is extensive, and there are a host of valuable sources to use to support this volume. We would signpost the reader to use *Ionic Channels of Excitable Membranes* (Hille) and *Microelectrode Techniques: The Plymouth Workshop Handbook* (<http://plymsea.ac.uk/id/eprint/7954/>) as complementary texts. Our focus of this volume was to add to these and provide a timely update to existing books and articles, building on these foundations to hopefully become a routine reference guide for current and future ion channel physiologists.

Researchers from a wide range of disciplines will benefit from this volume, which sets out to simplify the perceived complexities of electrophysiology and provide some advances in methods for more experienced ion channel researchers. With an increasing demand for the submission of complete stories to journals and funding bodies, the scope for inclusion of these highly technical procedures is becoming a fundamental part of scientific enquiry. We hope you find this a useful addition to the ion channel literature canon.

*Reading, UK  
Ballerup, Denmark*

*Mark Dallas  
Damian Bell*

---

# Contents

Preface .....	v
Contributors .....	ix
1 An Introduction to Patch Clamp Recording..... <i>Charlotte L. Hill and Gary J. Stephens</i>	1
2 Patch Clamp Technology in the Twenty-First Century .....	21
<i>Jan Dolzer</i>	
3 Heterologous Expression of Ion Channels in Mammalian Cell Lines .....	51
<i>Alistair Mathie, Emma L. Veale, and Robyn G. Holden</i>	
4 Electrophysiology on Channel-Forming Proteins in Artificial Lipid Bilayers: Next-Generation Instrumentation for Multiple Recordings in Parallel .....	67
<i>Ekaterina Zaitseva, Alison Obergrussberger, Conrad Weichbrodt, Mordjane Boukhet, Frank Bernhard, Christopher Hein, Gerhard Baaken, Niels Fertig, and Jan C. Behrends</i>	
5 Perforated Whole-Cell Recordings in Automated Patch Clamp Electrophysiology .....	93
<i>Kadla R. Rosholm, Kim Bodrum, and Anders Lindquist</i>	
6 Multielectrode Arrays.....	109
<i>Russell Burley and Jenna R. M. Harvey</i>	
7 Utilising Automated Electrophysiological Platforms in Epilepsy Research .....	133
<i>Carol J. Milligan and Svenja Pachernegg</i>	
8 Dynamic Clamp on a Windows PC.....	157
<i>Lorin S. Milescu and Joël Tabak</i>	
9 Combining Whole-Cell Patch-Clamp Recordings with Single-Cell RNA Sequencing .....	179
<i>Kashif Mahfooz and Tommas J. Ellender</i>	
10 Bioluminescence Methodology for Ion Channel Studies .....	191
<i>Paul A. Wadsworth, Aditya K. Singh, Ngibi Nguyen, Clifford Stephan, and Fernanda Laezza</i>	
11 Nucleated, Outside-Out, Somatic, Macropatch Recordings in Native Neurons .....	229
<i>Francesco Tamagnini</i>	
12 Preparation of Rat Organotypic Hippocampal Slice Cultures Using the Membrane-Interface Method .....	243
<i>Timothy W. Church and Matthew G. Gold</i>	
13 In Vivo Patch-Clamp Studies.....	259
<i>Ti Zhou, He Li, and Zhongju Xiao</i>	
14 In Vivo Optogenetics with Stimulus Calibration .....	273
<i>Luke T. Coddington and Joshua T. Dudman</i>	

15	Single or Double Patch-Clamp Recordings In Ex Vivo Slice Preparation: Functional Connectivity, Synapse Dynamics, and Optogenetics .....	285
	<i>Jean Simonnet, Louis Richevaux, and Desdemona Fricker</i>	
16	Optogenetics and Optical Tools in Automated Patch Clamping .....	311
	<i>Kim Boddum, Peder Skafte-Pedersen, Jean-Francois Rolland, and Sandra Wilson</i>	
	<i>Index</i> .....	331

---

## Contributors

- GERHARD BAAKEN • *Ionera Technologies GmbH, Freiburg, Germany*
- JAN C. BEHRENDT • *Laboratory for Membrane Physiology and Technology, Department of Physiology, Faculty of Medicine, University of Freiburg, Freiburg, Germany*
- FRANK BERNHARD • *Institute of Biophysical Chemistry & Center for Biomolecular Magnetic Resonance, Goethe University Frankfurt, Frankfurt am Main, Germany*
- KIM BODDUM • *Sophion Bioscience A/S, Ballerup, Denmark*
- MORDJANE BOUKHET • *Ionera Technologies GmbH, Freiburg, Germany*
- RUSSELL BURLEY • *Cerevance Ltd., Cambridge, UK*
- TIMOTHY W. CHURCH • *Department of Neuroscience, Physiology and Pharmacology, University College London, London, UK*
- LUKE T. CODDINGTON • *Janelia Research Campus, Howard Hughes Medical Institute, Ashburn, VA, USA*
- JAN DOLZER • *Sutter Instrument Company, Novato, CA, USA*
- JOSHUA T. DUDMAN • *Janelia Research Campus, Howard Hughes Medical Institute, Ashburn, VA, USA*
- TOMMAS J. ELLENDER • *Department of Pharmacology, University of Oxford, Oxford, UK*
- NIELS FERTIG • *Nanion Technologies GmbH, Munich, Germany*
- DESDEMONA FRICKER • *CNRS (Integrative Neuroscience and Cognition Center, UMR 8002), Paris, France; Université de Paris, Paris, France*
- MATTHEW G. GOLD • *Department of Neuroscience, Physiology and Pharmacology, University College London, London, UK*
- JENNA R. M. HARVEY • *Cerevance Ltd., Cambridge, UK*
- CHRISTOPHER HEIN • *Institute of Biophysical Chemistry & Center for Biomolecular Magnetic Resonance, Goethe University Frankfurt, Frankfurt am Main, Germany*
- CHARLOTTE L. HILL • *Metrian Biosciences Ltd, Cambridge, UK*
- ROBYN G. HOLDEN • *Medway School of Pharmacy, University of Kent and University of Greenwich, Chatham Maritime, UK*
- FERNANDA LAEZZA • *Department of Pharmacology and Toxicology, The University of Texas Medical Branch, Galveston, TX, USA*
- HE LI • *Department of Physiology, Southern Medical University, Guangzhou, Guangdong, China*
- ANDERS LINDQUIST • *Sophion Bioscience A/S, Ballerup, Denmark*
- KASHIF MAHFOOZ • *Department of Pharmacology, University of Oxford, Oxford, UK*
- ALISTAIR MATHIE • *Medway School of Pharmacy, University of Kent and University of Greenwich, Chatham Maritime, UK*
- LORIN S. MILESCU • *Department of Biology, University of Maryland at College Park, College Park, MD, USA*
- CAROL J. MILLIGAN • *Florey Institute of Neuroscience and Mental Health, Melbourne Brain Centre, Parkville, VIC, Australia*
- NGHI NGUYEN • *HTS Screening Core, Center for Translational Cancer Research, Texas A&M Health Science Center: Institute of Biosciences and Technology, Houston, TX, USA*
- ALISON OBERGRUSSBERGER • *Nanion Technologies GmbH, Munich, Germany*

- SVENJA PACHERNEGG • *Florey Institute of Neuroscience and Mental Health, Melbourne Brain Centre, Parkville, VIC, Australia; Reproductive Development Group, Murdoch Children's Research Institute, Parkville, VIC, Australia*
- LOUIS RICHEVAUX • *CNRS (Integrative Neuroscience and Cognition Center, UMR 8002), Paris, France; Université de Paris, Paris, France*
- JEAN-FRANCOIS ROLLAND • *Axxam SpA, Milan, Italy*
- KADLA R. ROSHOLM • *Sophion Bioscience A/S, Ballerup, Denmark*
- JEAN SIMONNET • *Bernstein Center for Computational Neuroscience, Humboldt-Universität zu Berlin, Berlin, Germany*
- ADITYA K. SINGH • *Department of Pharmacology and Toxicology, The University of Texas Medical Branch, Galveston, TX, USA*
- PEDER SKAFTE-PEDERSEN • *Sophion Bioscience A/S, Ballerup, Denmark*
- CLIFFORD STEPHAN • *HTS Screening Core, Center for Translational Cancer Research, Texas A&M Health Science Center: Institute of Biosciences and Technology, Houston, TX, USA*
- GARY J. STEPHENS • *Reading School of Pharmacy, University of Reading, Berkshire, UK*
- JOËL TABAK • *Institute of Biomedical and Clinical Science, University of Exeter Medical School, Exeter, Devon, UK*
- FRANCESCO TAMAGNINI • *School of Pharmacy, University of Reading, Whiteknights Campus, Reading, UK*
- EMMA L. VEALE • *Medway School of Pharmacy, University of Kent and University of Greenwich, Chatham Maritime, UK*
- PAUL A. WADSWORTH • *Biochemistry and Molecular Biology Graduate Program, The University of Texas Medical Branch, Galveston, TX, USA; Department of Pharmacology and Toxicology, The University of Texas Medical Branch, Galveston, TX, USA*
- CONRAD WEICHBRODT • *Nanion Technologies GmbH, Munich, Germany*
- SANDRA WILSON • *Sophion Bioscience A/S, Ballerup, Denmark*
- ZHONGJU XIAO • *Department of Physiology, Southern Medical University, Guangdong, Guangzhou, China*
- EKATERINA ZAITSEVA • *Ionera Technologies GmbH, Freiburg, Germany*
- YI ZHOU • *Department of Neurobiology, School of Basic Medical Sciences, Army Medical University, Chongqing, China*



# Chapter 1

## An Introduction to Patch Clamp Recording

Charlotte L. Hill and Gary J. Stephens

### Abstract

Electrophysiology is an essential tool aiding the study of the functions and dysfunctions of electrically excitable cells and their networks. The patch clamp method is a refined electrophysiological technique that can directly measure the membrane potential and/or the amount of current passing across the cell membrane. The patch clamp technique is also incredibly versatile and can be used in a variety of different configurations to study a range of properties, from spontaneous cell firing activity in native tissue to the activation and/or deactivation kinetics of individual channels expressed in recombinant cell lines. In this chapter we give an overview of patch clamping and how the different configurations can be set up and applied to electrophysiological research.

**Key words** Electrophysiology, Ion channels, Patch clamp, Voltage clamp, Current clamp, Single-channel recording

---

### 1 Introduction

Electrophysiology is an essential tool to aid the study of the functions and dysfunctions of electrically excitable cells (typically neurons) and their networks and, increasingly, nonexcitable cells. Correct application of electrophysiological techniques requires understanding of the physical and chemical properties of the cell and how these contribute to the physiology of ion transport across the cell membrane. The pivotal electrophysiology experiments of Alan Hodgkin and Andrew Huxley in the early 1950s, which provided the first complete description of the ionic mechanisms underlying the action potential, used crude glass electrodes to measure the membrane potential in squid giant axons [1]. This advance was honored with the Nobel Prize in Physiology and Medicine in 1963. Further developments included the use of very fine glass electrodes to puncture the cell membrane and perform intracellular recordings of changes in membrane potential. However, these “sharp” electrodes were largely unsuitable to record ion channel activity, as the electrode had to both measure the

membrane potential and inject current instantaneously. This problem was overcome by Bert Sakmann and Erwin Neher, who used relatively large-bore pipettes to make a tight seal with the surface of the cell, rather than penetrate the membrane. This method was originally named “extracellular patch clamp” and provided the first measurements of currents flowing through individual ion channels in the cell membrane [2, 3]. Sakmann and Neher were awarded the Nobel Prize in Physiology and Medicine in 1991. The method has been further developed into a number of different recording configurations which allow the high-resolution study of either all ion channels in the cell membrane or individual ion channels in cell-attached or excised patches, as discussed more fully below.

### **1.1 The Cell Membrane and Its Electrical Properties**

The cell membrane tightly controls the osmolarity of the extracellular and intracellular fluids, which produce large differences in the concentration gradients of specific ions, such as sodium ( $\text{Na}^+$ ), potassium ( $\text{K}^+$ ), chloride ( $\text{Cl}^-$ ), and calcium ( $\text{Ca}^{2+}$ ). The cell membrane is essentially a thin insulating layer between two conductive solutions, which separates the unequal distribution of such ions and creates a difference in the charge of the intracellular and extracellular solutions. The equilibrium potential of individual ions, as measured by the Nernst equation, results in an electrical potential across the cell membrane and is measured as voltage, whereby the inside of the cell is more negative than the outside. As the cell membrane can separate and store charge, it acts electrically as a capacitor, which takes time to charge and discharge and therefore slows down changes in membrane potential.

Despite the cell membrane being impermeable to charged particles, it is possible for ions to traverse the membrane via specialized ion channels and transporters. The movement of charge due to conformational changes in voltage-gated ion channels permits the flow of ions, this movement forms the basis of electrical activity in neurons and is measured as current. The size and flow of current is determined by the driving force (voltage) and amount of opposition (resistance) to the passage of ions across the cell membrane. Therefore, current ( $I$ ) through the cell membrane (a resistor) is directly proportional to the electrical potential ( $V$ ) across it and inversely proportional to the resistance ( $R$ ) according to Ohm’s law:

$$I = V/R$$

The electrical potential and flow of current across the cell membrane can be measured by a variety of either direct (intracellular) or indirect (extracellular) electrophysiological methods [4]; here, we focus on the patch clamp technique as the major intracellular method.

---

## 2 The Patch Clamp Method

The patch clamp method is an electrophysiological technique that uses a glass electrode with a relatively large bore (micropipette) to make a tight seal on the surface of the cell and record activity of ion channels in the cell membrane [2, 3]. This method can be used to directly measure the amount of current passing through the cell membrane at a fixed voltage and is otherwise known as *voltage clamp* (see Subheading 2.1.1). Alternatively, the membrane potential of a cell can be determined and the amount of voltage moving across the cell membrane at a fixed current can be measured in the *current clamp* mode (see Subheading 2.1.2). Prior to the development of patch clamp, the conventional method of measuring the membrane potential of a cell was to use the sharp microelectrode (“sharps”) technique; this used high resistance glass electrodes with a very small tip diameter to penetrate the cell membrane. A major disadvantage of the “sharps” technique is that penetration and damage of the cell membrane introduces a significant leakage current around the microelectrode that necessitates injection of additional current; another disadvantage is the inability to adequately compensate for the capacitance of the microelectrode. Not only is patch clamp considered a refinement of the “sharps” method, but it is also more versatile, specifically due to the ability to adapt use for a variety of different configurations [5] (see Fig. 1). The different patch clamp configurations have facilitated the study of all ion channels in the cell membrane (whole-cell mode) as well as individual ion channels, either in the intact cell membrane (cell-attached mode) or in excised patches of membrane (“outside-out” and “inside-out” configurations). As discussed elsewhere in this book, the patch clamp methodology has been adapted for higher-throughput automated (typically whole-cell) recording. This chapter will focus on manual patch clamp as the gold-standard technique, often used to confirm and extend automated patch data, and will highlight its versatility in terms of application to recording from somatic, dendritic, and presynaptic compartments, as well as membranes on internal organelles. We will also consider how the patch clamp technique has been used to advance knowledge of electrical and broader physiological function.

### 2.1 Electrical Considerations in Patch Clamp Recording

When the patch pipette tip, which contains conductive pipette solution, makes contact with the bath solution, current flows through the tip and goes straight to the ground electrode in the recording chamber. Resistance of the pipette tip ( $R_p$ ) can be calculated using Ohm’s law by measuring the flow of current in response to an amplifier-controlled voltage step (i.e., a small oscillating “test pulse”; e.g., 5 mV, 5 ms), which is measured with respect to the ground electrode. Every patch clamp experiment essentially starts

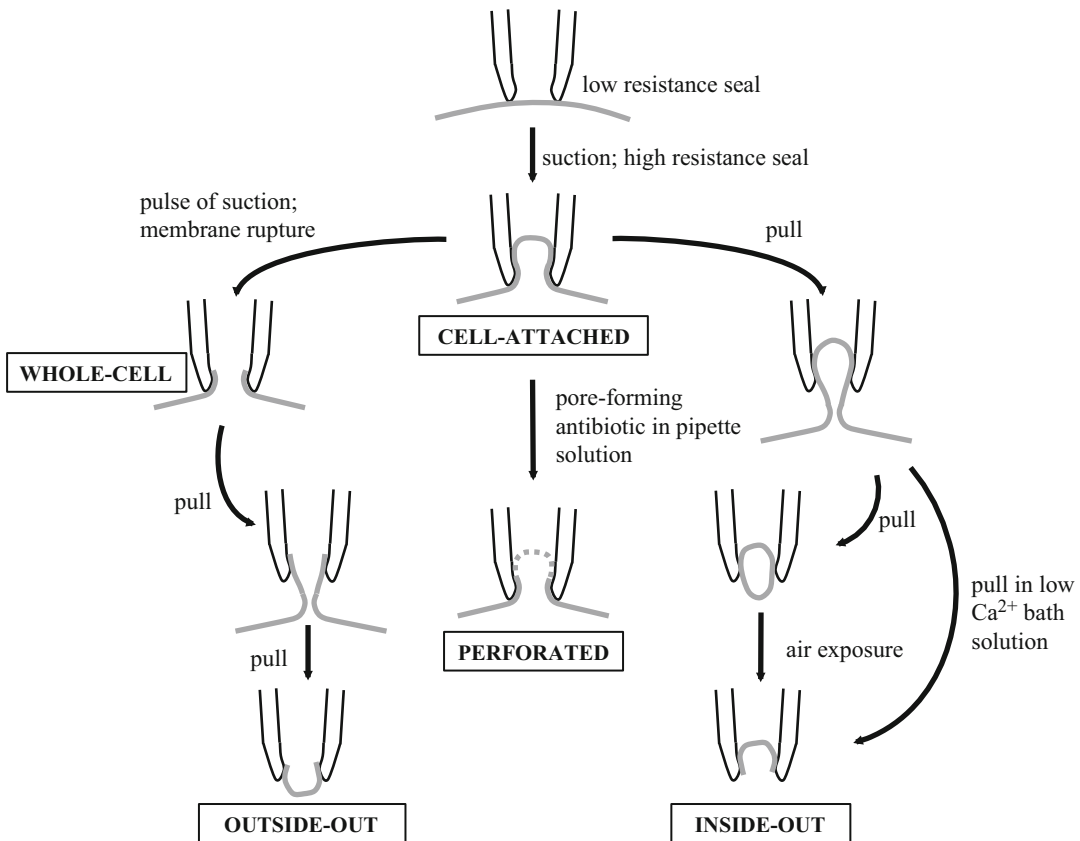


**Fig. 1** Patch clamp configurations. This schematic illustrates the interaction of the patch pipette tip with the surface of the cell membrane and the procedures that lead to various recording configurations within the patch clamp setup. (Adapted from [5])

with the cell-attached configuration (*see* Fig. 1), in which the patch pipette comes into close contact with the cell surface membrane to form a seal. Ohm's law can also be applied during the sealing process, as occlusion of the pipette tip with the cell surface reduces the current flow dramatically and ideally forms a high-resistance "gigaohm" ( $>1 \text{ G}\Omega$ ) seal.

The patch pipette tip is an insulator between two conductive solutions and therefore introduces pipette capacitance ( $C_p$ ), which produces fast transients at the beginning and end of the test pulse when a giga-ohm seal is established. These fast transients are compensated using a resistive headstage by injecting current, whose waveform negates the effect of  $C_p$ , until the test pulse ideally resembles a straight line (i.e., no voltage step). Once the cell-attached configuration is established and the fast transients compensated, the operator can then attempt to "break in" to the cell and obtain whole-cell configuration (*see* Subheading 3.3). As for the test pulse, slow transients appear as a consequence of the introduction of membrane capacitance ( $C_m$ ) from the lipid

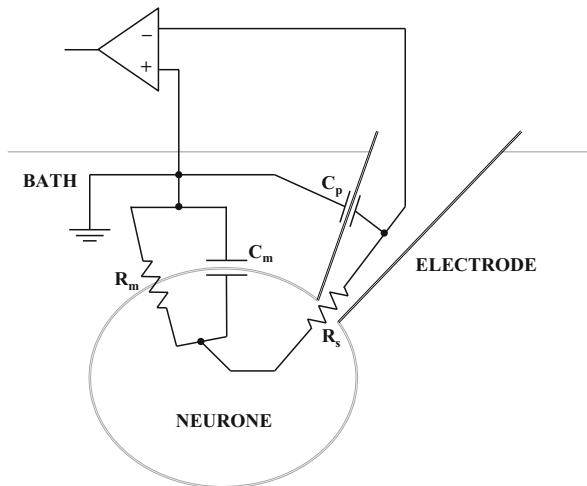


**Fig. 2** Equivalent electronic circuit for the whole-cell patch clamp configuration. This schematic demonstrates that membrane resistance ( $R_m$ ) and membrane capacitance ( $C_m$ ) are in parallel with each other, but are in series with the pipette capacitance ( $C_p$ ) and series resistance ( $R_s$ ). Not to scale. (Adapted from [6])

membrane upon obtaining the whole-cell configuration.  $C_m$  is compensated in a similar way to  $C_p$ . The formation of the whole-cell configuration also introduces series resistance ( $R_s$ ) between the glass and lipid compartments; predominantly,  $R_s$  represents the sum of  $R_p$  and any access resistance ( $R_a$ ) introduced between the pipette tip and the cell interior.  $R_s$  is also compensated to minimize voltage and time errors during experiments. In a compensated configuration, the current that flows down the pipette, into the cell and across the membrane to ground or earth can be accurately measured. Figure 2 is a schematic of the equivalent circuit of the whole-cell configuration.

During all modes of patch clamp recording, analog signals are digitized by the patch clamp amplifier with a built-in digitizer or an amplifier in combination with a separate “digidata” device. Signals are acquired or “sampled” at a particular frequency, typically ~5–20 kHz, with the higher sampling rates used for ionic currents that switch on and off more rapidly, such as inactivating, transient  $\text{Na}^+$  currents, or for rapid waveforms such as nerve action potentials. Signals are typically low-pass filtered, at approximately one-fifth to one-third of the sampling rate, to reduce intrinsic electrical system noise.

### 2.1.1 Voltage Clamp

Through the use of intracellular recording techniques, the activity of ion channels can be measured in the form of changes to the membrane potential, which reflect the permeability of the membrane to particular ions entering or leaving the cell. However, investigation of ion channel behavior can be a challenge, as changes

in the membrane potential are coupled to the gating mechanisms of some ion channels. Therefore, it is desirable to fix (“clamp”) the membrane potential at a constant value and record the current through the cell membrane directly. This can be achieved by voltage clamp, which is a technique that uses a feedback circuit to set the membrane potential to a desired value. Voltage clamp works by injecting current that is opposite and equal to the current flowing through the ion channels in the cell membrane. The amount of current required to keep the membrane potential constant provides a direct measure of the current flowing across the membrane. Different conductances can be activated by specific “step” protocols, where voltage increments are applied for an appropriate duration, or by voltage “ramp” protocols, whereby a continually increasing voltage is applied across an appropriate range to activate the conductance of interest. As part of current-activating protocols, “leak” current due to ohmic responses can be activated by applying voltage pulses ( $P$ ), often in hyperpolarizing direction, at a fixed integer ( $N$ ) of  $P$ ; this contaminating leak current can be subtracted from  $P$ . Typically, leak currents are subtracted using a  $P/N$  protocol where  $N = 4$  (i.e., leak current is activated by hyperpolarizing pulses at  $1/4$  of the magnitude of the associated activating depolarizing pulse). As described further below, voltage clamp is commonly used to record current movement through voltage-gated or ligand-gated ion channels at the whole-cell or single channel level, or to record postsynaptic currents due to neurotransmitters acting on ionotropic receptors. The movement of ions through electrogenic transporter proteins can also be measured in this mode.

### 2.1.2 Current Clamp

If the membrane potential is not clamped and a fixed amount of current is injected instead, the voltage change across the pipette and cell resistors in series can be measured using the current clamp mode. Cells are typically clamped close to their resting membrane potential by direct current (DC) injection.  $R_s$  in current clamp can be estimated easily and adjusted using “bridge balance” circuitry to compensate for voltage errors. The minimal current required to generate firing activity is referred to as the “rheobase” and is a useful measure of excitability and quality of seal/recording. During recording, measures such as input resistance can be monitored using small current injection (~10–20 pA from holding current). The current clamp mode can be used to monitor the resting membrane potential, which can provide useful information about the health of the patched cell and, as described further below, current clamp is commonly used to record regenerative cell firing or synaptic potentials in electrically excitable isolated cells such as neurons, or in neuronal networks, particularly in *ex vivo* brain slices.

---

### 3 Patch Clamp Configurations

#### 3.1 Cell-Attached Configuration

Prior to the patch pipette entering the bath solution, a small oscillating test pulse (e.g., 5 mV, 5 ms) is applied to monitor  $R_p$  (typically  $\sim 2\text{--}7 \text{ M}\Omega$  for a pipette of  $1\text{--}3 \mu\text{m}$  tip diameter) when the pipette is lowered into the bath. The application of positive pressure can be used to expel very small volumes of solution from the pipette tip; when opposed to the cell this often causes a slight “dimple” indent in the membrane and can also effectively “clean” the surface of the target cell, this is often essential when attempting to patch cells in an acute or organotypic tissue slices [7]. Direct contact between the target cell and the patch pipette is encouraged by releasing the positive pressure, but often it is necessary to apply a small amount of suction; at this stage the pipette can be said to be “on-cell” and activity can be recorded from ion channels in the intact membrane patch. A “loose” seal (of  $\text{M}\Omega$  rather than  $\text{G}\Omega$  order) can be used to monitor cell firing activity; the advantage of this configuration is that it is possible to reuse the patch pipette, for example, when searching for an active presynaptic input in paired recording. Related to a loose patch, macropatches (or “giant” patches) can be used to isolated larger areas of membrane; this configuration can be used to record ion channels or transporters with low channel density and is useful to record from large cells which are not amenable to good voltage clamp, such as *Xenopus* oocytes or plant cells. Macropatch recording necessitates use of lower resistant pipettes (typically  $<2 \text{ M}\Omega$ ) with relatively large tip diameters ( $\sim 10 \mu\text{m}$ ) and is inevitably associated with larger leak currents and higher noise. However, it is more common to proceed to a “tight” seal configuration to facilitate good voltage or current control. Thus, suction is typically applied to cause a rapid increase in  $R_p$  and the formation of a high-resistance seal (i.e.,  $>1 \text{ G}\Omega$ ), this process can be facilitated by hyperpolarizing the membrane toward the resting membrane potential. Fast transients associated with  $C_p$  (typically  $<10 \text{ pF}$ ) are cancelled. It is now possible to perform cell-attached recording or to advance to other configurations such as excised inside-out patches, whole-cell recording, perforated whole-cell or excised outside-out patches (as described below).

The tight seal cell-attached configuration is typically used to measure spontaneous cell firing, but can also be used to record single-channel currents, or summed activity of such. In this mode, cellular constituents are not “washed out” and agents can be added to a standard pipette solution (rather than the extracellular solution) to isolate conductances or to investigate activity at the ion channel of interest. Cell-attached recording may be used to study ion channels that are dependent on diffusible second messengers for their activity and/or those channels subject to high degrees of “run-down.” Spontaneous cell firing activity can be recorded in

voltage or current clamp mode, with cells typically held at 0 mV or zero-current levels to measure activity in a noninvasive manner.

### **3.2 Inside-Out Configuration**

In the inside-out mode, following establishment of the cell-attached configuration and achievement of a stable gigaohm seal, instead of setting the holding potential to a negative value in preparation for whole-cell recording, the holding potential is typically left at 0 mV. Inside-out patches are created by carefully pulling the patch pipette away from the cell to excise the membrane; as the seal between the pipette glass and the membrane forms a very strong bond, the membrane around the pipette tip will tear and leave an intact patch (*see Fig. 1*). If the edges of the patch come together and form a vesicle, the “outward-facing” section of cell membrane can be disrupted by exposing it briefly to air. However, the excised patch will not form a vesicle if the recording chamber is perfused with low or  $\text{Ca}^{2+}$ -free solution. As the patch electrode is on the extracellular side of the excised cell membrane, and given that the holding potential reflects the potential of the patch electrode in reference to ground, the holding potential should then be made positive. In the inside-out configuration, the cytoplasmic surface of the cell membrane is exposed to the bath solution; for example, this allows controlled concentrations of intracellular messengers to be added to the perfused bath solution and their effects to be investigated. Equally, ligands can be included in the pipette solution (which is typically composed of extracellular solution) and effects on extracellular ion channel domains investigated. Single-channel recording (*see Subheading 4.2.2*) is also frequently performed using excised inside-out patches, in particular, where the effects of intracellular messengers are under investigation. To facilitate the inside-out configuration, pipettes are typically pulled at slightly higher resistances than those used for whole-cell recording.

### **3.3 Whole-Cell Configuration**

From the cell-attached configuration, the command potential of the patch pipette is set to approximately resting membrane potential (i.e.,  $-60$  to  $-70$  mV) in preparation for obtaining the whole-cell configuration. Gentle suction, to produce negative pressure in the patch pipette, is applied to rupture the cell membrane under the pipette tip to provide low-resistance electrical access. As a result of “breaking in” to the cell, the current response to the test pulse will produce slow transients, which are associated with  $C_m$ ; typically,  $C_m$  is  $\sim 20\text{--}50$  pF (dependent on cell diameter) and is subsequently cancelled. The formation of the whole-cell configuration also introduces  $R_s$  between the glass and lipid compartments; practically, in the whole-cell mode  $R_s$  is synonymous with  $R_a$  and values  $<15\text{--}20$  M $\Omega$  (dependent on cell type and which can be subject to further percentage compensation) are typically considered acceptable. The fidelity of the final seal can also be gauged by the amplitude of the current flowing at rest in voltage clamp (the holding

current), which is a reflection of maintaining a giga-ohm seal and is ideally  $<10$  pA in the most favorable condition of an isolated cell. Whole-cell voltage or current clamp recording can now be performed. Throughout the experiment, parameters such as  $R_s$ ,  $R_a$  and holding current should be stable; often a small variation from starting values is set as a threshold to abandon the recording. Whole-cell recordings at different membranes/compartments are considered further below.

### **3.4 Perforated Patch Configuration**

Rather than using suction to rupture the patch membrane as in conventional whole-cell recording, perforated patch clamp recording permits electrical access between the cell and the patch pipette using pore-forming antibiotics such as nystatin, gramicidin or amphotericin B, which are included in the pipette solution. Pipette tips can be briefly dipped into standard intracellular solution before “back-filling” with the antibiotic solution to facilitate formation of a gigaohm seal prior to pore formation. Once the cell-attached configuration is formed and fast capacitances are cancelled, the appearance of slow capacitance (contributed due to formation of pores in the attached cell membrane) can be monitored; typically,  $R_a$  values of  $\sim 40\text{--}80$  M $\Omega$  indicate successful “perforation.” The danger is that the membrane ruptures completely to form the conventional whole-cell configuration, as indicated by lower  $R_a$  values. The perforated patch configuration generally allows monovalent ions to pass between the pipette solution and the cell interior, whereas second messenger molecules are retained rather than being “washed-out” of the cytoplasm; thus, this mode is ideal for studying ion channel regulation by endogenous cell signaling pathways. Perforated patches are usually more stable and can be the method of choice for ion channels subject to run-down, in particular, when investigated in the conventional whole-cell configuration.

### **3.5 Outside-Out Configuration**

For outside-out recording, following establishment of the whole-cell configuration, the pipette is gently “pulled off” the cell membrane to break the encapsulated membrane, which can then reform at the pipette tip with the external membrane exposed to the bathing solution (*see* Fig. 1). In this configuration, pipettes are typically pulled at slightly higher resistances than those used for whole-cell recording. Primarily, this allows the study of a smaller population of ion channels than in the whole-cell configuration. Thus, the behavior of individual channels can be investigated (*see* Subheading 4.2.2). Here, the intracellular solution within the patch pipette can be controlled to facilitate single-channel recording or to investigate the effects of agents acting at intracellular ion channel domains. Similarly, the effect of agents acting at extracellular ion channel domains can be investigated by adding them to the bath perfusate. This configuration can also facilitate greater voltage control than seen in whole-cell recording; in particular, when an ion

channel species is highly expressed in membranes of cells with small capacitance, high “current density” may preclude whole-cell recording due to space clamp issues (as discussed more fully in Subheadings 4.2.1 and 4.2.3).

---

## 4 Experimental Procedure of Voltage Clamp

### 4.1 Preparation of Patch Pipettes

Patch pipettes are typically fabricated from thin (or sometimes thick) borosilicate capillary glass or quartz using an electrode puller, which can be horizontal or vertical in orientation. Most typically, a single piece of glass is clamped around a filament, heated around its center, often in a multicyclic manner with application of a jet of air to cool the filament between cycles of pulls; this process ultimately pulls the glass apart, resulting in two pipettes with very fine (1–3  $\mu\text{m}$ ) tips. The temperature of the filament, the velocity, time and pressure of the pulling motion and the number of cycles in which this is repeated can be controlled to determine the taper of the pipette and the diameter of the final pipette tip. In order to achieve a completely clean and smooth tip and/or further adjust the diameter (typically to increase  $R_p$ ) of pulled patch pipettes, it is recommended to fire-polish the tip using a microforge device. For best overall results, patch pipettes should be produced in small batches, used the same day they are made and stored in a dust-free environment.

For the lowest noise, highest resolution recordings, such as for single-channel recording, the patch electrode can be thinly coated as close as possible to the tip with inert, hydrophobic agents such as beeswax, paraffin or, commonly, the proprietary agent Sylgard, which can be cured by heating. Such agents can be applied with backpressure to prevent enclosure of the tip itself; a coated pipette has reduced stray pipette capacitance that may arise across the pipette wall due to entry into the bath solution.

Patch pipettes are partially filled with a conductive solution, typically using a fine needle/tubing and a syringe. Backfilling can be used, whereby solution is introduced to the open end of the pipette. Capillary glass with a filament can be used to ensure that the solution flows smoothly into the tip without creating air bubbles when the pipette is held vertically. The pipette solution can be adapted according to recording configurations; in particular, establishment of the whole-cell configuration allows the contents of the cell to mix with the pipette solution. Pipette solutions can thus be designed as (pseudo)physiological intracellular solutions that facilitate isolation of different voltage-gated or ligand-gated ion channel conductances. Similarly, the pipette solution can be supplemented by ATP and/or GTP salts, agents such as phosphocreatine and buffers such as HEPES or EGTA. The pH (~7.4) and osmolarity (~300–320 mOsmol/l) of the intracellular solution can also be

adjusted to physiological values to attempt to improve cell health and longevity of recording. As described more fully below, the mixing of pipette solution with cell contents in the whole-cell configuration can be used to directly load the cell with diffusible drugs, second messenger compounds (such as cell signaling components) and/or labelling compounds. Similarly, agents can be added to the pipette solution to interact with extracellular domains (in cell-attached or inside-out configuration) or intracellular domains (in outside-out configuration). Moreover, as described in Subheading 3.4, in the specialist perforated patch configuration, pore-forming antibiotics are included in the pipette solution to facilitate formation of low access resistance seals.

Patch pipettes are tightly fixed to an airtight electrode holder containing a chlorided silver (Ag/AgCl) wire, which is immersed into the pipette solution and conducts ions efficiently. The holder is attached to the headstage and connected to a patch clamp amplifier. The headstage is mounted on a micromanipulator to facilitate the fine control of movement and positioning of the patch pipette with a high level of stability. The pipette is maneuvered to the recording site of interest, typically held within a recording chamber on the stage of an appropriate microscope as described more fully below. Application and release of pressure to form different recording modes can be achieved by use of an airtight syringe with a Luer lock three-way stopcock (or similar) connected to the electrode holder by a length of plastic tubing. It is possible to standardize this step by applying a known amount of pressure/suction measured via the graduated syringe or, even more accurately, by using a manometer to measure exact pressure.

## **4.2 Applications of Different Patch Clamp Recording Configurations**

### *4.2.1 Recording from Isolated Cells*

Patch clamp recordings are typically well achieved from small, isolated cells adhered to glass coverslips which are placed in a specialized recording chamber, typically with controlled inflow and outflow of extracellular solution and a facility to attach the grounding electrode (which can be via a ~3 M KCl agar salt-bridge to minimize any “drift” during electrical recordings). The recording chamber is fixed onto a moveable platform or onto the stage of an “inverted” microscope. Inverted microscopes have the light source above and objective lens below the recording chamber and allow an appropriately large working distance for patch pipette access. Micromanipulators are firmly attached either to a moveable platform or mounted on a separate, isolated platform; such manipulators are typically hydraulic or piezoelectric-controlled and may be motorized, and should be low noise and provide fine control of movement to allow the patch pipette to be moved into position with a high level of stability. A camera can be attached to the microscope and connected to a video monitor to facilitate identification of cells and positioning of the patch pipette. The whole setup is placed on an antivibration table surrounded by a Faraday cage to

shield electrical interference. Together this system provides for stable patch clamp recording, free from extraneous noise.

Cells (neurons, glia, muscle, etc.) may be dissociated from their native tissue and plated onto glass coverslips and recorded acutely, or may be maintained in primary culture prior to recording. Increasingly, cells such as genetically stable cell lines or stem cells can be similarly prepared for patch clamp recording. Commonly, ion channel or ionotropic receptor subunits or transporter proteins of interest can be transient or stably expressed in an appropriate cell expression system (e.g., HEK, CHO, COS, or similar). Such “recombinant” cells ideally lack similar contaminating endogenous proteins so that a “pure” ion channel population can be examined; by contrast, native (or natively derived) cells will typically contain a variety of different conductances, potentially including isoforms of the protein of interest. Therefore, the pipette solution can be manipulated to record the current of interest selectively, typically by adjusting the major internal cation concentration. For example, to record whole-cell K<sup>+</sup> currents, a physiological ~140 mM KCl-based intracellular solution (or K gluconate- or K aspartate-to avoid activation of Cl<sup>-</sup> conductances) can be used. To record whole-cell Na<sup>+</sup> currents, an intracellular solution containing physiological ~5 mM NaCl, with ~140 mM CsF or CsMeSO<sub>4</sub> to reduce outward K<sup>+</sup> current, can be used. To record whole-cell Ca<sup>2+</sup> currents, it is typically more important to negate contaminating conductances, such as inward Na<sup>+</sup> (in addition, Na<sup>+</sup> can also permeate Ca<sup>2+</sup> channels) and outward K<sup>+</sup> currents; therefore, ~140 mM CsCl can be used; Cs aspartate can also be used to avoid activation of additional Cl<sup>-</sup> conductances. Moreover, currents with additional activation requirements can be investigated; for example, BK<sub>Ca</sub> currents, which are both voltage-gated and Ca<sup>2+</sup>-dependent, can be recorded using ~140 mM KCl with free Ca<sup>2+</sup> concentration titrated using Ca<sup>2+</sup> buffers such as EGTA or BAPTA. Similarly, ligand-gated currents, such as those carried by Na<sup>+</sup> in excitatory ionotropic receptors or by Cl<sup>-</sup> in inhibitory ionotropic receptors, can be recorded using appropriate intracellular solutions. Such channels can be investigated either under selective expression in recombinant cells or in native cells, for the latter, current isolation is often aided by pharmacological agents.

Typically, physiological external solutions are used for patch clamp recording from isolated cells; however, these “extracellular” solutions can also be manipulated to aid recording. For example, for Ca<sup>2+</sup> current recording, Ba<sup>2+</sup> is often used as the charge-carrying ion as Ba<sup>2+</sup> permeability through Ca<sup>2+</sup> channels is high and this also avoids processes such as Ca<sup>2+</sup>-dependent inactivation. For Na<sup>+</sup> current recording, external Na<sup>+</sup> concentration can be reduced by (partial) substitution with salts, such as choline Cl<sup>-</sup>, which acts to reduce Na<sup>+</sup> current density. A more specialized example is for K<sup>+</sup> current recording, where physiological NaCl can be

partially replaced by Rb<sup>+</sup>, which acts to prolong the K<sup>+</sup> “tail” current and allow detailed interpretation of deactivation kinetics etc. Isolation of such conductances can be aided by pharmacological agents and also by use of specialized voltage clamp protocols; for example, the use of hyperpolarizing (pre)pulses to inactivate Na<sup>+</sup>, and sometimes transient K<sup>+</sup>, currents among a mixed population. Modification of extracellular solutions can also be used to investigate the ionic dependence of electrogenic transporter currents, in particular, when expressed selectively in recombinant cell systems.

For dissociated and, in particular, longer term cultured cells, there is often a tendency for cells to develop extensions (such as neurites in neurons), this can lead to issues with the fidelity of clamp (typically referred to as “space clamp” issues). Here, injected voltage can dissipate into these extensions, such that the errors in command voltage are read by the amplifier and the cell is not effectively voltage clamped. A related issue is when an ion channel species is highly expressed in membranes of isolated cells with small capacitance. Space clamp issues most commonly manifest in dramatic increases in current over small voltage increments, rather than the desirable graduated, smooth “switching on” of the current. As described elsewhere in this book, current–voltage relationships may be fitted by different Boltzmann functions; among the different parameters measured, the “slope factor”  $k$  (in mV/e-fold change in current) represents a measure of voltage-dependency of activation; a very low value of  $k$  (i.e., <2–3 mV) may be indicative of poor space clamp.

Cell-attached recordings can be performed in isolated cells. Typically, cell-firing activity is better recorded in tissue slices (*see* Subheading 4.2.3) where active inputs are better maintained; however, large isolated cells with lower ion channel/transporter density can be recorded using macropatches (or giant patches). A relevant example here is the use of *Xenopus* oocytes as an alternative to mammalian expression systems and the subsequent recording of macropatches to assess activity of the expressed protein.

Current clamp recording is typically used to monitor resting membrane potential and, in electrically excitable acutely dissociated or primary cultured neurons, to measure regenerative action potentials. For the latter, a family of hyperpolarizing and depolarizing current pulses are applied to measure passive and active membrane properties (typically in 50–100 pA step increments). For current clamp recording, the pipette and external solutions used mirror the physiological intracellular and extracellular solution, respectively.

More specialized patch clamp recordings can be made from intracellular membranes within isolated cells, often from nonexcitable cells. While specialized membrane preparations can often be used (*see* Subheading 4.2.4), recordings from isolated cells can also be made; an example here is “double patch clamp” recording from intracellular membranes (such as mitochondrial) within cells. In

this configuration, an inner, high resistance, electrode is surrounded by an outer electrode which is used to obtain an intracellular recording and then withdrawn, this exposes the inner electrode tip, which forms a giga-ohm seal on an intracellular membrane. Corresponding with the small size of the membrane to be patched, specialized, relatively high resistance pipettes are used in this mode.

Patch clamp techniques can be used in combination with imaging techniques in isolated cells to reveal physiological consequences of ion channel activation. For example, simultaneous patch clamp recording and  $\text{Ca}^{2+}$  imaging can be used in dissociated and cultured neurons to reveal the source and spatial regulation of this important second messenger.

#### *4.2.2 Single-Channel Recording*

The activity of individual ion channels can be studied using the single-channel recording technique, which can be performed in three configurations; cell-attached, outside-out patches and inside-out patches (*see* Subheadings 3.1, 3.2 and 3.4). In all cases, the seal between membrane and pipette is of very high quality ( $>20 \text{ G}\Omega$ ) and unlike whole-cell configuration, the membrane at the opening of the pipette is not ruptured [5, 8]. This is to ensure that the current that flows through the tip of the pipette originates from the ion channels embedded in the membrane beneath it. As the excised membrane patch is extremely small, there is likely to be very few ion channels present.

Single-channel currents are small (typically single figure pA), with conductances typically in the magnitude of 2–500 pS. Conductance can be calculated as the reciprocal of resistance; therefore it is essential that the seal resistance in single-channel recording is a lot higher than that normally required for the whole-cell configuration. A high resistmace seal is neceessary to reduce the level of noise and allow the resolution of small currents.

The current of a single ion channel can be identified as a seemingly instantaneous fluctuation between two levels of conductance as the channel transitions through states that correspond to being either open or closed. The opening and closing of ion channels is often described as a stochastic process, which means that these are random events with a probability distribution that can be statistically analyzed. It can also be described as a Markov process, whereby the probabilities of future states are dependent on the present state only and not the sequence of events that came before. Some ion channels may fluctuate between three or more levels of conductance, which can be indicative of intermediary states between fully open and fully closed.

The open and closed states of an ion channel are discrete events, the amplitude and durations of which can be analyzed and inferences made about its activity and kinetics. Different strategies for such analysis have been developed and are described in detail

elsewhere [9–12], although a slightly less technical review by Laver [13] may be a good starting point for the uninitiated.

#### 4.2.3 Recording from Acute and Organotypic Tissue Slices

Experiments that use acute ex vivo or organotypic tissue, typically brain, slices require a different “upright” microscope setup when compared to experiments that use isolated cells (*see Fig. 3*). To allow the experimenter to locate and record from a suitable cell, the upright microscope has the objective lens above the tissue with the light source below. Other than this key difference, the experimental setup is largely analogous to that used for isolated cells described above. Within the recording chamber, it is often necessary to hold the tissue slice in position using a “harp” (often made from platinum wire and nylon string or mesh). Tissue is perfused with a carboxygenated solution such as artificial cerebrospinal fluid (aCSF) for brain slice recording to maintain viability; as with the intracellular solution, the pH and osmolarity of extracellular solution can be adjusted to physiological values. A low magnification objective lens is typically used to locate the tissue region of interest, and a water-immersion objective lens (~60 $\times$  magnification) is used to identify a suitable cell to record, often using differential interference contrast (DIC) optics in combination with infra-red illumination (IR-DIC). The objective lens can be carefully raised following cell identification whereby the surface tension of the extracellular solution will allow for a greater working distance in which to manoeuvre the patch pipette using a suitable micromanipulator.

Spontaneous cell firing activity in voltage or current clamp mode is commonly measured in brain slices, where network inputs

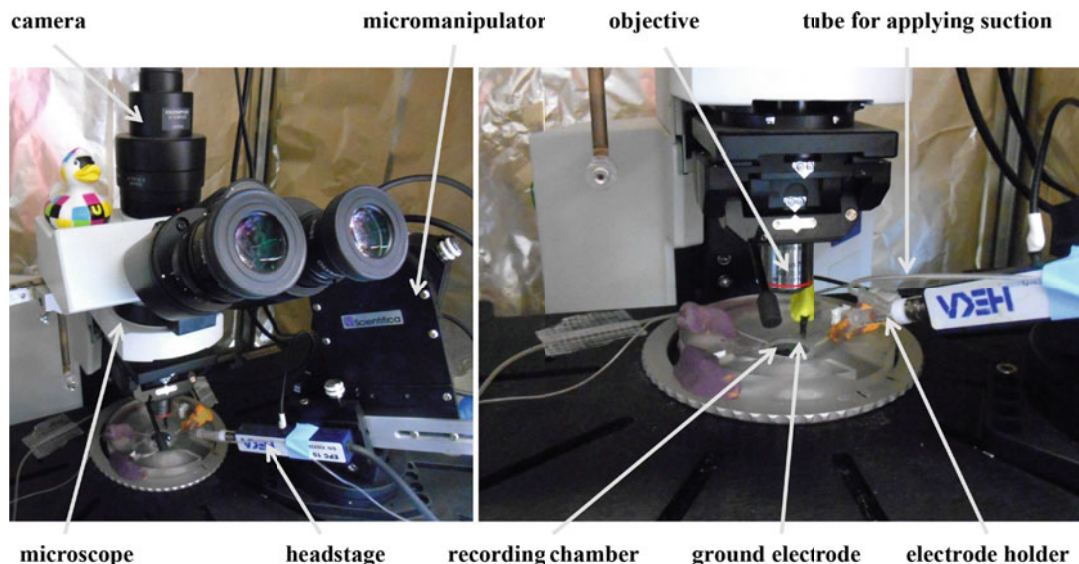


**Fig. 3** An overview of the patch clamp experiment setup with the main components labelled. This is an example of an upright microscope, which is best used for brain or organotypic slices

are maintained and, thus, a more physiologically relevant situation can be studied. Here, the cell-attached configuration is typically used. Somatic whole-cell recordings from identified principal cells in brain slices from regions such as hippocampus or cerebellum, are commonly used to record spontaneous postsynaptic currents generated by neurotransmitters, released (typically) from presynaptic terminals onto ionotropic postsynaptic receptors. Action potential-independent (the so-called miniature) postsynaptic currents can be recorded in the presence of tetrodotoxin to block voltage-gated  $\text{Na}^+$  channels and, thus, prevent action potential generation. A stimulating electrode (for example a bipolar tungsten electrode attached to a constant voltage stimulator) placed to activate inputs into principal neurons can be used to measure evoked postsynaptic currents. As described above for isolated cells, pipette solutions can be designed to isolate the desired response. For example, to record excitatory postsynaptic currents due to  $\text{Na}^+$  influx via ionotropic receptors, such as those gated by glutamate, acetylcholine, or 5-HT ligands, physiological extracellular aCSF and a ~5 mM NaCl with 140 mM K gluconate (or Cs gluconate)-based intracellular solution, typically in the presence of inhibitory (GABA/glycine) ionotropic receptor blockers, can be used. To record inhibitory postsynaptic currents due to  $\text{Cl}^-$  movement through ionotropic receptors, such as those gated by GABA or glycine ligands, extracellular aCSF and a ~140 mM CsCl-based intracellular solution, typically in the presence of excitatory (glutamate) ionotropic receptor blockers, can be used; here, as GABA and glycine ligand-gated currents have some similarities, the corresponding blocker is also typically used. In these cases, voltage clamp protocols record spontaneous, miniature or evoked postsynaptic currents in cells typically held around the resting membrane potential where driving force for respective charge-carrying ions is high.

Whole-cell somatic ligand-gated currents can also be recorded from cells in brain slices using similar solutions as described above for dissociated or cultured cells. Due to the presence of extensive dendritic trees (and/or axonal projections) there are clear potential space clamp problems associated with somatic recording of voltage-gated conductances, these issues largely preclude such voltage clamp measurements in principal neurons in brain slices using whole-cell recording. Therefore, perforated patch and, in particular, excised outside-out patches, are commonly “pulled” from principal neurons in brain slices to facilitate adequate voltage control of ion channels, in particular, those with high somatic expression.

#### 4.2.4 Advanced Recording from Acute and Organotypic Tissue Slices

More recent pioneering work has adapted the patch clamp technique to facilitate recording from specialized presynaptic terminals and, increasingly, from dendrites. Such recordings require higher resistance electrodes (typically up to 15–20 M $\Omega$ ) which can lead to

high  $R_s$  and, potentially, slow voltage clamp. However, such issues have been somewhat overcome to allow presynaptic recording in a limited number of preparations, such as the (relatively) large calyx of Held in the auditory brainstem, hippocampal/cerebellar mossy fiber terminals and basket cell terminals and granule cell boutons in the cerebellum. Recent advances have also allowed the application of different recording configurations to dendrites present in brain cells; in particular, production of high-quality tissue slice preparations and simultaneous use of advanced optical systems such as IR-DIC and, even more so, multiphoton microscopy, to facilitate better visualization of thin processes. Pipettes are typically fabricated with longer tapers (often by increasing the number of cycles in the pulling process), are of slightly higher resistance than for somatic recording and benefit more greatly from fire polishing to smooth the tip. Due to the small size of the pipette tips used,  $R_a$  is high (typically  $>100\text{ M}\Omega$ ), making accurate clamping more difficult; however, there are an increasing number of reports detailing patch clamp recording in dendrites. For both presynaptic terminals and dendrites, whole-cell recording is often confirmed, and/or morphology visualized, via inclusion of fluorescent dyes or similar markers such as biocytin in the pipette solution.

Advances have also permitted dual (or multiple) patch clamp recording from pre- and postsynaptic neurons and also somatodendritic recording. Thus, the cell-attached mode can be used to record presynaptic activity in voltage or current clamp, while postsynaptic activity can be measured simultaneously using the whole-cell mode. For example, changes in the presynaptic waveform in a defined interneuron can be correlated with postsynaptic activity of a major principal neuron, such as Purkinje cells in the cerebellum or pyramidal neurons in the hippocampus, without the need to use a stimulating electrode to activate a larger, less well-defined area. Moreover, simultaneous activity at specialized presynaptic sites and the corresponding postsynaptic response can be correlated using different recording modes.

A further specialization, often used in tissue slice recording, but also prevalent in dissociated/cultured cells, is the recording of so-called nucleated patches. These can be formed by an extension of the technique used in outside-out patch formation, with the major technical difference being that suction is continually applied through the patch pipette during the excision of the patch. This suction serves to pull the cell nucleus toward the pipette tip so that it is retained following excision of the membrane, which typically forms as a spherical inclusion in the patch pipette. There is comparative evidence that nucleated patches show larger conductances and agonist responses, and greater recording longevity than conventional outside-out recordings.

Increasingly, patch clamp techniques are used together, or in combination, with other pioneering technological advances to reveal further detail of ion channel network function in tissue slices. For example, optogenetics can be used to guide the experimenter to cell(s) of interest within networks to unravel their function using patch clamp recording. Such investigations are aided by multiphoton imaging techniques, as are use of ion-, pH-, or voltage-sensitive dyes and measurement of drug effects, using “caged” compounds, whereby a residue that prevents bioactivity can be cleaved off by UV light. As with isolated cells, patch clamp recording can be used in tissue slices simultaneously with techniques such as  $\text{Ca}^{2+}$  imaging in order to correlate physiological function. New techniques are also expanding the reach of patch clamp recording. For example, scanning ion conductance microscopy is an imaging technique that uses a glass micropipette which can also be used for patch clamp recording subsequent to identification of a cell of interest. Such techniques have pioneered the mapping of ion channels that have proved difficult to localize using conventional techniques; this has led to this combination being dubbed the “smart-patch” technique [14].

#### 4.2.5 Intracellular Membranes

Recent advances have further facilitated patch clamp recording from intracellular membranes. Several previous studies have used lipid bilayer membranes in which purified ion channels are reconstituted and activity of single channels is recorded via a patch clamp amplifier. However, such activity, in particular for intracellular membranes, is highly artificial and has tended to produce equivocal data. It is also possible to record from intracellular membranes within isolated cells (*see* Subheading 4.2.1 for a description of recording from mitochondrial membranes within an intact cell). Such recordings are technically demanding and an increasing number of specialized intracellular membrane preparations, including mitochondria, endolysosomes, and sarcoplasmic/endoplasmic reticulum, and subsequent patch clamp recordings from such, are now being reported. Prevalent examples here are the use of mitoplasts prepared from intracellular mitochondrial membranes and whole-lysosome preparations, such preparations require higher resistance patch electrodes and may benefit from modifications to the external solution to best mirror the environment experienced by the intracellular membrane, such as an acidic solution ( $\text{pH} \sim 5.0$ ) for lysosomal membranes. It is possible to make recording in all major patch clamp configurations in such isolated membrane preparations.

#### 4.2.6 In Vivo Patch Clamp Recording

Finally here, the most obvious required extension of isolated cell and tissue slice recording is an advancement to the *in vivo* situation and the ability to perform patch clamp recording in anesthetized and in awake, head-fixed or freely moving animals. This is

beginning to be achieved with whole-cell recordings that overcome issues with low success rate, largely associated with poor access resistance recordings [15]. To record in the CNS, craniotomy and delicate removal of the meninges is typically required; careful application of the principles of seal formation and pressure/suction facilitate patch clamp recording. Interventions such as the use of perforated whole-cell recording are useful to maintain stability and prolong in vivo recording.

## References

- Hodgkin AL, Huxley AF (1952) A quantitative description of the membrane current and its application to conduction and excitation in nerve. *J Physiol* 117:500–544
- Neher E, Sakmann B (1976) Noise analysis of drug induced voltage clamp currents in denervated frog muscle fibres. *J Physiol* 258:705–729
- Neher E, Sakmann B, Steinbach JH (1978) The extracellular patch clamp: a method for resolving currents through individual open channels in biological membranes. *Pflugers Arch* 375:219–228
- Hille B (2001) Ion channels of excitable membranes. Sinauer, Sunderland, MA
- Hamill OP, Marty A, Neher E, Sakmann B, Sigworth F (1981) Improved patch-clamp techniques for high-resolution current recording from cells and cell-free membrane patches. *Pflugers Arch* 391:85–100
- Molleman A (2003) Patch clamping: an introductory guide to patch clamp electrophysiology. Wiley, Chichester
- Edwards FA, Konnerth A, Sakmann B, Takahashi T (1989) A thin slice preparation for patch clamp recordings from neurones of the mammalian central nervous system. *Pflugers Arch* 414:600–612
- Sigworth FJ, Neher E (1980) Single  $\text{Na}^+$  channel currents observed in cultured rat muscle cells. *Nature* 287:447–449
- Colquhoun D, Sigworth FJ (1983) Fitting and statistical analysis of single-channel records. In: Sakmann B, Neher E (eds) Single-channel recording, 2nd edn. Springer, New York
- Sigworth FJ, Sine SM (1987) Data transformations for improved display and fitting of single-channel dwell time histograms. *Biophys J* 52:1047–1054
- Hawkes AG, Jalali A, Colquhoun D (1992) Asymptotic distributions of apparent open times and shut times in a single channel record allowing for the omission of brief events. *Philos Trans R Soc Lond B Biol Sci* 337:383–404
- Tveito A, Lines GT, Edwards AG, McCulloch A (2016) Computing rates of Markov models of voltage-gated ion channels by inverting partial differential equations governing the probability density functions of the conducting and non-conducting states. *Math Biosci* 277:126–135
- Laver DR (2001) The power of single channel recording and analysis: its application to ryanodine receptors in lipid bilayers. *Clin Exp Pharmacol Physiol* 8:675–686
- Dutta AK, Korchev YE, Shevchuk AI, Hayashi S, Okada Y, Sabirov RZ (2008) Spatial distribution of maxi-anion channel on cardiomyocytes detected by smart-patch technique. *Biophys J* 94:1646–1655
- Wang Y, Liu YZ, Wang SY, Wang Z (2016) In vivo whole-cell recording with high success rate in anaesthetized and awake mammalian brains. *Mol Brain* 9:86



# Chapter 2

## Patch Clamp Technology in the Twenty-First Century

Jan Dolzer

### Abstract

In the almost four decades since its inception, the patch clamp technique has transitioned from a specialist skill to a method commonly used among many others in a lab. Development of patch clamp instrumentation has not been steady: A boost of product releases in rapid succession by multiple manufacturers in the 1990s had slowed to a trickle by the mid-2000s. In 2016, Sutter Instrument's entry into the market of turnkey patch clamp amplifier systems, defined as an amplifier with matching data acquisition hardware and software, caused a fresh breeze in a field in danger of going stale. Sutter has meanwhile completed the product line, culminating in the flagship dPatch® Ultra-fast, Low-noise Digital Amplifier. The dPatch System constitutes a contemporary, digital design that features many firsts, including digital signal compensation, an extremely high bandwidth and fully integrated dynamic clamp capability, paired with the increasingly popular SutterPatch® Software.

This chapter compares feature sets of the new Sutter instrumentation with the established platforms by the other two providers of turnkey systems, Axon Instruments by Molecular Devices and HEKA Elektronik by Harvard Bioscience. A variety of products from other manufacturers, who rely on combination with components from other sources rather than offering turnkey systems, are listed, but for their conceptual diversity not compared at a great level of detail. The chapter further covers architectural considerations for patch clamp systems, headstage design, data acquisition strategies and efficient structuring of the recorded data, controlling and monitoring periphery, advanced technologies, such as software lock-in amplifier capability and dynamic clamp features, and application modules for efficient analysis of action potentials and postsynaptic events.

**Key words** Patch clamp amplifier, Data acquisition, Whole-cell, Single-channel recording, dPatch, IPA, SutterPatch, Dynamic clamp

---

### 1 Introduction

In the decades since its invention [1, 2], patch clamp electrophysiology has fared a similar fate to many other scientific techniques: From a bleeding-edge skill, mastered by a relatively small number of well-trained specialists, it has matured and proliferated to a widely used method. Patch clammers used to recognize one another after exchanging a few sentences, a substantial level of electronics skills was part of what was needed to be successful, and an oscilloscope was a mandatory part of each electrophysiology rig. There were

quite a number of laboratories that defined themselves as patch clamp labs or electrophysiology labs in a broader sense.

Today, patch clamp experiments are usually performed as one out of a wide spectrum of scientific techniques to investigate a problem or a question associated with a particular model system. Researchers do not typically define themselves as patch clampers or electrophysiologists anymore and, consequently, often lack the detail knowledge of the intricacies of the instrumentation they use. Progress in instrumentation design and technology has made this paradigm shift possible for the majority of scientific applications of the patch clamp technique.

The automobile industry today delivers products that do not routinely require roadside repair or maintenance anymore. A car user can easily perform their daily commute and everyday shopping without so much as knowing how to open the hood—even though they will not likely become a successful race driver. Very similarly, the makers of today’s patch clamp systems must provide hardware and software that perform the majority of everyday tasks without requiring detailed electronics knowledge or an advanced degree in computer science. Algorithms that automatically set resistance and capacitance compensation to a degree that enables a meaningful recording are expected, as are application modules that facilitate data acquisition and analysis following published and established standards.

Among the suppliers for patch clamp amplifier and data acquisition systems, only three offer turnkey packages, consisting of an amplifier component, a more or less integral data acquisition system, and a software package: Axon Instruments/Molecular Devices, LLC. [3], HEKA Elektronik Dr. Schulze GmbH [4], and Sutter Instrument Company [5]. For the purposes of this chapter, instrumentation and software by these three major suppliers shall be discussed in more detail. Several smaller patch clamp amplifier manufacturers, such as Alembic [6], Dagan [7], npi electronic [8], and Warner Instruments [9], serve niche sectors of the market. A number of laboratories use National Instruments Corporation interfaces for data acquisition [10], often in conjunction with software programmed in-house or in the public domain. Common development platforms for this type of software are MatLab [11] or LabView [12]. The British company Cambridge Electronics Design (CED; [13]) makes computer interfaces and software, including products that can be used for patch clamp. A number of software packages that operate with various mainstream hardware models are available commercially, open-source, or as freeware. A few examples, without any claim of completeness, include Axograph [14], Ephus [15], jClamp [16], NeuroMatic [17], QuB [18], or WinWCP [19]. Since most of these products either serve niche applications, have limited feature sets, or require a substantial amount of customization and programming, an

exhaustive discussion is beyond the scope of this chapter. Many of the principles discussed in the context of the hardware and software systems by the three major providers analogously still apply to these products.

---

## 2 Headstage Design Considerations

To minimize current noise and maximize signal bandwidth, virtually all current patch clamp amplifiers consist of a separate headstage and a main unit. The headstage contains the feedback amplifier circuitry for voltage clamp operation as well as the current clamp/voltage follower circuit, and acts as the physical link between a micromanipulator and a pipette holder. Connection to the micromanipulator is typically established through a standard dovetail fitting. The dovetail connection was originally agreed on between Sutter Instrument and Axon Instruments in the early 1990s (Dale Flaming and Alan Finkel, personal communication) and has since been adopted by virtually all manufacturers of micromanipulators for electrophysiology and patch clamp amplifiers.

Two common formats for pipette holder fittings to the headstage are Axon Instruments' HL-U standard and HEKA Elektronik's BNC-based connection. Sutter Instrument and several other amplifier manufacturers use connections that are compatible with the HL-U standard. If a threaded connector made of Teflon® is used on the headstage side, as with Axon Instruments headstages and several others, considerable mechanical movement of the joint is possible, which manifests itself as drift of the pipette tip. Since this is often falsely attributed to the micromanipulator, troubleshooting the wrong component can waste precious time. To avoid this effect, Sutter Instrument headstages use a threaded collar that is machined of metal, and the pipette holder is firmly seated against it (Fig. 1). A welcome side effect is substantially better noise shielding of the headstage input. Several third-party suppliers make pipette holders as replacements, or for special applications, which are compatible with one of the two common standards. For the HL-U standard, Sutter Instrument also offers a pipette holder with a barrel made of quartz, which minimizes thermal expansion and may improve noise performance in certain applications [20].

Ground connector receptacles are typically placed at the back of the headstage. With most manufacturers, the headstage case is connected to signal ground and constitutes one of the ground connections to the micromanipulator system. The HEKA EPC 10 headstage case is driven, and therefore the ground connector and the dovetail fitting are insulated. The Sutter Instrument dPatch System comes with headstages that are divided into the analog recording headstage and a preamplifier module that contains the analog-to-digital and digital-to-analog converters, as well as the



**Fig. 1** The pipette holder fitting on Sutter Instrument amplifiers is compatible with Axon Instruments' HL-U standard, which has been adopted by several other manufacturers. The threaded collar on Sutter headstages is executed in metal rather than the commonly used Teflon®. This provides both greater mechanical stability and better electrical shielding

compensation circuitry, most of which operates in the digital realm. The preamplifier is designed to be placed inside the Faraday cage (if equipped), and all communication to the main unit is digital, which makes it completely immune to noise interference.

---

### 3 Feedback Elements

#### **3.1 Noise Performance in Voltage Clamp**

Most experimenters form the gigaseal in voltage clamp mode, irrespectively of whether they are planning a single-channel recording or move on to whole-cell mode and, eventually, may switch to current clamp mode. Currents through individual ion channels are small, typically in the range between 0.1 pA and several tens of pA, depending on the identity of the ion channel, the membrane potential, and the solutions. The demands to noise performance are therefore most stringent in voltage clamp mode. While the experimenter is, obviously, interested in the noise level during an actual recording, having an electrode holder, a pipette, a cell or patch and a bath connected to the headstage is not an appropriate way to determine the noise performance of an amplifier. These components act as antennas, and the noise they pick up describes the environment rather than the amplifier. The established method of measuring the noise specification of a patch clamp amplifier is therefore with the headstage in open-circuit condition, inside a grounded enclosure. The noise specification is given as root mean

square (RMS) noise by convention, since that metric is a good descriptor of broadband noise. However, among amplifier manufacturers, there is no consistent bandwidth at which the noise performance is measured. For single-channel recordings, the RMS noise of the amplifier system should be around 200 fA in a 0.1 Hz–10 kHz band. For whole-cell recordings, a noise level of 1–2 pA<sub>RMS</sub> in the same frequency band is acceptable.

### 3.2 Resistive Feedback

The most common headstage design uses the resistor feedback technology, in which a high-MΩ resistor  $R_f$  and an operational amplifier  $A_1$  form a sensitive current-to-voltage converter [21]. The feedback circuit is connected to the inverting input of the operational amplifier, and the command voltage to the non-inverting input (Fig. 2a). A second operational amplifier  $A_2$  subtracts the command voltage from the output of  $A_1$ , which is proportional to the feedback current. The output of  $A_2$  is, therefore, a voltage that is proportional to the current through the tip of the pipette ( $V_I$ ). The limited bandwidth of  $R_f$  makes it necessary to boost the high-frequency gain at the output of  $A_2$ . The principle, its limitations, and further design considerations are discussed in great detail in [21] and shall not be reiterated here.

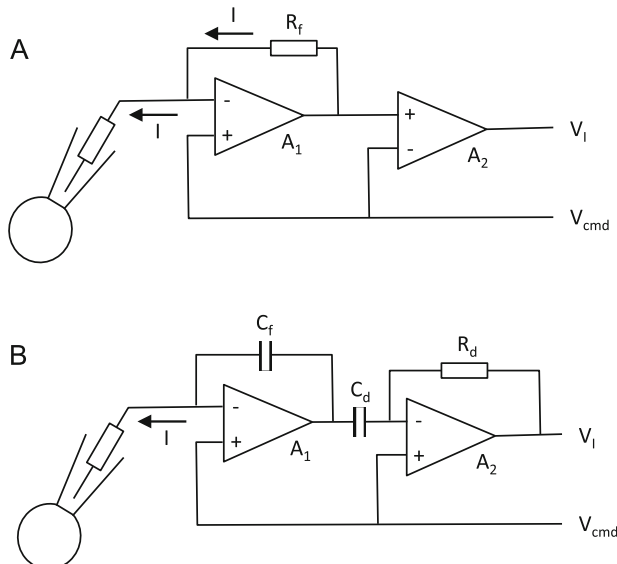


**Fig. 2** Resistive and capacitive feedback circuits used in patch clamp headstages. **(a)** Resistive feedback circuit.  $I$ : The current injected into the pipette is converted into a proportional voltage by operational amplifier  $A_1$  and feedback resistor  $R_f$ . Operational amplifier  $A_2$  subtracts the command potential  $V_{cmd}$  and puts out voltage  $V_I$ , which is proportional to the current  $I$ . **(b)** Capacitive feedback circuit. The feedback capacitor  $C_f$  configures operational amplifier  $A_1$  as an integrator. The following circuit of operational amplifier  $A_2$ , capacitor  $C_d$  and feedback resistor  $R_d$  form a differentiator, which puts out the voltage signal proportional to  $I$

### 3.3 Capacitive Feedback

To minimize noise in the feedback circuit, the Molecular Devices Axopatch 200B amplifier and the Sutter dPatch system feature capacitive feedback stages in addition to resistive ranges. Replacing the feedback resistor  $R_f$  with a capacitor  $C_f$  creates an integrating headstage circuit, which then must be followed with a differentiator (Fig. 2b). A capacitive feedback circuit provides lower noise when compared to resistive feedback, a greater bandwidth, better linearity and a larger dynamic range. Particularly the better noise performance makes capacitive feedback designs the best choice for single-channel recordings. A capacitive feedback circuit is not suitable for current clamp recordings, however. Therefore, both the Axopatch 200B and the dPatch systems are equipped with two resistive ranges, in addition. The dPatch system also features dedicated voltage follower circuitry, which enable current clamp recordings with minimal distortion. This is not the case for the Axopatch 200B (*see* Sect. 4 below).

#### 3.3.1 Resetting Transients

Large steady-state offsets in the recorded current would drive the integrator circuit in capacitive mode into saturation. Therefore, the capacitor needs to be reset when the circuit gets close to saturation. During this reset, a transient occurs, and the signal is not valid for a short period of time (typically  $\ll 1$  ms). *See* ref. 21 for an exhaustive discussion of this principle. While the Axopatch 200B uses a sample-and-hold circuit and puts out a “not-valid” signal on a dedicated connector, the digital design of the dPatch system allows for directly flagging the reset to the SutterPatch Software. The user can then decide to mask the resets with a straight line, equivalent to the way the Axopatch 200B treats them, to insert a blank into the recorded data, which may make it easier to exclude the invalid portion from further analysis, or to record the reset transients as they are. The reset transients further comprise a slow component with a complex time course, which can take several ms to fully decay. These are compensated with analog circuitry or by digital subtraction in the Axopatch 200B and dPatch amplifiers, respectively.

## 4 Voltage Follower Circuitry in Current Clamp

It is important to note that the Axopatch 200 amplifier was designed for ultimate noise performance, but high-fidelity current clamp recordings were not among the design goals. The lack of a dedicated voltage follower circuit in the headstage causes waveform distortions in current clamp mode, which must be taken into consideration when action potential waveform analysis is performed [22]. All other currently available amplifiers by the major providers have dedicated voltage follower circuits and are suitable for recordings in current clamp mode. While there are minute differences in bandwidth and phase correlation between various

amplifier models, which may affect high-resolution analysis of action potential waveforms (e.g., [23]), a detailed discussion is beyond the scope of this chapter.

---

## 5 Mode Switching/Smart Switching

A patch clamp amplifier whose command input is connected to a separate computer interface needs special attention when the experimenter switches from voltage- to current clamp mode. Since the recorded cell is most likely held at a hyperpolarizing potential, typically in the vicinity of the presumable resting potential, the command for that potential would be interpreted as an inward current after switching. To avoid either having to depolarize to 0 mV before the switch, or injecting current after the switch, amplifiers with a separate interface have an “ $I = 0$ ” setting at which the external command input is ignored. Amplifier systems with an integrated interface, such as the HEKA EPC 10 and the Sutter amplifier systems, do not need this setting, since the holding potential in voltage clamp is under entirely independent control from the holding current in current clamp mode. An integrated interface also allows to more accurately control the sequence of events during the switch from voltage to current clamp. Both HEKA’s EPC 10 and the Sutter amplifier systems utilize this principle for proprietary features, which are called Gentle Switch and Smart Switch, respectively, to avoid transients that are potentially damaging to the cells.

---

## 6 Compensation and Correction Circuitry

In patch clamp recordings, a number of signal modifications are common in order to reveal components of the recorded signal that would otherwise be obscured by passive capacitive or ohmic responses originating from the electrical circuit that consists of the pipette, the pipette holder, and the cell membrane. Several capacitive components and the series resistance  $R_s$  cause capacitive transients in voltage clamp mode and form low-pass filters in current clamp mode. It is important to understand that series resistance correction is the only method described in this section which alters the command signal sent out to the cell. Offset and capacitance compensation methods are applied to the recorded signal only and do not affect the command stimulus. They are, therefore, sometimes referred to as “cosmetic” measures. Nevertheless, they constitute effective ways of revealing fast currents, such as voltage-gated  $\text{Na}^+$  currents, which might otherwise be hidden in the capacitive transient elicited by a depolarizing step. Capacitance compensation circuitry also prevents the capacitive transient after a voltage

step from driving the headstage circuit into saturation. All compensation and correction methods described in Sects. 6–8 are applied before the signal is stored, and a copy of the untreated signal is not typically retained.

### **6.1 Offset Compensation**

After lowering the recording pipette into the bath in voltage clamp mode, a steady-state offset current is measured. This offset is caused by the sum of offset potentials from several sources. The half-cell potentials of the bath and recording electrodes can be one of the largest sources of an offset potential. Particularly when solutions with large organic anions substituting most of the chloride are used in conjunction with Ag/AgCl electrodes, offset potential amplitudes of well over 100 mV are not unusual.

The current offset is compensated by applying a potential that reduces it to zero. Computer-controlled amplifiers have a function that automatically zeroes the offset potential. The offset potential is not considered part of the command potential, but the potential after offset compensation is defined as 0 mV. While modern patch clamp amplifiers, such as the Sutter Instrument amplifier systems, do keep a record of the offset potential, few researchers routinely pay attention to it.

If a slow drift of the signal is observed, the most likely cause is a deterioration of the chloride coat on the electrode wire or the bath electrode. Another common cause is bath solution that gets in contact with the nonchlorided portion of an electrode wire or the wire portion of an Ag/AgCl pellet. Rechloriding the silver wire should be done in regular intervals. Blank silver portions can be insulated with Sylgard®, epoxy, or glue that remains elastic and does not leach solvents.

Some amplifiers have a feature called Track, which continuously eliminates the offset. This becomes problematic if Track is accidentally left enabled during and after seal formation. Since the reference point for the command potential is lost then, the recording is invalidated. The main reason for enabling Track is a slow drift in the signal, which is preferably addressed by eliminating its root cause (see above).

### **6.2 Capacitance Compensation**

Capacitance compensation is applied at two stages in the process of forming a seal and a whole-cell recording. Depending on the manufacturer of the amplifier the terminology varies. Sutter Instrument and Axon Instruments use the terms Electrode or Pipette Compensation and Cell or Whole-cell Compensation, respectively. Axon Instruments further divides the Pipette Capacitance into its fast and slow component. Both Sutter Instrument and HEKA Elektronik use fixed parameters for the slow component of the electrode capacitance compensation. HEKA Elektronik uses the term C-fast to describe the electrode capacitance, while C-slow refers to the whole-cell capacitance. These differences in terminology can lead to confusion.

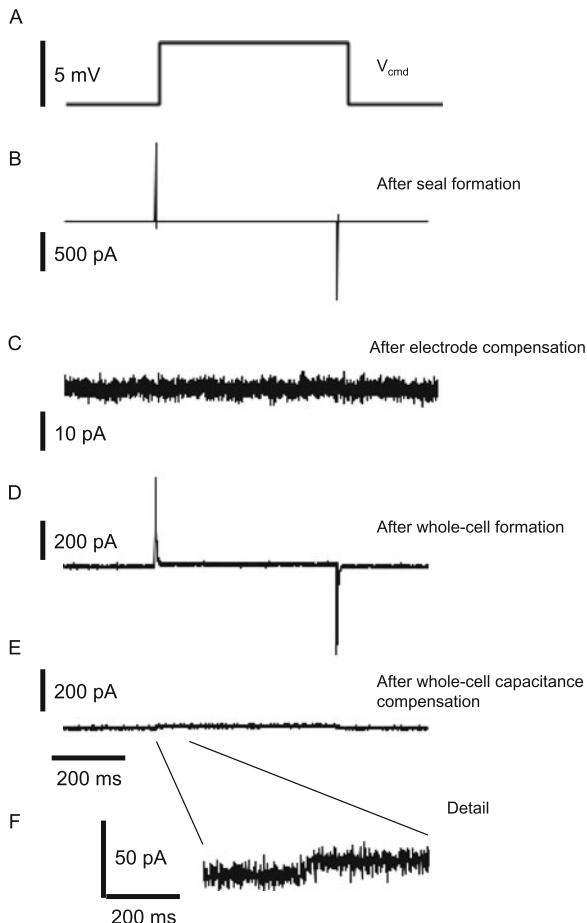


**Fig. 3** Capacitance compensation recorded on a Sutter dPatch Amplifier system with a model cell connected. Analog bandwidth: 10 kHz, resistive range  $\pm 20$  nA. After seal formation, the current response (**b**) to voltage command step (**a**) is a straight line with short capacitive transients. After automatic electrode compensation the capacitive transients virtually disappear in the noise (**c**). The longer capacitive transients after proceeding to whole-cell position (**d**) are compensated by the automatic cell compensation with minimal manual touch-up (**e**). (**f**) Detail of the rising step in **e**. The time scale is identical in **a–e**

### 6.3 Electrode Capacitance

#### 6.3.1 Voltage Clamp Mode

After seal formation (Fig. 3a–c), the capacitance of the recording circuitry is determined by the capacitance of the pipette and the, comparatively small, capacitance of the membrane patch. The latter disappears in comparison to the former. The electrode capacitance consists of two capacitive components, the slower one of which is relatively constant. Many researchers only adjust the faster component of the electrode capacitance, if separate controls are available. Sutter Instrument and HEKA Elektronik amplifier systems use fixed parameters rather than separate controls (see above).

In single-channel recordings and high-bandwidth applications, it is important to physically reduce the electrode capacitance as much as possible rather than compensating for it. This is done to both minimize the capacitive noise and maximize the recording bandwidth. The most commonly used methods are: (1) reducing the area of the capacitor that is formed by the glass pipette in the bath by coating it with wax or Sylgard®, or pouring oil on top of the bath solution, (2) maximizing the distance between the two conductive solutions by coating the pipette and giving it a stubby shape with a short taper, and (3) using quartz capillaries, which have a lower dielectric constant than the commonly used borosilicate. Quartz capillaries cannot be pulled with filament-based pipette pullers, however. Currently, the only commercially available puller that can handle quartz is the Sutter Instrument P-2000 laser-based micropipette puller.

### 6.3.2 Current Clamp Mode

Most researchers base the capacitance compensation applied in current clamp mode on the value that was determined in voltage clamp. To avoid oscillations that can be triggered by rapid changes in the recorded signal, such as action potentials, the magnitude is commonly reduced by 5–10%. Even though it is the same pipette property that is being compensated, it is not uncommon to refer to this method as Capacitance Neutralization when in current clamp mode.

## 6.4 Whole-Cell Capacitance

Once the electrode capacitance has been compensated, most experimenters proceed to the whole-cell configuration. This is done by applying stronger suction to the pipette. Some cell types or preparations break in more easily when a “Zap” pulse is applied, a depolarizing voltage step of several hundred mV and typically a duration in the submillisecond range.

The whole-cell configuration is indicated by the presence of much larger capacitive transients on the square membrane test response, since the membrane of the entire cell now contributes to the total capacitance of the system (Fig. 3d–f). All patch clamp amplifiers designed to perform whole-cell recordings have the capability of compensating for the membrane capacitance  $C_m$  and series resistance  $R_s$ . Note that HEKA Elektronik calls this compensation C-slow, which bears the risk of being confused with Axon Instruments’ fast and slow components of the electrode capacitance. Sutter Instrument’s amplifier systems explicitly refer to Electrode and Cell Compensation, respectively.

The automatic compensation feature, common in computer-controlled amplifiers, should constitute a good starting point for capacitance compensation. Manual touch-up may be required for highly sensitive applications.

## 7 Series Resistance Correction

The series resistance  $R_s$  between the inside of the recording pipette and the lumen of the cell is comprised of the pipette resistance and the resistance of cell membrane lining the inside of the pipette orifice, as well as organelles, vesicles, membrane fragments or other debris that may clog up the opening. Depending on the cell type, there is a variety of strategies to minimize the series resistance, including but not limited to choosing a large pipette opening and applying pressure-suction regimes after whole-cell formation. A rule of thumb is that the best that can be achieved is twice the electrode resistance. But with many preparations, a substantially higher  $R_s$  must be accepted.

The series resistance is the  $R$  component of a low-pass filter that slows down rapid changes in the command potential. In addition, the voltage drop across  $R_s$  causes a reduction of the amplitude of the command potential. Therefore, a command potential step gets both slowed down and reduced in amplitude (Fig. 4).

Two different methods have been applied to mitigate the effect of  $R_s$ , commonly referred to as Correction and Prediction. The principle of  $R_s$  Correction is adding a scaled version of the recorded current signal to the command potential and thus compensate both the slowing of edges and the voltage drop. Since this circuit constitutes a positive feedback loop, it introduces the risk of oscillation, also referred to as ringing. Series resistance Prediction, also known

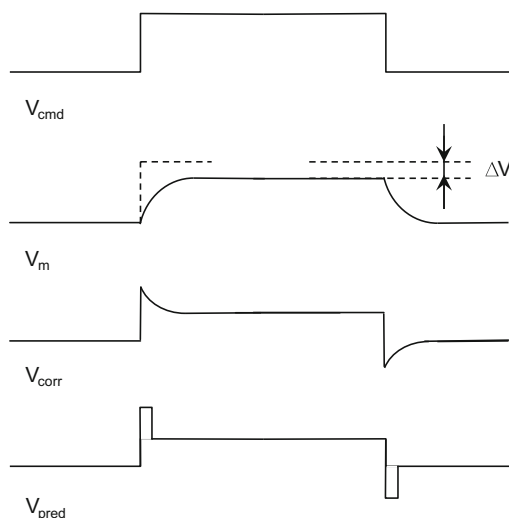


**Fig. 4** Series resistance correction and prediction. The command step  $V_{cmd}$  is both reduced in amplitude and slowed down by the series Resistance, which results in the membrane potential  $V_m$ . Series resistance correction ( $V_{corr}$ ) and prediction ( $V_{pred}$ ) mitigate this effect, depending on the percentage applied and square up  $V_m$  (not shown)

as Supercharging, adds a scaled and shaped version of the command potential, which is derived from the whole-cell capacitance compensation circuit. Since Prediction is not controlled by a positive feedback loop, it does not introduce the risk of ringing. It also does not correct the voltage drop across  $R_s$ . Unlike the other compensation circuitry, series resistance compensation is not applied to the recorded signal only but affects the signal that is applied to the pipette. Therefore, feedback ringing of the Correction circuit applies large command voltage oscillations to the cell membrane, which quickly destroys cells and makes the recording useless.

Both Prediction and Correction are typically combined and applied in a graduated fashion as a percentage. To avoid feedback oscillations and their detrimental effect on the cells, many experimenters keep the Correction under 70%. The Axon Instruments Multiclamp 700B features an oscillation detection feature, which disables  $R_s$  Correction as soon as a beginning oscillation is detected. The digital architecture of the Sutter Instrument dPatch system eliminates nonlinearities and tolerances of analog components, which significantly reduces the occurrence of feedback oscillation and minimizes the detrimental effect. With a model cell connected,  $R_s$  Correction of >95% does not cause feedback oscillations, even with a lag of only 2  $\mu$ s. Provoked oscillations (99% Correction, 1  $\mu$ s Lag) do not drive the circuit into rail-to-rail operation at an analog bandwidth of 10 kHz. While in theory that should prevent cell damage, this assumption still remains to be tested in wet-lab conditions and with a variety of cell types.

---

## 8 Bridge Balance Compensation

In current clamp mode, injected current waveforms cause a voltage drop across the resistance of the recording pipette. Since this voltage drop cannot readily be distinguished from a voltage signal originating from the preparation, bridge balance compensation is used to eliminate the Ohmic component. The name originates from the use of a circuit called a “Wheatstone bridge” in the days of early microelectrode amplifiers. Modern designs use operational amplifiers for this purpose. To adjust bridge balance, a current pulse is applied to the preparation. Then a scaled version of the current waveform is added to the recorded signal and adjusted until the steady-state portion of the voltage response disappears (Fig. 5).

---

## 9 Dynamic Holding

In current clamp recordings it is sometimes desirable to compensate for the weakening membrane resting potential of a deteriorating cell and hold it at a target potential by injecting current that

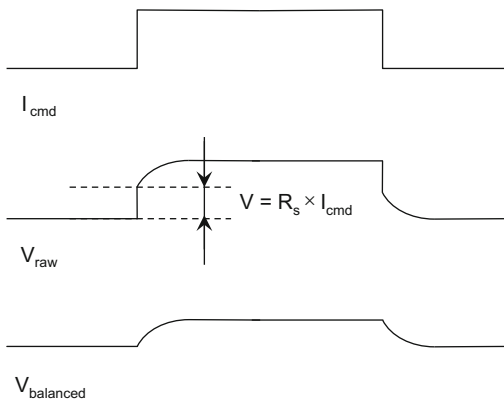


**Fig. 5** Bridge balance compensation. A command step applied in current clamp ( $I_{cmd}$ ) elicits a voltage drop across the pipette resistance, superimposed by the voltage response from the preparation ( $V_{raw}$ ). Bridge balance compensation eliminates the Ohmic portion and returns the isolated voltage response from the preparation ( $V_{balanced}$ )

updates with a long time constant. The computer-controlled amplifier systems from the three major providers have features that achieve this. Axon Instruments calls this function Slow Current Injection, HEKA Elektronik uses the term Low-frequency Voltage Clamp (LFVC), and Sutter Instrument calls it Dynamic Holding.

Care must be taken not to accidentally leave this feature enabled, however, when the uninfluenced resting potential of the cell is the subject of the experiment. Continuous current injection also constitutes a net movement of charges, which may lead to depletion or accumulation of ions inside the recorded cell or in its vicinity.

## 10 Data Acquisition

### 10.1 Data Acquisition Over the Years

In the early days of the patch clamp technique, it was common to continuously record the current and voltage signals on storage media such as FM tape or, once available, digital audio tape (DAT), using modified recorders. Regular audio recording equipment was not suitable, since it does not preserve DC offsets, either because the storage medium does not support it, or because the signal is purposely highpass-filtered. In addition, it was not uncommon to write the signal to a strip chart recorder for convenient overview. Stimulus waveforms were created using sophisticated stimulus generators, whose signal was recorded along with the elicited signal.

With the advent of more powerful computers and interfaces that had buffering capability and analog-to-digital and digital-to-analog converters (AD/DA boards), data acquisition became much

more streamlined, and stimulus waveforms were often created by software. Commercial amplifiers and data acquisition systems were launched, and the California-based company Axon Instruments Inc., as well as the German HEKA Elektronik Dr. Schulze GmbH established themselves as the market leaders. Both providers offered systems in a three-tier architecture consisting of a patch clamp amplifier, a computer interface, and software packages that controlled data acquisition and provided a certain level of data analysis capability.

It was not uncommon to combine one provider's amplifier with the other's computer interface, or use an amplifier made by one of the smaller manufacturers (see above). Both Axon and HEKA originally used interfaces made by third-party providers, Labmaster and Instrutech, respectively. In the early 1990s, Axon Instruments developed their first in-house interface, the Digidata 1200. HEKA Elektronik continued using Instrutech interfaces until they eventually acquired the company in 2007.

Axon Instruments was sold to Molecular Devices Corp. in 2004, and the company went through two more mergers until 2008. With a focus on high-throughput instrumentation and imaging platforms, not much development has been done for the conventional electrophysiology product line. The only somewhat recent hardware product by Axon Instruments/Molecular Devices is the Digidata 1550 interface. Only incremental updates were made to the pCLAMP software suite in varying intervals. The most recent version upgrade, pCLAMP 11, came with a minimal set of new features. Many long-standing issues and shortcomings have remained unresolved. It is still a 32-bit application, which more and more clearly shows its age.

HEKA Elektronik was acquired by Harvard Bioscience, Inc. in 2015. The established EPC 10 patch clamp amplifier was updated several times until the early 2010s and has since been available in its current revision. Patchmaster Software has continuously undergone development, both for bug fixes and new features. Patchmaster NEXT Software, released in 2018, presents much of the Patchmaster functionality in a more contemporary and intuitive graphical user interface, and on a more modern development platform.

In 2016, Sutter Instrument released the IPA<sup>®</sup> Integrated Patch Amplifier System, a patch clamp amplifier optimized for whole-cell recordings, with the data acquisition system integrated on the same circuit board, and SutterPatch<sup>®</sup> Data Acquisition, Management, and Analysis Software being part of the bundle. Over the following few years, the product family was broadened. It currently includes the Double IPA<sup>®</sup>, a dual-headstage version of the IPA system, the dPatch<sup>®</sup> Ultra-Fast, Low-Noise Patch Clamp Amplifier System with dynamic clamp capability, available with one or two headstages, and the recently released Dendrite<sup>™</sup> Data Acquisition

System. Each product includes SutterPatch Software, which is based on Igor Pro by WaveMetrics and undergoes constant development. A number of research papers about experiments using the IPA Family Amplifier Systems and the included SutterPatch Software have been published [24–32]. Both the dPatch and Dendrite systems are too new to have been used for any publications at the time of this writing.

## 11 Three-Tier Architecture Evolves into Integrated Systems

In the early days of recording patch clamp data to computers, often with the intermediate step of recording on tape recorders modified to be DC-capable, a three-tier architecture was common (Fig. 6): The amplifier puts out an analog signal, which is routed to the analog-to-digital/digital-to-analog (AD-DA) converter, often referred to as the computer interface, or simply the interface. The interface, under control of software, turns the analog signal into a digital representation, which the software stores in a structured fashion. The software can also generate a command waveform, which the interface turns into an analog signal that is sent to the amplifier. This traditional architecture is still used by Axon Instruments and, for compatibility with others' components, by providers of standalone amplifiers or data acquisition systems.

A contemporary approach integrates the data acquisition hardware with the amplifier. The HEKA Elektronik EPC 10 system combines amplifier and computer interface circuit boards in a single

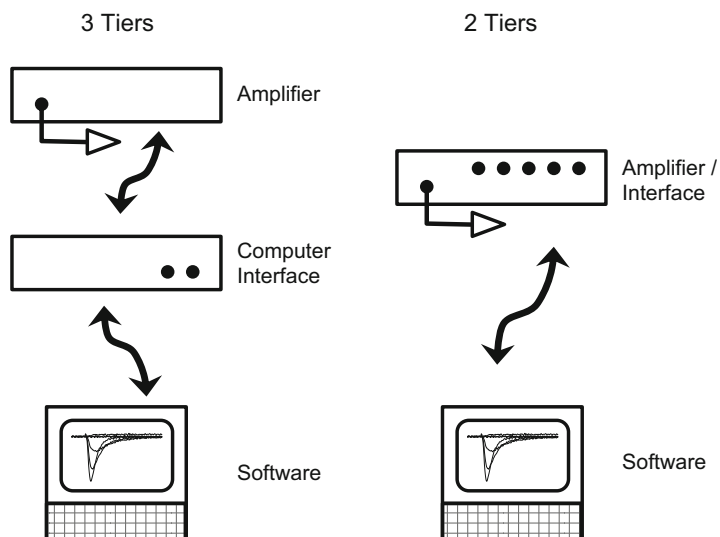


**Fig. 6** Comparison of the original three-tier architecture and the more modern two-tier architecture in patch clamp systems

case, with a common power supply. The Sutter Instrument IPA family devices combine both amplifier and interface circuitry on the same board, which reduces power consumption and keeps system cost low. The patented [33, 34] Sutter Instrument dPatch® system even takes it a step further by making the AD-DA converter circuitry part of the headstage assembly and performing all compensation and correction (see above) in the digital realm. Since reliable capacitance compensation requires a very high sampling rate to capture rapidly decaying transients, the dPatch system incorporates the ability to sample at 5 MHz per headstage channel. The analog bandwidth of the headstages lies between 500 kHz and 1 MHz.

Software applications for data acquisition constitute the third tier of the classic architecture. With all three major providers, the acquisition software is tied to the respective computer interface, whether integrated (HEKA, Sutter) or separate (Axon). Axon Instruments offers pCLAMP Software, a package that consists of the data acquisition application Clampex and the data analysis program Clampfit. AxoScope software, a drastically feature-reduced version of Clampex, comes bundled with the Digidata® 1550 interface. pCLAMP Software needs to be acquired separately. Starting with version 11, the Clampfit analysis program requires a separate license protection key.

Most HEKA users purchase Patchmaster Software for data acquisition as a separate item and perform data analysis in third-party software. The most popular third-party analysis platform among HEKA users is Igor Pro by WaveMetrics [35], a technical graphing and analysis software with extensive programming capability.

Sutter Instrument patch clamp systems integrate all three architectural tiers into a single package and provide the Igor Pro-based SutterPatch® data acquisition, management and analysis software as part of the system package.

---

## 12 Data Structure Determines Efficiency of Data Analysis

A structured storage format facilitates data management and streamlines analysis. Efficient batch analysis requires that the data structure is consistent between experiments, since it needs to be predictable in which portion of the data a particular family of currents is found, and what its structure is. The three major providers store data in different ways, and certain aspects of the terminology may create confusion.

### 12.1 Samples, Signals, Sweeps and Series in a Greater Context

The most common form of patch clamp data in voltage clamp mode constitutes a family of currents elicited by a family of voltage steps or more complex waveforms. This data pattern is commonly used, for example, to investigate a current–voltage relationship and create the respective plot, commonly referred to as an *I*–*V* curve.

**Table 1**  
**Terminology comparison between the three major software packages**

Axon Instrument pCLAMP	HEKA Patchmaster	SutterPatch
N/A	Compound Data	Experiment
Sequencing Key Sequence	Protocol	Paradigm
N/A	N/A	Paradigm Data
Protocol	PGF Sequence	Routine
Trial (data file)	Series	Series (Routine Data)
Signal	Signal	Signal
Sweep	Sweep	Sweep
Epoch	Segment	Segment
Sample	Sample	Sample

The data consists of one or multiple input signals, typically with multiple sweeps, between which a portion of the waveform is incremented.

Axon Instruments' pCLAMP software calls the set of instructions that creates this dataset a Protocol. The resulting dataset is called a Trial and constitutes an individual data file (Table 1). Other than data file naming, which includes a prefix and an automatically incrementing numerical index, no context for the dataset is created, and it is up to the experimenter to write down where in the structure of their experiments the data file belongs.

HEKA Elektronik's Patchmaster software refers to the equivalent set of instructions as a Pulse Generator (File) Sequence. The resulting dataset is stored as part of a larger data file, which can contain data from an arbitrary number of executions of Pulse Generator Sequences. The data in a data file can be accessed in a tree-like structure. An infinite number of Pulse Generator Sequences can be stored in a Pulse Generator File.

Sutter Instrument's SutterPatch Software uses the term Routine for the corresponding instruction set and calls the resulting dataset Routine Data or a Series (Fig. 7a). If the recording is started by executing a Routine, a container for the dataset is automatically created, which is called a Paradigm. The Paradigm Data contain various types of information, which is not based on samples, sweeps and signals, called Metadata (see below). Importantly, Paradigm Data also record the temporal context of each Series relative to others, if the same Routine is executed several times, or different Routines are executed successively. The data are organized in a configurable tree structure, represented in the Data Navigator, which provides random access to any Paradigm, Routine, Signal

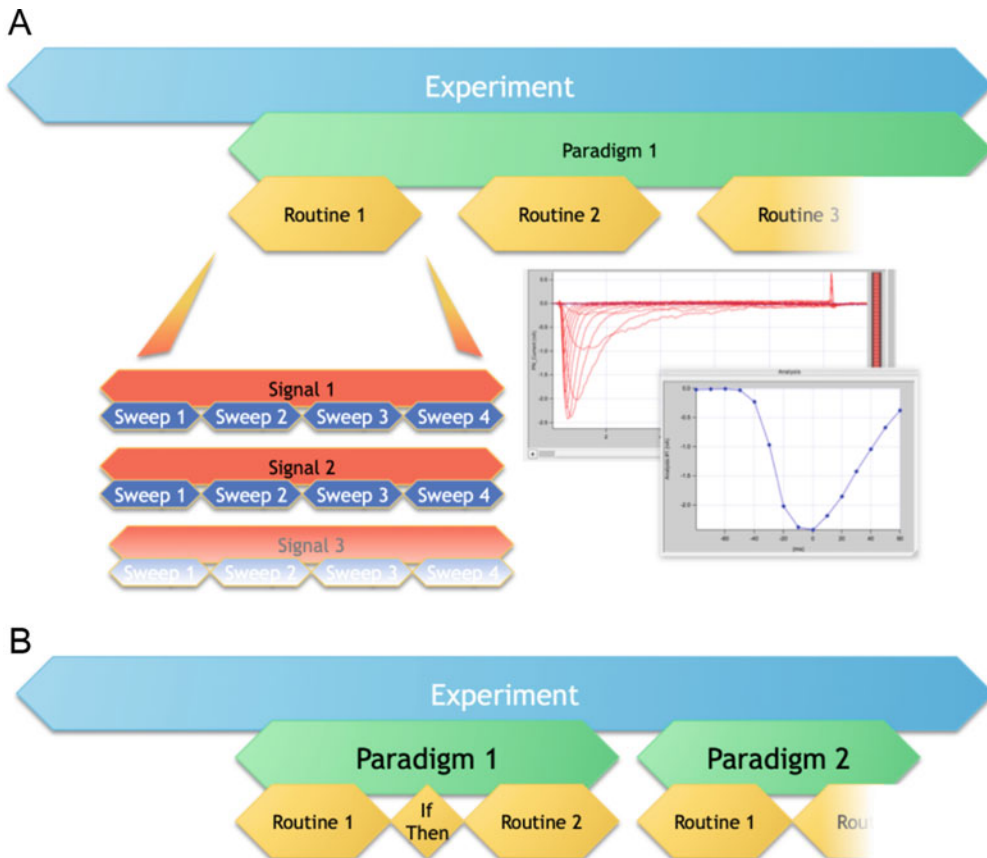


**Fig. 7** The data structure in SutterPatch® Software. **(a)** An “Auto-triggered Paradigm” is created by execution of a Routine, in this case a family of voltage steps that elicits voltage-gated sodium ( $\text{NaV}$ ) currents and creates an  $I$ - $V$  curve in real time. **(b)** An example of two “Planned Paradigms,” which can be used to partially automate an experiment. Routine 1 could be the same  $\text{NaV}$  Routine as in **a**. The flow control element (If-Then) accesses the real-time measurements in Routine 1 and determines whether the peak current is greater than an acceptance threshold. If so, Paradigm 1 proceeds to Routine 2, which is used to determine the half-inactivation potential  $V_{1/2}$ . Then Paradigm 1 sets the holding potential to  $V_{1/2}$  and chains to Paradigm 2, which generates the data for a concentration-response curve. If the acceptance criterion is not met, Paradigm 1 terminates the recording after the If step

or Sweep node. Multiple Series within a Paradigm can be displayed in a Scope Window on a continuous time axis and drilled down to for closer examination and analysis.

All three software packages feature a certain level of automation. The most basic approach is implemented in pCLAMP, where Sequencing Keys let the user load or execute Protocols, change inputs and outputs and link to other Sequences. Flow control is only realized as said links to other keys and Wait steps that block execution for a preset time, or until the user responds to a prompt. Execution of Sequencing Keys is in no way reflected in the data

structure: If a Protocol is executed, a corresponding, but isolated data file is created. If not, execution is only logged in the purely text-based Lab Book.

Patchmaster offers much more sophisticated scripting ability in what is called Protocols. The fact that pCLAMP and Patchmaster use the term Protocol for completely different structural entities leads to considerable confusion among users who switch from one platform to the other (Table 1). Patchmaster Protocols enable control of virtually all hardware settings and, importantly, provide If-Then-Else and Loop steps for advanced flow control and a substantial level of automation of the experiment.

SutterPatch Software also lets the user execute a scripted experiment, as defined by a Paradigm. Other than pCLAMP and Patchmaster, execution of a Paradigm does create a data entity as a subset of the data file, irrespectively of whether it is executed as an “auto-triggered Paradigm,” initiated by execution of a Routine (Fig. 7a; see above), or a “planned Paradigm” as a scripted portion of the experiment (Fig. 7b). Not only do SutterPatch Paradigms, much like Patchmaster Protocols, let the user control all hardware functions, provide advanced flow control, give access to real-time measurements and support execution of arbitrary mathematical equations, but they also let the user call Igor Pro commands, including custom code procedures, which enables execution of complex analysis procedures and creation of bespoke graphs or layouts. Last but not least, execution of a planned Paradigm creates an entity within the experiment, whose predictable data structure is the foundation for automated, efficient data analysis.

## 12.2 Handling Metadata

Besides the electrophysiological recording, which after digital conversion is stored in numerical sample points, the experimenter typically wants to record information about the specimen, instrumentation or environmental parameters. These metadata have traditionally been written down in a lab journal, a separate text document or a text window in the data acquisition software. This unstructured approach results in metadata that are difficult to mine and, in the case of a paper-based journal or a separate file, are at risk of being separated from the associated electrophysiological data. Only SutterPatch Software comes with features that enable storing user-defined metadata in a highly structured fashion.

## 12.3 Automatically Determined

Most of the metadata that describe the instrumentation used during the recording can be determined automatically. Traditionally, amplifiers transmitted certain settings to dedicated input connectors on a data acquisition interface. This was referred to as Telegraphing and is naturally limited to only a small number of parameters. The only amplifier by a major manufacturer still using this technique is the Axopatch 200B amplifier. All other systems by the major providers either use software telegraphing (MultiClamp

700B), or the amplifier circuitry is directly controlled by the same software that also accomplishes data acquisition (HEKA, Sutter).

But it is not only the amplifier settings that can be stored along with the recorded signals without requiring input from the experimenter. The identity of hardware, such as model and serial numbers, firmware revision, the software configuration that was employed, the identity of the user who was logged into the operating system, and many other parameters can be determined in the background and stored without requiring user intervention.

#### **12.4 User-Defined**

Contemporary platforms, such as SutterPatch Software, enable the experimenter to store other information they may find relevant, such as the animal species, genotype, sex, weight or age, as well as parameters of the tissue or cell preparation, such as prep time, dissociation solution or storage conditions. Even parameters that cannot traditionally be recorded with electrophysiology data, such as the recording solutions, or information about the micropipette electrodes, can be stored in a structured way. The user can opt to be prompted to review and confirm parameter values at the beginning of an experiment, or before a data recording commences.

Two aspects are important when it comes to storing metadata in a way that facilitates efficient analysis: (1) Each metadata parameter must be stored in its own, dedicated field. Extracting information from a free-text comment field or a shared space is inefficient and highly error-prone. (2) A measure, such as the animal weight or age, must be recorded separately in two fields, as the numerical quantity and the corresponding unit. Storing the weight of a mouse as “22.3 g” requires parsing of a string parameter for analysis. If the unit is recorded separately, however, the software can prompt for the numerical weight in g at the beginning of an experiment. The unit, “g” in this example, will likely stay the same between experiments.

#### **12.5 Dynamically Updated During Acquisition**

While parameters associated with the experimental animal or the preparation do not usually change during an experiment, other metadata parameters may change, and their stored values may need to be dynamically updated. That is naturally the case for amplifier settings if they are changed in the course of long experiments, for example, to account for changes in the series resistance of a whole-cell recording. The amplifier bandwidth and the corresponding sampling rate may be different for different types of acquisition Routines.

Potentially more critical is the capability to record changes in a stimulus, such as the addition of a test compound. The key here is the ability to record a parameter change, with a time stamp, even if it occurs while no signal data is stored to disk. This enables the researcher to more accurately reproduce under which environmental conditions the next dataset was recorded, while accounting for

possible delays in the stimulus delivery system. The most common delays are introduced by switching solutions with a perfusion system, since dead volumes cannot be completely eliminated, the full exchange of the bath solution takes some time, and slow receptor binding may cause additional delays. A time-tagged record of when a solution change was initiated is the most reliable way of ensuring complete solution exchange. Display of a sequence of Routine data sets on a continuous time axis, with tagged events during or between them, provides a convenient overview over an experiment or a portion of it. Among software packages by the major providers, only SutterPatch Software has this ability. Both pCLAMP and Patchmaster software rely on purely text-based tags generated by the user. If they occur outside signal acquisition, they are not in temporal association with the data but merely exist as comments in the respective Lab- or Notebook windows. That makes the analysis unnecessarily inefficient and error-prone, since it involves parsing of plain text entries.

---

## 13 Controlling and Monitoring Periphery

A variety of hardware for control or monitoring of environmental parameters, cell identification or stimulus delivery can be associated with a patch clamp setup. From the view of the amplifier and data acquisition system, these devices are considered periphery. Even though a microscope manufacturer will very likely disagree and view their advanced fluorescence lamp as something other than periphery, the term shall be used for the purposes of this chapter.

Peripheral instrumentation is typically controlled by either a graduated, analog voltage signal, or a series of digital pulses. By convention, most commercially available data acquisition systems put out an analog range of  $\pm 10$  V. These are typically referred to as Auxiliary Outputs or similar. The same amplitude range of  $\pm 10$  V is commonly used for Auxiliary Input channels. Digital Outputs either follow the TTL logic level standard, or the more modern CMOS standard [36]. These standards are designed to be compatible with each other. Most common electrophysiology periphery known to the author accepts CMOS signals as digital input.

An important consideration in the decision of whether to use analog or digital control of peripheral instrumentation is the question whether or not the amplitude of the event generated by the peripheral instrument plays a role for the recorded signal. If, for example, a liquid-filament switch system bathes the cell in either one solution, or the other, only the timing of the signal is relevant, and a digital output line can be used. Similarly, if a bank of pinch valves in a solution switcher is controlled individually. However, if the stimulus amplitude is of relevance for the recorded signal, analog control is preferred. That is also the case if the respective peripheral

instrument provides the capability to trigger sophisticated stimulus waveform patterns through a short digital pulse: Unless that waveform pattern is recorded together with the data, valuable information about the applied stimulus may be irrevocably lost.

One scenario commonly seen in the field is triggering a light stimulus by opening a shutter, while controlling the intensity with a manual dial. Without meticulous documentation, nothing is known about stimulus intensity. Even if the dial setting is diligently written down for each trigger, precision is limited by the dial, and accuracy depends on proper calibration procedures. The record is usually either made in a paper journal or a separate text document. In neither case is a permanent link to the recorded signal created. Most modern light sources accept an analog signal to control the light intensity. An LED light source has short enough switching times to not require a shutter, and the same analog signal also controls the duration. Therefore, an Auxiliary Output should be used to control light intensity, if possible, together with the duration.

Another common scenario is the use of an electric stimulator or stimulus isolator. Some of these devices can create sophisticated waveforms or stimulus trains, triggered by a single, short TTL pulse. If the connection is implemented in that way, the stimulus signal must be recorded on a separate input channel of the data acquisition system. Otherwise, it is virtually impossible to efficiently keep track of a complex stimulus. The much-preferred way is controlling a stimulus isolator through a Digital Output in case the amplitude is irrelevant, or an Auxiliary Analog Output if amplitude does matter.

When a solution switcher is used in pharmacology experiments, it streamlines data analysis if the acquisition software supports mapping a particular configuration of the outputs to a reservoir of the solution switcher and its contents, as characterized by compound identity, concentration and other factors, such as whether it is a control or test compound solution. At present, SutterPatch Software is the only commercially available package that features this ability.

---

## 14 Capacitance Measurements/Lock-In Amplifier

Both the Patchmaster and SutterPatch software packages feature software lock-in functionality. For high-resolution capacitance measurements during a voltage clamp recording a sine wave voltage is applied. The phase relation between the stimulus and the elicited current response are used to compute membrane parameters of the three-state model [37–40]. This enables highly sensitive recordings of exo- and endocytotic processes. pCLAMP software does not have this functionality.

---

## 15 Dynamic Clamp

The dynamic clamp technique was first introduced in 1993 as a method for simulating ionic conductances in neurons during patch clamp recordings [41, 42] and was later found to be applicable in cardiac and endocrinology research [43], as well as potentially other fields. This method typically involves recording the cell's membrane potential, transmitting the data either to an external computer, or using an interface with the necessary computing power built in, calculating the appropriate current to be injected into the recorded cell, and sending this value back to the amplifier. An external computer needs to run a real-time operating system, or at least an operating system with minimal jitter to ensure timely response to changes in the recorded signal. That precludes simple use of an existing computer interface and a purely software-based addition of dynamic clamp to existing platforms [44]. Communication between the computer and amplifier limits the rate at which the dynamic clamp calculations can be updated. Moreover, the additional hardware and software needed to do dynamic clamp have limited its application.

Unlike conventional platforms, which require either an external computer, or real-time processing power in the computer interface, the patented digital architecture of the Sutter Instrument dPatch amplifier provides an ideal platform for integral dynamic clamp. Utilizing parallel processing across a field programmable gate array (FPGA) and two high-speed ARM core processors, several sophisticated dynamic clamp models are implemented within this architecture. In each model, the update of the applied current values occurs without requiring any communication between the dPatch system and the data acquisition computer. Depending upon the complexity of the model, update rates of up to 500 kHz can thus be achieved.

Simulation of a population of channels within the cell membrane involves modeling the kinetics of the channel's gating mechanisms. The channel kinetics can either be modeled using multiple independent gates as in the Hodgkin–Huxley model [45], or a multistate Markov model [46]. For Hodgkin–Huxley style models, the dPatch system provides up to 16 individual gates per simulated channel, with up to 8 simulated channels running simultaneously per headstage. For Markov models, up to four 14-state models can be run simultaneously, or eight models with 10 or fewer states can be executed.

The values derived from the gating equations are then used to calculate the current applied to the cell. The calculation of current can either be defined in terms of conductance, or permeability. For conductance models, the value defined from the gating calculations is combined with the reversal potential of the ions passing through

the simulated channels, as well as the conductance of the simulated channels. Furthermore, channel conductance values can be voltage-dependent. For permeability models, the value defined from the gating calculations is combined with the intracellular and extracellular concentrations of the ions passing through the simulated channels. These models simulate the Goldman-Hodgkin-Katz equations [47, 48]. A comprehensive overview of the Dynamic Clamp feature in the dPatch amplifier system was given in a 2020 webinar presentation [49]. Since Dynamic Clamp capability is a feature that has been newly introduced to SutterPatch Software at the time of this writing, there is no scientific publication about its use in the laboratory yet.

---

## 16 Application Modules

The growing demand for more integrated solutions in patch clamp software has been met with the addition of several application modules to SutterPatch Software. The discussion here shall be limited to two methods of event detection in SutterPatch Software. A 2019 webinar presentation demonstrates the use of the SutterPatch Application modules in everyday laboratory operation [50]. A single-channel analysis module was recently added to SutterPatch Software [51]. Since it is very likely to undergo further development and changes based on user feedback, this application module shall not be discussed here. pCLAMP Software provides similar event detection functionality, while Patchmaster Software does not have event detection features.

### 16.1 Event Detection

#### 16.1.1 Action Potentials

Action potential detection is typically threshold-based. When applied to patch clamp recordings in current clamp mode, the signal-to-noise ratio is normally good enough to ensure reliable detection of action potentials without false positives or negatives. With juxtacellular *in vivo* recordings or other extracellular recording techniques, detection may be more involved, and using the event length as an additional detection criterion may be useful. SutterPatch Software puts out a number of standard waveform analysis parameters for each action potential, such as the threshold potential and the time of threshold crossing, the peak amplitude, the action potential duration (APD) at a user-defined level of repolarization, and the greatest afterhyperpolarization as well as its time of occurrence. In addition, a phase plane plot ( $\partial V / \partial t$  vs. voltage) for each action potential or the average is generated, and event count and frequency are put out (Fig. 8).

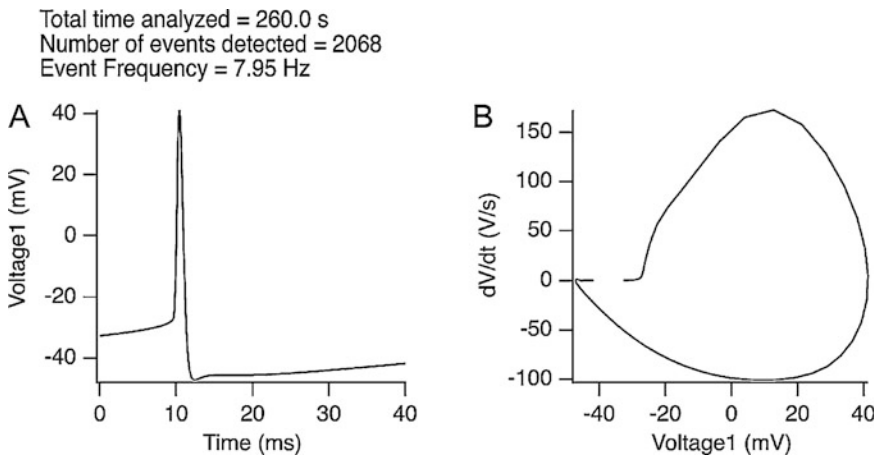


**Fig. 8** Graphical output of the SutterPatch Action Potential Analysis Module applied to a recording of spontaneous activity in a brain slice. **(a)** Average action potential waveform across all detected events. **(b)** Phase-plane plot of the averaged action potentials. Above the plots, basic statistics of the analyzed dataset are put out. In addition to the layout, the numerical results for each action potential are compiled and displayed as a table (not shown)

#### 16.1.2 Postsynaptic Events

Depending on the quality of the recording, detection of postsynaptic events can be a lot more demanding than action potential analysis. SutterPatch Software employs a deconvolution algorithm [52, 53], which has proven rather robust to poor signal-to-noise ratio and overlapping events. The event template is defined through rise and decay time, as well as the event polarity. The detection threshold is defined in multiples of the standard deviation and can optionally be further constrained by an amplitude threshold. After event detection, the events can be reviewed individually, and invalid events can be excluded from further analyses. The averaged waveform can be compared to the template for iterative fine tuning if desired. The results are put out in numerical form and as a summary page, which can be used in a workgroup presentation or, with little further editing, be the basis of a publication figure (Fig. 9, [50, 54]).

Other common analysis software for postsynaptic events includes pCLAMP Clampfit, Axograph [14] and Mini Analysis by Synaptosoft Inc. [55]. The latter, although popular, does not seem to have been updated in many years and may not run on modern computer systems. Only the SutterPatch and Axograph software packages run on both Windows and MacOS.

---

## Acknowledgments

The author would like to thank countless scientific contacts, customers, and coworkers for stimulating and often challenging discussions over the years. Many colleagues at Sutter Instrument have

Total time analyzed = 3999999.0 s  
 Number of events detected = 749  
 Event Frequency = 1.87e-4 Hz  
 Average Event Amplitude = -10.25 pA  
 Standard Deviation of Event Amplitude = 5.60 pA

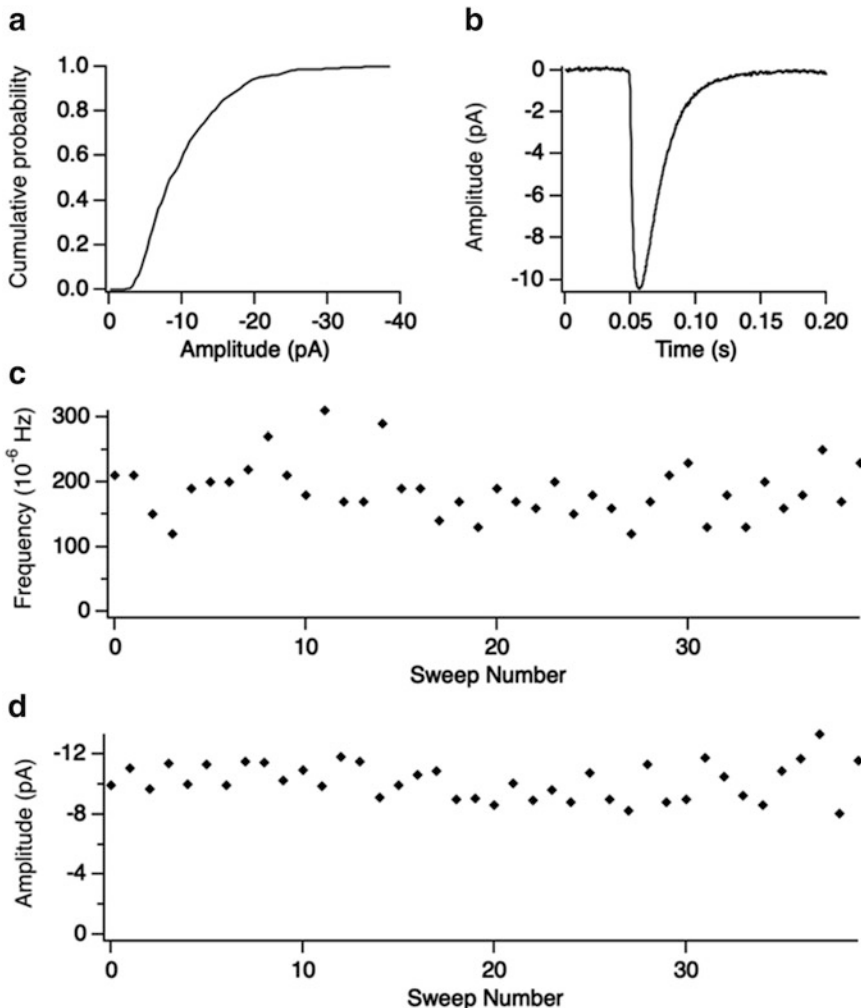


**Fig. 9** The graphical results generated by the SutterPatch Event Detection Module from a recording of spontaneous postsynaptic events in a brain slice recording. In addition to basic statistics of the analyzed dataset, four plots are created. (a) Amplitude distribution histogram. (b) Average waveform of all detected events. (c) Frequency distribution plot, showing the average frequency in each 20-s sweep. (d) Amplitude distribution plot. c and d indicate that the recording was stable regarding both frequency and amplitude

contributed to the manuscript with information, short text passages, discussion, and critique. Particular thanks go to Rich Lobbill, Hubert Affolter, Telly Galiatsatos, Greg Hjelmstad, Aaron Best, and Burt Maertz. Last but not least, Dale and Mark Flaming,

owners of Sutter Instrument Company, have provided funding for development of the Patch Clamp Systems, an entirely new product line in the portfolio. This constitutes a substantial financial risk, which will hopefully be mitigated by blowing a fresh breeze into an instrumentation market that has not been particularly innovative over the past 15 years.

*Declaration Regarding Potential Conflicts of Interests:* The author is the Product Manager for Patch Clamp Systems at Sutter Instrument Company, one of the three providers of complete patch clamp systems. In the past, he worked for both major competitors, Axon Instruments/Molecular Devices LLC and HEKA Elektronik Dr. Schulze GmbH. Every attempt was made to describe features, advantages, and disadvantages of the products made by these three competitors in a factual, fair, and unbiased manner, assuming the point of view of a patch clamp researcher. No insider knowledge that is not in the public domain was revealed in this chapter.

## References

1. Hamill OP, Marty A, Neher E, Sakmann B, Sigworth FJ (1981) Improved patch-clamp techniques for high-resolution current recording from cells and cell-free membrane patches. *Pflügers Arch* 391(2):85–100. <https://doi.org/10.1007/BF00656997>
2. Sakmann B, Neher E (eds) (1983) Single-channel recording. Plenum, New York
3. <https://www.moleculardevices.com>. Accessed 29 Oct 2019
4. <http://heka.com>. Accessed 29 Oct 2019
5. <https://www.sutter.com>. Accessed 29 Oct 2019
6. <http://www.alembicinstruments.com>. Accessed 29 Oct 2019
7. <https://www.dagan.com>. Accessed 29 Oct 2019
8. <http://www.npielectronic.de>. Accessed 29 Oct 2019
9. <https://www.warneronline.com>. Accessed 29 Oct 2019
10. <http://www.ni.com>. Accessed 29 Oct 2019
11. <https://www.mathworks.com>. Accessed 29 Oct 2019
12. <https://www.ni.com/labview>. Accessed 29 Oct 2019
13. <http://ced.co.uk>. Accessed 29 Oct 2019
14. <https://axograph.com>. Accessed 29 Oct 2019
15. <https://www.janelia.org/open-science/ephus>. Accessed 29 Oct 2019
16. <http://www.scisoftco.com/jclamp.html>. Accessed 29 Oct 2019
17. <http://www.neuromatic.thinkrandom.com>. Accessed 29 Oct 2019
18. <https://milesclabs.biology.missouri.edu/QuB.html>. Accessed 29 Oct 2019
19. [http://spider.science.strath.ac.uk/sipbs/software\\_ses.htm](http://spider.science.strath.ac.uk/sipbs/software_ses.htm). Accessed 29 Oct 2019
20. Minimizing thermal expansion with the Sutter Instrument Quartz Pipette Holder (2017). <https://www.youtube.com/watch?v=iF4RLWxuDv4>. Accessed 20 Nov 2019
21. Sherman-Gold R (ed) (1993) The Axon guide for electrophysiology & biophysics laboratory techniques. Axon Instruments, Inc., Foster City, CA
22. Magistretti J, Mantegazza M, Guatteo E, Wanke E (1996) Action potentials recorded with patch-clamp amplifiers: are they genuine? *Trends Neurosci* 19(12):530–534. [https://doi.org/10.1016/S0166-2236\(96\)40004-2](https://doi.org/10.1016/S0166-2236(96)40004-2)
23. Eshra A, Hirrlinger P, Hallermann S (2019) Enriched environment shortens the duration of action potentials in cerebellar granule cells. *Front Cell Neurosci* 13:289. <https://doi.org/10.3389/fncel.2019.00289>
24. Aimino MA, Coker CR, Silberman Y (2018) Acute ethanol modulation of neurocircuit function in the nucleus of the tractus solitarius. *Brain Res Bull* 138:5–11. <https://doi.org/10.1016/j.brainresbull.2017.07.019>
25. Anderson EM, Gomez D, Caccamise A, McPhail D, Hearing M (2019) Chronic unpredictable stress promotes cell-specific plasticity in prefrontal cortex D1 and D2 pyramidal

- neurons. *Neurobiol Stress* 10:100152. <https://doi.org/10.1016/j.ynstr.2019.100152>
26. Avelar AJ, Akers AT, Baumgard ZJ, Cooper SY, Casinelli GP, Henderson BJ (2019) Why flavored vape products may be attractive: green apple tobacco flavor elicits reward-related behavior, upregulates nAChRs on VTA dopamine neurons, and alters midbrain dopamine and GABA neuron function. *J Neuropharm* 158(1):107729. <https://doi.org/10.1016/j.neuropharm.2019.107729>
  27. Hutto RA, Bisbach CM, Abbas F, Brock DC, Cleghorn WM, Parker ED, Bauer BH, Ge W, Vinberg F, Hurley JB, Brockerhoff SE (2019) Increasing  $\text{Ca}^{2+}$  in photoreceptor mitochondria alters metabolites, accelerates photoreponse recovery, and reveals adaptations to mitochondrial stress. *Cell Death Differ.* <https://doi.org/10.1038/s41418-019-0398-2>
  28. Oda K, Vierock J, Oishi S, Rodriguez-Rozada S, Taniguchi R, Yamashita K, Wiegert JS, Nishizawa T, Hegemann P, Nureki O (2018) Crystal structure of the red light-activated channelrhodopsin Chrimson. *Nat Commun* 9 (1):3949. <https://doi.org/10.1038/s41467-018-06421-9>
  29. Oppermann J, Fischer P, Silapetere A, Liepe B, Rodriguez-Rozada S, Flores-Uribe J, Peter E, Keidel A, Vierock J, Kaufmann J, Broser M, Luck M, Bartl F, Hildebrandt P, Wiegert JS, Béjà O, Hegemann P, Wietek J (2019) Mer-MAIDs: a family of metagenomically discovered marine anion-conducting and intensely desensitizing channelrhodopsins. *Nat Commun* 10(1):3315. <https://doi.org/10.1038/s41467-019-11322-6>
  30. Qneibi M, Hamed O, Natsheh AR, Jaradat N, Emwas N, AbuHasan Q, Al-Kerm R (2019) Inhibition and assessment of the biophysical gating properties of GluA2 and GluA2/A3 AMPA receptors using curcumin derivatives. *PLoS One* 14(8):e0221132. <https://doi.org/10.1371/journal.pone.0221132>
  31. Qneibi M, Jaradat NA, Hawash M, Zaid AN, Natsheh AR, Yousef R, AbuHasan Q (2019) The neuroprotective role of *Origanum syriacum* L. and *Lavandula dentata* L. essential oils through their effects on AMPA receptors. *Biomol Res Int* 2019:1–11. <https://doi.org/10.1155/2019/5640173>
  32. Wietek J, Rodriguez-Rozada S, Tutas J, Tenedini F, Grimm C, Oertner TG, Soba P, Hegemann P, Wiegert JS (2017) Anion-conducting channelrhodopsins with tuned spectra and modified kinetics engineered for optogenetic manipulation of behavior. *Sci Rep* 7:14957. <https://doi.org/10.1038/s41598-017-14330-y>
  33. Lobdill R (2019) Digital patch-clamp amplifier. US Patent 10,393,727 B2 [Note: It is unclear, whether application or publication year shall be quoted: <https://patents.google.com/patent/US10393727B2>]
  34. Lobdill R, Best A, Hjelmstad G (2019) Digital patch-clamp amplifier. US Patent 20,190,072,509 A1 [Note: It is unclear, whether application or publication year shall be quoted: <https://patents.google.com/patent/US20190072509A1>]
  35. <http://www.igorpro.net>. Accessed 19 Nov 2019
  36. Logic Signal Voltage Levels (2019) All about circuits. <https://www.allaboutcircuits.com/textbook/digital/chpt-3/logic-signal-voltage-levels>. Accessed 21 Nov 2019
  37. Neher E, Marty A (1982) Discrete changes of cell membrane capacitance observed under conditions of enhanced secretion in bovine adrenal chromaffin cells. *Proc Natl Acad Sci U S A* 79:6712–6716
  38. Lindau M, Neher E (1988) Patch-clamp techniques for time-resolved capacitance measurements in single cells. *Pflugers Arch* 411:137–146
  39. Gillis KD (1995) Techniques for membrane capacitance measurements. In: Sakmann B, Neher E (eds) Single-channel recording. Plenum Press, New York, pp 155–198
  40. Lindau M (2012) High resolution electrophysiological techniques for the study of calcium-activated exocytosis. *Biochim Biophys Acta* 1820:1234–1242
  41. Sharp AA, O’Neil MB, Abbott LF, Marder E (1993) The dynamic clamp: artificial conductances in biological neurons. *Trends Neurosci* 16(10):389–394. [https://doi.org/10.1016/0166-2236\(93\)90004-6](https://doi.org/10.1016/0166-2236(93)90004-6)
  42. Prinz AA, Abbott LF, Marder E (2004) The dynamic clamp comes of age. *Trends Neurosci* 27(4):218–224. <https://doi.org/10.1016/j.tins.2004.02.004>
  43. Goaillard JM, Marder E (2006) Dynamic clamp analyses of cardiac, endocrine, and neural function. *Physiology* 21:197–207. <https://doi.org/10.1152/physiol.00063.2005>
  44. Bettencourt JC, Lillis KP, Stupin LR, White JA (2008) Effects of imperfect dynamic clamp: computational and experimental results. *J Neurosci Methods* 169(2):282–289. <https://doi.org/10.1016/j.jneumeth.2007.10.009>
  45. Hodgkin AL, Huxley AF (1952) A quantitative description of membrane current and its application to conduction and excitation in nerve. *J*

- Physiol 117:500–544. <https://doi.org/10.1113/jphysiol.1952.sp004764>
46. Milescu LS, Yamanishi T, Ptak K, Mogri MZ, Smith JC (2008) Real-time kinetic modeling of voltage-gated ion channels using dynamic clamp. *Biophys J* 95(1):66–87. <https://doi.org/10.1529/biophysj.107.118190>
47. Goldman DE (1943) Potential, impedance, and rectification in membranes. *J Gen Physiol* 27(1):37–60. <https://doi.org/10.1085/jgp.27.1.37>
48. Hodgkin AL, Katz B (1949) The effect of sodium ions on the electrical activity of the giant axon of the squid. *J Physiol* 108 (1):37–77. <https://doi.org/10.1113/jphysiol.1949.sp004310>
49. Hjelmstad G (2020) Dynamic Clamp - Modeling Conductances with the dPatch® Amplifier System. Webinar recording. <https://www.youtube.com/watch?v=T2fKGV-eQl8&t=620s>. Accessed 1 May 2020
50. Snyder A (2019) Analysis of spontaneous excitatory and inhibitory postsynaptic currents and action potentials. Webinar recording. <https://www.youtube.com/watch?v=Il-kaZZDcY4&t=773s>. Accessed 18 Nov 2019
51. Dolzer J (2019) Single-channel analysis with SutterPatch® software. Webinar recording. <https://www.youtube.com/watch?v=Il-kaZZDcY4&t=309s>. Accessed 21 Nov 2019
52. Neher E, Takeshi S (2001) Combining deconvolution and noise analysis for the estimation of transmitter release rates at the calyx of held. *J Neurosci* 21(2):444–461
53. Pernía-Andrade AJ, Goswami SP, Stickler Y, Fröbe U, Schlögl A, Jonas P (2012) A deconvolution-based method with high sensitivity and temporal resolution for detection of spontaneous synaptic currents in vitro and in vivo. *Biophys J* 103(7):142939
54. SutterPatch Walk-Through: #5 Application Modules (2019). [https://youtu.be/hpu\\_UJmJ3nM](https://youtu.be/hpu_UJmJ3nM). Accessed 1 May 2020
55. <http://www.synaptosoft.com/MiniAnalysis>. Accessed 19 Nov 2019



# Chapter 3

## Heterologous Expression of Ion Channels in Mammalian Cell Lines

Alistair Mathie, Emma L. Veale, and Robyn G. Holden

### Abstract

Heterologous expression of recombinant ion channel subunits in mammalian cell lines allows for characterization of their functional properties and pharmacological regulation. In this chapter, we describe methods for thawing, refreezing, passaging, cell culture, and transfection of tsA201 cells suitable for electrophysiology and imaging experiments. Furthermore, we discuss the strengths and limitations of using these methods.

**Key words** tsA201 cells, Ion channels, Electrophysiology, Imaging, Cell culture, Transfection, Calcium phosphate, TurboFect

---

### 1 Introduction

Mammalian cell lines have been used as an expression tool for recombinant proteins, including ion channels, for many years [e.g., 1–6]. Characteristically, these cell lines are capable of carrying out most of the posttranslational folding and processing required to generate functional, mature protein from mammalian DNA. Human embryonic kidney (HEK) cells (and modified HEK cells, such as tsA201) are commonly utilized by electrophysiologists since they are easily maintained and can support a wide variety of transfection methods [7, 8]. Moreover, HEK cells provide the cellular machinery for protein processing that is efficient, reproducible, and affordable. tsA201 cells have an epithelial morphology with a pyramidal or rhombic shape and their small cell size and minimal processes mean they are appropriate for voltage-clamp experimentation. These properties allow for the heterologous expression of ion channel proteins and the functional properties of expressed wild-type (WT) and mutated ion channel proteins to be studied in detail, both to understand the physiological properties of these channels and to characterize their pharmacological regulation. An

excellent description of the properties of HEK293 cells and their use for studying heterologously expressed ligand-gated ion channels was given by Thomas and Smart in 2005 [7].

Most of our electrophysiological experiments on heterologously expressed recombinant ion channels are carried out using tsA201 cells [9–14]. The tsA201 cell line is produced from a modified HEK293 cell line, which has been stably transfected with a temperature sensitive SV40 large T antigen [15, 16] by the transformation of HEK cell cultures with sheared adenovirus 5 DNA. Although these cells contain endogenous proteins, including ion channels such as potassium (K) channels, which may cause background interference in electrophysiological experiments (*see Note 1*), tsA201 cells have been used in a variety of functional expression assays due to their ability to produce high levels of recombinant protein [8]. For our studies, tsA201 cells are purchased from the European Collection of Authenticated Cell Cultures (ECACC): [www.phe-culturecollections.org.uk](http://www.phe-culturecollections.org.uk), catalogue number: tsA201 (ECACC 96121229). Cells can be purchased as frozen ampoules or growing cultures.

In the sections below, we describe methods for thawing, refreezing, passaging, and transfection of tsA201 cells suitable for electrophysiology and imaging experiments of recombinant WT and mutated ion channel proteins.

---

## 2 Materials

### 2.1 Recovery of Frozen Cells

1. Ampoule of frozen tsA201 cells.
2. Dulbecco's Modified Eagle's Medium (DMEM) containing 10% HIFBS, 1% NEAA, 2 mM L-glutamine, 1% penicillin and streptomycin (*see Note 2*). Prepare the medium in advance using the following components. The medium is stored at 4 °C until required.  
DMEM—high glucose (4500 mg/L).  
Heat-inactivated foetal bovine serum (HIFBS) (*see Note 3*).  
Nonessential amino acid solution (NEAA) (*see Note 4*).  
L-Glutamine–penicillin–streptomycin stock solution (200 mM L-glutamine, 10,000 U penicillin, and 10 mg streptomycin/mL) (*see Note 5*).
3. 15 mL centrifuge tubes, 75 cm<sup>2</sup> filter capped flask, sterile Pasteur pipette, 70% ethanol.
4. Autoclave bags, beaker for waste, blue/white roll, latex gloves, and lab coat.

**2.2 Freezing Cells**

1. Two 75 cm<sup>2</sup> flasks containing tsA201 cells at 70–90% confluence.
2. DMEM containing: 10% HIFBS, 1% NEAA, 2 mM L-Glutamine, 1% penicillin and streptomycin.
3. Trypsin–EDTA (ethylenediaminetetraacetic acid) solution (10×)—(0.5% trypsin, 0.2% EDTA) or Cell Dissociation solution (1×).
4. Cryogenic Freezing Medium: 90% HIFBS and 10% dimethyl sulfoxide (DMSO).
5. 15 mL centrifuge tubes (×2), sterile Pasteur pipettes, serological Stripette pipettes, cryotubes (×10), Pipettor Aid, Nalgene cryogenic freezing container “Mr Frosty Box.”
6. Cryogenic storage vials (2 mL).
7. Autoclave bags, beaker for waste, blue/white roll, latex gloves, and lab coat.

**2.3 Preparation of Poly-D-Lysine Plates**

1. Poly-D-lysine (PDL) hydrobromide (0.5 mg/mL) prepared by adding 5 mg of PDL to 10 mL sterile water.
2. Nunclon™ 4-well (1.9 cm<sup>2</sup>) multidishes.
3. 13 mm circular glass coverslips.
4. Safety glasses, heatproof gloves, lab coat, blue/white roll, forceps.

**2.4 Tissue Culture and Cell Counting**

1. DMEM containing: 10% HIFBS, 1% NEAA, 2 mM L-glutamine, 1% penicillin and streptomycin.
2. Trypsin–EDTA Solution (10×) (*see Note 6*).
3. 70% Ethanol.
4. Virkon®—1% solution (add one scoop to 1 L of water—dissolve by stirring). Color should be pink. Color will fade with age. Discard any colorless solution and make fresh. The solution should be stable for 1–2 weeks (*see Note 7*).
5. Four-well multidishes containing poly-D-lysine-coated glass coverslips (*see Subheading 3.3*).
6. Serological Stripette pipettes: 5 mL, 10 mL, 25 mL.
7. Nunclon™ 75 cm<sup>2</sup> flask with filter cap.
8. Centrifuge tubes (15 mL).
9. Pipettor Aid (Pipette Filler).
10. Hemocytometer.
11. “FastRead” disposable counting chambers (ImmuneSystems BVS100).
12. Inverted light microscope.
13. Autoclave bags, beaker for waste, blue/white roll, latex gloves, and lab coat.

**2.5 Calcium Phosphate Transfection**

1. 2 M CaCl<sub>2</sub> (MW 147.02) = 14.7 g in 50 mL H<sub>2</sub>O.
2. 2× phosphate-free HEPES buffered saline (HBS): (pH to 6.95).
3. 280 mM NaCl (MW 58.44) = 818.16 mg in 50 mL H<sub>2</sub>O.
4. 50 mM HEPES (MW 238.3) = 595.75 mg in 50 mL H<sub>2</sub>O.
5. 100 mM Na<sub>2</sub>HPO<sub>4</sub> (MW 141.96) = 709.8 mg in 50 mL H<sub>2</sub>O (pH to 6.95).
6. Phosphate buffered saline (PBS) = 1 tablet in 200 mL of autoclaved <sub>dd</sub>H<sub>2</sub>O.

Store solutions at 4 °C.

---

### 3 Methods

**3.1 Recovery of Frozen Cells**

1. Prewarm newly prepared DMEM medium in a water bath at 37 °C for 30 min.
2. In a microbiological safety cabinet, hold a tissue soaked in 70% ethanol around the cap of the frozen ampoule and turn the cap a quarter turn to release any residual liquid nitrogen that may be trapped. Retighten the cap.
3. Quickly transfer the ampoule to a 37 °C water bath until only one or two small ice crystals, if any, remain. This should take no more than 1–2 min (*see Note 8*).
4. Slowly transfer the contents of the ampoule into a 15 mL centrifuge tube, containing 5 mL of prewarmed medium, using a sterile Pasteur pipette or by pipetting.
5. Centrifuge the cells at 100–120 × *g* for 3 min (*see Note 9*) to remove any cryoprotectant.
6. Pour away all the supernatant, using a sterile Pasteur pipette to remove any residual medium.
7. Resuspend cells in 5 mL of medium and transfer the contents to a 75 cm<sup>2</sup> filter capped flask.
8. Place in 5% CO<sub>2</sub> incubator overnight at 37 °C.

Following Day

9. Check that the cells are adhering to the flask. There should be a mixture of fixed and floating (dead) cells. If they are all floating, it is unlikely that they will succeed in growing.
10. Pour away the medium containing dead cells from the flask and carefully add 5 mL of prewarmed medium. (Hopefully, this selects the healthiest cells at this stage.)
11. Leave cells to grow in incubator until 70–80% confluent (*see Note 10*), then passage as normal (*see Subheading 3.4*).

### 3.2 Freezing Cells

Once healthy cells have been grown in the laboratory, it is useful to freeze aliquots for future use.

1. Prewarm newly prepared DMEM medium in a water bath at 37 °C for ~30 min.
2. While the medium is warming prepare cryogenic medium. For two flasks we would normally prepare 10 mL (9 mL HIFBS and 1 mL DMSO).
3. Remove flasks from the incubator and assess density and cell viability under the microscope. Ideally, cells should be 70–90% confluent and free of any bacterial or fungal contaminants.
4. Spray with 70% ethanol and transfer flask to microbiological cabinet.
5. Pour off supernatant from flasks into a waste beaker and add 2 mL of cell dissociation solution or equivalent volume of trypsin–EDTA. Agitate flasks gently and replace back in CO<sub>2</sub> incubator for 3–5 min.
6. After short incubation, remove cells from incubator and place back in fume hood. Ensure that all adherent cells are dissociated from bottom of flask, using agitation or pipetting.
7. Add 10 mL of medium to each flask. Pipet up and down repeatedly to dislodge any remaining adherent cells and to ensure cells are mixed and not clumped (trying not to create too many air bubbles).
8. Transfer 10 mL from each flask to a 15 mL centrifuge tube.
9. Spin down in centrifuge at 100–120 ×  $\text{g}$  for 3 min.
10. Pour away supernatant, leaving just the pellet. Resuspend each pellet in 5 mL of medium and spin again at 100–120 ×  $\text{g}$  for 3 min. A small aliquot of cells can be removed to perform a cell count if required (*see Subheading 3.5*).
11. Remove all the supernatant using a sterile Pasteur pipette to remove any residual medium.
12. Resuspend each pellet in 5 mL of the cryogenic medium or enough to give a concentration of 2–4 × 10<sup>6</sup> cells per mL. Transfer 1 mL of suspension to each cryogenic vial which has been labelled with the cell line name, passage number and date.
13. Place cryogenic vials into the “Mr Frosty” box containing isopropyl alcohol and place in –80 °C freezer overnight.
14. For long term storage, transfer ampoules to the vapor phase of a liquid nitrogen storage vessel, until required.

### 3.3 Preparation of PDL Plates

#### 3.3.1 Preparation of Coverslips

1. Place the glass coverslips into a petri dish containing distilled water. This helps to remove any glass or particle debris. Using tweezers transfer individual glass coverslips to blue roll and blot-dry.
2. Transfer dried coverslips to a foil tray and lightly cover with ethanol. Transfer to sink area and flame-sterilize (*see Note 11*). Alternatively transfer to petri dish containing ethanol and blot-dry on blue roll.
3. Transfer flamed coverslips to four-well plates.

#### 3.3.2 PDL Coating of Coverslips

1. In a microbiological safety cabinet, using a sterile Pasteur pipette, drop PDL onto each coverslip. Ensure central area has a good coating. Alternatively, pipet 300 µL onto the coverslip (*see Note 12*).
2. Leave for 20–30 min with the lids off (*see Note 13*).
3. Remove as much PDL as possible from the coverslips using the Pasteur pipette and allow to dry completely.
4. Transfer the plates to the UV cabinet and irradiate with lids off for 1–2 h.
5. Store plates in fridge until required. Always ensure plates are stored upright to prevent coverslips falling out.

### 3.4 Tissue Culture

1. Preheat medium and cell dissociation solution (or trypsin–EDTA) in water bath (37 °C) for approximately 30 min before starting. Do not attempt to use cold solutions.
2. Open the microbiological safety cabinet and sanitize surfaces using 70% ethanol, including the glass (*see Note 14*).
3. Place all the materials that you will require in the hood, spraying them all with 70% ethanol to reduce the introduction of contaminants. Do not overcrowd the hood or block the front grill.
4. After spraying hands with 70% ethanol remove large 75 cm<sup>2</sup> flask from incubator and check cells under microscope. Cells should be 70–80% confluent at this stage (*see Note 10*).
5. Check that cells are healthy and there is no sign of contamination. (A very yellow flask could be a sign of infection or over-confluent cells, which may not recover.)
6. Spray the flask with 70% ethanol and place into the safety cabinet. Pour off supernatant into waste beaker. Add 2 mL of cell dissociation medium or trypsin–EDTA to the flask. Agitate flask gently. Replace flask back into the incubator and incubate for 3–5 min.

7. Remove cells from incubator and place back in fume hood. Ensure cells have completely dispersed from the bottom of the flask. You can use agitation or pipetting at this stage.
8. Add 10 mL of medium to the flask. Pipet up and down repeatedly to ensure thorough mixing and removal of cells from bottom of flask (try not to create too many air bubbles). Transfer 5 mL to 2 × 15 mL centrifuge tube (10 mL total).
9. Transfer tubes to centrifuge. Spin at 100–120 ×  $\text{g}$  at room temperature for 3 min to pellet cells. Ensure tubes are balanced in centrifuge.
10. Transfer tubes back into safety cabinet, spraying with 70% ethanol.
11. Remove all the supernatant, leaving just the pellet in the tubes.
12. Tap tubes to dislodge pellets from the bottom of the tube and add ~5 mL of medium to each tube. Pipet up and down thoroughly to resuspend cells (again, try not to create too many air bubbles).

#### 3.4.1 Plates

1. Using resuspended cells from **step 12**, Subheading 3.4, remove a small aliquot to count cells (*see* Subheading 3.5), then make a further dilution equivalent to  $7 \times 10^4$  cells per mL. Ensure cells are thoroughly mixed, by pipetting up and down. This prevents cells clumping together in big groups during plating. Transfer 0.5 mL of resuspended cells to each well of the plate (2 mL of resuspended cells per 4-well plate).
2. Ensure the coverslip is covered by cells. Press glass coverslip down with a clean tip or end of the Stripette to ensure coverslip is firmly positioned at the bottom of the plate and not floating. Cells prefer to grow between two surfaces, which can cause a lot of cells to grow on the bottom of the coverslip, rather than the top, if it is floating.
3. Spray with 70% ethanol and place in 5% CO<sub>2</sub> incubator at 37 °C and leave to grow overnight.

#### 3.4.2 Flasks

1. Using resuspended cells from **step 12**, Subheading 3.4, calculate how much you would need to add to 20 mL of medium in order to achieve a density of  $1.5 \times 10^5$  cells per mL.
2. In 75 cm<sup>2</sup> flask, add 20 mL of fresh medium. To this, add volume of cells calculated in **step 1**.
3. Place in incubator. The flask should be 70–80% confluent in 3–4 days.

Transfer waste beaker to sink and add enough 1% Virkon to turn solution yellow (50:50 ratio). Ensure any used Stripette pipettes, flasks, and so on are discarded into the autoclave bags. Disinfect safety cabinet with 70% ethanol and close.

### 3.5 Cell Counting

1. Transfer 9  $\mu\text{L}$  of cell solution to one chamber of a “FastRead” plate (*see Note 15*).
2. Each chamber contains ten  $4 \times 4$  counting grids. Using a handheld tally counter and a regular light microscope, count the number of cells in one  $4 \times 4$  grid.
3. The volume in the chamber above each  $4 \times 4$  grid is  $10^{-4}$  mL, so cell concentration in each grid (expressed as cells per mL) is calculated by multiplying the number of cells counted by  $10^4$ .
4. It is recommended to count multiple  $4 \times 4$  grids and calculate an average value.

### 3.6 Calcium Phosphate Transfection

tsA201 cells can be transiently transfected using a modified calcium-phosphate protocol. Calcium phosphate is a quick, simple, efficient, and inexpensive method of DNA transfection [17, 18]. The procedure allows for introduction of a desired recombinant DNA sequence into eukaryotic cells via the use of a calcium phosphate–DNA precipitation (*see Note 16*). The protocol is less labor-intensive than other transfection methods such as electroporation and is applicable to large-scale production of transfected cells [17] (*see Note 17*). In our experiments we transfect cDNA for the ion channel of interest together with cDNA for a reporter gene (normally Green Fluorescent Protein (GFP)) to identify which cells have been successfully transfected (*see Note 18* and Fig. 1a–c).

In this protocol, a HEPES-buffered saline solution containing phosphate ions is combined with a calcium chloride solution containing the DNA to be transfected. When the two are combined, a fine precipitate of the positively charged calcium and the negatively charged phosphate will form, binding to the surface of the DNA to be transfected. The suspension of the precipitate is then added to the cells to be transfected. The DNA complex then enters the cell via endocytosis [18].

Optimal conditions seem to be 225 mM  $\text{CaCl}_2$  and 0.9 mM  $\text{Na}_2\text{HPO}_4$ . One can reoptimize by adjusting phosphate and calcium concentrations.

1. Take out prepared solutions from fridge 30 min before using, to allow them to warm up to room temperature. Defrost DNA and GFP if using, just before beginning.
2. Into a rack, label two Eppendorf tubes (1.5 mL), A and B. Calculate what needs to be added to Tube A.

NB. Example template below is for one 4-well plate, so if more than one plate of cells or plates with larger wells, containing larger volumes of medium are used, then it is necessary to multiply everything up accordingly, including Tube B.

Example: If DNA has a concentration of 0.5  $\mu\text{g}/\mu\text{L}$ , then add 1  $\mu\text{L}$  per well. So, for four wells, add 4  $\mu\text{L}$  of the DNA to tube A.

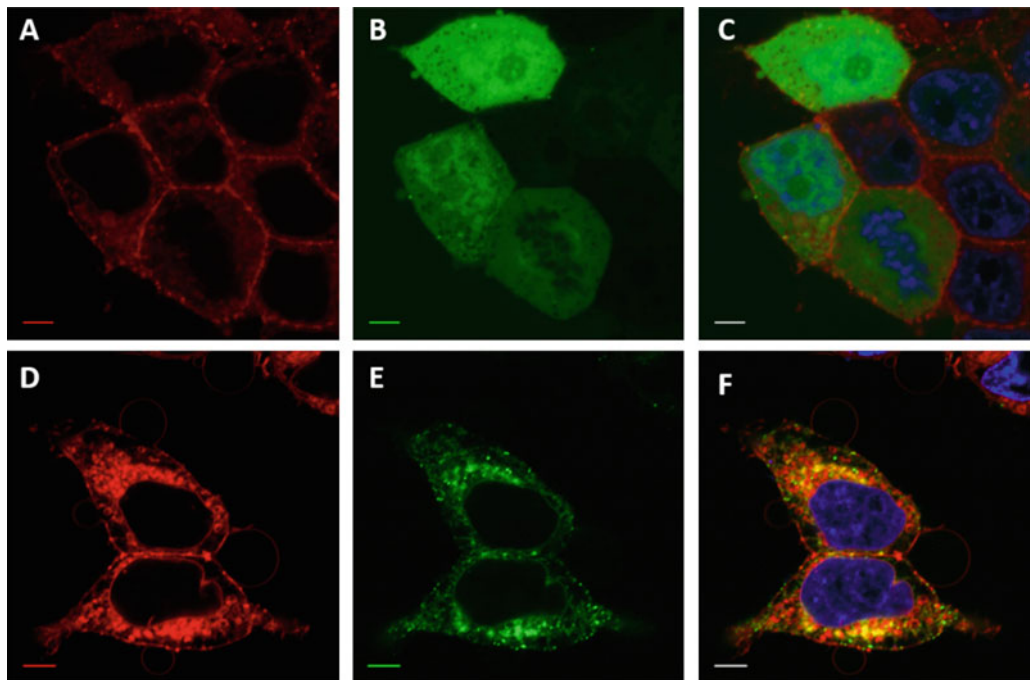


**Fig. 1** Localization of GFP. Confocal images of tsA201 cells with red plasma membrane stain (Cell Mask Deep Red) (**a**) and transiently transfected with GFP alone (**b**). (**c**) is the overlay of (**a**) and (**b**) and this shows that GFP is expressed throughout the cytoplasm of transfected cells but not in the cell membrane. The nuclei are stained blue. Panels **d-f** show the localization of GFP-tagged channels (in this case human TASK-3 channels, termed TASK-3\_GFP) at the plasma membrane. (**d**) shows red plasma membrane stain, (**e**) shows cells transiently transfected with TASK-3\_GFP and (**f**) shows the overlay. A yellow signal signifies GFP (and therefore channels) expressed at the plasma membrane. All scale bars are 5  $\mu$ m

Tube A	Tube B
4 $\mu$ L DNA (0.5 $\mu$ g)	98.2 $\mu$ L phosphate-free Buffer (HEPES)
4 $\mu$ L GFP (0.5 $\mu$ g)	1.8 $\mu$ L of 100 mM phosphate buffer ( $=1.8$ mM)
22.5 $\mu$ L of 2 M CaCl <sub>2</sub> $(=450$ mM)	
69.5 $\mu$ L H <sub>2</sub> O	
$\Sigma = 100$ $\mu$ L for 4 wells	$\Sigma = 100$ $\mu$ L for 4 wells

3. Working inside hood, make up tubes A and B according to the calculations above. Remember to vortex and spin down DNA and GFP before using.
4. Vortex each tube A and B briefly. Spin down briefly.
5. Add contents of tube B to tube A (dropwise). Do not vortex.

6. Incubate at room temperature for 5–15 min to form calcium phosphate/DNA precipitate.
7. Mix contents of tube by pipetting up and down gently, before dripping, 50 µL of the mix evenly into each well of the plate.
8. Place cells back in incubator for 4–6 h (4 h minimum, longer than 8 h is also not ideal for cells).
9. After 4–6 h, warm up the PBS and medium in the water bath at 37 °C for 30 min. Wash cells twice with warmed PBS. (Aspirate medium with a sterile Pasteur pipette, add 1 mL warmed PBS, aspirate and then repeat. After second wash, add 0.5 mL of warmed medium.) Place plate back into the incubator.
10. Cells can be used the following day for electrophysiology, imaging, and other measurements (but *see Note 1*).

### **3.7 Adapted Protocol for TurboFect Transfection**

TurboFect (Thermo Scientific) transfection is a fast and highly efficient transfection method for the expression of DNA plasmids within eukaryotic cells. TurboFect Transfection Reagent consists of sterile solution and a cationic polymer, which interacts with negatively charged cDNA, forming small complexes that are highly diffusible and easily endocytosed. Once within intercellular space, the reagent acts as a “proton-sponge,” inducing osmotic swelling of the endocytosed complexes. This leads to their rupture, releasing the cDNA which is then translocated to the cell nucleus. In our laboratory, we use TurboFect for imaging experiments as it appears to be gentler on cells than calcium phosphate transfection (*see Note 19*).

1. Take out prepared solutions from fridge 30 min before using and allow them to warm up to room temperature. Defrost required DNA just before beginning.
2. 0.5 µg of the fluorescent vector (e.g., pAcGFP-N1) (*see Note 20*) encoding the relevant cDNA is diluted in 100 µL serum-free DMEM prior to the addition of 1.5 µL of the transfection reagent.
3. The DNA mixture is vortexed immediately to resuspend any precipitate that may have formed and then incubated at room temperature for 20 min.
4. Following incubation, 100 µL is added to the appropriately labelled well of the plate and incubated for 24 h at 37 °C in a humidified atmosphere of 95% O<sub>2</sub> and 5% CO<sub>2</sub>.

## **4 Notes**

1. tsA201 cells express endogenous currents from voltage gated potassium (K<sub>V</sub>) channels, which are essential for the cell’s survival. This is illustrated in Fig. 2. The endogenous K<sub>V</sub> currents activate at voltages positive to –20 mV (Fig. 2a) and are blocked by 5 mM TEA (Fig. 2b). For this reason a suitable

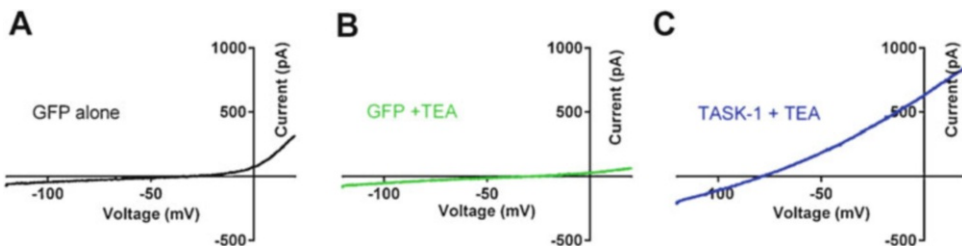


**Fig. 2** Endogenous K current in tsA201 cells. (a) Current voltage relationship in tsA201 cells transfected with GFP alone. There is little endogenous current at voltages negative to  $-20$  mV but an endogenous  $K_V$  current is activated at voltages positive to  $-20$  mV. (b) The endogenous  $K_V$  current is blocked by 5 mM TEA. (c) Currents through expressed channels (in this case human TASK-1 channels) can be recorded in the presence of TEA and quantified at voltages negative to  $-20$  mV to minimize contamination by endogenous currents

electrophysiological protocol and/or pharmacological separation needs to be employed to minimize contamination by these during current recordings (*see Fig. 2c*).

2. DMEM is a modification of MEM, containing increased levels of amino acids and vitamins, an ideal medium for a whole range of cell types including hybridomas. The glucose in the medium provides the main source of carbohydrates to promote cell growth. Using higher glucose levels supports a wider range of cell types.
3. Fetal bovine serum is probably the most important and expensive component of the cell culture medium. It is a complex mix of albumins, growth factors and growth inhibitors. The quality, type and concentration of serum can all affect the growth of the cells. Serum can be contaminated, so using heat-inactivated serum can reduce the risk of contamination by viruses. Production of FBS is regulated by the International Serum Industry Association (ISIA, [www.serumindustry.org](http://www.serumindustry.org)) and it is important to obtain FBS from an ethically approved supplier.
4. Essential amino acids are already present in the cell culture medium, as cells are unable to synthesize these themselves and are required to promote growth. The concentration of amino acids in the culture medium will determine the maximum cell density that can be achieved. Once the amino acids are depleted the cells will no longer be able to proliferate. The exception is glutamine, which degrades quite quickly, so is added to the medium separately. Nonessential amino acids are also added separately to the medium and help stimulate growth and prolong the viability of the cells.
5. Antibiotics are added to try and prevent contamination from bacteria, fungi, or mycoplasma, usually contracted from poor sterile techniques and contaminated reagents. Their use is generally frowned upon, due to the development of resistant strains—however, they are routinely used in cell culture.

6. Trypsin–EDTA is commonly used for the dissociation and disaggregation of adhered mammalian cells and tissues. Trypsin is a porcine pancreas-derived protease that dislodges cells. Ethylenediaminetetraacetic acid (EDTA) is a chelating agent, which is added to trypsin solutions to enhance enzymatic activity, however, proteases can be harmful and remove membrane markers/receptors of interest from the cells. In this case a nonenzymatic form of trypsin should be used, such as cell dissociation solution.
7. Virkon™ is effective against a large number of bacteria, viruses, and fungi strains. All waste should be treated with Virkon™, before disposal.
8. Avoid completely immersing the ampoule as this may result in contamination. Hold between thumb and finger and move around in bath.
9. The centrifuge procedure is expressed in terms of relative centrifugal force (rcf) times gravity ( $\text{g}$ ) rather than centrifuge rotor speed (revolutions per minute, rpm). Since the rcf depends on both the rotor speed and the rotor radius, it will vary from centrifuge to centrifuge for an identical speed. The relationship between  $\text{g}$  and speed ( $s$ ) is described by the following equation:

$$\mathcal{g} = (1.118 \times 10^{-5}) rs^2$$

where “ $r$ ” is the radius of the rotor in cm and “ $s$ ” the speed in rpm.

In the procedures described here, a relatively low centrifugal force is used, so there is some latitude in the  $\text{g}$  value chosen. The range recommended here ( $100\text{--}120 \times \text{g}$ ) will correspond to a rotor speed of around 800–1000 rpm for most bench centrifuges.

10. An example of healthy 70%-confluent tsA-201 cells can be seen here: [https://www.phe-culturecollections.org.uk/media/56718/96121229\\_tsA201\\_72hr\\_post\\_seeding.jpg](https://www.phe-culturecollections.org.uk/media/56718/96121229_tsA201_72hr_post_seeding.jpg)
11. TAKE CARE! Wear goggles to protect eyes from flying glass. Alternatively transfer to petri dish containing ethanol and blot-dry on blue roll.
12. Try to only get PDL on coverslip and not fill the whole well. If you are making PDL plates (minus glass), cover bottom of well with a layer of PDL and follow as above. Remember you will use more PDL than normal.
13. Try not to leave longer than an hour, as drying out of PDL on the glass, leads to large crystals of PDL on the plates which can affect the cells.

14. All work must be performed in a microbiological safety cabinet to prevent contamination of cells and to protect the operator from any aerosols, protection being provided through HEPA (high-efficiency particulate air) filters. Ensure the front and the rear of the cabinet are free of items to maximize airflow.
15. This is enough solution to fill the chamber. The cell solution is introduced by placing the pipette tip against the sample application area (see [www.immunesystems.co.uk/catalog/pdf/fastread.pdf](http://www.immunesystems.co.uk/catalog/pdf/fastread.pdf) for an illustration of this) and slowly dispensing. Sample liquid is drawn into the chamber by capillary action and excess liquid is expelled into the overflow reservoir, leaving the correct volume of fluid in the well for cell counting.
16. For optimal success it is proposed that plates are of 70% confluence and covered by approximately  $5 \times 10^3$  cells [7]. Additionally, it is advised that the cDNA intended for transcription, is produced in an endotoxin free buffer.
17. As a method, calcium phosphate transfection has proven efficiencies above 50% depending on the cell lines used [18]; however, these can vary based on pH due to the maturity of the culture medium [7]. Furthermore, the efficiency of the procedure can be hindered by the density of the initially seeded cells. If low, success rates can be unpredictable.
18. The ion channel cDNA of interest is usually cloned into pcDNA3.1 vector (Invitrogen, Carlsbad, CA, USA). When more than one transcript is cotransfected together (e.g., GFP with a channel of interest) it is important to determine the degree of cotransfection. Coexpression is verified using simultaneous transfection of GFP (green) and DsRed (red) transcripts. Random selection of 50 cells that expressed one transcript (e.g., GFP) revealed that >95% of these successfully transfected cells also expressed the other (DsRed) transcript [19].
19. The different methods of transfection do not appear to alter the number of functional channels expressed at the membrane. For TASK-1 channels, transfected with either calcium phosphate or TurboFect on the same day current density was 8.0 pA/pF,  $n = 5$  cells, 95% CI = 5.8–10.1 for calcium phosphate transfection vs. 9.5 pA/pF,  $n = 5$  cells, 95% CI = 8.3–10.7 for TurboFect transfection [13].
20. For imaging experiments, WT sequence was cut from the pcDNA3.1 vector and cloned into the MCS of pAcGFP1-N1 vector (Clontech-Takara Bio Europe, Saint-Germain-en-Laye, France) to create a fusion construct with the N-terminus of AcGFP1. Terminating stop codons were removed by site-directed mutagenesis using a QuikChange site-directed mutagenesis kit and procedure (Agilent Technologies, Santa Clara,

CA) and maintained within the same reading frame with the start codon of AcGFP1. Constructs were fully sequenced to ensure correct sequence incorporation (Eurofins MWG Operon, Huntsville, AL, USA). The GFP tag allows for visualization of TASK-3 expression (*see Fig. 1d-f*).

Electrophysiological recordings showed that the GFP tag (9.7 pA/pF,  $n = 9$  cells, 95% CI = 6.8–12.7 for WT TASK-1 channels vs. 8.2 pA/pF,  $n = 8$  cells, 95% CI = 4.9–11.5 for pACGFP TASK-1 channels) did not alter the current density for TASK-1 K2P channels expressed in tsA201 cells measured in temporally matched experiments [13]. Indeed, the WT TASK-1 channel current density was consistent throughout all experiments in this study: 7.8 pA/pF ( $n = 44$  cells from 17 days, 95% CI = 5.8–9.7). However, this is not always the case. In another series of experiments with a different K2P channel, TASK-3, locating GFP within the channel on the M1P1 loop and therefore located on the extracellular face of the channel significantly reduced channel current density from  $64 \pm 1$  pA/pF (mean  $\pm$  SEM,  $n = 197$ ) to  $32 \pm 6$  pA/pF ( $n = 10$ ) [20].

## References

- Chahine M, Plante E, Kallen RG (1996) Sea anemone toxin (ATX II) modulation of heart and skeletal muscle sodium channel alpha-subunits expressed in tsA201 cells. *J Membr Biol* 152:39–48
- Shen ES, Cooke GM, Horlick RA (1995) Improved expression cloning using reporter genes and Epstein-Barr virus ori-containing vectors. *Gene* 156:235–239
- Yang N, Ji S, Zhou M, Ptácek LJ, Barchi RL, Horn R, George AL Jr (1994) Sodium channel mutations in paramyotonia congenita exhibit similar biophysical phenotypes in vitro. *Proc Natl Acad Sci U S A* 91:12785–12789
- Chahine M, Bennett PB, George AL Jr, Horn R (1994) Functional expression and properties of the human skeletal muscle sodium channel. *Pflugers Arch* 427:136–142
- O’Leary ME, Horn R (1994) Internal block of human heart sodium channels by symmetrical tetra-alkylammoniums. *J Gen Physiol* 104:507–522
- Margolskee RF, McHendry-Rinde B, Horn R (1993) Panning transfected cells for electrophysiological studies. *Biotechniques* 15:906–911
- Thomas P, Smart TG (2005) HEK293 cell line: a vehicle for the expression of recombinant proteins. *J Pharmacol Toxicol Methods* 51:187–200
- Chen C, Okayama H (1987) High-efficiency transformation of mammalian cells by plasmid DNA. *Mol Cell Biol* 7:2745–2752
- Veale EL, Al Moubarak E, Bajaria N, Omoto K, Cao L, Tucker SJ, Stevens EB, Mathie A (2014) Influence of the N-terminus on the biophysical properties and pharmacology of TREK1 potassium channels. *Mol Pharmacol* 85:671–681
- Veale EL, Hassan M, Walsh Y, Al Moubarak E, Mathie A (2014) Recovery of current through mutated TASK3 potassium channels underlying Birk Barel syndrome. *Mol Pharmacol* 85:397–407
- Veale EL, Mathie A (2016) Aristolochic acid, a plant extract used in the treatment of pain and linked to Balkan Endemic Nephropathy, is a regulator of K2P channels. *Br J Pharmacol* 173:1639–1652
- Al-Moubarak E, Veale EL, Mathie A (2019) Pharmacologically reversible, loss of function mutations in the inner pore helices of TREK-1 K2P channels. *Sci Rep* 9:12394
- Cunningham KP, Holden RG, Escrivano-Subias P, Cogolludo A, Veale EL, Mathie A (2019) Characterisation and regulation of

- wild type and mutant TASK-1 two pore domain potassium channels indicated in pulmonary arterial hypertension. *J Physiol* 597:1087–1101
14. Cunningham KP, MacIntyre DE, Mathie A, Veale EL (2020) Effects of the ventilator stimulant, doxapram, on human TASK-3 (KCNK9, K2P9.1) and TASK-1 (KCNK3, K2P3.1) channels. *Acta Physiol* 228:e13361
  15. Graham FL, van der Eb AJ (1973) A new technique for the assay of infectivity of human adenovirus 5 DNA. *Virology* 52:456–467
  16. Graham FL, Smiley J, Russell WC, Nairn R (1977) Characteristics of a human cell line transformed by DNA from human adenovirus type 5. *J Gen Virol* 36:59–74
  17. Batard P, Jordan M, Wurm F (2001) Transfer of high copy number plasmid into mammalian cells by calcium phosphate transfection. *Gene* 270:61–68
  18. Chen CA, Okayama H (1988) Calcium phosphate-mediated gene transfer: a highly efficient transfection system for stably transforming cells with plasmid DNA. *Biotechniques* 6:632–638
  19. Veale EL, Rees KA, Mathie A, Trapp S (2010) Dominant negative effects of a non-functional TREK1 splice variant expressed in brain. *J Biol Chem* 285:29295–29304
  20. El Hachmane MF, Rees KA, Veale EL, Sumbayev VV, Mathie A (2014) Enhancement of TWIK-related acid sensitive potassium channel 3 (TASK3) two pore domain potassium channel activity by TNF $\alpha$ . *J Biol Chem* 289:1388–1401



# Chapter 4

## Electrophysiology on Channel-Forming Proteins in Artificial Lipid Bilayers: Next-Generation Instrumentation for Multiple Recordings in Parallel

**Ekaterina Zaitseva, Alison Obergrussberger, Conrad Weichbrodt,  
Mordjane Boukhet, Frank Bernhard, Christopher Hein,  
Gerhard Baaken, Niels Fertig, and Jan C. Behrends**

### Abstract

Artificial lipid bilayers have been used for several decades to study channel-forming pores and ion channels in membranes. Until recently, the classical two-chamber setups have been primarily used for studying the biophysical properties of pore forming proteins. Within the last 10 years, instruments for automated lipid bilayer measurements have been developed and are now commercially available. This chapter focuses on protein purification and reconstitution of channel-forming proteins into lipid bilayers using a classic setup and on the commercially available systems, the Orbit mini and Orbit 16.

**Key words** Reconstituted ion channels, Artificial lipid bilayer, Orbit mini, Orbit 16, Protein purification

---

### 1 Introduction

*“Indeed, I can see no justification for ripping a channel protein out of the comfortable home of its native membrane and transferring it to a foreign and artificial environment other than to enable the posing of molecular questions about ion-channel behaviour, questions that simply cannot be asked in the complicated cellular environment”* Christopher Miller, Foreword to *Ion Channel Reconstitution*; Miller, C., Ed.; New York, 1986 [1].

Artificial or synthetic lipid bilayers, also known as black lipid membranes (BLMs), have been used for more than half a century to study biological pores and channels using voltage clamp electrophysiology. Very early on it had been shown that BLMs made from

---

**Electronic supplementary material** The online version of this chapter ([https://doi.org/10.1007/978-1-0716-0818-0\\_4](https://doi.org/10.1007/978-1-0716-0818-0_4)) contains supplementary material, which is available to authorized users.

lipid emulsions in organic solvents could be “doped” with more or less well-defined and/or purified proteinaceous materials like “excitability-inducing material” (EIM) and the antibiotics alamethicin and gramicidin to modify membrane conductance and reproduce excitability and ion selectivity phenomena found in biological membranes [2–4]. Importantly, it could be shown subsequently that this modification was due to the formation of discrete pores [5–9], which was influential for the development of the idea that ion channels in the sense of individual pore-forming molecular entities underlie bioelectric phenomena such as the membrane and action potential [10]. Work on gramicidin, especially, also gave important clues as to the mechanism by which selective ion flux over membranes might occur [11].

The two decades following these seminal discoveries brought the reconstitution (i.e., the isolation and reincorporation in free-standing BLMs) of more complex and more well-defined channel or pore-forming proteins such as nicotinic acetylcholine receptors, voltage-dependent sodium channels, calcium-dependent potassium channels, sarcoplasmic reticulum potassium channels, calcium channels from skeletal-muscle T-tubules, synaptosomal calcium channels, mitochondrial voltage-dependent anion channels (VDAC), and a number of bacterial porins. A good overview of what had been achieved by ion channel reconstitution by the mid-1980s is given in a volume thus entitled published in 1986 [1].

At that time, which roughly coincided with pipette-based patch-clamp electrophysiology reaching maturity [12], the hope was that reconstitution of membrane proteins in BLMs could bring about a new era in which ion channels might be studied in a radically reduced system to clarify the relation between molecular structure and function of the channel proteins, in analogy to biochemical analysis of enzyme function. However, it seems fair to say that, in fact, in the developments that led to today’s considerably enhanced understanding of structure–function relationships in ion channels, recordings from channels reconstituted in BLMs has only played a minor role compared to patch clamping cellular membranes. While from a reductionist standpoint the advantages of a synthetic lipid system as opposed to a cellular environment remained clear, the technical difficulty of both forming a stable synthetic membrane and purifying and reconstituting membrane proteins probably prevented a success story similar to that of patch clamping.

Accounts by some of the most successful practitioners of the art strongly suggest that a large part of the reason for the somewhat stunted growth of a promising technology was the fickle nature of the BLM itself: One author confesses to having on several occasions vented his frustration with the lack of stability of BLMs by deliberately and violently destroying glassware [13], while others wryly pretend to have, by their sufferings, been led from the straight path of reason toward a voodooesque rite involving socks [14, 15].

Furthermore, in contrast to the purified porins—including VDAC—which can be incorporated from detergent solution, membrane channels with alpha-helical structure typically first need to be reconstituted into vesicles [16, 17], or, more recently, mixed lipid–detergent micelles [18]. This first step is relatively well controlled. The real difficulty lies in transferring the channels from the vesicles into the BLM and for this step several strategies have coexisted for many decades, none of them having developed into a standard, generic method. Again, a large part of the reason for the limited progress in ion channel reconstitution likely is that the formation of a BLM, which is the prerequisite for any experiment, has been a notoriously laborious and unreliable process by any of the classical methods, while in order to systematically optimize reconstitution protocols, very many trials are necessary.

In this chapter, we will introduce next-generation instrumentation for (automated) formation of and parallel recording from BLM arrays, which we have developed to increase throughput for experiments involving reconstitution of ion channels and pore-forming membrane proteins. Our approach is based on the micro-electrode-cavity array (MECA) [19, 20] first reported in 2008 and made commercially available in 2014. Other approaches for enhanced throughput in BLM recordings by parallelization either miniaturize a classical bilayer setup or involve relatively intricate microfluidics. In contrast, the MECA device contains an array of microcavities containing Ag/AgCl microelectrodes, thus minimizing stray capacitances and enabling parallel recordings with high resolution and low noise [21, 22].

We describe methods used for lipid bilayer formation on these devices as well as on classic two-chamber setups (*see* Fig. 1). We provide short general overviews of methods of membrane protein expression and purification—including optimization of protein samples synthesized *in vitro*—as well as of their reconstitution in free-standing lipid membranes. As examples, detailed protocols will be given for the expression in *E. coli* and subsequent purification of the porin MspA and for reconstitution ranging from simple self-insertion of pore-forming antibiotics and water-soluble bacterial toxins to more complex detergent dilution and proteoliposome fusion approaches.

---

## 2 Materials

### 2.1 Bilayer Formation and Measurement on Classical Setups

1. Classical bilayer chamber containing a cuvette made from Delrin with an aperture diameter of 150 µm and a volume of 1 ml (e.g., from Warner Instruments LLC, Hamden, USA). Both volumes are connected (directly or through the salt-bridges) via Ag/AgCl-electrodes (e.g., World Precision Instruments, Sarasota, USA) to a current amplifier (e.g., Axopatch 200B,

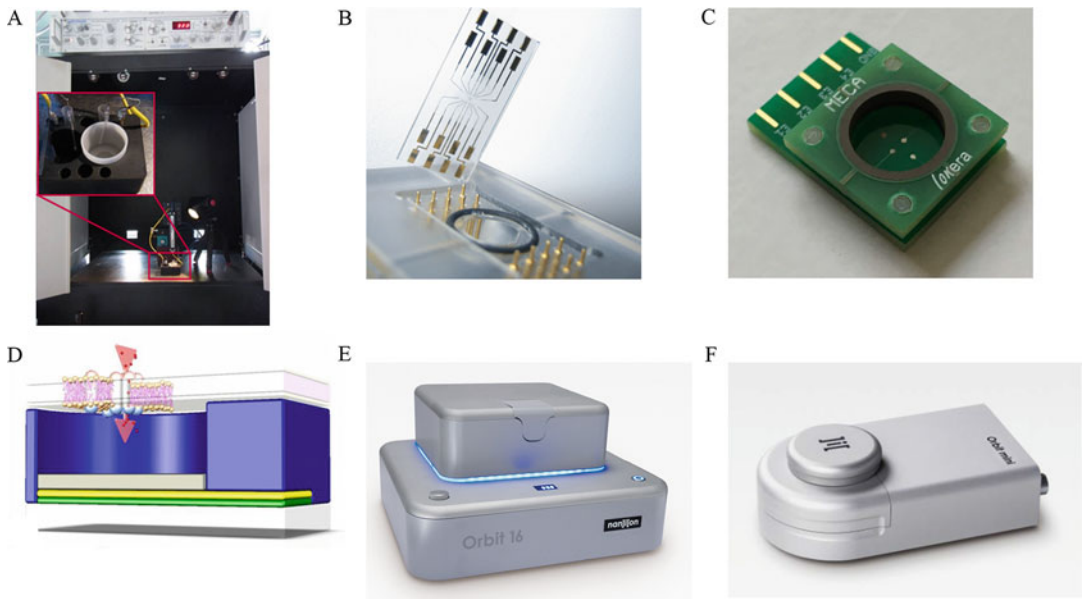


**Fig. 1** (a) Picture of a standard manual bilayer setup. (b) MECA-16 chip for the Orbit 16. (c) MECA-4 chip for the Orbit mini. (d) Schematic of the MECA chip. (e) The Orbit 16 instrument. (f) The Orbit mini instrument

Molecular Devices, San Jose, USA). The amplifier is connected to a PC via an AD/DA converter card (e.g., NI PCI 6036E, National Instruments, Austin, USA) with a connector block (e.g., BNC 2110, National Instruments, Austin, USA) controlled by appropriate software (e.g., GePulse, Michael Pusch, Genoa, Italy)—see Fig. 1a.

2. Tool for painting the membrane (e.g., thin paintbrush or a thin sharpened Teflon strip cut from 500  $\mu\text{m}$  thick foil).
3. Lipids for bilayer formation: 1,2-diphytanoyl-*sn*-glycero-3-phosphocholine (DPhPC; e.g., Avanti polar lipids Inc., Alabama, USA) (see Note 1).
4. Other synthetic or natural bilayer-forming lipids: e.g., egg phosphatidylcholines (PC); Asolectin; *E. coli* polar lipid extract; 1-palmitoyl-2-oleoyl-*sn*-glycero-3-phosphoethanolamine (POPE); 1-palmitoyl-2-oleoyl-*sn*-glycero-3-phosphoglycerol (POPG); 1-palmitoyl-2-oleoyl-glycero-3-phosphocholine (POPC).
5. Buffer solution: typically KCl or NaCl at various molarity (0.1–4 M) buffered with 10–25 mM HEPES, Tris-HCl, or MES depending on the desired pH (see Note 2).
6. “Milli-Q” or double distilled water (see Note 2).
7. N-decane (e.g., Sigma-Aldrich) for preparation of lipid solutions.
8. Chloroform (e.g., Sigma Aldrich) for cleaning chamber and cuvette.

## 2.2 Bilayer Array Formation on the MECA Chips

1. Lipids for bilayer formation: 1,2-diphytanoyl-*sn*-glycero-3-phosphocholine (DPhPC; Avanti Polar Lipids Inc., Alabama, USA) (*see Note 1*).
2. Other bilayer-forming lipids: e.g., egg PC; Asolectin; *E. coli* polar lipids extract; POPE; POPG; POPC.
3. Cholesterol or ergosterol (*see Note 3*).
4. Buffer solution typically KCl or NaCl with different molarities (100 mM–4 M) buffered with HEPES, Tris, or MES depending on pH range.
5. “Milli-Q” or double distilled water (*see Note 2*).
6. Organic solvents for preparation of lipid solutions: *n*-octane/nonane/decane.
7. Ethanol, isopropanol for cleaning the MECA chips.
8. Wetting plunger for MECA chips.
9. Orbit mini or Orbit-16 device (Fig. 1e, f; Nion Technology, Munich, Germany) with Elements Data Reader (EDR) software.
10. MECA-4 or MECA-16 chips (Fig. 1b–d; Ionera Technologies, Freiburg, Germany, available through Nion Technology).

## 2.3 *MspA* Protein Expression and Purification

1. Shaking incubator.
2. Thermal mixer.
3. Ice box.
4. Sterile spreading device.
5. LB agar selection plates with kanamycin.
6. Competent BL 21 cells.
7. Plasmid with PET47b + vector encoding *MspA* M2 Mutant with N-terminal His tag.
8. TB media.
9. LB media.
10. Isopropyl- $\beta$ -D-thiogalactopyranoside (IPTG).
11. Spectrometer.
12. Sonicator.
13. Ultracentrifuge.
14. Water bath.
15. Ni-NTA purification Column or beads.
16. Centrifugal ultrafiltration units with 100 kDa MWCO.
17. SDS-PAGE/Western Blot equipment for analysis.
18. Lysis Buffer: 20 mM Tris pH 7.5, 300 mM NaCl.

19. Equilibration Buffer: 20 mM Tris, 150 mM KCl, 0.5% n-Octylpolyoxyethylene (OPOE), 20 mM Imidazole, pH 8.
20. Elution Buffer: 20 mM Tris, 150 mM KCl, 0.5% n-Octylpolyoxyethylene (OPOE), 400 mM Imidazole pH 8.
21. Dilution Buffer: 20 mM Tris, 150 mM KCl, 0.5% n-Octylpolyoxyethylene (OPOE).

---

### 3 Methods

#### 3.1 Lipid Bilayer Formation

Voltage-clamp is the most powerful and versatile electrophysiological technique to study ion channels and pores. Resistive current can be measured under conditions of constant potential and therefore constant driving force so that conductance can be directly computed. Conductance changes can be related in real time to voltage-dependent gating, ligand binding, and channel block. Single-channel resolution or even recording from a single channel/pore (the two are not the same) is possible as well as ensemble recording from hundreds or thousands of pores.

The first prerequisite for voltage clamp recordings of the current through channels and pores reconstituted in an artificial lipid membrane is a configuration in which the synthetic membrane forms an interface of molecular dimensions between two electrolyte-filled compartments, both of which must be connected to an electronic voltage clamp circuit by nonpolarizable second order electrodes (typically Ag/AgCl). Classically, this is realized using an arrangement of two liquid containers separated by a septum made of a hydrophobic plastic such as poly(tetrafluoroethylene) (Teflon), poly(oxymethylene) (Delrin), or poly(styrene) containing an aperture  $\leq 100 \mu\text{m}$  diameter over which the bilayer is formed. A popular commercial version is the cup in a chamber design available from Warner Instruments, where the aperture is machined in the wall of a cylindrical cup which fits tightly in one half of a double chamber thus defining an inner (*trans*) and an outer (*cis*) volume [23]. However, other viable designs have become available (e.g., see ref. 24).

Lipid membranes are essentially self-organized molecular arrangements stabilized by the so-called hydrophobic effect [25], that is, the attractive interactions mutually between water molecules and between them and the polar headgroups of lipids. Spontaneously, this will lead to micelles and vesicles. To produce a free-standing bilayer, the experimenter has to provide the initial conditions for a metastable state to be reached, which is essentially a thin film covering the aperture.

Regarding methods of bilayer formation, the novice is confronted with some ancient and sometimes misleading terminology: the classical method first used by Müller, Rudin and colleagues is called the “painting” or “Müller-Rudin” method. Here, the bilayer

formation is initiated by spreading a lipid-in-alkane suspension over the aperture with a brush or small spatula. This results in a lipid-solvent plug filling the aperture which then gradually thins out under the influence of Marangoni force (also called Plateau-Gibbs border suction). When the layer becomes thinner than a few 100 nm, van-der-Waals forces become dominant leading to the final bimolecular membrane, which is connected to the rim of the aperture by an annulus or torus of lipid-solvent suspension. The membrane itself is at quasi-equilibrium with this torus and is generally thought to contain some residual solvent [13].

The second method for bilayer formation starts with applying lipid in volatile organic solvent onto the air–water interface on both sides of the partition while the levels of solution are kept below the aperture. Once the solvent has evaporated and lipid monolayers are formed, the solution levels are raised, which, according to the original interpretation leads to the formation of bilayers by apposition or “folding” of monolayers. In this idealized view, the method does not require solvent and the membranes formed by the Montal–Müller technique are therefore still often called “solvent-free bilayers” to contrast with the “solvent-containing bilayers” obtained with the Müller–Rudin technique. However, it was conclusively shown long ago that they are not free of solvent, requiring local pretreatment of the aperture with an alkane to enable formation of a torus or annulus to mediate continuity with the septum [26] and that they also form by thinning of a lipid plug [27]. The “folded, solvent free” Montal–Müller bilayer is, therefore, more of a myth than a reality.

In what follows, we will describe a pragmatic approach in which elements of the two techniques are combined and that has worked well in our hands.

### 3.1.1 Preparation of Lipid Solutions

1. Lipid powder can be directly dissolved in organic solvents listed in the Subheadings 2.1 and 2.2 or the lipids can be stored at -20 °C as dry films overlaid with argon.
2. To prepare a lipid film, place aliquots of the lipid solution in chloroform (eg. 1 mg) in a glass vial. Place the glass vial in a vacuum desiccator connected to a pump for at least 4 h to remove the solvent completely.
3. Overlay the lipid film with argon, close, seal with parafilm. Store at -20 °C.
4. To make 5 mg/ml lipid solution, add 200 µl of the octane to the lipid film, vortex and store the sealed vial at -20 °C (*see Note 4*).

The final lipid concentration used for the formation of lipid bilayers can be in a range of 5–20 mg/ml; *n*-octane, nonane, or *n*-decane can be used as solvents with MECA Chips. Optimal lipid

solution for automated bilayer formation is 5 mg/ml in octane. For manual formation a higher lipid concentration can be used. Note that for higher lipid concentration the membrane formation time usually increases.

### 3.1.2 Bilayer Formation Using the Classical Setup

1. Dissolve lipids in *n*-decane at a concentration of 5–10 mg/ml.
2. Pretreat the aperture in the cuvette by dispensing 1–2 µl of lipid solution with a pipette before starting bilayer formation around the aperture. Allow solvent to evaporate in air for at least 2 h.
3. Dispense 1 ml of buffer solution with a pipette in each the cuvette and the chamber.
4. Dip the thin painting brush into the lipid solution and paint over the aperture. Monitor the electrical resistivity of the aperture. It should be in the range of several hundreds of MΩ to 1 GΩ. Let the bilayer thin out for about 10 min and monitor the capacitance. Capacitance should increase to attain the range of 50–80 pF for an aperture of 150 µm diameter. If the values for capacitance and resistivity match the ranges given above continue with Subheading 3.3. However, often a bilayer is not spontaneously formed with this first step. In most of these cases, the aperture remains clogged with a thick layer of lipid solution. In that case, continue with **step 5**.
5. Reopen the aperture by applying a high voltage pulse (1.6 V) through the “Zap”-button on the Axopatch 200B. The resistivity should change back to a couple of kΩ (depending on the ionic strength of the buffer solution).
  - (a) Using a pipette, lower the water level of the buffer solution in one cuvette to below the aperture.
  - (b) Use a pipette to again raise the water level back to the initial level at which the aperture is totally covered with the buffer solution.
6. Again check the electrical resistivity and capacitance of the seal. The values should be in the ranges mentioned in **step 4**. Otherwise repeat **step 5**.
7. After the experiment, empty and thoroughly wash the cuvette, the chamber and the electrodes with water and chloroform. Eliminate all traces of lipids, salt solution and other residues of experimentation (protein, polymer, etc.) which might contaminate the following experiment.

### 3.1.3 Bilayer Array Formation on MECA-4 Chips (For Use on Orbit Mini)

The easiest way to form lipid bilayers on the MECA-4 chips is to use an air bubble covered with a thin lipid film as illustrated in Fig. 2 and Supplementary Video 1.

1. Add buffer solution to the MECA-4 chip and wet the cavities by gently pressing with the wetting plunger.

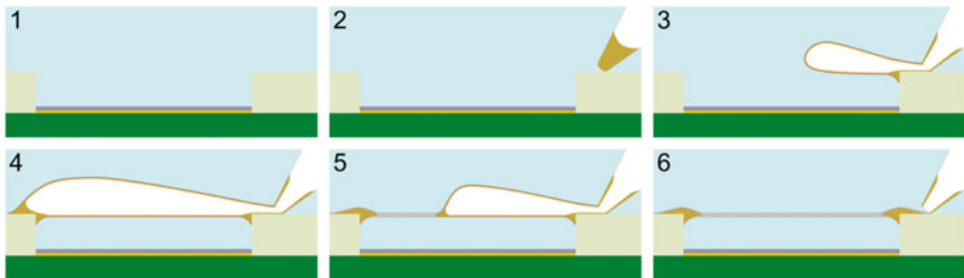


**Fig. 2** Schematic cartoon (not to scale) illustrating lipid bilayer formation on the MECA-4 chip with the air bubble technique

2. Touch the lipid solution with the 10  $\mu\text{l}$  pipette tip. Remove the solution which has remained in the tip due to the capillary force. Now the top of the pipette tip is coated with a thin film of the lipid solution (*see Notes 5 and 6*).
3. Place the tip on the chip surface close to one of the cavities. Form an air bubble on the chip surface under water using 3–5  $\mu\text{l}$  of air (Fig. 2; *see Note 7* and Supplementary Video 1).
4. Move the bubble and spread the lipid film over the chip surface around and over the cavities. Blow and slowly retract the bubble over the cavities one by one.
5. Take a fresh pipette tip, load lipid solution into the tip for a second time. Form membranes by blowing and slowly retracting the bubble over the cavities one by one. Bilayers will be formed spontaneously within seconds.
6. Destroy the membranes with a voltage pulse and repaint bilayers by forming and retracting the bubbles without changing the pipette tip.
7. Check membrane stability at 100 mV and the capacitance (*see Note 8*). Capacitances should be in a range of 7–11 pF for the 50  $\mu\text{m}$  apertures. The measured membrane capacitance depends on the amount of lipid on the surface and the actual bilayer size. With air bubbles, it is easy to add and remove lipid from the chip surface and thereby stabilize or thin-out the membranes.
8. If necessary, destroy and repaint the membranes. A reservoir of lipid remains on the surface. Lipid bilayers can be reformed by spreading lipid from this reservoir over the cavity with a “clean” air bubble made with a fresh pipette tip (*see Note 9*).
9. At the end of the experiment, remove the MECA chip from the recording chamber; rinse the MECA chip with distilled water.
10. Rinse the MECA chip with ethanol followed by isopropanol and finally water again. Blow dry with a stream of pressed air or nitrogen. The chip can be used for further experiments.

*3.1.4 Bilayer Array  
Formation on MECA-16  
Chips (For Use on Orbit-16)*

1. Add 150  $\mu\text{l}$  of the buffer solution into the well on top of the chip and place the pellet of the bath electrode in it. Make sure it does not obstruct the path of the spreading bar later on.
2. Use the wetting plunger to make sure that all sixteen cavities are filled with buffer, thus establishing contact of the driven electrodes with the ground electrode: apply a small voltage (e.g.,  $\pm 30$  mV) and observe the current signal in the oscilloscope window of the EDR software. The signal should be in overload (e.g., at 200 pA at 200 pA gain) if the cavities are filled with buffer.
3. Add the spreading bar and push the button on the Orbit to rotate the bar. Make sure that the spreading bar can rotate freely and that its trajectory is not blocked by the external electrode.
4. Add 0.1  $\mu\text{l}$  of DPhPC dissolved in octane at concentrations of 2–10 mg/ml with a micropipette directly on the chip’s surface between the spreading bar and the cavities so the spreading bar can take up the lipid and spread it over the cavities while performing a full rotation.
5. Start spreading the lipids by turning the spreading bar at a relatively fast speed (e.g., –40 a.u.) until most cavities are covered with a bilayer. Bilayer formation can be followed via the acquisition software as the resistance rises up to the  $\text{G}\Omega$  region and the current drops to zero.
6. If an insufficient number of bilayers is formed, redo **steps 2 and 3** several times if necessary (*see Notes 10 and 11*). Do not add too much lipid solution at once as the cavities will get clogged with lipid plugs, which then requires termination of the experiment and cleaning of all parts.
7. If a satisfactory amount of bilayers has accumulated, turn the magnet slowly (e.g., –3 a.u.) several times to “thin out” and stabilize the bilayers.
8. Run a capacitance test from the acquisition software to monitor the capacitance of the 16 individual bilayers. When 50  $\mu\text{m}$  diameter cavities are used the values should be in the range of 7–11 pF. Alternatively, apply a zap pulse (refer to the software manual) to break the bilayers. The resistivity should decrease from  $\text{G}\Omega$  to several  $\text{M}\Omega$ . This is a commonly used test to make sure you have bilayers and not lipid plugs covering the cavities. After zapping the membranes, you can re-form new bilayers as often as necessary by pushing the button to rotate the spreading bar again.
9. After each experiment, and before starting a new experiment, every part of the module that was in contact with the solution, lipids, and proteins has to be cleaned thoroughly with ethanol or isopropanol and DI water and dried afterwards e.g., on a hotplate ( $<70$  °C) or with pressurized air.

### 3.2 Preparation of Protein Samples for Reconstitution

High quality and purity membrane protein (MP) preparations are crucial for lipid bilayer recordings. Four different expression systems can be used for recombinant expression of membrane proteins: *E. coli*, yeast cells, insect cells, and mammalian cells [28]. The choice of expression system depends on the properties of the target protein. Overexpression of membrane proteins in *E. coli* (the most frequently used system), generally leads to growth inhibition and perturbs cell metabolism more strongly than overexpression of cytosolic proteins, resulting in low yields of MPs.

There are two principally different approaches for production of MPs in *E. coli*: native expression in the cytoplasmic membrane or expression into insoluble and inactive protein aggregates, commonly referred to as inclusion bodies, with subsequent refolding. The expression into inclusion bodies is best suited, but not restricted to, monomeric proteins with  $\beta$ -barrel architecture [29]. Prior to refolding, inclusion bodies are solubilized with strong protein denaturants (urea, sodium dodecyl-sulfate or guanidine hydrochloride) giving unfolded protein structure. The method may yield hundreds of mg of pure unfolded protein per liter of culture medium [30]. The critical step in the protein production is the selection of the refolding media and mode of transfer. Details of refolding conditions for different MPs are reviewed in [29].

Although many MPs were shown to be brought to their native-like structure from the inclusion bodies, refolding of oligomeric MPs remains particularly challenging. Therefore, expression of MPs in functional form is usually preferred but is often hampered by saturation of the capacity of the Sec-translocon. The yield of native MP can be significantly improved by controlling plasmid copy numbers and optimization of cell growth conditions (medium, temperature) and inducer concentration [31].

Protocols for MP purification by affinity and size exclusion chromatography are well established and have been extensively used in the past decades (*see, e.g.*, overview [32] and a protocol [33]). Screening of detergent, pH, and ionic strength conditions may be needed to optimize homogeneity and stability of purified MP. By choosing the appropriate detergent and optimal solubilization conditions it is possible to maintain native protein structure and prevent aggregation. It should be noted that when using recombinant proteins expressed in *E. coli* a two-step purification procedure should be implemented due to the high probability of contamination with *E. coli*-porins which are very abundant, stable and will easily insert into lipid bilayers. Below we describe the method for recombinant expression and purification of the octameric porin MspA from *Mycobacterium smegmatis* in *E. coli* using metal-chelation affinity chromatography.

**3.2.1 Expression and Purification of *Mycobacterium smegmatis* Porin A**

*Mycobacterium smegmatis* porin A (MspA) forms a channel in the outer membrane of this nontuberculous and generally nonpathogenic mycobacterium [34, 35]. It has an octameric beta-barrel structure [36]. MspA has gained prominence as the first biological nanopore successfully used for DNA-sequencing [37, 38]. In order to be suitable for this, however, negative charges in the pore lumen had to be removed. Here, we describe the expression and purification of this mutant (D90N/D91N/D93N/D118R/E139K/D134R) for subsequent lipid bilayer recordings.

**3.2.2 Transformation of *E. coli* BL21 Cells**

1. Thaw competent cells on ice.
2. Put 50 ng of the pET-47b(+) DNA coding for the mutant of MspA (1–2 µl) in a sterile 1.5 ml microcentrifuge tube.
3. Add 50 µl of competent cells to the DNA. Gently flick the tube 4–5 times to mix the cells and DNA.
4. Place the mixture on ice for 20 min.
5. Heat shock at 42 °C for 45 s.
6. Add 400 µl of room temperature LB media.
7. Place the tube at 37 °C for 1 h into a thermal shake.
8. Warm two selection plates with Kanamycin (50 µg/ml) to room temperature.
9. Spread 100–200 µl of the cells onto the selection plates.
10. Incubate overnight at 37 °C.

**3.2.3 Cell Culture Growth and Induction**

1. Pick a single colony and transfer into 5 ml of TB medium supplied with 50 µg/ml Kanamycin to grow a starter culture.
2. Incubate with shaking at 37 °C overnight.
3. Expand the starter culture by adding 0.5 ml of the starter culture to 250 ml TB medium supplied with 50 µg/ml Kanamycin.
4. Incubate for 1–4 h until culture density of OD600 reaches 0.5–0.6.
5. Cool down the culture to room temperature OD600 ~ 0.6–0.7.
6. Thaw IPTG Stock solution.
7. Induce expression by adding IPTG to a final concentration of 0.1 mM.
8. Induce overnight (16–18 h) at room temperature with shaking (180 rpm).

**3.2.4 Cell Collection and Lysis**

1. Centrifuge the cells at  $4000 \times g$  for 20 min at 4 °C.
2. Discard supernatant and resuspend cells in 100 ml of ice-cold PBS and recentrifuge in an appropriately sized tube.

3. Remove the supernatant and freeze pellet in liquid nitrogen for later processing or place on ice to proceed with lysis.
4. Resuspend the cells (~4 g from 250 ml culture) in 25 ml Lysis Buffer.
5. Sonicate the cell suspension on ice with five times of 20 short burst of 5 s followed by intervals of 30 s for cooling. Avoid foaming.
6. Remove cell debris by slow centrifugation at 4 °C for 10 min at  $3000 \times g$ .

### *3.2.5 Protein Purification*

1. Add *n*-octylpolyoxyethylene (OPOE) to the lysate supernatant to a final concentration of 5%, mix thoroughly.
2. Place the glass beaker with the lysate into a water bath at 100 °C for 20 min to denature all the soluble proteins and misfolded MspA oligomers.
3. Cool down and centrifuge at 120,000 × *g* for 30 min at 4 °C.
4. Load the supernatant to a Ni-NTA column ore beads equilibrated with Equilibration Buffer.
5. Wash with Equilibration Buffer and elute with Elution Buffer. Collect the protein-containing fraction.
6. Dilute the protein-containing fraction 20 times with Dilution Buffer and place into an ultrafiltration centrifugal concentrator with MWCO 100,000 kDa. Spin down to a 1 ml volume. Alternatively, use size exclusion chromatography (Superdex S200 column using Dilution Buffer as the column buffer).
7. Control the protein purity and integrity with SDS-PAGE and Western Blot (Anti-his).
8. Determine the protein concentration. Dilute to obtain stock solution of 20 µg/ml in Dilution Buffer.
9. Aliquot and freeze in liquid nitrogen. Store at –80 °C (*see Note 12*).

### *3.2.6 Optimization of Protein Samples Synthesized In Vitro*

In vitro translation of membrane proteins is a powerful alternative strategy to heterologous expression in cellular systems [39, 40]. Several ion channels have been successfully translated in vitro and subsequently reconstituted into lipid bilayers after purification [40–44]. *E. coli* based cell-free expression systems allow the synthesis of membrane proteins with high protein yields of up to several milligrams per milliliter [45]. Typically the reaction mixture is supplied with liposomes or preformed nanodiscs to enable cotranslational insertion and folding of the synthesized ion channel into suitable hydrophobic environments. To minimize contamination of the synthesized sample with residual bacterial porins still present in standard S30 lysates [46], an additional ultracentrifugation step should be included (*see Note 13*). A potential decrease in the

protein production efficiency of the resulting lysates could be compensated by increasing their final concentration in the cell-free reactions (*see Note 14*) and background activities of contaminating outer membrane porins can thus be reduced or completely eliminated.

If the protein of interest is expressed *in vitro* in the presence of nanodiscs [40, 44, 47], it can easily be purified by using small affinity-tags attached to the membrane protein (*see Note 15*). Purified membrane protein/nanodiscs complexes can be used directly for the transfer into other lipid bilayers [44, 48, 49], *see Note 16*. If the reaction mixture is supplied with liposomes, the harvested proteoliposomes can be optimized for subsequent electrophysiological recordings. The general scheme of this procedure is shown in Fig. 3.

1. Add large unilamellar vesicles to the cell-free reaction mixture (Asolectin; 200 nm; final concentration 6 mg/ml) to enable cotranslational insertion of the synthesized ion channel (Fig. 3, step 1).
2. After expression, first centrifuge the reaction mixture to separate the soluble fraction from the precipitate ( $22,000 \times g$ , 4 °C, 5 min). Separate proteoliposomes containing synthesized protein via centrifugation at  $100,000 \times g$  for 30 min at 4 °C. Wash the obtained pellet with buffer containing 2 M urea to remove attached but not-inserted proteins. Check the protein content in the sample using SDS-PAGE (Fig. 3, step 2).
3. For single-channel recordings and high protein concentration in the collected proteoliposomes the protein–lipid ratio can be adjusted by additional enrichment with lipids. Incubate the resuspended proteoliposomes with lipid vesicles (1–5 µg protein–mg of lipids) in buffer 50–200 mM hypertonic to the measurements buffer for bilayer recordings, sonicate and extrude through polycarbonate filter of 100 nm (Fig. 3, steps 3 and 4).
4. Fuse the proteoliposomes with preformed lipid bilayers as described in Subheading 3.3.3 (Fig. 3, steps 5 and 6).

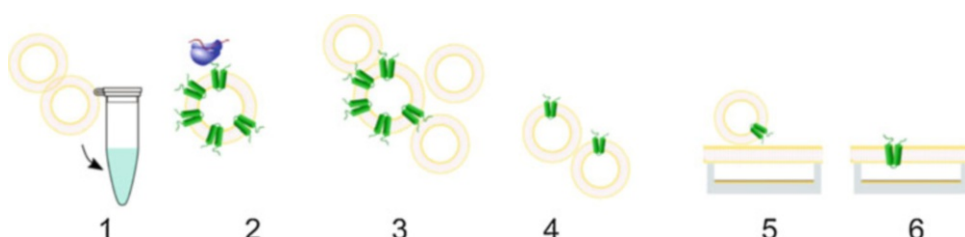


**Fig. 3** Schematic cartoon illustrating optimization of *in vitro* expressed protein samples for single-channel recordings

### 3.3 Protein Reconstitution

There are different types of channel-forming proteins which can be used for experiments involving planar lipid bilayers. That is why there are very different strategies for preparing and reconstituting them. There are four principally different cases:

1. Water soluble monomers of self-assembling toxins (e.g., hemolysin, aerolysin)—these are self-inserting by nature.
2. Antimicrobial peptides (e.g., gramicidin, tyrocidins)—these are inserted from DMSO or ethanol/methanol containing solutions.
3. Membrane proteins with predominantly beta-barrel structures (e.g., OMPs, VDAC, TOM complex)—these are purified and reconstituted directly from detergent micelles (typically Octyl-POE or n-Dodecyl β-D-maltoside (DDM)).
4. Membrane proteins with predominantly alpha-helical structures (e.g., Ion channels—KcsA, KvAP, ryanodine receptor)—these are purified in mild detergents (DDM; Fos-Choline-14, beta-OG) and reconstituted from mixed micelles (detergent-lipid); proteoliposomes or transferred from nanodiscs (*see Note 16*).

In all cases, the most important step for single-channel electrophysiological recordings is the adjustment of the protein concentration in the measurement chamber. Final protein concentration depends on the type of protein and is usually in the pM–nM range. It also depends on the lipid bilayer area (MECA-chip cavity size), that is, the probability of protein insertion increases in larger membranes. For a successful reconstitution, DMSO/methanol or detergent concentration, as well as protein–detergent or protein–lipid ratio should be individually adjusted for each protein target.

There are three main protocols for reconstitution of protein into lipid bilayers depending of the type of protein used. The main steps for the different methods are outlined in this section below.

#### 3.3.1 Self Insertion of Water-Soluble Multimeric Bacterial Toxins and Peptide Antibiotics

1. Predilute protein stock in recording buffer solution to reach the desired protein concentration after the addition of 0.2–1 µl of the solution to the recording chamber. In general, for single-channel recordings with 50 µm-membranes the final protein concentration is typically in the nano- to picomolar range (e.g., for Hemolysin 1–2 ng/ml and Gramicidin about 2 pg/ml).
2. Add the desired volume of the protein solution to the measurement chamber above the membranes. Carefully mix the solution in the recording chamber by repeatedly and carefully drawing at least 30 µl of the solution in and out of the pipette tip.

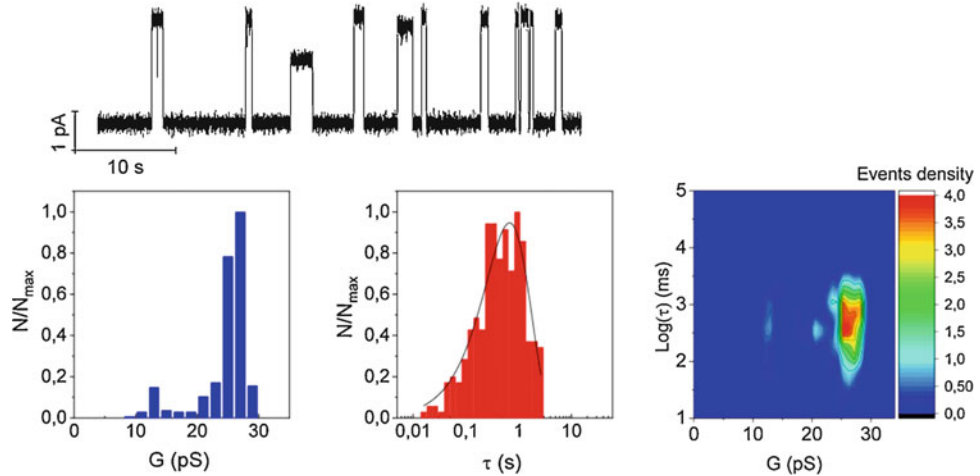


**Fig. 4** Example of single-channel current recording of gramicidin A and the data analysis. Upper row: representative ion current trace through single gramicidin A channels. Second row: (a) Conductance histograms (normalized event counts vs. single-channel conductance). (b) Channel lifetime log-binned histograms fitted by single exponential distributions. (c) Two-dimensional events density contour map of the gramicidin A channels lifetime and conductance distributions.  $V_{\text{hold}} = 100 \text{ mV}$ ;  $25^\circ \text{C}$  [50]

3. Apply 40 mV and wait for insertions, which will be visible as rectangular current steps. You may additionally apply short voltage pulses just below the bilayer electroporation threshold (e.g., 200 mV/200 ms for 50  $\mu\text{m}$  MECA-chips) to facilitate spontaneous insertion.
4. Ion channel activity normally appears after several minutes which are needed for the individual subunits to reach the membrane. As seen for example in Fig. 4, the formation and disappearance of conducting gramicidin A channels are observed as rectangular current transitions when a trans-bilayer potential difference is applied.
5. Record current traces at desired voltages for at least 2 min. The EDR software allows conversion of the data in popular formats, such as axon binary (ABF). Various well-established software tools [e.g., Clampfit (Molecular Devices, Sunnyvale, CA, USA), IgorPro (Wavemetrics, Lake Oswego, OR, USA) or Origin (Origin Lab Corporation, Northampton, MA, USA)] can then be used for data analysis. Representative single-channel current traces and data analysis for gramicidin A in a DPhPC-membrane are presented in Fig. 4. The “All-point histogram” and “Event detection” functions in the Clampfit software can be used to obtain a rough overview on channel statistics and to detect channel opening events. A typical analysis includes a calculation of the distribution of single-channel conductance (estimated from fits to all-point current histograms), and determining a mean open time distribution via an exponential fit to the distribution of the duration of

conducting states (the dwell time histogram), which reflects the stochastic nature of the channels. Two-dimensional event density contour map of the channels lifetime and conductance distribution can be plotted to analyze properties of individual channel populations (Fig. 4).

### 3.3.2 Membrane Protein Reconstitution via Detergent Dilution

The method of directly incorporating proteins into a bilayer array from detergent micelles is suitable for membrane proteins with predominantly beta-barrel structures, solubilized in nonionic detergents (e.g., octyl-POE; DDM).

1. Add a very small amount of protein solution in detergent micelles, ~0.1–0.2  $\mu$ l at 1–100  $\mu$ g/ml (see Note 17) protein concentration and a double of the detergent critical micelle concentration (CMC) into the chamber with mixing (see Notes 18 and 19). Rapid dilution of the detergent below the CMC results in a disassembly of the micelles. Some of the protein molecules will reach the lipid bilayers and incorporate, but most of them will denature and aggregate. Alternatively, you may first quickly predilute ~0.5  $\mu$ l of the protein stock in 10  $\mu$ l buffer and immediately add it to the measurement chamber above the membranes.
2. Apply voltage pulses (200 mV/200 ms) or 100 mV DC to facilitate protein insertion (see Subheading 3.3.1, step 3). Individual insertions will be seen as stepwise changes in ionic current. Figure 5 shows an example of recordings of the porin MspA on the Orbit 16 reconstituted via detergent dilution.

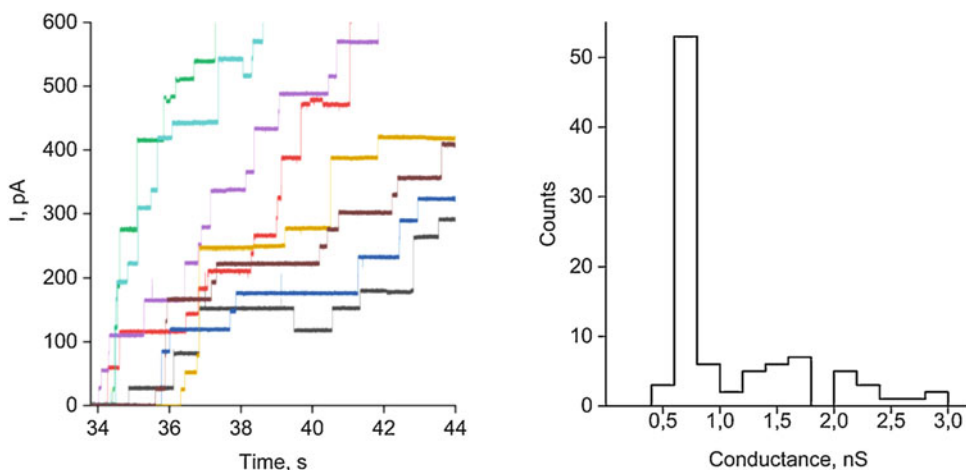


**Fig. 5** Assay of channel-forming activity (left) and Histogram of single-channel conductance (right) of recombinant MspA mutant porin in a diphytanoyl phosphatidylcholine bilayer. Traces from a single experiment recorded in parallel from 16 lipid bilayers. Addition of MspA in OPOE detergent micelles (0.5%) resulted in insertion of 97 pores within 10 s after addition of the protein. Analysis of rMspA single-channel conductance distribution derived from one parallel recording from 12 bilayers on the Orbit-16. Recording buffer: 20 mM HEPES, 350 mM KCl, pH 7.5; rMspA final concentration ~20 ng/ml;  $V_{hold}$  40 mV

3. After a sufficient number of single-channel insertions on the membrane array is reached, perfuse the chamber 2–3 times by withdrawing 50 µl buffer solution from the measurement chamber and replacing it with the fresh buffer to remove traces of detergent and prevent further protein insertions.
4. If membranes become unstable in the presence of detergent repaint them and wait for insertions for 3–5 min without adding more of the protein solution.

### 3.3.3 Proteoliposome Fusion

Membrane proteins with mostly alpha-helical structures (e.g., ion channels) cannot usually be directly transferred from detergent micelles into the lipid bilayers. For efficient electrophysiological recordings from ion channels, they should be first reconstituted into proteoliposomes by adding lipids to the ion channel preparation followed by detergent removal, either by dilution, dialysis, or addition of biobeads. In a second step the proteoliposomes are then fused with the preformed bilayers (*see Notes 20 and 21*). Details on proteoliposome preparation can be found in [51, 52].

Most successful strategies for reconstitution from proteoliposomes rely on two factors: (1) enhanced binding (docking) of the vesicles to the target membrane, which can be electrostatically encouraged by divalent cations ( $\text{Ca}^{2+}$ ) or the use of charged lipids (*see Note 22*); and (2) osmotic destabilization by the application of a salt gradient [1, 16]. The latter effect is brought about by making the side of addition of the vesicles hypertonic, supposedly leading to water flow through the bilayer and swelling and fusion of docked vesicles, provided that the osmolyte used can permeate the vesicle membrane. This can be ensured, if necessary, by incorporation in the liposomes of the weakly anion-selective channel nystatin together with its cofactor ergosterol. Upon fusion, ergosterol is strongly diluted and the nystatin channels close, leaving only the desired protein active in the membrane [53, 54].

1. To fuse the proteoliposomes with lipid bilayers, add vesicles as close to the membranes as possible.
2. Apply 30–50 mV and wait for 2–3 min.
3. If they do not fuse spontaneously (appearance of a current), add about 0.5 µl of 1–3 M KCl above the membranes to osmotically destabilize the system for a short time and encourage the proteoliposomes to fuse (*see Fig. 3*, steps 5 and 6; *see Notes 23–25*).
4. Carefully perfuse the cis chamber with buffer to remove a salt gradient.
5. Record ionic current at different applied potentials for at least 1 min (*see Fig. 6*). Single-channel conductance can be calculated from the amplitude of current during openings. Open probability ( $P_o$ ) at different voltages and time points, as well as

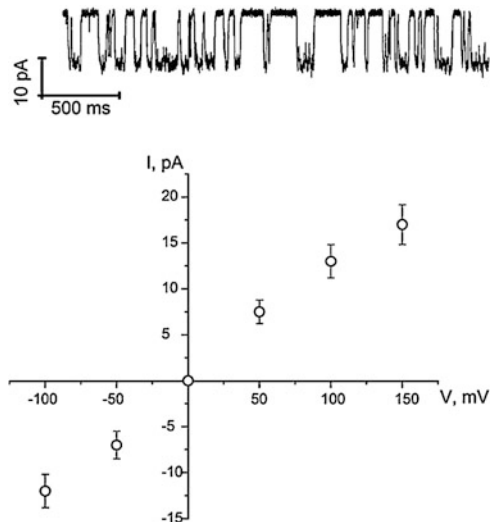


**Fig. 6** Representative single-channel current trace and mean single-channel current amplitude as a function of applied voltage from in vitro-translated KcsA<sub>E71A</sub> purified and reconstituted using nanodiscs. Recorded in symmetric solution containing 200 mM KCl, 20 mM MES, pH 4.5

dwell time in open and closed states can be determined using appropriate software (e.g., Clampfit). See “Single Channel Search” and “Event Detection” functions of Clampfit Tutorial (Axon Instruments, Molecular Devices; *see Note 26*).

### 3.4 Data Acquisition, Storage, and Analysis

Data acquisition follows the general rules of the electrophysiological trade which are exhaustively laid out in several texts [55, 56], of which the “Axon Guide” [57] is particularly recommended. Briefly, care should be taken to use preamplification as high as possible without saturating the AD-converter: it is a common error to acquire, for example, single-channel data with current levels well below 200 pA with too low a gain setting, for example, 5 mV/pA instead of 50 mV/pA (corresponding to  $\pm 2$  nA and  $\pm 200$  pA full scale, respectively for a  $\pm 10$  B output) which results in a loss of precision (30.5 fA instead of 3.5 fA/bin at 16 bit) and even possibly added digitization noise.

The rate of digitization (the inverse of the sampling interval) should significantly exceed the Nyquist criterion ( $>2 \times$  the analog low pass filter cut-off frequency,  $f_c$ ). Just meeting it is often insufficient, especially if event detection algorithms or off-line digital filtering is used; we routinely digitize at  $10 \times f_c$ , as current data storage devices easily handle data files of several gigabytes.

Another important point is holding potential control by the output of a digital to analog (DA) converter, as commonly used. Here, the lowest possible gain on the voltage command input of the voltage-clamp amplifier should be used to minimize the influence



**Fig. 7** Parallel single-channel recordings on the MECA-16 chip with corresponding all points histograms showing current distribution for in vitro-translated KcsA<sub>E71A</sub> channels reconstituted via proteoliposome fusion. Gray lines indicate the channel open (O) and closed (C) states respectively. KcsA<sub>E71A</sub> was translated in the presence of Asolectin liposomes, which were subsequently enriched with POPG lipids and fused with POPE–POPG (3:1) bilayers on the MECA-16 chip.  $V_{hold} = 100$  mV. Recorded in symmetric solution containing 200 mM KCl and 20 mM MES, pH 4.5 on the *cis*-side and 10 mM MOPS pH 7.5 on the *trans* side of the bilayers

of noise on the DA output, as any fluctuation on the voltage command input will create a capacitive current response on the recording. In addition, pipette capacitance cancellation on the Axopatch or HEKA amplifiers can be used to further suppress this noise component.

All points histograms as shown in Fig. 7 is a good way of getting an overview of data: they contain information on preferred current levels, if any (position of maxima on the current ( $x$ ) axis), as well as roughly on the total time spent on the particular level (the areas under the peaks). Further analysis usually requires event detection and creation of an idealized record. Algorithms of varied complexity and power are available in free or commercial software (Ana, Michael Pusch, Genova, Italy), Clampfit (Molecular Devices), or Mosaic [58, 59].

As shown in Fig. 4, standard analysis involves the measurement of dwell times (durations of closed, open, or intermediate states), which can be fitted with (sums of) exponentials to obtain characteristic (mean) values. While the analysis of single-channel data is more demanding than that of ensemble currents, the advantage is that dwell time distributions carry more information than time constants of ensemble currents and their characteristic values can be directly related to the rate constants of mechanisms underlying the observed dynamics [60–63].

Two-parameter scatter- or density plots as shown in Fig. 4 are particularly useful in identifying subpopulations or substates of pores or channels.

---

## 4 Notes

1. Lipid bilayers can be formed from a range of different lipid compositions. A branched chain phospholipid 1,2-diphytanoyl-*sn*-glycero-3-phosphocholine (DPhPC) is the most widely used lipid due to exceptional stability of DPhPC bilayers. DPhPC membranes are in the fluid lamellar phase in a very wide temperature range. Formation of stable bilayers from natural lipids and lipid mixtures is generally more difficult due to lipid oxidation, phase separation, and a possible contamination of natural lipids.
2. “Milli-Q” or double distilled water should be used to prepare all buffer solutions. After preparation, all solutions should be filtered through a 0.2-μm filter. Reducing or oxidizing agents capable of reacting with Ag/AgCl (dithiothreitol, hydrogen peroxide, hydrogen sulfide, hydroxylamine, etc.) should never be added to the buffer solutions. High-molarity chloride buffers (above 3 M) should be additionally saturated with AgCl to prevent electrode depletion.
3. Up to 30% w:w of cholesterol or ergosterol can be added to the lipid solution. For example, the planar model lipid system mimicking gram-positive membranes is a 3:1 mixture of 1-palmitoyl-2-oleoyl-*sn*-glycero-3-phosphoglycerol [POPG] and 1-palmitoyl-2-oleoyl-*sn*-glycero-3-phosphoethanolamine [POPE]; a possible mammalian membrane mimic is POPC-POPE (3:1).
4. DPhPC stock solution can be stored at -20 °C for several months. We recommend keeping the lipid stock solution in the freezer and working with aliquots made weekly to minimize freeze-thaw cycles.
5. While filling the pipette tip with a dip of lipid solution make sure to only touch the surface of the lipid stock solution and not to insert the tip too deep as residuals of lipid solution on the exterior of the tip will result in “unzappable” membranes or lipid plugs.
6. After the pipette tip has been filled with lipid solution, blow the pipette tip completely dry by using the full pipette volume of 10 μl.
7. Generate the air bubble (around 2 mm in diameter) not directly over the cavity, but a little bit aside and subsequently move it over the cavity.
8. After forming a membrane, perform a capacitance measurement. Ensure that during this measurement the current range is set to ±2 nA instead of the 200 pA you may be using as default.

9. If too much of the lipid solution was brought to the cavity the membrane cannot be destroyed with a voltage pulse (zap-pulse). Such membranes which cannot be zapped away can be made “zappable” by repeatedly moving an air bubble made with a fresh pipette tip over the cavity back and forth or “bursting” a bubble above the membrane. It is not necessary to remove the buffer or to clean the chip (*see* Supplementary Video 1).
10. Check the trajectory of the spreading bar; make sure it can rotate freely without hitting the bath electrode.
11. If you experience a poor yield of bilayers during bilayer formation: (a) lift the spreading bar at one end, for example, with a pipette tip for a short time. This will remove residing micro bubbles resulting from air dispensed unintentionally while loading the lipid solution on the chip. (b) Adjust trajectory of the spreading bar. It should cover all microelectrodes in the center of the chip. (c) Clean or replace the spreading bar.
12. Stability and storage conditions of proteins vary. Aliquots of proteoliposomes should be flash-frozen and kept at  $-80^{\circ}\text{C}$  or at least  $-20^{\circ}\text{C}$ . Antimicrobial peptides, soluble toxins, or porins can be kept in solution at  $4^{\circ}\text{C}$  for several months.
13. Standard S30 lysates are optimized for high expression efficiency but still contain certain amounts of residual small membrane vesicles containing membrane proteins such as OmpX, OmpA, and OmpC [46]. If background activities of these membrane proteins are problematic for specific assay conditions, the S30 lysate could be further cleared by additional ultracentrifugation steps at higher  $\text{g}$ -forces. Centrifuge the S30 lysate for 30 min at 70,000 to 100,000  $\times \text{g}$  at  $4^{\circ}\text{C}$ . After centrifugation two separate phases will be visible. Carefully collect the upper phase (S70 or S100 lysate) and discard the lower phase. This procedure will usually remove most or even all of residual porin background activity in common electrophysiological assays. For high sensitivity assays, the S100 lysate could be further incubated with POPC liposomes (6 mg/ml; 200 nm) for 1 h at  $4^{\circ}\text{C}$  to fuse any residual membrane vesicles. The liposomes can then be quantitatively removed by an additional centrifugation at 100,000  $\times \text{g}$  for 30 min at  $4^{\circ}\text{C}$  and used for *in vitro* expression.
14. Centrifugation of cell-free lysates at  $\text{g}$ -forces  $>30,000$  may increasingly result in the removal of a certain number of ribosomes. In particular the protein expression efficiency of S100 lysates may be 10–30% lower if compared with intact S30 lysates. If necessary, this can be compensated by increasing the final concentration of S100 lysates in the cell-free reaction up to 50%.

15. The membrane scaffold proteins used to preform nanodiscs contain a His<sub>6</sub>-tag. In order to rapidly separate nanodiscs filled with the target protein from empty nanodiscs after cell-free expression reactions, using a differential affinity-tag such as the StrepII-tag attached to the target protein would be most straightforward. Alternatively, the His<sub>6</sub>-tag could be cleaved off from the membrane scaffold proteins by TEV protease before nanodiscs assembly.
16. Addition of the purified KcsA-containing nanodiscs to the preformed bilayer array on the MECA chip results in the appearance of typical KcsA channel activity in several membranes. However, in our experience, the channel reconstitution efficiency and stability of the resulting membranes were not as good as in the optimized proteoliposome samples.
17. Higher protein concentration results in simultaneous insertion of multiple channels, which is seen in appearance of steps with the double or triple conductance value. *See Fig. 5* with multi-channel recordings of MspA—final concentration 20 ng/ml (added from the stock solution of 200 µg/ml in 0.5% OPOE).
18. Rapid dilution of the detergent below the CMC results in a disassembly of the micelles therefore, when diluting protein stock solution in detergent, the detergent concentration should always be kept above the CMC.
19. The concentration of the protein stock solution and the final dilution factor must be optimized individually to improve the rate of single-channel insertions and to minimize the influence of the detergent on the membrane. Protein injection in the vicinity of a lipid bilayer and thorough mixing of the solution are decisive factors for the homogeneous distribution of functional proteins.
20. Proteoliposome density is crucial for efficient fusion. The proteoliposomes must be heavier than the surrounding solution to sink to the membranes and not to float. Addition of sucrose (200 mM) to the proteoliposome preparations helps to reach the proper density. As an alternative, the proteoliposomes with a higher salt concentration (1 M KCl) can be prepared.
21. Proteoliposomes with the protein–lipid ratio about 1:1000 w:w or less should be used for single-channel recordings in lipid bilayers.
22. Lipids with opposite charges in membranes and liposomes can be used to ease docking and fusion. Supplementation with 1–2% PG in membranes and DOTAP in proteoliposomes usually helps fusion.
23. 40 mM CaCl<sub>2</sub> can be used additionally to 1 M KCl to induce fusion.

24. Note that only proteoliposomes containing open channels permeable to at least one component of the salt will swell and therefore fuse. Otherwise nystatin–ergosterol channels can be used to force the proteoliposome fusion.
25. Proteoliposome fusion efficiency depends on the proteoliposome size and the membrane surface. If fusion efficiency is insufficient you may extrude the proteoliposomes through a 100 nm polycarbonate filter and use MECA chips with 100 or 150  $\mu\text{m}$  cavities.
26. For a single-channel opening, the conductance is calculated using Ohm's law:  $G = I/V$ . While plotting the current amplitude as a function of voltage (an  $I/V$  curve) the channel conductance is the slope of the graph.

## References

1. Miller C (1986) Ion channel reconstitution, 1st edn. Springer, New York, NY
2. Mueller P, Rudin DO (1963) Induced excitability in reconstituted cell membrane structure. *J Theor Biol* 4:268–280. [https://doi.org/10.1016/0022-5193\(63\)90006-7](https://doi.org/10.1016/0022-5193(63)90006-7)
3. Mueller P, Rudin DO (1967) Action potential phenomena in experimental bimolecular lipid membranes. *Nature* 213:603–604. <https://doi.org/10.1038/213603a0>
4. Mueller P, Rudin DO (1967) Development of  $\text{K}^+$ - $\text{Na}^+$  discrimination in experimental bimolecular lipid membranes by macrocyclic antibiotics. *Biochem Biophys Res Commun* 26:398–404. [https://doi.org/10.1016/0006-291x\(67\)90559-1](https://doi.org/10.1016/0006-291x(67)90559-1)
5. Bean RC, Shepherd WC, Chan H, Eichner J (1969) Discrete conductance fluctuations in lipid bilayer protein membranes. *J Gen Physiol* 53:741–757
6. Ehrenstein G, Lecar H, Nossal R (1970) The nature of the negative resistance in bimolecular lipid membranes containing excitability-inducing material. *J Gen Physiol* 55:119–133. <https://doi.org/10.1085/jgp.55.1.119>
7. Hladky SB, Haydon DA (1970) Discreteness of conductance change in bimolecular lipid membranes in the presence of certain antibiotics. *Nature* 225:451–453. <https://doi.org/10.1038/225451a0>
8. Gordon LG, Haydon DA (1972) The unit conductance channel of alamethicin. *Biochim Biophys Acta Biomembr* 255:1014–1018. [https://doi.org/10.1016/0005-2736\(72\)90415-4](https://doi.org/10.1016/0005-2736(72)90415-4)
9. Eisenberg M, Hall JE, Mead C (1973) The nature of the voltage-dependent conductance induced by alamethicin in black lipid membranes. *J Membr Biol* 14:143–176
10. Behrends JC (2012) Evolution of the ion channel concept: the historical perspective. *Chem Rev* 112:6218–6226. <https://doi.org/10.1021/cr300349g>
11. Hille B (2001) Ion channels of excitable membranes, 3rd edn. Sinauer Associates, Inc, Sunderland, MA
12. Sakmann B, Neher E (1995) Single-channel recording. Springer, New York, NY
13. White SH (1986) The physical nature of planar bilayer membranes. In: Miller C (ed) Ion channel reconst., 1st edn. Springer, Boston, MA, pp 3–35
14. Finkelstein A (1974) Bilayers: formation, measurements, and incorporation of components. *Methods Enzymol* 32:489–501. [https://doi.org/10.1016/0076-6879\(74\)32049-6](https://doi.org/10.1016/0076-6879(74)32049-6)
15. Ehrlich BE (1992) Planar lipid bilayers on patch pipettes: bilayer formation and ion channel incorporation. *Methods Enzymol* 207:463–470. [https://doi.org/10.1016/0076-6879\(92\)07033-k](https://doi.org/10.1016/0076-6879(92)07033-k)
16. Miller C (1983) First steps in the reconstruction of ionic channel functions in model membranes. In: Barker JL, McKelvy JF (eds) *Curr. methods cell. neurobiol.* Wiley, New York, NY, pp 1–37
17. Williams AJ (1994) An introduction to the methods available for ion channel reconstitution. In: Ogden D (ed) *Microelectrode Tech* Plymouth work. Handbook. Company of Biologists Limited, Cambridge, UK, pp 79–99
18. Mittermeier L, Demirkhanian L, Stalbauer B et al (2019) TRPM7 is the central gatekeeper of intestinal mineral absorption essential for postnatal survival. *Proc Natl Acad Sci U S A* 116:4706–4715. <https://doi.org/10.1073/pnas.1810633116>

19. Baaken G, Sondermann M, Schlemmer C et al (2008) Planar microelectrode-cavity array for high-resolution and parallel electrical recording of membrane ionic currents. *Lab Chip* 8:938–944. <https://doi.org/10.1039/b800431e>
20. Baaken G, Ankri N, Schuler A-K et al (2011) Nanopore-based single-molecule mass spectrometry on a lipid membrane microarray. *ACS Nano* 5:8080–8088. <https://doi.org/10.1021/nn202670z>
21. Baaken G, Halimeh I, Bacri L et al (2015) High-resolution size-discrimination of single nonionic synthetic polymers with a highly charged biological nanopore. *ACS Nano* 9:6443–6449. <https://doi.org/10.1021/acsnano.5b02096>
22. del Rio Martinez JM, Zaitseva E, Petersen S et al (2015) Automated formation of lipid membrane microarrays for ionic single-molecule sensing with protein nanopores. *Small* 11:119–125. <https://doi.org/10.1002/smll.201402016>
23. Warner. <https://www.warneronline.com/classic-bilayer-cups-chambers>. Accessed 23 July 2019
24. Elements. <https://elements-ic.com/blmkit-page/>. Accessed 23 July 2019
25. Tanford C (1980) The hydrophobic effect: formation of micelles and biological membranes. Wiley Interscience, New York, NY
26. White SH, Petersen DC, Simon S, Yafuso M (1976) Formation of planar bilayer membranes from lipid monolayers. A critique. *Biophys J* 16:481–489. [https://doi.org/10.1016/S0006-3495\(76\)85703-7](https://doi.org/10.1016/S0006-3495(76)85703-7)
27. Niles WD, Levis RA, Cohen FS (1988) Planar bilayer membranes made from phospholipid monolayers form by a thinning process. *Biophys J* 53:327–335. [https://doi.org/10.1016/S0006-3495\(88\)83110-2](https://doi.org/10.1016/S0006-3495(88)83110-2)
28. He Y, Wang K, Yan N (2014) The recombinant expression systems for structure determination of eukaryotic membrane proteins. *Protein Cell* 5:658–672. <https://doi.org/10.1007/s13238-014-0086-4>
29. Popot J-L (2014) Folding membrane proteins *in vitro*: a table and some comments. *Arch Biochem Biophys* 564:314–326. <https://doi.org/10.1016/j.abb.2014.06.029>
30. Schwarzer TS, Hermann M, Krishnan S et al (2017) Preparative refolding of small monomeric outer membrane proteins. *Protein Expr Purif* 132:171–181. <https://doi.org/10.1016/j.pep.2017.01.012>
31. Jensen HM, Eng T, Chubukov V et al (2017) Improving membrane protein expression and function using genomic edits. *Sci Rep* 7:13030. <https://doi.org/10.1038/s41598-017-12901-7>
32. Ishchenko A, Abola EE, Cherezov V (2017) Crystallization of membrane proteins: an overview. In: Wlodawer A, Dauter Z, Jaskolski M (eds) *Protein crystallogr, Methods mol. Biol.*, vol 1607. Humana, New York, NY, pp 117–141
33. Kubicek J, Block H, Maertens B et al (2014) Expression and purification of membrane proteins. *Methods Enzymol* 541:117–140. <https://doi.org/10.1016/B978-0-12-420119-4.00010-0>
34. Niederweis M, Ehrt S, Heinz C et al (1999) Cloning of the *mspA* gene encoding a porin from *Mycobacterium smegmatis*. *Mol Microbiol* 33:933–945. <https://doi.org/10.1046/j.1365-2958.1999.01472.x>
35. Niederweis M (2003) Mycobacterial porins - new channel proteins in unique outer membranes. *Mol Microbiol* 49:1167–1177. <https://doi.org/10.1046/j.1365-2958.2003.03662.x>
36. Faller M, Niederweis M, Schulz GE (2004) The structure of a mycobacterial outer-membrane channel. *Science* 303:1189–1192. <https://doi.org/10.1126/science.1094114>
37. Derrington IM, Butler TZ, Collins MD et al (2010) Nanopore DNA sequencing with *MspA*. *Proc Natl Acad Sci U S A* 107:16060–16065. <https://doi.org/10.1073/pnas.1001831107>
38. Manrao EA, Derrington IM, Laszlo AH et al (2012) Reading DNA at single-nucleotide resolution with a mutant *MspA* nanopore and phi29 DNA polymerase. *Nat Biotechnol* 30:349–353. <https://doi.org/10.1038/nbt.2171>
39. Rues R-B, Henrich E, Boland C et al (2016) Cell-free production of membrane proteins in *Escherichia coli* lysates for functional and structural studies. In: Mus-Vetœau I (ed) *Heterologous expr. membr. proteins, Methods Mol. Biol.*, vol 1432. Humana, New York, NY, pp 1–21
40. He W, Felderman M, Evans AC et al (2017) Cell-free production of a functional oligomeric form of a *Chlamydia* major outer-membrane protein (MOMP) for vaccine development. *J Biol Chem* 292:15121–15132. <https://doi.org/10.1074/jbc.M117.784561>
41. Kovácsová G, Gustavsson E, Wang J et al (2015) Cell-free expression of a functional pore-only sodium channel. *Protein Expr Purif* 111:42–47. <https://doi.org/10.1016/j.pep.2015.03.002>

42. Focke PJ, Hein C, Hoffmann B et al (2016) Combining in vitro folding with cell free protein synthesis for membrane protein expression. *Biochemistry* 55:4212–4219. <https://doi.org/10.1021/acs.biochem.6b00488>
43. Renauld S, Cortes S, Bersch B et al (2017) Functional reconstitution of cell-free synthesized purified Kv channels. *Biochim Biophys Acta Biomembr* 1859:2373–2380. <https://doi.org/10.1016/j.bbamem.2017.09.002>
44. Winterstein L-M, Kukovetz K, Rauh O et al (2018) Reconstitution and functional characterization of ion channels from nanodiscs in lipid bilayers. *J Gen Physiol* 150: jgp.201711904. <https://doi.org/10.1085/jgp.201711904>
45. Henrich E, Peetz O, Hein C et al (2017) Analyzing native membrane protein assembly in nanodiscs by combined non-covalent mass spectrometry and synthetic biology. *Elife* 6: e20954. <https://doi.org/10.7554/elife.20954>
46. Foshag D, Henrich E, Hiller E et al (2018) The *E. coli* S30 lysate proteome: a prototype for cell-free protein production. *New Biotechnol* 40:245–260. <https://doi.org/10.1016/j.nbt.2017.09.005>
47. Rues R-B, Gräwe A, Henrich E, Bernhard F (2017) Membrane protein production in *E. coli* lysates in presence of preassembled nanodiscs. In: Burgess-Brown N (ed) *Heterologous gene expr. E. coli*, Methods Mol. Biol., vol 1586. Humana, New York, NY, pp 291–312
48. Banerjee S, Nimigean CM (2011) Non-vesicular transfer of membrane proteins from nanoparticles to lipid bilayers. *J Gen Physiol* 137:217–223. <https://doi.org/10.1085/jgp.201010558>
49. Patriarchi T, Shen A, He W et al (2018) Nano-delivery of a functional membrane receptor to manipulate cellular phenotype. *Sci Rep* 8:3556. <https://doi.org/10.1038/s41598-018-21863-3>
50. Reiter R, Zaitseva E, Baaken G et al. (2019) Activity of the Gramicidin A Ion Channel in a Lipid Membrane with Switchable Physical Properties. *Langmuir* 35:14959–14966. <https://doi.org/10.1021/acs.langmuir.9b02752>
51. Stockbridge RB, Tsai M-F (2015) Lipid reconstitution and recording of recombinant ion channels. *Methods Enzymol* 556:385–404. <https://doi.org/10.1016/bs.mie.2014.12.028>
52. Knol J, Sjollema K, Poolman B (1998) Detergent-mediated reconstitution of membrane proteins. *Biochemistry* 37:16410–16415. <https://doi.org/10.1021/bi981596u>
53. Woodbury DJ (1999) Nystatin/ergosterol method for reconstituting ion channels into planar lipid bilayers. *Methods Enzymol* 294:319–339. [https://doi.org/10.1016/S0076-6879\(99\)94020-X](https://doi.org/10.1016/S0076-6879(99)94020-X)
54. de Planque M, de Planque M, Mendes G et al (2006) Controlled delivery of membrane proteins to artificial lipid bilayers by nystatin-ergosterol modulated vesicle fusion. *IEE Proc Nanobiotechnol* 153:21–30. <https://doi.org/10.1049/ip-nbt:20050039>
55. Sakmann B, Neher E (2009) Single-channel recording, 2nd edn. Springer, New York, NY. <https://doi.org/10.1007/978-1-4419-1229-9>
56. Ogden D (1994) Microelectrode techniques: the Plymouth workshop handbook, 2nd edn. Company of Biologists Limited, Cambridge, UK
57. Sherman-Gold R (2012) The Axon guide. <https://mdc.custhelp.com/euf/assets/content/AxonGuide3rdedition.pdf>. Accessed 23 July 2019
58. Forstater JH, Briggs K, Robertson JWF et al (2016) MOSAIC: a modular single-molecule analysis interface for decoding multistate nanopore data. *Anal Chem* 88:11900–11907. <https://doi.org/10.1021/acs.analchem.6b03725>
59. MOSAIC. <https://pages.nist.gov/mosaic/>. Accessed 23 July 2019
60. Wyllie DJ, Behe P, Colquhoun D (1998) Single-channel activations and concentration jumps: comparison of recombinant NR1a/NR2A and NR1a/NR2D NMDA receptors [published erratum appears in *J Physiol (Lond)* 1998 Nov 1;512(Pt 3):939]. *J Physiol* 510:1–18
61. Lape R, Colquhoun D, Sivilotti LG (2008) On the nature of partial agonism in the nicotinic receptor superfamily. *Nature* 454:722–727. <https://doi.org/10.1038/nature07139>
62. Colquhoun D, Hawkes AG (2009) The principles of the stochastic interpretation of ion-channel mechanisms. In: Sakmann B, Neher E (eds) *Single channel rec.*, 2nd edn. Springer Science+Business Media LLC, New York, NY, pp 397–482
63. Colquhoun D, Hawkes AG (1994) The interpretation of single channel recordings. In: Ogden DC (ed) *Microelectrode tech. Plymouth work. Handbook.*, 2nd edn. Company of Biologists Limited, Cambridge, UK, pp 141–188



# Chapter 5

## Perforated Whole-Cell Recordings in Automated Patch Clamp Electrophysiology

Kadla R. Rosholm, Kim Boddum, and Anders Lindquist

### Abstract

The automated patch clamp (APC) technology is used for increasing the data throughput of electrophysiological measurements, especially in safety pharmacology and drug discovery. Typically, electrical access to the cells are obtained using standard whole-cell formation by rupturing the membrane, thereby causing a rapid washout of cytosolic components. In contrast the perforated whole-cell configuration provides electrical access to the cell interior while limiting intracellular wash-out. This method allows for recordings of ion channels that are gated by intracellular modulators (e.g., ATP, cyclic nucleotides, or  $\text{Ca}^{2+}$ ), prevents channel current “run down,” and maintains a physiological membrane potential for action potential recordings. Here we present some practical approaches to the use of perforated patch clamp for APC recordings. Our findings from these high-throughput, data-rich measurements (e.g., defining optimized concentrations and practical recommendations for four different perforating agents) can be more broadly applied to perforated patch clamp experiments in general (automated and manual), improving success rates, experimental conditions, and applications.

**Key words** Automated patch clamp, Perforated patch clamp, Perforating agent, Pore-forming agent, Nystatin, Amphotericin B,  $\beta$ -Escin, Gramicidin, Qube 384

---

### 1 Introduction

Automated patch clamp (APC) is used to increase data throughput of electrophysiological experiments within a wide range of areas, such as pain research [1], cardiac safety [2], and compound screening [3], and has the capability of recording in standard whole-cell or perforated patch whole-cell configuration [1] (*see Fig. 1*).

In traditional patch clamp electrical access to the cell is ensured by sealing the cell membrane to the patch hole followed by applying suction, thereby rupturing the membrane. The rapid dialysis of the cytosol with the intracellular (IC) solution allows the experimenter to have complete control of the intracellular composition [4].

In perforated patch clamp, the membrane patch in the patch hole is not ruptured as in standard whole-cell patch clamp

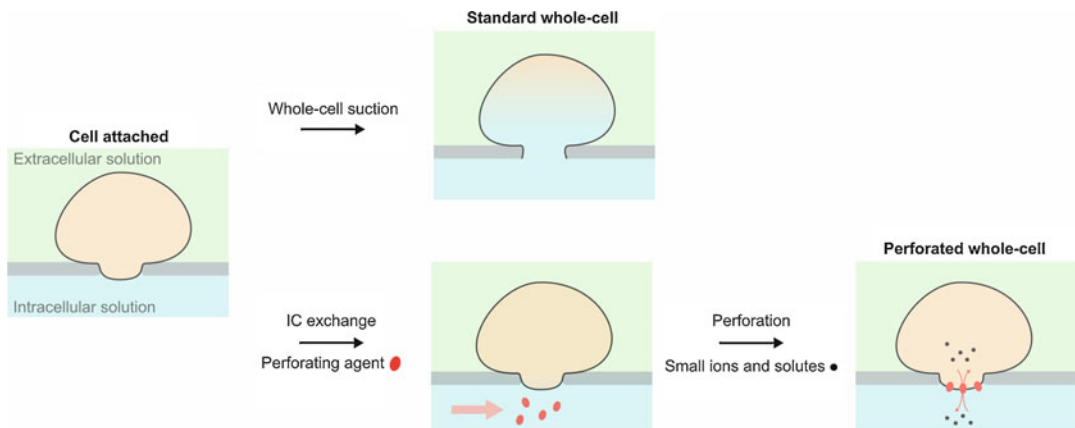


**Fig. 1** Scheme depicting standard whole-cell configuration (top) and perforated whole-cell configuration (bottom) on an automated planar patch clamp setup. The layout of the consumable ensures complete exchange of the intracellular solution, which can be an advantage when running perforated patch experiments

recordings. Instead perforating agents are introduced to the IC solution. The perforating agent inserts into the membrane patch and form pores that provide electrical access to the cell interior, while maintaining endogenous levels of larger ions and signaling molecules (*see* Fig. 1). This method allows for recordings of ion channels that are gated by intracellular modulators (e.g., ATP, cyclic nucleotides or  $\text{Ca}^{2+}$ ) prevents channel current “run down” (loss of current) and is often the preferred configuration for measuring action potentials in cardiomyocytes and neurons [4]. Commonly used perforating (or pore-forming) agents are the antibiotics nystatin and amphotericin B (polyene antibiotics), gramicidin (a linear polypeptide antibiotic), and  $\beta$ -escin (a saponin derivative) [5]. For an overview of their properties *see* Table 1.

A major challenge of perforated patch experiments is that the perforating agent disrupts seal formation. In manual patch clamp this issue is minimized by reducing the seal formation time and the concentration of perforating agent. In APC the perforating agent can be introduced after seal formation by exchanging the IC solution (IC exchange).

Here we provide some practical guidelines for performing perforated patch clamp experiments using an APC instrument, the Qube 384, with or without the use of IC exchange. Qube 384 (Fig. 2, top) is a fully automated screening system that uses the planar patch clamp technique for parallel ion-channel measurements on living cells. It consists of a 384-channel pipetting robot, a worktable for placing compounds and consumables, 384 individual patch clamp amplifiers and an automated cell preparation module. The QChip 384 (Fig. 2, bottom) is the measurement plate on which all experiments are performed. It contains 384 individual measurement sites, each with: individual flow channels for the

**Table 1**

**Properties of perforating agents used in perforated patch clamp experiments and our experimental recommendations**

Perforant	Nystatin	Amphotericin B	Gramicidin	$\beta$ -Escin
Class <sup>a</sup>	Polyene antibiotic	Polyene antibiotic	Linear polypeptide antibiotic	Saponin derivative
Pore radius <sup>a</sup>	(0.4–0.5) nm	(0.4–0.5) nm	$\leq 0.35$ nm	>10 kDa
Selectivity <sup>a</sup>	Weakly cationic	Weakly cationic	Highly cationic	Nonselective
Conductance <sup>a</sup>	5 pS	6 pS	50 pS	?
Stock concentration	30 mM (DMSO)	30 mM (DMSO)	25 mM (DMSO)	10 mM ( $H_2O$ )
Final concentration	(100–200) $\mu M$	(100–200) $\mu M$	(10–25) $\mu M$	(5–50) $\mu M$
Delivery method	IC exchange	IC exchange	Directly in IC	Directly in IC/IC exchange

<sup>a</sup>From Ishibashi et al. [5]



**Fig. 2** Qube 384 (top) and the QChip 384 measurement plate (bottom)

application of cells and external solutions; and individual electrode pairs for voltage/current control and data recording.

This chapter includes a thorough analysis of perforated patch quality and spontaneous whole-cell formation, both critical measures to ensure successful experiments. The high-throughput data collection that is possible on an APC instrument allows the efficient generation of large datasets. These standardized data allow direct comparison of four commonly used perforating agents, removing many of the confounding factors that previous comparisons may have encountered. For instance, the following list of factors would likely cause significant differences in key parameters measured: lab-to-lab variations; culturing conditions and media; cell line differences; handling and storage. Even the specific architecture, shape, diameter, and materials used to fabricate manual patch clamp recording pipettes alters the diffusion rate, and hence apparent activity, of a perforating agent. Consequently, armed with this standardized data we envision the reported recommendations, regarding for example concentration of perforating agent, are of general interest for perforated patch experiments using either manual or automated patch clamp, allowing researchers to select the perforating agent most suitable to their experimental requirements—see the summary in Table 3.

---

## 2 Materials

### 2.1 Cell Culture

#### 2.1.1 Cells

1. CHO hERG DUO (B'SYS B.6.0).
2. T175 cm<sup>2</sup> cell culture flasks.

#### 2.1.2 Solutions and Reagents

1. Phosphate-buffered saline (PBS) without Ca<sup>2+</sup> and Mg<sup>2+</sup>.
2. TRYPSIN solution containing 180 µg ethylenediaminetetraacetic acid (EDTA) per mL.
3. Trypan blue.

#### 2.1.3 Culture Media

1. Dulbecco's Modified Eagle's Medium/Nutrient Mixture F-12 (DMEM/F-12) 500 mL.
2. Fetal bovine serum (FBS) 10%.
3. Geneticin (G418) 100 µg/mL.
4. Hygromycin B 100 µg/mL.
5. L-Glutamine solution 2 mM.

#### 2.1.4 Serum-Free Media (SFM)

1. CHO Cell Culture Media (C5467, Sigma) 25 mL.
2. 4-(2-hydroxyethyl)-1-piperazineethanesulfonic acid (HEPES) solution (1 M) 25 mL.
3. Penicillin/Streptomycin (P/S) 100 U/mL.
4. Soybean trypsin inhibitor (SBTI) 0.04 mg/mL.

## **2.2 Preparation of Perforating Agent Stock Solution**

1. Amphotericin B powder.
2. Nystatin powder.
3.  $\beta$ -Escin powder.
4. Gramicidin powder.
5. Dimethylsulfoxide (DMSO, *see Note 1*).

## **2.3 Solutions**

1. Extracellular (EC) solution, in mM: CaCl<sub>2</sub> 2, MgCl<sub>2</sub> 1, HEPES 10, KCl 4, NaCl 145, pH = 7.4 with KOH, Osmolarity = 305 mOsm with glucose.
2. Intracellular (IC) solution, in mM: KF 120, KCl 20, HEPES 10, EGTA 10, pH = 7.2 with KOH, Osmolarity = 270–280 mOsm.

## **2.4 Electro-physiology**

1. Qube 384 (Sophion).
2. Microtiter plates (MTPs) 1 × 1 (Sophion, SB2260), 1 × 16 (Sophion, SB2261), 384-well plate (Greiner Bio-One, 781280).
3. QChip 384 (1 patch clamp hole per site) (Sophion, SB2110).
4. Cell transfer plate (CTP) (Sophion, SB3301).
5. Magnet for QStirrer (Sophion, SB3070).
6. QStirrer cup (Sophion, SB2050).
7. QFuge tube (Sophion, SB2251).
8. Cell preparation unit (ACP) tip (Sophion, SB2210).
9. Cell preparation unit (ACP) reservoir for EC solution (Sophion, SB2255).
10. Cell waste bottle (Sophion, SB2253).
11. Liquid management system (LMS) supply containers (Sophion, SB3331).
12. Liquid management system (LMS) waste containers (Sophion, SB3332).
13. Pipette tips for 384-robot (Sophion, SB2200).

## **3 Methods**

### **3.1 Cell Culture for APC**

#### **3.1.1 Cell Culture (175 cm<sup>2</sup> Cell Culture Flask)**

CHO hERG DUO cells are cultured in culture media (*see sect. 2*) in a standard incubator at 37 °C with humidified atmosphere (5% CO<sub>2</sub>). We recommend passaging the cells every 2–3 days using trypsin and keeping the confluence at 70–80%.

### *3.1.2 Harvest of Cells for APC (175 cm<sup>2</sup> Cell Culture Flask)*

In APC the cells are randomly captured onto the measurement site and thus a homogeneous cell suspension with a high percentage of viable cells is essential for reaching high success rates. It is therefore important to follow the harvest recommendations as closely as possible.

1. Remove culture media and wash with 7 mL PBS.
2. Add 3 mL Trypsin, gently swirl the flask and aspirate (leave about 1 mL).
3. Place the culture flask in a 37 °C incubator for ~2 min (ensure that the cells have reached a rounded, spherical shape).
4. Gently tap on the side of the flask and add 5 mL SFM and resuspend the cells by working the cell suspension up and down 5–10 times.
5. Determine the cell density and viability by diluting an aliquot 1:2 in Trypan Blue and count the cells in a hemocytometer.
6. Make sure that the final cell density is 2–5 million/mL.

## **3.2 Solutions of Perforating Agent**

### *3.2.1 Nystatin and Amphotericin B*

1. On the day of the experiment a 30 mM stock solution is made by addition of ~180 µL DMSO (*see Note 2*) to 5 mg nystatin or amphotericin B powder.
2. Dissolve by vortexing for 1 min followed by sonication for 2–3 min. Keep in foil during these stages since nystatin and amphotericin B are light sensitive.
3. Dilute in IC solution to desired concentration (100–200 µM) immediately before starting the experiment.

### *3.2.2 β-Escin*

1. On the day of the experiment a 10 mM stock solution is made by addition of 454 µL IC solution to 5 mg β-escin powder.
2. Dissolve by vortexing until the solution is clear.
3. Dilute in IC solution to desired concentration (5–50 µM) immediately before starting the experiment.

### *3.2.3 Gramicidin*

1. On the day of the experiment a 25 mM stock solution is made by addition of 106 µL DMSO (*see Note 2*) to 5 mg gramicidin powder.
2. Dissolve by vortexing until solution is clear.
3. Dilute in IC solution to desired concentration (10–25 µM) immediately before starting the experiment.

### 3.3 Perforated Patch Whole-Cell Recordings Using Qube 384

#### 3.3.1 Experimental Setup

ViewPoint is the software used to setup and execute experiments on Qube 384, which let you specify and choose the following five protocols: Worktable, Cell preparation, Whole-cell, Experiment, and Cleanup. All protocols are built by inserting one or more blocks based on predefined block templates. When a block is selected, some of them will have a parameter field box where changes to the block can be made.

1. *Worktable.* Choose the block template: “4 × Qchip 1 × Compound 1 1 × Compound 2.” Make sure that the reservoir types are defined as described in Table 2.
2. *Cell preparation.* Choose the block template: “Cell Preparation: Standard.” Set the following parameters:  
*Centrifuge G-force:* 150 ×  $g$   
*No. of cell washes:* 2  
*Centrifuge time:* 120 s
3. *Whole-cell protocol.* Choose the block template: “Whole-cell block: Standard” and change the whole-cell pressure to constant negative pressure (see Fig. 3a):  
*Start time:* 0 ms  
*Duration:* 16,000 ms  
*Start/End:* -10 mbar (see Note 3)

Set the following parameter:  
*Pressure during positioning:* -40 mbar

For the purpose of demonstration, we here used a specialized whole-cell protocol in which standard whole-cell suction (Fig. 3b) was applied in the first six columns of the QChip.

*Column 1–6:* Standard whole-cell suction (Fig. 3b).

*Column 7–24:* No whole-cell suction (Fig. 3a).

**Table 2**  
**Reservoir types chosen for perforated patch experiments with or without IC exchange**

Position	Type	
	IC exchange	Addition in IC
Compound 1	384 plate	1 × 1 reservoir
Compound 2	1 × 1 reservoir	1 × 1 reservoir
Extracellular saline	1 × 1 reservoir	1 × 1 reservoir
Intracellular saline	16 rows × 1 column reservoir	384 plate

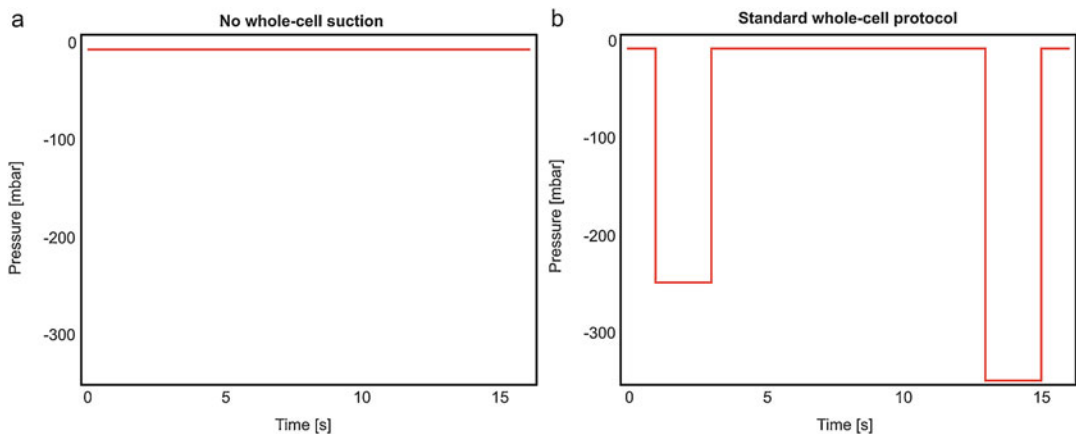


**Fig. 3** Applied whole-cell protocols. (a) No whole-cell suction ( $P = -10$  mbar) applied in column 7–24. (b) Standard whole-cell suction protocol applied in column 1–6

Running multiple whole-cell protocols within the same QChip is not possible for the general APC user (see Note 4).

4. *Experiment protocol.* For the experiments using IC exchange choose the following two block templates:

Block 1: “*Voltage gated: One liquid, recording after addition.*” In this block the voltage protocol is defined. The cells are voltage clamped at  $-80$  mV and hERG currents are elicited by 15 pulses comprised of a 5 s depolarization to  $+20$  mV followed by a 5 s tail step to  $-50$  mV (Fig. 4, red).

Block 2: “*Exchange intracellular saline.*”

First, the hERG current is recorded to evaluate the electrical access to the interior of the cell (block 1). Subsequently, the intracellular solution is exchanged (block 2), followed by three additional recordings of hERG current to evaluate the electrical access to the cell interior as the perforating agent inserts into the membrane. Note, that a 5 min incubation break was inserted between the first and second run of block 1 after the IC exchange.

For the experiments without IC exchange use repeated runs of block 1 to evaluate the electrical access to the interior of the cell over time.

5. *Cleanup.* Choose the block template “*Standard.*”

### 3.3.2 Preparing Qube 384 for Experiments

Detailed information on how to operate Qube 384 can be found in the user manual [6]. Here we list in short how to prepare the Qube 384 for perforated patch experiments:

1. Wake Qube 384 from standby.
2. Make sure all LMS supply containers are full and all LMS waste containers as well as the cell waste bottle are empty.

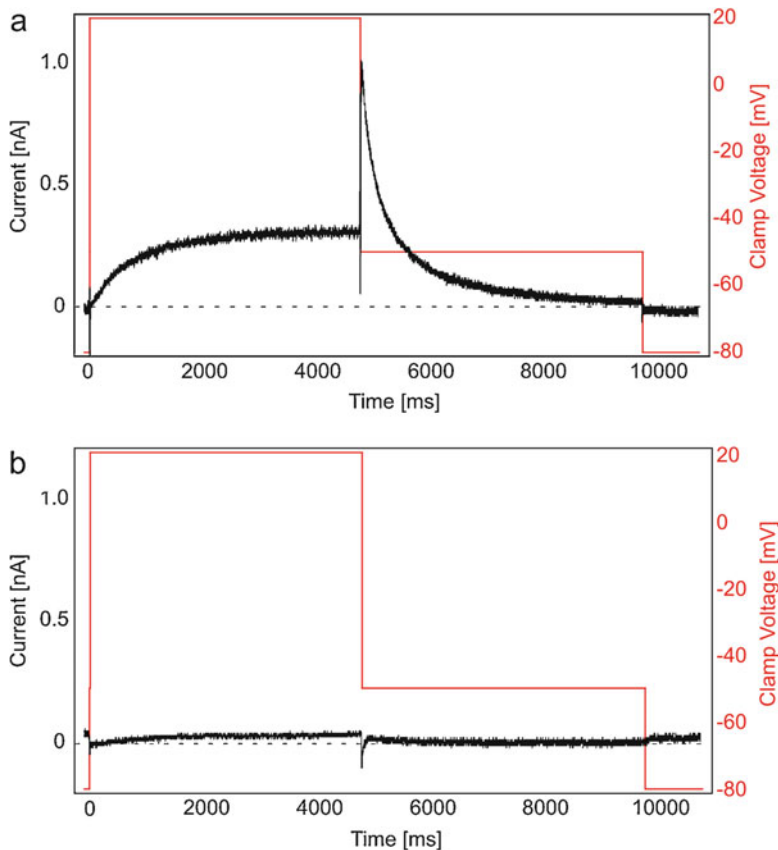


**Fig. 4** Representative recordings of hERG current (black) recorded on cells in standard whole-cell (**a**) and cell-attached (**b**) configuration in response to a voltage protocol (red) comprising a 5 s depolarization to +20 mV followed by a 5 s step −50 mV

3. Place consumables. The workplane positions are displayed in Fig. 5. Load 384-robot pipette tips in the assigned positions, place a QFuge tube in the centrifuge and load the ACP pipette. Place the CTP and the EC solution reservoir for the ACP at the cell preparation unit. Place reservoirs of the types defined in Table 1 at the assigned positions and place a QChip 384 in the first QChip position.
4. Add solutions (*see Note 5*). Place the harvested cells in the QStirrer with a magnet. For experiments using IC exchange, add EC solution to  $1 \times 1$  reservoirs in compound 2 and extracellular saline positions. Add IC solution to the top row of the  $16 \times 1$  intracellular saline reservoir. In the top row of the 384-well plate the perforating agent is added at increasing concentrations as illustrated in Fig. 6.

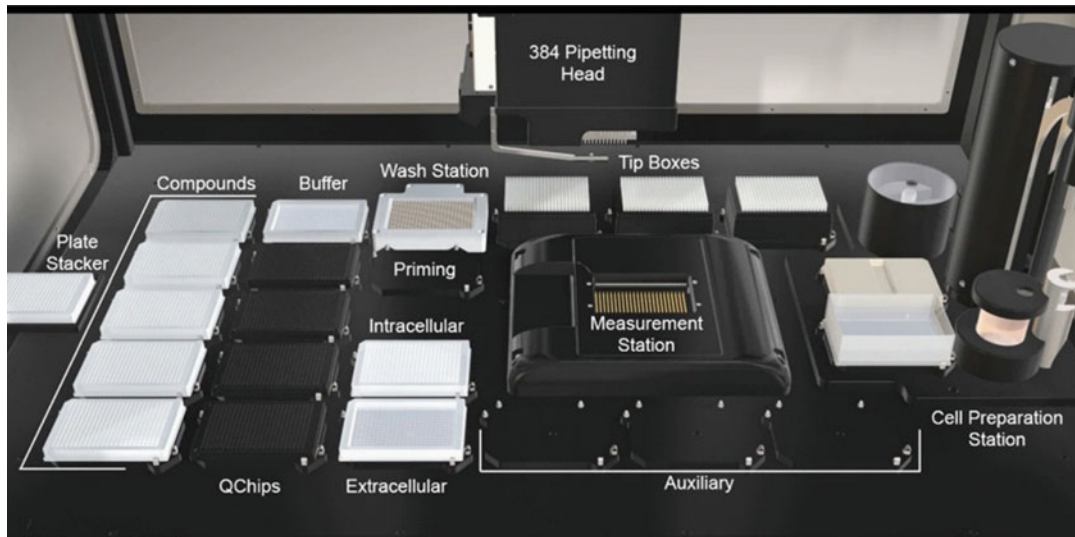


**Fig. 5** Workplane layout. Compound plates are placed in the left row, QChip 384 measurement plates are placed in the second row from the left and the intracellular and extracellular solutions are placed in the third row from the left. The 384 robot pipette tips are placed in tip boxes behind the measurement station. The cell preparation station is situated on the right side of the workplane. For more details see the Qube 384 user manual [6]

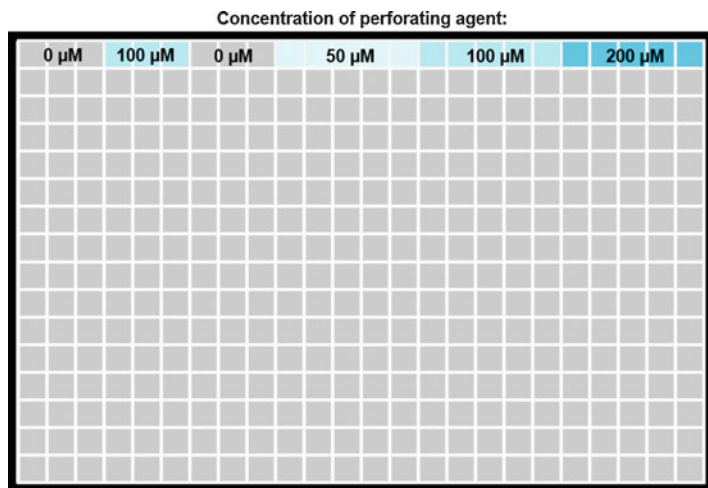


**Fig. 6** Compound plate layout for evaluating the concentration of perforating agent. The perforating agent was prepared just before commencing the experiment and added to the 24 top row wells of a 384-well plate. The displayed example is for nystatin or amphotericin B: 0 µM (column 1–3 and 7–9), 50 µM (column 10–14), 100 µM (column 4–6 and 15–19), and 200 µM (column 20–24)

For experiments without IC exchange the perforating agent is added in the 384 plate in the intracellular solution reservoir.

### 3.4 Data Analysis:

#### Perforated Patch Whole-Cell Recordings Using IC Exchange

##### 3.4.1 Evaluation of Cell-Attached Configuration

When performing perforated patch experiments, it is important to make sure that the majority of the cells are in the cell-attached mode following the whole-cell protocol and have not spontaneously ruptured into the standard whole-cell configuration (see Note 6). In order to evaluate the electrical access to the cell interior analyze the electrical capacitance of the cell membrane ( $C_{\text{slow}}$ ) and the hERG current ( $I_{\text{hERG}}$ ) in the first run of the experiment protocol.

The electrical capacitance of a cell membrane results from the lipid bilayers ability to store charges and is directly proportional to the membrane surface area ( $\sim 1 \mu\text{F}/\text{cm}^2$ ) [7]. A measure of the entire cell membrane can only be obtained when there is proper electrical contact to the intracellular environment and consequently  $C_{\text{slow}}$  is much larger for a cell in whole-cell configuration than for a cell in cell-attached configuration. The histograms of  $C_{\text{slow}}$  values recorded for cells in cell-attached (blue) or in whole-cell (red) configuration (Fig. 7) illustrate that the two populations are clearly separated and that  $C_{\text{slow}}$  can be used as an indicator for whether the cells are in cell-attached ( $C_{\text{slow}} < 9 \text{ pF}$ ) or whole-cell mode ( $C_{\text{slow}} > 9 \text{ pF}$ ).

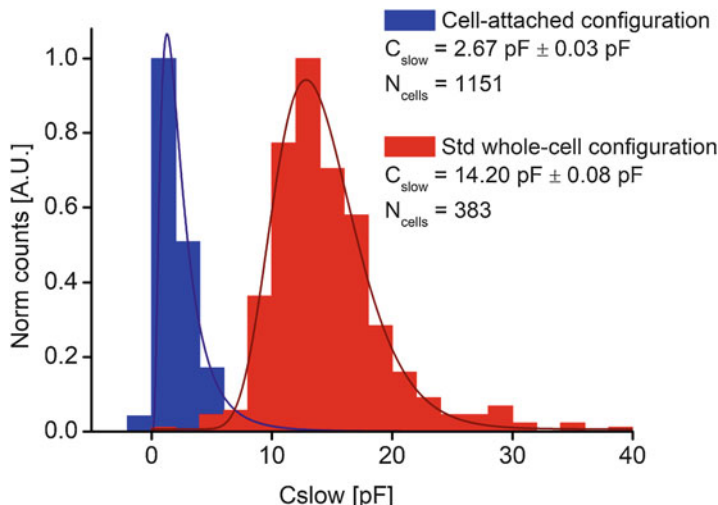


**Fig. 7** Histograms of cell capacitance ( $C_{\text{slow}}$ ) values recorded for cells in standard whole-cell configuration (red) and cell-attached configuration (blue). Fitting of a lognormal function to the histograms (lines) allows quantification of the mean  $C_{\text{slow}}$  of the populations

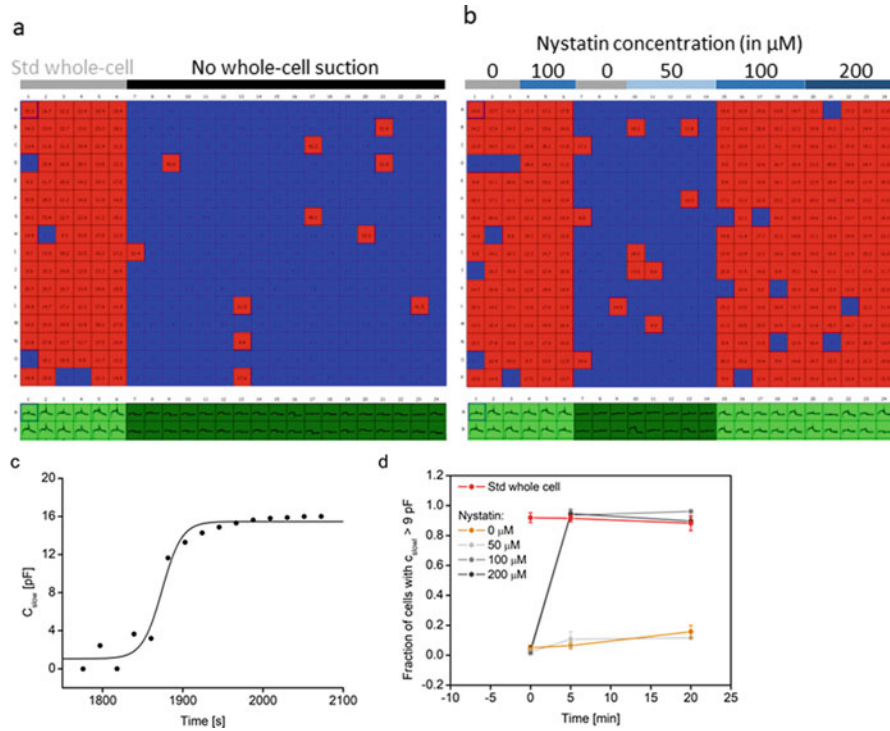


**Fig. 8** QChip plate view displaying cell capacitance ( $C_{slow}$ ) measurements before (a) and after (b) addition of nystatin, 0  $\mu\text{M}$  (column 1–3 and 7–9), 50  $\mu\text{M}$  (column 10–14), 100  $\mu\text{M}$  (column 4–6 and 15–19), and 200  $\mu\text{M}$  (column 20–24), by exchange of the intracellular solution. Sites with  $C_{slow} > 9 \text{ pF}$  are color coded red and sites with  $C_{slow} < 9 \text{ pF}$  are color coded blue. Below the plate view the corresponding hERG current measurements from the top two rows are displayed (green). (c) The development of single cell capacitance over time upon the addition of 100  $\mu\text{M}$  nystatin using IC exchange. (d) Fraction of cells in standard or perforated whole-cell configuration ( $C_{slow} > 9 \text{ pF}$ ) quantified before, 5 min after and 20 min after exchange of the intracellular solution. The colors represent the addition of 0  $\mu\text{M}$  (orange), 50  $\mu\text{M}$  (light grey), 100  $\mu\text{M}$  (grey), or 200  $\mu\text{M}$  (black) nystatin to cells in cell-attached mode as well as cells in standard whole-cell mode (red) for comparison. Values are average  $\pm$  SEM between three experiments and the number of cells investigated per concentration were 80–240

A QChip site view of single cell  $C_{slow}$  values is displayed in Fig. 8a, together with the corresponding hERG currents measured in the two top rows. The majority of the cells exposed to standard whole-cell suction (column 1–6) are in whole-cell mode ( $C_{slow} > 9 \text{ pF}$ , red) whereas the majority of the cells that were exposed to constant pressure ( $P = -10 \text{ mbar}$ , column 7–24) are in cell-attached mode ( $C_{slow} < 9 \text{ pF}$ , blue).

The configuration of the cells is reflected in the corresponding hERG currents displayed below the QChip site view. Cells in standard whole-cell configuration are expected to display standard

hERG currents (Fig. 4a), whereas the poor electrical access to the cell interior in cell-attached mode result in very small currents (Fig. 4b).

### 3.4.2 Evaluation of Perforated Whole-Cell Configuration Using Nystatin

Next, evaluate the perforated whole-cell configuration in the three runs of the voltage protocol following IC exchange. The IC exchange takes approximately 5 min, during which the intracellular solution is exchanged with solutions of increasing concentration of the perforating agent (Fig. 6). The configuration of the cells will be reflected in the measured cell capacitance and hERG current.

Figure 8b shows a QChip site view of  $C_{\text{slow}}$  values (top) and hERG current (bottom) recorded 5 min after nystatin addition using IC exchange. Upon the addition of nystatin most of the cells exposed to 100 and 200  $\mu\text{M}$  nystatin (column 15–19 and 20–24, respectively) enter perforated whole-cell configuration ( $C_{\text{slow}} > 9 \text{ pF}$ , red) and display large hERG currents.

The rate of nystatin insertion varies from cell to cell.  $C_{\text{slow}}$  versus time is plotted in Fig. 8c for a single cell in cell-attached mode upon the addition of 100  $\mu\text{M}$  nystatin in the intracellular solution. The figure shows how  $C_{\text{slow}}$  increases from  $\sim 2 \text{ pF}$  in cell-attached mode to  $\sim 15 \text{ pF}$  in perforated whole-cell mode.

Plotting the fraction of cells in standard or perforated whole-cell configuration ( $C_{\text{slow}} > 9 \text{ pF}$ ) before, 5 min after and 20 min after addition of perforating agent (Fig. 8d), illustrates that nystatin at 100  $\mu\text{M}$  and above promotes perforated whole-cell formation in cell-attached cells. No effect can be observed upon the addition of 50  $\mu\text{M}$  nystatin as compared to the baseline (orange and grey data points in Fig. 8d). The same procedure can be used for evaluation of amphotericin B and  $\beta$ -escin (data not shown).

### 3.4.3 Data Quality Assessment

To examine the data quality, extract the following experiment parameters: the average membrane resistance ( $R_{\text{mem}}$ ), series resistance ( $R_{\text{series}}$ ), hERG peak current ( $I_{\text{max}}$ ) and cell membrane capacitance ( $C_{\text{slow}}$ ) in the last run of the voltage protocol. The parameters are summarized in Table 3 for nystatin, amphotericin B, and  $\beta$ -escin (see Note 7). To ensure high-quality data, the experiments are filtered using the following criteria:

$$R_{\text{mem}} > 100 \text{ M}\Omega \text{ per cell}$$

$$9 \text{ pF} < C_{\text{slow}} < 50 \text{ pF}$$

$$I_{\text{peak}} > 100 \text{ pA}$$

## 3.5 Data Analysis: Perforated Patch Whole-Cell Recordings Without IC Exchange

The perforating agent gramicidin is relatively slow acting (30 min) [4] and consequently not feasible for experiments with IC exchange, in which the agent is introduced relatively late in the experiment. Instead gramicidin should be added in the IC solution from the beginning of the experiment.

**Table 3**

**List of parameters determined for cells in perforated and standard whole-cell configuration, respectively**

	$R_{\text{mem}}$ (MΩ)	$R_{\text{series}}$ (MΩ)	$I_{\text{max}}$ (pA)	$C_{\text{slow}}$ (pF)	$N_{\text{cell}}$	Success rate (%)	Delivery method
Nystatin (200 μM) <sup>a</sup>	954 ± 61	13.3 ± 0.5	350 ± 21	16.0 ± 0.7	75	78	
Amphotericin B (200 μM) <sup>a</sup>	1194 ± 97	25 ± 1	274 ± 11	15.1 ± 0.5	135	53	IC exchange
β-Escin (10 μM) <sup>a</sup>	1152 ± 86	17 ± 1	500 ± 28	16 ± 1	54	68	
<b>Standard whole-cell<sup>a</sup></b>	<b>1303 ± 48</b>	<b>11.4 ± 0.7</b>	<b>491 ± 20</b>	<b>15.1 ± 0.3</b>	<b>151</b>	<b>86</b>	
Gramicidin (25 μM) <sup>b</sup>	201 ± 7	26 ± 1	336 ± 14	14.4 ± 0.4	139	48	Directly in IC
<b>Standard whole-cell<sup>b</sup></b>	<b>749 ± 50</b>	<b>9.3 ± 0.4</b>	<b>517 ± 24</b>	<b>14.0 ± 0.4</b>	<b>74</b>	<b>77</b>	

Values are average ± sem of  $N_{\text{cell}}$

<sup>a</sup>Quantified 10 min after the addition of perforating agent using IC exchange

<sup>b</sup>Quantified in the first voltage protocol of the experiment

Except from abstaining the IC exchange, experiment protocols, data analysis and data quality assessment are similar to the previously described methods. Gramicidin provides electrical access to the cell interior, however, as might be expected it disturbs seal formation, resulting in reduced seal resistances. The average  $C_{\text{slow}}$ ,  $R_{\text{mem}}$  and  $R_{\text{series}}$  values are listed in Table 3.

#### 4 Notes

1. DMSO in IC solution during seal formation should be kept as low as possible. Having DMSO (0.1%) in the IC solution during seal formation causes an increase in the number of cell-attached cells spontaneously entering whole-cell mode. Therefore, it is recommended to keep the DMSO concentration in the IC solution as low as possible, for experiments in which the perforating agent (e.g., gramicidin) is added in the IC solution from the beginning of the experiment.
2. DMSO stability. DMSO is hygroscopic and adsorbs moisture from the surrounding environment over time which might cause decreased compound solubility and contamination. To avoid this, either freeze it in aliquots upon opening or make sure to replace the solution often.
3. Influence of holding pressure. In case of problems with spontaneous whole-cell formation this can in some cases be remedied by lowering the holding pressure from standard (-10 mbar) to -3 mbar (see Fig. 9).

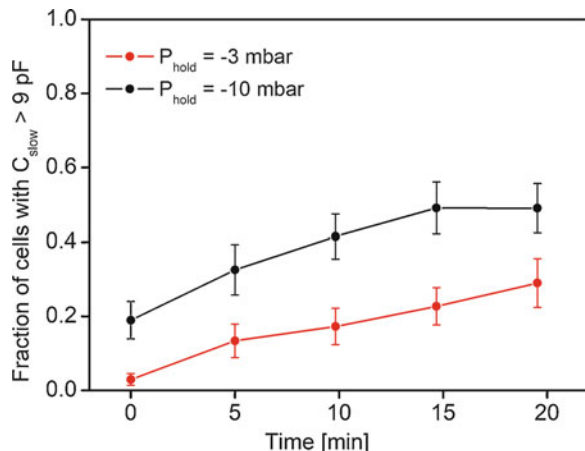


**Fig. 9** The holding pressure affects cell propensity to spontaneous whole-cell formation. The fraction of cells (native HEK293 cells) in cell-attached configuration ( $C_{slow} < 9 \text{ pF}$ ) that spontaneously rupture into the standard whole-cell configuration ( $C_{slow} > 9 \text{ pF}$ ) was plotted versus time after IC exchange. The experiments were run without whole-cell suction using a constant holding pressure  $P_{hold} = -10 \text{ mbar}$  (black, standard) or  $P_{hold} = -3 \text{ mbar}$  (red). Values are average  $\pm$  sem of three experiments and the number of cells investigated were 144 per condition

4. Using standard whole-cell protocols. In general, it is not possible to use different whole-cell protocols within the same experiment and a comparison of different whole-cell protocols should be performed in subsequent experiments.
5. Optimizing automated perforated patch assay to a specific target. Since every cell line is unique, we strongly recommend testing a range of concentrations of perforating agent across the QChip 384 measurement plate, to identify the one best suitable for the specific target in question. Remember to include the relevant control columns with the appropriate amount of solvent (e.g., DMSO) to be sure the cells in cell-attached configuration are not affected by the solvent.
6. Spontaneous rupture into the standard whole-cell configuration. When performing perforated patch experiments, a small proportion (<10%) of the cells spontaneously rupture into standard whole-cell configuration. However, some transfected cell lines are fragile (depending on cell type and ion channel) and more prone to spontaneous whole-cell formation. As part of perforated patch assay optimization, this should be evaluated by including control columns without perforating agent, in which the majority of the cells should maintain in cell-attached mode during the time span of the experiment.

7. Influence of perforating agents on data quality. In general,  $R_{\text{mem}}$  and  $I_{\text{max}}$  are slightly lower for cells in perforated as compared to standard whole-cell, likely due to the perforating agents interfering with the seal (see Table 3). As expected,  $R_{\text{series}}$  is elevated for cells in perforated whole-cell, due to the increased amount of membrane in the patch hole. Note that large-amplitude fast-gating ion channels such as voltage-gated sodium channels are more susceptible to the voltage errors associated with large  $R_{\text{series}}$  values and therefore more suitable for conventional whole-cell [4].

## References

1. Bell DC, Dallas ML (2018) Using automated patch clamp electrophysiology platforms in pain-related ion channel research: insights from industry and academia. *Br J Pharmacol* 175:2312–2321
2. Sube R, Ertel EA (2017) Cardiomyocytes derived from human induced pluripotent stem cells: an in-vitro model to predict cardiac effects of drugs. *J Biomed Eng* 10:527–549
3. Chambers C, Witton I, Adams C et al (2016) High-throughput screening of Nav1.7 modulators using a giga-seal automated patch clamp instrument. *Assay Drug Dev Technnol* 14:93–108
4. Linley JE (2013) Perforated whole-cell patch-clamp recording. In: Gamper N (ed) Ion channels, Methods in molecular biology (methods and protocols), vol 998. Humana, Totowa, NJ, pp 149–157
5. Ishibashi H, Moorhouse AJ, Nabekura J (2012) Perforated whole-cell patch-clamp technique: a user's guide. In: Okada Y (ed) Patch clamp techniques, Springer protocols handbooks. Springer, Tokyo, pp 71–83
6. Sophion Bioscience A/S (2019), Qube user manual, Revision 2.4.2. <http://sophion.com/>
7. Golowasch J, Nadim F (2014) Capacitance, membrane. In: Jaeger D, Jung R (eds) Encyclopedia of computational neuroscience. Springer, New York, NY



# Chapter 6

## Multielectrode Arrays

Russell Burley and Jenna R. M. Harvey

### Abstract

Multielectrode arrays (MEAs) are grids of substrate-integrated microelectrodes that allow for electrophysiological interrogation of dissociated cell cultures or tissue slices. Here we discuss the use of nonimplantable electrodes for studies. The methods described attempt to provide a starting point for researchers new to the field who wish to begin to utilize this powerful, but daunting technology and quickly apply the basic principles to their own research interests.

**Key words** Multielectrode array, Microelectrode, Cell culture, Organotypic slice, Acute tissue slice, Neuronal network, Electrophysiology

---

### 1 Introduction

The 1970s and 1980s saw the development and first use of planar arrays of microelectrodes to measure the spontaneous electrophysiological activity from dissociated neurons (reviewed in [1]). Since this pioneering period of research, the affordability of computing power, the commercial supply of MEA chips and chambers, and software development have facilitated the greater accessibility of MEA techniques to a wider section of the research community. Complementary to conventional single electrode methods like the patch clamp, use of MEAs allows for the noninvasive study of continuously growing cell cultures and ex vivo tissue slices, permitting simultaneous recording and stimulation at multiple sites across the preparation. Parallel, multisite extracellular recordings allow for a population view of intact circuits and neuronal networks. Such recordings give an insight into the spatiotemporal aspects of the functional network that reflects the highly orchestrated neuronal activity that contributes to neural processing.

With cultures of dissociated neurons, the structure of the brain is lost as the damaged or axotomized cells mature and form new connections at random. While this is a disadvantage, such a simplified model system has other benefits. If attention to the

maintenance of optimal growing conditions is given, the advantage of such networks growing on MEAs is that they may be maintained for long periods of time and may be recorded from many times, or even continuously. This opens up a whole world of experimental avenues that can be used to study development, synaptic organization and integration, and the properties of the emergent spontaneous active network. Furthermore, because the culture is extremely accessible to pharmacological manipulation in a way that the whole brain is not, the response to a chemical or pharmacological challenge can be easily analyzed at a global level where the changes in the spatiotemporal pattern of action potentials give a surprisingly close correlation to responses *in vivo* that are a reflection of behavioral phenomena.

To preserve the local architecture of the circuitry, acute tissue slices may be prepared from whole brain and kept viable for a number of hours during which time, short duration recordings may be carried out in a tissue chamber [2]. This achieves a situation very close to the *in vivo* setting useful for short-term, but immediate study. Good experimental access is allowed, and slices can be prepared from transgenic animals or those modelling a disease state. The advantages here that MEA recording has in comparison to conventional single electrode recording techniques are that once the preparation is established there is no need to position recording and stimulating electrodes in order to access all areas of the slice, and more importantly, in the same experiment, behavior of the tissue can be sampled simultaneously across many regions allowing responses to be observed and correlated very easily.

For extended periods of recording from slices in which much of the network connections remain intact, brain slices have also been cultured organotypically (reviewed in [3]). Such long-term use has value in providing a three-dimensional environment for neuronal recordings but requires time during which the slices are allowed to mature and stabilize. Cocultures of different brain regions have been achieved where neurite extension occurs and axonal processes contact neighboring tissue samples as the cells mature [4, 5]. This allows for the recapitulation of circuit connections between separate structures and the study of their synaptic associations. Chronic, or long-term effects of drugs, models of disease or transgenic manipulation in a more realistic living brain circuit that better represents the *in vivo* behavioral setting is where MEA organotypic slice cultures find a niche utility.

The variety of experimental paradigms that can be supported using MEA electrophysiology are broad and varied, with the advantages over single-microelectrode techniques that MEAs provide, an integrated view of circuit function is simply attainable. The state of the art is seeing continuous improvement in array design and peripheral hardware allowing more recording sites and more detailed analytical tools accessible in a more user-friendly and fully integrated package.

The application of MEA electrophysiology to create experimental platforms for drug discovery through the development of protocols and analytical software amenable to higher-throughput testing of compounds is a goal that is also being delivered [6, 7]. Increased automation and turnkey applications for parallel recording are providing the opportunity for stable and reproducible long-term study of pharmacological and toxicological agents aligned to the requirements of the pharmaceutical industry.

The future will no doubt see further innovation and accelerated take-up of MEA recording as a standard laboratory technique in both academic and industrial settings. This will have a significant, and highly valuable impact on the quality of studies modelling circuit function and will succeed in further bridging the gap between *in vitro* and *in vivo* study.

---

## 2 Materials

Water of the highest purity available should be used for all solutions. Ultrapure water with a resistivity of  $18 \text{ M}\Omega \text{ cm}^{-1}$  at  $+25^\circ\text{C}$  is a basic requirement throughout.

### **2.1 Dissociated Cell Culture**

1. Animals: timed-mated dam with E18 embryos.
2. Fetal bovine serum (FBS).
3. 0.005% polyethylenimine (PEI) in borate buffer: dissolve 4.77 g  $\text{Na}_2\text{B}_4\text{O}_7 \cdot 10\text{H}_2\text{O}$  in 450 mL of sterile distilled water. Adjust the pH to 8.4 using HCl. Top up with distilled water to make a final volume equal to 500 mL. Dilute PEI in sterile distilled water to produce a stock solution of 1% PEI in water. Using the 1% stock of PEI dilute to produce a 0.005% working solution of PEI in borate buffer.
4. 50  $\mu\text{g}/\text{mL}$  poly-D-lysine  $>300 \text{ kDa}$ : dilute 5 mg poly-D-lysine hydrobromide in 100 mL distilled water, pass the solution through a 0.22  $\mu\text{m}$  filter unit to sterilize.
5. 5  $\mu\text{g}/\text{mL}$  laminin: dilute 1 mg laminin in 200 mL plating medium and pass through a 0.22  $\mu\text{m}$  filter unit to sterilize.
6. 1% Terg-A-Zyme: prepare a 1% w/v solution of Terg-A-Zyme in distilled water.
7. Dissection tools: large straight scissors, scalpel and No. 11 blade, iridectomy or spring scissors, fine curved forceps, fine straight forceps, small spatula. Sterilize by autoclaving or soaking in 70% ethanol before use.
8. Dissection microscope.
9. Hank's balanced salt solution (HBSS) without calcium and magnesium.

10. Dissection medium: 500 mL HBSS without calcium and magnesium, 5 mL Penicillin-Streptomycin (final 100 units/mL and 100 µg/mL), 5 mL 1 M HEPES (final 10 mM), 5 mL 100 mM sodium pyruvate (final 1 mM), 2.3 mL of 7.5% sodium bicarbonate (final 0.035%).
11. Papain Dissociation System (Worthington).
12. 70 µm sterile mesh filter.
13. Plating medium: 10 mLs B-27® Electrophysiology supplement added to 500 mLs Neurobasal® Medium. Can be stored at +4 °C for up to 2 months.
14. MCS arrays in a standard 8 × 8 layout of 30 µm Ti electrodes with 200 µm spacing and an internal reference electrode with a 0.5 cm culture ring height (60MEA200/30iR-Ti) or MED64 probes in a standard 8 × 8 layout of 50 × 50 µm platinum black electrodes and 150 µm spacing and indium tin oxide transparent conducting tracks, incorporating 4 × 200 µm reference electrodes and a 1 cm ring (MED-P515A).
15. Zero evaporation Teflon™ lids with a semipermeable membrane (ALA Scientific Instruments Inc.).

## **2.2 Acute Tissue Slice**

1. Animals: juvenile rats 3–4 weeks of age.
2. 4% agar: dissolve 4 g agar in 100 mL of hot water, heating the solution in a glass beaker and stirring continuously. When completely dissolved pour into 10 cm petri dishes to a depth of about 1 cm and cool to allow setting. The dish of agar can be kept for repeated use if stored at +4 °C and sealed in a plastic bag to prevent dehydration.
3. Dissection tools: large straight scissors, small straight scissors, small tweezers with serrations, smooth edged, broad metal spatula, straight forceps.
4. Cutting solution: 110 mM sucrose, 60 mM NaCl, 28 mM NaHCO<sub>3</sub>, 1.25 mM NaH<sub>2</sub>PO<sub>4</sub>, 3 mM KCl, 7 mM MgSO<sub>4</sub>·7H<sub>2</sub>O, 0.5 mM CaCl<sub>2</sub>, 5 mM glucose, 0.6 mM sodium ascorbate, 0.015 mM phenol red, pH 7.2–7.3 when bubbled with 95:5% O<sub>2</sub>–CO<sub>2</sub>.
5. Artificial cerebrospinal fluid (aCSF) in: 124 mM NaCl, 25 mM NaHCO<sub>3</sub>, 1 mM NaH<sub>2</sub>PO<sub>4</sub>, 4.4 mM KCl, 1.2 mM MgSO<sub>4</sub>·7H<sub>2</sub>O, 2 mM CaCl<sub>2</sub>, 10 mM glucose, 0.015 mM phenol red, pH 7.3–7.4 when bubbled with 95:5% O<sub>2</sub>–CO<sub>2</sub>.
6. Transfer pipette (*see Note 1*).
7. Vibratome: we routinely use both the Leica Biosystems VT1000P and VT1200S with Julabo FL300 recirculating cooler. Steel, double-edged razor blades snapped in half.
8. Slice storage chamber (*see Note 2*).

9. MCS arrays in a standard  $8 \times 8$  layout of  $30 \mu\text{m}$  Ti electrodes with  $200 \mu\text{m}$  spacing, an internal reference electrode and a  $0.5 \text{ cm}$  glass ring (60MEA200/30iR-Ti).
10. Harp slice grids for MEA electrophysiology:  $9.5 \text{ mm}$  internal diameter,  $0.5 \text{ mm}$  thick,  $0.2 \text{ g}$  in weight,  $1 \text{ mm}^2$  spaced nylon mesh (ALA Scientific Instruments).
11. For perfusion tubing use 3350 Tygon®  $3/32''$  outer diameter,  $1/32''$  inner diameter, and for peristaltic tubing in the outflow F117943 blue-blue,  $1.65 \text{ mm}$  internal diameter and for return, inflow tubing F117949 black-white,  $3.18 \text{ mm}$  internal diameter.

### **2.3 Organotypic Slice Culture**

1. Animals: mouse pups at postnatal day 4–5.
2. Sterilized dissection tools: Small and large scissors, and fine and coarse straight forceps. Sterility can be achieved by autoclaving or soaking in  $70\%$  ethanol.
3. Petri dishes:  $35 \text{ mm}$  and  $60 \text{ mm}$ , sterile.
4. Glass transfer pipette with tapered end cut off and smoothed with heat from a flame (*see Note 1*).
5. Sterile No. 11 scalpel and blade.
6. 2 fine gauge needles.
7. Circular filter paper of  $55 \text{ mm}$  diameter to fit in  $60 \text{ mm}$  dish.
8. Single-edged steel razor blade for blocking brain tissue.
9. Cutting solution (Subheading 2.2, item 4). Solution can be filter-sterilized if not prepared from sterile components.
10. Vibratome: Leica Biosystems VT1200S with Julabo FL300 recirculating cooler to keep the cutting solution at around  $+4^\circ\text{C}$ . Steel, double edged razor blades.
11. Culture medium:  $75\%$  MEM,  $25\%$  horse serum,  $2 \text{ mM}$  glutamine,  $100 \text{ U/mL}$  penicillin– $100 \mu\text{g/mL}$  streptomycin,  $25 \text{ mM}$  HEPES and  $5 \text{ mg/mL}$  glucose. Cytosine  $\beta$ -D-arabinofuranoside ( $20 \mu\text{M}$ ) can be added to inhibit glial proliferation if necessary.
12.  $0.1\%$  PEI in water.
13. Semipermeable membranes: we culture slices for use on MEAs as interface explants on PTFE cell culture inserts;  $0.4 \mu\text{m}$  pore size,  $30 \text{ mm}$  diameter.
14. Dissection microscope for placing slices onto arrays.
15. MED64 probes in a standard  $8 \times 8$  layout of  $50 \times 50 \mu\text{m}$  platinum black electrodes and  $150 \mu\text{m}$  spacing, indium tin oxide transparent conducting tracks,  $4 \times 200 \mu\text{m}$  reference electrodes, and a  $1 \text{ cm}$  ring (MED-P515A).

---

### 3 Methods

#### 3.1 Basics of MEA Use and Preparation

##### 3.1.1 Choice of Arrays for Culture and Acute Slices

MED64 probes for a basic 64 channel or Plex system and MCS MEAs with 60 electrodes are available in array sizes with different sized electrodes and electrode spacing, and also fabricated from different materials to produce opaque or transparent contact pads and tracks. Choice of configuration will be dependent on use. An internal reference electrode will be necessary for use with tissue culture applications, but is not essential for acute slice preparations if a ground wire is being used as a reference. 100 µm electrode spacing may be used for mouse hippocampal slices, whereas rat tissue will be better sampled from an array with 150–200 µm spacing. Hippocampal pattern arrays, multisampling probes and hexagonal arrays may be more suited to the specific needs of the study where the investigator may want to sample from separate subregions of the tissue, where the shape of the cell fields may be more linear or nucleated, or when tissue cultures may be established in multichamber probes where the electrodes are spread between isolated sections of the chamber. Glass or plastic rings forming the perimeter of the chamber are also produced in a range of heights and this will need to be considered when sealing the chamber with lids or better access is required to the chamber if perfusing.

##### 3.1.2 Preparation of Arrays

Newly purchased MEAs have a surface that is hydrophobic, preventing the successful adherence of cells. It is advisable to treat new arrays to render them hydrophilic to allow for better attachment to the growing surface. This property can be easily assessed by placing a drop of water onto the surface and ensuring that it spreads to wet the chamber. A number of treatments are suggested for improving the surface properties prior to use. If access to a plasma chamber is available, exposing the chambers to a gaseous plasma will render the surface hydrophilic (*see Note 3*). Alternatively, precoating with a protein solution (FBS) for a short time will also be effective. Some users prefer to preculture cells on new arrays allowing the growing cells to modify the surface and creating a more hydrophilic environment. This culture is usually grown for a brief period and then discarded.

##### 3.1.3 Sterilization

For use with acute tissue slices it is not necessary to sterilize arrays. For tissue culture, methods need to be considered so that damage to the MEA chamber and the electrodes does not occur. For electrodes made of TiN and gold these may be washed with 70% alcohol, exposed to UV radiation, autoclaved or oven-sterilized in dry heat at no greater than +125 °C. Electrodes made of platinum black and carbon nanotubes should not be autoclaved, sterilization should be achieved only using 70% ethanol and UV illumination.

### 3.1.4 Coating MEA Probes Before Use

The most effective probe coating will depend on the nature of the cells or tissue being studied. For each primary cell, immortalized cell line, iPSC-derived neuronal culture or tissue slice preparation, the long-term viability and growth parameters of the culture will need to be carefully monitored and assessed. Conditions can then be optimized appropriately. Many of these can be modified from standard protocols developed for routine tissue culture of the chosen cell type.

Apply 0.005% PEI in 25 mM borate buffer to cover the whole surface of the chamber for 10 min at room temperature. Aspirate the PEI and wash the MEA three times with sterile distilled water. To prevent the MEAs becoming hydrophobic again the MEA probes can be stored in petri dishes sealed with parafilm with the growing surface of the chamber submerged in distilled water at +4 °C until required.

Add 1 mL of poly-D-lysine to the center of the array and incubate at +37 °C for 1 h. Aspirate the PDL and rinse three times with sterile distilled water. Allow the probe to air-dry.

### 3.1.5 Reuse of MEAs

Recovering MEAs for reuse should use methods that are as gentle as necessary to avoid damage to the electrodes and chamber. The following use of MEAs for acute slice recording it is usually sufficient to remove the tissue and just rinse the MEA with distilled water. Following tissue culture applications, the surface will need to be cleaned with a detergent or enzymatic treatment. The MEAs can be soaked in a 1% Terg-A-Zyme solution overnight and agitated by gentle shaking or rocking. After treatment, the MEAs should be rinsed thoroughly with distilled water and dried prior to repeating the hydrophilic surface treatment and sterilization. It is vital to remove any residue from treatment with detergent since failure to do so may cause damage to the electrodes and carrier glass.

### 3.1.6 Monitoring the Viability of MEAs

MEAs treated with care, cleaned, and recoated should be usable for many subsequent studies. Degradation of the electrode surface will inevitably accumulate over repeated use and the noise level when attached to the amplifier will reflect this change in performance. Noise levels are affected by electrode size, material and configuration. Generally, the smaller the electrode, the higher the noise, but where the electrode fabrication is designed to create a greater surface area due to deposition to form a three-dimensional surface, lower impedance is accompanied by a lower noise level. Make a note of the peak-to-peak noise when attached to the recording system for the first time filled with a buffer solution, or aCSF and track the performance over repeated use. Attached to the amplifier, an MCS TiN MEA with 10 µm electrodes should have noise in the range ±40 µV, and 30 µm may have peak-to-peak noise around ±10 µV. If individual electrodes suffer from degradation or become

faulty they can be inactivated in the acquisition software. If performance looks unusually poor across the whole array, clean the contact pads on the MEA and the headstage with methanol and if the noise persists inspect the rest of the equipment for problems. If individual electrodes appear faulty it may be useful to rotate the array in the headstage to check that they move with the MEA. If they do not, then the fault is with the connector and headstage.

### 3.1.7 *Impedance Check*

For some MEAs, easy monitoring of electrode impedance over time can be achieved through the use of an impedance testing device. All of the electrodes in the array may be tested simultaneously and displayed using a software driven measurement. Data can be stored and tracked over the lifetime of the array and allow the user to evaluate the effect of various substrate treatments and to decide when a chip needs to be discarded. Impedance is affected by the size of the electrode, thus for MCS arrays, a 30 µm electrode typically has an impedance of 30–50 kΩ, whereas a 10 µm electrode has an impedance of 250–400 kΩ. A hydrophobic electrode surface will also increase the impedance of the electrodes in the array. Make sure to place the MEA in the tester in the correct orientation, since chips with an internal reference electrode have modified electrodes to connect to ground.

### 3.1.8 *Recording Hardware*

Multichannel Systems produces a versatile, compact and powerful in vitro system with integrated amplifier, stimulus generator, temperature control and a real-time signal detection/feedback processor. It is suitable for many different in vitro, high-throughput and in vivo applications and can take input from different types of headstage. Recordings can be made from four MEAs in parallel, all sampling at 50 kHz per channel but can also record from different electrode configurations. MEAs with 32, 60, 120, and 256 electrodes can be used. The flexibility of the interface board is unsurpassed, allowing for the hardware to be switched between different uses depending on need. Amplifiers are built into the headstage so that noise is reduced by having amplification close to the signal source. The downside of this approach however is that the active electronics incorporated into the headstage prevents placement of the headstage in a humidified environment. Longer-term recordings could make use of recording chambers with semi-permeable membrane covers and it is possible to shroud the headstage assembly in a gassed chamber but for long-term recording from cell cultures or organotypic slices where there is a requirement for permanent residency in a tissue culture environment, other systems may be more appropriate.

Alpha MED Scientific produces the MED64 microelectrode recording system which can be used for acute slices, cultured cells and slice cultures. The basic system records from 64 channels simultaneously with an impressive signal-to-noise ratio. Additional

recording sites can be added to expand the system to record from up to  $8 \times 64$  electrode samples by multiplexing, stimulation through 1 or 2 electrodes being applied sequentially to each MED connector.

### **3.2 Preparation of Cell cultures on MEAs**

For the study of network electrophysiology, neuronal cells on MEAs provide an ideal technology. The growing culture gives a reductionist view of complex brain cytoarchitecture on a scale that is amenable to observation and manipulation via pharmacological or genetic methods, or electrical stimulation.

For those unfamiliar with rodent brain dissection Spijker [8] provides an excellent place to start and for the basic fundamentals of neuronal tissue culture see Dreyfus and Black, [9]. The following describes the preparation of rodent hippocampal or cortical neurons for culture onto MEAs but other methods can be easily adapted [10]. We have found that this method is equally successful for both types of cells, establishing robust, enduring cultures that develop quickly and may be maintained for long culture periods.

1. Dissection of tissue should be carried out in a laminar flow hood. Prepare the area for dissection by sterilising all dissection tools and microscope. Chill separate 50 mL tubes, half-filled with dissection medium on ice to collect dissected tissue. Keep an additional tube chilled to provide solution for washing.
2. Heads are removed from embryonic day 18 (E18) rat foetuses from a timed-mated female rat following euthanasia, carried out according to local ethical guidelines and cooled immediately by immersion in a large volume (25–30 mL) of cold HBSS. The heads should be washed a couple of times in fresh, cold HBSS to remove any traces of blood.
3. Dissection of cortex, hippocampus or other brain regions is carried out using standard techniques following gross anatomical landmarks and natural boundaries between tissue regions. This should be carried out using a stereoscopic dissection microscope placed in a laminar flow hood. To keep tissues cold during dissection the procedure can be carried out in a petri dish containing dissection medium placed over ice, or on a precooled metal plate.
4. First, expose the skull with a scalpel by making an incision in the skin along the midline surface of the skull, parting each fold of skin away to the side. From the caudal end, cut through the soft bone close to the midline along the dorsal surface using small iridectomy scissors, taking care not to cut into the underlying brain tissue. Splay open the cut halves of the skull. Remove the brain by scooping up with a small spatula, being aware of attached meninges which could hinder, or tear the brain as it is being lifted from the skull. Peel off any remaining meninges and remove blood.

5. Remove the cerebellum. Dissect away each of the two cortices from the hippocampus using the tips of the forceps to gently pare away from the underlying structure which can be distinguished by the difference in colour. Place the dissected cortices into a separate dish or tube of cold dissection medium. If the hippocampus is required, it can now be identified easily with the cortex removed. Straight forceps can be used to hold the brain steady and using a second pair of curved forceps, always with closed tips, tease away the whole hippocampus in one piece by rolling it away from the unwanted tissue beneath. Areas can be detached by opening and closing the forceps to cut through. Once separated, remove any cortex that has been retained with the hippocampus. Collect into fresh, cold dissection medium. Repeat for all the remaining embryos.
6. We favour a papain digestion of tissue to dissociate cortical and hippocampal cells for plating MEAs that is less damaging than other proteases, and use a commercial papain dissociation system for cell isolation. The method is based on those of Huettner and Baughman [11] and refinements by Finkbeiner and Stevens adapting their earlier protocols for hippocampal tissue [12]. Cell yield and viability are improved over digestion using trypsin. The protocol is described here in brief, but the user should also be familiar with the manufacturer's instructions. The papain dissociation kit contains all reagents used below except HEPES.
7. Add 2 mL of 1 M HEPES buffer to 100 mL of EBSS (vial 1 from kit). This can be stored at +4 °C in between uses and needs to be equilibrated with 95:5 O<sub>2</sub>–CO<sub>2</sub> before use, this solution is used to reconstitute the other components of the kit.
8. Prepare solution A: add 5 mL of EBSS to the papain vial (vial 2 in kit, containing 20 units papain per mL in 1 mM L-cysteine with 0.5 mM EDTA) just before use and briefly incubate at +37 °C to maximize solubility and activity. The kit contains a color chart to assess the pH, if this solution appears dark red or purple indicating alkalinity equilibrate with 95:5 O<sub>2</sub>–CO<sub>2</sub>.
9. Prepare solution B: add 500 µL of EBSS to the DNase vial (vial 3 in kit, giving 2000 units DNase per mL), mix gently just before use.
10. Prepare solution C, ovomucoid protease inhibitor with bovine serum albumin: add 32 mL EBSS to the albumin-ovomucoid inhibitor mixture (vial 4 in kit, containing 10 mg ovomucoid and 10 mg albumin per mL) and allow to dissolve. Keep cold and equilibrate at +37 °C and 95:5 O<sub>2</sub>–CO<sub>2</sub>.
11. Take the cold brain tissue and mince with a scalpel after removing from the dissection medium, chopping on a flat surface such as a petri dish over ice, or on the side of the tube used in

the next step. Transfer 250  $\mu$ L of DNase solution (solution B) to the papain vial (solution A) just before use and mix gently. Add the minced tissue to the papain solution. Equilibrate with 95:5 O<sub>2</sub>–CO<sub>2</sub> and cap the tube. Incubate at +37 °C for 10 min with gentle agitation.

12. Vigorously triturate tissue with a 10 mL tissue culture pipette until devoid of clumps.
13. Strain cell suspension through a 70  $\mu$ m mesh filter to remove any pieces of undissociated tissue.
14. Centrifuge at 1000  $\times g$  for 5 min at room temperature.
15. While cells are centrifuging, mix 2.7 mL EBSS with 0.3 mL solution C and 0.15 mL solution B (3.15 mL total).
16. Following centrifugation, discard the supernatant and resuspend the cell pellet in the DNase, dilute ovomucoid inhibitor solution EBSS above (Subheading 3.2, step 10).
17. Place 5 mL solution C in a 15 mL tube and using a 5 mL pipette, carefully layer the cell suspension on top of the 5 mL ovomucoid solution.
18. Centrifuge over the ovomucoid gradient at 300  $\times g$  for 5 min at room temperature. Discard the supernatant and resuspend the cell pellet in plating medium.
19. Count the cells and dilute to the required plating density in plating medium.
20. Density of cells will vary according to the neuronal culture. Two different approaches are recommended which can be adapted to the culture being prepared and the growth of the cells. A high density, small volume can be applied to the center of the MEA chamber around the electrode grid, taking care not to touch the electrodes while dispensing from the pipette. A 50  $\mu$ L volume of cell suspension at a density of 2 million cells/mL will produce an area of high-density neurons and glia. This plating procedure may be a necessity when small brain areas are being prepared containing rare populations of the cell type of interest. Where larger brain areas are being dissected for dissociation, cell numbers may allow for the entire chamber to be flooded with a cell suspension. Seeding the chamber with 1 mL of a 100,000 cells/mL suspension is a good starting point for establishing cortical or hippocampal cultures (see Fig. 1).
21. If plating a high-density spot of cells, top up the media very gently 60 min later, after the cells have become adherent. The growing culture can then be fed approximately every 5 days by replacing half of the volume of media in the chamber (0.5 mL). We also like to replace the media 24 h after plating to remove any nonadherent cells or debris from the dissociation.

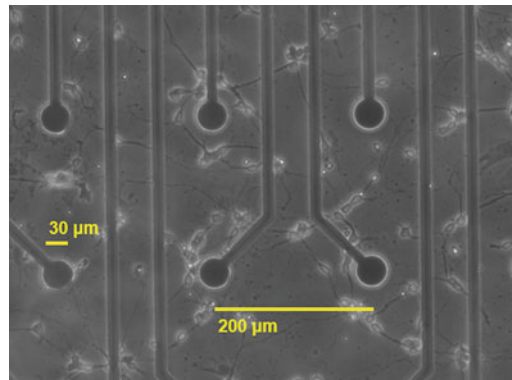


**Fig. 1** Photomicrograph of rat cortical neurons cultured from E18 embryos and plated onto an MCS multielectrode array according to the protocol described in Subheading 3.2. Chambers were sealed with zero evaporation lids. The 30  $\mu\text{m}$  electrodes have an interelectrode spacing of 200  $\mu\text{m}$ . The cells are shown at just 2 days in culture and are already beginning to extend long neuritic processes

22. To maintain good growth conditions, monitor the pH and volume of the growing cells. If media is being lost by evaporation despite a humidified cell culture environment, additional media changes may be required. To minimize the effects of evaporation a number of steps can be taken. If the MEAs are housed individually in petri dishes, sterile water can be added directly to the petri dish surrounding the chamber. Alternatively, a tidier solution is to use zero evaporation lids to enclose the culture. Depending on culture ring options chosen it is possible to fit a Teflon™ cap with an airtight seal to the chamber with a transparent semipermeable membrane. This allows for gaseous exchange but no loss of water vapor. These lids are essential to preserve the sterility of the growing cells if the chambers are removed from the sterile environment for recording where they may be exposed to airborne pathogens.
23. Cortical and hippocampal cultures prepared in this way will begin to extend neuritic processes almost immediately and within the first week will begin to show isolated spikes on individual electrodes. As the culture matures, activity will begin to be observed on more electrodes and the behavior of the cells will change such that tonic spike activity will become more “bursty,” bursts will synchronize into population events and the structure of spikes within the burst will change. Figure 2 shows example recordings made during the fourth week of culture when these population bursts are being recorded on many of the electrodes in the array.

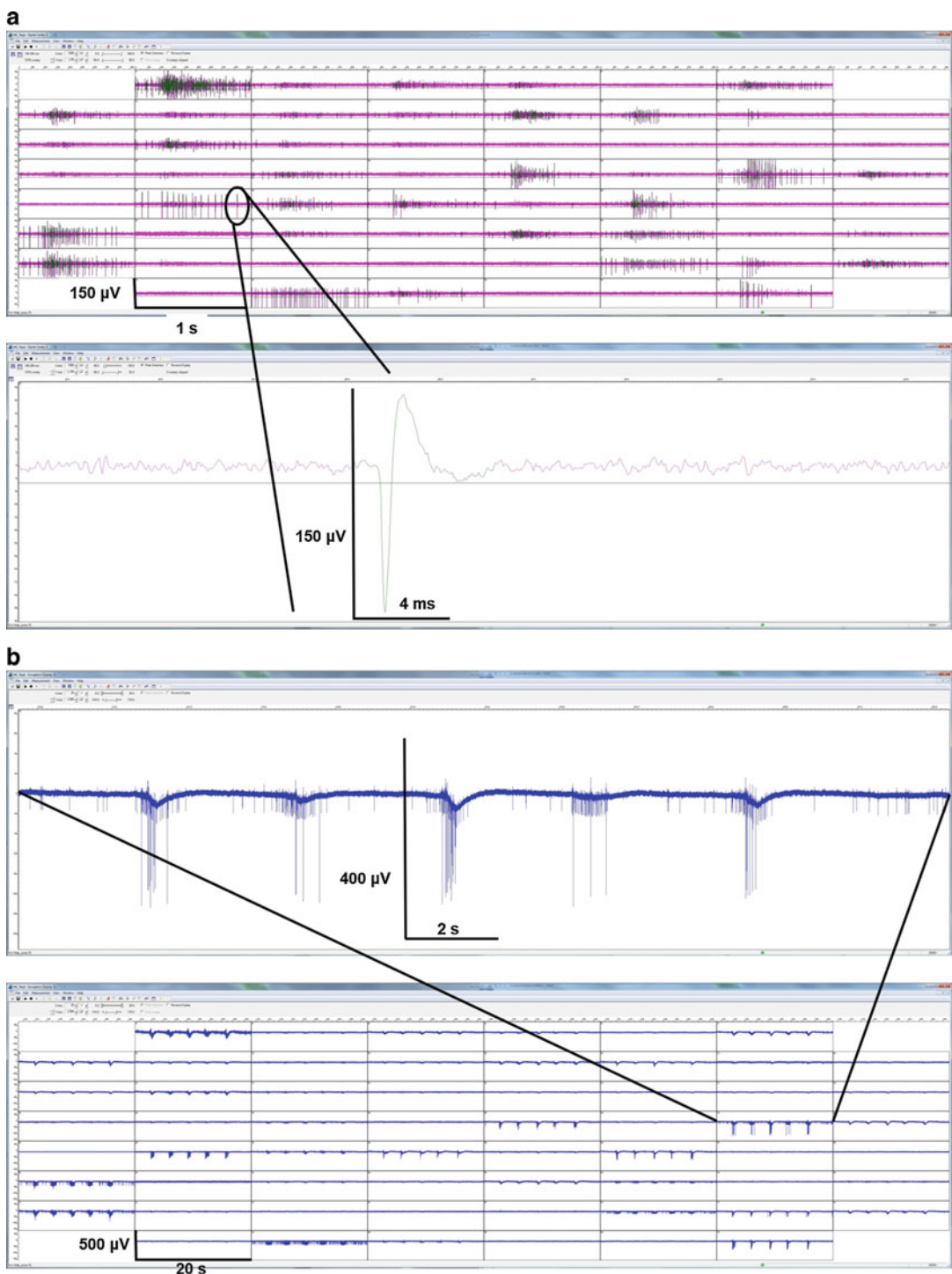


**Fig. 2** Screenshot of spontaneous network activity recorded from a rat cortical neuron culture at 25 days in vitro. The culture was prepared according to the methods described and the recordings were carried out using the equipment outlined in Note 9. The 60 electrodes were sampled at 25 kHz,  $\times 1200$  gain with the

### 3.3 Acute Tissue Slice

Hippocampal slices have long been used in the study of synaptic function due to their well characterized circuitry and involvement in learning and memory. Slices recorded on MEAs have many of the attractive features of conventional acute slice electrophysiology but have additional advantages due to the versatility and ease of selecting stimulation sites and the benefit of multiple recording sites. Many good discussions of methodology have been published recently which explore the technical aspects of how to prepare high-quality tissue slices for conventional electrophysiological applications. Well preserved tissue is the fundamental challenge for brain slice electrophysiology and the reader is referred to a number of excellent discourses that examine the basic procedures required for routine preparation of brain slices [2, 13, 14]. The following methods focus more closely on how the methods may be modified and optimized to obtain good MEA recordings from the acute tissue slice. As with acute brain slices for single microelectrode techniques, the overall health of the slice dictates the success of the experiment. It is vital to cause as little physical and chemical trauma to the tissue during removal and slicing of the brain as possible. Since direct damage to the surface of the slice and underlying layers caused by the cutting blade is inevitable, minimizing the detrimental effect of sodium influx and cell swelling is attempted by cutting the tissue in a solution in which sodium is replaced with sucrose. Relatively thin slices are usually employed to permit a good level of oxygenation of the tissue.

1. Cut a block of agar from the plate with a blade, of dimensions  $1 \times 0.5 \times 1$  cm. Mount onto the vibratome stage with cyanoacrylate adhesive and allow to dry.
2. Sacrifice rats at an age of 21–35 days by cervical dislocation and remove the brains quickly into ice cold, gassed cutting solution. Remove the head using the large scissors by cutting close to the back of the skull.
3. Place the decapitated head on a level surface where it will not slip, facing away from you. Using the scalpel or small scissors, make an incision in the skin from the middle of the back of the head to between the eyes. Spread both halves of the skin away from the skull to each side. Insert the tip of the small scissors

---

**Fig. 2** (continued) temperature maintained at +37 °C on the headstage. In (a) the data are high-pass filtered at 300 Hz. Each window in the top panel shows a 1 s trace of activity. The exploded view below is a single spike recorded on electrode 25 to show a typical spike morphology. The line shows a threshold marker representing five times the standard deviation of the noise. Individual electrodes can be seen to show tonic spike firing, bursting, and one or two examples of electrodes recording multiunits. (b) Shows longer 20 s traces without filtering. Here the highly synchronized network bursts are clearly seen with more than half of the electrodes on the array participating in this coordinated activity. The exploded view above shows electrode 74 and the structure of spikes within a typical burst

into the foramen magnum and keeping the points of the scissors away from the brain, tight against the bone, snip low down around each side ending above each eye. When both cuts have been made, grasping the back of the skull with the serrated tweezers will allow you to lift away the upper skull and flip it over the front of the head. Free the exposed brain from any clearly visible meninges, and then carefully scoop the brain from the rear, underneath the cerebellum onto the spatula taking care not to deform the tissue and being aware of any residual meningeal tissue that may stop the brain being lifted out or even cut into the tissue when doing so. Rapidly cool the brain by gently sliding off the spatula and immersing the brain in a 50 mL tube half-filled with iced cutting solution (*see Note 4*) to quickly bring the tissue down to temperature. The whole brain removal and cooling should be carried out in around 30 s to preserve the health of the tissue.

4. Before sectioning the tissue prepare the vibratome slicing chamber by filling the chamber with iced cutting solution and bubbling with 95:5 O<sub>2</sub>–CO<sub>2</sub> leaving to cool and equilibrate. Similarly, the slice storage chamber should be set up so that it is at the desired temperature and aCSF is well equilibrated with 95:5 O<sub>2</sub>–CO<sub>2</sub>. To prepare the brain for the vibratome, the brain can be gently removed into fresh cutting solution into a 10 cm petri dish placed over ice (*see Note 5*). For dissection, a single edged razor blade is preferred. With the brain on its ventral surface, a coronal cut across both hemispheres immediately anterior to the cerebellum and a coronal cut through the striatum at a position approximately beneath the bregma is carried out. Then the blade can be used to separate the hemispheres down the midline. Each hemisphere is then positioned on the flat medial surface and the dorsal cortical region removed with a cut in the horizontal plane to provide a stable surface to stick down to the slicing stage. Next flip the hemispheres onto the dorsal surface and place them together, next to each other as they would be if the hemispheres were not separated. Draining solution away from the tissue, the blade can be used to lift both sections together off the dish onto the blade and then the tissue can be placed on the prepared slicing stage with its agar block fixed in position and a small blob of cyanoacrylate adhesive on the stage mount in front of the agar. The tissue can be encouraged to slip off the blade onto the stage with the side of a pair of forceps.
5. Mount the tissue sections with their rostral flat edge against the agar so that the blade approaches the tissue from the caudal edge. Once in position on the stage leave to dry for just a few seconds before mounting onto the vibratome, submerged in

ice cold cutting solution. Set to slice at 350  $\mu\text{m}$  on the vibratome (*see Note 6*), discard the first slices until the hippocampus begins to appear.

6. Use the transfer pipette to gently remove the cut sections as they separate from the cut tissue block and begin to float away. Slices are then stored for approximately 120 min in continuously gassed aCSF at +28 °C in a submerged storage chamber. This will allow the slices to recover and equilibrate with the recording solution (*see Note 2*).
7. To mount slices on arrays for recording, view an empty MEA under a stereoscopic dissection microscope in the orientation that it will be in when inserted onto the headstage. Gently lift a hippocampal slice from the recovery chamber with a transfer pipette and deposit with a little solution onto the center of the array. While it is wet it will be easy to turn using a paintbrush or the closed, blunt ends of a pair of forceps. Depending on how much surrounding tissue is present it may be possible to manipulate the slice by an area distant from the region of interest. To encourage the slice to adhere to the glass surface in the correct position, allowing the investigator to know with some certainty where stimulating electrodes may need to be set and where the cell fields are in relation to the array as a whole, short narrow strips of filter paper can be used to wick away the solution under the slice. This action will suck the slice across the glass surface in the direction of the movement of the solution. With a little practice and experience it will be possible to quickly move the slice into the correct position on the array as the solution is removed from the tissue. Allowing just a few moments for the slice to adhere will keep it in position. Then quickly use the same transfer pipette to hold approximately 1 mL of aCSF and dispense the solution directly on top of the slice to submerge it. Touch the slice with the meniscus of the solution in the pipette as pressure is begun to be applied to the pipette bulb. If solution is introduced down the edge of the chamber the slice will be removed from its position and float away. Dripping the solution onto the slice will similarly detach the tissue. Figure 3 shows a hippocampal slice positioned onto a MEA.
8. Next, use a slice grid to hold the slice in position more firmly to protect it from movement during perfusion. Prewet the harp slice grids in aCSF and make sure bubbles have not formed on the mesh. If they have, knock them off before lifting the grid with straight forceps. Introduce the grid into the MEA chamber directly over the tissue slice, lower and release when the grid will gently sit over the tissue without dropping onto it or moving the slice in the process.

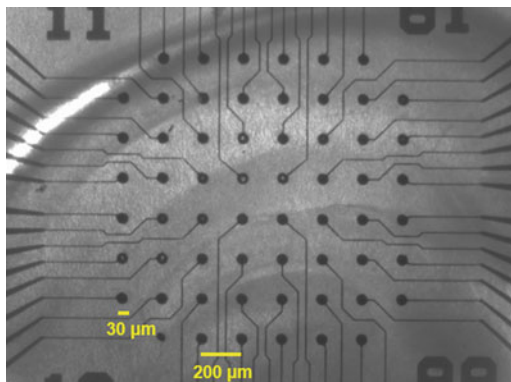


**Fig. 3** Photomicrograph of a rat hippocampal slice positioned onto an MCS multielectrode array according to the protocol described in Subheading 3.3. The array carries 30  $\mu\text{m}$  electrodes with an interelectrode spacing of 200  $\mu\text{m}$ . The dentate gyrus is toward the bottom right of the picture and the dendritic field of the CA1 region is the lighter area sweeping across the top half of the electrode array. The choroidal fissure is visible just passing over the top of the array from the left side

9. Perfusion of the slice should be started as soon as the slice is positioned appropriately in the MEA chamber it should be attached carefully onto the prewarmed headstage and clamped firmly, taking care not to dislodge it in the process. If the array has been handled or solution has dripped onto the contacts outside of the culture ring dry off the glass and then wipe with 100% methanol to clean them. Begin perfusion with prewarmed and gassed aCSF as soon as possible (*see Note 7*).
10. Not all experimental paradigms will require electrical stimulation of the slice. Activity may be spontaneous or induced by chemical or pharmacological means. The example data shown in Fig. 4 shows local field potentials recorded in a hippocampal slice rendered epileptic. Note the excellent signal-to-noise ratio and the amplitudes that are maximal at almost 1 mV peak-to-peak.

### 3.4 Organotypic Slice Culture

The organotypic slice culture preparation preserves much of the structure and synaptic aspects of the tissue, creating a more *in vivo*-like platform compared to a dissociated primary neuronal culture. The structure of the slice changes over time in culture as the tissue develops; however, in contrast to the acute slice, experiments can be performed over several days, weeks or months. Cerebellar slices can be maintained in culture for several months and spontaneous activity of Purkinje cells detected over this time [15]. This section describes a method for preparing mouse cerebellar brain slices for maintenance in culture, allowing the recording of network level activity on MED64 MEAs. This recording system can operate

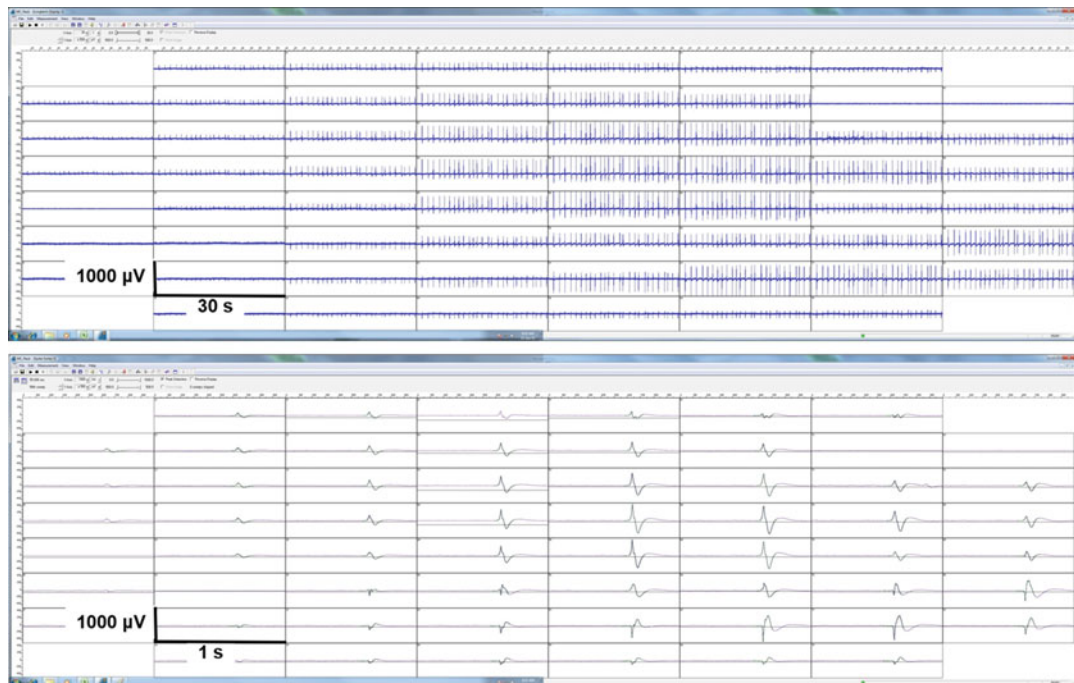


**Fig. 4** Screenshot showing epileptiform bursting activity from an acute rat hippocampal slice prepared from a P28 rat attached to an MCS multi-electrode array. The recording was carried out with the hardware detailed in **Note 10**. The slice was exposed to 100  $\mu$ M 4-aminopyridine with temperature maintained at +28 °C. The data were sampled at 10 kHz,  $\times 1200$  gain and filtered between 3 Hz and 300 Hz. The top panel shows traces covering 1 s of recording and the panel below shows 30 s recording periods

within a humidified incubator, allowing continuous recording to take place over long time periods. If specific requirements of the tissue are taken into account, the following method can be adapted for rodent brain slices from other regions. Humpel provides a general overview of organotypic brain slice methodology [3].

1. Prepare cutting solution (*see Subheading 2.2, item 4* for composition). Sucrose-containing cutting solution should be a slushy consistency and pregassed with 95:5% O<sub>2</sub>-CO<sub>2</sub> (*see Note 4*). Fill the buffer tray of the vibratome with iced cutting solution and bubble with 95:5% O<sub>2</sub>-CO<sub>2</sub> gas to maintain pH and O<sub>2</sub> saturation throughout.
2. Prepare culture medium (*see Subheading 2.3, item 11* for composition). Prepare without AraC, and pipet 1.2 mL culture medium into the required number of 35 mm petri dishes or wells in a 6-well plate. Place a cell culture insert into each dish or well and put in a +37 °C incubator with 5% CO<sub>2</sub> to pre-equilibrate. The number of dishes you require will depend on how many slices you need to culture. We suggest no more than 4 or 5 slices per insert.

3. Sacrifice mouse pups by cervical dislocation, decapitate and carefully remove the brain into ice-cold, slushy, pregassed cutting solution in a half-filled 50 mL tube on ice. We dissect and slice two brains at a time.
4. The brains should be blocked on a circular piece of filter paper in the lid of a 60 mm dish, wetted with cutting solution and using a single-edged razor blade. Approximately half of the forebrain should be removed and a parasagittal cut made at the peripheral edge of one hemisphere of the remaining forebrain. This provides a flat surface for gluing the brain block to the slicing platform. It is important that cuts are made perpendicular so that the block can be mounted onto the platform in a perfectly straight orientation. This allows for consistency of slices between brains and the easy identification of anatomical landmarks.
5. Apply cyanoacrylate adhesive to the platform and transfer two blocks of tissue, from two brains, onto the glue on the cut edge, drawing moisture away from the edge of each block carefully with a piece of filter paper first. Excessive glue can be drawn up the sides of the tissue and make slicing difficult; therefore, a minimal amount should be applied.
6. Place the platform in the vibratome buffer tray, submerging the tissue in cold solution.
7. Cut 300  $\mu\text{m}$  thick sections.
8. As each slice comes off the blade transfer it, using a glass transfer pipette (Subheading 2.2, item 6), into a 60 mm dish filled with cutting solution. Use two needles to carefully pull the cerebellum from the rest of the slice.
9. As each slice comes off the blade transfer it, using the transfer pipette into a 60 mm dish filled with cutting solution. Use two needles to carefully pull the cerebellum from the rest of the slice.
10. Transferring as little liquid as possible, place the cerebellar slice onto the cell culture insert surface with the transfer pipette. Remove the excess solution from the membrane with another pipette. Put the dish back in the incubator.
11. Perform a half media change every 2–3 days using culture medium (containing AraC if preferred) for 2 weeks.
12. The day before slice placement, prepare MEAs by adding 1 mL of 0.1% PEI in water. Leave overnight then rinse the arrays thoroughly. Arrays should not be left to dry.
13. Transfer 500  $\mu\text{L}$  culture medium to each MEA dish and place in the incubator for preequilibration (at least 1 h). We place each array in a lidded 60 mm petri dish with sterile distilled water in the bottom to increase humidification.

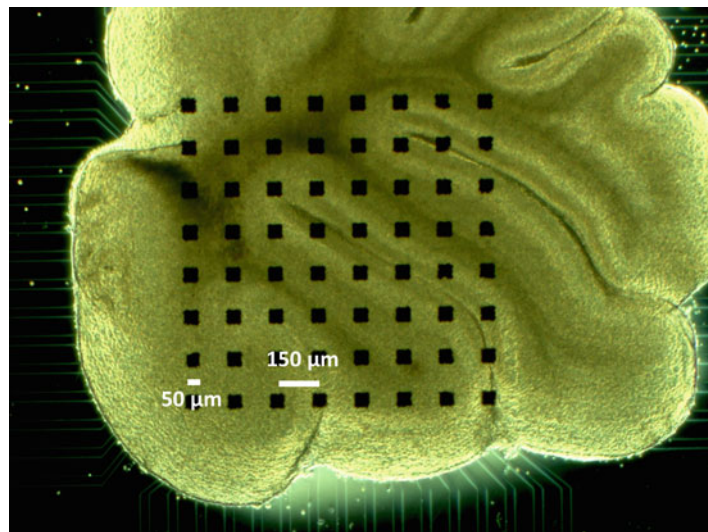


**Fig. 5** Photomicrograph of a mouse cerebellar slice positioned onto an MED64 multi-electrode array according to the protocol described in Subheading 3.4. The array covers a 1 mm × 1 mm area and carries 50  $\mu\text{m}$  electrodes with an interelectrode spacing of 150  $\mu\text{m}$ . The slice has been placed to cover an area from the central white matter to the edge of the cerebellar cortex, covering the Purkinje cell layer from which spontaneous activity can be recorded

14. Using a sterile No. 11 blade scalpel cut around each slice through the membrane using fine straight forceps to stabilize it as you cut along each of the four sides. Pinch one corner of the cut-out piece of membrane with the forceps and place the slice in the MEA dish, slice-side down.
15. Position the slice with your area of interest over the array, we use a fine paintbrush to move the slice, and carefully reduce the volume of medium in the dish to 150  $\mu\text{L}$ . Place back in the incubator for 1 h.
16. Increase the volume of medium to 250  $\mu\text{L}$ . At this point the slice can easily float off the array if not sufficiently adhered. If this happens placement can be attempted again, and the process repeated. Figure 5 shows a cerebellar slice positioned on an MEA.
17. Perform a half media change every 2–3 days. The slice will have adhered sufficiently to record activity after a minimum of 48 h. It is important not to perform a media change within 12 h of recording to avoid artefactually increasing activity. Slices can remain in culture with cells spontaneously firing for weeks to months if maintained correctly. Figure 6 shows typical spontaneous action potentials recorded from Purkinje cells in a cerebellar slice.



**Fig. 6** Screenshot showing spontaneous firing activity from an organotypic cerebellar slice prepared from a P4 mouse attached to an MED64 multielectrode array. The recording was carried out with the hardware detailed in **Note 11**. The data were sampled at 20 kHz,  $\times 1000$  gain, and high-pass filtered at 100 Hz. The top panel shows 64 traces covering 1 s of recording and the panel below shows a 5 s recording period from a single electrode. Downward deflections represent spontaneous action potentials recorded from the Purkinje cell layer

#### 4 Notes

1. Take a glass Pasteur pipette and using a diamond tipped pen, score around the middle, snapping off the front half of the pipette and discarding. Melt the cut surface of the back of the pipette in a blue Bunsen flame to smooth any sharp areas. Insert the cut end into the rubber bulb so that the wide, smooth rear of the pipette can be used to lift slices with a little solution very delicately, without folding, or causing any mechanical compression.
2. For recovering and storing tissue slices a number of brain slice chambers for submerged and interface storage are commercially available. As an alternative, slice storage chambers are easily made by bubbling gas into a large glass beaker. Suspending a second vessel in the beaker, made out of a 50 mL plastic syringe barrel with a plastic mesh glued onto the bottom allows for the slices to be arranged on the mesh where they will be well perfused by the circulating solution.
3. Plasma cleaner: to achieve good plasma surface activation and cleaning to improve adhesion we use a Diener electronic Zepeto Plasma Cleaner. The cylindrical chamber can house about 12 MEAs in one session. Set the device to produce a low-vacuum plasma for 5 min at 0.2 mbar and 100 W.
4. To produce an ice cold cutting solution for preparation of the tissue and sectioning with a vibratome, gas 500 mL of solution with 95:5 O<sub>2</sub>-CO<sub>2</sub> until equilibrated in a soft plastic cylinder

with a screw top. Freeze the solution quickly in a freezer at  $-80^{\circ}\text{C}$ . As ice begins to form, but before it is frozen solid, crush the ice to a slush by squeezing the bottle and shaking vigorously. Use this icy slush to cool the brain before dissection, and to fill the tissue chamber of the vibratome ready to receive the blocked-up tissue for sectioning.

5. Orientation of slice: hippocampal slices can be prepared in different cutting planes. We prefer the horizontal plane for Schaffer collateral stimulation and recording responses in CA1. Coronal slices and hippocampal slices with entorhinal cortex intact may be preferred depending on which afferent pathways are required to be preserved. Xiong et al. provide an excellent discussion of these considerations [16].
6. Begin with the vibratome blade set to a low advance speed (0.05–0.1 mm/s), a wide amplitude (0.75–1 mm) and a frequency of 65–70 Hz, or close to the instrument's maximum vibration.
7. The experimenter will be required to trial and develop effective ways to introduce and remove solution from the MEA chamber that minimize mechanical disturbance of the tissue, prevent introduction of bubbles, do not transmit pulsatile flow of solution from the pump, prevent “breathing” of the solution level in the chamber, effectively bathe the slice without solution flowing around the perimeter of the chamber leaving an unperfused area in the middle, and minimize electrical noise. From the metal inlet perfusion cannula we melt capillary glass to produce an L-shaped glass nozzle of 2 mm outside diameter, with each arm just 1 cm long and the cut ends polished in a blue flame to smooth them off, attached using a short piece of Tygon® tubing. The tubing allows the glass to be turned into an upright position when it is not in the bath, and produces a little flexibility to avoid knocking the chamber when positioning the inlet.
8. To obtain the correct temperature in the chamber, the in-line heating temperature should be set slightly higher than is required. This can be worked out simply by running the perfusion and measuring the temperature in the bath with a thermometer or a digital meter with a thermocouple probe. Begin with the temperature set 1–2  $^{\circ}\text{C}$  above the desired recording temperature and adjust until the reading is stable at the required level.
9. Recording equipment for cultures used a Multi Channel Systems USB-MEA240-Up-4 System-E which features four MEA 1060-BC amplifiers (with blanking circuit for stimulus artefact suppression) and a 256-channel data acquisition system capable of recording simultaneously from up to 240 electrodes.

Temperature was maintained at +37 °C on the headstage using a TC02 temperature controller. Typically four MEA chambers were recorded from simultaneously. Software control was provided by four copies of MEA\_Select, four copies of MC\_Rack, and TCX temperature controller. MC\_Rack was used for analysis.

10. Recording equipment was a Multi Channel Systems USB--MEA240-Up-4 System-E which features four MEA 1060-BC amplifiers (with blanking circuit for stimulus artefact suppression) for upright microscope and a 256-channel data acquisition system capable of recording simultaneously from up to 240 electrodes. Stimuli were delivered using a 4000 series STG stimulus generator with eight independent channels. Perfusion was maintained with a Gilson Minipuls3 8-channel peristaltic system with four channels for perfusion. Solution reservoirs stood in a +28 °C circulating water bath each bubbled with a mixture of 95:5 O<sub>2</sub> and CO<sub>2</sub> delivered through a gas distribution stone. Each headstage had temperature independently monitored and controlled using a TC02 temperature controller and each perfusion inlet was warmed to +28 °C using an inline perfusion cannula (*see Note 8*). To examine individual recording sites, a long working distance, stereo zoom microscope with illumination ring was mounted on a boom arm that could be brought into position over each of the recording sites. Software control was provided by four copies of MEA\_Select, four copies of MC\_Rack, MC\_Stimulus II, and TCX temperature controller. MC\_Rack was used for analysis.
11. Recording setup for organotypic slices was composed of eight MED-C03 connectors housed on the shelves of a tissue culture incubator with the cables ported out of the rear of the incubator. Incubation was maintained at +37 °C, 5% CO<sub>2</sub>, and 100% humidity. The main amplifier (MED-A64MD1) and Head Amplifier (MED-A64HE1S) took the output from a MED64 multiplexer (MED-A64SF1 and MED-A64SF2) allowing for the time-sequenced acquisition from the eight samples. Data acquisition and analysis was controlled using MED64 Mobius Software.

## References

1. Pine J (2006) A history of MEA development. In: Taketani M, Baudry M (eds) Advances in network electrophysiology using multi-electrode arrays. Springer, New York
2. Lein PJ, Barnhart CD, Pessah IN (2012) Acute hippocampal slice preparation and hippocampal slice cultures. Methods Mol Biol 758:115–134
3. Humpel C (2015) Organotypic brain slice cultures: a review. Neuroscience 305:86–98
4. Berdichevsky Y (2009) Microfluidics and multielectrode array-compatible organotypic slice culture method. J Neurosci Methods 178 (1):59–64
5. Plenz D (2011) Multi-electrode array recordings of neuronal avalanches in organotypic

- cultures. *J Vis Exp* 54:e2949. <https://doi.org/10.3791/2949>
6. Johnstone AFM (2010) Microelectrode arrays: a physiologically based neurotoxicity testing platform for the 21<sup>st</sup> century. *Neurotoxicology* 31:331–350
  7. Stett A (2003) Biological application of micro-electrode arrays in drug discovery and basic research. *Anal Bioanal Chem* 377:486–495
  8. Spijkers S (2011) Dissection of rodent brain regions. In: Li KW (ed) *Neuroproteomics*. Humana Press, New York/Heidelberg, pp 13–26. [https://doi.org/10.1007/978-1-61779-111-6\\_2](https://doi.org/10.1007/978-1-61779-111-6_2)
  9. Dreyfus CF, Black IB (1990) Multiple approaches to brain culture. In: Conn PM (ed) *Cell culture methods in neuroscience*, vol 2. Elsevier, pp 3–16. <https://doi.org/10.1016/B978-0-12-185254-2.50005-X>
  10. Pacifici M, Peruzzi F (2012) Isolation and culture of rat embryonic neural cells: a quick protocol. *J Vis Exp* 63:e3965. <https://doi.org/10.3791/3965>
  11. Huettner JE, Baughmann RW (1986) Primary culture of identified neurons from the visual cortex of postnatal rats. *J Neurosci* 6 (10):3044–3060
  12. Finkbeiner S, Stevens CF (1988) Application of quantitative measurements for assessing glutamate neurotoxicity. *Proc Natl Acad Sci U S A* 85:4071–4074
  13. Papouin T, Haydon PG (2018) Obtaining acute brain slices. *Bio Protoc* 8(2):e2699. <https://doi.org/10.21769/BioProtoc.2699>
  14. Ting JT, Daigle TL, Chen Q et al (2014) Acute brain slice methods for adult and aging animals: application of targeted patch clamp analysis and optogenetics. *Methods Mol Biol* 1183:221–242
  15. Kessler M (2008) Spontaneous activity in Purkinje cells: multi-electrode recording from organotypic cerebellar slice cultures. *Brain Res* 1218:54–69
  16. Xiong G, Metheny H, Johnson BN et al (2017) A comparison of different slicing planes in preservation of major hippocampal pathway fibers in the mouse. *Front Neuroanat* 11:107. <https://doi.org/10.3389/fnana.2017.00107>. eCollection 2017



# Chapter 7

## Utilising Automated Electrophysiological Platforms in Epilepsy Research

Carol J. Milligan and Svenja Pachernegg

### Abstract

Genetic mutations have long been implicated in epilepsy, particularly in genes that encode ion channels and neurotransmitter receptors. Among some of those identified are voltage-gated sodium, potassium and calcium channels, and ligand-gated gamma-aminobutyric acid (GABA), neuronal nicotinic acetylcholine (CHRN), and glutamate receptors, making them key therapeutic targets. In this chapter we discuss the use of automated electrophysiological technologies to examine the impact of gene defects in two potassium channels associated with different epilepsy syndromes. The *hKCNC1* gene encodes the voltage-gated potassium channel hK<sub>V</sub>3.1, and mutations in this gene cause progressive myoclonus epilepsy (PME) and ataxia due to a potassium channel mutation (MEAK). The *hKCNT1* gene encodes the weakly voltage-dependent sodium-activated potassium channel hKCNT1, and mutations in this gene cause a wide spectrum of seizure disorders, including severe autosomal dominant sleep-related hypermotor epilepsy (ADSHE) and epilepsy of infancy with migrating focal seizures (EIMFS), both conditions associated with drug-resistance. Importantly, both of these potassium channels play vital roles in regulating neuronal excitability. Since its discovery in the late nineteen seventies, the patch-clamp technique has been regarded as the bench-mark technology for exploring ion channel characteristics. In more recent times, innovations in automated patch-clamp technologies, of which there are many, are enabling the study of ion channels with much greater productivity than manual systems are capable of. Here we describe aspects of Nexion NPC-16 Patchliner, examining the effects of temperature on stably and transiently transfected mammalian cells, the latter of which for most automated systems on the market is quite challenging. Remarkable breakthroughs in the development of other automated electrophysiological technologies, such as multielectrode arrays that support extracellular signal recordings, provide additional features to examine network activity in the area of ion channel research, particularly epilepsy. Both of these automated technologies enable the acquisition of consistent, robust, and reproducible data. Numerous systems have been developed with very similar capabilities, however, not all the systems on the market are adapted to work with primary cells, particularly neurons that can be problematic. This chapter also showcases methods that demonstrate the versatility of Nexion NPC-16 Patchliner and the Multi Channel Systems (MCS) multielectrode array (MEA) assay for acutely dissociated murine primary cortical neurons, enabling the study of potassium channel mutations implicated in severe refractory epilepsies.

**Key words** Automated electrophysiology, Planar patch clamp, Planar chip, Microfluidics, Multielectrode arrays, Temperature sensitivity, Voltage-gated ion channels, Voltage-clamp, Current clamp, Primary neurons, Epilepsy

## 1 Introduction

Discoveries of ion channel gene mutations in epilepsy have advanced considerably since the identification of the first, in the CHRNa4 ( $\alpha 4$  subunit) gene back in 1995 [1], and this acceleration is due to the advent of more cutting-edge sequencing techniques [2, 3]. Determining the functional consequences of gene mutations and their associated molecular deficits is a vital step in understanding the therapeutic implications [4]. hKv3.1 and hKCNT1 ( $K_{Na}1.1$ , Slo2.2, Slack) belong to the voltage-gated potassium channel superfamily that share a common structure comprising four subunits surrounding a central aqueous pore, with each subunit consisting of six hydrophobic transmembrane segments (S1–S6), flanked by intracellular amino and carboxyl termini. The S4 segment consists of conserved basic residues and plays an important role in voltage sensing by the channel. The linker between the S5 and S6 segments (H5 or P region) contains a highly conserved sequence that forms the selectivity filter [5]. These channels are thought to be enablers of high frequency firing, neurotransmitter release and neuronal endurance [6–8]. They are widely expressed throughout the nervous system [9], making them ideally positioned to play important roles in controlling neuronal excitability.

Symptoms of MEAK begin between 3 and 15 years, with progressively severe myoclonus and rare tonic–clonic seizures [10]. Patients carry a recurrent loss-of-function mutation (R320H) in the hKCNC1 gene ( $K_v3.1^{R320H}$ ). The condition is often associated with immobility and mild cognitive decline. Autosomal dominant causative variants in the hKCNT1 gene result in a spectrum of severe epilepsy phenotypes [11], the majority of which result in channels displaying a gain-of-function, regardless of the epilepsy type [12]. KCNT1-related epilepsies are commonly associated with severe seizures that are drug-resistant.

Developed in the late 1970s, the manual patch-clamp technique [13, 14], the paradigm for measuring ionic currents through ion channel proteins, revolutionized the electrophysiological study of ion channels in excitable cells. Because of the throughput limitations of the manual technique, many automated devices have been developed [15] and are now commonly used in academic research and extensively used for drug discovery by the pharmaceutical industry.

The Patchliner has built-in temperature control capabilities allowing the user to heat solutions and compounds or cool solutions, compounds, and cells via heating modules such as the pipette, the measuring head, and the chip wagon or cooling modules on the cooling plate (Fig. 1), respectively, making it ideally suited for temperature sensitive ion channels or modulators. One

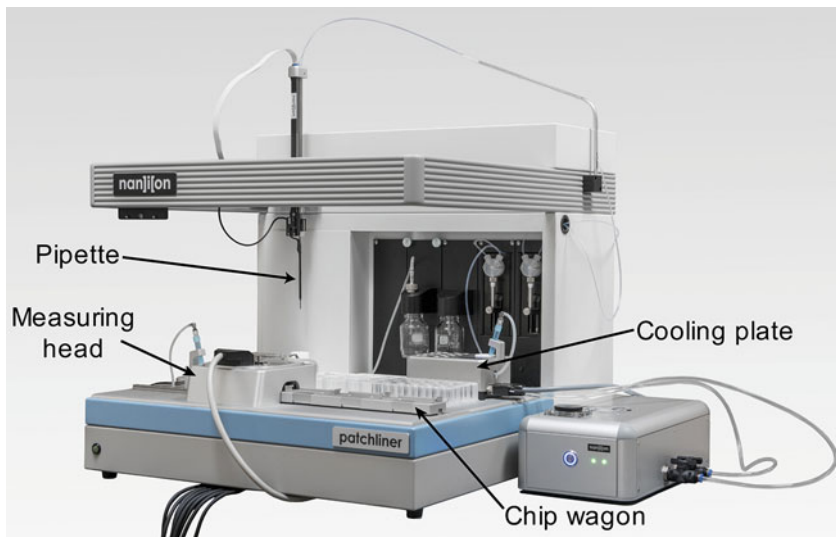


**Fig. 1** Annotated Image Showing the Temperature Modules on Patchliner. Arrows indicate robotic pipette, measuring head, and chip wagon, which can be heated simultaneously or independently, and the Cooling plate. (Image supplied by Nanon Technologies, GmbH)

particularly unusual feature of MEAK, that we were keen to explore, was a transient clinical improvement with fever. Protocols that describe elevated temperature *in vitro* Patchliner recordings using HEK 293 cell stably transfected with wild-type (WT) hKCNC1 ( $Kv3.1^{WT}$ ) and transiently cotransfected with hKCNC1 R320H ( $Kv3.1^{WT+R320H}$ ) are discussed in this chapter.

We have previously demonstrated that recordings from native ion channels in primary mammalian cells can be acquired using planar patch-clamp technology [16, 17], but the biggest hurdle to overcome here handling primary neurons, was to preserve intact neuronal processes when preparing cell suspensions. This is vital because the sodium channels that are important for propagation of the action potential reside in the axon initial segments [18].

Another approach for examining cell/network/tissue excitability is multielectrode array (MEA) electrophysiology. The first planar multielectrode extracellular recording systems were described in the 1970s and 1980s [19–21] although a generation of platforms with improved capabilities have subsequently been developed [22]. There are numerous MEA systems currently available on the market, including Multi Channel Systems (Reutlingen, Germany), Axion BioSystems (Atlanta, USA), MaxWell Biosystems (Basel, Switzerland), NMI TT Microdevices (Reutlingen, Germany), and Alpha MED Scientific (Osaka, Japan), all of which offer parallel recording capabilities enabling high throughput screening. In contrast to patch clamp, MEAs record extracellular signals, making them the assay of choice for primary cell research. Protocols are well established for murine and human cardiomyocytes [23–25]

and certain protocols for dissociating embryonic and neonatal rodent primary neurons have been described [26–29]. This chapter describes in more detail a protocol for acutely dissociating mouse primary cortical neurons and the application of MEA technology to record activity from these neurons using Multi Channel Systems platform as an example.

The primary neuron preparation involves dissection of the mouse brain as well as dissociation and culture of the cortical neurons. Here, MEA data acquired from wild-type mouse neuronal cultures is compared to that acquired from neurons of the KCNT1 transgenic mouse model of epilepsy. This approach involves neurons being cultured directly onto MEA plates that contain substrate-integrated recording electrodes, and because the neurons grow into complex neuronal networks within a few weeks [30, 31], it is possible to capture the electrical activity from hundreds to thousands of cells over periods of weeks to months.

The MCS Multiwell-MEA system described in this chapter comprises three hardware components: the interface board, the headstage, and the MEA-multiwell plates (Fig. 2a). The latter are made from epoxy or glass substrates and contain gold recording electrodes as well as an additional circular reference electrode per well (Fig. 2b). To make recordings from the neuronal cultures, the 24-well-epoxy-MEA plates are inserted into the recording headstage, which contains 288 channel amplifiers, integrated heating element and stimulator, and an analogue/digital conversion unit. The headstage is connected to the data acquisition computer via the interface board.

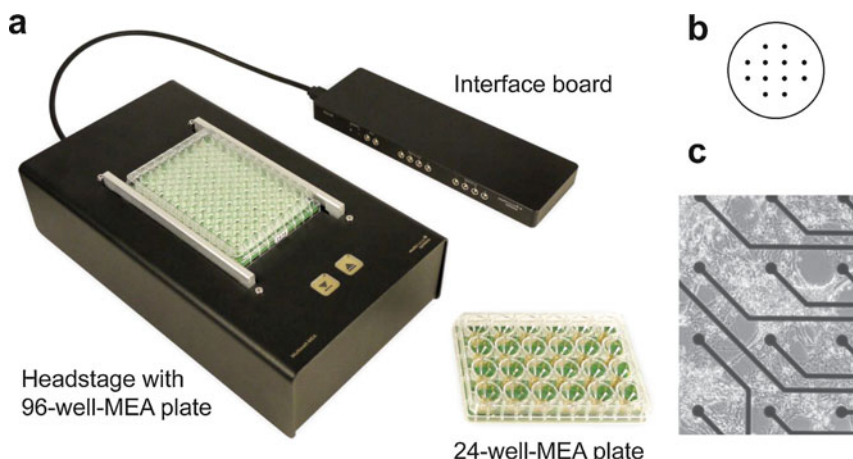


**Fig. 2** The Multiwell-MEA recording system by Multi Channel Systems. (a) Image of the recording headstage (holding a 96-multiwell-MEA, epoxy-based plate) connected to the interface board. Inset: a 24-multiwell-MEA plate (Images courtesy of Multi Channel Systems, Reutlingen, Germany). (b) Schematic showing the configuration of the 12 recording electrodes in one well of a 24-well MEA plate. (c) Neonatal cortical mouse neurons after 14 days in culture on a transparent glass-based single-well-MEA plate

In recent years, MEAs have been increasingly used in epilepsy research. Spontaneous synchronous bursting patterns, epileptiform electrical activity, and responses to antiepileptic drugs are tested both in epileptic mouse models and in human induced pluripotent stem cell-derived neurons [32–36].

Here we describe protocols using the first-generation platform Patchliner and Multi Channel System's multiwell-MEA assay, as examples, to measure evoked and spontaneous electrical output of mouse primary cortical neurons from wild-type mice and a murine model of epilepsy.

---

## 2 Materials

### 2.1 Equipment

1. Pipettes 10, 20, 200, and 1000 µL and tips with filters (Eppendorf South Pacific).
2. Easypet pipetting aid with 1, 5, and 10 mL maxitips (Eppendorf South Pacific).
3. 5, 10, and 25 mL graduated pipettes (Corning).
4. 1 mL transfer pipettes (Sigma-Aldrich).
5. 1.5 mL microcentrifuge tubes (Eppendorf South Pacific).
6. Conical centrifuge tubes (15 mL and 50 mL, Corning).
7. Vented flasks for cell culture (T25, BD Falcon).
8. 24-multiwell-plates (Corning).
9. 10 cm petri dishes (Nunc).
10. Razor blades.
11. 40 µm cell strainers (Corning).
12. Millex® syringe 50 mL with 0.22-µm-pore diameter filter (Sigma-Aldrich).
13. Dissection set: two curved ceramic coated Dumont forceps (0.07 × 0.04 mm); two straight, extra fine, Graefe forceps (0.5 × 0.5 mm); one pair of extra narrow scissors with sharp tips.
14. 24-well-plates for Multiwell-MEA system gold electrodes on epoxy material; 12 recording electrodes per well; electrode diameter 100 µm; electrode distance 700 µm (24W700/100F-288) (Multi Channel Systems, Reutlingen, Germany).
15. Parafilm® (Sigma).
16. Cell culture hood and incubator (set to 37 °C and 5% CO<sub>2</sub>).
17. Water bath (set to 37 °C).
18. Stereoscopic microscope.

19. High speed bench top centrifuge (CT15RT Techcomp Holdings Ltd.).
20. Countess™ automated cell counter (Thermo Fisher Scientific) or a haemocytometer.
21. Heating pad for small laboratory animals set to 37 °C (*see Note 1*).
22. Plasma cleaner (*see Note 2*).
23. UltraBasic bench top pH metre (Denver Instrument).
24. Advanced Instruments Osmo1, single sample microosmometer (Thermo Fisher Scientific).
25. NPC®-16 Patchliner Octo (*see Note 3*), PatchControl<sup>HT</sup> software, single-hole, 4-hole ensemble or 8-hole ensemble NPC®-16 chips (*see Note 4*). NPC®-16 electrode set (*see Note 5*) (Nanion Technologies GmbH).
26. Two EPC 10 USB Quadro patch-clamp amplifiers, multichannel stimulation/acquisition software with programmable experiment control and automation (PATCHMASTER, HEKA Instruments).
27. Computers (64 bit) with 24-inch thin film transistor monitors (*see Note 6*).
28. Multiwell-MEA workstation; includes Multiwell-MEA headstage (with 288 recording channels, integrated heating element and stimulator) and interface board (3.0 Multiboot). Software: Multiwell Screen (data acquisition), DataManager (data export), and Analyzer (data analysis) (MCS, Reutlingen, Germany).
29. Analysis packages including Microsoft Excel, MatLab R2018a (Mathworks), Igor Pro 6.37 (WaveMetrics Inc., USA), Adobe Illustrator CS5.1 (Adobe Systems) and GraphPad Prism 7 (Molecular Devices).

## **2.2 Cells and Reagents**

### **2.2.1 Human Embryonic Kidney Cells**

1. Human embryonic kidney (HEK) 293 cells stably expressing the human Kv3.1<sup>WT</sup> (*see Note 7*).
2. hKCNC1 R320H mutant cDNA (*see Note 8*).
3. Cell culture media: Modified Eagles Medium, 2 mM L-glutamate, 10% fetal bovine serum (FBS), 100 U/mL penicillin and 100 mg/mL streptomycin (P/S), and 400 g/mL geneticin (GIBCO Invitrogen™).
4. Dulbecco's phosphate buffer saline Ca<sup>2+</sup> and Mg<sup>2+</sup> free (D-PBS) (GIBCO Invitrogen™).
5. Accutase® cell detachment solution (GIBCO Invitrogen™).
6. Opti-MEM I reduced serum media (Thermo Fisher Scientific).

7. Lipofectamine 2000 transfection reagent (GIBCO Invitrogen™).
8. Sodium chloride (NaCl), potassium chloride (KCl), magnesium chloride ( $MgCl_2$ ), calcium chloride ( $CaCl_2$ ), D-glucose, 4-(2-hydroxyethyl)piperazine-1-ethanesulfonic acid, N-(2-hydroxyethyl)piperazine-N'-(2-ethanesulfonic acid) (HEPES  $Na^+$  salt), potassium fluoride (KF), ethylene glycol-bis(2-aminoethyl ether)-N,N,N',N'-tetraacetic acid (EGTA), sodium hydroxide (NaOH), hydrochloric acid (HCl), potassium hydroxide (KOH) (Sigma-Aldrich).

#### *2.2.2 Primary Cortical Mouse Neurons*

1. Postnatal day one (P1) or two (P2) WT (C57BL/6) or KCNT1 mice (*see Note 9*).
2. Minimal Essential Media containing: 10 mM HEPES, 0.6% D-glucose, 10% FBS and 1% P/S (GIBCO Invitrogen™).
3. Neurobasal-A media containing: 2% B27 supplement, 1% GlutaMAX, and 1% P/S (Thermo Fisher Scientific).
4. Trypsin-EDTA (Thermo Fisher Scientific).
5. Deoxyribonuclease I (DNase I) from bovine pancreas (Sigma-Aldrich).
6. Hank's Balanced Salt Solution containing 10 mM HEPES (HBSS/HEPES; Sigma-Aldrich).
7. Accutase® cell detachment solution (GIBCO Invitrogen™).
8. Tergazyme (Alconox).
9. Poly-D-lysine (PDL) hydrobromide (Sigma-Aldrich).
10. Laminin (Sigma-Aldrich).
11. Ethanol (Sigma-Aldrich).
12. Cytosine beta-D-arabinofuranoside hydrochloride (Ara-C; Sigma-Aldrich).
13. Trypan blue solution (Thermo Fisher Scientific).

#### *2.2.3 Recording Solutions*

1. Standard extracellular recording solution: 140 mM NaCl, 4 mM KCl, 1 mM  $MgCl_2$ , 2 mM  $CaCl_2$ , 5 mM D-glucose, 10 mM HEPES (pH 7.4 with NaOH).
2. Standard extracellular solution for enhancing seals: 80 mM NaCl, 3 mM KCl, 10 mM  $MgCl_2$ , 35 mM  $CaCl_2$ , 10 mM HEPES (pH 7.4 with HCl) (*see Note 23*).
3. Standard intracellular recording solution: 50 mM KCl, 60 mM KF (*see Note 24*), 10 mM NaCl, 10 mM EGTA, 10 mM HEPES (pH 7.2 with KOH).

### 3 Methods

#### 3.1 HEK 293Cell Culture and Transient Transfection

Conduct the following procedures in a sterile tissue culture fume hood.

1. HEK 293 cells stably expressing hKv3.1<sup>WT</sup> should be cultured in cell culture media (*see Subheading 2.2.1, item 3*) in standard T25 tissue culture flasks and incubated at 37 °C and 5% CO<sub>2</sub>, until subconfluent (*see Note 10*).
2. Passage the cells every 2–3 days using Accutase® cell detachment solution (*see Note 11*) and maintain them at a subconfluent level (*see Note 12*).
3. For each transfection, add 5 µg of selected cDNA to Opti-MEM I reduced serum media to make a total volume of 200 µL in a 1.5 mL tube. In a second tube, add 30 µL Lipofectamine 2000 Reagent to 170 µL Opti-MEM I reduced serum media and mix the contents of each tube thoroughly by gentle pipetting. Incubate the two tubes at room temperature (r.t.) for 5 min, then combine the contents of the two tubes and mix thoroughly by gentle pipetting and incubate at r.t. for a further 20 min. Add the combined transfection mixture to a T25 flask of HEK 293 cells cultured to 60% confluence and incubated at 37 °C and 5% CO<sub>2</sub> for 24 h, following which the transfection media should be replaced with normal culture media and returned to the incubator for a further 24 h (*see Note 13*).

#### 3.2 24-Multiwell Plate Preparation

1. Add 0.5 mL tergazyme per well and incubate at r.t. for at least 12 h. Discard tergazyme and rinse twice with 0.5 mL distilled H<sub>2</sub>O (*see Note 14*).
2. To PDL coat plates add 500 µL PDL per well and incubate at 4 °C for at least 16 h or at 37 °C for 3 h. Following incubation remove PDL and wash plates twice with distilled H<sub>2</sub>O and then dry and UV-sterilize the plates for at least 1 h in a fume hood with the lids removed.
3. Three hours prior to seeding cells, coat the plates with laminin (diluted 1:50 in MEM media *see Subheading 2.2.2, item 2*) using 250 µL per well and incubate at 37 °C.

#### 3.3 Dissection of Mouse Cortex

1. Use newborn mouse pups between P1 and P2.
2. Prewarm MEM media with 0.25% trypsin to 37 °C. Use 1 mL of trypsin in a 50 mL centrifuge tube per mouse pup.
3. Sterilize dissection set with 80% ethanol.
4. Anesthetize mouse pups using appropriate anesthetic (Institutional Animal Care Facility) and perform decapitation with sharp scissors.

5. Use Graefe forceps to hold the head of the mouse pup and remove the skin and skull using Dumont forceps. Gently transfer the brain into a petri dish containing 1 mL of ice-cold solution of HBSS/HEPES.  
Use a stereoscopic microscope and the second set of Graefe and Dumont forceps for steps 6–9 (see Note 15).
6. Use Graefe forceps to hold the cerebellum and gently remove the meninges and the olfactory bulbs using the Dumont forceps.
7. Separate both hemispheres of the brain and gently cut out the hippocampi from the cortices using the Dumont forceps.
8. Transfer cortices to a fresh petri dish containing 1 mL of ice cold HBSS/HEPES.
9. Cut cortices into small pieces with a razor blade and transfer into a 50 mL centrifuge tube using a 1 mL transfer pipette. Keep on ice until the dissection of all pups is complete.
10. Repeat steps 3–9 for each pup, using fresh solutions and consumables (see Note 16).

### **3.4 Dissociation of Mouse Primary Cortical Neurons**

Conduct the following steps in a sterile tissue culture fume hood.

1. Using transfer pipettes, transfer dissected cortical tissue into the 5 mL prewarmed 0.25% trypsin in 50 mL centrifuge tubes and incubate for 6 min in a water bath at 37 °C.
2. Add 500 µL DNase I (diluted in MEM/FBS solution to 640 U/mL) to each tube and incubate for a further 4 min in a water bath at 37 °C.
3. Add 10 mL MEM media to each tube and centrifuge for 5 min at 400 RCF.
4. Discard all, but 0.5 mL media, before adding 6 mL fresh MEM media to each tube and gently triturate the cell pellet using a 1000 µL pipette until a single-cell homogenate is achieved (see Note 17).
5. Place a 40 µm cell strainer onto a fresh 50 mL centrifuge tube and pipet 1 mL MEM media to wet the strainer, then transfer 6 mL of the cell homogenate into the strainer followed by 3 mL MEM media and centrifuge for 5 min at 400 RCF.
6. Mix 10 µL of cell homogenate (from step 4) with 10 µL trypan blue solution in a 1.5 mL microcentrifuge tube and count the cell number using the Countess™ automated cell counter or a haemocytometer.
7. Carefully aspirate media and discard, then resuspend cell pellets in MEM media to a concentration of  $3 \times 10^6$  cells per mL.
8. Take the precoated 24-multiwell MEA plates and the regular 24-multiwell plates (Subheading 3.2, step 3) and aspirate the laminin.

9. Carefully plate 120  $\mu$ L cell suspension, directly over the electrodes in the 24-multiwell MEA plate (approximately  $3.5 \times 10^5$  cells per well) of each well. For patch-clamp experiments, use the regular 24-multiwell plates and seed  $1.0 \times 10^6$  cells per well in 0.5 mL MEM media. Count this as days in vitro 0 (div0). Incubate the MEA plates for 1 h at 37 °C, then add 0.5 mL MEM media per well to the MEA plates.
10. After 24 h (div1), remove all of the MEM media and add 1 mL Neurobasal-A media (containing neurobasal-A media with 2% B27 supplement, 1% GlutaMAX, and 1% P/S) per well.
11. On div3, add 1 mL neural media per well containing 5  $\mu$ M Ara-C.
12. On div5, remove media containing Ara-C and add 1 mL neural media per well.
13. Following div5, change 2/3 of the media with neural media three times a week (*see Note 18*).
14. Neuronal activity can be assessed using MEA recordings at around div7 and synchronized electrical activity is apparent around div14 (*see Note 19*).

### **3.5 Planar Patch-Clamp Solutions**

Electrophysiological solutions should always be prepared with deionized H<sub>2</sub>O and the osmolarity (*see Note 20*) and the pH (*see Note 21*) measured before filtering (*see Note 22*). Solutions can be stored at 4 °C for up to 5 days, but should be warmed to r.t. (20–22 °C) before use.

1. Standard extracellular recording solution (mM): 140 NaCl, 4 KCl, 1 MgCl<sub>2</sub>, 2 CaCl<sub>2</sub>, 5 d-glucose, 10 HEPES (pH 7.4 with NaOH).
2. Standard extracellular solution for enhancing seals (mM): 80 NaCl, 3 KCl, 10 MgCl<sub>2</sub>, 35 CaCl<sub>2</sub>, 10 HEPES (pH 7.4 with HCl) (*see Note 23*).
3. Standard intracellular recording solution (mM): 50 KCl, 60 KF (*see Note 24*), 10 NaCl, 10 EGTA, 10 HEPES (pH 7.2 with KOH).

PatchControlHT software has preprogrammed protocols for liquid handling that is performed by the built-in robotic pipette. The pipette aspirates and dispenses solutions and compounds according to the programmed positions on the system.

### **3.6 Harvesting Cells for Planar Patch Clamp**

For automated planar patch-clamp recordings, an essential feature that determines the success rate is the health of the cells, and to achieve healthy cell cultures, they should be maintained at subconfluent levels. Cells are prepared in suspension and therefore the process of capturing them is completely random, making it impossible to visually select the healthiest looking ones. Furthermore, the

seal formed between the planar chip and the cell membrane, which ultimately influences the standard of the recording, relies on good tissue culture practices.

### 3.6.1 HEK 293 Cells

- Once the cells reach 80% confluence, remove and discard the media from the T25 culture flask, then using 5 mL D-PBS gently wash the cells twice.
- Discard the D-PBS and add 0.5 mL prewarmed Accutase cell detachment solution and gently tilt the flask from side to side to cover all the cells. Incubate for 3 min at 37 °C and 5% CO<sub>2</sub>.
- Add 5 mL culture media to neutralize the Accutase and gently pipet 2–3 times.
- Transfer the cell suspension into a 15 mL conical centrifuge tube and centrifuge at 180 ×  $\text{g}$  for 2 min at r.t. and then discard the supernatant by decanting (*see Note 25*). 180 ×  $\text{g}$
- To resuspend the cell pellet, add a mixture (50:50 ratio) of extracellular recording solution and culture media (*see Note 26*) to attain a density of between 1 × 10<sup>6</sup> and 5 × 10<sup>7</sup> mL. Cells can be counted using a Countess automated cell counter or standard haemocytometer.
- Transfer the cell suspension into the cell hotel (*see Note 27*) and allow the cells to rest for 10 min.

### 3.6.2 Primary Cortical Mouse Neurons

- Seven days after seeding mouse primary cortical neurons, discard the neural media from one well of a 24-well plate (*see Note 28*) and gently wash twice with 0.5 mL D-PBS, using a 1000 µL pipette.
- Dissociate cells with 0.5 mL prewarmed Accutase solution for 8–10 min at r.t.
- Add 1 mL neural media to neutralize the Accutase and gently pipet twice (*see Note 28*).
- Transfer the cell suspension to a 1.5 mL Eppendorf tube and centrifuge at 40 ×  $\text{g}$  for 1 min at r.t., without brake and then discard the supernatant.
- To resuspend the cell pellet, add a 0.5 mL mixture of extracellular recording solution and neural media (50:50 ratio) and pipet gently twice (*see Note 29*).
- Transfer the cell suspension to the cell hotel, disable the automated pipette and allow the cells to rest for 15 min before making recordings.

## 3.7 Automated Planar Patch Clamp Using Patchliner

An optical PCI card in the computer couples ‘PatchControl<sup>HT</sup>’, the Patchliner software to “Patchmaster,” the HEKA amplifier software. The communication between the two software enables PatchControl<sup>HT</sup> to control HEKA amplifier functions through preprogrammed protocols (*Trees*) that can be loaded and modified

for optimisation with different cells. Selection of the appropriate planar chip is determined by the size of the aperture and the number of apertures, which, in turn, influences the resistance (*see Note 30*). The workstation of the Patchliner houses cells, solutions, and compounds, all positioned according to the *Tree* settings and dispensed/aspirated via a robotic pipette that detects changes in capacitance. Chip cartridges are housed on the motorized carriage (“chip wagon”; Fig. 1) which holds up to three chips, allowing for data acquisition of 48 recordings, sequentially, without operator intervention. Microfluidic chambers and planar glass chips are embedded into the cartridges. The measuring head, housing eight headstages, contains the pneumatic and electrical contacts and moves up and down to address the chip cartridge, allowing acquisition of data from eight cells simultaneously. The pipette dispenses intracellular and extracellular recording solutions and a small positive pressure is applied to each chip chamber, independently, and the offsets are corrected. Cells are dispensed from the cell hotel and a –50 mBar suction is applied to attract cells onto each of the eight individual chip apertures. This leads to a small increase in the seal resistance. Seal enhancing solution and additional suction pulses, together with application of negative voltage assist in gigaohm seal formation. External recording solution replaces the seal enhancing solution and additional short suction pulses are applied to obtain whole-cell access. PatchControl<sup>HT</sup> applies negative pressure according to chip resistance, series resistance and slow capacitance and disables any cells that do not meet quality control specifications of seal resistance and series resistance. Once the whole-cell configuration has been established, the experimental part of the protocol commences.

### 3.7.1 General Experimental Setup

1. Open PatchControl<sup>HT</sup> and load a preprogrammed *Tree* (File □ load □ *Tree*). To make any necessary adjustments select the edit mode (⌘□ Edit) (*see Note 31*).
2. Select appropriate chip cartridges and place three chips onto the chip wagon.
3. Compounds should be prepared directly before use (*see Note 32*).
4. Place compounds and recording solutions on the workstation according to the positions defined by the joblist (*see Note 33*).
5. Cells are housed in the cell hotel, where they are aspirated at regular intervals throughout the experiment to prevent clumping and sedimentation (*see Note 34*).
6. It is important to initialize the robot, at the beginning of each day of experiments, to assure that all modules are correctly positioned and a data file is opened within Patchmaster.

7. Activate the *Tree*, to commence an experiment, by selecting the start ►. At the end of each run, the software will loop back and restart, until all chips on the chip wagon have been utilised.

### 3.7.2 Transient Transfection Combined with Temperature with HEK 293 Cells

1. Load a preprogrammed *Tree* for HEK 293 cells to record current–voltage relationship curves ( $K_V IV$ ) combined with temperature control. Modify the protocol so that the temperature of the chip wagon, measuring head, and pipette are elevated simultaneously (e.g., 27 °C, 36 °C, and 39 °C) before each  $K_V IV$  voltage protocol is applied (see Note 35).
2. Select medium resistant single-hole chips (2–4 MΩ) and load three chips onto the chip wagon.
3. Follow steps 5–7 in Subheading 3.7.1.

In the examples shown in Fig. 3, HEK293 cells stably expressing the  $K_V 3.1^{WT}$  and transiently coexpressing  $K_V 3.1^{WT+R320H}$  were captured on a single-hole chip and voltage-clamped at a holding potential of –80 mV and 2 s test depolarizations were applied in 10 mV increments, from –80 mV to +80 mV, every 7 s. When the cells were exposed to increasing temperatures (27 °C, 36 °C, and 39 °C), the unusual shape of the raw current traces reveals the channels temperature sensitivity (Fig. 3a). It is also apparent that transient transfection of the hKCNC1 R320H mutant cDNA affects both the evoked current amplitudes as well as the temperature sensitivity of the channel (Fig. 3a, b).

### 3.7.3 Current- and Voltage-Clamp Recordings with Primary Cortical Mouse Neurons

The electrophysiological properties (e.g., ionic current and action potential (AP) firing) of mouse primary cortical neurons can be measured using the Patchliner in both the voltage-clamp and current-clamp modes, respectively.

1. Load a preprogrammed *Tree* for neurons combined with temperature control. Modify the protocol so that the temperature of the chip wagon and measuring head are at a constant temperature of 27 °C. Potassium ( $I_K$ ) and sodium ( $I_{Na}$ ) are recorded first in the voltage-clamp mode and then APs are subsequently recorded in the current-clamp mode (see Note 36).
2. Select high resistant single-hole chips (5–6 MΩ) for recordings with mouse primary cortical neurons and load three chips onto the chip wagon.
3. Follow steps 5–7 in Subheading 3.7.1.

To induce  $I_K$  and  $I_{Na}$  ionic currents, mouse cortical neurons were held at a holding potential –100 mV and stepped in 5 mV increments to +30 mV. The sampling rate for these recordings was 50 kHz. Typical current recordings of  $I_{Na}$  and  $I_K$  in the voltage-clamp mode are shown in Fig. 4a. Mean normalized current–

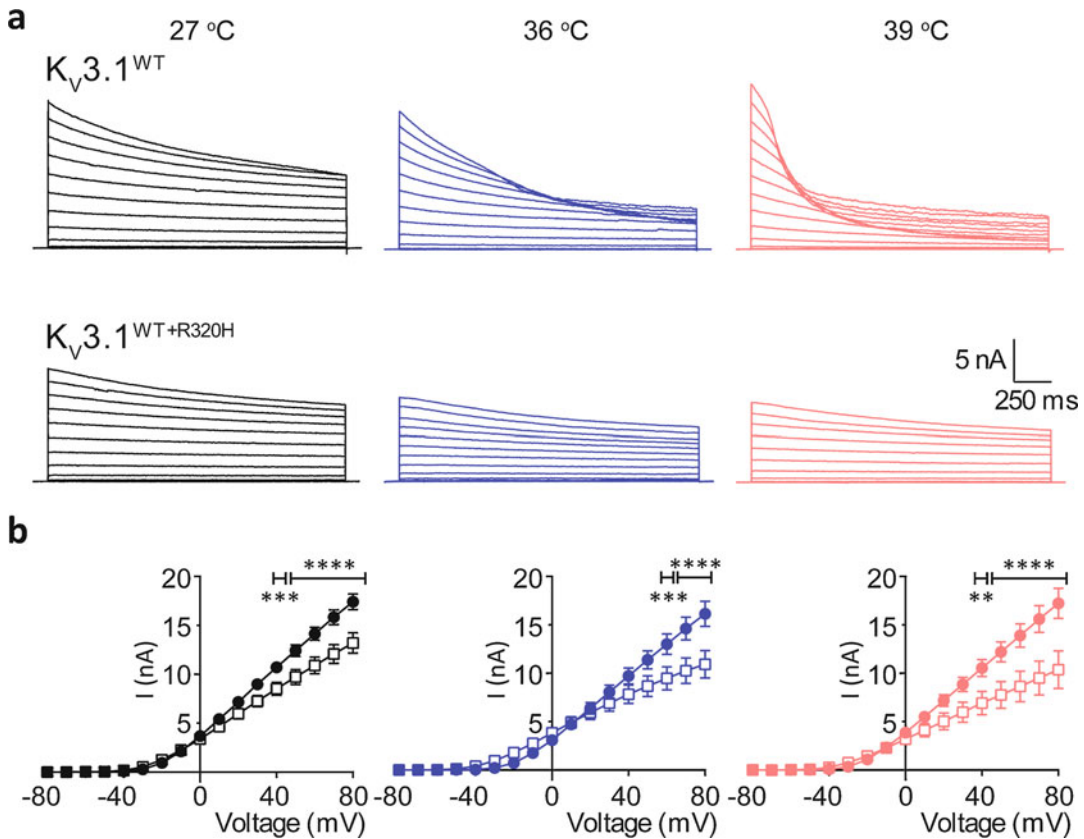


**Fig. 3** Effect of increased temperature on Kv3.1<sup>WT</sup> and Kv3.1<sup>WT+R320H</sup> mutant channels. **(a)** Representative current family traces, for Kv3.1<sup>WT</sup> (top panel) and Kv3.1<sup>WT+R320H</sup> (bottom panel) at 27 °C (black), 36 °C (blue), and 39 °C (pink). Scale bars apply to all traces. **(b)** Average peak current–voltage relationship curves for Kv3.1<sup>WT</sup> (closed circles) and Kv3.1<sup>WT+R320H</sup> (open squares) at 27 °C (black), 36 °C (blue) and 39 °C (pink). Kv3.1<sup>WT</sup> ( $n = 45$ ), 36 °C ( $n = 25$ ) and 39 °C ( $n = 20$ ) and Kv3.1<sup>WT+R320H</sup> channels 27 °C ( $n = 41$ ), 36 °C ( $n = 19$ ) and 39 °C ( $n = 14$ ). Statistical significance marked as \*\*  $p < 0.01$ ; \*\*\*  $p < 0.001$ ; \*\*\*\*  $p < 0.0001$ . (Reproduced from ref. 10 with permission from John Wiley & Sons)

voltage relationship curves for  $I_{\text{Na}}$  and  $I_K$  can be seen in Fig. 4b. A representative trace from a single mouse cortical neuron demonstrates AP firing in response to a 1000-ms square pulse current injection (Fig. 4c).

### 3.8 MEA Recordings

1. Turn on Multiwell-MEA headstage and open the Multiwell Screen software. In the software, set temperature to 37 °C and wait until the headstage reaches the set temperature, which takes approximately 10 min.
2. Remove the cover from the headstage and open its brackets using either the “eject” button in the software or the “>” button on the headstage. Insert MEA plate into the headstage, close the brackets either using the software (“insert”) or the “<” button on the headstage and replace the cover.

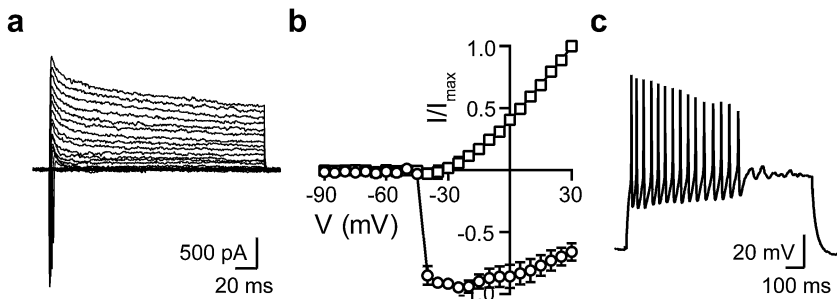


**Fig. 4** Voltage-clamp and current-clamp recorded from primary mouse cortical neurons. (a) Representative raw current responses to a voltage-step protocol. (b) Mean normalized current–voltage relationship curves for inward current (open circles) and outward current (open squares) in response to a voltage-step protocol ( $n = 3$ ). (c) Representative raw trace of AP firing, of a primary mouse cortical neuron, in response to a depolarizing current injection

3. The Multiwell Screen Software should automatically detect the type of MEA plate inserted into the headstage. Otherwise, a pop-up menu will open from which the correct MEA plate type can be selected manually.
4. To record baseline spontaneous electrical activity (see Note 37), edit the following settings in the software:
  - (a) Type your filename into the “lab book” window.
  - (b) To save your file, type in the file path in the “recorder” window.
  - (c) Select the recording time in the “experimental flow” window (typically 5–15 min).
  - (d) In the “data source settings” window, select a sampling rate (typically 10,000–20,000 Hz) and a high- and low-pass filter (typically 1 and 3500 Hz, respectively).
  - (e) Before starting the recording, equilibrate the MEA plate on the headstage for at least 3 min.
  - (f) To start recording, press the “go” button in the software (see Note 38).
  - (g) Once the preselected recording time has elapsed, the recording will automatically stop.
  - (h) To retrieve the MEA plate, remove the cover from the headstage, open the headstage brackets and lift out the MEA plate.

Typical MEA results obtained from cultures of WT (C57BL/6) and transgenic KCNT1 cortical neurons are shown in Fig. 5. Neurons were cultured for 4 weeks and MEA recordings were acquired every second to third day. Spike detection was achieved using in-house MatLab scripts based on precision timing spike detection [37], and single

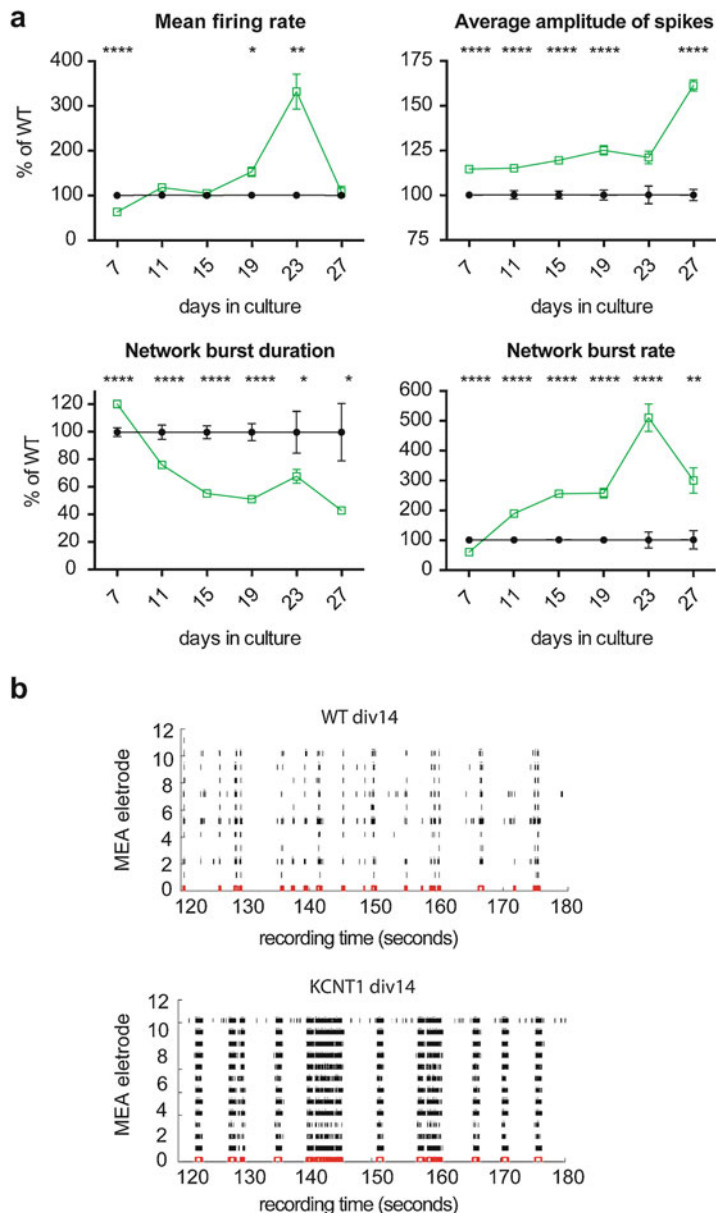


**Fig. 5** MEA recordings of spontaneous electrical activity from primary mouse cortical neurons. **(a)** Mean firing rate, average amplitude of spikes, network burst duration, and network burst rate in neurons derived from WT (black closed circles;  $n = 11$ ) and KCNT1 transgenic (green open squares;  $n = 21$ ) neonatal mice. Statistical significance marked as \*  $p < 0.05$ ; \*\*  $p < 0.01$ ; \*\*\*  $p < 0.001$ ; \*\*\*\*  $p < 0.0001$ . **(b)** Representative raster plots showing spontaneous electrical activity, over a 1-min recording window, for WT (top panel) and KCNT1 transgenic (bottom panel) primary mouse neuronal networks

channel and network bursts were also analyzed using in-house MatLab scripts [29, 38]. Figure 5a shows the mean firing rate, average spike amplitude, network burst duration, and network burst rate of cortical neurons derived from WT and transgenic KCNT1 mice. Neurons derived from KCNT1 transgenic mice have a greater mean firing rates and higher average spike amplitudes, when compared to WT neurons, suggestive of greater spontaneous electrical activity. Furthermore, the shorter duration of individual network bursts and significantly increased network burst rate, observed with these transgenic neurons, is indicative of more synchronized firing. All of these features are nicely illustrated in the representative raster plots (Fig. 5b), obtained over a 1 min recording window, which show very clearly that the transgenic neurons display more spontaneous, synchronized activity than the WT neurons. Overall, MEA technology is a useful tool for investigating phenotypical differences between primary neurons derived from different epilepsy mouse models.

---

## 4 Notes

1. To avoid hypothermia, keep the mouse pups either with their mother or on a heating pad for small laboratory animals, set to 37 °C.
2. Reuse of the MEA plates is not recommended by the manufacturer, but they can be used up to three times when treated with Tergazyme and plasma cleaned for 3.5 min after each use.
3. The NPC®-16 Patchliner Octo is being used here, but other automated patch-clamp platforms with similar capabilities have also been validated.
4. NPC®-16 chips are single use and are generally manufactured with three different resistance: low (1–2 MΩ), medium (2–4 MΩ), and high (5–6 MΩ). Nanonix will produce customer specific chips, according to cell size, upon request. Chips are also available with single holes or ensembles of 4 or 8 holes. Ensemble chips are ideal for ligand-gated channels, especially if currents are small in amplitude, because the currents are summated.
5. Chloride electrodes in bleach-filled chambers for 30–60 min and then rinse with deionized water and air-dry before use.
6. Minimum specifications for the computer include Windows 10 (Microsoft) with a 64-bit operating system and an optical PCI card for communication with the HEKA amplifiers, but any brand can be used.
7. For these experiments, a stable cell-line expressing Kv3.1<sup>WT</sup> was used, but any stable cell-line can be used on this system.

8. hKCNC1 R320H cDNA was used here, but any cDNA clone can be substituted. The mutation c.959G>A (p.R320H) was inserted in the hKCNC1 cDNA (NM\_004976) cloned in a pCMVEntry vector (OriGene Technologies, Rockville, MD) using Quick Change kit (Stratagene, San Diego, CA) according to the manufacturer's instructions.
9. One litter (usually between four and eight pups) will yield sufficient cells for three to four 24-well-MEA plates.
10. Cells should be grown to a maximum confluence of 70–80%.
11. Accutase® cell detachment solution gently dissociates mammalian cells from support substrates and from each other; however, other detachment agents can be used (e.g., trypsin or detachin).
12. When cells are allowed to grow to a confluence greater than 80%, aggregates tend to form, which in turn leads to lower capture rates, poor seal formation and difficulties breaking into the whole-cell configuration.
13. A Lipofectamine 2000 Reagent protocol, available at (<https://www.ecu.edu/cs-dhs/biochemistry/upload/Transfection-Protocol.pdf>), was used to transiently transfet the cells. It should be noted that other transfection kits are also suitable for transient expression of ion channel proteins.
14. The preparation of the 24-multiwell MEA plates and the regular 24-multiwell plates is exactly the same. Be careful not to let any liquid get into the outer casing of the MEA plates as this will lead to noisy recordings.
15. Skull removal dulls the forceps, so it is important to keep one set for skull removal and the second set for hippocampi dissection.
16. Cortices from 4 to 5 mouse pups can be pooled in one 50 mL centrifuge tube, but be sure to maintain the correct ratios of trypsin, DNase I solution, and MEM/FBS media.
17. Achieving a single-cell homogenate can take up to 30–40 titration steps.
18. Take care not to detach the cells during media changes when culturing the neurons over a prolonged time. Using a graduated pipette to remove media works better than a vacuum aspirator.
19. Electrical outputs alter significantly directly following media changes, so it is recommended that recordings are made 24–48 h after media change.
20. Use a freezing-point osmometer to measure the osmolarity (external solutions ~298 mOsm/L and internal solution ~285 mOsm/L) of all patch-clamp solutions.

21. Generally, the pH of solutions should not require adjustment when pH adjusted stock solutions of each salt are used. External solutions should be pH 7.4 whilst internal solutions should be pH 7.2.
22. Recording solutions should be sterile filtered using a 50 mL syringe with a 0.22- $\mu\text{m}$ -pore diameter filter attached. This is particularly important for the internal recording solution.
23. To obtain a gigaohm seal, it is usually necessary to use an external solution that contains a high concentration of  $\text{Ca}^{2+}$  ions. This seal enhancing solution is replaced once a gigaohm seal is achieved, but before establishing whole-cell access. Calcium can be replaced by barium as the charge carrier to avoid calcium-dependent inactivation when working with voltage-gated calcium channels, since most voltage-gated calcium channels also conduct barium ions [39, 40].
24. Although the mechanism is not fully understood, it has long been known that fluoride ions in the intracellular solution improve gigaohm seal formation and stabilize the cell membrane [41].
25. To avoid shearing the cell membranes, it is recommended to set the centrifuge acceleration rate to 6 and deceleration rate to 3 (0 is the slowest and 9 is the fastest acceleration rate and 9 is the shortest and 0 to longest brake time).
26. When cells are resuspended in a mixture of recording solution and culture media (50:50), their bench life is greatly improved, and they remain viable for up to 4 h at room temperature.
27. Cells are housed in the “cell hotel,” where they are kept from clumping and sedimenting by gentle automated pipetting, which improves cell viability. The pipetting volume and speed is preprogrammed, but can be changed by the operator.
28. Primary neurons are extremely fragile and therefore must be handled very gently, so minimize the number of times that they are pipetted.
29. When working with primary cells, it is often challenging to harvest cells in large numbers; however, good cell capture rates can still be achieved with as few as 1000 cells/mL [42].
30. The capacitance of the cell, determines the size of the aperture (chip resistance) required. As an example, medium resistance chips are ideal for use with HEK293 cells and CHO cells [43] and high resistance chips are ideal for use with mouse osteoblasts [17] and neurons. For example, if the capacitance of the cell is low, they will pass through a low resistance chip aperture when suction is applied, and conversely, high capacitance cells will not form good seals on high resistance chips.

31. PatchControl<sup>HT</sup> comes with a range of preprogrammed *Trees* with different experimental conformations (e.g., Voltage-clamp, Current-clamp, Cell-attached) and experimental paradigms (e.g., Voltage-gated, Ligand-gated) for specific cellular characteristics (e.g., cell capacitance, membrane stability) and channel types (e.g., Na<sup>+</sup>, K<sup>+</sup>, Ca<sup>2+</sup> channels or P2X, GABA, NMDA receptors) in which, via easy drag-and-drop commands, parameters such as pressure and voltage can be adjusted. Application notes are available at <http://www.nanion.de>.
32. Compounds should be prepared directly before use to avoid precipitation. Certain compounds adhere to other substrates; therefore, it is best to use glassware rather than plastic to avoid underestimation of compound concentration.
33. The joblist defines the position of the compounds, the volume and speed of application and the selection of the appropriate HEKA pulse generator file within Patchmaster.
34. Regular aspiration of cells retains viability for at least 4 h after preparation in suspension, although some deterioration in success rates has been observed after 3 h. Furthermore, if cells are placed in the cell hotel of the cooling plate (Fig. 1) at 15 °C, seal resistance and whole-cell stability, and subsequently data quality, are improved.
35. The recording chamber, chip wagon, and pipette can be heated simultaneously or independently. These modules can be heated to 80 °C, however, it is not recommended to increase the temperature above 55 °C. It can take some time for the modules to heat up so leave sufficient time to reach the set temperature. The temperature of the cells and the solutions can also be cooled via an add-on cooling plate (Fig. 1).
36. After evaluation of ionic currents in the voltage-clamp mode, the *Tree* switches the amplifiers into current-clamp mode and proceeds on to AP measurements. To induce AP responses in neurons, they were held at a constant membrane potential of −70 mV. The program then finds the stimulus threshold for each individual cell by applying a 1 ms depolarizing pulse. The values for the thresholds are then set in the pulse generator file (pgf) in Patchmaster. PatchControl<sup>HT</sup> then loads another pgf and the current-clamp protocol uses these set values so that each individual cell is stimulated accordingly.
37. Within the Multiwell Screen software, several experimental conditions can be defined (e.g., stimulation electrodes and protocols, chemical compound dosing protocols, and compound dilution series).

38. If recordings are particularly noisy, try removing the plate and wiping the underside with 80% ethanol. Residual moisture will lead to noisy channels.

## Acknowledgments

The authors wish to thank Professor S Petrou, whose National Health and Medical Research Council (NHMRC) Project Grant (1106027) supported the research using mouse primary cortical neurons. The Florey Institute of Neuroscience and Mental Health is supported by Victorian State Government infrastructure funds.

## References

1. Steinlein OK, Mulley JC, Propping P et al (1995) A missense mutation in the neuronal nicotinic acetylcholine receptor alpha 4 subunit is associated with autosomal dominant nocturnal frontal lobe epilepsy. *Nat Genet* 11:201–203
2. Helbig I, Heinzen EL, Mefford HC et al (2016) Primer part 1—the building blocks of epilepsy genetics. *Epilepsia* 57:861–868
3. Perucca P (2018) Genetics of focal epilepsies: what do we know and where are we heading? *Epilepsy Curr* 18:356–362
4. Epi PMC (2015) A roadmap for precision medicine in the epilepsies. *Lancet Neurol* 14:1219–1228
5. Barros F, Pardo LA, Dominguez P et al (2019) New structures and gating of voltage-dependent potassium ( $K_v$ ) channels and their relatives: a multi-domain and dynamic question. *Int J Mol Sci* 20:E248
6. Markham MR, Kaczmarek LK, Zakon HH (2013) A sodium-activated potassium channel supports high-frequency firing and reduces energetic costs during rapid modulations of action potential amplitude. *J Neurophysiol* 109:1713–1723
7. Rudy B, McBain CJ (2001)  $Kv3$  channels: voltage-gated  $K^+$  channels designed for high-frequency repetitive firing. *Trends Neurosci* 24:517–526
8. Sierra F, Comas V, Buno W et al (2005) Sodium-dependent plateau potentials in electrocytes of the electric fish *Gymnotus carapo*. *J Comp Physiol A Neuroethol Sens Neural Behav Physiol* 191:1–11
9. Bhattacharjee A, Gan L, Kaczmarek LK (2002) Localization of the slack potassium channel in the rat central nervous system. *J Comp Neurol* 454:241–254
10. Oliver KL, Franceschetti S, Milligan CJ et al (2017) Myoclonus epilepsy and ataxia due to KCNC1 mutation: analysis of 20 cases and  $K(+)$  channel properties. *Ann Neurol* 81:677–689
11. Oyrer J, Maljevic S, Scheffer IE et al (2018) Ion channels in genetic epilepsy: from genes and mechanisms to disease-targeted therapies. *Pharmacol Rev* 70:142–173
12. Milligan CJ, Li M, Gazina EV et al (2014) KCNT1 gain of function in 2 epilepsy phenotypes is reversed by quinidine. *Ann Neurol* 75:581–590
13. Hamill OP, Marty A, Neher E et al (1981) Improved patch-clamp techniques for high-resolution current recording from cells and cell-free membrane patches. *Pflugers Arch* 391:85–100
14. Neher E, Sakmann B, Steinbach JH (1978) The extracellular patch clamp: a method for resolving currents through individual open channels in biological membranes. *Pflugers Arch* 375:219–228
15. Bell DC, Dallas ML (2018) Using automated patch clamp electrophysiology platforms in pain-related ion channel research: insights from industry and academia. *Br J Pharmacol* 175:2312–2321
16. Milligan CJ, Li J, Sukumar P et al (2009) Robotic multiwell planar patch-clamp for native and primary mammalian cells. *Nat Protoc* 4:244–255
17. Petty SJ, Milligan CJ, Todaro M et al (2016) The antiepileptic medications carbamazepine

- and phenytoin inhibit native sodium currents in murine osteoblasts. *Epilepsia* 57:1398–1405
18. Alexander SP, Catterall WA, Kelly E et al (2015) The concise guide to PHARMACOL-OGY 2015/16: voltage-gated ion channels. *Br J Pharmacol* 172:5904–5941
  19. Droege MH, Gross GW, Hightower MH et al (1986) Multielectrode analysis of coordinated, multisite, rhythmic bursting in cultured CNS monolayer networks. *J Neurosci* 6:1583–1592
  20. Gross GW, Rieske E, Kreutzberg GW et al (1977) A new fixed-array multi-microelectrode system designed for long-term monitoring of extracellular single unit neuronal activity in vitro. *Neurosci Lett* 6:101–105
  21. Thomas CA Jr, Springer PA, Loeb GE et al (1972) A miniature microelectrode array to monitor the bioelectric activity of cultured cells. *Exp Cell Res* 74:61–66
  22. Pine J (2006) A history of MEA development. In: *Advances in network electrophysiology*. Springer, New York, pp 3–23
  23. Banach K, Halbach MD, Hu P et al (2003) Development of electrical activity in cardiac myocyte aggregates derived from mouse embryonic stem cells. *Am J Physiol Heart Circ Physiol* 284:H2114–H2123
  24. Sala L, Ward-Van Oostwaard D, Tertoolen LGJ et al (2017) Electrophysiological analysis of human pluripotent stem cell-derived cardiomyocytes (hPSC-CMs) using multi-electrode arrays (MEAs). *J Vis Exp* 123:1–15
  25. Tertoolen LGJ, Braam SR, Van Meer BJ et al (2018) Interpretation of field potentials measured on a multi electrode array in pharmacological toxicity screening on primary and human pluripotent stem cell-derived cardiomyocytes. *Biochem Biophys Res Commun* 497:1135–1141
  26. Berdondini L, Massobrio P, Chiappalone M et al (2009) Extracellular recordings from locally dense microelectrode arrays coupled to dissociated cortical cultures. *J Neurosci Methods* 177:386–396
  27. Jimbo Y, Kawana A, Parodi P et al (2000) The dynamics of a neuronal culture of dissociated cortical neurons of neonatal rats. *Biol Cybern* 83:1–20
  28. McSweeney KM, Gussow AB, Bradrick SS et al (2016) Inhibition of microRNA 128 promotes excitability of cultured cortical neuronal networks. *Genome Res* 26:1411–1416
  29. Mendis GDC, Berecki G, Morrisroe E et al (2019) Discovering the pharmacodynamics of conolidine and cannabidiol using a cultured neuronal network based workflow. *Sci Rep* 9:121
  30. Bettencourt LM, Stephens GJ, Ham MI et al (2007) Functional structure of cortical neuronal networks grown in vitro. *Phys Rev E Stat Nonlinear Soft Matter Phys* 75:021915
  31. Gullo F, Maffezzoli A, Dossi E et al (2009) Short-latency cross- and autocorrelation identify clusters of interacting cortical neurons recorded from multi-electrode array. *J Neurosci Methods* 181:186–198
  32. Grosser S, Queenan BN, Lalchandani RR et al (2014) Hilar somatostatin interneurons contribute to synchronized GABA activity in an in vitro epilepsy model. *PLoS One* 9:e86250
  33. Gullo F, Manfredi I, Lecchi M et al (2014) Multi-electrode array study of neuronal cultures expressing nicotinic beta2-V287L subunits, linked to autosomal dominant nocturnal frontal lobe epilepsy. An in vitro model of spontaneous epilepsy. *Front Neural Circuits* 8:87
  34. Ishii MN, Yamamoto K, Shoji M et al (2017) Human induced pluripotent stem cell (hiPSC)-derived neurons respond to convulsant drugs when co-cultured with hiPSC-derived astrocytes. *Toxicology* 389:130–138
  35. Odawara A, Katoh H, Matsuda N et al (2016) Physiological maturation and drug responses of human induced pluripotent stem cell-derived cortical neuronal networks in long-term culture. *Sci Rep* 6:26181
  36. Odawara A, Matsuda N, Ishibashi Y et al (2018) Toxicological evaluation of convulsant and anticonvulsant drugs in human induced pluripotent stem cell-derived cortical neuronal networks using an MEA system. *Sci Rep* 8:10416
  37. Maccione A, Gandolfo M, Massobrio P et al (2009) A novel algorithm for precise identification of spikes in extracellularly recorded neuronal signals. *J Neurosci Methods* 177:241–249
  38. Mendis GD, Morrisroe E, Petrou S et al (2016) Use of adaptive network burst detection methods for multielectrode array data and the generation of artificial spike patterns for method evaluation. *J Neural Eng* 13:026009
  39. Ferreira G, Yi J, Rios E et al (1997) Ion-dependent inactivation of barium current through L-type calcium channels. *J Gen Physiol* 109:449–461
  40. Veselovskii NS, Fedulova SA (1986) Effect of replacing calcium ions with barium ions in studies of the inward currents of mammalian neurons. *Neurofiziologiya* 18:313–318

41. Kostyuk PG, Krishtal OA, Pidoplichko VI (1975) Effect of internal fluoride and phosphate on membrane currents during intracellular dialysis of nerve cells. *Nature* 257:691–693
42. Becker N, Stoelzle S, Gopel S et al (2013) Minimized cell usage for stem cell-derived and primary cells on an automated patch clamp system. *J Pharmacol Toxicol Methods* 68:82–87
43. Richards KL, Milligan CJ, Richardson RJ et al (2018) Selective NaV1.1 activation rescues Dravet syndrome mice from seizures and premature death. *Proc Natl Acad Sci U S A* 115: E8077–E8085



# Chapter 8

## Dynamic Clamp on a Windows PC

Lorin S. Milescu and Joël Tabak

### Abstract

Dynamic clamp is a powerful tool for interfacing computational models and real cells. We describe here how to set up and carry out dynamic clamp experiments using a patch clamp amplifier, a National Instruments data acquisition card, and the freely available QuB software that operates on a PC running MS Windows.

**Key words** Dynamic clamp, Patch clamp, Real-time computation, QuB, Ion channels, Action potential

### Abbreviations

AI	analog input
AO	analog output
DAQ	data acquisition
DCE	dynamic clamp engine
MC	model cell
NI	National Instruments;

---

### 1 Introduction

Dynamic clamp is a powerful tool for studying the contribution of ion channels to the electrical activity of live, excitable cells. It is a hybrid method, combining patch-clamp electrophysiology with mathematical models of ion channels [1–4]. This allows the investigator to easily manipulate any parameter of an ion channel model, as in a computer simulation, and to immediately observe how the change affects the electrical activity of a real cell. Thus, dynamic clamp bypasses the weaknesses of both experimental electrophysiology, where a channel can be blocked but its key parameters cannot be modified, and mathematical modelling, where channel parameters can be arbitrarily changed but the model may not

represent real cells accurately. As a result, dynamic clamp has been used to directly show how voltage-dependent ion channels influence the properties of action potentials and spiking patterns in individual cells, and to artificially connect pairs of cells to determine how cell-to-cell connections affect the activity of the coupled cells [4, 5].

Dynamic clamp is a real-time control loop, where the following steps are repeated at high throughput rates: (1) read the membrane voltage from the patch-clamp amplifier through a digital acquisition card, (2) send that voltage value to the mathematical model, (3) advance (solve) the model over a small time step, (4) calculate an output current, and (5) inject that current into the cell through the data acquisition card and patch-clamp amplifier. These operations can be implemented with dedicated hardware or in software. Hardware solutions are generally easy to use and run at high rates but are inherently limited in terms of model complexity, and they are more expensive because they require custom electronics (but a low-cost, Arduino-based dynamic clamp exists [6]). Software solutions require only a general-purpose data acquisition card and a computer and thus can be cheaper, and the mathematical models that can be approached are typically more complex. Historically, dynamic clamp software has relied on real-time computer operating systems, which are more difficult to manage but maintain a tight real-time performance [7, 8]. However, advances in CPU and digitizer technology have enabled more user-friendly dynamic clamp programs that run on Microsoft Windows [9–11] but perform just as well as real-time Linux applications [12].

In this chapter, we introduce the reader to dynamic clamp with QuB [13], a freely available software that has been tested over many years in multiple labs, and is being actively maintained and developed. QuB runs on common Windows PC computers and features state-of-the-art real-time performance and a sophisticated scripting language that allows the user to develop complex models, including Markov models of ion channels and compartmental models of neurons, and solve them with fast deterministic or stochastic algorithms [14]. With QuB, one can add dynamic clamp functionality to an existing patch-clamp rig for the cost of a National Instruments data acquisition card, which can be as little as \$1000. We describe here how to set up QuB for dynamic clamp, including calibrating the gains and offsets, and discuss a step-by-step example where a physical model cell connected to the headstage of the amplifier is converted into a spiking neuron. The script used in this example can be taken as a starting point for more complex applications, together with the other examples available on the QuB website. For more information on the computational methods used in QuB for dynamic clamp, consult [13, 14]. For dynamic clamp applications with QuB, consult, for example, [15–18].

---

## 2 Materials

### 2.1 Patch-Clamp Amplifier

A patch-clamp amplifier with true current clamp capability and typical compensation circuitry (pipette capacitance, series resistance, etc.). Although performance and convenience may vary, any amplifier that has these two features should work well with QuB. In our labs, we tested EPC 9 and 10 (HEKA) and Multiclamp 700B (Molecular Devices) amplifiers. We also tested an Axon 200B amplifier (Molecular Devices) and found it satisfactory, if not ideal.

### 2.2 Model Cell

A physical model cell (MC) with switchable RC circuitry that emulates bath, on-cell, and whole-cell configurations. Patch-clamp amplifiers are typically sold with a model cell. If not available, consider making one.

### 2.3 Computer

A PC running a Windows version compatible with QuB (XP, 7, 8, or 10). The computer must have a PCIe or PCI slot available for the National Instruments (NI) data acquisition (DAQ) card. Dynamic clamp performance is commensurate with the characteristics of the processor, but any newer generation Intel or AMD processor with four cores (two is the absolute minimum) should be adequate for simulating complex models at high rates. For ultimate real-time performance, we recommend a dedicated computer with a dual Intel Xeon processor.

### 2.4 Data Acquisition Card

A NI DAQ card compatible with the most recent NIDAQmx drivers. We have used PCIe-6351 and PCIe-6361 cards with excellent results. Together with the card, purchase a BNC connector box (e.g., BNC 2110) and the cable that connects them.

### 2.5 Connecting Cables

Two BNC cables for connecting the amplifier to the DAQ card, via the BNC connector box.

---

## 3 Methods

### 3.1 Install the Data Acquisition Card

Follow the procedure outlined by NI in their card installation brochure. Go through the following steps: (1) install the driver; (2) restart the computer and verify that the NI software has been installed and the computer operates properly; (3) shut down the computer; (4) physically install the NI card in the computer; and (5) restart the computer. The NIDAQmx driver will automatically detect the card and install it. Verify the proper operation of the card by running the Test Panels utility provided by NI in their Measurement and Automation Explorer software. By default, the card is named *Dev1* if it is the very first installed on the computer. You

must refer to this name when you set up the dynamic clamp engine (DCE) in QuB.

### **3.2 Connect the Data Acquisition Card to the Patch-Clamp Amplifier**

First, use the NI cable to hook the BNC connector box to the DAQ card installed on the computer. Then, use BNC cables to make two connections between the BNC box and the patch clamp amplifier: (1) connect the voltage output of the amplifier to one of the analog input (AI) channels (e.g., AI0) of the BNC box; and (2) connect one of the AO channels (e.g., AO0) of the BNC box to the current command input of the amplifier. Depending on your electrophysiology equipment, you may want to use a switchbox for actual dynamic clamp experiments (*see Note 1*).

### **3.3 Connect the Model Cell to the Amplifier**

For the purpose of this tutorial, connect the MC to the amplifier’s headstage. For dynamic clamp experiments with live cells, replace the MC with the electrode holder.

### **3.4 Install the QuB Software**

Go to the QuB website (<http://milesculabs.org/qub.html>) and follow instructions for how to install QuB. Download the example files that will be used in this tutorial. You will also find materials that describe the scripting language. If you encounter difficulties during the installation process, given the existing variety of Windows versions and user configurations, contact the authors for assistance.

### **3.5 Set up the Real-Time Interface in QuB**

For convenience, QuB has a number of predefined user interfaces, each displaying a layout of windows appropriate for a given task, including dynamic clamp experiments. These predefined interfaces can be further customized, and new ones can be created (*see Note 2*). For our purpose, select the *Real-time* interface, which by default brings in view the *Script*, *Scriptlets*, *Chart*, *TriggerGraph*, and *Report* windows, as shown in Fig. 1. The *Script* window is where we write the code that creates and customizes the DCE and defines the experiment. To the right of the *Script* window there is a *Parameter editor*, where script parameters are listed and their values are displayed and can be modified. The *Scriptlets* window contains optional user-defined macros (“scriptlets”) to change several parameters at once or to define complex dynamic clamp protocols and run them automatically. The *Chart* window provides a real-time display of data streams containing acquisition variables, such as membrane voltage or injected current, or any other quantity that needs to be continuously visualized and saved to file, as desired by the user. The *TriggerGraph* window can be used to visualize in real-time action potentials or other signals detected in the charted data streams. Finally, the *Report* window is a text interface used by the DCE (and other functions) to communicate status and performance.

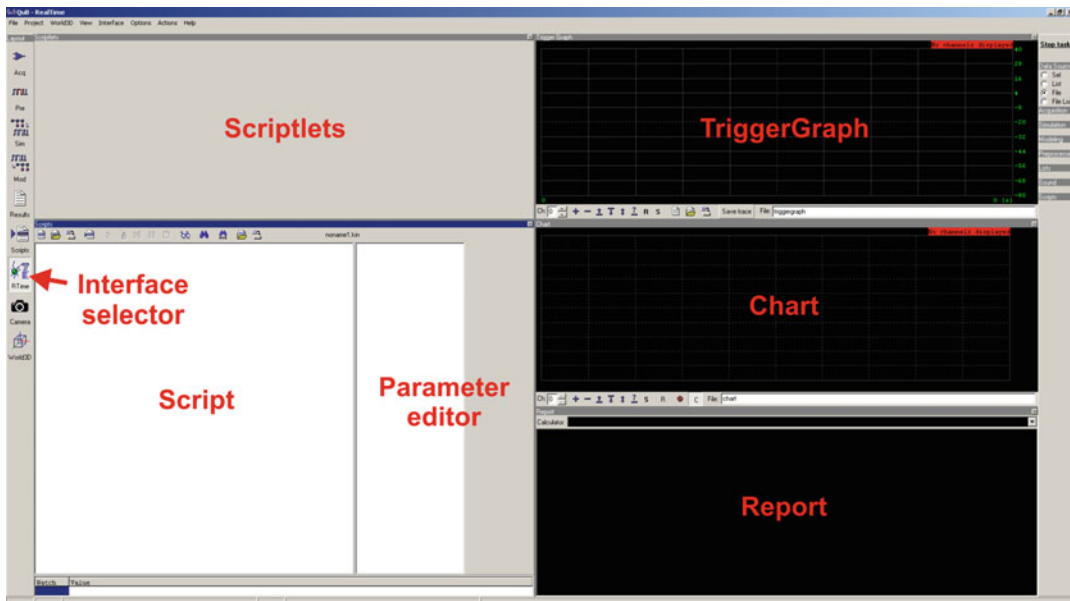


**Fig. 1** Setting up the real-time interface in QuB

### 3.6 Calibrate Gains and Offsets

The patch-clamp amplifier interfaces with the DAQ card via voltage signals that encode the physical quantity measured (e.g., membrane voltage, sent by the amplifier to the DCE) or are used as a command (e.g., the injected current, sent by the DCE to the amplifier). The conversion between a physical quantity and voltage is subject to a scaling factor (intended) and an offset (typically an artifact). These values must be accurately provided to the DCE, to ensure that a given quantity takes the same value at both sending and receiving ends. For example, artifactual offsets of as much as a few tens of pA are not uncommon, and these errors in the injected current can have dramatic effects on the spiking activity of some neurons. Also, errors of a few mV in the measured voltage can be important when using dynamic clamp to inject voltage-dependent conductances (e.g., sodium channels) into the cell.

To conveniently determine the scaling and offset for the two amplifier/DAQ card connections described above, we provide a simple script, called “Calibration.kin”, the content of which is listed at the end of this chapter. Load this file in QuB (*Main Menu>File>Open Kinetic script*). The code performs the following steps: (1) creates the DCE; (2) declares a variable  $V$  that represents the membrane voltage read from the amplifier, and a parameter  $I_{out}$  that represents the injected current sent to the amplifier; (3) sets up the DCE input and output parameters, including the AI and AO channel numbers and the scaling and offset factors; (4) instructs the DCE to stream  $V$  and  $I_{out}$  to the *Chart* window; and (5) starts the DCE. Note that the *TriggerGraph* and *Scriptlets*



**Fig. 2** Calibration of gains and offsets. Chart window displays the input voltage and the output current

windows are not used here. Compile the script by pressing the *Compile* button at the top of the *Scripts* window. If successful, the *Run* button becomes active and the script is ready to be executed.

With the MC connected to the headstage, switch the amplifier into voltage-clamp mode and then take both the MC and the amplifier through the sequence of bath, on-cell, and whole-cell configurations. For each configuration, perform the necessary compensations (pipette offset, fast and slow capacitance, series resistance, etc.). Then, switch the amplifier into current-clamp mode and enable external current command. Set a gain that you will normally use later on for current clamp and dynamic clamp experiments. Run the calibration script in QuB. The DCE starts and you will now see two streams of data being displayed in the *Chart* window, one for *V* and one for *I\_out*, as you see in Fig. 2. The value of *I\_out* is also shown in the parameter editor window, at the right of the *Scripts* window. This value can be modified in real-time and the amplifier will respond immediately.

You are now ready to calibrate. Basically, you have to find a set of scaling and offset factors that allow QuB and the amplifier software to “see” the same values for *V* and *I\_out*. We start with *V*. Use the software that controls the amplifier (e.g., PatchMaster or pClamp) to apply a holding current of, say, +100 pA. Make sure that this value does not saturate the amplifier, given the resistance of your specific model cell. If necessary, reduce this value. Now read and write down the values of the membrane voltage, as reported by the amplifier’s software and by QuB. In our own test, the amplifier (EPC10) reports 46 mV, whereas QuB reports 4.393 mV, as in Fig. 2. Repeat these steps with a negative value for the holding current (e.g., -100 pA). In our test, the amplifier now reports -54 mV, whereas QuB reports -5.079 mV. Thus, over the tested range of the holding current, the amplifier reports an excursion in voltage  $\Delta V_{\text{Amp}} = 100 \text{ mV}$ , whereas QuB reports  $\Delta V_{\text{QuB}} = 9.472 \text{ mV}$ . From these values, we calculate a new scaling factor of  $\Delta V_{\text{Amp}} / \Delta V_{\text{QuB}} = 100 / 9.472 = 10.557$ . Do your own calculation, then stop the script and type your value in the code:

```

...
ode.setinput(
...
scale = 10.557,      //Type your scaling value here
offset      = 0,
...
);

```

Restart the script (first hit *Compile*, then *Run*) and verify that now the amplifier and QuB report equal voltage ranges (but not necessarily the same individual values). Repeat this procedure as necessary. Once the scaling is correctly assigned, calculating the offset for  $V$  is simple: set the holding current to zero and calculate the difference between the voltage value reported by the amplifier  $V_{Amp} = -4$  mV and the value reported by QuB  $V_{QuB} = -3.6$  mV. The offset is equal to  $V_{Amp} - V_{QuB} = -0.4$  mV. Type this value in the code:

```

ode.setinput(
...
scale = 10.557,
offset      = -0.4,      //Type your offset value here
...
);

```

Now restart the script and verify that QuB and the amplifier report the same value for  $V$ , for whatever value you assign to the holding current. Aim for a sub-mV error.

To calibrate for  $I_{out}$ , use QuB to set different values for  $I_{out}$  (e.g.,  $\pm 100$  pA), and compare them with what the amplifier reports for the external current. Make sure that the amplifier itself injects no current, other than the external command ( $I_{out}$ ) received from QuB. Follow a similar procedure as for  $V$ , to calculate first the scaling and then the offset for  $I_{out}$ . Depending on your amplifier and your settings (e.g., the external command gain), you may find that the initial scaling factor of 1 is too large and the amplifier is saturated. In this case, start the calibration with a smaller gain, e.g., 0.001. Type this value in the code:

```

...
ode.setoutput(
...
scale = 0.001, //Type your initial scaling value here
offset      = 0,
...
);

```

Now restart the script, set  $I_{out}$  first to +100 and then to -100 pA in QuB, and read the current values reported by the amplifier. In our case, these are 93 and -108 pA, respectively. The new scaling factor is equal to  $0.001 \times \Delta I_{QuB}/\Delta I_{Amp} = 0.001 \times 200/201 = 0.9975 \times 10^{-3}$ . Type this value in the code:

```

ode.setoutput(
...
scale = 0.9975e-3, //Type your scaling value here
offset      = 0,
...
);

```

Now restart, set  $I_{out} = 0$  in QuB and read the value reported by the amplifier,  $I_{Amp} = -7.5$  pA. The offset can be calculated as  $I_{out} - I_{Amp} = 7.5$  pA. Type this value in the code:

```

ode.setoutput(
...
scale = 0.9975e-3,
offset      = 7.5, //Type your offset value here
...
);

```

Restart and verify that QuB and the amplifier report the same value for current. Aim for a sub-pA error. The calibration is now complete and you are ready for dynamic clamp experiments (see Note 3).

### 3.7 Convert the Model Cell into a Spontaneously Spiking Neuron

To understand the general principles of dynamic clamp, as well as the details of implementation in QuB, it is easier to use a physical model cell instead of a real cell. To the neuroscientist, the MC is equivalent to a neuron that has been stripped of all conductances,

except for a leak with a reversal voltage of 0 mV and a conductance equal to  $1/R_{MC}$ , where  $R_{MC}$  is the resistance of the MC in whole-cell mode. This “inert” model cell can be easily transformed into a spiking neuron. To do so, you will add a voltage-gated  $\text{Na}^+$  channel, a voltage-gated  $\text{K}^+$  channel, and a leak (background) channel. At the same time, you will strip the MC of its own zero-reversal leak, which would otherwise make the converted MC behave like a very leaky patch.

To run this example, download and open the “SpikingNeuron.kin” script in QuB. Make sure that the accompanying file “SpikingNeuron.kint” is downloaded in the same folder (see Note 4). In the section of the script that sets up the DCE input and output parameters, enter your own scaling and offset values, as determined in the previous calibration example, as well as the AI and AO channel numbers. Compile the script to confirm that your edits were successful, in which case the *Run* button should become active.

The *SpikingNeuron* script can be run in three different ways:

1. As a *pure computer simulation* of a spontaneously spiking neuron model defined by a system of ordinary differential equations, with one for voltage and additional ones for the voltage-sensitive channels (see Note 5). In this mode, QuB acts as any other simulation software.
2. As a *hybrid simulation* of a spiking neuron created by transforming the MC. In this mode, the ion channels are simulated but the voltage is read from the amplifier, and the total current is injected into the model cell. The intrinsic conductance of the model cell is subtracted.
3. As a *dynamic clamp application*, where a number of ionic conductances are added to a real cell (or subtracted from it). In this mode, the ion channels are simulated but the voltage is read from the amplifier, and the total current is injected into the real cell.

To switch between these modes, you must change the value of the *RunMode* parameter in the parameter editor window (see comments in the "SpikingNeuron.kin" file in the Appendix). In pure simulation and dynamic clamp modes, the total output current, as written in the code, has the expression:

```

...  

I_out := I_Inj - (
    + icK.current
    + icNa.current
    + icLeak.current
)*Cm;
...

```

For convenience, the ion channel currents are multiplied by the value of the membrane capacitance, which makes it possible to use conductance densities, rather than absolute values that vary with cell size. In hybrid simulation mode, the total current expression is modified to subtract the MC "leak":

```

...
I_out := I_Inj - (
    + icK.current
    + icNa.current
    + icLeak.current
) * Cm
+ I_MC; //Subtract the MC leak
...

```

For the purpose of this tutorial, you will use the first two operation modes to test the correct operation of your dynamic clamp setup. First, use the pure simulation mode to generate action potentials and display them in the *TriggerGraph* window. These action potentials are used as the “reference.” Then, use the hybrid simulation mode to generate a new set of action potentials that are now potentially affected by a series of artifacts caused by the model cell, the patch-clamp amplifier, and the data acquisition process. If these two sets of action potentials overlap, then you know that your dynamic clamp setup operates correctly. First, set RunMode = 0 to enable the pure simulation mode. Using the parameter editor, change the membrane capacitance parameter  $C$  and the MC resistance  $R_{MC}$  to be equal to the corresponding nominal values of your specific model cell (e.g.,  $C = 22 \text{ pF}$ ,  $R_{MC} = 0.5 \text{ G}\Omega$ ). Press the Enter key after you type in a new value. Set  $I_{inj} = 0$  and  $Ch = 0$ , then compile and run the script. The simulation should look as in Fig. 3. In the *Chart* window you will see four streams of data, corresponding to  $V$ , the  $\text{Na}^+$  and  $\text{K}^+$  currents ( $I_{\text{Na}}$  and  $I_K$ ), and the current predicted to flow through the MC ( $I_{MC}$ ). Note that  $I_{MC}$  is calculated but not injected in pure simulation mode. In the *TriggerGraph* window you see the same four traces but on a very short time scale. Stop the script, change the value of the  $Ch$  parameter from 0 to 10, and restart the script. This change will display the four traces in the *TriggerGraph* window starting on channel 10, instead of zero. Rescale the traces appropriately (right-click on the *TriggerGraph* window and use the property editor), so matching pairs of traces overlap exactly. Stop the script.

Next, set RunMode = 1 to enable the hybrid simulation mode and restart the script. Now the physical model cell—via the patch clamp amplifier and the DAQ card—is included in the simulation. As can be seen in Fig. 4a, the action potential and the ionic currents are almost perfectly overlapping between the two modes, which means that we have set up and calibrated correctly our dynamic clamp system. If you see any differences with your setup, make sure

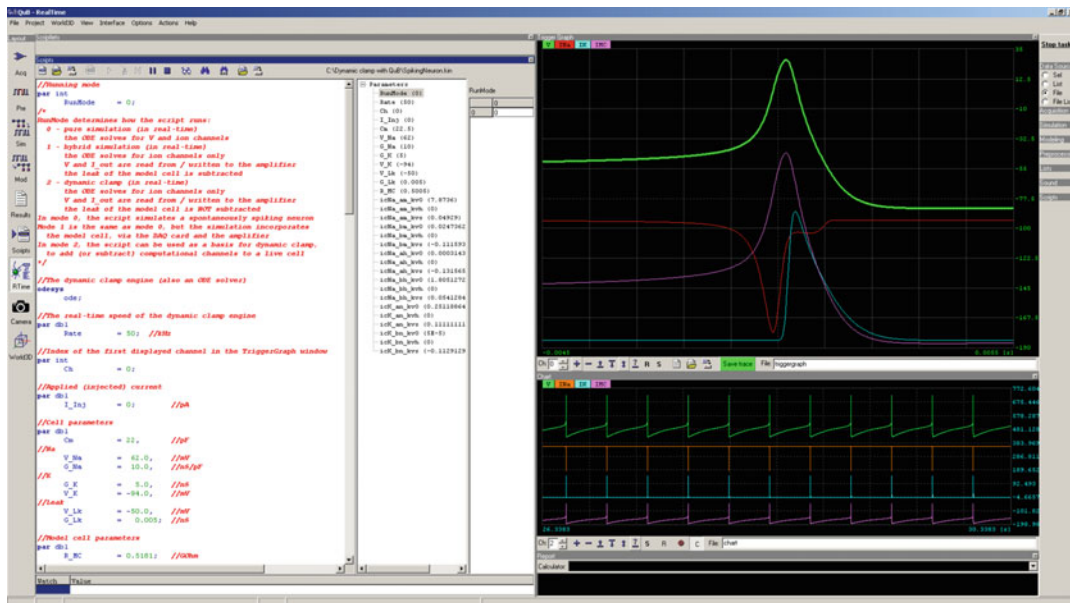


**Fig. 3** Using QuB to simulate a spontaneously spiking neuron. Note the changes in the window layout, relative to Fig. 1

the patch-clamp amplifier compensates for series resistance, and adjust the compensation values for pipette capacitance (too high a value may result in oscillations) and series resistance. Also adjust the  $R_{MC}$  parameter in QuB, which strongly affects spiking frequency.

When you are satisfied that your dynamic clamp system functions properly, you can start testing the effects of different model parameters on action potential shape and firing frequency. Change any parameter in the model, via the parameter editor window, and you can immediately observe the effects in the *Chart* and *Trigger-Graph* windows. For example, if you change the sodium channel conductance  $G_{Na}$  from 10 to 5 nS, action potentials become less tall and wider, as shown in Fig. 4b. If you shift the voltage dependence of the activation particle  $m$  by  $-5$  mV, the spiking threshold becomes lower and there is more  $I_{Na}$  available to generate the action potential, which becomes taller and narrower (Fig. 4c). In contrast, if you shift the inactivation by  $-5$  mV, there is more closed-state inactivation and action potentials become wider, in almost the same way as when you reduce  $G_{Na}$ .

When you stop the script, examine the output generated by the DCE in the *Report* window, to understand the real-time performance. On our test computer (a dual processor Intel Xeon with NI PCIe-6361 card) the results are as follows:

```
ODE stats (RT) EULER
Main thread rate 49.58 kHz, step avg/std 20.17us/0.01167us, CV
0.05786, min/max 20.17us/27.93us, run time 10.394s, IErrCnt
0, OErrCnt 0, DErrCnt 0, DOErrCnt 0.
```

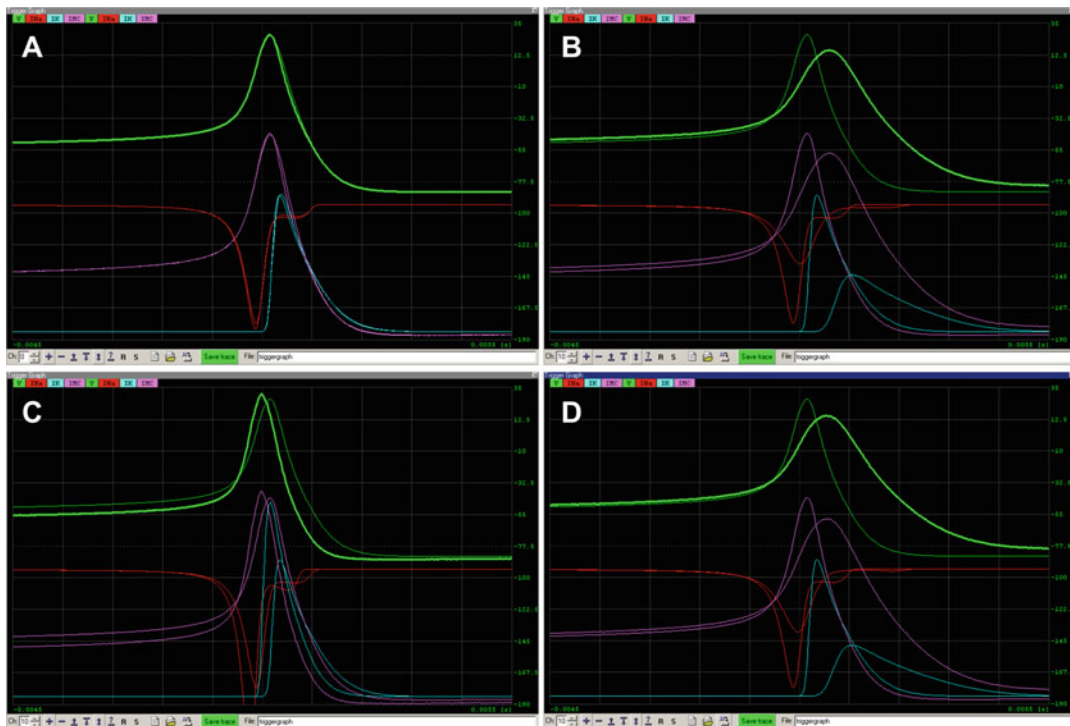


**Fig. 4** Transforming the physical model cell into a spontaneously spiking neuron. **(a)** The action potential and the ionic currents are virtually identical when generated in pure simulation mode or in hybrid simulation mode, when the model cell, the patch clamp amplifier, and the digital acquisition card are interconnected. **(b)**, As in **(a)**, but the sodium channel conductance was changed from 10 to 5 nS. **(c)** Sodium channel activation was shifted by  $-5$  mV. **(d)** Sodium channel inactivation was shifted by  $-5$  mV

```

Main thread step histogram [ms] (Min 0.0001, Max 0.1, Bin
0.000999)
Bin[ms] Bin[kHz] Count Frac.(count) Frac.(time)
0.001099 909.918 0 0 0
0.002098 476.644 0 0 0
...
0.019081 52.4082 0 0 0
0.02008 49.8008 0 0 0
0.021079 47.4406 515296 0.99992 0.999917
0.022078 45.294 39 7.56786E-5 7.83949E-5
0.023077 43.3332 1 1.94048E-6 2.1793E-6
0.024076 41.5351 0 0 0
0.025075 39.8804 0 0 0
0.026074 38.3524 0 0 0
0.027073 36.9372 0 0 0
0.028072 35.6227 0 0 0
0.029071 34.3985 1 1.94048E-6 2.6868E-6
0.03007 33.2557 0 0 0
0.031069 32.1864 0 0 0
...
0.099001 10.1009 0 0 0
0.1 10 0 0 0

```

This step histogram indicates outstanding real-time performance, with virtually constant time steps of 0.021 ms.

### **3.8 Running a Dynamic Clamp Experiment**

If you followed our tutorial so far and managed to convert the RC model cell into a spiking neuron, you will find that running an actual dynamic clamp experiment is very straightforward. Basically, you can take the example script described above (“SpikingNeuron.kin”), set RunMode = 2 to enable the dynamic clamp mode, and run the script while you patch a (whole) cell in current clamp mode. Of course, you will need to adapt the script to your specific problem. Let’s say, for example, that you want to investigate how voltage-gated sodium channels influence the firing activity of a certain type of neuron [15, 18]. For this, you will eliminate the computer-generated potassium and leak currents by zeroing their conductance values (make G\_K = 0 and G\_Leak = 0 in the parameter editor window, or completely eliminate these currents from the script). Ideally, you would also modify the simplistic Hodgkin-Huxley sodium channel kinetic model that we have provided in this tutorial to a model that matches the properties of the sodium currents expressed in your neurons of interest. Then, starting with zero sodium channel conductance (make G\_Na = 0 in the parameter editor), you will patch a cell and examine its spiking pattern under control conditions, with the endogenous sodium channels functional. Then, you will apply TTX to block sodium channels and replace the endogenous current with a computer-generated current, via dynamic clamp. You will now be able to change the values of the conductance and kinetic parameters of your sodium channel model to test how they affect the spiking pattern of the cell. Data acquired during dynamic clamp, before and after TTX application, can be saved with QuB and/or with the software that controls the patch-clamp amplifier, such as pClamp (Molecular Devices) or Patchmaster (HEKA) (*see Note 6*). To take advantage of the many advanced features provided by the QuB software, such as designing dynamic clamp protocols, consult the QuB website, the published papers that used QuB, and contact the authors.

---

## **4 Notes**

1. Most patch-clamp amplifiers (e.g., Multiclamp 700B) require an external data acquisition card (e.g., Digidata 1440a) for normal operation. That card is normally connected to the command input of the amplifier. However, for dynamic clamp experiments, this input must be used by the NI DAQ card. If you have such a configuration, consider a switch box for the convenience of simultaneously connecting the main digitizer

and the NI card to the command input of the amplifier. Use the switch box to alternate between dynamic clamp and any other mode, instead of repeatedly connecting and disconnecting cables. Alternatively, EPC 10 amplifiers feature an internal digitizer and a circuit that summates external and internal inputs. In this case, the NI DAQ card can be permanently connected to the current command input and no switching is necessary.

2. Detailed instructions for showing or hiding, resizing, and setting window properties are given on the QuB website. Briefly, to turn on or off a window, go to *MainMenu>View* and select one of the available viewports. By default, QuB offers a layout mode where windows are mutually resizable (to switch, select *MainMenu>Interface>Floating windows*). In this mode, to change the size of a window use the spacer bar between that window and the adjacent one. To reposition a window, left-click on the caption bar of that window, hold the mouse button down, and move it around. You will see a rectangle that indicates where the window will be positioned when you release the mouse button: at either the top, bottom, left, or right of another window. If you have multiple monitors, you can also grab a window from one monitor and drop it onto another. If the layout appears broken—for example the windows seem to overlap, or you see the background, try to resize a little any of the windows. In most cases, this fixes the layout. If not, reset the layout to its default state (go to *MainMenu>Interface>Restore Interface defaults*) and rearrange the windows.
3. In principle, the scaling and offset factors should be calculated only once. However, any change in the physical setup, such as a new instrument or even a new grounding connection, can modify these factors, particularly the offsets. Recalibrate upon changes in hardware, and check the offsets whenever you start a new set of experiments.
4. Parameters (variables declared with the “par” keyword) can be initialized in the code for the very first time they are declared and used, but after that their values should only be modified in the parameter editor window. Between runs, parameter values are stored in the automatically generated “.kint” file that has the same name as the script file (“.kin”).
5. In this example, the ordinary differential equations for the  $\text{Na}^+$  and  $\text{K}^+$  channels are not written explicitly in the script, but instead are internally constructed by the scripting language compiler, using the *ode.addchannel* function. In contrast, the equation for  $V$  is coded explicitly in the script.
6. The *Chart* can save live, unlimited data to disk, including not only the continuous streams of data (e.g.,  $V$ ) but also any interactive change in parameter values (e.g.,  $I_{\text{Inj}}$ ). These

data files use a QuB-specific format but they can be exported in other formats (including text), to be opened for analysis in other programs.

## 5 Appendix

The “Calibration.kin” script file contains the following code:

```
//Declare the dynamic clamp engine (also an ODE solver)
odesys
    ode;

//Declare input variable V
var dbl
    V          = 0.0;    //mV

//Declare output parameter I_out
par dbl
    I_out      = 0.0;    //pA
/*
Note about parameters:
- they are automatically saved between runs in the .kint file
- modify their values in the Parameter Editor, not in the code
*/

//Set the I/O device name
ode.devicename = "Dev1";
/*
This name should match the DAQ device name set with the NI
Measurement and Automation Explorer utility. Default name is "Dev1"
*/

//Set up AI
ode.setinput(
    input      = V,      //Input variable, read from DAQ
    scale     = 1,      //The scaling factor
    offset   = 0.0,    //The offset
    channel   = 0,      //Read from this AI channel
    filter    = 1.0    //1 raw signal, 0..1 filtered
);

//Set up AO
ode.setoutput(
    output = I_out, //Output variable, written to DAQ
    scale  = 1,      //The scaling factor
    offset = 0.0,    //The offset
    channel = 0,      //Write to this AO channel
    filter  = 1.0,    //1 raw signal, 0..1 filtered
    default = 0.0    //The last value written to DAQ
);

//Add output to the Chart window
ode.addout(V,      "V",      "mV");
ode.addout(I_out, "I_out", "pA");

//Start the dynamic clamp engine
ode.solve(
    tstart = 0, tend = 1000,           //Run for 1000 s
    method = SOLVE_EULER + SOLVE_RT, //Use the real-time mode
    minstepsize = 0,                 //Run at maximum rate
    graphthreadaffinity = 1,         //Assign the GUI thread to core 1
    mainthreadaffinity = 2,          //Assign the main thread to core 2
    dohistogram = true,             //Display a histogram of the step
    histogrambincount = 100, histogrammin = 1e-7, histogrammax = 1e-4
);
```

The “SpikingNeuron.kin” script file contains the following code:

```

//Running mode
par int
    RunMode      = 0;
/*
RunMode determines how the script runs:
0 - pure simulation (in real-time)
    the ODE solves for V and ion channels
1 - hybrid simulation (in real-time)
    the ODE solves for ion channels only
    V and I_out are read from / written to the amplifier
    the leak of the model cell is subtracted
2 - dynamic clamp (in real-time)
    the ODE solves for ion channels only
    V and I_out are read from / written to the amplifier
    the leak of the model cell is NOT subtracted
In mode 0, the script simulates a spontaneously spiking neuron
Mode 1 is the same as mode 0, but the simulation incorporates
    the model cell, via the DAQ card and the amplifier
In mode 2, the script can be used as a basis for dynamic clamp,
    to add (or subtract) computational channels to a live cell
*/

//The dynamic clamp engine (also an ODE solver)
odesys
ode;

//The real-time speed of the dynamic clamp engine
par dbl
Rate      = 50; //kHz

//Index of the first displayed channel in the TriggerGraph window
par int
Ch        = 0;

//Applied (injected) current
par dbl
I_Inj     = 0;           //pA

//Cell parameters
par dbl
    Cm      = 22,          //pF
//Na
    V_Na    = 62.0,         //mV
    G_Na    = 10.0,          //nS/pF
//K
    V_K     = -94.0,         //mV
    G_K     = 5.0,           //nS
//Leak
    V_Lk    = -50.0,          //mV
    G_Lk    = 0.005;          //nS

//Model cell parameters
par dbl
R_MC      = 0.5;          //GOhm

//Input, output, and other variable
var dbl
    V        = -60.0,         //mV
    I_out   = 0,              //pA
    I_MC    := V / R_MC; //pA

//Ion channel models, contained in separate "include" files
//Na
includefile "icNa_HH.kin"
//K
includefile "icK_HH.kin"
//Leak
includefile "icLeak.kin"

```

```

//Set Voltage
icK.setvoltage(V);
icNa.setvoltage(V);
icLeak.setvoltage(V);

//Set Vrev
icK.setvrev(V_K);
icNa.setvrev(V_Na);
icLeak.setvrev(V_Lk);

//Set Conductance
icK.setconductance(G_K);
icNa.setconductance(G_Na);
icLeak.setconductance(G_Lk);

//Equilibrate
icK.calcpEq;
icNa.calcpEq;

//Set up the expression of the total current
if (RunMode = 0) or (RunMode = 2) then {
    I_out := I_Inj - (
        + icK.current
        + icNa.current
        + icLeak.current
    ) * Cm;
} else {
    I_out := I_Inj - (
        + icK.current
        + icNa.current
        + icLeak.current
    ) * Cm
    + I_MC; //Subtract the MC leak
};

//Set up DAQ, if not in pure simulation mode
if RunMode <> 0 then {
    //AI
    ode.setinput(
        input      = V,      //Input variable, read from DAQ
        scale     = 1,      //The scaling factor
        offset   = 0.0,    //The offset
        channel  = 0,      //Read from this AI channel
        filter   = 1.0     //1 raw signal, 0..1 filtered
    );
    //AO
    ode.setoutput(
        output   = I_out, //Output variable, written to DAQ
        scale    = 1,      //The scaling factor
        offset   = 0.0,    //The offset
        channel  = 0,      //Write to this AO channel
        filter   = 1.0,    //1 raw signal, 0..1 filtered
        default  = 0.0     //The last value written to DAQ
    );
    //Device name
    ode.devicename = "Dev1";
};

//Set up the ODEs

//Time
var dbl
    t;

//Set t as the independent variable
ode.setindvar(t);

//ODE for V, if in pure simulation mode
if RunMode = 0 then{
    ode.adddiff(V, I_out/Cm);
};

```

```

//Add ion channels to the ODE solver
ode.addchannel(channel = icK, amatrix = true);
ode.addchannel(channel = icNa, amatrix = true);
/*
Notes:
- the ODE equations are constructed internally by the compiler
- the "amatrix" option solves the channels as in Milescu et al, 2008
- Markov models require changes in the code
*/

//Add output to Chart
ode.addout(V, "V");
ode.addout(icNa.current, "INa");
ode.addout(icK.current, "IK");
ode.addout(I_MC, "IMC");

//Set up four linked triggers to detect APs
var dbl triggerthreshold = -30;
//V
ode.addouttrigger(
    name = "V",
    triggerchannel = 0,
    value = triggerthreshold, slope = 1,
    copydata = true,
    copyfromchannel = 0,//copies from this channel in Chart
    copytochannel = Ch, //to this channel in TriggerGraph
    copyleft = 0.05, copyright = 0.05,//seconds
    filter = TRIGGER_FILTER_NONE
);
//INa
ode.addouttriggeraction(
    name = "V", actionname = "INa",
    copydata = true, copyfromchannel = 1, copytochannel = Ch + 1,
    copyleft = 0.05, copyright = 0.05
);
//IK
ode.addouttriggeraction(
    name = "V", actionname = "IK",
    copydata = true, copyfromchannel = 2, copytochannel = Ch + 2,
    copyleft = 0.05, copyright = 0.05
);
//IMC
ode.addouttriggeraction(
    name = "V", actionname = "IMC",
    copydata = true, copyfromchannel = 3, copytochannel = Ch + 3,
    copyleft = 0.05, copyright = 0.05
);

//Model time in ms, real time in seconds
var dbl
    TimeScale = 1000;

//Start the dynamic clamp engine
ode.solve(
    tstart = 0, tend = 3600,
    timescale = TimeScale,
    method = SOLVE_EULER + SOLVE_RT,
    minstepsize = 1/(Rate*1000),//the real-time step
    graphhreadaffinity = 1, mainthreadaffinity = 2,
    reltol = 1e-6, abstol = 1e-6,
    dohistogram = true, histogrambincount = 100, histogrammin = 1e-7,
    histogrammax = 1e-4
);

```

The “icNa\_HH.kin” script file contains the following code:

```

/*
The Hodgkin-Huxley Na+ channel model:

    am
    (1 - m) <--> m
        bm

    ah
    (1 - h) <--> h
        bh

    I_Na = ccount * g(0) * m^3 * h * (V - V_Na)
*/

//Declare the ion channel model icNa
ionchannel hh           //hh = Hodgkin-Huxley
icNa;

icNa.statecount         = 2;      //Two "particle" types (m and h)

//The index refers to m (=0) or h (=1)
icNa.g(0)               = 1;      //m is conducting, h is not
icNa.power(0)            = 3;      //Three equal and independent m particles
icNa.power(1)            = 1;      //One h particle

//Declare rate constant parameters
par dbl
    icNa_am_kv0          = 7.8736,
    icNa_am_kvh           = 0.0,
    icNa_am_kvs           = 0.04929,

    icNa_bm_kv0           = 0.024736,
    icNa_bm_kvh           = 0.0,
    icNa_bm_kvs           = -0.11159,

    icNa_ah_kv0           = 0.31432e-3,
    icNa_ah_kvh           = 0.0,
    icNa_ah_kvs           = -0.131565,

    icNa_bh_kv0           = 1.805127,
    icNa_bh_kvh           = 0.0,
    icNa_bh_kvs           = 0.054128;

//Set up rate constant expressions as
// k = kv0*exp((V - kvh) * kvs)
// where k and kv0 are in 1/ms,
// kvh is in mV, and kvs is in 1/mV
// and assign the parameters
//First index refers to m or h
//Second index refers to forward or backward
//am
icNa.ratetype(0, 0) = RATE_EXPVHALF;
icNa.setkv0(0, 0, icNa_am_kv0);
icNa.setkvh(0, 0, icNa_am_kvh);
icNa.setkvs(0, 0, icNa_am_kvs);
//bm
icNa.ratetype(0, 1) = RATE_EXPVHALF;
icNa.setkv0(0, 1, icNa_bm_kv0);
icNa.setkvh(0, 1, icNa_bm_kvh);
icNa.setkvs(0, 1, icNa_bm_kvs);
//ah
icNa.ratetype(1, 0) = RATE_EXPVHALF;
icNa.setkv0(1, 0, icNa_ah_kv0);
icNa.setkvh(1, 0, icNa_ah_kvh);
icNa.setkvs(1, 0, icNa_ah_kvs);
//bh
icNa.ratetype(1, 1) = RATE_EXPVHALF;
icNa.setkv0(1, 1, icNa_bh_kv0);
icNa.setkvh(1, 1, icNa_bh_kvh);
icNa.setkvs(1, 1, icNa_bh_kvs);

```

The “icK\_HH.kin” script file contains the following code:

```

/*
The Hodgkin-Huxley K+ model:

      an
(1 - n) <--> n
      bn

I_K = ccount * g(0) * n^4 * (V - V_K)
*/

//Declare the ion channel model icK
ionchannel hh          //hh = Hodgkin-Huxley
icK;

icK.statecount= 1;    //One "particle" type (n)

icK.g(0)            = 1;    //n is conducting
icK.power(0)        = 4;    //Four equal and independent n particles

//Declare rate constant parameters
par dbl
    icK_an_kv0     = 0.251189,
    icK_an_kvh     = 0.0,
    icK_an_kvs     = 0.111111,
    icK_bn_kv0     = 5e-5,
    icK_bn_kvh     = 0.0,
    icK_bn_kvs     = -0.112912;

//Set up rate constant expressions as
// k = kv0*exp((V - kvh) * kvs)
// where k and kv0 are in 1/ms,
// kvh is in mV, and kvs is in 1/mV
// and assign the parameters
//First index refers to n
//Second index refers to forward or backward
//an
icK.ratetype(0, 0) = RATE_EXPVHALF;
icK.setkv0(0, 0, icK_an_kv0);
icK.setkvh(0, 0, icK_an_kvh);
icK.setkvs(0, 0, icK_an_kvs);
//bn
icK.ratetype(0, 1) = RATE_EXPVHALF;
icK.setkv0(0, 1, icK_bn_kv0);
icK.setkvh(0, 1, icK_bn_kvh);
icK.setkvs(0, 1, icK_bn_kvs);

```

The “icLeak.kin” script file contains the following code:

```

//A Hodgkin-Huxley leak (background) channel

//Declare the leak channel model icLeak
ionchannel hh          //hh = Hodgkin-Huxley
icLeak;

icLeak.statecount      = 1;    //One "particle" type
icLeak.g(0)            = 1;    //Conducting
icLeak.power(0)        = 1;    //One particle

```

## References

1. Tan RC, Joyner RW (1990) Electrotonic influences on action potentials from isolated ventricular cells. *Circ Res* 67:1071–1081
2. Sharp AA, O’Neil MB, Abbott LF, Marder E (1993) Dynamic clamp: computer-generated conductances in real neurons. *J Neurophysiol* 69:992–995
3. Robinson HP, Kawai N (1993) Injection of digitally synthesized synaptic conductance transients to measure the integrative properties of neurons. *J Neurosci Methods* 49:157–165
4. Prinz AA, Abbott LF, Marder E (2004) The dynamic clamp comes of age. *Trends Neurosci* 27:218–224
5. Goaillard JM, Marder E (2006) Dynamic clamp analyses of cardiac, endocrine, and neural function. *Physiology (Bethesda)* 21:197–207
6. Desai NS, Gray R, Johnston D (2017) A dynamic clamp on every rig. *eNeuro* 4(5):ENEURO.0250-17.2017.
7. Butera RJ Jr, Wilson CG, Delnegro CA, Smith JC (2001) A methodology for achieving high-speed rates for artificial conductance injection in electrically excitable biological cells. *IEEE Trans Biomed Eng* 48:1460–1470
8. Dorval AD, Christini DJ, White JA (2001) Real-time linux dynamic clamp: a fast and flexible way to construct virtual ion channels in living cells. *Ann Biomed Eng* 29:897–907
9. Kullmann PH, Wheeler DW, Beacom J, Horn JP (2004) Implementation of a fast 16-bit dynamic clamp using LabVIEW-RT. *J Neurophysiol* 91:542–554
10. Yang Y, Adowski T, Ramamurthy B, Neef A, Xu-Friedman MA (2015) High-speed dynamic-clamp interface. *J Neurophysiol* 113:2713–2720
11. Nowotny T, Szucs A, Pinto RD, Selverston AI (2006) StdpC: a modern dynamic clamp. *J Neurosci Methods* 158:287–299
12. Patel YA, George A, Dorval AD, White JA, Christini DJ, Butera RJ (2017) Hard real-time closed-loop electrophysiology with the real-time eXperiment Interface (RTXI). *PLoS Comput Biol* 13:e1005430
13. Milescu LS, Yamanishi T, Ptak K, Mogri MZ, Smith JC (2008) Real-time kinetic modeling of voltage-gated ion channels using dynamic clamp. *Biophys J* 95:66–87
14. Salari A, Navarro MA, Milescu LS (2016) Modeling the kinetic mechanisms of voltage-gated ion channels, in *Advanced patch-clamp analysis for neuroscientists*, Korngreen A (ed), Springer, New York, pp 267–304
15. Milescu LS, Yamanishi T, Ptak K, Smith JC (2010) Kinetic properties and functional dynamics of sodium channels during repetitive spiking in a slow pacemaker neuron. *J Neurosci* 30:12113–12127
16. Tabak J, Tomaiuolo M, Gonzalez-Iglesias AE, Milescu LS, Bertram R (2011) Fast-activating voltage- and calcium-dependent potassium (BK) conductance promotes bursting in pituitary cells: a dynamic clamp study. *J Neurosci* 31:16855–16863
17. Adams CE, DeFazio RA, Christian CA, Milescu LS, Schnell S, Moenter SM (2019) Changes in both neuron intrinsic properties and neurotransmission are needed to drive the increase in GnRH neuron firing rate during estradiol-positive feedback. *J Neurosci* 39:2091–2101
18. Navarro MA, Salari A, Lin JL, Cowan LM, Pennington NJ, Milescu M, Milescu LS (2020) Sodium channels implement a molecular leaky integrator that detects action potentials and regulates neuronal firing. *eLife* 9:e54940



# Chapter 9

## Combining Whole-Cell Patch-Clamp Recordings with Single-Cell RNA Sequencing

Kashif Mahfooz and Tommas J. Ellender

### Abstract

To understand how the brain functions we need to understand the properties of its constituent cells. Whole-cell patch-clamp recordings of neurons have enabled studies of their intrinsic electrical properties as well as their synaptic connectivity within neural circuits. Recent technological advances have now made it possible to combine this with a sampling of their transcriptional profile. Here we provide a detailed description how to combine whole-cell patch-clamp recordings of neurons in brain slices followed by extraction of their cytoplasm suitable for single-cell RNA sequencing and analysis.

**Key words** Single-cell RNA sequencing, In vitro Electrophysiology, Patch clamp, Brain slice, Gene expression

---

### 1 Introduction

Whole-cell patch-clamp recordings both in vitro and in vivo have provided great insights into the electrical diversity that exists amongst neurons in the brain. Similarly, recent high-throughput single-cell RNA sequencing efforts have provided greater understanding of the transcriptional diversity that exists amongst neurons of the brain [1–7]. Such efforts have provided a transcriptomic-based taxonomy of cell types, for example, in cortical structures comprising over 100 distinct cell classes [5–7]. These recent endeavors have often used high throughput approaches using suspensions of cells [1, 4–6, 8] or nuclei [3] derived from dissociated brains, which does not allow for the characterization of electrical properties of neurons. Previous approaches combining whole-cell patch-clamp recordings with genetic analysis often used RT-PCR techniques and was limited to predetermined subsets of genes [9]. To provide an unbiased assessment of gene expression, as well as being able to interrogate the electrical and circuit properties of mature neurons, we and other groups have used an approach that combines whole-cell patch-clamp electrophysiology with

subsequent single-cell RNA sequencing [2, 10, 11]. In particular, we used *in utero* electroporation techniques to fluorescently label cortical neurons derived from distinct progenitor pools and combined this with a characterization of their intrinsic and circuit properties as well gene expression [11]. Here we provide a detailed step-by-step instruction on how to progress from making acute brain slices to performing whole-cell patch-clamp recordings under conditions that allow for the successful extraction and processing of the mRNA from the cytoplasm of the patched neurons (Fig. 1).

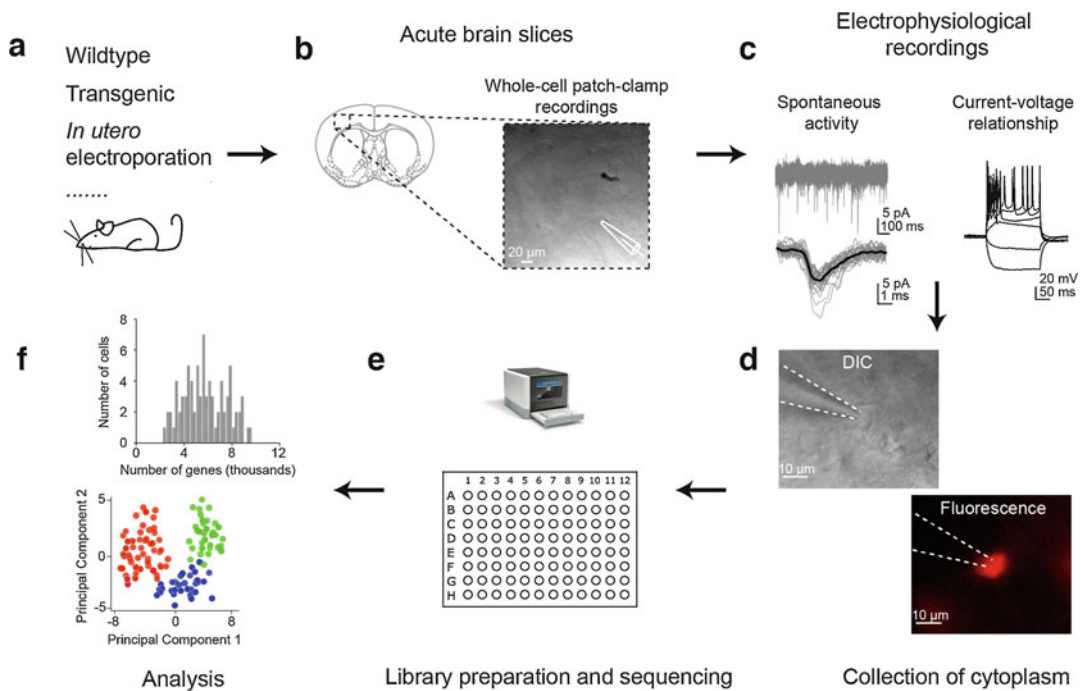


**Fig. 1** From whole-cell patch-clamp recordings to single-cell RNA sequencing workflow (a, b) Acute brain slices were prepared as described in the Subheading 3.2 and transferred to a storage chamber. Slices can come from any wildtype or transgenic animal and in our case came from animals that had undergone *in utero* electroporation to label neurons derived from distinct progenitor pools (c) Whole-cell patch-clamp recordings were performed from neurons in somatosensory cortex and included recordings of spontaneous activity as well as current–voltage relationships. (d) After recordings the cytoplasmic content of the neuron was extracted as described in the Subheading 3.4. The example shown here is a tdTomato expressing Layer 2/3 pyramidal neuron. Top image is a Dodt contrast image for visualization while patching and the bottom image (red) is in fluorescent light. (e) The extracted cytoplasmic content was transferred to a 96-well plate. Further slots were filled in the same manner as described above and once the plate was completed, cDNA synthesis, library preparation, and sequencing were performed as described in Subheading 3.5. (f) The sequencing and analysis can provide information on the differential expression of thousands of genes

## 2 Materials

### 2.1 Solutions

1. Prepare all solutions under RNase-free conditions (*see Note 1*) in deionised water ( $\text{dH}_2\text{O}$ ) treated with 0.1% diethyl pyrocarbonate (DEPC) and autoclaved, or separately purchased DNase/RNase-Free distilled water can be used. Store all the solutions at 4 °C, unless mentioned otherwise.
2. Extracellular cutting solution: 230 mM D-sucrose, 26 mM  $\text{NaHCO}_3$ , 3.5 mM KCl, 10 mM glucose, 1.25 mM  $\text{NaH}_2\text{PO}_4$ , 1.3 mM  $\text{CaCl}_2$ , 2.6 mM  $\text{MgCl}_2$ , pH 7.2–7.3 and 310 mOsmol/l, bubbled with carbogen (95% oxygen, 5% carbon dioxide) and chilled on ice for at least 45 min prior to use (*see Note 2*).
3. Extracellular recording solution: 126 mM NaCl, 2.5 mM KCl, 1.25 mM  $\text{NaH}_2\text{PO}_4$ , 26 mM  $\text{NaHCO}_3$ , 2 mM  $\text{MgCl}_2$ , 2 mM  $\text{CaCl}_2$ , 10 mM D-glucose, pH 7.2–7.3; osmolarity, 300–310 mOsmol/l, continuously bubbled with carbogen gas, and for at least 30 min before the start of electrophysiological recordings.
4. Intracellular solution (current clamp): 123 mM potassium gluconate, 12 mM KCl, 10 mM HEPES, 0.2 mM EGTA, 4 mM MgATP, 0.3 NaGTP, 10 mM sodium phosphocreatine, 1 U/ $\mu\text{l}$  recombinant RNase inhibitor, pH 7.2–7.3; osmolarity, 290–295 mOsmol/l (*see Note 3*). Add the RNase inhibitor on the day of recording. The EGTA in the intracellular solution will scavenge free calcium and reduce potential RNase activity [12].
5. Smart-seq2 cell lysis buffer: 1.3  $\mu\text{l}$  of 0.2% v/v Triton X-100 containing 2 U/ $\mu\text{l}$  RNase inhibitor, 1  $\mu\text{l}$  of 10 mM dNTP Mix (10 mM each dATP, dGTP, dCTP, and dTTP at neutral pH), and 1  $\mu\text{l}$  of 100  $\mu\text{M}$  Oligo-dT<sub>30</sub>VN primer (*see Note 4*).
6. Reverse transcription mix: 10 U/ $\mu\text{l}$  SuperScript IV reverse transcriptase, 5 mM DL-dithiothreitol (DTT), 1× SuperScript IV Buffer, 1 M betaine, 1  $\mu\text{M}$  locked nucleic acid-template-switching oligonucleotide (LAN-TSO) (*see Note 5*), 1 U/ $\mu\text{l}$  recombinant RNase inhibitor, 6 mM  $\text{MgCl}_2$ .
7. cDNA amplification PCR mix: 1× KAPA HiFi HotStart ReadyMix, 0.1  $\mu\text{M}$  IS PCR oligos (5'-AAGCAGTGTTATC AACGCAGAGT-3').

### 3 Methods

#### 3.1 Preparation for RNase-Free Workspace

1. All the chemicals and glassware should be RNase-free and kept separately as “RNA only.” Any handling of equipment should be done using gloves to minimize contamination.
2. Empty the electrophysiology patch-clamp rig of all nonessential pieces of equipment (Fig. 2) and replace all existing tubing on the perfusion system. During the period of experiments involving cytoplasm extraction, clean the rig regularly and thoroughly by spraying with RNaseZAP and wiping the surfaces using RNase Decontamination Wipes followed by final spraying with DEPC-treated dH<sub>2</sub>O and a wipe using sterile RNase-free paper towels.
3. Prepare a dedicated space in the lab that should be used to process all RNA related work and clean this space once a week by following the same cleaning protocol described in the previous step.
4. Before making brain slices, clean the vibratome using a similar procedure. Briefly, spray with RNaseZAP and surface clean using RNase Decontamination Wipes and finally spray with DEPC-treated dH<sub>2</sub>O and wipe clean with RNase-free paper towel. Make sure to clean the metal/ceramic blades and brain stage also.

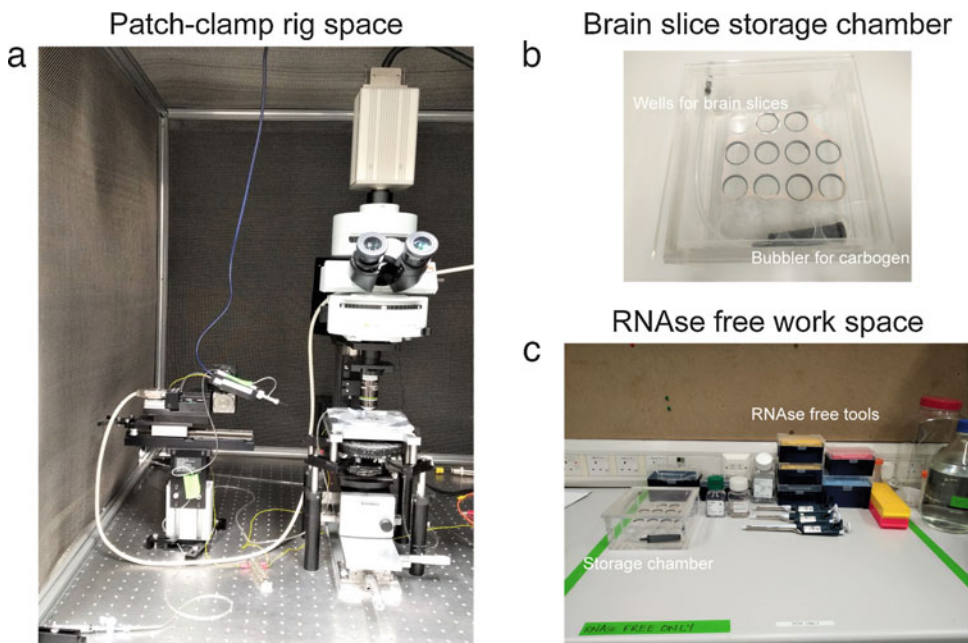


**Fig. 2** Electrophysiology rig space and equipment (a) The rig space should be clean and kept clear of any unnecessary items. (b) Acute brain slice storage chamber containing bubbler for carbogen gas. (c) RNase free and tidy dedicated workspace for sample processing

- The storage chamber to store brain slices should be cleaned the day before use by spraying with RNaseZAP and adding a 10% bleach solution. Leave the solution mix for at least 5 min to prevent any bacterial/fungal growth. Subsequently rinse the chamber out with DEPC-treated dH<sub>2</sub>O and leave to air-dry, ready for use the next day.

### **3.2 Preparation of Acute Brain Slices**

- Deeply anaesthetise the rat/mouse using 3–4% isoflurane and decapitate rapidly. Drop the head directly in ice-cold cutting solution (*see Note 2*). Wait for approximately 30 s while the head is still submerged in the cutting solution to help it cool down.
- Dissect out the brain and keep this in the ice-cold cutting solution.
- Glue the brain on the vibratome stage (*see Note 6*).
- Make 300–400 µm brain slices using the vibratome while the brain is continuously submerged in ice-cold cutting solution (*see Note 7*).
- The vibratome setting for acute brain slicing in our hands is 0.5–0.6 mm/s forward speed, 0.9 mm amplitude and 90 Hz frequency.
- Immediately transfer the slices to the storage chamber with recording solution maintained at 35 °C for 30 min (*see Note 8*). Move the chamber to room temperature afterward. Let the slices rest for at least 20 min before starting recordings and use the brain slices within the next 4 h when collecting cytoplasm to avoid potential transcriptional changes that might occur with prolonged storage.

### **3.3 Electrophysiological Recordings**

- Transfer one slice to the clean patch-clamp recording setup with oxygenated solution flowing at 3 ml/min.
- Neurons can be visualised at 20× and 40× using video assisted infrared differential interference contrast (DIC) or Dölt contrast imaging (Fig. 3).
- Identify the target neuron as standard for whole-cell patch-clamp recordings; taking into consideration the size, shape and depth of the neuron.
- It is important to backfill the patch pipette with approximately 1 µl intracellular solution just prior to patching a neuron (Fig. 4) to avoid evaporation of the intracellular solution. The resistance of the patch pipette should approximately be 3–4 MΩ.
- Make sure that the length of the silver chloride wire in the patch electrode is precise and just long enough to encounter the intracellular solution (Fig. 4).

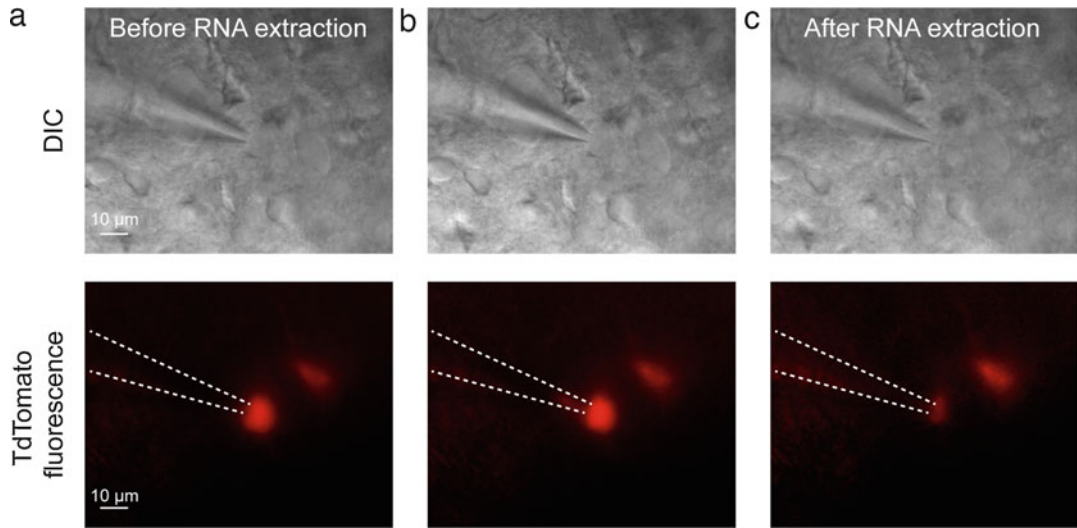


**Fig. 3** Collecting cytoplasm from patched neurons (a) DIC and fluorescent (tdTomato) image while performing whole-cell patch-clamp recording. (b) Extraction of cellular content (see Subheading 3.4). The fluorescent protein can be seen moving into the patch pipette along with cytoplasm. (c) DIC and fluorescent image after the extraction of cellular content

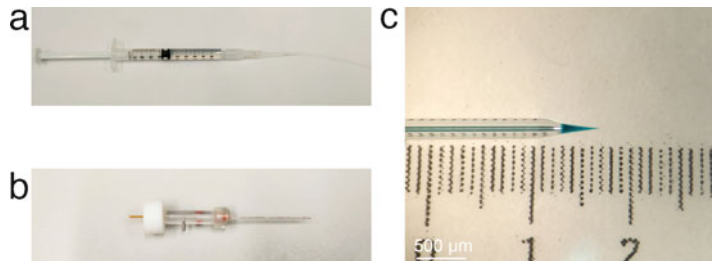


**Fig. 4** Preparing glass recording pipets (a) To backfill the micropipette with internal solution a microloader tip was attached to a filled 1 ml syringe and intracellular solution was filtered through a 0.22  $\mu$ m syringe filter. (b) Micropipette holder with relatively long silver wire. (c) Micropipette with ~1  $\mu$ l intracellular solution (fast green dye was added for demonstration purpose only)

6. Approach the cell with positive pressure (~10 mbar) (see Note 9). After contacting the cell, achieve a giga-seal configuration by releasing the positive pressure combined with gentle suction. Voltage-clamp the cell at -70 mV.
7. Wait for a minute before breaking open the cell by applying sudden negative pressure (see Note 10).
8. Perform whole-cell patch-clamp recordings to assess electrical and circuit properties and any other parameters of interest.

### 3.4 Cytoplasm Collection for RNA Sequencing

- After finishing the electrophysiological recordings (*see Note 11*) aspirate the entire cellular contents of the cell into the patch pipette by applying light suction sustained over the period of 1–2 min (*see Note 12*).
- The transfer of the cytoplasm should be confirmed by visualization under DIC and/or fluorescent light. The patched cell should shrink completely and the cytoplasm along with nucleus should move inside the patch pipette (Fig. 3).
- Equilibrate the pressure after completing the transfer of cellular content by releasing the negative suction and withdraw the patch pipette from perfusion chamber. It is crucial to equilibrate the pressure and make sure to lock the stopcock valve while taking the pipet out from the slice to avoid losing the extracted cytoplasm.
- Expel the content of the patch pipette into an RNA-free microcentrifuge tube prefilled with ~3.3 µl Smart-seq2 cell lysis buffer.
- This is a critical step and extra care should be taken. Apply strong positive pressure once the tip is located near the bottom of the microcentrifuge tube. To ensure that the content is transferred, break the tip of the patch pipette near the side and bottom of the microcentrifuge tube (*see Note 13*).
- Transfer the sample to dry ice immediately and store at –80 °C for further processing (*see Note 14*).
- Clean the silver wire before patching the next cell to get rid of previous mRNA. This is done through the usual steps as outlined above, that is, spray with RNaseZAP, clean using RNase Decontamination Wipes and spray with DEPC-treated dH<sub>2</sub>O and wipe clean with RNase-free paper towel.
- Now it is possible to record from the next neuron.
- It is important to interleave the collection of neurons if one is comparing two different populations, for example to control for changes in expression related to storage of slices in the holding chamber or other factors such as time of day.

### 3.5 Single-Cell RNA Sequencing

#### 3.5.1 Reverse Transcription

- Use Smart-seq2 protocol to convert the collected RNA sample into complementary DNA (cDNA) [13]. The steps are briefly described below.
- Remove the samples from –80 °C storage and centrifuge at 700 × g in a microcentrifuge for 30 s at 4 °C and transfer the tubes on ice.
- Set up the thermal cycler at 72 °C and incubate the collected RNA samples at 72 °C for 3 min. Transfer the tubes back on ice after completing the incubation. This step denatures the mRNA and help oligo-dT primer to hybridize with the poly (A) tail.

4. Prepare the reverse transcription (RT) master mix by combining the components listed in the table below. To avoid any shortage, prepare one extra reaction mix.

<b>Components</b>	<b>Volume (<math>\mu</math>l)</b>	<b>Final concentration in 10 <math>\mu</math>l reaction mix</b>
SuperScript IV reverse transcriptase (200 U/ $\mu$ l)	0.50	10 U/ $\mu$ l
DTT (0.1 M)	0.50	5 mM
SuperScript IV buffer (5 $\times$ )	2.00	1 $\times$
Betaine (5 M)	2.00	1 M
LAN-TSO (100 $\mu$ M)	0.1	1 $\mu$ M
Recombinant RNase inhibitor (40 U/ $\mu$ l)	0.25	1 U/ $\mu$ l
MgCl <sub>2</sub> (1 M)	0.06	6 mM
Ultrapure nuclease free water	0.29	—
Total volume	5.70	—

5. Add 5.70  $\mu$ l of RT mix to each of the 0.2 ml microcentrifuge tube and mix gently three times to avoid any bubble formation. This will make up the total volume of 10  $\mu$ l. Centrifuge the sample at 700  $\times$  g in a microcentrifuge for 10 s at 4 °C and transfer the tubes on ice.
6. Transfer the reaction mix to a thermal cycler with a preheated lid and incubate the sample using the program described in the table below.

<b>Cycle</b>	<b>Temperature (°C)</b>	<b>Time</b>
1	42	90 min
2–11	50	2 min
	42	2 min
12	70	15 min
13	4	Hold

### 3.5.2 cDNA Amplification

7. At this stage, cDNA can be stored at 4 °C for further processing.
1. Mix the components listed in the table below to prepare a PCR master mix. It is always a good practice to prepare for a few extra reactions.

<b>Components</b>	<b>Volume (<math>\mu</math>L)</b>	<b>Final concentration in 25 <math>\mu</math>L reaction mix</b>
KAPA HiFi HotStart ReadyMix (2 $\times$ )	12.50	1 $\times$
IS PCR primers (10 $\mu$ M)	0.25	0.1 $\mu$ M
Ultrapure nuclease-free water	2.25	–
Total volume	15	–

2. Add the 15  $\mu$ L PCR master mix to the 10  $\mu$ L cDNA sample obtained from the reverse transcription step. This will make for a final PCR reaction volume of 25  $\mu$ L. Mix the sample and centrifuge at 700  $\times$   $g$  for 10 s.
3. Set up the thermal cycler with the following program and run the sample.

<b>Cycle</b>	<b>Temperature (°C)</b>	<b>Time</b>
1	98	3 min
2–19	98	20 s
	67	15 s
	72	6 min
20	72	5 min
21	4	Hold

4. At this point we would send of the samples to a sequencing facility, which aided with further processing, quality check and sequencing following the Smart-seq 2 protocol [13]. Randomize the location of samples on the plate to avoid location effects.

## 4 Notes

1. RNase-free conditions involve the use of glassware and tools that are completely RNase free. Handling items with gloves and autoclaving prior to use and/or thorough cleaning by spraying with RNaseZAP followed by a wipe down with RNase Decontamination Wipes, and finally a spray with DEPC-treated dH<sub>2</sub>O and a wipe with sterile paper towels, guarantee this.
2. Putting cutting solution in a –20 °C freezer for 10 min before cutting allows for a colder mixture containing ice. This seems to produce better and more viable slices especially when working with tissue from older animals (> 1 month).

3. Filter the solution using 0.22 µm syringe filter. Measure the osmolality before storing the intracellular solution in 500 µl tubes at -80 °C. Thaw one tube on the day of recording and use it the same day and discard anything left over. Check the osmolality again after adding the RNase inhibitor and adjust by adding RNase-free dH<sub>2</sub>O. Do not refreeze the solution for future use.
4. The Oligo-dT<sub>30</sub>VN (5'-AAGCAGTGGTATCAACGCAGAG TACT<sub>30</sub>VN-3') primer specifically binds to all the RNA containing poly(A) tail. The 3' end contains 30 thymine bases; A, C, or G is represented by "V" and "N" is any of the four nucleotides. Prepare a 100 µM stock solution by dissolving the oligonucleotides in TE buffer. They can be stored in small aliquots (40–50 µl) at -20 °C for a year.
5. There are two riboguanosines (rG) and one locked nucleic acid (LAN)-modified guanosine (+G) at the 3' end of template switching oligonucleotide (5'-AAGCAGTGGTATCAACGC AGAGTACATrGrG +G-3'). These nucleotides facilitate template switching by utilizing the terminal transferase activity of reverse transcriptase at the time of reaction. Dissolve the TSO in TE buffer to prepare a 100 µM stock solution and store at -80 °C.
6. For coronal brain sections containing cortical and subcortical regions the cerebellum is removed and the cut surface is glued down.
7. Based on experience of using both metal blades and ceramic blades we find that slices are better using reusable ceramic blades. However, make sure to clean ceramic blades before every use to get rid of any potential RNase activity.
8. Storing the brain slices at 35 °C for 30 min produced slices that had a clearer surface and improved visibility making it easier to find healthy neurons to patch.
9. A manometer is initially useful for this. Later on a fixed volume in a 1 ml syringe can also be used.
10. Approach the cell diagonally and not from the top as this would avoid any compression of the cell or tissue. When the patch pipette comes in proximity of the cell, a dimple should appear on the cell membrane because of the positive pressure. Apply negative pressure to achieve gigaseal configuration only after the appearance of a dimple. Pull the patch pipette slightly backward to relax the membrane before breaking in to achieve whole-cell configuration. Discard the cell if the health deteriorates or the membrane ruptures immediately after breaking in.
11. In our experiments it has been possible to record for up to 30 min in whole-cell configuration and still be able to successfully extract the cytoplasm.

12. It does not matter whether this is in current-clamp or voltage-clamp mode. Maintain visual inspection of the neuron to control how much suction needs to be applied. When the nucleus of the neuron gets stuck at the tip a longer period of suction might be needed, or we often resorted to applying suction using a 2.5 ml syringe to increase the amount of suction.
13. Strong positive pressure should be applied before breaking the tip and not after. Best results are achieved when the patch pipettes are broken while continuously applying positive pressure.
14. Samples stored at  $-80^{\circ}\text{C}$  for 2 months were still usable and yielded good data.

## Acknowledgments

This work was supported by a MRC Career Development Award (MR/M009599/1) to TJE.

## References

1. Gokce O, Stanley GM, Treutlein B et al (2016) Cellular taxonomy of the mouse striatum as revealed by single-cell RNA-Seq. *Cell Rep* 16:1126–1137
2. Munoz-Manchado AB, Bengtsson Gonzales C, Zeisel A et al (2018) Diversity of interneurons in the dorsal striatum revealed by single-cell RNA sequencing and PatchSeq. *Cell Rep* 24 (2179–2190):e2177
3. Rosenberg AB, Roco CM, Muscat RA et al (2018) Single-cell profiling of the developing mouse brain and spinal cord with split-pool barcoding. *Science* 360:176–182
4. Saunders A, Macosko EZ, Wysoker A et al (2018) Molecular diversity and specializations among the cells of the adult mouse brain. *Cell* 174(1015–1030):e1016
5. Tasic B, Menon V, Nguyen TN et al (2016) Adult mouse cortical cell taxonomy revealed by single cell transcriptomics. *Nat Neurosci* 19:335–346
6. Tasic B, Yao Z, Graybuck LT et al (2018) Shared and distinct transcriptomic cell types across neocortical areas. *Nature* 563:72–78
7. Zeisel A, Munoz-Manchado AB, Codeluppi S et al (2015) Brain structure. Cell types in the mouse cortex and hippocampus revealed by single-cell RNA-seq. *Science* 347:1138–1142
8. Macosko EZ, Basu A, Satija R et al (2015) Highly parallel genome-wide expression profiling of individual cells using nanoliter droplets. *Cell* 161:1202–1214
9. Toledo-Rodriguez M, Markram H (2014) Single-cell RT-PCR, a technique to decipher the electrical, anatomical, and genetic determinants of neuronal diversity. *Methods Mol Biol* 1183:143–158
10. Cadwell CR, Palasantza A, Jiang X et al (2016) Electrophysiological, transcriptomic and morphologic profiling of single neurons using patch-seq. *Nat Biotechnol* 34:199–203
11. Ellender TJ, Avery SV, Mahfooz K et al (2019) Embryonic progenitor pools generate diversity in fine-scale excitatory cortical subnetworks. *Nat Commun* 10:5224
12. Eberwine J, Yeh H, Miyashiro K et al (1992) Analysis of gene expression in single live neurons. *Proc Natl Acad Sci U S A* 89:3010–3014
13. Picelli S, Faridani OR, Bjorklund AK et al (2014) Full-length RNA-seq from single cells using smart-seq2. *Nat Protoc* 9:171–181



# Chapter 10

## Bioluminescence Methodology for Ion Channel Studies

**Paul A. Wadsworth, Aditya K. Singh, Nghi Nguyen, Clifford Stephan, and Fernanda Laezza**

### Abstract

As key players in cell function, ion channels are important targets for drug discovery and therapeutic development against a wide range of health conditions. Thus, developing assays to reconstitute ion channel macromolecular complexes in physiological conditions and screen for chemical modifiers of protein–protein interactions within these complexes is timely in drug discovery campaigns. For most ion channels, expressing their pore-forming subunit in heterologous mammalian cells has now become a routine procedure. However, reconstituting protein-channel complexes in physiological environments is still challenging, limiting our ability to identify tools and probes based on allosteric mechanisms, which could lead to more targeted and precise modulation of the channel function. Here, we describe the assay development steps to stably reconstitute the interaction between voltage-gated  $\text{Na}^+$  (Nav) channel Nav1.6 and its accessory protein, fibroblast growth factor 14 (FGF14) using the split-luciferase complementation assay (LCA), followed by assay miniaturization and optimization in 384-well plates for in-cell high-throughput screening (HTS) against protein-channel interactions. This optimized LCA can subsequently be used for rapid estimation of hit potency and efficacy via dose-dependency studies, enabling ranking of hits prior to more labor-intensive validation studies. Lastly, we introduce the methodology for rapid functional hit validation studies using semi-automated planar patch-clamp electrophysiology. Our robust, in-cell HTS platform can be adapted to any suitable ion channel complex to explore regulatory pathways of cellular signaling using kinase inhibitors, as well as to screen small molecules for probe development and drug repurposing toward new targets/areas of medicine. Overall, the flexibility of this assay allows users to broadly explore therapeutic options for channelopathy-associated diseases at a fast pace, enabling rapid hypothesis generation in early phase drug discovery campaigns and narrowing down targets prior to more labor-intensive *in vivo* studies.

**Key words** Assay development, Assay optimization, HTS, Bioluminescence, Port-a-Patch, Nav channels

---

### 1 Introduction

Voltage-gated sodium (Nav) channels are the molecular determinant of the action potential, which underlies electrical signaling in the brain [1] and as such are attractive targets for drug development [2, 3]. Protein–protein interactions (PPI) between Nav channels and their accessory proteins fine-tune neuronal excitability and are

essential for mechanisms of plasticity and neural adaptations at the cell, circuitry, and behavioral level [4–8]. Subtle changes in the composition of these ion channel complexes can be disruptive for the entire organism. Although mutations in either the channel itself or these regulatory proteins give rise to channelopathies with few viable treatment options [9, 10], PPI interfaces are specific and flexible, making them ideal scaffolds for probe and drug design, especially within the CNS where selectivity and specificity are vital for limiting side effects. The split-luciferase complementation assay (LCA) is a robust method for interrogating interactions between ion channels and their regulatory proteins [11–14], enabling rapid screening of compounds prior to more labor-intensive orthogonal assays. The LCA can be adapted for high-throughput screening (HTS) of large chemical libraries against protein-channel complexes to facilitate hypothesis generation and testing of mechanisms associated with neuronal plasticity and other forms of cellular adaptations. Such endeavors lay the groundwork for medication development against a wide array of diseases associated with ion channel dysfunction [15].

The goal of this chapter is to: (1) provide specific technical information for generating a double stable cell line that can be used to assess protein-channel regulators in live cells; (2) provide guidance for miniaturizing this assay from 96-well to 384-well plates with regard to optimization of parameters that both maximize hit detection and selection, and reduce total costs during screening campaigns; (3) provide an overview of HTS data analysis to exemplify how this assay lends itself for rapid validation of hits via analysis of in-cell potency and efficacy; and (4) explain the methodology for expedited functional validation of hits using the Nanion Port-a-Patch, a portable planar patch-clamp electrophysiology device for rapid functional validation of hits [16].

### **1.1 Development of a Robust Assay to Assess Protein-Channel Interactions in a Double Stable HEK293 Cell Line**

We have previously introduced the LCA to detect the assembly of FGF14 with the intracellular C-terminal tail of the Nav1.6 channel in live cells using transient transfection [13, 17–20]. The assay was designed with the intent of reconstituting the protein-channel complex in cells using a minimal functional domain (MFD) approach, namely, restricting the target for screening only to key residues mediating interactions within binding partners. While the MFD approach has been integral to vaccine development strategies in immunology [21], it has been poorly explored in other fields of therapeutic development with few exceptions for G-protein coupled receptors [22], microtubule proteins [23] and the STIM-Orail channel complex [24–26]. Thus, MFD represents a novelty in the ion channel drug discovery field. In the LCA, the C-terminal and N-terminal fragments of the *P. pyralis* luciferase are fused, respectively, to FGF14 (CLuc-FGF14), and a chimera expressing CD4 fused to the Nav1.6 C-tail (CD4-Nav1.6-NLuc).

Construction of LCA constructs requires cloning of the two interacting partners of interest into suitable mammalian expression vectors. The vectors are designed to express the target proteins in frame with complementary luciferase fragments spaced by a flexible linker region [13]. Following co-expression of these constructs in transiently transfected HEK293 cells, FGF14:Nav1.6 C-terminal tail complex formation can be detected in the presence of the luciferase substrate, D-luciferin, with light production as a read-out of relative binding of the two proteins. However, while transient transfection is suitable for establishing new assays and is still the preferred mode for directly comparing the impact of mutations on protein-channel interactions, stable cell lines are vastly superior, if not necessary, for large screening campaigns against a unique target. Thus, with the intent of developing an assay suitable for HTS, the first goal is to develop a double stable cell line to circumvent the need for high volume transient transfections, reducing variability and labor-related costs. A double stable HEK293 cell line can be generated using linearized CLuc- and -NLuc constructs under the control of selective antibiotics, such as neomycin and puromycin, as for CLuc-FGF14 and CD4-Nav1.6-NLuc, respectively.

## **1.2 Assay Miniaturization and Optimization in 384-Well Plates**

This assay should be adapted from a 96-well to 384-well plate format with the intent of achieving a satisfactory  $Z$ -factor ( $\geq 0.5$  for in-cell assays) and the minimal resource consumption required for maintaining robust assay performance. The  $Z$ -factor (also known more simply as  $Z$ ) is a well-accepted statistical parameter utilized to determine assay performance; it is defined as the ratio between the sum of the standard deviation of the positive and the negative control groups, and the difference between the arithmetic means of the two groups, respectively [27]. An overall  $Z$  of  $\geq 0.5$  signifies that the assay is sufficiently robust for hits to be reliably identified as statistically significant despite well-to-well and plate-to-plate variability. With this in mind, we explored two criteria to maximize  $Z$ ; cell density and efficacy of positive controls. Greater signal separation between these controls compared to the vehicle (i.e., DMSO which is used to dissolve compounds) improves  $Z$  and increases confidence in hit detection. Finding reliable and robust positive and negative controls can be a challenge, especially when little is known about a given target. For instance, for our target, positive controls were selected from kinase inhibitors, which presumably affect the FGF14:Nav1.6 complex formation indirectly through posttranslational modifications (no changes are observed in protein expression). Even when the ultimate goal of the screening campaign is to identify small molecules that modify the PPI interface of a protein complex directly, it may be necessary to select positive controls from separate classes of compounds, if no chemical modifiers of the desired group are available at the time.

### 1.2.1 Miniaturization

To miniaturize the assay from 96-well to 384- or 1536-well plates, parameters for optimization should include cell density, positive and negative controls, reagent volumes, substrate incubation times, cell adhesion, and media composition. In previous versions of our LCA, based on transient expression of cDNA plasmids, transfected cells were transferred from the original 24-well plate format, chosen for optimal transfection efficiency, into either 96-well or 384-well plates 24 h prior to the assay. We found that to be necessary to facilitate protein production, as well as maximizing cell adhesion prior to exchange of media for compound treatments [14]. However, plating cells in advance ( $>18$  h) necessitates the use of complete cell culturing medium including 10% FBS and phenol red, which we found reduce compound effectiveness and inhibit luminescence signal, respectively. Thus, to limit interference with LCA performance, cells need to be washed and medium replaced with serum-free/phenol red-free medium prior to the assay. We attempted washing cells (in 384-well plates) with either warm medium or saline phosphate buffer but observed significant and highly variable levels of cell loss (i.e., large patches of detached cells) during aspiration with the automated Multidrop Combi reagent dispenser on the slowest dispensing speed settings, and also found that  $\sim 5\text{--}10\ \mu\text{L}$  of medium (final volume per well =  $40\ \mu\text{L}$ ) remained in each well following aspiration. Though deviations from the desired volume by 5% [28] are commonly accepted for liquid handling devices, any residual volume from washes constitutes an additional source of variation. Furthermore, it is not feasible for liquid handling devices to completely aspirate all reagent in 384-wells, leading to dilution of the fresh  $40\ \mu\text{L}$  of serum-free media by  $\sim 20\%$  ( $10\ \mu\text{L}$ ) and resulting in variable compound concentrations during screening (final concentration  $> 30\ \mu\text{M}$  in a volume of  $>40\ \mu\text{L}$ ). We tested the assay using cells in suspension (cells plated 1–4 h prior to plate reading) and observed superior raw luminescence values compared to adherent cells, with positive controls exerting similar effects. Thus, for the assay presented here, we recommend using cells in suspension to increase reliability and reduce costs during HTS campaigns.

### 1.2.2 Optimization

The primary criterion to consider for optimization of LCA is cell density per well, which should be evaluated with respect to signal–background (S:B) ratio and  $Z'$  when treated with the positive controls. We observed that  $Z'$  improves with increasing cell density and extended D-luciferin incubation ( $\geq 45$  min) due to greater signal separation between positive and negative controls, and thus recommend reading plate luminescence for a sustained duration to identify optimal plate reading time-points for subsequent screening campaigns. Additionally, we have observed a significant relationship between cell density and dose of the inhibitory positive control MNS: the inhibitor dose–response curve shifts to the left with

decreasing cell density, indicating increased drug efficacy. This is an extremely useful point, as during compound screening, each plate should include an eight-point dose response of the positive control, enabling evaluation of plate-to-plate variability and rapid identification of faulty experiments. For instance, errors in cell plating that lead to excess cells per well can be recognized by reduced potency of the negative control (dose-response curve rightward-shift). Potency of screened compounds can be extrapolated by mapping their respective well's luminescence against this curve, thereby improving hit detection due to an additional layer of “normalization” with respect to changes in cell density.

Users should also be aware that  $Z'$  will likely increase with increasing cell density, largely due to greater S:B. However, we recommend using the absolute minimum cell density that demonstrates satisfactory assay sensitivity for two reasons: (1) during compound screening, lower cell density translates into increased probability of a potent inhibitor to cross the hit threshold due to increased efficacy and (2) a reduction in cell density significantly cuts cell culture resource requirements when large volumes are required for HTS. Thus, if two cell densities yield similar  $Z'$  values, the lesser density should be used. A similar rationale should also be applied when optimizing other variables, such as volume per well.

### **1.3 Limitations of the LCA System for Screening Ion Channel Regulators, and Possible Solutions**

One major drawback of LCA and other luminescence-based screenings is the relatively high number of false positives (very high sensitivity with comparatively lower specificity) compared to other screening modalities, a phenomenon that has been attributed in some cases to the spurious activity of compounds on the reporter (luciferase). In the LCA, a false positive hit could bind to the reconstituted luciferase interfering with the enzyme's ability to emit light leading to target-unrelated signal reduction. It is necessary to control for this by including counter-screenings by which putative hits are tested against the full luciferase enzyme. However, our experience is that counter-screenings can eliminate valuable compounds. In an early screening campaign aimed at identifying kinase pathways regulating the FGF14:Nav1.6 channel complex, we triaged the casein kinase 2 (CK2) inhibitor 4,5,6,7-tetrabromobenzotriazole (TBB) on the basis of full luciferase-based counter-screening [29]. A subsequent analysis of the FGF14 coding sequence identified a putative CK2 sequence recognition motif and spurred further evaluation of structurally diverse CK2 inhibitors. Not only did these follow-up studies reveal potent regulation of the FGF14:Nav1.6 complex by the CK2 enzyme [18], but they also enabled integration of the results with a broader signaling pathway analysis that revealed convergence of CK2 and the enzyme glycogen-synthase kinase 3 (GSK3) on the same region (aa226-231) of FGF14 [19]. Thus, although we recognize the need for counter-screenings, we advise making hit selection an

integrated process encompassing chemoinformatic as well as domain-expert and pathway analysis. Another limitation of the LCA is that it does not allow for identification of toxic compounds nor selection of hits based on functional activity. In both cases, these limitations can be overcome by integrating counter-screenings for cell toxicity and orthogonal assays, such as manual or planar patch-clamp electrophysiology, for functional validation of hits.

#### **1.4 Advantages of the Cell-Based LCA Approach to Discovering New Ion Channel Regulators**

The foremost advantages of the LCA are its flexibility for choosing what targets will be used, as well as its ability to be implemented in live cells, allowing reconstitution of protein-channel interactions in a physiological environment (i.e., maintaining channel domains at the cell membrane where specific ionic concentrations or presence of region-specific signaling mediators may have a significant impact on protein conformation).

Additionally, using an in-cell assay like the LCA for primary screening enables simultaneous filtering of poorly permeable or cytotoxic compounds, providing initial ADMET information for hits at an early phase of the drug discovery campaign. The microplate format of the LCA enables multiplexing by which following luminescence reading, cells can be assayed with other screening modalities, such as in-cell Western and imaging-based high-content phenotypic screenings [30, 31], providing a comprehensive read-out of compound performance. For screening campaigns of 2000–100,000 compounds where there is need for multiple assays, we recommend using a 384-well plate format (working volume per well of 15–110 µL). In the 384-well format, the final volume of the LCA components alone can range from 40 to 80 µL depending on optimized conditions, leaving room for 30–70 µL of additional reagents, such as a fluorescent-based cell viability assay (i.e., CellTiter-Blue) or high-content screening dyes. Furthermore, the optimized LCA used for HTS can subsequently be used for rapid validation of hits via dose-dependency studies, enabling ranking of hits by potency and efficacy prior to more labor-intensive validation studies. Using conditions identical to that of the primary screening, 8–20 hits can be tested per 384-well plate using 8–10 doses with  $n = 2–4$  replicates per concentration. During follow-up studies, this system also facilitates confirmation of repurchased hit potency, preliminary evaluation and comparison of analogs to parent compounds, as well as mechanistic investigations through transient transfection with LCA constructs containing rationally guided point mutations.

---

## 2 Materials

Prepare all solutions using ultrapure water ( $18\text{ M}\Omega\text{-cm}$  at  $25\text{ }^{\circ}\text{C}$ ) and analytical grade reagents. Prepare and store all reagents at  $4\text{ }^{\circ}\text{C}$  (unless indicated otherwise). Diligently follow all waste disposal regulations when disposing of waste materials. We do not add sodium azide to reagents as it might interfere with the assay results.

### 2.1 Cell Lines and Bacterial Strains

1. HEK-293 cells.
2. Chemically competent *E. coli* (such as One Shot TOP10 Chemically Competent *E. coli*, Invitrogen).

### 2.2 Tissue Culture

1. *Complete medium*: Dulbecco's Modified Eagle's Medium (DMEM) and F12 (Ham's) nutrient mixture in 1:1 ratio supplemented with 10% Fetal bovine serum (FBS), 100 U/mL penicillin, and 100  $\mu\text{g}/\text{mL}$  streptomycin. To prepare  $\sim 500\text{ mL}$ , combine 220 mL DMEM, 220 mL F12, 50 mL FBS, and 5 mL of 1000 $\times$  penicillin–streptomycin solution. Store 50 mL aliquots at  $4\text{ }^{\circ}\text{C}$  for up to 4 weeks.
2. *Preconditioned medium*: complete medium (fresh) supplemented with 10–40% complete medium collected from healthy HEK293 cells maintained in dishes or flasks. The cells used for generating preconditioned medium should be washed and medium replaced no less than every 48 h. After collecting medium from flasks, it should be filtered through sterile 0.22  $\mu\text{m}$  filters to remove cells and other contaminants.
3. 1 $\times$  phosphate-buffered saline (PBS): 0.02 M phosphate (0.0038 M  $\text{NaH}_2\text{PO}_4$ , 0.0162 M  $\text{Na}_2\text{HPO}_4$ ), 0.15 M NaCl, pH 7.4, titrated with HCl.
4. 0.25% trypsin–EDTA, diluted at a ratio of 1:6 for 0.25% trypsin–EDTA to PBS.
5. 75  $\text{cm}^2$  and 150  $\text{cm}^2$  cell culture flasks.
6. 10  $\text{cm}^2$  tissue culture dishes.
7. 6-well and 24-well cell culture plates.
8. 96-well and 384-well cell culture white/ $\mu$ Clear<sup>®</sup> bottomed plates with lid (Greiner Bio-One, 655098 and 781098) (see Note 3).
9. Transfection reagent (such as Lipofectamine 3000, Invitrogen).
10. Geneticin (G418), 100 mg/mL, dissolved in sterile water or PBS.
11. Puromycin, 1 mg/mL, dissolved in sterile water or PBS.
12. 150  $\mu\text{L}$  cloning cylinders, glass (Millipore Sigma, C1059).
13. Trypan blue.

### 2.3 Cloning and DNA Preparation

1. pcDNA3.1-CD4-Nav1.6 C-tail-NLuc [13].
2. pEF6-CLuc-FGF14 [13].
3. pcDNA4-TO-Puromycin-mVenus-MAP (ECFP variant; Addgene, plasmid # 44118).
4. pGL3 firefly luciferase plasmid (Promega).
5. Phusion High-Fidelity DNA Polymerase (New England Biolabs).
6. High-fidelity BamHI, NotI, and XbaI restriction enzymes (New England Biolabs).
7. Custom cDNA Primers (Integrated DNA Technologies).
8. T4 DNA ligase (New England Biolabs).
9. Gel Extraction Kit (Qiagen).
10. Luria broth (LB): 10 g of Bacto tryptone, 5 g of yeast extract, and 10 g of NaCl dissolved in 1 L of distilled or deionized H<sub>2</sub>O and sterilized by autoclaving.
11. Luria agar: 10 g of Bacto tryptone, 5 g of yeast extract, 10 g of NaCl, and 15 g of agar dissolved in 1 L of distilled or deionized H<sub>2</sub>O with heating and sterilized by autoclaving.
12. Ampicillin.
13. Selection media: LB agar plates supplemented with 100 µg/mL ampicillin.
14. QIAprep Spin Miniprep Kit (Qiagen).
15. EndoFree Plasmid Maxi Kit (Qiagen).

### 2.4 Luciferase Assay

1. *LCA cell medium*: combine 245 mL of DMEM without phenol red with 245 mL of F12, 5 mL of 1000× nonessential amino acids, and 5 mL of 1 M HEPES. Store 50 mL aliquots at 4 °C. HEPES is added to prevent pH changes during long periods outside of CO<sub>2</sub> atmosphere (i.e., while reading plate luminescence for >1 h). The presence of phenol red may reduce luminescence signal, and FBS may interfere with compound effects during screening; thus, they are not recommended as components of medium for assaying.
2. *30 mg/mL D-luciferin stock solution*: dissolve 1 g of D-luciferin (potassium salt, GoldBio) in 33.33 mL of cold PBS. Store 1.25 mL aliquots at -20 °C. Keep solutions containing luciferin protected from light.
3. *50 mM Coenzyme A stock solution*: dissolve 100 mg of Coenzyme A (trilithium salt, Sigma) (*see Note 1*) in 2547 µL of cold PBS. Store 75 µL aliquots at -20 °C.
4. *LCA substrate solution (2×)*: For one 96-well plate (minimum required volume of 9.6 mL for 100 µL/well), combine 1.25 mL of 30 mg/mL D-luciferin, 75 µL of 50 mM

Coenzyme A, and 11.2 mL of warmed (37 °C) PBS (*see Note 2*) to yield a final concentration (2×) of 3 mg/mL d-luciferin and 0.3 mM Coenzyme A. For one 384-well plate (minimum required volume 15.36 mL for 40 µL/well), scale up volume for one 96-well plate by 1.5× (1.875 mL of 30 mg/mL d-luciferin, 112 µL of 50 mM coenzyme A, and 16.8 mL PBS). Thoroughly mix and keep protected from light. Solutions should be used within 1 h. Volumes can be scaled up proportionally. Prepare an additional half recipe for priming if using an automated liquid dispenser. Dispense an equal volume of this 2× solution to wells prior to luminescence reading; final well concentration (1×) during luminescence reading: 1.5 mg/mL d-luciferin and 0.15 mM coenzyme A.

5. Dimethyl sulfoxide (DMSO).
6. *Positive control (inhibitor)*: Dissolve 4 mg of MNS (3,4-methylenedioxy-beta-nitrostyrene) in 518 µL of DMSO to yield a 20 mM stock. Store 20 µL aliquots at –20 °C.
7. *Positive control (enhancer)*: Dissolve 10 µg of recombinant human tumor necrosis factor-α (TNF-α) protein in 995 µL of cold PBS and supplement with 5 µL of 20 mg/mL BSA to yield a final concentration of 10 µg/mL TNF-α with 0.1 mg/mL BSA. Store 20 µL aliquots at –20 °C.
8. White plate bottom tape seals (*see Note 3*).
9. Targeted compound libraries resuspended in 100% DMSO (*see Note 4*).

## **2.5 Cell Viability Assay**

1. Cell Proliferation Assay Kit (such as CellTiter-Blue, Promega).

## **2.6 Electro-physiology**

1. *Nanion standard Intracellular (internal) solution for Na<sup>+</sup> channels*: 50 mM CsCl, 10 mM NaCl, 60 mM Cs-Fluoride 20 mM EGTA, 10 mM HEPES; osmolarity: 285 mOsmol. Adjust pH to 7.2 using CsOH. Sterilize using 0.22 µm filters, and store 1 mL aliquots at 4 °C for up to 1 week or at –20 °C for up to 6 months.
2. *Nanion standard extracellular (external) solution for Na<sup>+</sup> channels*: 140 mM NaCl, 4 mM KCl, 1 mM MgCl<sub>2</sub>, 2 mM CaCl<sub>2</sub>, 5 mM d-glucose monohydrate, 10 mM HEPES; osmolarity: 298 mOsmol, or at least 10 mOsmol greater than the intracellular solution. Adjust pH to 7.4 using NaOH. Sterilize using 0.22 µm filters, and store 10–50 mL aliquots at 4 °C for up to 1 week or at –20 °C for up to 6 months.
3. *Seal enhancing solution (SES)*: 80 mM NaCl, 3 mM KCl, 10 mM MgCl<sub>2</sub>, 35 mM CaCl<sub>2</sub>, 10 mM HEPES; osmolarity: 298 mOsmol. Adjust pH to 7.2 using HCl. Sterilize using 0.22 µm filters, and store 1 mL aliquots at 4 °C for up to 1 week or at –20 °C for up to 6 months.

4. *Suspension medium*: DMEM and F12 (Ham's) nutrient mixture in 1:1 ratio supplemented with 15 mM HEPES. Combine 246 mL of DMEM, 246 mL of F12, and 7.5 mL of 1 M HEPES. Store 50 mL aliquots at 4 °C.
5. TrypLE Express Enzyme (1×).
6. NPC-1, 3–5 MΩ Chips (Nanion #061103).

## 2.7 Instrumentation

1. Thermal cycler.
2. Gel imaging system (i.e., Alpha Imager).
3. UV/Vis spectrophotometer (i.e., Nanodrop).
4. Multimode microplate reader (i.e., Tecan Infinite M1000 or Bioteck Synergy Neo2).
5. Liquid dispenser, preferably automated (i.e., Multidrop Combi); alternatively, a multichannel pipet (12 channels) may be used.
6. LabCyte Echo 550 acoustic liquid handler.
7. Hemocytometer, preferably automated (i.e., Bio-Rad TC 10).
8. Port-a-Patch (Nanion).

---

## 3 Methods

Described below are (1) the steps to create a double stable cell line using linearized vectors and (2) how to optimize an assay in 384-well plates for HTS to screen regulators of Nav channels. The previously known interacting pair of FGF14 and Nav1.6 intracellular C-terminal tail will be used to demonstrate the use of this assay to screen regulators or small molecule probes, but this system is well suited for investigating other similar targets (i.e., binding between an ion channel and other regulatory proteins, such as CaMKII). For those intending to screen relatively small libraries (<5000 compounds), transient transfection may be adequate, and Subheading 3.2 may be skipped. However, the use of a stable cell line will significantly reduce plate-to-plate variability and allow for lower cell densities/well, enabling more robust hit detection.

### 3.1 DNA Cloning and Linearization of Constructs

First, coding regions for proteins of interest are cloned in frame with the CLuc or NLuc fragments and must be inserted into vectors containing resistance genes for the selective antibiotics puromycin or G418. The methodology for the initial generation of both the pcDNA3.1-CD4-Nav1.6-NLuc and pEF6-CLuc-FGF14 constructs has been described previously [13]; the pcDNA3.1 vector contains the neomycin gene, which enables resistance to G418. However, the CLuc-FGF14 fragment must be excised from pEF6 and inserted in the pcDNA4-TO-

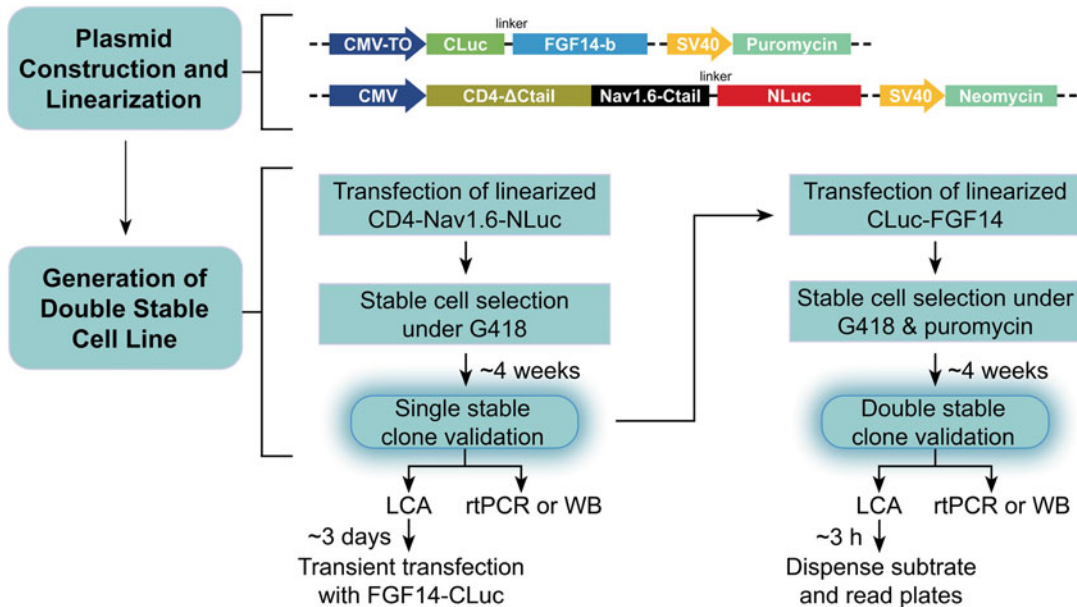


**Fig. 1** Overview of procedure for generating a double stable cell line. Plasmids for expression of the luciferase constructs are linearized prior to sequential transfection in HEK293 cells (Subheading 3.1), and cells are selected using the antibiotics G418 (resistance encoded by the Neomycin gene) and puromycin. Following successful insertion of the first expression vector (encoding CD4-Nav1.6-NLuc), cells are validated using either rtPCR or WB (to confirm presence of recombinant protein), as well as by LCA, whereby the single stable cells are transiently transfected with CLuc-FGF14. In contrast, double stable cells can be rapidly validated by administration of the substrate solution and reading luminescence. Lack of luminescence indicates a non-useful cell line, and alternate clones should be selected. *LCA* luciferase complementation assay, *WB* Western blot

Puromycin-mVenus-MAP vector to enable resistance to puromycin. Additionally, we recommend excision of the ECFP component through addition of a single XbaI restriction site. Finally, the two constructs are linearized prior to transfection to improve integration of DNA into the cell genome for stable cell creation (Fig. 1).

### 3.1.1 Excise ECFP from pcDNA4-TO-Puromycin-mVenus-MAP

- To excise ECFP from pcDNA4-TO-Puromycin-mVenus-MAP, first insert an additional XbaI restriction site at the N-terminus of ECFP using two site-directed mutagenesis steps with the following primers:
  - Forward pcDNA4.XbaI.1FW: 5'-GGCGGCCGCGTCT GCAGCAT-3'.
  - Reverse pcDNA4.XbaI.1RV: 5'-CCGCCGGCGCAG TCGTCGTA-3'.
  - Forward pcDNA4.XbaI.2FW: 5'-GCGGCCGCGTCTA GAGCATGG-3'.
  - Reverse pcDNA4.XbaI.2FW: 5'-GCGGCCGCGTCTA GAGCATGG-3'.

2. Digest pcDNA4-TO-Puromycin-mVenus-MAP (~5–10 µg) using XbaI (1 µL or ~10 Units) to excise the ECFP fragment and yield linearized DNA with sticky ends. Perform in triplicate with a final volume of 50 µL per reaction, and incubate at 37 °C for 1 h.
  3. Religate the vector using T4-DNA ligase (100 ng in 20 µL volume), and incubate for 16 h at 16 °C.
- 3.1.2 Insert CLuc-FGF14 into pcDNA4-TO-1; Puromycin-mVenus-MAP*
1. Excise the cDNA fragment corresponding to the coding sequence for the CLuc-FGF14 from pEF6-CLuc-FGF14 using the BamHI and NotI restriction enzymes: combine 10 µg of pEF6-CLuc-FGF14 plasmid DNA and 1 µL of each enzyme with their respective 1× reaction buffers for a final reaction volume of 50 µL. Incubate at 37 °C for 1 h. Perform this reaction in triplicate. Resolve products by electrophoresis using a 1% agarose gel and purify using a gel extraction kit according to the manufacturer's instructions.
  2. A directional cloning strategy can be used to insert the excised and purified CLuc-FGF14 fragment into the pcDNA4-TO-Puromycin-mVenus-MAP vector at 5' BamHI and 3' NotI sites. Ligate the purified CLuc-FGF14 fragment (insert) into the pcDNA4-TO-Puromycin-mVenus-MAP vector at 5' BamHI and 3' NotI sites, with a 1:3 molar ratio of vector to insert, using T4 DNA ligase, and incubate for 16 h at 16 °C.
  3. Use 0.5–5 µL of the ligation reaction mixture to transform 50 µL of high efficiency DH5 $\alpha$  *E. coli* cells. Add 450 µL of LB broth to transformation reaction and incubate at 37 °C for 1 h prior to plating on selective LB agar plates supplemented with 100 µg/mL ampicillin.
  4. Select individual colonies and grow 5 mL overnight cultures in LB broth containing 100 µg/mL ampicillin.
  5. Purify plasmid DNA using a Miniprep Kit and confirm the identity of the recombinant plasmid by restriction digestion using BamHI and NotI restriction enzymes.
  6. Finally, verify the construct pcDNA4-TO-Puro-CLuc-FGF14 by DNA sequencing with the following primers:
    - (a) Sequencing primer 1: 5'-GACCTCCATAGAAGACA CCGG-3'.
    - (b) Sequencing primer 2: 5'-GCAGGCAAGGCTACTAC TTG-3'.
  7. Select colonies which yielded correct recombinant plasmids and grow 100 mL cultures in LB broth containing 100 µg/mL ampicillin using the verified clones and purify plasmid DNA using an EndoFree Plasmid Maxi Kit.
  8. Quantify the purified constructs by UV spectrophotometry (i.e., optical density at 260 nm using the Nanodrop).

### 3.1.3 Linearize the Constructs Containing *C*luc-*FGF14* and *CD4*-*Nav1.6-NLuc*

- Linearize the pcDNA3.1-CD4-Nav1.6 C-tail-NLuc and pcDNA4-TO-Puromycin-CLuc-FGF14 constructs with single cutter restriction enzyme NotI and XbaI, respectively, according to the manufacturer's instructions.
- Resolve the digested reaction mix by electrophoresis using a 1% agarose gel, and visualize linear bands using a gel imaging system. Purify linear bands using a gel extraction kit according to the manufacturer's instructions. Elute the linearized DNA fragments in 30  $\mu$ L of sterile, molecular biology grade water to obtain an expected final yield of ~300–500 ng/ $\mu$ L.

## 3.2 HEK293 Cell Transfection and Selection of Stable Clones

The primary goal of this section is to generate a monoclonal cell line that expresses both recombinant LCA constructs. First, one linearized construct will be transfected into HEK293 cells and clones will be selected using G418 over 3–5 weeks, and then validated by LCA, as well as WB and/or rtPCR (Fig. 1). These single stable clones should be expanded and used for transfection of the second linearized construct, and the clone selection process repeated using both G418 and puromycin. Due to slow cell growth in the presence of these antibiotics, this process may take between 3 and 6 months.

- Maintain HEK293 cells in 75 cm<sup>2</sup>-tissue culture flasks in a 5% CO<sub>2</sub> incubator at 37 °C using complete medium. These flasks must be maintained to provide preconditioned medium for generation of the first single stable clones.
- Plate  $3.5 \times 10^5$  HEK293 cells per well (6 wells total) of a 24-well tissue culture plate and incubate overnight to give monolayers at ~80% confluence.
- The next day, gently wash the HEK293 cells two times with prewarmed DMEM/F12 without serum or antibiotics and transfect (with Lipofectamine 3000) using either 1 or 2  $\mu$ g of linearized pcDNA3.1-CD4-Nav1.6 C-tail-NLuc plasmid DNA, at least two 24-wells per transfection (*see Note 5*). Use 1  $\mu$ L of the transfection reagent per 1  $\mu$ g of plasmid DNA, with a final transfection volume of 200  $\mu$ L per well, as described previously [13]. Leave two wells non-transfected as controls (for when media with antibiotics is added, to make sure non-transfected cells die).
- After 24 h, aspirate media, wash cells with 400  $\mu$ L PBS, and dispense 1 mL of 30% preconditioned medium (*see Note 6*) supplemented with 0.5 mg/mL G418 to all wells (including two control wells). Allow cells to grow for 24 h.
- After 24 h, wash each well briefly with 400  $\mu$ L of PBS and dispense 100  $\mu$ L of 0.04% trypsin solution (0.25% trypsin diluted with PBS) per well. Stop trypsinization using 800  $\mu$ L of complete medium, and carefully wash the cells off the plate

and dispense all wells for each transfection ratio into separate 15 mL tubes. Centrifuge for 5 min at  $800 \times g$  and resuspend in 5 mL complete medium.

6. Plate cells at a low density (~20% confluence) in 6-well plates using a final volume of 4 mL of 30% preconditioned medium (supplemented with G418) per well.
7. Replace medium every 2–3 days to remove dead cells, provide fresh nutrients, and replace degraded antibiotics. When few to no viable cells are observed in control wells (non-transfected cells in medium containing antibiotics) or when wells contain healthy stable cells that have grown to  $\geq 30\%$  confluence, wash and split cells to new 6-well plates or 6 cm<sup>2</sup> dishes.
8. After 2–3 weeks, wash and split wells containing healthy cells to 10 cm<sup>2</sup> dishes at an extremely low density (*see Note 7*) using a final volume of 8 mL of 20% preconditioned medium (supplemented with G418) per dish.
9. After 1–2 days, use an inverted light microscope to identify the healthiest cells. Gently mark their location on the dish bottom using a permanent marker. Use cloning cylinders to isolate  $\geq 5$ –10 single cells as follows:
  - (a) Place cloning cylinders (glue side down) onto marked colonies on plate.
  - (b) Using a gloved, sterile hand press gently on top of the cylinders to secure them around the colonies.
  - (c) Add 50 µL trypsin–EDTA/PBS (1:6) to each cylinder and incubate for 1–3 min.
  - (d) Add 50 µL complete medium to each cylinder and use a 1000 µL tip pipette to triturate and disperse cells.
  - (e) Transfer 100 µL from cylinder into 24-well plates, and dispense 1 mL of 20% preconditioned medium (supplemented with G418) to each well.
10. Grow for ~1 week or until cells reach  $>70\%$  confluence, *gently* changing media (take care to not detach cells) every 3 days.
11. Validate clones using LCA, in addition to either WB [13] or rtPCR [32]. For LCA, split each clone into 4 wells of a 24-well plate, and subsequently transfect with 1 µg of pEF6-CLuc-FGF14 per well. After 24 h, split into 96-well plate and read plate luminescence, as described previously [13]. Expand 1–2 clones (*see Note 8*) that yield the highest luminescence, as well as exhibit presence of the CD4-Nav1.6-NLuc construct (by WB or rtPCR).
12. Using single stable clones, repeat Subheading 3.2, steps 1–10. At this stage, medium should always contain 0.5 mg/mL G418, and should be supplemented with 1 µg/mL puromycin following transfection with linearized pcDNA4-TO-Puromycin-CLuc-FGF14 plasmid DNA.

13. Validate clones using LCA, in addition to either WB [13] or rtPCR [32]. To validate double stable clones by LCA:
  - (a) Expand each clone in at least two wells of 24-well plates.
  - (b) Trypsinize cells as in Subheading 3.2, step 5. Resuspend cells from one 24-well in 450  $\mu$ L of LCA medium, and dispense 100  $\mu$ L to four 96-wells. Incubate at 37 °C for 2 h.
  - (c) Dispense 100  $\mu$ L of LCA substrate solution to each 96-well, and read plate luminescence for  $\geq$ 30 min, as described previously [13].
14. Expand 1–2 clones that yield the highest luminescence, as well as exhibit presence of both the CD4-Nav1.6-NLuc and CLuc-FGF14 constructs (by WB or rtPCR). Proceed to Subheading 3.3 using a single clone, and store alternate clones at –80 °C.

### **3.3 Assay Miniaturization and Optimization in 384-Well Plates**

For the purpose of screening large chemical libraries in a high-throughput and economically viable manner, the assay must be scaled from a 96-well to 384- or 1536-well plate format (Fig. 2). Assay parameters should then be finely tuned in a manner that leads to satisfactory assay performance while minimally impacting assay sensitivity. This is assessed by measuring the signal separation between the mean of positive and negative controls and the variance between replicates to calculate  $Z$ . Thus, to improve  $Z$ , the inhibitory positive control should reduce the signal to as close to zero percent as possible, while the enhancer control should increase the signal by  $\geq$ 2-fold and  $\geq$ 3 SDs (i.e.,  $\geq$ 200% luminescence when normalized to DMSO controls). For more in-depth understanding of this and related concepts during optimization, we recommend consulting the Assay Guidance Manual [33].

The positive controls MNS and TNF- $\alpha$  are used here due to their effects on the FGF14:Nav1.6 interaction, but alternative controls should be used based on the protein: channel interaction of interest. Additionally, while our assay optimization experiments led us to select 384-well plates containing  $3 \times 10^4$  cells per 40  $\mu$ L per well, these conditions may not be ideal for other cell lines and are described here with the sole purpose of exemplifying the technical details involved with each step.

All optimization experiments should be tested in triplicate (i.e., three independent 384-well plates with identical conditions) to ensure that plate-to-plate variability can be monitored (through calculation of  $Z$ -factor standard error). The order of steps mentioned here should not be taken as absolute. All components of assay development are deeply intertwined, and thus it may not always be practical to separate optimization into discrete, consecutive experiments as described here. Additionally, it may be necessary to retest previous optimization experiments following significant downstream modifications (i.e., more potent positive control identified, change in volume per well, new brand of substrate reagents).

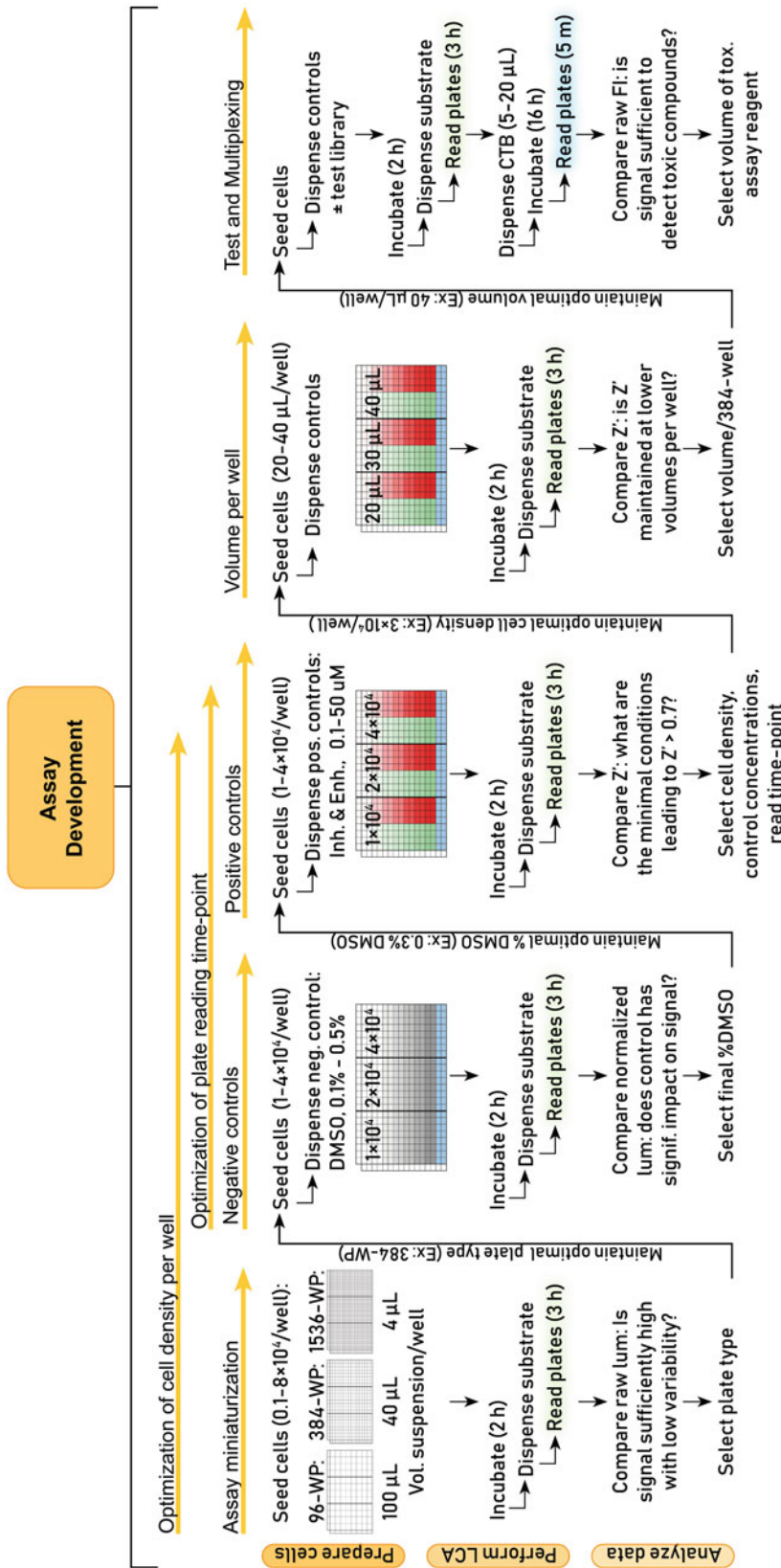


**Fig. 2** Assay development. Schematic of the procedure for developing an assay to screen compounds against protein-channel interactions in a high-throughput format, representing the methodological procedure discussed in Subheading 3.3. *F*/fluorescence intensity, *LCA* luciferase complementation assay, *WP* well-plate

### 3.3.1 Cell Culture

Cell health is fundamental to any in-cell screening campaign. Cell culture conditions (flask type, media composition, cell handling, and schedule for passing cells) must be kept constant to reduce variability during assay development and screening.

1. Expand double stable cells in 150 cm<sup>2</sup> cell culture flasks. Wash cells with 10 mL of warm PBS and provide 25–30 mL of complete medium (supplemented with appropriate antibiotics) every other day. To ensure cells do not reach >95% confluence (may change gene expression), pass cells every 3–4 days using the following protocol:
  - (a) Aspirate media.
  - (b) Dispense 10 mL warm PBS to wash *briefly* (<5 s); aspirate PBS.
  - (c) Dispense 4 mL of trypsin-EDTA (1:6) and incubate at 37 °C for 1–2 min; observe cells under microscope to ensure all cells are detached and in solution.
  - (d) Dispense 8 mL of complete medium, collect all cells in a 15 mL tube, and centrifuge.
  - (e) Aspirate supernatant and resuspend in complete medium.
2. To prepare cells on the day of assaying, trypsinize 3–5 flasks of ~75–90% confluence following Subheading 3.3.1, step 1a–d but using a 50 mL tube to collect cells from all flasks (of similar passage number). Resuspend cells initially using ~6 mL of LCA medium and thoroughly triturate using a 5 mL serological pipette. Ensure all cell clumps have been removed using a light microscope or cell counter, then add ~40 mL of LCA medium, gently mix, and incubate at RT for 30 min (or no more than 5 h) prior to counting and dispensing cells for assaying.

### 3.3.2 Assay Miniaturization

Following generation of the stable cell line, the assay can be scaled down depending on (1) the intended volume of the screening campaign, and (2) the basal luminescence that can be generated by the stable cell line. Luminescence increases approximately linearly with cell density, and a minimum of ~0.5–1 × 10<sup>4</sup> cells may be required to detect appreciable signal (Fig. 3), although surface area per well may also play a role. Additionally, the required cell concentration to achieve a cell density in smaller wells may be prohibitive; suspensions with high cell concentrations to dispense a large number of cells in a very low volume (i.e., 5 µL per 1536-well) may result in excessive variability due to fluctuations in cell concentration throughout the suspension being dispensed. This may occur when dispensing cells at a concentration ≥~1000 cells/µL. We recommend beginning with at least 3 cell densities covering a

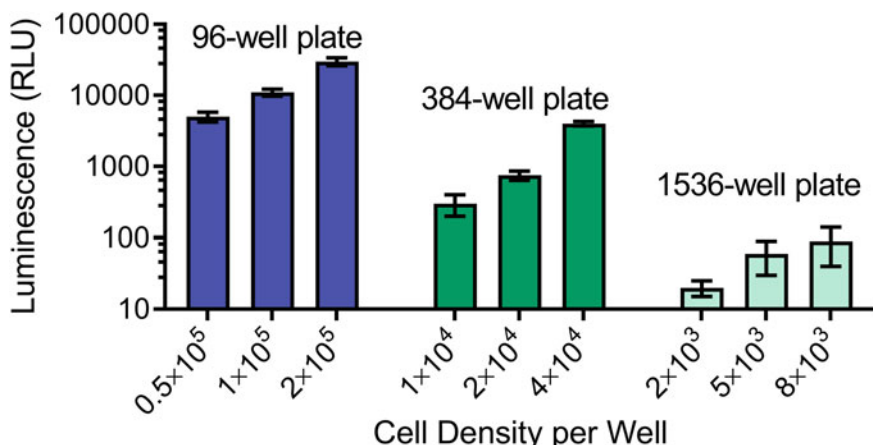


**Fig. 3** LCA signal strength and variability in 96, 384, or 1536-well plates. Plot of luminescence (RLU, relative luminescence units) by cell density in 96, 384, or 1536-well plates. Luminescence was detected after 1 h incubation with luciferin. While luminescence output has an approximately linear relationship with cell density, numerous other factors also play a role, including surface area per well and volume of cell suspension dispensed per well (60–120  $\mu\text{L}$ /well, 20–50  $\mu\text{L}$ /well, or 3–8  $\mu\text{L}$ /well for 96, 384, or 1536-well plates, respectively). There is often a balance between cell density and volume per well that results in optimal luminescence values with low SD. In our experience, variability increases when too minimal of volumes are used or cell density is too low, leading to inconsistency in actual number of cells dispensed per well

broad range per plate format. This step will serve as an initial guide for subsequent steps where cell density per well can be further refined.

1. Quantify cell viability (using trypan blue) and cell density using a cell counter to ensure there is sufficient cell suspension volume (*see Note 9*) containing >90% live cells.
2. For each plate format, serially dilute cells into equal volumes of 3–6 different densities (*see Note 10*). Dispense each cell suspension across 4, 8, or 16 columns of 96-, 384-, or 1536-well plates, respectively, either manually or with an automated liquid dispenser using the following conditions (*see Note 11*):
  - (a) 96-well plates:  $0.5\text{--}1.5 \times 10^5$  cells/well using 100  $\mu\text{L}$  of cell suspension/well.
  - (b) 384-well plates:  $1\text{--}4 \times 10^4$  cells/well using 40  $\mu\text{L}$  of cell suspension/well.
  - (c) 1536-well plates:  $1\text{--}10 \times 10^3$  cells/well using 4  $\mu\text{L}$  of cell suspension/well.
3. Set up the experimental protocol for the Microplate Reader with the following parameters (*see Note 12*):
  - (a) Maintain temperature at 37 °C.
  - (b) End Point Assay: perform kinetic reading (luminescence) at 5 min intervals for 3 h.

4. Prepare LCA substrate solution ( $2\times$ ), dispense to wells using a 1:1 ratio of cell suspension to substrate solution, and immediately begin reading plates.
5. Plot luminescence over time (as in Fig. 2c) for each condition to determine when the signal peaks and plateaus.
6. Choose the plate format that had a reasonable and feasible cell density that output an appreciable luminescence signal with low variability (SD < 20% when normalized to the mean luminescence for all wells).

### 3.3.3 Selection of the Negative Control

Following plate selection, the negative control type and concentration must be selected prior to optimization of positive controls (which require a negative control for comparison). For most ion channel studies, DMSO is the natural choice, as compound libraries (both drug-like scaffolds and kinase inhibitors) are generally dissolved in DMSO. Alternative negative controls may be required for screening of other library types (RNA, etc.). At this stage, it is also necessary to have a general idea of the desired compound screening concentration, which may govern the minimum DMSO concentration needed: the stock concentration of commercially available compound libraries is generally 10 mM. A screening concentration of 20  $\mu$ M will yield 0.2% DMSO following dispensing a compound to cells, thus this is the minimum concentration of DMSO that should be used for negative controls. If higher concentrations may be desired for either screening or subsequent validation studies, then use this test to determine the maximal dose that has no significant impact on either cell health or luminescence signal. Concentrations greater than 0.5–1% DMSO may be toxic.

Additionally, this test can be used to further refine an optimal cell density range that generates a sufficiently high signal with low variability. Based on the signal from cell densities in the plate type from Subheading 3.3.2, those densities with low signal should be eliminated. Use the cell density that resulted in sufficient signal, as well as densities with either 50% fewer and 50% greater cells per well. As an example, we describe using 384-well plates.

1. Quantify cell viability (using trypan blue) and cell density using a cell counter.
2. Dilute cells into 3 different densities from  $1 \times 10^4$  cells/ $40 \mu\text{L}/\text{well}$  to  $4 \times 10^4$  cells/ $40 \mu\text{L}/\text{well}$  (see Note 13). Dispense 40  $\mu\text{L}$  of each cell suspension across 8 columns of a 384-well plate manually or using an automated liquid dispenser.
3. Prepare 100% DMSO solution in 384-wells of the source plate for an acoustic liquid dispenser. Test the effect of 0.05% to 0.5% DMSO (see Note 14) for each cell density by dispensing

20–200 nL of DMSO per well using  $n \geq 4$  wells per condition; leave one column of cells with no DMSO (cells in media alone) as a negative control.

4. Set up the experimental protocol for the Microplate Reader with the following parameters:
  - (a) Maintain temperature at 37 °C.
  - (b) End Point Assay: perform kinetic reading (luminescence) at 5-min intervals for 3 h.
5. Prepare LCA substrate solution (*see Subheading 2.4*), dispense 40 µL per well, and immediately begin reading plates.
6. Plot luminescence over time (as in Fig. 2c) for each condition to determine when the signal peaks and plateaus, and whether DMSO had a significant impact.
7. Proceed to the next optimization experiment using the maximum required concentration of DMSO that had minimal impact on luminescence.

### 3.3.4 Optimization of Assay Positive Controls and Cell Density per Well

Following selection of the negative control concentration, the cell density per well should be optimized with respect to the positive controls (Fig. 4), as assessed by calculation of  $Z'$ . As an example, we use a final concentration of 0.3% DMSO, which is maintained for all wells including positive controls.

1. Quantify cell viability and cell density using a cell counter.
2. Dilute cells into three different densities from  $1 \times 10^4$  cells/40 µL/well to  $1 \times 10^4$  cells/40 µL/well. Dispense 40 µL of each suspension across 8 columns of a 384-well plate manually or using automated liquid dispenser.
3. Prepare positive assay control compounds in 384-wells of the source plate to test an appropriate concentration range for each cell density. For example, for the inhibitor MNS and enhancer TNF- $\alpha$ , we recommend using eight concentrations (0.1, 0.5, 1, 2.5, 5, 10, 20, and 30 µM for MNS; 0.1, 0.5, 1, 5, 10, 20, 30, 40, and 50 ng/mL for TNF- $\alpha$ ) with  $n \geq 4$  wells per concentration per cell density; additionally, include two columns of negative controls for every cell density (*see Note 15*). The final concentration of DMSO should be maintained at 0.3% for all wells (excluding those containing cells with medium alone) by using the acoustic liquid dispenser to backfill with 100% DMSO (i.e., for 20 µM MNS, dispense 40 nL of 20 mM MNS and backfill with 80 nL of 100% DMSO).
4. Set up the experimental protocol for the microplate reader as in **step 4** in Subheading 3.3.2.
5. Prepare LCA substrate solution, dispense 40 µL per well, and immediately begin reading plates.

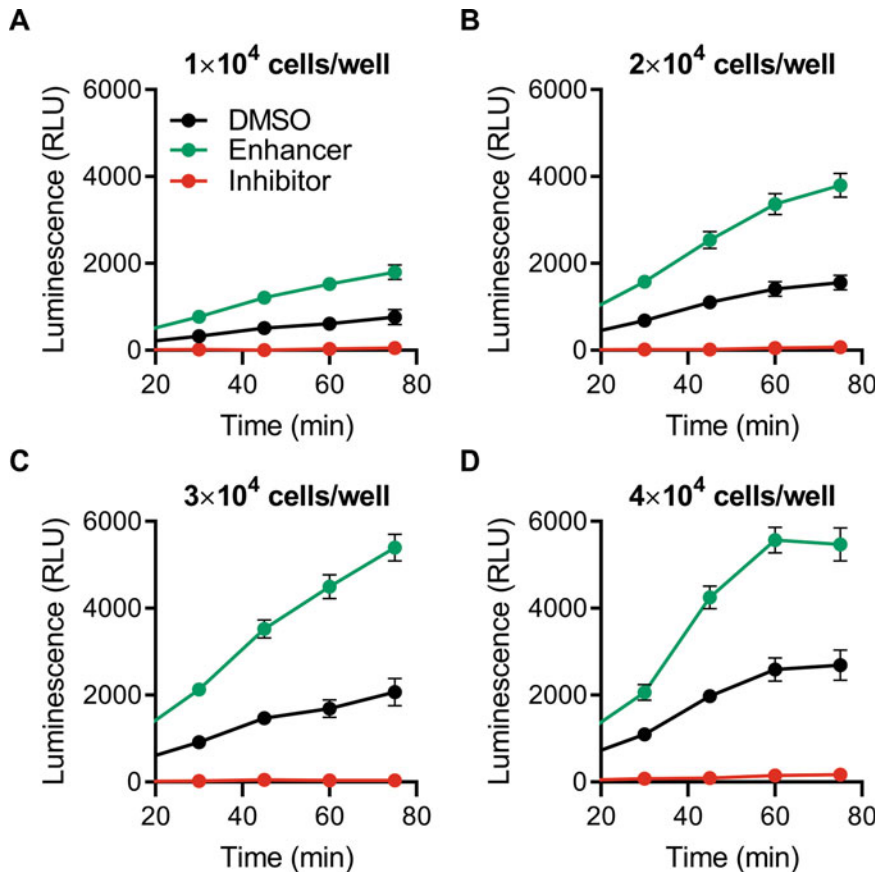


**Fig. 4** Signal separation for positive controls varies with time and cell density per well. (a–d) Plot of luminescence (RLU, relative luminescence units) signal in 384-well plates for  $1\text{--}4 \times 10^4$  cells per well over 30–75 min following dispensing of the LCA substrate solution containing  $\alpha$ -luciferin. Luminescence increases over time and with increasing cell density. The S:B ratio and corresponding  $Z$  values calculated at each time-point also tend increase over time but not necessarily proportionally with either time or cell density. Thus, optimization of the luminescence reading time-point should be thoroughly explored throughout assay development

## 6. Data analysis:

- Export relative luminescence values into Microsoft Excel.
- Plot luminescence over time (as in Fig. 4) for each condition to determine when the signal peaks and plateaus (*see Note 16*). Subsequent normalization to the mean maximal luminescence from wells treated with 0.3% DMSO (Fig. 5) enables rapid visualization of how fold change of controls varies with time.
- For each time point, plot the raw luminescence values for all replicates of each condition (0.3% DMSO, MNS, and TNF- $\alpha$ ) using a scattered dot plot (*see Note 17*).

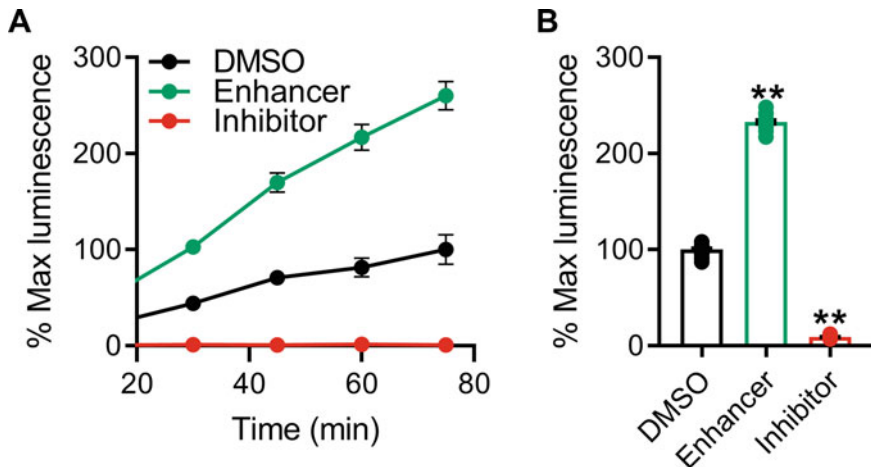


**Fig. 5** Final assay conditions in 384-well plates. **(a)** Plot of percent luminescence (normalized to the maximal mean signal from negative control wells,  $n = 16$ ) in 384-well plates containing  $3 \times 10^4$  cells per well over 30–75 min following dispensing of the LCA substrate solution. Cells were treated with either the negative control (0.3% DMSO, vehicle) or positive controls (Enhancer, 50 ng/mL TNF- $\alpha$ ; Inhibitor, 25  $\mu$ M MNS). **(b)** Plot of percent luminescence from **(a)** at 60 min showing individual replicate values for each condition. We selected a plate read time-point of 60 min due to optimal  $Z$  ( $0.7 \pm 0.1$ ) and S:B ratios, which arose in part due to lesser SD compared to later time-points

- (d) Plot the individual values of TNF- $\alpha$  compared to control by cell density (Fig. 2a); the effect of TNF- $\alpha$  increases with increasing cell density, yielding higher  $Z$  values.
- (e) Plot the dose response of the MNS by cell density; the dose–response curve shifts to the left with decreasing cell density, indicating increased drug potency.
  - Maintaining a dose response of control compounds on every screening plate may be beneficial to compare screened compound potency to that of the control dose response curve.
- (f) Identify the concentration.
- (g) The positive control concentration yielding the greatest potency and lowest standard deviation should be used for all subsequent studies.
- (h) Using the most potent MNS and TNF- $\alpha$  concentration, calculate the following (*see Note 18*):

$$Z' \text{ factor} = 1 - 3 \times \frac{(\delta_p + \delta_n)}{(\mu_p - \mu_n)} \quad (1)$$

$$S : B = \frac{\mu_p}{\mu_n} \quad (2)$$

$$S : N = \frac{(\mu_p - \mu_n)}{\sqrt{\sigma_p^2 + \sigma_n^2}} \quad (3)$$

$$SW = \frac{\mu_p - \mu_n - 3 \times (\sigma_p + \sigma_n)}{\sigma_p} \quad (4)$$

7. We recommend selecting a final assay cell density based on the following criteria:
- $Z$ -factor  $> 0.5\text{--}0.7$  (*see Note 19*).
  - Reproducibility (similar  $Z$ -factor between independent runs/plates).
  - Minimum necessary cell density (i.e., if two densities have similar  $Z$ -factors and reproducibility, choose the lower cell density to reduce costs and increase apparent potency of screened compounds).

### 3.3.5 Optimization of Assay Volume per Well

Following selection of cell density and optimization of controls, total reagent volume per 384-well can be optimized. For large screening campaigns, smaller volumes can translate to large cost reductions. For example, reducing the volume of cell suspension by 25% (to 30  $\mu\text{L}/384\text{-well}$ ) would similarly reduce the volume of LCA substrate solution ( $2\times$ ) to 30  $\mu\text{L}/384\text{-well}$ , as well as potentially the toxicity assay reagent, which constitutes one of the highest cost reagents. Additionally, a volume reduction would allow greater flexibility for multiplexing of additional assays that may require additional reagents, such as high-content imaging dyes.

1. Quantify cell viability and cell density using a cell counter.
2. Dilute cells into 3 different cell concentrations such that dispensing either 20, 30, or 40  $\mu\text{L}$  of cell suspension per 384-well results in the same cell density per well based on Subheading 3.3.2 (i.e., all wells in the plate contain  $3 \times 10^4$  cells, but the final volume of media in each well is 20, 30, or 40  $\mu\text{L}$ . Dispense 20, 30, or 40  $\mu\text{L}$  of each suspension across 8 columns of a 384-well plate manually or using automated liquid dispenser).
3. For each of the 3 groups (20, 30, or 40  $\mu\text{L}$ ), dispense positive controls as in step 3 in Subheading 3.3.3, with compound volumes appropriately adjusted.
4. Set up the experimental protocol for the Microplate Reader as in step 4 in Subheading 3.3.2.
5. Prepare LCA substrate solution, dispense 20, 30, or 40  $\mu\text{L}$  per well, and immediately begin reading plates.
6. Analyze data similarly to step 6 in Subheading 3.3.3.

7. We recommend reducing the assay volume per 384-well if the following criteria are met compared to control (40  $\mu$ L per well):
  - (a)  $Z$ -factor is not significantly reduced.
  - (b)  $Z$ -factor standard error is not significantly increased.
  - (c) Luminescence peak and plateau timepoints are not significantly extended.

### 3.3.6 Optimization of Additional Assay Variables

There are many variables in every assay that can be similarly optimized, and a fraction of these are briefly described here. While the order of steps and conditions exemplified here worked optimally for our assay, we encourage the testing of many conditions to further improve an assay on a case-to-case basis. When assessing any condition, always maintain a full spectrum of controls (negative and positive, multiple doses), sufficient biological replicates (independent plates) and technical replicates (independent wells, consecutive luminescence readings), and consistency of other conditions to enable comparison of runs.

1. Repeat Subheading 3.3.5, substituting the following for change in final volume per well:
  - (a) *Volume of substrate solution per well.* Keep cell suspension volume per well constant. Dispense a reduced volume of substrate solution with proportionally increased stock concentrations.
  - (b) *Substrate brand.* Alternate sources of luciferin are available (at potentially increased cost) that may have features such as increased stability/longevity, greater output, or not impaired by phenol red.
  - (c) *Multiplexing.* The LCA lends itself to multiplexing with other tests using a single well. For instance, cytotoxicity can be assessed directly following LCA luminescence reading (discussed in Subheading 3.3.8). However, morphological effects of compounds can also be assessed by imaging of plates in a high-throughput manner [31, 32]. Brightfield imaging can be used alone, or dyes/stains (i.e., DAPI or high-content imaging dyes) can be dispensed for high-content analysis, which monitors phenotypic changes such as morphology and organelle localization that can be both visualized and quantified and in real time.

### 3.3.7 Troubleshooting: Assessment of Well-to-Well Variability, Plate Effects and Streaking

For optimal results, the effect of well position on luminescence output for a given plate reader should be tested to ensure that plate location does not impact results. Additionally, high well-to-well variability will result in an inability to accurately detect hits during compound screening, and this will be apparent by low  $Z$  values.

1. To determine if poor assay performance (low  $Z'$ ) is due to high well-to-well variability, trypsinize cells from 3 independent flasks and keep cell suspensions separate. Count cells and seed into three 384-well plates (one plate per cell suspension) using a single cell density and no treatment (40  $\mu\text{L}$  of cells in media alone per well). Perform LCA. If the normalized SD for all wells exceeds ~10–15%, examine the following:
  - (a) Cell clumping; check by visualizing cells using cell counter. Cell clumping may occur due to microbial contamination or excessive swirling/tapping of flasks during trypsinization. Use syringe (i.e., 18–20 gauge) to triturate cells prior to cell seeding.
  - (b) Gain/sensitivity setting too high during luminescence reading; systematically reduce gain in small intervals (*see Note 12*).
2. To test the effect of well position, seed cells into all wells of 96- or 384-well plates in triplicate using a single cell density with no treatment (40  $\mu\text{L}$  of cells in media alone per well), and perform LCA.
  - (a) If streaking (i.e., odd rows have decreased luminescence compared to even rows) or other row/column effects are observed, or if the effect is limited to one plate (i.e., the first or last plate to which cells were dispensed), then the issue likely originates with the automated liquid dispenser or lack of sufficient dead volume.
  - (b) If a particular region on the plate is affected, such as plate sides, center, or bottom right, the issue likely originates with the plate reader.

### 3.3.8 Cell Viability Testing

To ensure that change in luminescence signal is not a result of compound cytotoxicity, a cell viability assay should be run in parallel with screening campaigns to quickly eliminate potential false positives. One major advantage of the in-cell LCA in 384-well plates is its ease of use for multiplexing additional assays. Immediately following luminescence reading, the cell viability assay reagent can be dispensed without aspiration of existing media. The CTB cell viability assay is used as an example; this assay measures fluorescence produced when resazurin is reduced (by NADH) to resorufin in cells. Cell cytotoxicity (i.e., induced by drugs) leads to decreased NADH production (and thereby, the capacity to reduce resazurin), which is then detected as a drop fluorescence intensity. At this stage of development, we recommend introducing additional compounds of interest for testing with LCA that can be used as guides to select cutoffs for cell viability. For instance, use a known cytotoxic compound (i.e., tamoxifen) and possibly other compounds that do not adversely affect cell viability.

1. Perform LCA identically to Subheading 3.3.4 using the optimized cell density and reagent volume for all wells; however, dispense LCA medium without cells and substrate solution for one column in each 8-column set (i.e., columns 1, 9, and 17). Treat cells with positive controls as well as known cytotoxic compounds (*see Note 20*).
2. Immediately following luminescence reading, dispense either 5, 10, or 20  $\mu$ L of CTB reagent across 8-column sets in the 384-well plates.
3. Incubate plates for 10–16 h at 37 °C with 5% CO<sub>2</sub> and subsequently detect fluorescence signal intensity (FI) using a plate reader with the following settings:
  - (a) Excitation  $\lambda = 560$  nm; emission  $\lambda = 590$  nm.
  - (b) Gain 100 (or use optimal gain).
4. Data analysis to determine compound toxicity:
  - (a) Plot all individual wells on a scatterplot in order of well number to ensure there are no plate effects.
  - (b) To obtain the corrected fluorescence intensity for viable cells, subtract the mean fluorescent signal intensity of wells with no cells (background fluorescence) from the mean of negative controls (cells treated with 0.3% DMSO alone). Next, use this value to normalize sample fluorescent signal intensity for each set.
  - (c) The toxicity cutoff can be set as follows:
    - Compounds that cause a reduction in fluorescence by  $\geq 50\%$  compared to negative controls.
    - Compounds that cause a reduction in fluorescence by  $\geq 3$  SDs ( $Z$ -score  $> 3$ ) compared to negative controls (*see Note 21*).
    - Set the fluorescence of the known cytotoxic compound as 0%, and the negative control as 100%. Choose a cutoff in this range depending on the target application. Note that this method should yield a similar result as subtracting the background fluorescence.
  - (d) Compare the mean and standard error of raw fluorescence signal intensities for each volume of CTB reagent. For screening, use the lowest volume of CTB reagent that had sufficient signal and low error to accurately identify toxic compounds in a single well (one replicate). High fluorescence values are less important than the well-to-well variability.

### **3.4 High-Throughput Screening of Small Molecule Libraries and Hit Selection Using Z-Scores**

Following successful completion of assay development and selection of final parameters in 384-well plates (Fig. 5), the assay is ready to be used for screening of large chemical libraries in 384-well plates. Depending on the selected incubation times, up to 10–20 plates containing can be screened per day, yielding a total of 3200–6400 compounds screened per day (320 compounds per plate). If no plate effects were observed in Subheading 3.3.5 (i.e., lower luminescence along plate sides), then we recommend using a screening plate layout with 320 experimental compounds in columns 3–22 and all controls in columns 1–2 and 23–24 (*see Note 22*).

1. Dispense screening compounds, DMSO, and positive controls into 384-well plates using an acoustic liquid dispenser (*see Note 23*).
2. Quantify cell viability and cell density using a cell counter and dispense cells into prepinged plates according to the optimized cell density and reagent volumes. Incubate plates for 2 h at 37 °C with 5% CO<sub>2</sub>, dispense LCA substrate solution, and read plate luminescence.
3. Immediately following luminescence reading, dispense CTB reagent. After incubating plates for ~16 h at 37 °C with 5% CO<sub>2</sub>, read plate fluorescence (excitation  $\lambda = 560$  nm, emission  $\lambda = 590$  nm).
4. Data analysis:
  - (a) Calculate  $Z$  for each plate. Plates with  $Z < 0.4$  should be thoroughly reviewed for potential problems and repeated if results appear spurious.
  - (b) Plot the MNS dose response (mean normalized luminescence versus log [M]) for each plate. Plates with significant shifts in the dose response should be thoroughly reviewed for potential problems and repeated if results appear spurious.
  - (c) To determine compound toxicity, normalize sample fluorescent signal intensity to the mean fluorescence of per plate negative controls. Exclude compounds from further analysis based on cutoffs determined in Subheading 3.3.6.
  - (d) Calculate  $Z$ -scores for all screened compounds according to the following formula:

$$Z \text{ score} = \frac{\mu_i - \mu_{\text{DMSO}}}{\delta_{\text{DMSO}}} \quad (5)$$

where  $\mu_i$  is the luminescent signal of the sample (i.e., any particular screened compound), and  $\mu_{\text{DMSO}}$  and  $\delta_{\text{DMSO}}$  are the mean and standard deviation, respectively, of the per plate 0.3% DMSO controls for that sample.

- (e) Examine the distribution of screening results and select hits. Traditionally, hits are those compounds with  $Z$ -scores  $>3$  or  $<-3$ . However, thresholds can be adjusted based on the  $Z$ -score distribution, which is dependent on the compound library and system of interest.
- 5. Counter-screen hits against the full-length luciferase to identify false positives using transiently transfected HEK293 cells in 96-well plates (*see Note 24*) as described previously [13, 14].

### **3.5 High-Throughput Hit Validation Via Dose-Dependency Studies**

Once selected, hits should be repurchased to confirm compound identity and to assess dose dependency. Using the newly optimized assay, this can be rapidly achieved under conditions identical to that of the primary screening. Here, expanded dose responses of compounds can be rapidly tested in variable formats depending on the number of hits. Each hit should be validated using  $\geq 8$  doses over  $\geq 2$  log dilutions (i.e., 0.1–30  $\mu\text{M}$ ). For larger sets of hits, 20 compounds can be tested per 384-well plate using eight concentrations of  $n = 2$  replicates per concentration (each hit in separate columns). For smaller sets, eight compounds can be tested using 10 concentrations with  $n = 4$  replicates per concentration.

1. Dispense compounds, DMSO, and positive controls into 384-well plates using an acoustic liquid dispenser and perform LCA as in Subheading 3.4.
2. Data analysis to determine hit dose-dependency:
  - (a) Plot mean normalized luminescence versus  $\log [M]$  for each compound concentration.
  - (b) Fit the data using a nonlinear regression (using software such as GraphPad Prism):

$$A + \frac{B - A}{1 + 10^{\log \log(x_0-x)/H}} \quad (6)$$

where  $x$  is  $\log_{10}$  of the compound concentration in  $M$ ,  $x_0$  is the inflection point ( $\text{EC}_{50}$  or  $\text{IC}_{50}$ ),  $A$  is the bottom plateau effect,  $B$  is the top plateau effect, and  $H$  is the Hill slope.

- (c) Compound potency is defined by the  $\text{EC}_{50}/\text{IC}_{50}$ , whereas the compound efficacy is defined by the maximal compound effect (i.e., percent luminescence at the bottom or top plateau effect, for inhibitors and enhancers, respectively).
- (d) Kinase inhibitors that increase the FGFI4:Nav1.6 interaction with increasing doses are classified as agonists; kinase inhibitors that decrease FGFI4:Nav1.6 interaction with increasing doses are classified as antagonists or inverse agonists [15, 19].

### 3.6 Functional Hit Validation Via Planar Patch-Clamp Electrophysiology

Hits discovered using LCA can be rapidly validated using the Port-a-Patch to conduct planar patch-clamp electrophysiology [16] with cell lines stably expressing the ion channel of interest, such as Nav channels [35, 36] (Fig. 6). The only required equipment includes the Port-a-Patch with Suction Control Unit (Fig. 6), an amplifier, and a computer to operate the included PatchControl software. Multiple add-ons are also available to increase functionality or automation, such as internal and external perfusion systems, temperature control, a low capacitance holder to reduce noise, and a microscope slide kit to simultaneously visualize (i.e., fluorescence) and record cells. Overall, the ease-of-use of this instrument makes functional validation of hits possible even to those laboratories without extensive experience in electrophysiology. Once proficient, 25–50 cells can be patched in a single day, enabling testing of relatively large sets of hits (~10–20) in a short period.

1. Culture HEK293 cells stably expressing both the human Nav1.6 channel and FGF14-1b (*see Note 25*) in 75 cm<sup>2</sup> flasks using complete medium supplemented with 100 mg/mL G418. Cells should not be grown above ~80% confluence.
2. Harvest one 75 cm<sup>2</sup> flask at 60–80% confluence using the following protocol (*see Note 26*) to obtain a cell suspension that can be used for 2–4 h (*see Note 27*). The optimal cell density is  $\geq$ 1 million cells/mL, but only 5  $\mu$ L of cell suspension is used per experiment (one cell).
  - (a) Gently wash the cells 2× using 5 mL of warmed PBS.
  - (b) Dispense 5 mL of TrypLE and tilt the dish/flask gently to distribute the enzyme evenly. Immediately aspirate ~3 mL to leave only a thin coating but ensure that all cells remain moist.

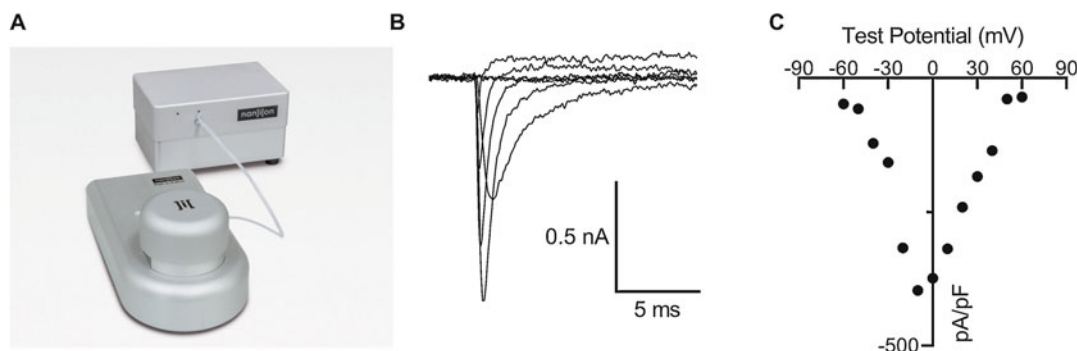


**Fig. 6** Planar patch-clamp electrophysiology using the Port-a-Patch. (a) The small, yet highly versatile Port-a-Patch connected to the Suction Control Unit. (b) Raw Na<sup>+</sup> transient current traces of a HEK293 cell expressing the human Nav1.6 recorded on the Port-a-Patch. Currents were elicited using a voltage step protocol from a holding potential of -80 mV to -60 mV increasing in 10 mV steps up to 60 mV. (c) Corresponding IV activation plot for a single cell

- (c) Incubate for 3–5 min at 37 °C. Observe cells using light microscope to confirm that cells have detached and are loose in media. If cells are not yet detached, incubate for ~1–2 min longer.
  - (d) Dispense 5 mL of resuspension medium and centrifuge cells at 500 ×  $\text{g}$  for 4 min.
  - (e) Aspirate supernatant and triturate cells in 0.5 mL of resuspension medium and 0.5 mL of extracellular solution.
  - (f) Allow cells to recover for 10–20 min at 4–10 °C before use. During patching, cells should be kept on a gentle shaking or rotating platform at very low speed to prevent formation of a cell pellet.
3. Launch the PatchControl software and load the appropriate suction protocol (i.e., intermediate.ppf for cells with typical membrane quality/robustness).
  4. Fill the inside of an NPC-1 chip with 5  $\mu\text{L}$  of intracellular solution (*see Note 28*).
  5. Screw chip onto mount of the Port-a-Patch, ensuring that the internal solution is in contact with the internal electrode (*see Note 29*).
  6. Place the Faraday shielding unit on top.
  7. Dispense 5  $\mu\text{L}$  of extracellular solution onto the chip and ensure that it is in contact with the external electrode. In PatchControl, press the “Play” button.
  8. Gently rotate cell suspension to mix, and aspirate 5  $\mu\text{L}$ . In a separate pipette, aspirate 20  $\mu\text{L}$  of SES.
  9. When the “Add Cells!” button appears, click the button and dispense the 5  $\mu\text{L}$  of cell suspension directly over the center of the chip.
  10. When the resistance has increased to 20–40 M $\Omega$  (indicating cell attachment; **Note 30**), gently dispense 20  $\mu\text{L}$  of SES with the pipette tip facing *away* from the center.
  11. Once sealing procedure is complete (i.e.,  $R > 1 \text{ G}\Omega$ ), gently wash off SES by pipetting 20  $\mu\text{L}$  of external solution on one side of the chip (i.e., right side) with pipette tip facing *away* from the cell. Then, slowly aspirate 20  $\mu\text{L}$  from the other side (i.e., left side), again with the tip facing *away* from the cell. Repeat three more times to ensure that solution is completely washed.
  12. Start the experiment using the following preloaded protocols:
    - (a) NaPharmP4leak.
    - (b) Na-IV-P4leak.
    - (c) Na\_Inact.

13. Repeat steps 4–11 using extracellular solution containing the compound of interest at a concentration based on the IC/EC<sub>50</sub> calculated from dose responses in Subheading 3.5. Use  $n \geq 10$  cells per condition.
14. Analyze data:
  - (a) Export data from PatchMaster using the ASCII format.
  - (b) Open in Microsoft Excel.
  - (c) Calculate the mean and standard error for corresponding data values from each cell.
  - (d) Fit the averaged data for both the IV and inactivation IV using the Boltzmann equation using Igor (or an equivalent electrophysiological data analysis software).

---

## 4 Notes

1. Coenzyme A is useful for increasing the signal, as well as increasing the length of time that the signal plateaus. This may be useful when reading a large number of plates in a single day during screening, especially where it is not feasible to read every plate at an extremely precise time-point.
2. LCA cell medium supplemented with HEPES can be used as an alternative to PBS when plates will be read for an extended period without the presence of CO<sub>2</sub> to maintain a more stable pH. We have observed that use of LCA cell medium for substrate solution yields moderately higher raw luminescence values without significantly altering the effect of compounds on normalized luminescence.
3. We recommend using clear bottom plates to visualize cells throughout assay development (i.e., ensure that no odd cell morphology is observed, cells are not in clumps, cells appear evenly distributed across wells). However, using solid white bottom plates (Greiner #781080) or sealing plates with white tape seals prior to reading will significantly increase raw luminescence values and decrease the apparent well-to-well variation due to reduced backscatter of light through the plate bottom.
4. During assay development, we recommend using a small library (<320 compounds on a single 384-well plate) to assess how assay parameters (i.e., varying cell density or reagent volumes) impact compound effectiveness (i.e., relative Z-scores), as well as to determine reproducibility between independent experiments. Libraries should contain well-annotated compounds, such as targeted kinase inhibitors or FDA-approved drugs, such as the Broad Institute Collection.

5. Especially when attempting transfection of new plasmid DNA, it is wise to test multiple quantities of plasmid DNA (i.e., 0.5, 1, 2, or 3 µg). As the goal is to generate a single, healthy clone that stably expresses the cDNA constructs of interest, multiple conditions should be tested to find the optimal method.
6. To prepare 50 mL of 20% preconditioned media, combine 40 mL complete medium supplemented with appropriate antibiotics (i.e., 500 µg/mL G418 for the first stable transfection) with 10 mL of sterile filtered medium from subculture of HEK293 cells. The final concentration of selective antibiotics is reduced by the same percentage as it is comprised of preconditioned medium. By slowly increasing the antibiotic concentration over 3 weeks (30%, 20%, and finally 10% during week 3), the initial stress to transfected cells is reduced to promote faster and healthier growth for stable cells while simultaneously preventing growth of non-stable cells.
7. Cells should be seeded extremely sparsely in dishes such that individual clones can be discretely selected (i.e., only one cell visible at a given location when observed with a light microscope). Over-seeding cells can occur easily and will necessitate subsequent splitting and reseeding at lower density.
8. At this stage, the single stable cell line should be immediately expanded, and aliquots frozen at –80 °C. These cells can be used for subsequent generation of multiple double stable cell lines expressing alternative complementary cDNA plasmids expressing protein pairs of interest (i.e., numerous regulators of a single ion channel, such as FGF13 or spectrins). For instance, while this chapter describes the subsequent insertion of CLuc-FGF14, other regulatory proteins fused to CLuc could be used to generate alternative double stable cell lines. This would enable rapid cross-screening of small molecules against multiple related protein complexes to discover highly specific probes against a single target of interest.
9. Cell suspensions need to be continually mixed by gentle pipetting/swirling prior to counting and plating, and all solutions should always have at least 20% dead volume, or a minimum of 4 mL when dispensing with a multichannel pipette from reagent reservoir, or a minimum of 15–20 mL dead volume when dispensing with an automated dispenser to account for priming. The minimum volume for 128 wells of a 384-well plate (8 columns) is 5120 µL but should be brought to ~10 mL to account for dead volume if using a multichannel pipette. The use of insufficient dead volumes can significantly impact results and lead to higher well-to-well variability, for instance due to plate streaking (every other row having reduced cells, causing reduced signal output; results from such plates must be discarded).

10. For example, to obtain a density of  $4 \times 10^4$  in 40  $\mu\text{L}/384\text{-well}$ , the cell suspension will need to have a concentration of  $1 \times 10^6$  cells/mL ( $1000,000$  cells/mL  $\times 0.04$  mL = 40,000 cells) with sufficient volume for  $n = 128$  wells (8 columns) using 40  $\mu\text{L}$  per well accounting for dead volumes. Obtain a cell suspension volume of 100 mL with a density of  $1 \times 10^6$  cells/mL. Use 25 mL of this suspension for seeding the first 8 columns. Dilute the remaining 75 mL of suspension by 25% by adding 25 mL of media, mix, and use 25 mL of this suspension for seeding  $3 \times 10^4$  cells into the second 8 columns. Repeat as necessary. See table below for examples of the necessary cell concentrations to achieve a particular cell density for a given volume:

<b>Cell Suspension concentration needed for a volume of:</b>		
<b>Cell #/well</b>	<b>30 <math>\mu\text{L}/\text{well}</math></b>	<b>40 <math>\mu\text{L}/\text{well}</math></b>
1000	$\sim 3.3 \times 10^4$	$2.5 \times 10^4$
10,000	$\sim 3.3 \times 10^5$	$2.5 \times 10^5$
30,000	$1 \times 10^6$	$7.5 \times 10^5$
40,000	$1.25 \times 10^6$	$1 \times 10^6$
50,000	$1.5 \times 10^6$	$1.25 \times 10^6$

11. We recommend starting with these volumes for each plate type, but this step is also amenable to testing several volumes of suspension per well in addition to multiple cell densities. However, bear in mind that the volume of cell suspension dispensed is only half of the final working volume (an equal volume of LCA substrate solution (2 $\times$ ) will be dispensed prior to reading plates). We have found that increasing the substrate solution concentration to 4 $\times$  yielded reduced luminescent signal.
12. Recommended initial settings for luminescence reading using various plate readers:
- Synergy H1: open hole; integration time 0.5 s, gain 200.
  - Tecan Infinite M1000: open hole; integration time 0.1 s, settle time 0.01 s.

Please note that while increasing the gain/sensitivity setting will increase the raw luminescence values, an excessively high gain setting may result in high well-to-well variability. In this case, the apparent high standard deviation between replicates within a given plate is a result of technical errors rather than biological problems. Low raw luminescence values (i.e., <500 in a 384-well plate or <2000 in a 96-well plate) may not be cause for concern if the well-to-well variability is low. If

luminescence appears low, multiple gain settings should be tested to find an optimal assay sensitivity prior to troubleshooting the biological experimental parameters

13. Depending on the baseline luminescence generated by the stable cell line and results from Subheading 3.3.2, plate cell densities ranging from  $1 \times 10^3$  to  $1 \times 10^5$  with each cell density having 8 columns of the plate (thus, a maximum of 3 different cell densities per 384-well plate). The expected optimal cell density will likely range from  $2 \times 10^4$  to  $4 \times 10^4$ .
14. Test at least the maximum DMSO concentration that will be required for the assay, which depends on the stock concentration of library drugs (generally 10 mM from commercial suppliers). Thus, if the screening concentration will be 20  $\mu\text{M}$ , then the DMSO concentration can be no less than 0.2%. Concentrations greater than 0.5–1% DMSO may be toxic.
15. This includes one column of cells treated with media alone and one column of cells treated with media and DMSO alone. Especially during assay development, maintain an excess of negative controls on every plate to monitor well-to-well variation and to ensure that the parameters being optimized are not misrepresented by normalization to outlier controls.
16. The time required for signal peak and plateau is also useful for determining how long plates can be incubated prior to plate reading, which is one limiting factor for the number of plates that can reasonably be assayed in a single day during HTS.
17. Plotting all individual replicate values, rather than mean  $\pm$  SD alone, enables rapid visualization of the spread between wells.
18.  $\delta_p$  and  $\delta_n$  are the SD of the positive (p) and negative (n) control groups, and  $\mu_p$  and  $\mu_n$  are the arithmetic means of the two groups, respectively; S:B, signal to background; S:N, signal-to-noise; and SW, signal window. For cell-based assays, generally, a  $Z$  of  $\geq 0.5$  signifies that outliers can be reliably identified as statistically significant despite well-to-well and plate-to-plate variability. Based on Eq. (1),  $Z$  is improved by greater signal separation between the mean of positive and negative controls, as well as by reducing variance between replicates. In practical terms, consistency between replicates would improve confidence in a single well outlier being truly significant (i.e., compound treatment in a single well resulted in a significant change in complex formation rather being due to well-to-well variability).  $Z$  can be calculated separately using the enhancer and inhibitor positive controls (using the absolute value in the denominator), demonstrating the assay sensitivity for essentially two separate assays (one to detect FGF14:Nav1.6 enhancers, one to detect inhibitors) using a single system.

19. If  $Z$  is low, we recommend the following for these potential causes:
  - (a) High well-to-well variability: repeat experiment; ensure that cell viability is >90% and that cells do not form clumps prior to seeding cells.
  - (b) Lack of potent controls: repeat experiment using fresh controls; dissolve controls in DMSO rather than water-based solvents to ensure sample viscosity is not an issue for acoustic liquid dispenser; search literature for more potent modulators of the ion channel target of interest.
20. The dose makes the poison: all compounds may be cytotoxic at high concentrations. Test multiple doses of suspected cytotoxic compounds to confirm cytotoxicity (or lack of).
21. Using SDs as a threshold for toxicity may not be advisable due to typically relatively low SD (~3–6%) in negative controls. Thus, a compound that reduces fluorescence by only 20% may have a  $Z$ -score of -6. Small reductions in fluorescence may indicate an outlier, or cytotoxicity due to high concentrations (i.e., if screening concentration is high). Furthermore, if the negative control SD is low for the toxicity assay, then experimental compound  $Z$ -scores may be less relevant than normalized mean change in fluorescence.
22. Controls should include a minimum of  $n = 8$  wells for cells treated with media alone (negative control as quality check for DMSO), and  $n = 16$  wells for cells treated with 0.3% DMSO or positive controls ( $n = 8$  wells for each condition on each side of the plate). Alternatively, the positive controls can be split into  $n = 8$  wells of the maximal concentration and  $n = 8$ –16 wells of the positive control dose response ( $n = 2$  wells per concentration). This will enable mapping of screened compounds against a standard curve for either inhibition or stimulation.
23. Depending on the acoustic liquid dispenser's processing speed and number of screening plates, it may be necessary to “prepping” dissolved screening compounds, DMSO, and positive controls into 384-well plates in advance. Seal plates with foil to prevent evaporation and store at  $-20^{\circ}\text{C}$  until ready for use. Warm to room temperature prior to dispensing cells.
24. This assay can be scaled up to 384-well plates using conditions similar or identical to those optimized in Subheading 3.3. To identify false positives in this assay, calculate  $Z$ -scores using negative controls as in Subheading 3.4, step 4d. Exclude those compounds with  $Z$ -scores of  $>3$  or  $< -3$ .
25. HEK293 cells stably expressing the Nav1.6 channel are commercially available. These cells can be used to create a double stable cell line expressing the protein of interest by following a

protocol similar to Subheading 3.2. Stable cells should be validated using WB and/or rtPCR, as well as patch-clamp electrophysiology (rather than LCA).

26. This relatively quick procedure should be viable for most cell lines. However, if poor seals are obtained, it may be caused by excess stress during cell harvesting. Nanon has optimized the following procedure has been optimized for gently harvesting cells to achieve improved seals for patching:
  - (a) Prewarm 10 mL HBSS to 37 °C and 5 mL 30% Accutase to RT.
  - (b) Aspirate medium and dispense 5 mL of 37 °C HBSS and incubate for 1 min at RT. Aspirate HBSS and repeat.
  - (c) Dispense 5 mL of 30% Accutase (prewarmed to RT), and quickly remove 4 mL. Incubate at 37 °C for ~10 min.
  - (d) Observe cells using light microscope to confirm that cells have detached and are loose in media. If cells are not yet detached, incubate for ~1–5 min longer.
  - (e) Add 8 mL of cold (4–8 °C) HBSS-EDTA and gently pipette cells using a large pipette (i.e., 5 mL serological pipette), and incubate at 4–8 °C for 10 min to allow cells to recover.
  - (f) Carefully aspirate off 8 mL medium, add fresh 4–8 °C 8 mL BHK-HEPES, and incubate 5 min at RT. Carefully aspirate off 8 mL medium.
  - (g) Add 3 mL external solution, and transfer the cells to Eppendorf low-binding tubes (1 mL/tube) and keep at 4–10 °C. Let cells recover for 15–30 min.
27. Additional flasks can be harvested as needed to continue patching in a single day, but cells should not be used after 4 h of incubation in extracellular solution. To patch for an extended duration, you may alternatively triturate centrifuged cells in 4 mL of resuspension medium and aliquot into 4 separate Eppendorf tubes to maintain sterility. Medium can be aspirated and changed to extracellular solution immediately prior to patching.
28. Hold chips by grasping only the sides (do not touch the surface) to avoid contamination by grease or dust, which could compromise cell sealing or data quality.
29. Ensure that both the internal and external electrodes are well chlorided. Depending on frequency of usage, we recommend rechloriding electrodes at least once per week.
30. It may be necessary to optimize the suction protocol depending on the particular cell type and overall health; if the suction is too strong (i.e., weaker membrane breaks too early using intermediate.ppf) or too weak, adjust the suction protocol to weak.ppf or strong.ppf, respectively.

## References

1. Ahern CA, Payandeh J, Bosmans F et al (2016) The hitchhiker's guide to the voltage-gated sodium channel galaxy. *J Gen Physiol* 147:1–24
2. Xu L, Ding X, Wang T et al (2019) Voltage-gated sodium channels: structures, functions, and molecular modeling. *Drug Discov Today* 24:1389–1397
3. Stoilova-Mcphie S, Ali S, Laezza F (2013) Protein-protein interactions as new targets for ion channel drug discovery. *Austin J Pharmacol Ther* 1(2):5
4. Leterrier C, Brachet A, Fache MP et al (2010) Voltage-gated sodium channel organization in neurons: protein interactions and trafficking pathways. *Neurosci Lett* 486:92–100
5. Di Re J, Wadsworth PA, Laezza F (2017) Intracellular fibroblast growth factor 14: emerging risk factor for brain disorders. *Front Cell Neurosci* 11:1–7
6. Molinarolo S, Granata D, Carnevale V et al (2018) Mining protein evolution for insights into mechanisms of voltage-dependent Sodium Channel auxiliary subunits. *Handb Exp Pharmacol* 246:33–49
7. Hoxha E, Marcinnò A, Montarolo F et al (2019) Emerging roles of Fgf14 in behavioral control. *Behav Brain Res* 356:257–265
8. Wildburger NC, Ali SR, Hsu W-CJ et al (2015) Quantitative proteomics reveals protein–protein interactions with fibroblast growth factor 12 as a component of the voltage-gated Sodium Channel 1.2 (Nav1.2) macromolecular complex in mammalian brain. *Mol Cell Proteomics* 14:1288–1300
9. Li MCH, O'Brien TJ, Todaro M et al (2019) Acquired cardiac channelopathies in epilepsy: evidence, mechanisms, and clinical significance. *Epilepsia* 60:1753–1767
10. Symonds JD, Zuberi SM (2018) Genetics update: Monogenetics, polygene disorders and the quest for modifying genes. *Neuropharmacology* 132:3–19
11. Azad T, Tashakor A, Hosseinkhani S (2014) Split-luciferase complementary assay: applications, recent developments, and future perspectives. *Anal Bioanal Chem* 406:5541–5560
12. Wehr MC, Rossner MJ (2016) Split protein biosensor assays in molecular pharmacological studies. *Drug Discov Today* 21:415–429
13. Shavkunov AS, Ali SR, Panova-Elektronova NI et al (2015) Split-luciferase complementation assay to detect channel-protein interactions in live cells. *Methods Mol Biol* 1278:497–514
14. Shavkunov A, Panova N, Prasai A et al (2012) Bioluminescence methodology for the detection of protein–protein interactions within the voltage-gated Sodium Channel macromolecular complex. *Assay Drug Dev Technol* 10:148–160
15. Wadsworth PA, Folorunso O, Nguyen N et al (2019) High-throughput screening against protein:protein interaction interfaces reveals anti-cancer therapeutics as potent modulators of the voltage-gated Na<sup>+</sup> channel complex. *Sci Reports* 9 (1)
16. Fertig N, Blick RH, Behrends JC (2002) Whole cell patch clamp recording performed on a planar glass chip. *Biophys J* 82:3056–3062
17. Ali SR, Singh AK, Laezza F (2016) Identification of amino acid residues in fibroblast growth factor 14 (FGF14) required for structure-function interactions with voltage-gated sodium channel Nav1.6. *J Biol Chem* 291:11268–11284
18. Hsu WCJ, Scala F, Nenov MN et al (2016) CK2 activity is required for the interaction of FGF14 with voltage-gated sodium channels and neuronal excitability. *FASEB J* 30:2171–2186
19. Hsu WC, Nenov MN, Shavkunov A et al (2015) Identifying a kinase network regulating FGF14:Nav1.6 complex assembly using split-luciferase complementation. *PLoS One* 10:1–21
20. Ali S, Shavkunov A, Panova N et al (2014) Modulation of the FGF14:FGF14 homodimer interaction through short peptide fragments HHS public access. *CNS Neurol Disord Drug Targets* 13:1559–1570
21. Kanduc D (2013) Pentapeptides as minimal functional units in cell biology and immunology. *Curr Protein Pept Sci* 14:111–120
22. Deriu D, Gassmann M, Firbank S et al (2005) Determination of the minimal functional ligand-binding domain of the GABAB (1b) receptor. *Biochem J* 386:423–431
23. Wang W, Jiang Q, Argentini M et al (2012) Kif2C minimal functional domain has unusual nucleotide binding properties that are adapted to microtubule depolymerization. *J Biol Chem* 287:15143–15153
24. Zhou Y, Nwokonko RM, Cai X et al (2018) Cross-linking of Orai1 channels by STIM proteins. *Proc Natl Acad Sci U S A* 115: E3398–E3407

25. Zhou Y, Cai X, Nwokonko RM et al (2017) The STIM-Orai coupling interface and gating of the Orai1 channel. *Cell Calcium* 63:8–13
26. Ma G, Zheng S, Ke Y et al (2017) Molecular determinants for STIM1 activation during store-operated  $\text{Ca}^{2+}$  entry. *Curr Mol Med* 17:60–69
27. Inglese J, Johnson RL, Simeonov A et al (2007) High-throughput screening assays for the identification of chemical probes. *Nat Chem Biol* 3:466–479
28. Chai SC, Goktug AN, Chen T (2013) Liquid handling devices in drug discovery: when, what, why? *Eur Pharm Rev* 18:11–14
29. Shavkunov AS, Wildburger NC, Nenov MN et al (2013) The fibroblast growth factor 14-voltage-gated sodium channel complex is a new target of glycogen synthase kinase 3 (GSK3). *J Biol Chem* 288:19370–19385
30. Szabat M, Modi H, Ramracheya R et al (2015) High-content screening identifies a role for  $\text{Na}^+$  channels in insulin production. *R Soc Open Sci* 2:150306
31. Rajwa B (2017) Effect-size measures as descriptors of assay quality in high-content screening: a brief review of some available methodologies. *Assay Drug Dev Technol* 15:15–29
32. Wang YL, Wang Y, Tong L et al (2008) Over-expression of calcineurin B subunit (CnB) enhances the oncogenic potential of HEK293 cells. *Cancer Sci* 99:1100–1108
33. Sittampalam GS, Grossman A, Brimacombe K et al (2019) *Assay Guidance Manual*. Eli Lilly & Company and the National Center for Advancing Translational Sciences, Bethesda (MD)
34. Trask OJ (2018) Guidelines for microplate selection in high content imaging. *Methods Mol Biol* 1683:75–88
35. Obergrussberger A, Haarmann C, Rinke I et al (2014) Automated patch clamp analysis of nACh $\alpha$ 7 and Nav1.7 channels. *Curr Protoc Pharmacol* 65:11.13.1–48
36. Oliva MK, McGarr TC, Beyer BJ et al (2014) Physiological and genetic analysis of multiple sodium channel variants in a model of genetic absence epilepsy. *Neurobiol Dis* 67:180–190



# Chapter 11

## Nucleated, Outside-Out, Somatic, Macropatch Recordings in Native Neurons

Francesco Tamagnini

### Abstract

Patch-clamp recordings are a powerful tool for the live measurement of the plasma membrane biophysical properties, with the ability to discriminate fast events such as fast inactivating  $\text{Na}^+$  currents ( $<1$  ms c.a.). It can be used in virtually every cell-type, including cardiomyocytes, skeletal muscles, neurons, and even epithelial cells and fibroblasts. Voltage-clamp, patch-clamp recordings can be used to measure and characterize the pharmacological and biophysical profile of membrane conductances, including leak, voltage-gated, and ligand-gated ion channels. This technique is particularly useful in studies carried out in cell-lines transfected with the gene expressing the conductance under investigation. However, voltage-clamp measures conducted on the soma of a native, adult neuron, for example in an acute brain slice or in the brain of a live individual, are subject to three major limitations: (1) the branching structure of the neuron causes space-clamp errors, (2) ion channels are differentially expressed across different neuronal compartments (such as soma, dendrites, and axons), and (3) the complex geometry of neurons makes it challenging to calculate current densities. While not preventing the experimenter to conduct patch-clamp, voltage-clamp recordings in native neurons, these limitations make the measures poorly standardized and hence often unusable for testing specific hypotheses.

To overcome the limitations outlined above, outside-out, patch-clamp recordings can be carried out instead (See Chap. 1, Sect. 3.5); however, the signal-to-noise ratio in outside-outs from native, adult neurons is usually too low for obtaining accurate measurements.

Here we describe how to carry out nucleated, outside-out, somatic, macropatch recordings (from now on abbreviated into “macropatch recordings”) to obtain accurate and standardized measures of the biophysical and pharmacological properties of somatic, neuronal membrane conductances.

**Key words** Macropatch, Voltage-clamp, Outside-out, Native neurons, Somatic membrane, Voltage-gated channels

## 1 Introduction

### 1.1 The Use of Patch-Clamp, Voltage-Clamp to Characterize Voltage-Gated Channels Biophysical Properties

The electrical properties of the plasma membrane are key factors driving the function of cells and tissues and they are central for the computational abilities of neurons and other excitable cells, such as muscle cells and glandular epithelia [1]. The pioneering and seminal work of Hodgkin and Huxley [2] demonstrated that neuronal plasma membranes work like equivalent electrical circuits, characterized by a charge separation between two poles, the intracellular and the extracellular space, and a condenser (the phospholipid bilayer) in parallel with a resistor (the membrane leak conductances, such as nongated  $K^+$  and  $Cl^-$  channels) (Fig. 1a). In addition, voltage-gated (and analogously ligand-gated) ion channels are responsible for the electrogenic, active membrane electrical properties of a cell (Fig. 1b).

For example, the action potential is generated via the activation of  $Na^+$  and  $K^+$  voltage-gated channels [3, 4], while the release of neurotransmitter is triggered by the  $Ca^{2+}$  influx in the presynaptic terminal caused by the activation of voltage-gated  $Ca^{2+}$  channels [5, 6]. To study the biophysical properties of these channels, it is necessary to measure the changes of conductance in presence of different levels of the stimulating factors (i.e., increasing depolarization steps for voltage-gated ion channels activated by depolarization). To this end, the voltage-clamp technique was developed (*see* Chap. 1 for details). Briefly, in voltage-clamp, a voltage recording electrode is placed in the intracellular space and is paired to a current generator. Both the recorder and the generator are connected to an integration system, which controls the current generator by pumping charges intracellularly in order to keep the membrane voltage at the set value (Fig. 2a), *known as holding potential* ( $V_{hold}$ ), following Ohm's law ( $V = RI$ ). Voltage-clamp, whole-cell patch-clamp works following the same principle, but the voltage recorder and the current generator coexist in the same

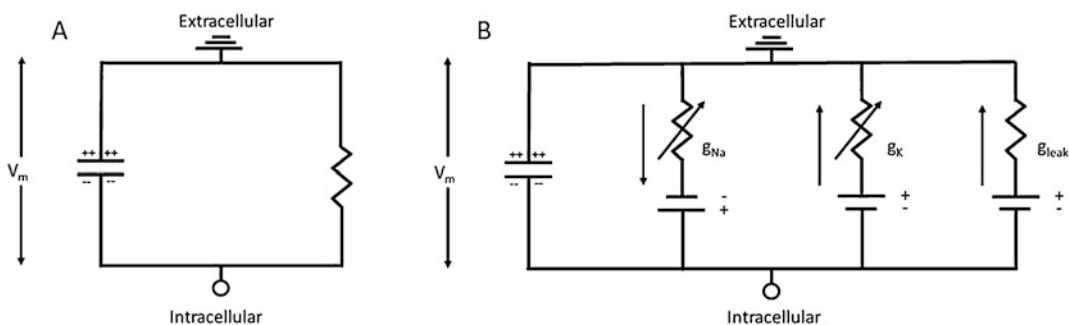


**Fig. 1** (a) Equivalent circuit representing the resistive and capacitive nature of the biological plasma membrane. (b) Excitable neurons possess voltage-gated conductances (such as  $g_{Na}$  and  $g_K$ ) responsible for the generation of action potentials upon depolarization of the plasma membrane

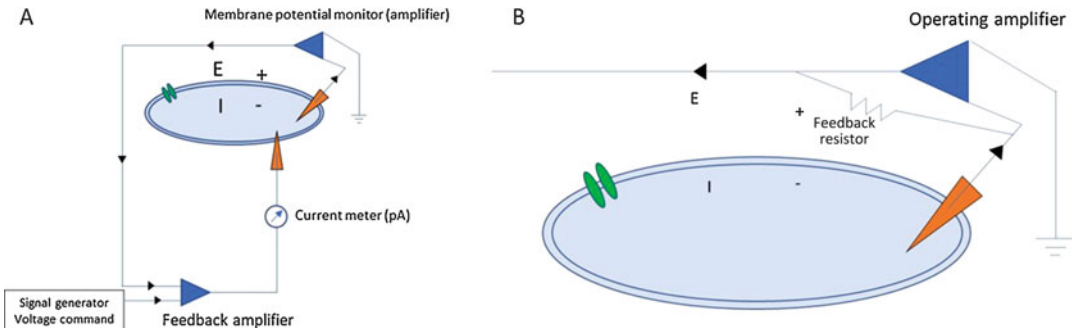


**Fig. 2** (a) Voltage-clamp can be reached with a two-electrode configuration, one to monitor voltage, one to measure/generate current, coordinated by a signal generator integrated with a voltage-command box. (b) However, neuronal membranes are usually too delicate to allow two electrode recording configurations. Single-electrode, voltage-clamp recordings can also be carried out: the same electrode is connected to an operating amplifier, to measure voltage, and a feedback resistor to generate the current needed for voltage-clamping

electrode and it is known as single electrode voltage-clamp (Fig. 2b). The opening of ion channels will generate a current, in presence of an electrochemical driving force for that ion. To counteract the effects of that current on the membrane potential, according to the Ohm's law the system will have to generate a current which has the same shape but inverse direction to the one generated by the ion channels. The generated current, divided by the driving force, will correspond to the conductance. Plotting the conductance versus the voltage deflection, will result in the generation of data-points that can be fit by a Boltzmann sigmoid curve, describing the activation of voltage-gated channels across different voltages. The cell-to-cell Boltzmann fit can, in turn, be used to calculate the channel's half-activation potential ( $V_{1/2}$ ) and its maximal conductance ( $G_{max}$ ) (as in Fig. 5).

### 1.2 Limitations of Voltage-Clamp Recordings in Adult Neurons

The intensity of the currents recorded via voltage-clamp patch-clamp are directly related to the total number of current generating channels present on the plasma membrane. Such number depends on two factors: (1) the channel density and (2) the total extension of the plasma membrane. In whole-cell configuration, this can represent a problem. In fact, to avoid biases arising from cell-to-cell natural variability in cell size, the current values should be expressed as current densities ( $pA/\mu m^2$ ). In practical terms, current densities are expressed in  $pA/pF$ : In fact, the capacitance value of a condenser is directly proportional to the surface extension of the armor

$$C = \frac{A\epsilon_0}{d}$$

where  $C$  = capacitance,  $A$  = area of the armor,  $d$  = distance between plates (in this case the thickness of the phospholipid bilayer), and  $\epsilon_0$  equals the dielectric constant of the phospholipid bilayer. Assuming that  $d$  and  $\epsilon_0$  do not significantly change from cell to cell, the current density can be equally expressed as  $I/A$  ( $\text{pA}/\mu\text{m}^2$ ) or  $I/C$  ( $\text{pA}/\text{pF}$ ). Since in whole-cell patch clamp the  $C$  of a cell can be directly measured, current densities are usually expressed in  $\text{pA}/\text{pF}$ . However, one needs to be careful with this approach. In fact, the complex geometry of neurons may result in a reduction in the accuracy of the  $C$  reading. This is due to reduced space clamping in large, geometrically complex cells [7].

The current injected to maintain the  $V_{\text{hold}}$ , spreads radially from the point of injection and it exponentially decays with distance. This phenomenon is known as *space clamp*. In turn, this results in the lack of control of the membrane potential in those parts of the cell which are distant from the point of current injection [8].

Finally, ion channel subtypes are often differentially expressed across different parts of an adult, native neuron. Hence, the currents recorded in the point of patch (usually the soma), may be the result of a heterogeneous population of ion channels with different biophysical properties, reducing the relevance of the recording. For example, voltage-gated  $\text{Na}^+$  ( $\text{Na}_v$ ) 1.6 channels are mostly expressed in the axonal initial segment and on the axon (especially in the nodes of Ranvier, in myelinated fibers), where they mediate the initiation and forward propagation of the action potential. On the other hand,  $\text{Na}_v$  1.2 channels are mostly expressed in the soma, where they mediate the back-propagation of the action potential [9].

### 1.3 Aim

To overcome the limitations outlined above, we will discuss here how to perform macropatch recordings. This method, while being technically challenging, can provide reliable and accurate data relative to the biophysical properties of both ligand- and voltage-gated channels on the neuronal somatic plasma membrane.

## 2 Materials

### 2.1 Brain Slices

Brain slices can be obtained from rodents at different ages, using standard methods as the ones described in [10, 11]. For the brain slicing process, you will need the following:

1. Cutting solution (see below for details).
2. Artificial cerebrospinal fluid (aCSF) (see below for details).
3. Scalpel (large belly blade preferred).
4. Surgical spring scissors.

5. Surgical tweezers.
6. Small bent spatula.
7. Larger bent spatula.
8. Modified Pasteur pipette for slices.
9. Ice bucket.
10. Carbogen mixture (95% O<sub>2</sub>, 5% CO<sub>2</sub>).
11. Cutting matrix (optional).
12. Water bath (37 °C).

## 2.2 Solutions

### 2.2.1 Cutting Solution

All cutting operations are performed at low temperatures (0–4 °C), to help and reduce the damages arising from ischaemia, following decapitation and preceding the completion of slicing. Cutting solutions are used to help prevent the damages coming from both ischaemia and cold temperatures. For example, they can have low Ca<sup>2+</sup> and high Mg<sup>2+</sup>, to help preventing the excitotoxicity arising from NMDA receptor activation; sucrose or glycerol can be used, in substitution of the corresponding equivalents of NaCl, to reduce the nucleation of extracellular ice crystals which can damage the plasma membrane. Certain laboratories decide to use aCSF as a cutting solution. As all these solutions are based on a NaHCO<sub>3</sub> buffer system, cutting solutions need to be constantly bubbled with a gas mixture containing 95% O<sub>2</sub> and 5% CO<sub>2</sub> (Carbogen). Use the cutting solution you prefer and keep it consistent across the whole project. Here, we report the composition of the cutting solution we use in our laboratory (Table 1A).

### 2.2.2 Artificial Cerebrospinal Fluid (aCSF)

The composition of the cerebrospinal fluid slightly changes from one research group to another. However, there are certain characteristics which are usually common: (1) The aCSF has a NaHCO<sub>3</sub>-based buffer system and for this reason it needs to be constantly bubbled with Carbogen; (2) it contains high concentrations of NaCl (usually >100 mM) and low of KCl (usually <5 mM); (3) the relative concentrations of Ca<sup>2+</sup> and Mg<sup>2+</sup> can change (2:1 is very common) and they are commonly 2 mM or less; (4) glucose levels can variate between 1 and 10 mM. Below, the aCSF formula we use in our laboratory (Table 1B). The pH of the aCSF must be 7.4 and the osmolarity = 300 mOsm/L c.a.

### 2.2.3 Intracellular Solutions

Intracellular solutions can vary, depending on the kind of current that must be measured. For example, to record K<sup>+</sup>, outward currents, starting from a hyperpolarized  $V_{\text{hold}} = -100$  mV, a high K<sup>+</sup>, low Cl<sup>-</sup> internal solution is recommended. In our laboratory, we normally use K-gluconate based intracellular solutions. However, other counterions for K<sup>+</sup> can be used, such as methansulfonate (KMeSO<sub>4</sub>). The pH should be 7.4. The osmolarity of the internal solution needs to be 5% lower than the extracellular solution, to avoid cell swelling and weakening/loss of the seal.

**Table 1**  
**An example of cryoprotective, cutting solution (A) and artificial cerebrospinal fluid (B)**

Molecule	[Final] mM	Mr
<i>(A)</i>		
Sucrose	189	342.30
Glucose	10	180.16
NaHCO <sub>3</sub>	26	84.01
KCl	3	74.55
MgSO <sub>4</sub> .7H <sub>2</sub> O	5	246.48
CaCl <sub>2</sub>	0.1	
NaH <sub>2</sub> PO <sub>4</sub>	1.25	137.99
<i>(B)</i>		
NaCl	124	58.44
KCl	3	74.55
NaHCO <sub>3</sub>	24	84.01
NaH <sub>2</sub> PO <sub>4</sub>	1.25	137.99
MgSO <sub>4</sub> .7H <sub>2</sub> O	1	246.48
CaCl <sub>2</sub>	2	110.98
Glucose	10	180.16

Note that in the cutting solution, in comparison with aCSF, the sucrose replaces NaCl (to prevent the formation of ice crystals), the [Mg<sup>2+</sup>] is higher and the [Ca<sup>2+</sup>] is lower (to reduce NMDA-R dependent excitotoxicity)

So, for an aCSF with an osmolarity of 300 mOsm/L, the intracellular solution should have an osmolarity comprised between 280 and 290 mOsm/L. If an intracellular marker needs to be added to the internal solution (i.e., biocytin for post-hoc reconstruction) the levels of the K<sup>+</sup> salt should be decreased accordingly, to keep the osmolarity constant. Below, an example of internal solution used in our laboratory, with (B) and without (A) biocytin, is given (Table 2).

### 2.3 Recording Setup

The recording setup to perform macropatches in acute slices needs to be built as follows.

1. *Microscope.* For visualizing cells in brain slices, you will need a fixed-stage, upright microscope, mounted on a translation table. To better visualize the cells within the brain parenchyma, we recommend using infrared, differential interference contrast (DIC) microscopy. Epifluorescence or confocal (1- or

**Table 2**  
**Example of KGluconate based internal solutions without (A) and with (B) biocytin**

Molecule	[Final] mM	Mr
<i>(A)</i>		
KGluconate	145	234.2
NaCl	5	58.44
HEPES free acid	10	238.3
EGTA	0.2	380
GTP-Na salt	0.3	523
ATP- Mg Salt	4	507
<i>(B)</i>		
KGluconate	135	234.2
NaCl	5	58.44
HEPES free acid	10	238.3
EGTA	0.2	380
GTP-Na salt	0.3	523
ATP-Mg Salt	4	507
Biocytin	13.4	372

Note that, to make space to the intracellular marker biocytin and keep the osmolarity constant, the concentration of KGluconate has been decreased in (B), in comparison to (A)

2-photon based) microscopy can also be implemented, to visualize specific subpopulations of neurons or patched neurons filled with a fluorescent probe, but this part is optional.

2. *Hydraulics.* During the recordings, the slices will have to be constantly perfused with carbogen-bubbled, heated (35–37 °C), aCSF. To this end, they will be placed in a submersion-style recording chamber, while the aCSF is pumped in and out the chamber by a pump system or let in and out via gravity.
3. *Micromanipulator.* A motorized or hydraulic or piezoelectric micromanipulator, with low drift and submicron resolution. This will be used to mount the amplifiers headstage and direct the micropipette to the cell.
4. *Isolation table.* The whole setup should be mounted on an antivibration table. This increases the stability of the patch and decreases the probability to lose the seal. The antivibration table can be an active control air table or a passive control one (i.e., a heavy metallic plate placed onto inflated tires/inner tubes).

5. *Amplifier.* We recommend using an amplifier designed for patch-clamp (Molecular Devices, HEKA, etc.). The amplifier is connected to a headstage, which is mounted directly on the micromanipulator. Patch-clamp amplifier headstages are designed to be connected to both an AgCl electrode via a micropipette holder and to an Ag/AgCl reference electrode which is placed in the recording chamber. The pipette holder allows to firmly place a micropipette, filled with internal solution, over the recording electrode. The Ag/AgCl will work as a bridge between the metallic circuitry within the amplifier (where electrons are the charge-bearing particles) and the solutions (where the ions are the charge bearing particles).
6. *Analog/Digital (A/D) interface.* This is needed to convert the amplified analog signal into a digital signal which can be visualized with a dedicated data acquisition software, such as pClamp (Molecular Devices), PatchMaster (HEKA), and Signal (Cambridge Electronic Design). A/D boards specifically designed for electrophysiology recordings are Digidata 1550 (and previous versions), from Molecular Devices and several adaptable boards from National Instrument.
7. *Glass micropipettes.* These pipettes can be purchased already pulled and polished. However, most electrophysiology laboratories pull them from borosilicate capillaries with the use of a horizontal/vertical puller. Narishige is one of the most common producers of these pullers. A Narishige microforge can be purchased separately to round up the sharp edges of the pulled pipette. The pipette diameter, after pulling and polishing, should be 1  $\mu\text{m}$  c.a., corresponding to a pipette access resistance of 2–7  $\text{M}\Omega$ .
8. *Faraday cage.* A Faraday cage should be placed around the recording system and every device directly connected to AC current should be left out of it. Reducing the noise via adequate shielding, cleanliness, and removing contacts with the space outside the cage (i.e., by introducing a dripper in the inlet perfusion if the reservoir is placed outside the cage) is always better and advisable, compared to filtering and active noise control. In fact, the latter instances can lead to data loss or, in certain cases, even add noise.
9. *Temperature control.* Temperature control within the recording chamber is of paramount importance, as the temperature has a dramatic effect on the electrical properties of the plasma membrane. An active temperature control system based on constant feedback (i.e., Scientifica Temp Controller) is advisable. However, a constant current system is also adequate, if the room T conditions remain stable.

### 3 Methods

#### 3.1 Overview

Manual patch-clamp techniques are known to be challenging. The experimental setup comprises many separate components and much can happen which can make the recordings unusable or the experiments inconclusive. A good rule of thumb is to get into the recordings as prepared as possible. For example, before starting an important experiment, make sure your technique is good by exercising on less important samples, such as the leftovers from someone else's experiment. In addition, make sure that your dissection technique is accurate and fast: the dissection time is a key factor in slice electrophysiology. In addition, plan your experiment well in advance: make sure you have a clear hypothesis in mind and the experimental protocol you are using is the most adequate to test it. Finally, make sure that both the rig and the laboratory are clean and tidy: Things tend to work out better in a well-ordered lab and, in case a problem occurs, it is usually easier to find a solution.

#### 3.2 Slice Preparation

The animal needs to be decapitated, following cervical dislocation. Subsequently, the brain is rapidly removed and placed into an ice-cold (0–4 °C) cryoprotective cutting solution (see above for details), which is constantly bubbled with Carbogen. Depending on the brain area of interest certain parts can be removed with single scalpel cuts. For example, if the prefrontal cortex is required, the cerebellum and the caudal part of the telencephalon can be removed with single scalpel cuts. To improve the accuracy and the precision of these cuts, a cutting matrix can be used. Depending on the anatomical plane required, the brain can be glued to a vibratome stage in different ways. For example, to cut horizontal slices containing striatum, hippocampus and temporal cortices, you should remove with single scalpel cuts the cerebellum, the prefrontal lobes and the dorsal part of the cortex; subsequently, the brain should be glued on the dorsal side (ventral side facing up). The sample should be quickly placed into a vibratome tray, covered with ice-cold carbogen-bubbled cutting solution and sections should be cut (*see Note 1*). The thickness of the slice can be comprised between 250 µm and 500 µm. While 400 µm is the thickness preferred for field potential or blind patch-clamp recordings, for visualized patch, using infrared DIC microscopy, we recommend to not exceed a thickness of 300 µm. Each slice should be immediately placed in Carbogen-bubbled, aCSF to recover. The recovery period should be carried out for 30 min at 37 °C, followed by >60 min at room temperature, prior to the beginning of the recordings (*see Note 2*).

#### 3.3 Patching

1. Place the slice in the recording chamber and make sure it is not moving. Using a harp to hold it down can help (Fig. 3a).
2. Use the 4× objective to choose the brain area of choice.

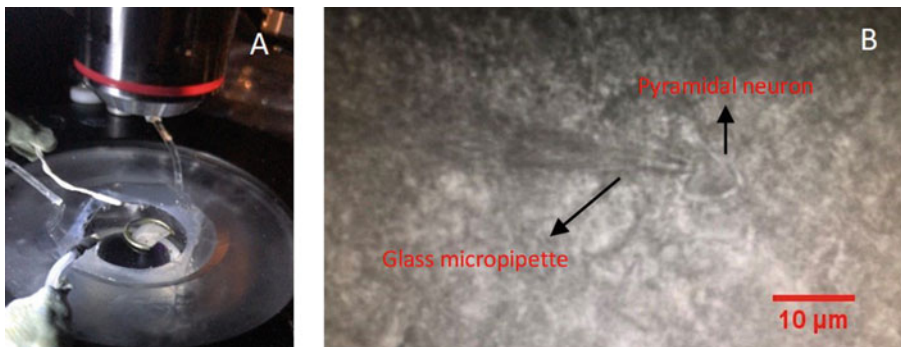


**Fig. 3** (a) Example of a brain slice placed in a submersion-style chamber and held down by a harp. (b) Example of a pyramidal neuron in whole-cell patch-clamp configuration in a brain slice, visualised with DIC, infrared microscopy

3. Once the iris has been closed on the area of interest, switch to the high magnification, salt-water dipping, long working distance objective (usually  $40\times$  or  $60\times$ ).
4. Use the focus to select a cell which looks healthy. A healthy cell, in adult slices, usually looks plump and with regular borders.
5. Fill the pipette half-way with intracellular solution, mount it on the pipette holder and place it just above the surface of the slice. Lock positive pressure inside the mounted pipette. Keep an eye on the pipette electrical resistance by constantly applying pulses of voltage difference between the recording and the reference electrode (1–5 mV). These will generate a current with an intensity inversely correlated to the access resistance of the electrode (Ohm's law:  $V = RI$ ). The amplifier, in this stage, should be in voltage-clamp mode; whole-cell capacitance and series resistance compensation should be switched off and the pipette offset should be kept around 0 mV.
6. Slowly lower the pipette in the brain parenchyma: You will see the internal solution being pushed out by positive pressure and moving debris away. The borders of the cell should now appear clearer.
7. Using an approach angle on the micromanipulator and the focus, approach the surface of the cell with the pipette. Once close enough to the plasma membrane, the access resistance to the electrode should increase and a dimple should appear on the surface of the plasma membrane. Immediately release the positive pressure.
8. Quickly switch on the voltage-clamping and set a  $V_{\text{hold}} = -70$  mV. Run a protocol enabling the transient passage of  $V_{\text{hold}}$  from  $-70$  mV to  $-65$  mV. The overall injected current and the current step between  $V_{\text{hold}} = -70$  mV and  $V_{\text{hold}} = -65$  mV will reveal the tightness of the seal.

9. Once the Gigaohm seal has been obtained, apply short pulses of negative pressure (i.e., you can apply brief and quick suctions to the pipeline connected to the pipette holder) paired to low intensity and short (25–100  $\mu$ s) electrical shocks (“Zap” function on most amplifiers) to reach the whole-cell configuration (Fig. 3b).
  10. Leave the cell to adjust for 1 or 2 min: Follow up the current injected to keep the  $V_{\text{hold}}$  ( $I_m$ ) and make sure it is stable.
1. Apply a light, negative pressure and lock it in the pipette. This will allow the nucleus of the cell to move toward the pipette opening.
  2. After 10–15 s, start to very slowly maneuver the micromanipulator and pull the pipette away from the cell, following an approach angle. The speed of pulling should not exceed 1  $\mu\text{m}/\text{s}$ .
  3. Monitor the  $I_m$  while pulling: Once the macropatch is pulled, the access resistance will be in the order of magnitude of G $\Omega$ s.
  4. Once the macropatch has been excised, keep on pulling until the macropatch has been completely removed from the slice. This will help the quality of the recording: In fact, the slice’s parenchyma is an environment which is less standardized, in comparison with the rest of the recording chamber. The excised macropatch, once pulled outside of the slice, should look like the ones in Fig. 4: You can see the nucleus enclosed within the excised macropatch. The size of a macropatch is usually comprised between 2 and 5  $\mu\text{m}$ .
  5. Compensate the whole cell’s capacitance and series resistance. Macropatches have usually a capacitance comprised between 1 and 5 pF. The series resistance of the macropatch should be under 20 M $\Omega$ .

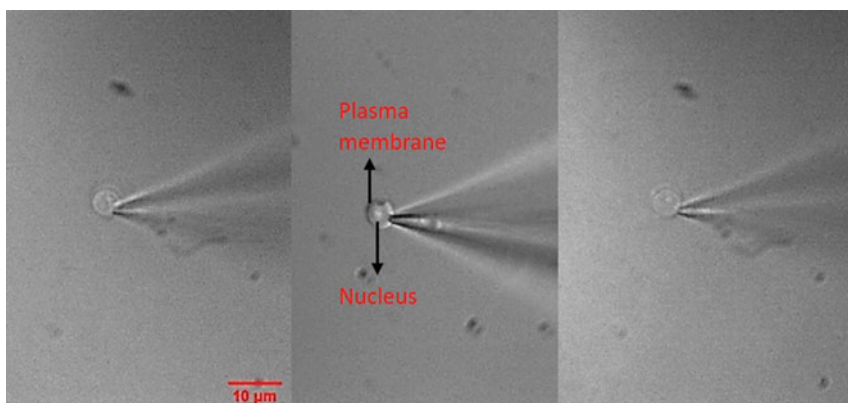


**Fig. 4** Three examples of somatic, nucleated, outside-out macropatches pulled from an adult neuron which was in a brain slice. In each image, the nucleus and the somatic membrane can be visualised

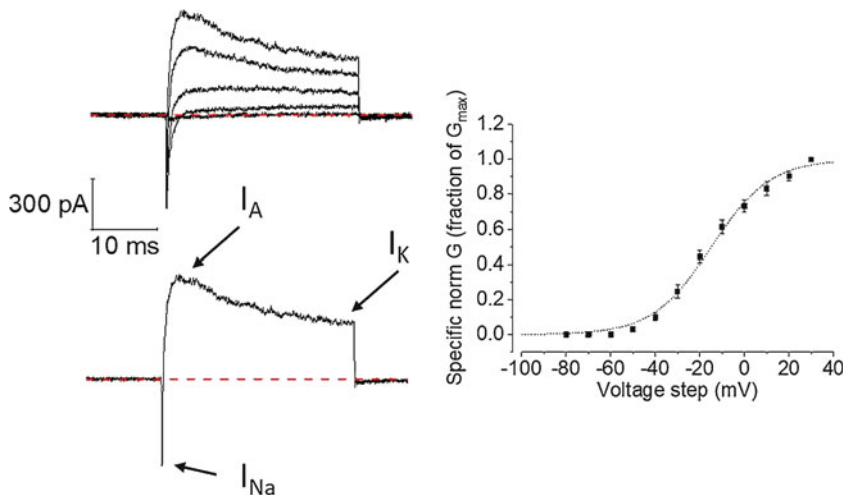


**Fig. 5 (a)** Example of inward  $\text{Na}^+$  and outward  $\text{K}^+$  currents. Among the outward currents, a fast-inactivating ( $I_A$ ) and a non-inactivating ( $I_K$ ) component, can be observed. These currents were evoked by progressive, 10 mV/30 ms, voltage steps, starting from an initial  $V_{hold} = -90$  mV. **(b)** Currents evoked by a 30 ms voltage step from  $-90$  mV to  $+10$  mV. **(c)** IV, Boltzmann curve generated by plotting the current amplitudes (or in this case mean  $\pm$  standard error of the mean specific conductances—modified from [12]) versus the applied change in  $V_{hold}$ . This curve can be used to calculate cell-to-cell (or in this case, macropatch-to-macropatch) values of the half-activation voltages and maximal conductance of the voltage-gated channel under investigation. (Modified from [12])

6. Record the signals. For example, if the biophysical, activation properties of voltage-gated, outward channels are being recorded, start from a  $V_{hold} = -75$  mV and apply short (i.e., 30 ms)  $V_{hold}$  depolarization steps (i.e., 10 mV, for 12 iterations). For each V step record multiple sweeps (at least 3) and remember to perform leak subtraction (see chapter...).
7. The current densities generated upon depolarization can be measured and IV curves can be generated for the calculation of the conductance activation properties ( $V_{1/2}$  and  $G_{max}$ ). Macropatches can be used to measure several currents, including voltage-gated  $\text{Na}^+$  and  $\text{K}^+$  currents, which are involved in action potential generation (Fig. 5) (see Note 3).
8. The rate of success of pulling macropatches is relatively low. Practice, persistence, and passion are key. Just keep on trying. A particular important point is to be very slow but constant while pulling away. Also, it is useful to respond to changes in  $I_m$  while pulling, to adjust the rate of pulling accordingly (slowing down or accelerating, depending on how wobbly the signal is) (see Note 4).

---

## 4 Notes

### 1. Brain areas and cell subtypes.

Our recordings have been carried out in hippocampal and cortical pyramidal neurons and interneurons, at both room temperature and 34 °C. Excising macropatches from interneurons has proved to be more challenging than from pyramidal neurons. This is probably due to the smaller size of interneuronal somas. For these reasons, we infer that macropatches are a viable technique for different cell types in virtually every brain area.

### 2. Slices recovery time.

Slice electrophysiology majorly relies on slice viability. Many factors affect it, including dissection time, the use of cryoprotective cutting solution and the temperature of the cutting solution. Each group tends to have its set of rules, which are equally valuable as long as they fit with an effective experimental plan. We recommend moving the slices directly from the ice-cold cutting solution to 37 °C aCSF, for 30 min. Subsequently, the slice can be left to recover for additional 60 min in aCSF at room temperature. The first temperature boost, in our experience, allows higher cell viability and, consequently, higher probability to excise macropatches.

### 3. Isolating individual currents in macropatches.

Native neuronal membranes contain a variety of different voltage-gated channels. For this reason, the currents recorded from macropatches may result from the activity of different channels. Teasing out the contribution of each one, to measure their respective biophysical properties, can be challenging. A viable approach can be using pharmacological tools to isolate each component: For example, TTX and 4-AP to block  $I_{\text{Na}}$  and  $I_{\text{A}}$ , respectively, can be used to isolate  $I_{\text{K}}$  currents. However, caution should be used in interpreting the results coming from these recordings, as the signal, as pharmacologically or biophysically isolated as it can be, may still arise from different channel subtypes.

### 4. Macropatches for the study of ligand-gated ion channels.

The focus of this chapter was on the use of macropatches for the characterization of voltage-gated channels biophysical properties. However, the same technique can be used for detecting currents generated by ligand-gated ion channels, such as GABA-A or AMPA-R dependent currents. This can be reached by pairing the patch-clamp equipment to a pico-/femto-spritzer, to apply localized chemical stimuli

directly on the macropatch. This approach would be preferred to bath application, to avoid biases due to the inactivation of these conductances associated with the persistent presence of the transmitter in the extracellular space [13].

## References

1. Mack S et al (2013) Principles of neural science, 5th edn. McGraw-Hill Education, New York
2. Hodgkin AL, Huxley AF (1952) A quantitative description of membrane current and its application to conduction and excitation in nerve. *J Physiol* 117:500–544
3. Armstrong CM (1981) Sodium channels and gating currents. *Physiol Rev* 61:644–683. <https://doi.org/10.1152/physrev.1981.61.3.644>
4. Hille B (1978) Ionic channels in excitable membranes. Current problems and biophysical approaches. *Biophys J* 22:283–294. [https://doi.org/10.1016/S0006-3495\(78\)85489-7](https://doi.org/10.1016/S0006-3495(78)85489-7)
5. Kandel ER (1981) Calcium and the control of synaptic strength by learning. *Nature* 293:697–700. <https://doi.org/10.1038/293697a0>
6. Katz B, Miledi R (1967) A study of synaptic transmission in the absence of nerve impulses. *J Physiol* 192:407–436. <https://doi.org/10.1113/jphysiol.1967.sp008307>
7. Bar-Yehuda D, Korngreen A (2008) Space-clamp problems when voltage clamping neurons expressing voltage-gated conductances. *J Neurophysiol* 99:1127–1136. <https://doi.org/10.1152/jn.01232.2007>
8. Hodgkin AL, Huxley AF, Katz B (1952) Measurement of current-voltage relations in the membrane of the giant axon of Loligo. *J Physiol* 116:424–448. <https://doi.org/10.1113/jphysiol.1952.sp004716>
9. Leterrier C, Brachet A, Fache MP, Dargent B (2010) Voltage-gated sodium channel organization in neurons: protein interactions and trafficking pathways. *Neurosci Lett* 486:92–100. <https://doi.org/10.1016/j.neulet.2010.08.079>
10. Tamagnini F et al (2013) Nitric oxide-dependent long-term depression but not endocannabinoid-mediated long-term potentiation is crucial for visual recognition memory. *J Physiol* 591:3963–3979. <https://doi.org/10.1113/jphysiol.2013.254862>
11. Tamagnini F et al (2015) Altered intrinsic excitability of hippocampal CA1 pyramidal neurons in aged PDAPP mice. *Front Cell Neurosci* 9:372. <https://doi.org/10.3389/fncel.2015.00372>
12. Tamagnini F et al (2017) Hippocampal neurophysiology is modified by a disease-associated C-terminal fragment of tau protein. *Neurobiol Aging* 60:44–56. <https://doi.org/10.1016/j.neurobiolaging.2017.07.005>
13. Ford CP, Phillips PEM, Williams JT (2009) The time course of dopamine transmission in the ventral tegmental area. *J Neurosci* 29:13344. <https://doi.org/10.1523/JNEUROSCI.3546-09.2009>



# Chapter 12

## Preparation of Rat Organotypic Hippocampal Slice Cultures Using the Membrane-Interface Method

Timothy W. Church and Matthew G. Gold

### Abstract

Cultured hippocampal slices from rodents, in which the architecture and functional properties of the hippocampal network are largely preserved, have proved to be a powerful substrate for studying healthy and pathological neuronal mechanisms. Here, we delineate the membrane-interface method for maintaining organotypic slices in culture for several weeks. The protocol includes procedures for dissecting hippocampus from rat brain, and collecting slices using a vibratome. This method provides the experimenter with easy access to both the brain tissue and culture medium, which facilitates genetic and pharmacological manipulations and enables experiments that incorporate imaging and electrophysiology. The method is generally applicable to rats of different ages, and to different brain regions, and can be modified for culture of slices from other species including mice.

**Key words** Organotypic, Hippocampus, Brain slice, Whole-brain cultures

---

### 1 Introduction

The first studies incorporating organotypic slice cultures utilized the roller tube technique [1, 2], in which brain slices attached to a coverslip are placed in a roller tube. This approach has been largely superseded by the membrane-interface method [3], which is the focus of this chapter. Since its introduction in 1991 by Stoppini, Buchs, and Muller, this simple and inexpensive method has been cited in over 4000 publications. The interface method involves placing brain tissue slices on a semipermeable membrane insert, which is placed in a well containing culture medium (Fig. 1). Nutrients in the slice culture medium reach the brain tissue via capillary action, and—since the tissue is only covered by a thin film of solution—sufficient oxygenation occurs with incubation in a humidified atmosphere.

Organotypic slices cultured using the membrane interface approach were first used to study neuronal development, synaptic plasticity and synaptogenesis [3–6]. These original studies

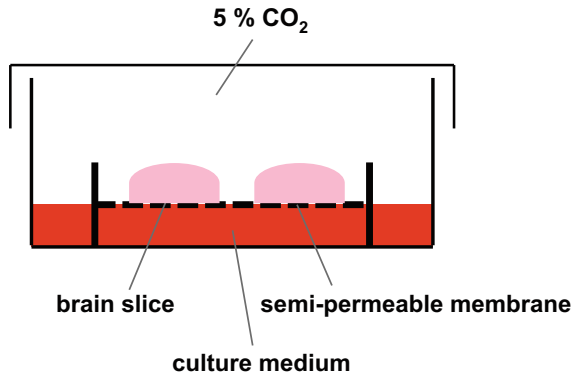


**Fig. 1** Schematic of membrane-interface method. The apparatus is incubated at 37 °C, in a humidified atmosphere of 5% CO<sub>2</sub>. The semipermeable membrane allows nutrients to reach the slice via capillary action without drowning the tissue in culture medium. The membrane-interface methodology affords the experimenter precise control over gene expression and culture conditions

revealed that the maturation of synaptic connections during ex vivo culturing is similar to in vivo maturation, highlighting the value of organotypic slices as a substrate for studies of development. Importantly, the interface method provides direct access to slices and their extracellular environment. As such, the technique is highly compatible with imaging and electrophysiology experiments and enables direct application of pharmacological compounds to either the slice or culture medium. For example, organotypic cultured slices have been used in high-content drug screening studies [7, 8]. Easy access to the brain tissue also provides the opportunity for genetic manipulations [9, 10], for example, to drive protein overexpression [11, 12] or knockdown [11]. Genetic manipulations can be induced by biolistic transfections [13], viral infection [11], or single-cell electroporation [14]. The use of organotypic brain slice cultures from animal models of neurodegenerative disease including Alzheimer's disease [15–17] is increasing. In addition, the culture medium may be monitored over time for the presence of diagnostic molecules. For example, levels of lactate dehydrogenase and inflammatory cytokines can be analyzed to evaluate cell damage, neuroprotective mechanisms, and ischemic events [18, 19].

It is worth considering the value and limitations of organotypic slice culturing compared to other methods for studying neurons. Primary cell cultures provide the most homogenous preparations that facilitate imaging of single neurons and are invaluable for functional analysis of, for example, ion channels and metabotropic receptors. However, they have limited utility for investigating neuronal circuitry and plasticity mechanisms. Studying neurons in living animals is technically very demanding, although there have been many recent developments in imaging [20, 21], electrical

recordings [22], and genetic manipulations [23] supporting research at this end of the complexity spectrum. Experiments with brain slices have the advantage that the number of animals required to test a hypothesis can be reduced in many cases since 10–15 hippocampal slices at a thickness of 300 µM can be collected per P17 male Sprague Dawley rat [17].

Acute brain slices are sufficient for many experiments, but viability is limited to about 24 h in the absence of culturing. There is ongoing debate concerning the suitability of organotypic cultures for studying the properties of neuronal networks. Clearly, slicing severs many axons and dendrites [24], but certain pathways may be well preserved following slicing [25]. The architecture of the hippocampus is particularly well suited to experimentation in slices. For example, intact Schaffer collaterals may be obtained by slicing in any of a number of different planes [25], including the horizontal plane as outlined in this chapter. Organotypic culturing enables some recovery of axonal projections, the dendritic arbor, and synaptic connections over time following slicing [26, 27], providing a potential advantage in comparison to acute slices. This perspective is supported by a comparative study, which showed that spontaneous spike firing rates and excitatory synaptic inputs are more similar to the *in vivo* hippocampal network in organotypic slices than acute slices [28]. However, this recovery in synaptic connections reaches a tipping point after about 2 weeks of organotypic culturing with rodent hippocampal slices, with excitability reaching levels that trigger epileptic events that preclude electrophysiology experimentation [5, 29]. Overall, organotypic culturing has clear value, and in many cases synergizes with studies at higher and lower levels of complexity.

In this chapter, we detail the materials required for the interface method of organotypic slice culture (Subheading 2) before laying out preparatory steps (Subheading 3.1), and protocols for dissection and slicing of hippocampus from rats (Subheading 3.2), and establishing organotypic cultures (Subheading 3.3). We also describe necessary steps during organotypic culture (Subheading 3.4), and explain how to remove slices from culture for experimentation (Subheading 3.5). Common pitfalls, potential modifications, and theoretical insights are highlighted in “Notes” (Subheading 4).

---

## 2 Materials

Prepare solutions using ultrapure water (e.g., by purifying deionized water with a MilliQ system to a resistivity of >18 MΩ), and analytical grade reagents.

## 2.1 Dissection and Slicing

1. Sprague-Dawley or Wistar rats aged postnatal day 17–19 (*see Note 1*).
2. Dissecting medium: 189 mM sucrose, 10 mM D-glucose, 26 mM NaHCO<sub>3</sub>, 3 mM KCl, 5 mM MgSO<sub>4</sub>·7H<sub>2</sub>O, 1.25 mM NaH<sub>2</sub>PO<sub>4</sub>, 0.1 mM CaCl<sub>2</sub>. Store at 4 °C for up to 1 week (*see Note 2*).
3. Artificial cerebral spinal fluid (aCSF): 124 mM NaCl, 3 mM KCl, 24 mM NaHCO<sub>3</sub>, 1.25 mM NaH<sub>2</sub>PO<sub>4</sub>·H<sub>2</sub>O, 1 mM MgSO<sub>4</sub>·7H<sub>2</sub>O, 10 mM D-glucose, 2 mM CaCl<sub>2</sub>. Store at 4 °C for up to 1 week (*see Note 3*).
4. Vibrating blade microtome (*see Note 4*) (e.g., Leica VT1200 S).
5. Stainless-steel blade (e.g., Wilkinson Sword double-edged blade) (*see Note 5*).
6. 70% ethanol.
7. Dissecting tools: large scissors, small dissecting scissors, dissecting tweezers, blunt rounded spatula, scalpel and blade.
8. Dissecting microscope (e.g., Zeiss Stemi 2000c stereomicroscope).
9. Parafilm.
10. Cyanoacrylate adhesive (e.g., Loctite superglue).
11. Slice holding chamber (e.g., from AutoMate Scientific Brain Slice Keeper series). A homemade holding chamber can be fabricated from a 50 mL syringe and a fine nylon mesh (Fig. 2, *see Note 6*).
12. 95% O<sub>2</sub>–5% CO<sub>2</sub> gas mixture (carbogen).

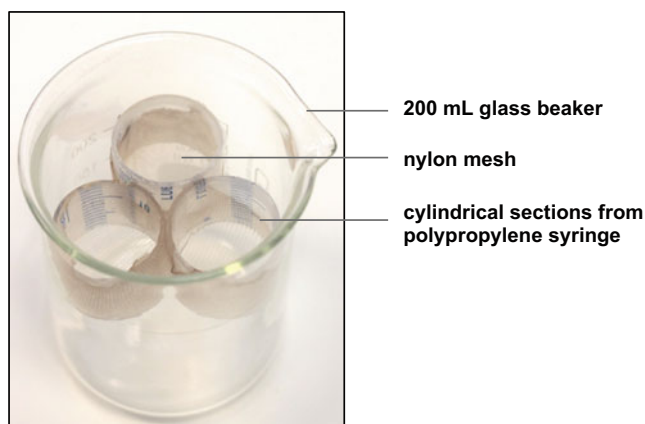


**Fig. 2** Slice chamber fabrication. A homemade slice chamber may be assembled by gluing stretched nylon tights to three cylindrical sections cut from a polypropylene syringe. Placing slices onto the porous nylon mesh enables sufficient oxygenation when slices are incubated in aCSF bubbled with carbogen

## 2.2 Slice Culture

1. Osmometer (e.g., Vapor Pressure Osmometer M5520 [Wescor]).
2. Penicillin (5000 U/mL)–streptomycin (5000 µg/mL).
3. Organotypic slice culture medium (OSM): 49.4% MEM, 12.5% heat-inactivated horse serum (Gibco, cat. no. [26050088](#)), 75 mM HEPES, 5 mM NaHCO<sub>3</sub>, 0.625 mM CaCl<sub>2</sub>, 1.25 mM MgSO<sub>4</sub>·7H<sub>2</sub>O, 1 mM L-glutamine, 32 mM D-glucose, 1 mg/L insulin from bovine pancreas (*see Note 7*), 0.425 mM ascorbic acid, 50 units (U)/mL penicillin, 50 µg/mL streptomycin. To prepare 200 mL OSM, add all components and bring up to ~150 mL before adjusting the pH to 7.28 with concentrated NaOH. Monitor the osmolarity when bringing up to the final volume using MilliQ water until a concentration of 320 mmol/kg is reached (*see Note 8*). Transfer OSM into a sterile tissue culture hood and sterile filter OSM through a 0.22 µm filter (e.g., Nalgene, cat. no. 568-0020). Store at 4 °C for up to 1 month (*see Note 9*).
4. Semipermeable cell culture inserts (Millipore, cat. no. PICM03050).
5. Polypropylene 6-well culture plates and 10 cm diameter dishes.
6. Modified Pasteur pipettes for the transfer of hippocampal slices. To fabricate wide-ended pipettes, first break off the tapering edge of a glass Pasteur pipette. Smooth the broken end with a naked flame then cover with a rubber bulb (e.g., Fisher Scientific, cat. no. 10746162) for drawing solution into the wide end of the glass pipette (diameter ~1 cm).

## 2.3 Lentiviral Infection

1. 5 µL Hamilton syringe (cat. no. 549-1231).
2. Fine 32 gauge Hamilton removable needle (cat. no. HAMI7762-05).
3. Lentivirus stored in 5 µL aliquots at –80 °C until required.
4. Prechilled OSM for diluting lentivirus.
5. 50 mL of 70% Ethanol in a 50 mL Falcon tube.

## 3 Methods

The following procedures should be carried out in a sterile tissue culture hood using aseptic technique, unless otherwise stated.

### 3.1 Preparatory Steps Prior to Dissection

1. Autoclave dissecting tools.
2. At least 30 min before dissection, add 1 mL OSM into each well of a 6-well tissue culture plate (*see Note 10*). Add a Millipore cell-culture insert into each well using sterile forceps. Ensure that the OSM is in contact with the semipermeable

membrane and that no air bubbles are trapped underneath the insert. Culture dishes can be prepared up to 24 h in advance of dissection.

3. Prepare slice washing plate: add 5 mL OSM supplemented with antibiotics into 3 wells of a 6-well plate, and transfer into an incubator at 37 °C with 5% CO<sub>2</sub>. Washing plates can also be prepared up to 24 h in advance. If the vibratome is cleaned diligently between slicings, it is possible to culture slices without antibiotics, but it is advisable to at least include penicillin and streptomycin in the initial washing solutions (*see Note 11*).
4. Spray the floor and walls of the tissue culture hood with 70% ethanol. If the tissue culture hood has a UV light for sterilization, turn on to further sterilize the tissue culture hood.
5. Spray dissecting area with 70% ethanol.
6. Pour 200 mL of prechilled dissecting medium into a 250 mL beaker and cover with Parafilm. Place solution in –20 °C for approximately 15 min until solution forms a slurry mix of frozen and liquid solution. Once a slurry has formed, place beaker in ice and bubble dissecting medium with carbogen for at least 30 min.
7. Prepare 500 mL aCSF supplemented with 2 mM CaCl<sub>2</sub> and bubble with carbogen for 30 min.
8. Prepare dissecting area by cleaning the work surfaces and vibratome with 70% ethanol.
9. Lay out dissecting tools and clean with 70% ethanol.
10. Remove the double-edged slicing blade from acetone and wash with 70% ethanol. Attach blade to vibratome mount and wash once more with 70% ethanol.

### **3.2 Brain Dissection and Hippocampal Slicing**

1. Cull rats (*see Note 12*) in accordance with local regulations, ideally by cervical dislocation followed immediately by decapitation with large surgical scissors.
2. Spray head with 70% ethanol to minimize contamination and keep contaminated hair fibers away from brain tissue.
3. Cut the skin using a scalpel blade in the rostral (anterior) to caudal (posterior) direction to reveal the skull.
4. Open the skull covering the cerebellum by first using the small dissecting scissors to cut from the vertebral foramen along the midline toward the sagittal suture. Next, cut at ~135° angles relative to the midline starting from the vertebral foramen toward each side of the skull covering the cortex (Fig. 3a). With fine blunted forceps, pull aside the skull to reveal the cerebellar tissue.

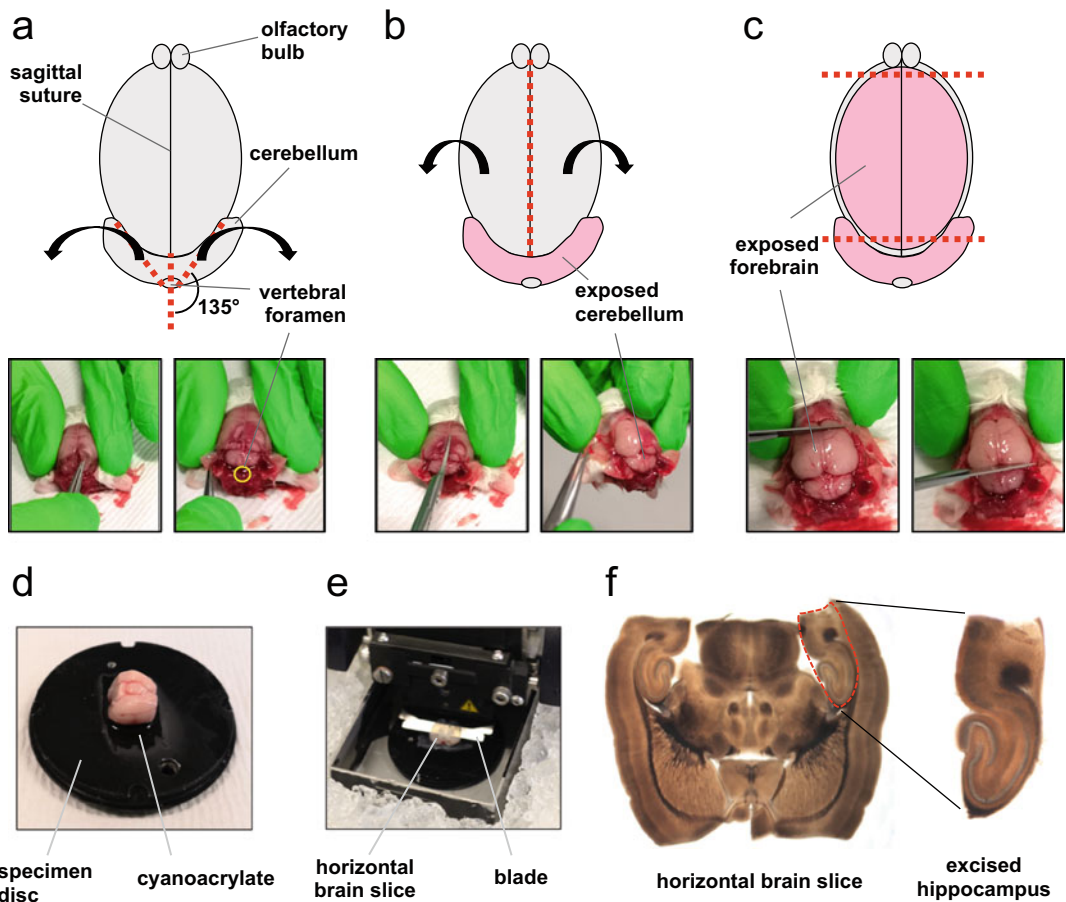


**Fig. 3** Brain dissection & slicing. Throughout the figure, incision lines are denoted by dotted red lines. Panels (a)–(c) show illustrations (upper row) and photographs (lower row) for dissection to remove skull around first the (a) cerebellum and then the rest of the (b) brain prior to removal of the (c) cerebellum and olfactory bulbs. (d) Dissected rat forebrain fixed to specimen disc. (e) Collection of horizontal brain slices using a vibratome. (f) Horizontal 300  $\mu\text{M}$ -thick brain slice (left) after vibratome slicing, and individual hippocampus (right) dissected from the larger slice

5. Cut the skull bilaterally along the midline from the caudal end of the brain toward the frontal lobe using small dissection scissors (Fig. 3b). Ensure the tips of the scissors are pressed lightly against the skull to avoid damaging the brain.
6. Using fine forceps, slightly raise one side of the skull from the brain. Use the forceps tips to detach the meninges from the underside of the skull before pulling back the skull to reveal the forebrain tissue (Fig. 3b). Repeat for the other side, and then remove the meninges from the exposed brain tissue with forceps.

7. Cut along the frontal plane at the division between the olfactory bulb and frontal lobes, and remove the cerebellum, using a scalpel blade (Fig. 3c).
8. Lift the dissected brain out with a rounded spatula and transfer into the slurry of dissection medium for ~1 min.
9. The following step should be performed as quickly as possible to prevent the brain from warming up or drying out: place a layer of cyanoacrylate superglue onto the prechilled slicing specimen disc. For horizontal slices (*see Note 13*), place the brain cortex-side down onto a flat spatula and gently tap the underside of the spatula on tissue paper to drain away excess solution that might prevent the brain adhering to the specimen disc. Using the flat side of a scalpel blade, slide the brain from the spatula and onto the center of the specimen disc in a smooth motion (Fig. 3d).
10. Rapidly slide the specimen disc into place in the slicing chamber, and fill the slicing chamber with the slurry of dissection medium. When filling the slicing chamber, gently pour the dissecting medium into the chamber to prevent the glue from wrapping around the brain.
11. Cut a thick ~2 mm section of brain to expose the hippocampus.
12. Set the vibratome to cut 300  $\mu\text{M}$  thick slices (Fig. 3e, *see Note 14*) at a speed of 0.04 mm/s when the blade has reached the hippocampus or region of interest. Use the modified Pasteur pipette to transfer slices to a 10 cm dish filled with aCSF bubbled with carbogen. Typically 10–15 good quality 300  $\mu\text{M}$  thick horizontal slices (Fig. 3f, left) can be obtained from one rat brain.
13. Trim hippocampal slices by cutting from the lateral ventricle located outside of the CA3/2 stratum oriens to the lateral sides. Make a second incision along the base of the hippocampus from the lateral ventricle. Transfer trimmed hippocampal slices (Fig. 3f, right) to a holding chamber filled with aCSF bubbled with carbogen.
14. Inspect slices under a dissecting microscope for signs of damage caused by dissection or handling. Damaged slices should be discarded.

### **3.3 Establishing the Organotypic Culture**

1. Spray outside of beaker containing slices with 70% ethanol before transferring into tissue culture hood. Rapidly proceed to next steps if a carbogen line is not available to continue bubbling the aCSF within the hood.
2. Transfer the 6-well plate containing culture inserts along with washing plate from the incubator to the tissue culture hood.

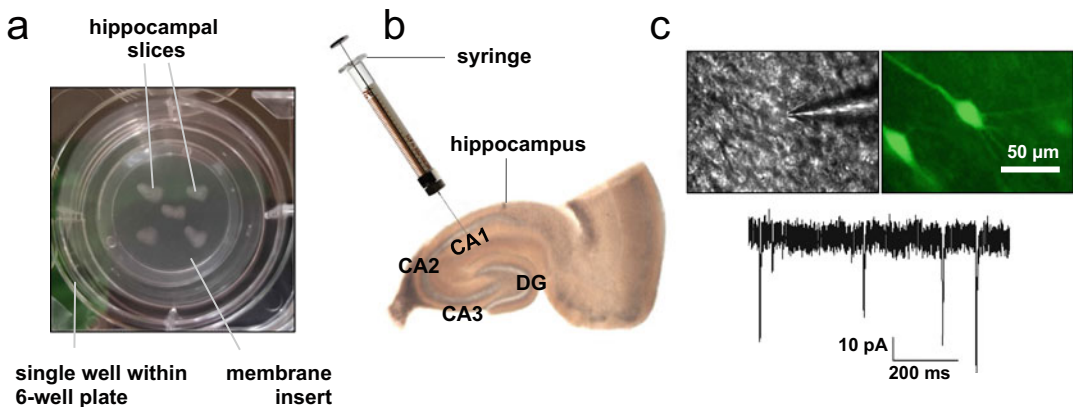


**Fig. 4** During and after organotypic culture (a) Bird's eye view of hippocampal slices inside Millipore semipermeable membrane insert. (b) Lentiviral injection using a fine gauge needle into the CA1 pyramidal layer. Subfields CA2, CA3, and the dentate gyrus (DG) are also labeled. (c) Example infrared (left) and GFP fluorescence (right) images of CA1 pyramidal neurons in hippocampal slices infected with lentivirus expressing GFP. (d) Recordings of spontaneous excitatory postsynaptic currents recorded from the GFP-labeled neuron shown in panel (c)

3. Transfer slices into the first well of the washing plate using the modified Pasteur pipette and gently shake the plate in a figure-of-eight motion for 10–20 s.
  4. Transfer slices into the second and then third well after gently shaking the plate in the same fashion (*see Note 11*).
  5. Gently transfer individual slices from the washing plate onto the membrane of the cell culture insert using the modified Pasteur pipette. Place 3–5 slices on each membrane (Fig. 4a) ensuring that the slices do not touch one another.
  6. Remove excess media covering slices with a pipette. Take care not to touch slices once they are placed on the membrane.
  7. Return the 6-well plate containing the slice inserts into the humidified incubator and culture at 37 °C and 5% CO<sub>2</sub>.
- ### 3.4 Steps During Organotypic Culturing
1. For experiments that involve lentiviral-mediated infection, slices should be infected within 2 h of placing in organotypic culture (*see Note 15*). Lentivirus may be administered using a Hamilton syringe fitted with a fine gauge needle (Fig. 4b, *see Note 16*).
  2. To maintain healthy slices in all cases, replace the media every 2–3 days with prewarmed OSM (*see Note 10*), taking care not to introduce air bubbles under the membrane. On returning the plate to the incubator, ensure that the humidification reservoir is filled to maintain a humidified atmosphere.
  3. Monitor slice viability every 4 days under the dissecting microscope. Viable slices should appear white with well-defined Dentate gyrus, CA3 and CA1 regions. Over the first few days

in vitro, dead cells and tissue debris are naturally cleared from the surface of the slice, resulting in slice thinning. Slices also flatten out over time in culture leading to noticeable broadening of the cell body layers. However, if cell bodies have ceased to be discernible this indicates that the slices are no longer viable and should be discarded. The appearance of black spots or webbing indicate bacterial or fungal contamination, in which case slices should be discarded immediately.

4. The Optimal timeframe to experiment with cultured hippocampal slices is between DIV6-18. Experiments become difficult due to slice thinning beyond DIV18 [30] (*see Note 17*).

### **3.5 Removing Slices from Organotypic Culture for Further Experimentation**

1. Clean a pair of thick tweezers by washing in 70% ethanol and leave to air dry.
2. Using the sterilized tweezers, remove a Millipore insert from a well and place onto a petri dish.
3. If the slices have been in culture for more than 3 days (*see Note 18*), cut through the interface membrane using a scalpel and around hippocampal slices leaving a 3–5 mm overhang of membrane around each slice. Hippocampal slices will remain attached to the interface membrane after embedding during culturing.
4. To continue to electrophysiology (*see Note 19*), transfer slices into a holding chamber filled with aCSF bubbled with carbon dioxide using a flat-ended spatula, and incubate for 1 h at room temperature prior to experimentation.
5. At high magnification, transduced neurons may be selected with the assistance of a fluorescence marker (Fig. 4c, *see Note 20*), and healthy cells can be identified using infrared differential interference contrast (IR-DIC) microscopy (*see Note 21*).

---

## **4 Notes**

1. Slices from more youthful rats (P5-P12) are more resilient to the culturing process [31, 32], especially to mechanical damage from slicing [33]. However, hippocampal morphology is better preserved when slices are taken from older rats, and culturing from P15 to P19 rats is possible when slices are treated carefully [12].
2. The dissecting medium can be modified to include N-methyl-D-glucamine (NMDG) in place of sodium [34]. The NMDG formulation can improve slice health in both acute [34] and organotypic preparations [35].

3. Prepare a 10× concentrated stock of aCSF in advance and store at 4 °C for up to 1 week. Working stocks of aCSF should be supplemented with CaCl<sub>2</sub> (2 mM) on the day of preparation to avoid calcium precipitation.
4. The McIlwain tissue chopper is an alternative to a vibratome. The tissue chopper is fast, easy to use, and allows for multiple hippocampi from a dozen rat brains to be cut simultaneously. However, brains are not maintained in medium during slicing, which can increase cell death, and the chopping motion compresses brain tissue, which can result in morphological changes and also cause cell death. In our experience, high quality slices are obtained using vibratomes operating at low speed (e.g., 0.04 mm/s). Serrated surfaces can be an issue using vibratomes due to *z*-axis blade deflection but advanced vibratomes can compensate for *z*-axis deflection for smoother slicing [36].
5. Commercial blades should be cleaned in acetone before use to remove any oils coating the blades.
6. Homemade slice chambers can be fabricated from a 50 mL polypropylene syringe that is 3 cm in diameter (e.g., Henke SOFT-JECT, VWR, cat. no. 613-1586). First, slice a 50 mL syringe (minus plunger) into three equal open cylinders ~2 cm in length. Glue the three cylindrical sections together using cyanoacrylate adhesive into a triangular assembly (Fig. 2). After setting for 1 h, glue a stretched nylon mesh material (e.g., tights) across one end of the triangular assembly. The slice chamber can be placed in a 200 mL beaker filled with aCSF and bubbled with carbogen to maintain healthy well-oxygenated brain slices [37, 38].
7. Prepare insulin stocks by dissolving at 1 mg/mL in 0.01 N HCl. Store at –20 °C in 250 µL aliquots. Insulin has been observed to improve neuronal survival rates and slice health when maintaining rat slices in culture [29].
8. Accurately titrating the pH and osmolarity (e.g., using a Vapor Pressure Osmometer M5520, Wescor) to pH 7.28 and 320 mmol/kg is critical for obtaining viable and reliable cultures. Small changes in pH and osmolarity will result in cell death.
9. Supplementing culture media with brain-derived neurotrophic factor (BNDF) has been observed to produce healthy, viable slices from adult rats [39]. Alternatively, aged hippocampal slice cultures can be prepared by embedding aged brain in agarose before slicing [40].
10. Culture media in excess of 1 mL per well will rise above the level of the semipermeable membranes and drown slices.

11. If good aseptic technique is applied, there is no need to include penicillin/streptomycin in the OSM. Penicillin is a GABA receptor antagonist at high concentration [41] so can be epileptogenic [42, 43]; however, at the concentration stated in this protocol (84  $\mu$ M) it should not induce epileptic activity [42]. To culture slices without antibiotics, first wash slices three times in wells filled with OSM supplemented with penicillin/streptomycin. Then wash three more times in wells filled with OSM without antibiotics before transfer onto membrane inserts sitting in medium without antibiotics.
12. The interface method is also routinely used to culture mouse brain slices [10, 31, 44].
13. Schaffer collaterals and mossy fibers are well preserved when hippocampal slices are cut in the horizontal (transverse) plane as described here. Coronal slices are obtained by fixing the brain to the specimen disc at the surface exposed after cutting between the frontal lobe and olfactory bulb (Fig. 3c). Sagittal slices are collected by first cutting the brain in half along the midline, and then attaching one hemisphere at a time to the specimen disc at the surface obtained from this cut [45]. Slicing along the horizontal-entorhinal cortex plane (12° tilt from the horizontal plane) is notable since Schaffer collaterals, mossy fibers and the perforant pathway are all preserved at this angle [46].
14. At thicknesses  $>400 \mu$ M, neuronal survival is compromised by deficient diffusion of nutrients and oxygen throughout the slice.
15. Beyond 2 h, a layer of astrocytes forms on the exposed upper surface of tissue once slices are placed in culture [47, 48]. This astrocyte layer acts as a barrier to lentiviral infection, which can be somewhat ameliorated by supplementing OSM with cytarabine (Ara-C) to reduce glial proliferation [49].
16. Lentivirus may be administered using the droplet method [12], or by injecting into the region of interest (e.g., CA1 layer, Fig. 4b). Injection may be achieved manually using a Hamilton syringe, or with an automated microinjector such as the Nanoject II Auto-Nanoliter Injector (Drummond Scientific) [50] or picospritzer (General Valve, Fairfield, NJ) [51].
17. Organotypic hippocampal slices have been reported to last for as long as 6–8 weeks when studying cell death or chronically treating slices with compounds *in vitro* [52].
18. If slices are maintained in organotypic culture for 3 days or less, they may be gently lifted from the inserts using the flat side of a scalpel blade after carefully pipetting 0.5 mL aCSF onto the top surface of the insert. Over time in culture, severed axons and

dendrites recover and form new synapses and projections [5, 53], some of which pass through the semipermeable membrane and anchor slices to the insert.

19. Organotypic cultured hippocampal slices are hyperexcitable. A few methods are available for reducing polysynaptic activity during electrical synaptic stimulation. An incision may be made in the CA2 region to sever Schaffer collateral connections and reduce polysynaptic activity on CA1 pyramidal neurons [54]. Alternatively, polysynaptic activity may be reduced by including the adenosine A1 receptor agonist 2-chloroadenosine in the recording solution [55, 56], or increasing  $\text{Ca}^{2+}/\text{Mg}^{2+}$  concentration in the aCSF [57].
20. If a fluorescent marker (e.g., green fluorescent protein) is being used to identify transduced neurons, then neurons exhibiting fluorescent blebbing along the axons or dendrites should be avoided as this is a sign of fluorescent protein aggregation.
21. Healthy neurons visualized by IR-DIC microscopy display a visible soma with smooth edges. Cells with a swollen morphology, which display dark/high contrast edges and a visible nucleus, should be avoided.

## Acknowledgments

This work was supported by a Wellcome Trust and Royal Society Sir Henry Dale fellowship to MGG (104194/Z/14/Z), and the BBSRC (BB/N015274/1).

## References

1. Hogue MJ (1947) Human fetal brain cells in tissue cultures; their identification and motility. *J Exp Zool* 106:85–107
2. Gähwiler BH (1981) Organotypic monolayer cultures of nervous tissue. *J Neurosci Methods* 4:329–342
3. Stoppini L, Buchs P-A, Muller D (1991) A simple method for organotypic cultures of nervous tissue. *J Neurosci Methods* 37:173–182
4. Muller D, Buchs P-A, Stoppini L (1993) Time course of synaptic development in hippocampal organotypic cultures. *Dev Brain Res* 71:93–100
5. De Simoni A, Griesinger CB, Edwards FA (2003) Development of rat CA1 neurones in acute versus organotypic slices: role of experience in synaptic morphology and activity. *J Physiol* 550:135–147
6. Mohajerani MH, Cherubini E (2005) Spontaneous recurrent network activity in organotypic rat hippocampal slices. *Eur J Neurosci* 22:107–118
7. Sundstrom L, Iii BM, Bradley M, Pringle A (2005) Organotypic cultures as tools for functional screening in the CNS to act as an important link between high-throughput approaches and animal models. *Drug Discov Today Targets* 10:993–1000
8. Cho S, Wood A, Bowlby MR (2007) Brain slices as models for neurodegenerative disease and screening platforms to identify novel therapeutics. *Curr Neuropharmacol* 5:19–33
9. Mildner M, Ballaun C, Stichenwirth M et al (2006) Gene silencing in a human organotypic skin model. *Biochem Biophys Res Commun* 348:76–82
10. Mikhaylova M, Bär J, van Bommel B et al (2018) Caldendrin directly couples postsynaptic calcium signals to actin remodeling in dendritic spines. *Neuron* 97:1110–1125.e14

11. Jurado S, Biou V, Malenka RC (2010) A calcineurin/AKAP complex is required for NMDA receptor-dependent long-term depression. *Nat Neurosci* 13:1053–1055
12. Church TW, Weatherall KL, Corrêa SAL et al (2014) Preferential assembly of heteromeric small conductance calcium-activated potassium channels. *Eur J Neurosci* 41:305–315
13. O'Brien JA, Lummis SCR (2006) Biolistic transfection of neuronal cultures using a hand-held gene gun. *Nat Protoc* 1:977–981
14. Rathenberg J, Nevian T, Witzemann V (2003) High-efficiency transfection of individual neurons using modified electrophysiology techniques. *J Neurosci Methods* 126:91–98
15. Mewes A, Franke H, Singer D (2012) Organotypic brain slice cultures of adult transgenic P301S mice: a model for tauopathy studies. *PLoS One* 7:e45017
16. Humpel C (2015) Organotypic vibrosections from whole brain adult Alzheimer mice (over-expressing amyloid-precursor-protein with the Swedish-Dutch-Iowa mutations) as a model to study clearance of beta-amyloid plaques. *Front Aging Neurosci* 7:1–10
17. Croft CL, Noble W (2018) Preparation of organotypic brain slice cultures for the study of Alzheimer's disease. *F1000Res* 7:592
18. Kunkler PE, Hulse RE, Kraig RP (2004) Multiplexed cytokine protein expression profiles from spreading depression in hippocampal organotypic cultures. *J Cereb Blood Flow Metab* 24:829–839
19. Su T, Paradiso B, Long YS et al (2011) Evaluation of cell damage in organotypic hippocampal slice culture from adult mouse: a potential model system to study neuroprotection. *Brain Res* 1385:68–76
20. Akassoglou K, Merlini M, Rafalski VA et al (2018) In vivo imaging of CNS injury and disease. *J Neurosci* 37:10808–10816
21. Jackson JS, Witton J, Johnson JD et al (2017) Altered synapse stability in the early stages of Tauopathy. *Cell Rep* 18:3063–3068
22. Kuhlman SJ, Olivas ND, Tring E et al (2013) A disinhibitory microcircuit initiates critical-period plasticity in the visual cortex. *Nature* 501:543–546
23. Shim G, Kim D, Park GT et al (2017) Therapeutic gene editing: delivery and regulatory perspectives. *Acta Pharmacol Sin* 38:738–753
24. Stepanyants A, Martinez LM, Ferecsko AS, Kisvárdy ZF (2009) The fractions of short- and long-range connections in the visual cortex. *Proc Natl Acad Sci U S A* 106:3555–3560
25. Xiong G, Metheny H, Johnson BN, Cohen AS (2017) A comparison of different slicing planes in preservation of major hippocampal pathway fibers in the mouse. *Front Neuroanat* 11:1–17
26. Bausch SB, McNamara JO (2000) Synaptic connections from multiple subfields contribute to granule cell hyperexcitability in hippocampal slice cultures. *J Neurophysiol* 84:2918–2932
27. Norberg J, Poulsen F, Blaabjerg M et al (2005) Organotypic hippocampal slice cultures for studies of brain damage, neuroprotection and neurorepair. *Curr Drug Targets CNS Neurol Disord* 4:435–452
28. Okamoto K, Ishikawa T, Abe R et al (2014) Ex vivo cultured neuronal networks emit in vivo-like spontaneous activity. *J Physiol Sci* 64:421–431
29. Liu J, Saponjian Y, Mahoney MM et al (2017) Epileptogenesis in organotypic hippocampal cultures has limited dependence on culture medium composition. *PLoS One* 12:1–25
30. Lein PJ, Barnhart CD, Pessah IN (2011) Acute hippocampal slice preparation and hippocampal slice cultures. *Methods Mol Biol* 758:115–134
31. Gogolla N, Galimberti I, DePaola V, Caroni P (2006) Preparation of organotypic hippocampal slice cultures for long-term live imaging. *Nat Protoc* 1:1165–1171
32. Humpel C (2015) Organotypic brain slice cultures: a review. *Neuroscience* 305:86–98
33. Legradi A, Varszegi S, Szigeti C, Gulya K (2011) Adult rat hippocampal slices as in vitro models for neurodegeneration: studies on cell viability and apoptotic processes. *Brain Res Bull* 84:39–44
34. Ting JT, Daigle TL, Chen Q, Feng G (2014) Acute brain slice methods for adult and aging animals: application of targeted patch clamp analysis and optogenetics. *Methods Mol Biol* 1183:221–242
35. Cilz NI, Porter JE, Lei S (2017) A protocol for preparation and transfection of rat entorhinal cortex organotypic cultures for electrophysiological whole-cell recordings. *MethodsX* 4:360–371
36. Geiger JRP, Bischofberger J, Vida I et al (2002) Patch-clamp recording in brain slices with improved slicer technology. *Pflugers Arch* 443:491–501
37. Edwards FA, Konnerth A, Sakmann B, Takahashi T (1989) A thin slice preparation for patch clamp recordings from neurones of the mammalian central nervous system. *Pflugers Arch* 414:600–612
38. Krimer LS, Goldman-Rakic PS (1997) An interface holding chamber for anatomical and physiological studies of living brain slices. *J Neurosci Methods* 75:55–58

39. Pringle AK, Sundstrom LE, Wilde GJCC et al (1996) Brain-derived neurotrophic factor, but not neurotrophin-3, prevents ischaemia-induced neuronal cell death in organotypic rat hippocampal slice cultures. *Neurosci Lett* 211:203–206
40. Arseneault J, O'Brien JA (2013) Optimized heterologous transfection of viable adult organotypic brain slices using an enhanced gene gun optimized heterologous transfection of viable adult organotypic brain slices using an enhanced gene gun. *BMC Res Notes* 6:1–8
41. Andersen P (1983) Basic mechanisms of penicillin-induced epileptiform discharges. *Prog Clin Biol Res* 124:3–13
42. Mtchedlishvili Z, Kapur J (2006) High-affinity, slowly desensitizing GABA<sub>A</sub> receptors mediate tonic inhibition in hippocampal dentate granule cells. *Mol Pharmacol* 69:564–575
43. Goodkin HP, Joshi S, Mtchedlishvili Z et al (2008) Subunit-specific trafficking of GABA<sub>A</sub> receptors during status epilepticus. *J Neurosci* 28:2527–2538
44. Driver JE, Racca C, Cunningham MO et al (2007) Impairment of hippocampal gamma ( $\gamma$ )-frequency oscillations in vitro in mice over-expressing human amyloid precursor protein (APP). *Eur J Neurosci* 26:1280–1288
45. Ullrich C, Daschil N, Humpel C (2011) Organotypic vibrosections: novel whole sagittal brain cultures. *J Neurosci Methods* 201:131–141
46. Rafiq A, DeLorenzo RJ, Coulter DA (2017) Generation and propagation of epileptiform discharges in a combined entorhinal cortex/hippocampal slice. *J Neurophysiol* 70:1962–1974
47. Lossi L, Alasia S, Salio C, Merighi A (2009) Cell death and proliferation in acute slices and organotypic cultures of mammalian CNS. *Prog Neurobiol* 88:221–245
48. Staal JA, Alexander SR, Liu Y et al (2011) Characterization of cortical neuronal and glial alterations during culture of organotypic whole brain slices from neonatal and mature mice. *PLoS One* 6:e22040
49. Rama S, Zbili M, Bialowas A et al (2015) Pre-synaptic hyperpolarization induces a fast analogue modulation of spike-evoked transmission mediated by axonal sodium channels. *Nat Commun* 6:10163
50. Kruger JM, Favaro PD, Liu M et al (2013) Differential roles of postsynaptic Density-93 isoforms in regulating synaptic transmission. *J Neurosci* 33:15504–15517
51. Kasri NN, Govek EE, Van Aelst L (2008) Characterization of Oligophrenin-1, a Rho-GAP lost in patients affected with mental retardation: lentiviral injection in organotypic brain slice cultures. *Methods Enzymol* 439:255–266
52. Routbort MJ, Bausch SB, McNamara JO (1999) Seizures, cell death, and mossy fiber sprouting in kainic acid-treated organotypic hippocampal cultures. *Neuroscience* 94:755–765
53. McKinney RA, Debanne D, Gähwiler BH, Thompson SM (1996) Lesion-induced axonal sprouting and hyperexcitability in the hippocampus in vitro: implications for the genesis of posttraumatic epilepsy. *Nat Med* 3:990–996
54. McKinney RA, Luthi A, Bandtlow CE et al (1999) Selective glutamate receptor antagonists can induce or prevent axonal sprouting in rat hippocampal slice cultures. *Proc Natl Acad Sci U S A* 96:11631–11636
55. Incontro S, Díaz-Alonso J, Iafrati J et al (2018) The CaMKII/NMDA receptor complex controls hippocampal synaptic transmission by kinase-dependent and independent mechanisms. *Nat Commun* 9:1–21
56. Lin J, Sann S, Zhou K, Nabavi S (2013) Optogenetic inhibition of synaptic release with chromophore-assisted light inactivation (CALI). *Neuron* 79:241–253
57. Bahia PK, Bennett ES, Taylor-Clark TE (2012) Reductions in external divalent cations evoke novel voltage-gated currents in sensory neurons. *PLoS One* 7:2



# Chapter 13

## In Vivo Patch-Clamp Studies

**Yi Zhou, He Li, and Zhongju Xiao**

### Abstract

Intact and functioning brain enables quantification of neural activities directly associated with real world such as visual and auditory information. In vivo patch clamp can record different types of neuronal activity, such as spiking responses, membrane potential dynamics, and synaptic currents (e.g., EPSC, IPSC) in either anesthetized or awake or even free moving animals. Researchers can not only directly measure these neuronal activities but also quantify and unravel synaptic contribution from excitatory and inhibitory circuits. Here, we describe the requirements and standard protocols to perform in vivo patch clamp recording. The key factors of successful recording based on references and our experiences are also provided.

**Key words** In vivo patch clamp, Neural circuits, Intracellular recording, Cell-attached recording, Whole cell recording

---

### 1 Introduction

In vivo patch clamp has been successfully applied in different regions of different species, including mouse [1, 2], rat [3, 4], cat [5], tadpoles [6], drosophila [7, 8], *C. elegans* [9], leopard frog [10], and zebrafish [11, 12]. In rat and mice, in vivo patch clamp has been widely used to study circuitry functions and mechanisms in sensory cortices, including barrel cortex [4], auditory cortex [13, 14], and visual cortex [15] as well as in the olfactory bulb [16], thalamus [17, 18], hippocampus [19, 20], inferior colliculus [1, 21], spinal cord [22], and dorsal root ganglion [2]. In Drosophila, in vivo patch clamp has been used to study sensory systems, such as the medulla cortex [23] and antennal lobe [7]. There are also applications of this method in zebrafish and *C. elegans* to study the properties of neurons and circuit function [9, 11]. Only a few related studies have been performed in primates, which could be due to technical risk [24, 25].

In this chapter, we introduced the standard protocols of in vivo patch clamp recording in mouse cortex for demonstration purpose.

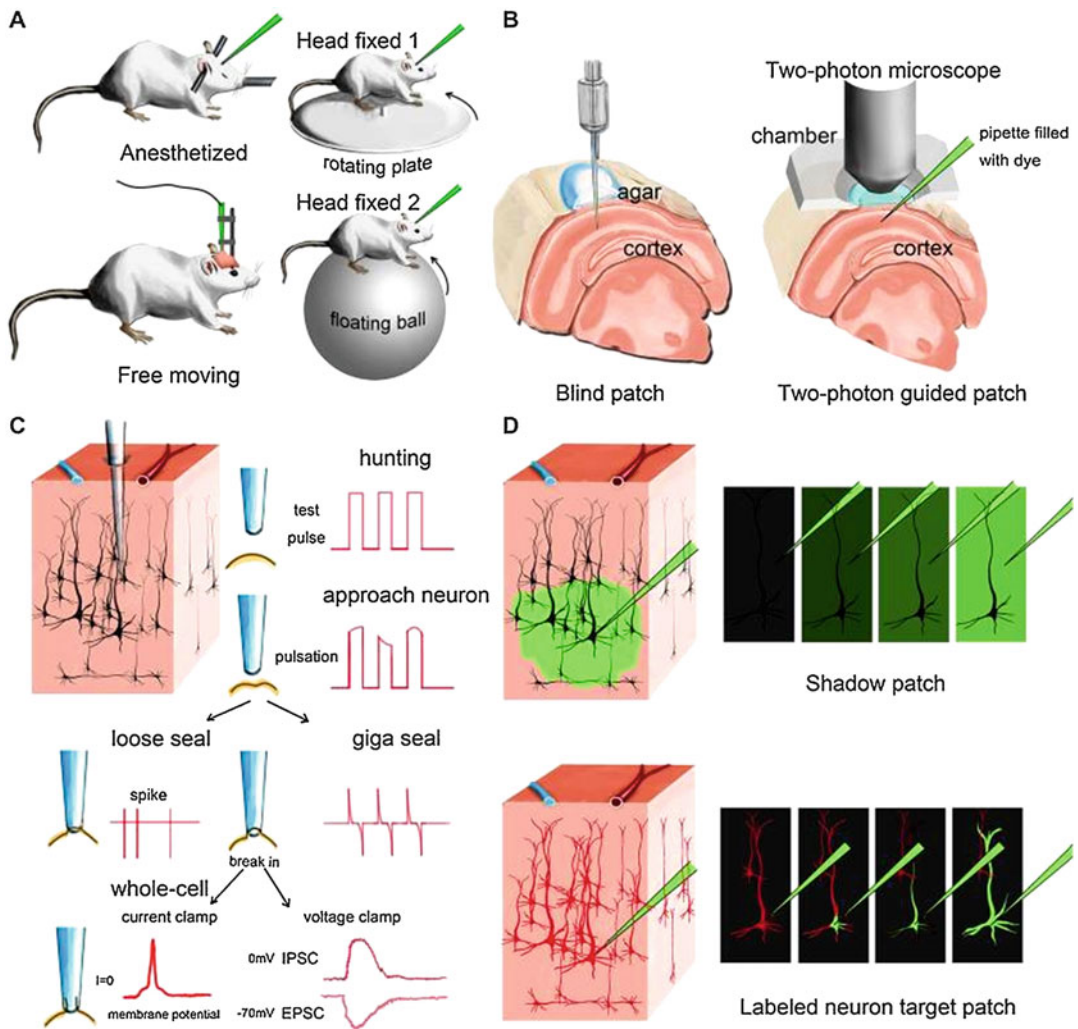


**Fig. 1** Different modes of in vivo patch clamp recording. **(a)** Representative in vivo patch clamp setups for anesthetized, awake, and moving animals. **(b)** Demonstration of blind patch and two-photon guided patch. **(c)** Procedures and different recording modes of in vivo patch clamp (blind patch). When the pipette approaches a nearby cell, heartbeat-associated changes become notable in test pulses. Releasing positive pressure allows the pipette tip to form a loose seal or a gigaseal for loose-patch recording or whole-cell recording, respectively. After gigaseal formation, the cell membrane can then be broken for either current-clamp recording or voltage-clamp recording. **(d)** Two different methods for visually guided in vivo patch clamp: shadow patch and labeled-neuron guided patch. (Modified from Tao et. al., 2015 with permission from Frontiers in Neural Circuits)

Operations in other regions or species might be different from this introduction but should be similar. Figure 1 showed different modes of in vivo patch clamp recording. To lower the technical challenge of in vivo patch clamp recording, some automated or semi-automated solutions have also been proposed [26–28].

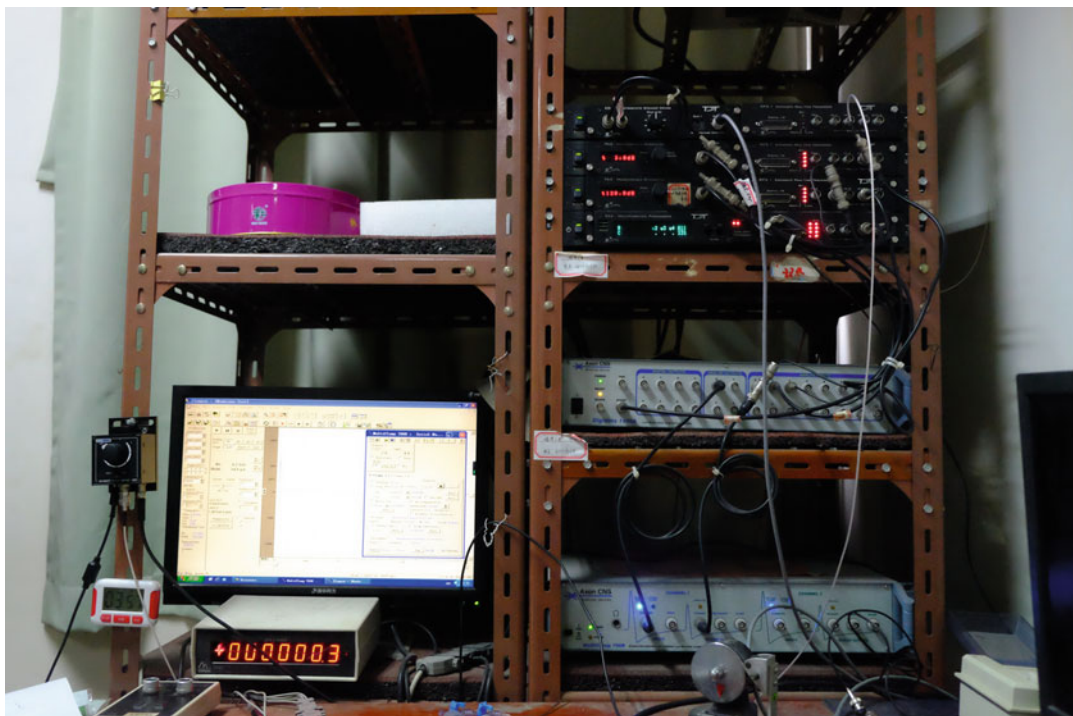


**Fig. 2** An example of patch clamp rig

Theoretically, any typical patch clamp rig that suits single cell or brain slice patch clamp recording should be ready for in vivo patch clamp study with minor upgrades. It worth noting that inverted microscope will not be necessary for blind in vivo patch clamp recording but a good stereoscope (e.g., Zeiss Stemi 508) with flexible swing arm is highly recommended. In this chapter, we used the following setup for demonstration: Axon Instrument700B amplifier (with1440A converter and CV-7B headstage, Fig. 2). Patch clamp systems from other providers (Heka, Sutter etc.) should also work well. Some customized accessories such as head plate/holder will also be needed [26, 28]. For reader who are not familiar with basic concepts of patch clamp technique, please check other chapters in this book for more details.

## 2 Materials

All solutions are prepared using ultrapure water (resistance  $>18\text{ M}\Omega$  at  $25\text{ }^{\circ}\text{C}$ ). All drugs should be stored following their instructions.

### 2.1 Internal Solutions

Two kinds of fluid can be used as internal solution: artificial cerebrospinal fluid (ACSF) can be used for in vivo cell-attached

**Table 1**  
**Recipe for preparing 1.0 L of ACSF (artificial cerebral spinal fluid)**

<b>Prepare 1 L of ACSF (1000 mL)</b>			
<b>Reagent name</b>		<b>Molecular weight (g/mol)</b>	<b>mL</b>
A (100 mL)	NaCl	58.44	126
	KCl	74.56	2.5
	NaH <sub>2</sub> PO <sub>4</sub> ·2H <sub>2</sub> O	156.01	1.25
	NaHCO <sub>3</sub>	84.01	26
B (50 mL)	MgCl <sub>2</sub> ·6H <sub>2</sub> O	203.3	1
	CaCl <sub>2</sub>	110.98	2
C	Vitamin C ( <i>see Note 2</i> )	176.14	0.5
	Sodium pyruvate	110.05	2
	Glucose	198.17	10

recording (a.k.a. loose patch recording or juxtacellular recording), and intracellular fluid can be used for *in vivo* whole cell recording.

## **2.2 Artificial Cerebrospinal Fluid (for In vivo Cell-Attached Recording)**

1. Table 1 showed the recipe of ACSF.
2. To simplify the procedures for ACSF preparation, two holding solutions (A, B) were recommended. Holding solutions can be prepared in advance and stored at 4 °C (*see Note 1*).
3. To obtain 1 L of ACSF, mix 100 mL solution A and 50 mL solution B together.
4. Add compound C to the mixed solution and adjust the total volume to 1 L with pure water.
5. Adjust the PH value of solution to 7.25–7.35 using NaOH solution (1 M).
6. Adjust the osmotic pressure of solution to 290–310 osm using pure water.

## **2.3 Intracellular Fluid (for In Vivo Whole Cell Recording)**

1. Prepare 50 mL Cs-Gluconate solution (0.5 M) (Table 2).
2. Prepare 50.0 mL of the following solution with 12.5 mL of Cs-Gluconate solution as base solution (*see Notes 3 and 4*) (Table 3).
3. Adjust total volume to 50 mL with pure water.
4. Adjust PH value to 7.25–7.45 using CsOH (1 M) (*see Note 5*).
5. Adjust osmotic pressure to 290–320 osm with pure water.
6. Filter the solution using a 0.22 µm filter for three times and disperse filtered solution (100 µL) into 1 mL tubes. Store tubes at –20 °C.

**Table 2**  
**Recipe for preparing 50.0 mL of Cs-gluconate (0.5 M)**

<b>Prepare 0.5 M Cs-gluconate(50 mL)</b>		
<b>Reagent name</b>	<b>Molecular weight (g/mol)</b>	<b>Solution volume</b>
CsOH	150	4.36 mL
Gluconic acid	196	7.94 mL

**Table 3**  
**Recipe for preparing 50.0 mL of intracellular fluid for in vivo whole cell recording**

<b>Reagent name</b>	<b>Molecular weight (g/mol)</b>	<b>50 mL (mg)</b>	<b>50 mL (g)</b>
Cs-gluconate	327.9	12.5 mL	12.5 mL
TEA-cl	165.7	41.425	0.0414
HEPES	238.3	119.15	0.1192
EGTA	380.35	190.175	0.1902
QX314	343.3	17.165	0.0172
Cs-cl	168.36	16.836	0.0168
ATP-mg	507.18	101.436	0.1014
GTP	523.18	7.848	0.0078
Phosphocreatine sodium	255.1	102.04	0.102
MK801	337.37	12.651	0.0127

#### 2.4 Glass Pipette

Either quartz, borosilicate or aluminosilicate capillary should be fine for preparation of patch clamp pipette. Either horizontal puller (e.g., P-97, P-1000 from Sutter, Inc.) or vertical puller (e.g., PC-10, PC-100 from Narishige Inc.) should be fine. Glass pipette with resistance between 5–7 MΩ is recommended. Always keep glass pipettes in covered containers such as large culture dish and use freshly pulled glass pipette if applicable (*see Notes 6–9*).

#### 2.5 Animal Preparation

For demonstration purpose, here we used C57BL/6 mice (females, 4–6 weeks, 14–20 g, housed under a 12-h light–dark cycle). Sterilization is recommended for all following procedures (*see Note 10*).

##### 2.5.1 Anesthesia

1. Intraperitoneal injection of sodium pentobarbital solution (a.k.a. Nembutal) (60–70 mg/kg) (*see Note 11*). Sodium pentobarbital solution (15 mg/mL) is prepared with saline.
2. Muscle injection of atropine sulfate (0.25 mg/kg) to inhibit respiratory secretions.

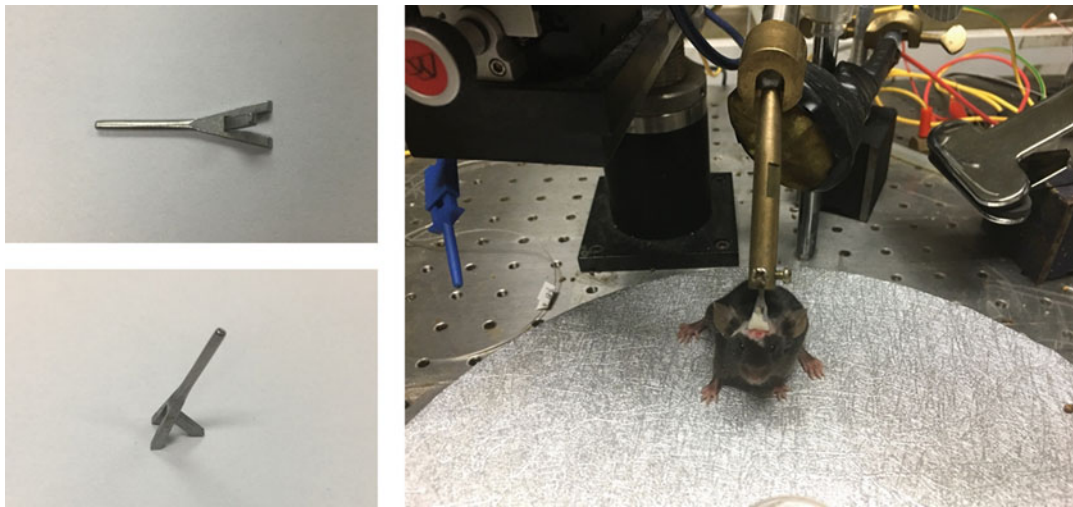


**Fig. 3** An example of customized holder

3. Check the anesthesia level of animal during the whole surgery regularly by testing paw withdrawal reflex. Provide supplemental anesthesia if needed.
4. Keep a continuous record of animal's vital signs (e.g., breath rate, heart rate, body temperature), if applicable.

#### 2.5.2 Craniotomy

1. Fix the anesthetized mouse on a stereotaxic apparatus.
2. Clean the skin and muscle above the target cortex using surgical tools.
3. Drill a small hole away from your target area for reference electrode using a dental drill. Use saline to cool down nearby skull and cortex to make sure they are not overheated by drilling.
4. Embed a small Ag-AgCl pellet into the hole for reference electrode and fix it using glass ionic cement.
5. Fix a customized holder (Fig. 3) to rough-polished skull surface using glass ionomer cement (*see Note 12*).

#### 2.5.3 Finishing and Recovery

1. Apply a small amount of erythromycin ointment (or other antibiotics) to the wound to prevent infection and inflammation.
2. Return the animal to a clean cage without other animals and provide adequate food and water for recovery.
3. Check the status of the animal regularly and treat the animal properly. It may take up to 1 week for the animal to fully recover. Mice with poor appetite or other abnormal behaviors (e.g., cowering in corner) should not be used for following experiment.

#### **2.5.4 Habituation and Training**

Because animal is head-fixed during in vivo patch clamp recording, habituation in a training room is highly recommended to ease nervous and anxious behaviors of animal. This is important to improve the success rate of recording in head-fixed awake animal. The training room should be like the recording environment. Good ventilation is recommended to keep the training room clean. Habituation/training can start the second day after surgery.

1. Place the animal above a running plate (or floating ball).
2. Fix the animal head by locking the head holder into a metal rod. Adjust the rod to make sure the animal is in an appropriate posture.
3. Train the animal to run in one direction by gently relocating the tail using a tweezer. After several sessions of training, the animals should be able to run in one direction on the running plate.
4. Train the animal for habituation 1–2 h each time and twice a day.
5. After 5–8 days of continuous training, the animal should be relaxed and quiet when head-fixed.

#### **2.5.5 Craniotomy**

1. Follow [2.5.1](#) to anesthetize animal again.
2. Fix the anesthetized mouse on a stereotaxic apparatus.
3. Clean the skin and muscle above the target cortex using surgical tools.
4. Drill a small hole above the target area using a dental drill. Use saline to cool down nearby skull and cortex to make sure they are not overheated by drilling.
5. Cover the exposed cortex with a small amount of Vaseline or silicone molding rubber (e.g., Body double). Then close the opened skull with polyethylene film.
6. Return the animal to its cage for 1 day recovery after animal is recovered from anesthesia.

### **2.6 Cell Hunting and Recording**

#### **2.6.1 Cell Hunting**

1. Repeat steps **1** and **2** in [2.5.4](#).
2. Repeat steps **1** and **2** in [2.5.5](#).
3. Turn on computer, patch clamp amplifiers, and other equipment.
4. Run patch clamp software (e.g., Clamplex, or Patch Master).
5. Use a sharp syringe needle (e.g., 31 gauge) to open a small portion (100–500  $\mu\text{m}$ ) of the dura and drain excessive cerebro-spinal fluid.

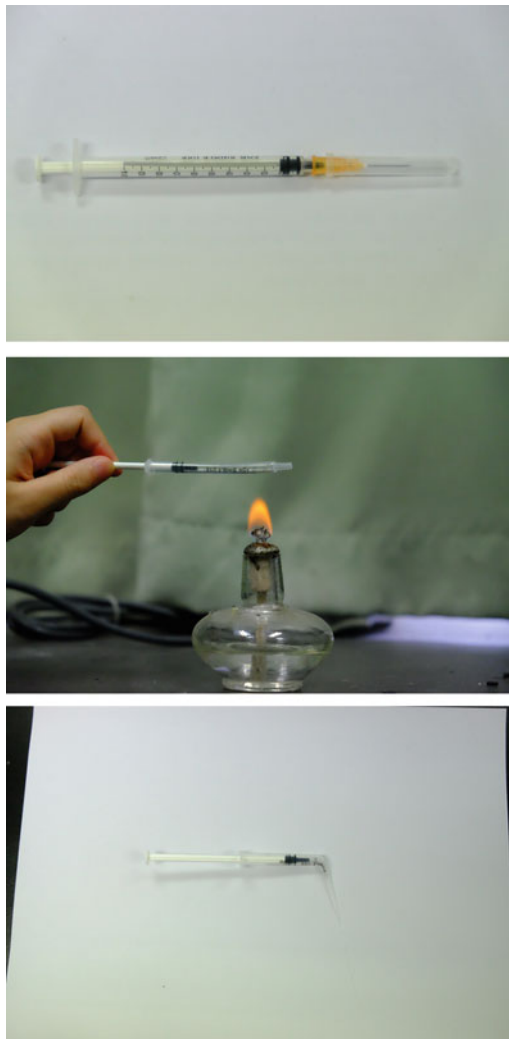


**Fig. 4** Simple steps to prepare a clean pipette injector using a 5 mL syringe

6. Use a freshly made solution injector (Fig. 4, *see Note 13*) to inject internal solution (ACSF or intracellular solution) into an unused pipette (*see Note 14*). Reusable injector is also acceptable but there is a higher risk of contamination.
7. Mount a glass pipette onto patch clamp headstage and apply a high pressure (1–3 psi) to pipette to prevent it from clogging.
8. Remove the Vaseline or molding rubber above the cortex.
9. Carefully move pipette tip to cortical surface using a manipulator (manually or electrically) under the guidance of a stereoscope. Reset the depth reader of manipulator to zero when pipette tip is contacting cortical surface then quickly lower the pipette to desired depth.

10. Reduce the pressure to 0.5–1 psi and lower the pipette as slow as possible toward target depth (1–2  $\mu\text{m}$ /step). Check the change of pipette resistance at the same time.
11. A sudden increase of pipette resistance (0.3–0.5  $M\Omega$ ) indicates the contact between pipette tip and other stuff (e.g., neuron, glia cells, blood vessels). Release the pipette pressure to 0 psi (*see Note 15*).

#### 2.6.2 Cell-Attached Recording

1. Do NOT apply holding voltage.
2. Apply a mild suction (−0.1 psi) to gradually increase the pipette resistance.
3. Stable pipette resistance between  $30\text{ M}\Omega$  and  $1\text{ G}\Omega$  indicates that cell is closely attached to the pipette and this is known as cell-attached recording. Clear and spontaneous action potential should be visible in the tracing window of patch clamp software.
4. Perform your designed experiment (e.g., deliver various stimuli) and record action potentials.
5. Slowly withdraw pipette from the tissue and prepare for the next recording start from **step 6** in Subheading 2.6.1.
6. Sacrifice the animal and finish the experiment(*see Note 16*).

#### 2.6.3 In vivo Whole Cell Recording

1. Set the clamping voltage to −40 mv.
2. Apply a mild suction (−0.1 psi) to obtain a stable giga-seal (Fig. 5) between pipette tip and cell membrane.
3. After giga-seal is stabilized, monitor the leaking current continuously. When the leaking current slowly changes from negative (outward) to positive (inward). Apply a mild suction until cell membrane is broke(Fig. 6, *see Note 17*).
4. EPSC (Excitatory postsynaptic current) or IPSP (Inhibitory postsynaptic current) can be recorded by clamping membrane potential at different levels (e.g., −70 mV for EPSC, 0 or +10 mV for IPSC). Please check previous publications for your reference.
5. Perform your designed experiment (e.g., deliver various stimuli) and record intracellular activities (e.g., synaptic currents).
6. Slowly withdraw pipette from the tissue and prepare for the next recording start from **step 6** in Subheading 2.6.1.
7. Sacrifice the animal and finish the experiment (*see Note 16*).

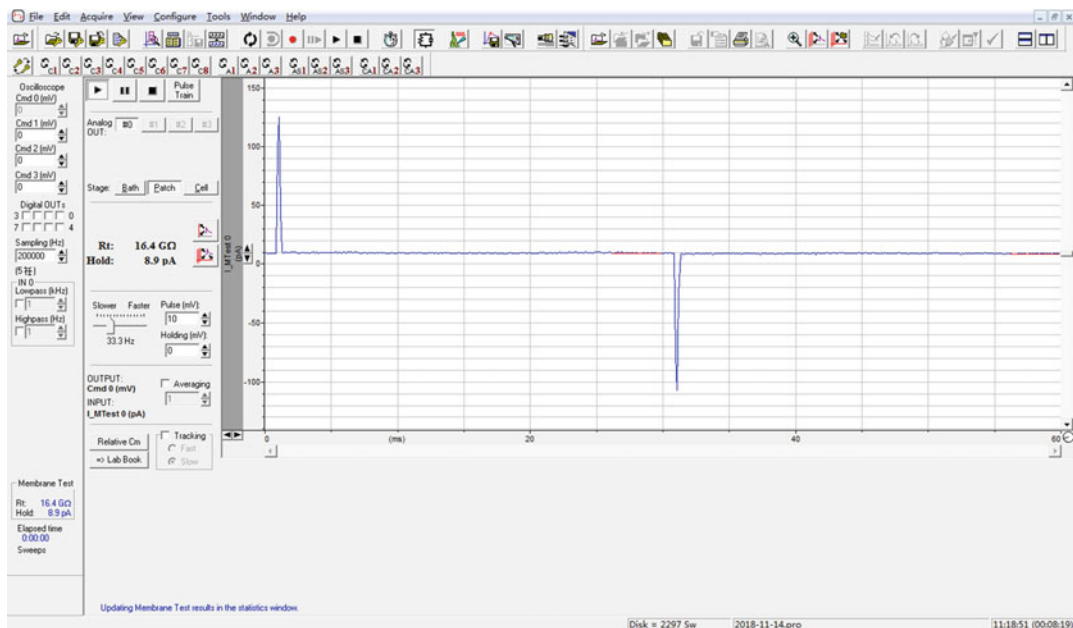


**Fig. 5** An example of in vivo patch clamp recording with gigaseal formed

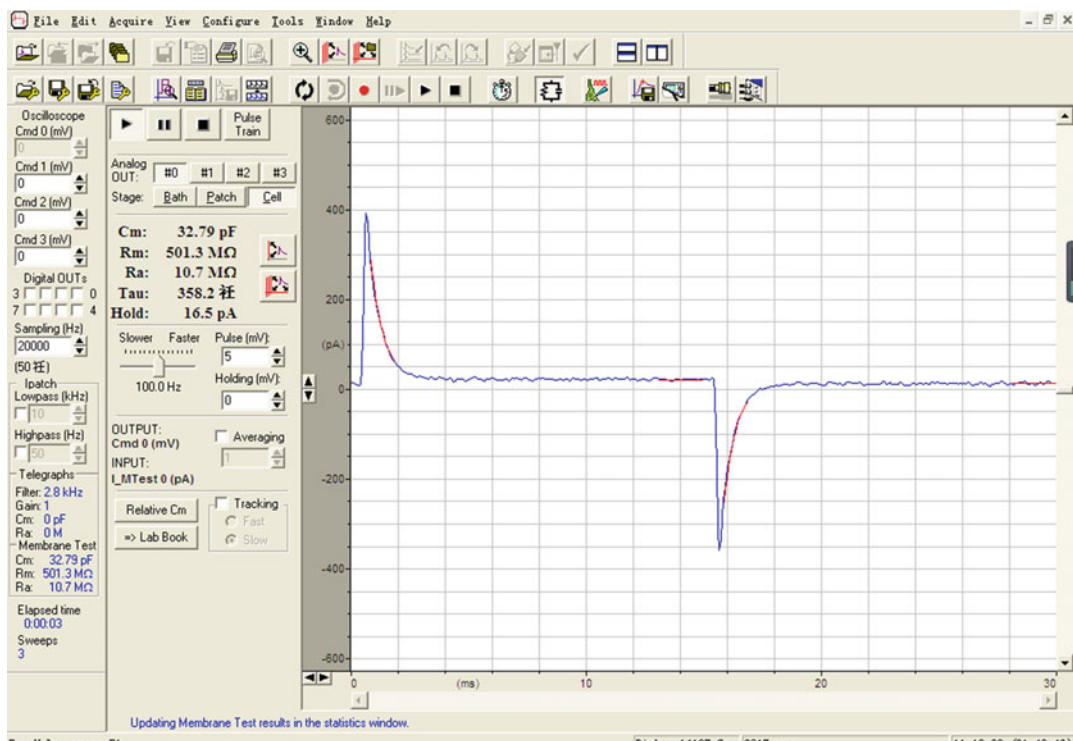


**Fig. 6** An example of in vivo patch clamp recording after breakthrough. Inward and outward currents are evoked by testing pulse

---

### 3 Notes

1. Subsidence might occur if solution A or B were kept for too long. Do not keep holding solution for more than 2 weeks.
2. Store at 4 °C.
3. ATP-Mg, GTP, and phosphocreatine sodium should be kept at -20 °C.
4. We recommend to add ATP-Mg, GTP, and phosphocreatine sodium sequentially with continuous and mild stirring. Keep the mixed solution at -20 °C.
5. Continuously monitor pH of solution when adding CsOH.
6. We recommend to quickly burn both ends of glass capillary on alcohol burner for cleaning purpose.
7. Always use freshly pulled glass pipettes for each experiment. Keep freshly pulled glass pipettes in a sealable container.
8. Pipette puller is sensitive to room temperature and moisture. Adjust the pulling parameters to make sure the opening/resistance of glass pipette is stable.
9. More details and tricks about how to pull proper glass pipette can be found from the guide book provided by Sutter Inc. for free:  
[https://www.sutter.com/PDFs/pipette\\_cookbook.pdf](https://www.sutter.com/PDFs/pipette_cookbook.pdf)
10. Gas anesthesia (e.g., isoflurane) is also recommended which is good for animal to recover from surgery.
11. Please always follow the instructions from a veterinary if you use anesthesia drug with experimental animals.
12. You can use some tools (e.g., used surgical blade) to rough the skull surface.
13. An easy way to make clean solution injector is using a 1 mL syringe. Warm the body part of syringe with heater and pull it gently to form a thin tube. Cut the tube using fine and clean razor to get a pipette injector.
14. Carefully check if there is any air bubble near the pipette tip after fluid was injected. Tap the pipette gently to remove air bubbles. You can also use glass capillary with filament to lower the chance of air bubbles.
15. Subheadings 2.6.2 and 2.6.3 are different choices following step 11 in 2.6.1.
16. You can mark or label the recording site for verification purpose if needed.

17. Pause the membrane breakthrough (suction) if giga-seal become unstable. Resume the suction after the giga-seal is stabilized.

---

## Acknowledgments

This work was supported by National Natural Science Foundation of China (NSFC) to Yi Zhou (31970932, 31771152) and Zhongju Xiao (31872769, 31671083).

## References

1. Nagtegaal AP, Borst JG (2010) In vivo dynamic clamp study of I(h) in the mouse inferior colliculus. *J Neurophysiol* 104:940–948
2. Ma C, Donnelly DF, LaMotte RH (2010) In vivo visualization and functional characterization of primary somatic neurons. *J Neurosci Methods* 191:60–65
3. Jacob V, Brasier DJ, Erchova I, Feldman D, Shulz DE (2007) Spike timing-dependent synaptic depression in the in vivo barrel cortex of the rat. *J Neurosci* 27:1271–1284
4. London M, Roth A, Beeren L, Häusser M, Latham PE (2010) Sensitivity to perturbations in vivo implies high noise and suggests rate coding in cortex. *Nature* 466:123–127
5. Yu J, Ferster D (2013) Functional coupling from simple to complex cells in the visually driven cortical circuit. *J Neurosci* 33:18855–18866
6. Zhang LI, Tao HW, Poo M (2000) Visual input induces long-term potentiation of developing retinotectal synapses. *Nat Neurosci* 3:708–715
7. Liu WW, Wilson RI (2013) Glutamate is an inhibitory neurotransmitter in the drosophila olfactory system. *Proc Natl Acad Sci U S A* 110:10294–10299
8. Murthy M, Turner G (2013) Whole-cell in vivo patch-clamp recordings in the drosophila brain. *Cold Spring Harb Protoc* 2013:140–148
9. Ramot D, MacInnis BL, Goodman MB (2008) Bidirectional temperature-sensing by a single thermosensory neuron in *C. elegans*. *Nat Neurosci* 11:908–915
10. Rose GJ, Alluri RK, Vasquez-Opazo GA, Odom SE, Graham JA, Leary CJ (2013) Combining pharmacology and whole-cell patch recording from CNS neurons, in vivo. *J Neurosci Methods* 213:99–104
11. Drapeau P, Ali DW, Buss RR, Saint-Amant L (1999) In vivo recording from identifiable neurons of the locomotor network in the developing zebrafish. *J Neurosci Methods* 88:1–13
12. Wei HP, Yao YY, Zhang RW, Zhao XF, Du JL (2012) Activity-induced long-term potentiation of excitatory synapses in developing zebrafish retina in vivo. *Neuron* 75:479–489
13. Zhou M, Liang F, Xiong XR, Li L, Li H, Xiao Z et al (2014) Scaling down of balanced excitation and inhibition by active behavioral states in auditory cortex. *Nat Neurosci* 17:841–850
14. Li LY, Li YT, Zhou M, Tao HW, Zhang LI (2013) Intracortical multiplication of thalamocortical signals in mouse auditory cortex. *Nat Neurosci* 16:1179–1181
15. Li YT, Liu BH, Chou XL, Zhang LI, Tao HW (2015) Strengthening of direction selectivity by broadly tuned and spatiotemporally slightly offset inhibition in mouse visual cortex. *Cereb Cortex* 25:2466–2477
16. Poo C, Isaacson JS (2011) A major role for intracortical circuits in the strength and tuning of odor-evoked excitation in olfactory cortex. *Neuron* 72:41–48
17. Brecht M, Sakmann B (2002) Whisker maps of neuronal subclasses of the rat ventral posterior medial thalamus, identified by whole-cell voltage recording and morphological reconstruction. *J Physiol* 538:495–515
18. Margrie TW, Brecht M, Sakmann B (2002) In vivo, low-resistance, whole-cell recordings from neurons in the anaesthetized and awake mammalian brain. *Pflugers Arch* 444:491–498
19. Atallah BV, Scanziani M (2009) Instantaneous modulation of gamma oscillation frequency by balancing excitation with inhibition. *Neuron* 62:566–577
20. Grienberger C, Chen X, Konnerth A (2014) NMDA receptor-dependent multidendrite Ca

- (2+) spikes required for hippocampal burst firing in vivo. *Neuron* 81:1274–1281
21. Kuo RI, Wu GK (2012) The generation of direction selectivity in the auditory system. *Neuron* 73:1016–1027
22. Sonohata M, Furue H, Katafuchi T, Yasaka T, Doi A, Kumamoto E et al (2004) Actions of noradrenaline on substantia gelatinosa neurones in the rat spinal cord revealed by in vivo patch recording. *J Physiol* 555:515–526
23. Behnia R, Clark DA, Carter AG, Clandinin TR, Desplan C (2014) Processing properties of ON and OFF pathways for drosophila motion detection. *Nature* 512:427–430
24. Joshi S, Hawken MJ (2006) Loose-patch-juxtacellular recording in vivo--a method for functional characterization and labeling of neurons in macaque V1. *J Neurosci Methods* 156:37–49
25. Mitchell JF, Sundberg KA, Reynolds JH (2007) Differential attention-dependent response modulation across cell classes in macaque visual area V4. *Neuron* 55:131–141
26. Kodandaramaiah SB, Franzesi GT, Chow BY, Boyden ES, Forest CR (2012) Automated whole-cell patch-clamp electrophysiology of neurons in vivo. *Nat Methods* 9:585–587
27. Suk HJ, van Welie I, Kodandaramaiah SB, Allen B, Forest CR, Boyden ES (2017) Closed-loop real-time imaging enables fully automated cell-targeted patch-clamp neural recording in vivo. *Neuron* 95:1037–1047
28. Holst GL, Stoy W, Yang B, Kolb I, Kodandaramaiah SB, Li L et al (2019) Autonomous patch-clamp robot for functional characterization of neurons in vivo: development and application to mouse visual cortex. *J Neurophysiol* 121:2341–2357



# Chapter 14

## In Vivo Optogenetics with Stimulus Calibration

Luke T. Coddington and Joshua T. Dudman

### Abstract

Optogenetic reagents allow for depolarization and hyperpolarization of cells with light. This provides unprecedented spatial and temporal resolution to the control of neuronal activity both in vitro and in vivo. In the intact animal this requires strategies to deliver light deep into the highly scattering tissue of the brain. A general approach that we describe here is to implant optical fibers just above brain regions targeted for light delivery. In part due to the fact that expression of optogenetic proteins is accomplished by techniques with inherent variability (e.g., viral expression levels), it also requires strategies to measure and calibrate the effect of stimulation. Here we describe general procedures that allow one to simultaneously stimulate neurons and use photometry with genetically encoded activity indicators to precisely calibrate stimulation.

**Key words** Optogenetics, Fiber photometry, Rodent, Behavior, Dopamine, Genetically encoded calcium indicators, Fluorescence, Transgenic

---

### 1 Introduction

Optogenetic modulation of neural activity [1] and fiber photometry [2, 3] have become routine experiments in neuroscience over the last decade. With appropriately flexible hardware [4, 5] they are readily compatible techniques but have been relatively infrequently used in complement. One clear potential for combined fiber photometry and optogenetics is to allow for the real-time calibration of exogenously stimulated neural signals [6].

Many published protocols for excitation or inhibition of specific subpopulations of neurons represent extreme manipulations of neural activity and thus may be complicated to interpret with respect to studying physiological function [7]. Extreme manipulations are defensible in part because negative results of milder manipulations are ambiguous in the absence of some independent measurement of the effectiveness of stimulation. Physiology-calibrated optogenetics (of which simultaneous fiber photometry is one approach) can (1) facilitate physiologically relevant circuit

manipulations, (2) increase confidence in the results of subtle circuit manipulations, and (3) allow for meaningful negative results.

As noted above simultaneous fiber photometry and optogenetics is a tractable extension to *in vivo* optogenetic experiments for most labs and can be accomplished with open source and relatively inexpensive hardware [4, 5]. Here we describe a method for combined fiberometry and optogenetics that allows for arbitrary calibration of optogenetic excitation using the example of midbrain dopamine (mDA) neurons as in our published work [6]. We note that this technique also allows for longitudinal measurements of mDA activity at somatic and axonal projection sites.

## 2 Materials

### **2.1 Expression of Optogenetic Actuators in Neuronal Tissue**

1. In some experiments a transgenic strategy may be employed in which case there is no additional requirement beyond procedures described below. In the specific experiments described here used mice heterozygous for both *Slc6a3-ires-cre* and *Ai-32* transgenes (*DAT<sup>cre</sup>*, [www.jax.org/strain/006660](http://www.jax.org/strain/006660); *Ai32*, [www.jax.org/strain/012569](http://www.jax.org/strain/012569)) aged 2–8 months. This scheme leads to selective expression of ChR2-YFP in midbrain dopamine neurons.
2. A strategy employing viral infection of tissue may be used to express optogenetic reagents and/or genetically encoded indicators for imaging. A wide variety of reagents are now available for such experiments. AddGene ([www.addgene.org/viral-service/aav-prep/](http://www.addgene.org/viral-service/aav-prep/)) and UPenn viral core ([gtp.med.upenn.edu/core-laboratories-public/vector-core](http://gtp.med.upenn.edu/core-laboratories-public/vector-core)) offer many options. Here we describe an approach using AAV2/1-CAG-FLEX-jRCaMP1a virus [8].

### **2.2 Making Custom Fiber Optics “Stubs” for Intracranial Implantation**

1. Fiber implants were custom-made from 0.48 NA, 200 µm core, 230 µm total outer diameter fiber optic fiber (Polymicro Technologies, Cat. #1068030133) and matched ceramic cannulas (Precision Fiber Products, Cat #MM-FER2007C-2300).
2. To make fiber implants, fiber casing was removed with fiber strippers (Fiber Optic Center Inc., Micro-Strip, 0.012 blade, 0.021 guide) and fiber was cut to length with an optic fiber cleaver (Fujikura).
3. Then fiber was inserted and made flush with dorsal edge of cannula before a small amount of light-cured glue (Opti-Bond Solo Plus) was applied to the ventral side of cannula and cured with a UV light source (Electro-Lite, ELC-410).

### **2.3 Light Delivery for Optogenetics**

1. A diverse range of possibilities for delivering light through fiber optics exist. The least expensive options tend to be fiber coupled light emitting diodes (LEDs). Some examples are fiber-

coupled LEDs from Thor Labs described below in our typical fiber photometry setup or the PlexBright modules from Plexon ([plexon.com/products/plexbright-led-modules/](http://plexon.com/products/plexbright-led-modules/)).

2. Alternatively, for some applications (often optogenetic inhibition experiments) substantial powers may be required—although care should be taken to control for effects mediated by heating the tissue [9, 10]). Fiber-coupled solid-state lasers can be purchased from a number of sources. Alternatively, free space optics can be used to launch a laser and generally achieve the most flexible and stable power output in our hands. We have often used fiber-coupled lasers from BlueSky ([blueskyresearch.com/products/fiber-coupled-lasers-and-systems/fiber-coupled-lasers/](http://blueskyresearch.com/products/fiber-coupled-lasers-and-systems/fiber-coupled-lasers/)) and free space lasers from Laser-Glow ([www.laserglow.com/product/byapplication/applications-optogenetics/](http://www.laserglow.com/product/byapplication/applications-optogenetics/)) or OEM Laser Systems ([www.oemlasersystems.com](http://www.oemlasersystems.com)). However, it is worth noting that many options are available and these are just a few sources that are used in our lab with success.
1. Two fiber photometry modules were built around 5-port filter cubes (FMC5, Doric Lenses) with two parallel excitation-emission channels to allow for simultaneous measurement of RCaMP1a and eYFP fluorescence, the latter channel having the purpose of controlling for the presence of movement artifacts.
2. 470 nm and 565 nm fiber-coupled LEDs (M470F3, M565F3, Thorlabs) were connected to Y-cables (Doric lenses, 200 μm, 0.22 NA, SMA-2xFC), with one branch of each Y-cable connected to the excitation ports on the five-port filter cube, and the other branch of each Y-cable connected to Si-based photodetectors (Thorlabs, DET100A) to give a direct readout of output power of the LED.
3. The filter cube excitation ports had acceptance bandwidths of 465–490 nm and 555–570 nm. Light was conveyed between the sample port of the cube and the animal by the sample patch cable, a 200 μm core, 0.48 NA fiber (Doric Lenses) terminating in a ceramic ferrule that was connected to the implanted fiber cannula by a ceramic mating sleeve (ADAL1, Thorlabs) using index matching gel to improve coupling efficiency (G608N3, Thorlabs).
4. Light collected from the sample fiber was measured at separate output ports (emission bandwidths 500–540 nm and 600–680 nm) by 600 μm core, 0.48 NA fibers (Doric Lenses) connected to silicon photoreceivers (2151, Newport). Signals from the receivers were streamed into a Cerebus Signal Processor (Blackrock Microsystems) at 30 kHz.

## **2.4 Hardware for Fiber Photometry**

5. The excitation LEDs were flickered on offset to each other at 100 Hz (1 ms on, 9 ms off), controlled by offset square waves generated at the analog output ports of the Cerebus processor. LED power was set so that at constant illumination the measured power from the tip of the sample patch cable was ~100 µW for each LED source.
6. Signals were extracted off-line with custom Matlab code by using the LED power measurements to define which regions of each signal should be kept, then interpolating across periods when the LEDs were off.
7. This gives a 100 Hz effective sample rate which is fast enough to measure Ca<sup>2+</sup>-sensor dynamics and offers improved signal-to-noise compared to source-separation methods that continuously modulate excitation sources at different frequencies. An important added benefit is the order-of-magnitude reduction in total excitation of the sample, leading to less photobleaching and increasing the power threshold at which 470 LED excitation would be expected to activate Chr2 currents.

### 3 Methods

#### 3.1 General Surgical Procedures

1. Spray stereotax and surrounding bench top area with an approved disinfectant. Wipe down all surfaces. Wipe down the metal with alcohol after the disinfectant so there is no residue left.
2. Turn on all machines including the glass bead sterilizer, co-ordinates display, self-regulating heating pad and light source.
3. Using aseptic technique, lay out the sterile field and open all sterile supplies onto it including suture, sterile absorbent triangles, sterile cotton-tip applicators, sterile scalpel, sterile 1/2 cm<sup>3</sup> syringe and sterile instrument pack.
4. Use a small petri dish to soak the implant in ethanol for at least 10 min before placing the implant onto the sterile field.
5. Place animal into the anesthesia induction chamber with an O<sub>2</sub> flow rate of 1 L/min and 2.5–3.0% Isoflurane for approximately 3–4 min, until the animal's breathing slows to about one breath per second.
6. Move animal to the nosecone on the stereotax.
7. Decrease anesthesia to maintenance level of ~1.75–2% Isoflurane with an O<sub>2</sub> flow rate of 0.5–0.8 L/min.
8. Monitor animal for anesthesia:
  - (a) Respiration Rate should be maintained at 1 breath every 1–2 s.
  - (b) Mucous Membranes should be pink in color (monitor color of ears and toes).

- (c) Loss of muscle tone.
  - (d) Loss of Pedal Reflex (see subsequent steps).
9. Fix animal into the head-bars and ensure that the head is stable, straight, and perpendicular to the nosecone.
  10. Administer Buprenorphine (general guideline: 0.1 mg/kg for mice; 0.05 mg/kg for rats).
  11. Shave the animal's head, allowing wide enough margins for the type of surgery being performed.
  12. Using a cotton-tip applicator, apply a coat of Puralube to each eye.
  13. Using a cotton-tip applicator or gauze, cleanse the surgical area by alternating with ethanol and betadine for a total of three times each, starting in the center of the site and being very careful to avoid the eyes.
  14. Utilize the toe-pinch method (pedal reflex) to ensure animal is in a surgical plane of anesthesia.
  15. Pinch both hind feet to observe any reaction and that breathing remains stable.
  16. If needed, increase Isoflurane by 0.25–0.5% before testing again after 30 s.
  17. Put on sterile gloves. *Note: here begins aseptic technique.*
  18. Using the sterile scalpel, make a midline incision just large enough for the particular surgery being performed.
  19. Graefe forceps can be utilized along with iris scissors to refine the incision and expose the skull, or to create a circular cut-out of skin for implant surgeries (Refer to “Mouse Head-bar Implant Surgery” Guideline).
  20. A sterile cotton-tip applicator can be used to clear the periosteum and other tissue or debris (utilize Hydrogen Peroxide 3% for surgeries involving implants).
  21. Locate bregma (*see Notes 1–11* for procedure).
  22. Zero both the *x*-axis and *y*-axis on the Coordinate Display Box. Make a small scratch with the needle directly under the cross hairs on the surface of the skull using the sterile needle to mark bregma.
  23. Move the *x*-axis and *y*-axis arms on the stereotax to locate the first coordinate and mark with another scratch under the cross-hairs. Continue moving the arms and marking the skull until all coordinates have been marked.
  24. Remove targeting scope.
  25. Focus microscope over each marked coordinate until it is magnified to the highest power, then begin to drill:

26. Sterilize tip of drill in glass bead sterilizer. Center drill over previously marked coordinate and ensure that drill is perpendicular to skull surface.
27. Begin drilling. Periodically check the depth of hole by lifting drill away from the skull, then continue drilling process as needed.
28. When almost through the skull, the edges of the hole will start to look clear and moist. At this point, discontinue drilling as the concave burr is designed to cut a thin wafer of skull and minimize damage.
29. Carefully remove skull wafer from the surface of the brain. It may be helpful to use an absorbable spear to clear area of blood/CSF to improve visibility. Be mindful not to puncture large vessels near the surface of the brain while removing the bone piece. These can bleed a lot if punctured.
30. Check Nanoject control box to make sure it is set to the correct volume and speed. We often use 23 nL/s achieving a total injected volume of ~100 nL of virus per site.
31. Secure the Nanoject onto the arm of the stereotax and while looking through the microscope, align the tip of the pipette over the small scratch made at bregma.
32. Zero the  $x$ -axis and  $y$ -axis on the digital coordinate machine and begin to move to the first coordinate.
33. Once the coordinate has been reached according to the digital coordinates, lower the pipette until it just touches the top of the brain (unless specified otherwise by researcher) and zero the  $z$ -axis on the coordinate machine.
34. Continue to lower the pipette until it reaches the deepest desired depth at this coordinate.
35. Inject virus.
36. If other depths are desired, move the  $z$ -axis up to the second deepest depth and repeat injection. If no other depths are desired, slowly bring pipette to the surface of the brain. You may need to wait up to 5 min from the time the injection was stopped depending upon number of sites and potential concern with spread of injection.
37. Continue to next coordinate and repeat the entire process.
38. Once all coordinates and depths have been injected, remove pipette from injector and discard.
39. Dispose of anything else that may be contaminated with virus into the sharps box.
40. If virus being injected has a very limited supply, it is ok to use one pipette on multiple animals (changing the pipette as often as possible based on the resources at hand). Always load

enough in the beginning for the total number of animals to be completed with that pipette.

41. *If fiber optics are to be implanted they can be implanted at this point. See Subheading 3.4 below for detailed procedures.*
42. *If implanting a head-fixation ring in a single surgery it can be performed at this stage. See Subheading 3.3 below for specific details.*
43. Apply Marcaine to incision.
44. Turn off Isoflurane and remove mouse from ear-bars. You may leave the oxygen on for a short period of time while the animal is still unconscious (especially if surgery has lasted more than 1 h).
45. Remove animal from stereotax and allow animal to recover on heating pad.
46. The animal is removed from the stereotaxis and administered injectable analgesic (Ketoprofen 5 mg/kg) immediately following surgery. Sub-cutaneous analgesic (Ketoprofen 5 mg/kg, SID) is provided for 2 days following recovery from surgery.
47. Administer warm fluids subcutaneously between the shoulder blades if surgery lasted longer than 60 min.

### **3.2 Attach a Rigid Plastic Ring to the Skull for Subsequent Head Restraint**

1. We generally use an open source 3D printed plastic ring attached to the skull for head fixation. This has been described in detail previously and open source designs are available ([dudmanlab.org/html/rivets.html](http://dudmanlab.org/html/rivets.html)). The exposed skull surface, if any, within the plastic ring is closed to air using a temporary silicone based adhesive (Kwik-Sil) and/or a small plastic cap fitted to the ring.
2. Lightly etch surface of the skull using No. 10 scalpel blade. This step is crucial to facilitate attachment of UV Glue/cement at subsequent stages of surgery.
3. A thin layer of biocompatible glue (VetBond or Loctite 454) is then applied to the surface of the skull and very minimally to the perimeter of the skin to reduce the fluid infusion into the surgical site postoperatively.
4. Using a sterile cotton tipped applicator that is broken in half to form a spatula, spread UV Optibond glue evenly across the skull, being careful to avoid any open craniotomies.
5. Wearing protective UV goggles, cure the Optibond glue for 20 s with the UV glue gun.
6. The dental cement is applied in two phases; first a thin layer is applied to the exposed skull surface and lower portion of the implant (or surrounding area for windows) and is allowed to

dry. The second layer is slightly thicker and is applied to the rest of the skull and over the edge head-fixation ring, avoiding the skin margins.

7. Wait at least 7–8 min for each layer of cement to dry before moving on to next step.
8. Apply Vetbond to adhere the skin margins to the edge of the dried dental cement.
9. Over the life of the animal and the exposed craniotomy, the underlying tissue is regularly flushed with sterile saline and monitored for irritation or infection.

### ***3.3 Implantation of Fiber Optics***

1. For fiber implantation, ~1.3 mm craniotomies were drilled through the skull at the above sites.
2. Fiber optic stubs were gripped in a stereotactic arm and lowered into place relative to the surface of the brain.
3. The fiber stub was initially cemented into place with a small droplet of VetBond directly where the base of the cannula entered the skull, followed by two layers of light-cured glue (Opti-Bond Solo Plus) applied to both the surrounding skull as well as the cannula to ensure fixation to the skull before removal of the stereotaxic arm.
4. Repeat for each implanted fiber stub (we have typically used 1–4 total).
5. After all fibers were implanted, dental acrylic (Lang Dental, Ortho-Jet package) was built up as high as possible around each cannula and the entire exposed skull surface, leaving enough of the dorsal ends of the cannulae exposed (~3 mm) to accommodate connection to fiber-mating sleeves during recording/stimulation. These procedures ensure a stable attachment of the cannula to the skull during repeated connections and disconnections from the patch cable across multiple recording sessions.
6. Mice were given post-operative care as described above and allowed to recover for 2 weeks following surgery before beginning training and recording.
7. This time allows virus expression levels to stabilize.
8. Exposed fiber faces were protected with dust caps (Precision Fiber Products, #BCDC-1300-W).

### ***3.4 Recording and Stimulation***

1. See Fig. 1 for example experimental results and configuration.
2. Somatic Chr2 excitation was performed with a 473 nm laser (100 mW, OEM Laser Systems) coupled by a branching fiber patch cord (200 µm, Doric Lenses) to the VTA-implanted fiber cannulas using a ceramic mating sleeve.

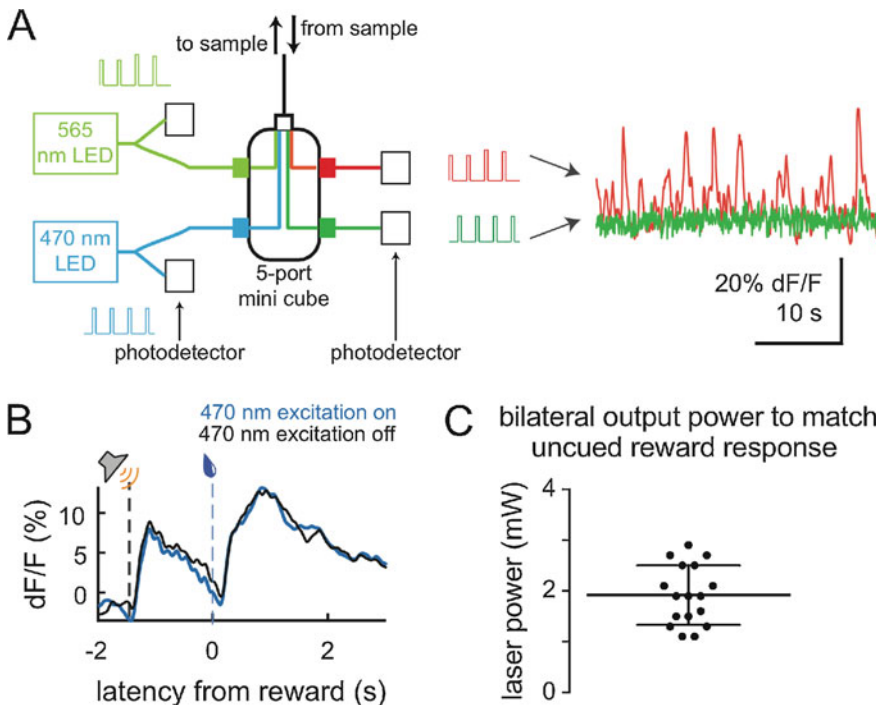


**Fig. 1** (a) Fiber photometry setup for measuring red-shifted calcium sensor signal from neurons also expressing YFP-Chr2. Two LED light sources are modulated at 100 Hz (1 ms on, 9 ms off), offset to each other. A Y-cable splits LED output between a photodetector and the band-filtered input ports of the 5-port minicube. Dichroic mirrors direct the two light sources into the sample patch cable, then direct the returning collected light into the band-filtered output ports, after which the signals are measured by photodetectors. The signal from the LED photodetectors is used to timestamp the signals that are to be recovered from the final photodetectors so that the continuous signals can be recovered from the flickered raw data. (b) A comparison of jRCaMP1b signal with and without 470 nm LED multiplexed, from the nucleus accumbens of a DAT<sup>cre</sup>::ai32 mouse injected with a virus to express jRCaMP1b bilaterally in VTA- and SNC-DA neurons. The effective power of 470 LED illumination at the tip with excitation on is ~10  $\mu$ W, well below the threshold at which Chr2-activation would be expected. (c) For bilateral VTA excitation, the 473 nm laser peak power output that elicited nucleus accumbens  $[Ca^{2+}]$  transients equivalent to those seen for uncued reward responses in mice ( $n = 17$ ) expressing jRCaMP1b and Chr2 in VTA- and SNC-DA neurons, with burst stimulation of 30 Hz (10 ms on, 23 ms off) for 150 ms. Peak power was measured from the tip of the sample cable after each experiment with the laser continuously on

3. On each recording day, LED light sources were turned on >10 min before recording began to ensure output stability. After head fixation, dust caps were removed and fresh index-matching gel (Thorlabs, G608N3) was applied to cannula faces. Gel reduces signal attenuation at the connection point as well as lubricates cannulae for smoother connection and disconnection.
4. Fiber mating sleeves (Thorlabs, ADAL1) were used to connect fiber cannulae to the patch cables for light delivery/collection. Signal amplitude and dynamics were checked immediately

following connection, and if significant differences were noted from the previous recording session, patch cable was disconnected and fiber faces were cleaned with lens paper and water, then ethanol, and then left to dry before reconnection with fresh index matching gel. NOTE: Relatively high- or low-amplitude signals with low dynamics rarely occurred, and usually indicated a dirty or improper connection that was resolved by cleaning and reconnecting the fibers. Given that signals were most often identical from session to session, fiber cleaning was not routinely done.

5. All fiber sites were plugged in and illuminated for 5–10 min before recording sessions began, in order to allow for initial photobleaching and behavioral responses to stabilize.
6. The inconstant, flickered illumination that allowed for multiplexing makes signals noisy to observe in real time. But even with relatively low signal-to-noise recording sites, observable dynamics were sufficient for evaluating recording quality during recording sessions, with detailed analysis done later, off-line.

---

## 4 Notes

### Locating Bregma

1. Localizing bregma with a zeroing scope/leveler affixed to the stereotax (e.g., [kopfinstruments.com/product/model-1915-centering-scope-40x/](http://kopfinstruments.com/product/model-1915-centering-scope-40x/)) has allowed us to produce the most reliable targeting of small structures and is recommended. Using the scope move the animal's head (utilizing knobs connected to u-bar, not X, Y, Z knobs) so that bregma lines up with the cross hairs in the scope (be mindful of which knobs have to be unlocked before they can move). Remove scope from stereotax after localizing bregma.
2. Make sure the instrument is locked into position along the M/L ( $x$ ) axis of the skull.
3. Gently lower the instrument until it touches the animal's skull.
4. Very slowly continue to lower the instrument to ensure that both needles hit zero simultaneously. If not, raise leveling tool and turn the knob that controls the mediolateral head tilt to slightly adjust the head as needed.
5. Continue steps 3 and 4 until both needles on the gauge reach zero at the same point.
6. Unlock plane adjustment on leveling tool and turn so it is now along the A/P ( $y$ ) axis.
7. Repeat steps 3–5.

8. If there was a large adjustment needed along the A/P axis, level M/L axis again before removing instrument.
9. Great care is taken to remove remaining tissue from the surface of the skull using a micro spatula when attaching a head-fixation ring. Adequacy of skull cleaning is monitored using application of sterile saline.
10. To achieve concomitant expression of a genetically encoded calcium indicator an AAV ( $\sim 5 \times 10^{12}$  titer, 150  $\mu\text{L}$ ) was injected bilaterally at two depths in the VTA ( $-3.2$  mm A/P,  $0.5$  mm M/L,  $-4.6$  and  $-4.3$  mm D/V) and one in the SNc ( $-3.1$  mm A/P,  $1.4$  mm M/L,  $-4.3$  mm D/V).
11. During the viral injection surgery, fibers were implanted bilaterally over the VTA ( $-3.2$  mm A/P,  $1.2$  mm M/L,  $-4$  mm D/V,  $6^\circ$  angle) as well as unilaterally over the DS ( $1$  mm A/P,  $1.8$  mm M/L,  $-2.3$  mm D/V,  $5^\circ$  angle) and the NAc ( $1.4$  mm A/P,  $0.9$  mm M/L,  $-4$  mm D/V). The angles indicated were used in order to allow sufficient space on top of the skull to couple fibers to patch cord.

## Acknowledgments

JTD is a senior group leader at the Janelia Research Campus of the Howard Hughes Medical Institute (HHMI). The work described here was funded by HHMI.

## References

1. Zhang F, Wang LP, Boyden ES, Deisseroth K (2006) *Nat Methods* 3:785
2. Kim CK, Yang SJ, Pichamoorthy N, Young NP, Kauvar I, Jennings JH, Lerner TN, Berndt A, Lee SY, Ramakrishnan C, Davidson TJ, Inoue M, Bito H, Deisseroth K (2016) *Nat Methods* 13:325
3. Gunaydin LA, Grosenick L, Finkelstein JC, Kauvar IV, Fenn LE, Adhikari A, Lammel S, Mirzabekov JJ, Airan RD, Zalocusky KA, Tye KM, Anikeeva P, Malenka RC, Deisseroth K (2014) *Cell* 157:1535
4. Akam T, Walton ME (2019) *Sci Rep* 9:3521
5. Owen SF, Kreitzer AC (2019) *J Neurosci Methods* 311:170
6. Coddington LT, Dudman JT (2018) *Nat Neurosci* 21:1563
7. Otchy TM, Wolff SBE, Rhee JY, Pehlevan C, Kawai R, Kempf A, Gobes SMH, Ölveczky BP (2015) *Nature* 528:358
8. Dana H, Mohar B, Sun Y, Narayan S, Gordus A, Hasseman JP, Tsegaye G, Holt GT, Hu A, Walpita D, Patel R, Macklin JJ, Bargmann CI, Ahrens MB, Schreiter ER, Jayaraman V, Looger LL, Svoboda K, Kim DS (2016) Sensitive red protein calcium indicators for imaging neural activity. *elife* 5:e12727
9. Owen SF, Liu MH, Kreitzer AC (2019) *Nat Neurosci* 22:1061
10. Stujenske JM, Spellman T, Gordon JA (2015) *Cell Rep* 12:525



# Chapter 15

## Single or Double Patch-Clamp Recordings In Ex Vivo Slice Preparation: Functional Connectivity, Synapse Dynamics, and Optogenetics

Jean Simonnet, Louis Richevaux, and Desdemona Fricker

### Abstract

Patch-clamp recordings are the method of choice to define cell-type specific electrophysiological properties of single neurons and the synaptic connectivity between pairs of connected neurons in brain slices. In combination with optogenetic tools, patch-clamp recordings allow for the investigation of long-range afferent connectivity from identified distant brain areas. Here we describe the necessary equipment to carry out patch clamp recordings, surgical methods for dissection and preparation of horizontal brain slices containing the hippocampus, and a step-by-step guide for establishing patch clamp recordings in the whole-cell configuration. We provide protocols for single neuron stimulation via the patch pipette and for photostimulation experiments that activate axon terminals expressing light sensitive ion channels.

**Key words** Whole-cell patch-clamp recording, Electrophysiology, Excitability, Inhibition, Channelrhodopsin, Optogenetics, Acute brain slice, Hippocampus, Synaptic transmission

---

### 1 Introduction

Action potential firing in central nervous system neuronal circuits underlies specific functions, including the integration of sensory information, the regulation of autonomous processes, and driving cognition or specific behaviors. Understanding how neural circuit activity is encoded requires knowledge of anatomy, single neuron and synaptic physiology, as well as local and brain wide functional connectivity.

The patch-clamp technique [1–3] is the gold standard for investigating ion channel behavior, single neuron physiology, and synaptic function. It has led to major discoveries in neuroscience. Patch clamping has been used to tackle a broad range of questions, from the characterization of intrinsic membrane currents [4–6], the firing properties of neurons [7] and synaptic properties [8] ex vivo, to the study of subthreshold membrane potential fluctuations and action potential firing in freely behaving animals [9]. In other

words, it has been and remains an essential method to study neurophysiology from the molecular level to the animal's behavior.

We have used patch-clamp recordings in acute slices from wild-type or transgenic mice, to study intrinsic neuronal properties [10, 11], cellular anatomy [12, 13], synaptic connectivity and dynamics as well as integration of long-range synaptic inputs [14, 15]. The present methods article focuses on the equipment and the procedures that we routinely use in our laboratory.

Specifically, we describe how to dissect the mouse brain for the preparation of acute hippocampal slices and how to carry out patch-clamp recordings, including a schematic of our setup dedicated to patch-clamp and optogenetics experiments. We describe how to prepare solutions used to immerse the brain tissue during slicing and during recordings, as well as the internal solutions used to fill the patch pipettes. We provide details about preparing the animal, the brain dissection, our slicing method, and slice handling procedures and we describe how to perform single or dual patch clamp recordings. We advise on key methods and protocols for recording intrinsic neuronal properties, testing the connectivity between pairs of neurons, investigating synaptic dynamics and studying the integration of long-range inputs using optogenetics tools.

---

## 2 Materials

### 2.1 External Solutions

Prepare two types of external solutions, a “cutting solution” and artificial cerebrospinal fluid (ACSF) for recording, from using ultrapure water (resistance 18 MΩ) from the lab’s water purification systems (Table 1; *see Note 1*).

To improve reproducibility and save time, prepare 10× stock solutions without the divalent cations, CaCl<sub>2</sub> and MgCl<sub>2</sub>, which should be prepared separately as 1 M solutions. Keep stock solutions at 4 °C. The final solutions (1×) must be prepared the day of the experiment.

These external solutions must be bubbled constantly with oxygen/carbon dioxide (O<sub>2</sub>–CO<sub>2</sub>, 95:5%).

### 2.2 Internal Solutions

The internal solution is used to fill the patch pipette and the cell’s interior. It is one of the most important factors determining the success of a whole-cell patch-clamp experiment.

1. Water quality: Use ultrapure water. We use cell culture graded distilled water (Gibco, ref. 15230089, Thermo Fisher).
2. Stability: As internal solutions contain temperature sensitive compounds, prepare them on ice. Aliquots can be stored in the freezer (–20 °C) for up to 1 year.

**Table 1**  
**Composition of cutting solutions and ACSF in mM**

<b>ref.</b>	<b>Product</b>	<b>Choline chloride</b>	<b>NaCl/Sucrose</b>	<b>ACSF</b>
Sigma—C7527	Choline chloride	110	/	/
Sigma—S7653	NaCl	/	125	124
Sigma—S0389	Sucrose	/	25	/
Sigma—P4504	KCl	2.5	2.5	2.5
Sigma—S9638	NaH <sub>2</sub> PO <sub>4</sub>	1.25	1.25	1
Sigma—S5761	NaHCO <sub>3</sub>	25	25	26
Sigma—G7528	Glucose	7	2.5	11
Fluka—21,114	CaCl <sub>2</sub>	0.5	0.1	2
Fluka—63,020	MgCl <sub>2</sub>	7	7	2

**Table 2**  
**Composition of internal solutions**

<b>ref.</b>	<b>Product</b>	<b>K-Gluc (mM)</b>	<b>For 25 ml</b>	<b>Cs-gluc (mM)</b>	<b>For 25 ml</b>
Sigma—G4500	K-gluconate	140	819.7 mg	/	/
Sigma—232,041	Cs-OH	/	/	135	610.1 µl
Sigma—G1951	D-gluconic acid	/	/	135	1112.7 µl
Sigma—P4504	KCl	1.2	2.2 mg	5	9.3 mg
Sigma—H3375	HEPES	10	59.6 mg	10	59.6 mg
Sigma—E4378	EGTA	0–0.2	0–1.9 mg	0–0.2	0–1.9 mg
Fluka—63,020	1 M MgCl <sub>2</sub>	2	50 µl	2	50 µl
Sigma—A9187	MgATP	4	50.7 mg	4	50.7 mg
Sigma—G9002	Na <sub>3</sub> -GTP	0.4	8.9 mg	0.4	8.9 mg
Sigma—P7936	Na phosphocreatine	10	63.8 mg	10	63.8 mg
Sigma—B4261	Biocytin	3%	75 mg	3%	75 mg
	pH 7.2–7.4		K-OH or K-gluconate	Cs-OH or D-gluconic acid	

3. Examples of internal solutions: Here we describe the composition of two types of solutions that we have used. Choose the internal depending on your scientific question and the type of recording that is appropriate (Table 2; see Note 2).
4. Low-chloride potassium gluconate-based (Low-Cl K-gluc) internal solution: 145 mM K-gluconate, 2 mM KCl, 10 mM HEPES, 0–0.2 mM ethylene glycol tetraacetic acid (EGTA), 2 mM MgCl<sub>2</sub>, 4 mM Mg-ATP, 0.4 mM Tris-GTP, 10 mM Na<sub>2</sub>-phosphocreatine.

5. Cesium gluconate-based (Cs-gluc) internal solution: 135 mM Cs-gluconate, 5 mM KCl, 10 mM HEPES, 0–0.2 mM EGTA, 2 mM MgCl<sub>2</sub>, 4 mM Mg-ATP, 0.4 mM Tris-GTP, 10 mM Na<sub>2</sub>-phosphocreatine.
6. Cellular anatomy: For post hoc recovery of the cellular anatomy, add biocytin (1–3 mg/ml, Tocris 3349 or Sigma B4261-50MG)—or alternatively Neurobiotin (Vector laboratories SP-1120)—to the internal solution.

### **2.3 Preparing Solutions**

1. Add the compounds one by one in ultrapure water (80% of the final volume in a beaker or an equivalent piece of glassware), following the order indicated above. Add the biocytin at the end and stir for 10–20 min.
2. Adjust the pH (in our hands it is too low initially) to 7.2–7.4 using the appropriate solution (Cs-OH for Cs-based solution or K-OH for K-based solution). This will also help to obtain complete dissolution of all compounds.
3. Transfer the solution to a container allowing precise measure of the volume (e.g., a burette) and adjust to the final volume with ultrapure water.
4. Control of Osmolality (Wescor Vapor Pressure Osmometer VAPRO, calibrate prior to measures). If high (most of the time), calculate the dilution factor to reach 290–300 MOsm and add the appropriate volume of ultrapure water. For instance, if the initial measure is 330 MOsm, for a total of 23 ml of internal solution, add 2.3 ml H<sub>2</sub>O. If too low, add the main compound (Cs Gluc or K Gluc). Adjust, stir for a minute, and then check the osmolality again. Repeat the procedure until an osmolality of 290–300 MOsm is reached.
5. Make aliquots (750 µl or 1 ml) and store at –20 °C to allow for a convenient use of 1 aliquot per day of experiment.

### **2.4 Pharmacology**

Prepare aliquots of pharmacological compounds and store them at –20 °C. When possible, we recommend stock concentrations of 1000× for easy calculation of final dilution the day of the experiment (e.g., final concentration obtained by diluting 20 µl in 20 ml; Table 3).

### **2.5 Anesthesia**

Prepare a mixture of ketamine and xylazine (100/15 mg/kg respectively).

### **2.6 Dissection and Slicing**

1. Versi-Dry bench absorbent paper (Fig. 1a).
2. 0.3–1 ml syringes.
3. 25G needles.
4. Curved forceps.

**Table 3**  
**Drugs used for pharmacology experiments**

Ref.	Product	Target	Stock (mM)	Use at ( $\mu$ M)	in 20 ml ( $\mu$ l)
Tocris—1078	TTX	Voltage-gated Na <sup>+</sup> channels	1	1	20
Sigma—A78403	4-AP	Voltage-gated K <sup>+</sup> channels	100	100	20
Tocris—0106/1	APV	NMDA receptors	50	100	40
Tocris—1044	NBQX	AMPA/kainate receptors	10	10	20

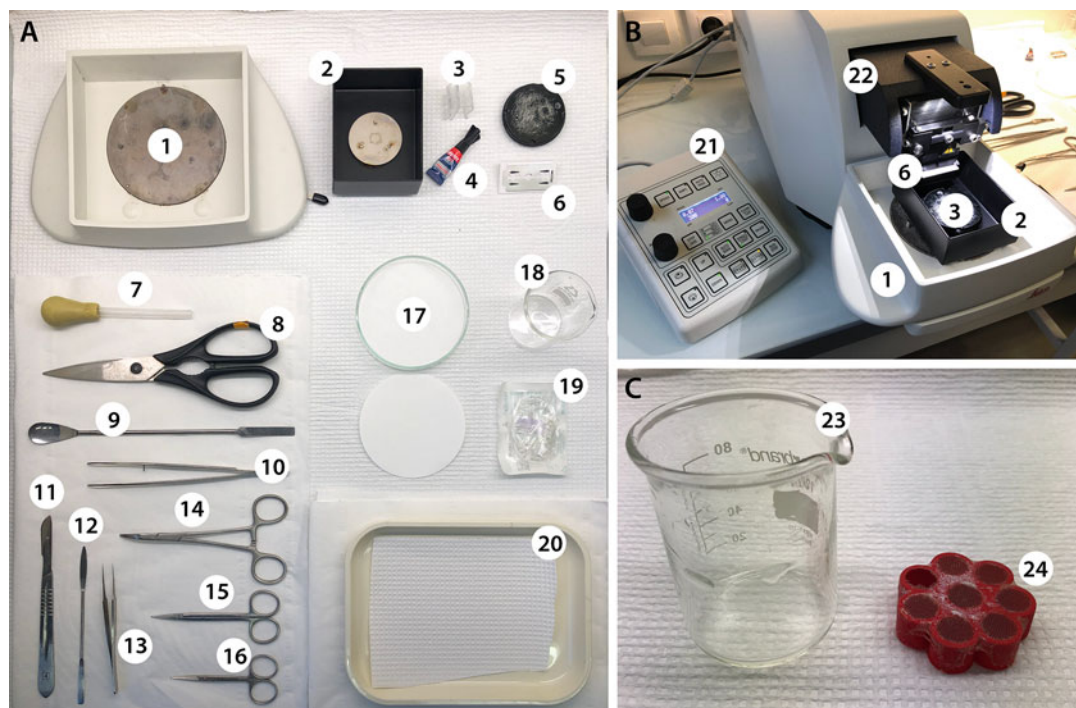


**Fig. 1** Dissection and slicing equipment. (a) 1, Vibratome outer chamber, to be filled with crushed ice. 2, Slicing chamber, to be filled with ice-cold, oxygenated cutting solution. 3, Tube holder for oxygenation. 4, Superglue. 5, Specimen holder. 6, Double edge stainless steel blade, use one half for slicing. 7, Transfer pipette with rubber bulb. 8, Big scissors. 9, Big spatula. 10, Curved forceps. 11, Scalpel. 12, Small round spatula. 13, Dumont forceps. 14, Curved hemostat. 15, Medium scissors. 16, Small scissors. 17, Absorbent paper. 18, 80 ml beaker. 19, Butterfly needle with tubing. 20, Versi-Dry bench absorbent paper. (b) 21, Vibratome control panel. 22, Leica VT1200S Vibratome. (c) 23, 80 ml beaker serving as slice storage chamber, with 24, 3D printed slice support with stretched and glued nylon stocking

- 5. Big scissors.
- 6. Medium and small scissors.
- 7. Curved hemostat.
- 8. Butterfly needle.

9. 60 ml syringe
10. Tubing with a roller clamp.
11. Vibratome (Fig. 1b; e.g., Leica VT1200S).
12. Double edged stainless steel razor blades.
13. Filter paper (Whatman).
14. Superglue.
15. Slice transfer pipette (shortened glass Pasteur pipette equipped with a rubber bulb).
16. Slice storage chamber: made from a nylon stocking stretched and superglued over a round support, held at midlevel in a beaker, later filled with ACSF and gently bubble with O<sub>2</sub>-CO<sub>2</sub> 95:5%). A 3D printer can be used for support shapes with individual wells (Fig. 1c).
17. Heated water bath.

## **2.7 Patch-Clamp Setup**

1. The patch-clamp setup needs to be installed on an antivibration air-table inside a Faraday cage (Fig. 2).
2. We use a BX51WI Microscope from Olympus, equipped with a 5× and a 60× objective, an infrared filter and DIC imaging.
3. A Multiclamp 700B amplifier with a pair of CV-7B headstages from Axon Instruments is interfaced via an Axon Digidata 1440A Digitizer with a PC, running pClamp (Molecular Devices) for data acquisition.
4. Wide-field blue and/or red illumination can be obtained via a twin OptoLED light source coupled into the microscope via a triple port (Cairn, UK). Appropriate filters for blue and/or red illumination are indicated in Fig. 3. The third port accommodates a laser for 1P focal illumination (Omicron LuxX laser: 405 nm, 300 mW; Fig. 3).
5. Optical stimulation is commanded via an isolated pulse stimulator (A-M Systems Model 2100) and triggered by the acquisition software.
6. A Luca EMCCD camera from Andor serves to visualize brain slices during patching.
7. Electrode holders for 1.5 mm glass are from G23 Instruments (ISO-S-1.5G microelectrode holders, Greenwich, London, UK). Inelastic polyethylene tubing to apply positive or negative pressure to the pipette is attached at the holder. Use electrophoresis of HCl solution to apply chloride to the silver wire that plunges in the internal solution in the patch pipette [16].
8. We use a pump for perfusion of the recording chamber (Gilson Minipuls 3 Peristaltic pump) to allow recycling of ACSF. This may be very useful if the ACSF contains expensive drugs.

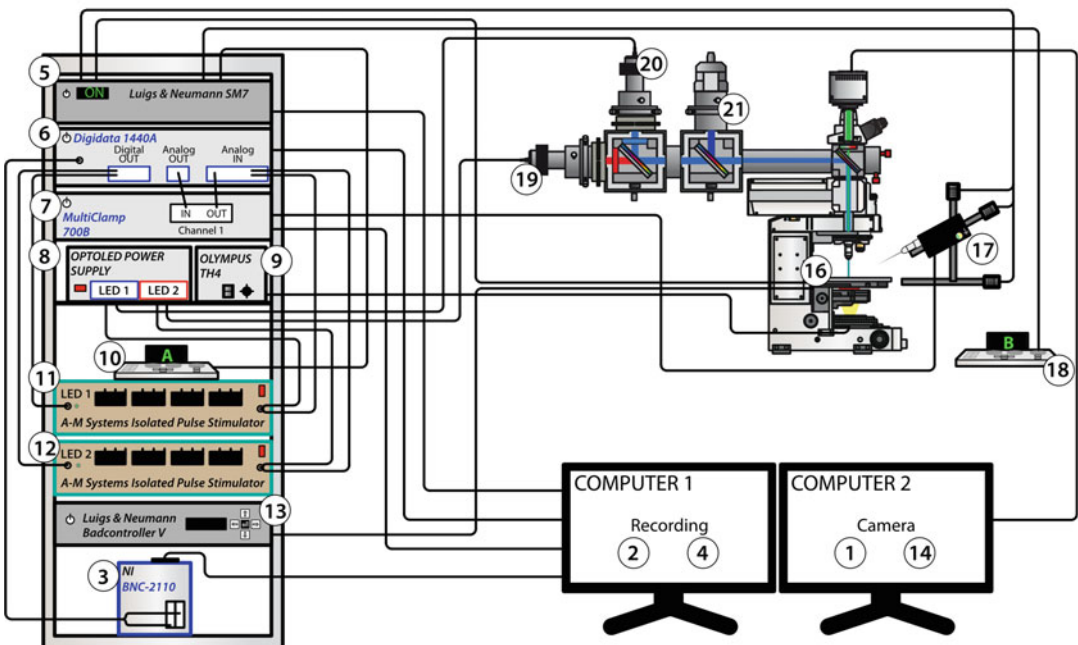
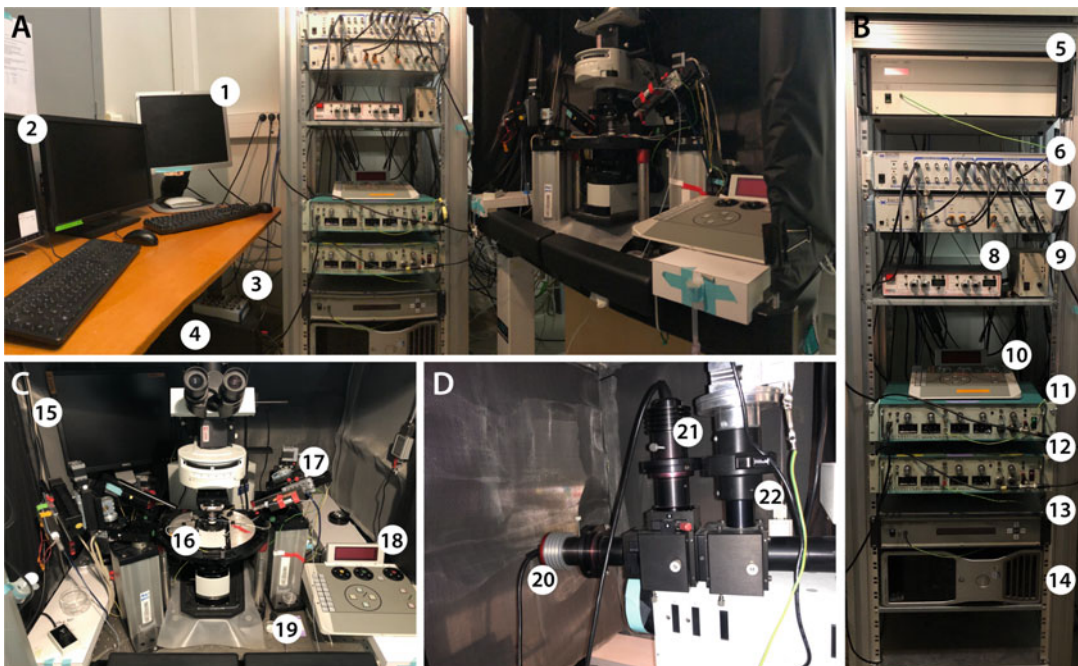


**Fig. 2** Electrophysiology setup (top) and schematic (bottom). **(a)** Overview of experimental set-up. **(b)** Electrophysiology instruments rack. **(c)** Recording chamber and Olympus BX51WI microscope, mounted on a Luigs & Neumann shifting Table. **(d)** Back view of the microscope with Cairn triple port microscope coupling. **1**, Camera screen. **2**, Electrophysiology screen. **3**, National Instruments BNC-2110. **4**, Computer. **5**, Luigs & Neumann SM7 micromanipulators controller. **6**, Digidata 1440A, Molecular Devices. **7**, Multiclamp 700B, Molecular Devices. **8**, Cairn OptoLED Power Supply. **9**, Olympus TH4 power supply. **10**, Luigs & Neumann micromanipulator keypad (x-y shifting table and microscope focus axis control). **11**, A-M Systems isolated pulse stimulator 1. **12**, A-M Systems isolated pulse stimulator 2. **13**, Luigs & Neumann Badcontroller V bath temperature controller. **14**, Camera computer. **15**, Second camera screen. **16**, Recording chamber. **17**, Pipette holder and micromanipulator. **18**, Luigs & Neumann micromanipulator keypad (pipette holder controller). **19**, Antivibration Table. **20, 21**, Cairn LED. **22**, 405 nm laser

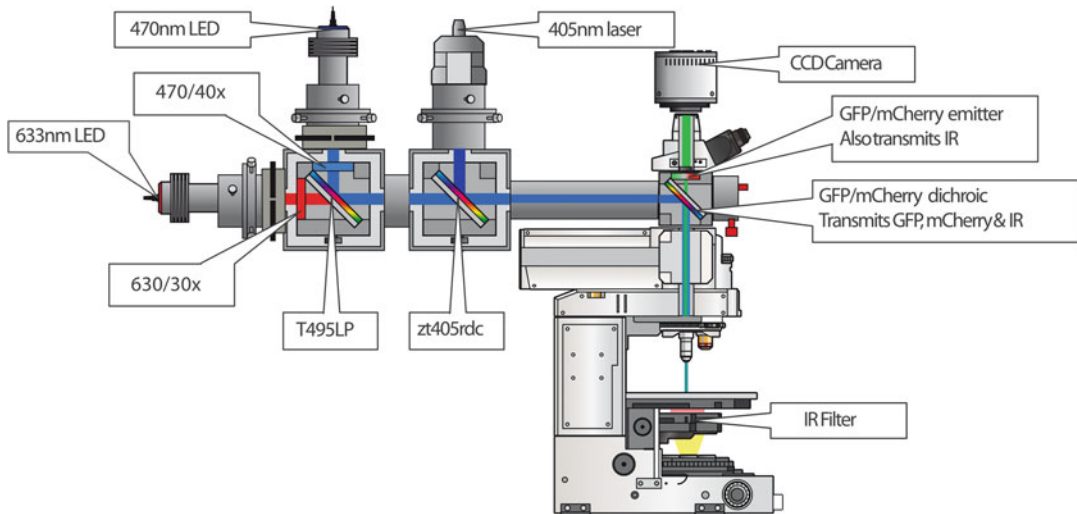


**Fig. 3** Microscope equipped for photostimulation. Two LEDs for 470 nm or 633 nm whole field light stimulation are coupled into the epifluorescence port. Combined dual wavelength stimulation with a multiband dichroic. The third port accommodates a 405 nm laser for focal 1P photostimulation [15]

Otherwise gravity-driven perfusion works well, combined with a suction at the outlet of the chamber. ACSF warmed to 35–37 °C and bubbled with 5% CO<sub>2</sub> in O<sub>2</sub>. ACSF perfusion speed, 2–3 ml/min in submerged chamber.

9. The Faraday cage and all electrically powered instruments need to be connected to a common ground reference on the table.
10. Harp to hold the slices down. Harps can be purchased from Warner instruments (metal slice anchor) or custom fabricated in the lab. Bend a platinum wire (Advent, Oxford, PT542104) to give it a U-shaped form, hammer it a bit to flatten it and reduce its height, then glue 4–8 thin nylon threads (from nylon stocking) on the two parallel bars of the U in a striped motif (Fig. 4).

## 2.8 Patch Clamp Pipettes

1. Borosilicate glass capillaries of external diameter 1.5 mm, thick walled with filament for easy filling (Fig. 4; Harvard Apparatus, GC150F-10).
2. Brown–Flaming Micropipette horizontal puller (P97 Sutter Instruments) with a 2.5 × 2.5 box filament (S-FB255B).
3. Follow the instructions written in the “pipette cookbook”, available for download from [sutter.com](http://sutter.com).
4. Custom pipette filling system: 1 ml syringe with a 0.2 µm syringe filter (Nalgene, ref. 171-0020); a shortened 200 µl pipette tip is used as an adaptor piece for the Microloader (20 µl, Eppendorf, ref. 5242 956.003; Fig. 4).

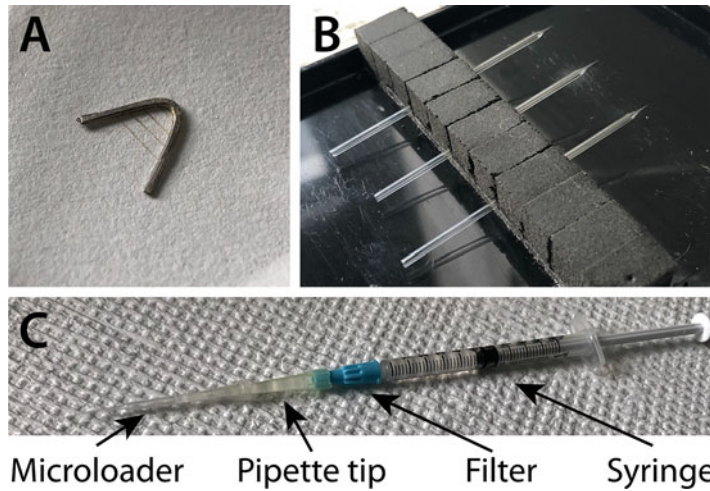


**Fig. 4** Electrophysiology accessories. (a) Slice holding harp made of platinum wire and nylon stocking. (b) three borosilicate glass patch pipettes. (c) Pipette filling system with microloader

### 3 Methods

#### 3.1 Preparations for Slicing

1. On the day of the electrophysiological recording experiment, prepare the cutting solution and ACSF (1×) by diluting the 10× stock solutions with ultrapure water, not adjusting to the final volume yet, and bubble the solutions with 95:5% O<sub>2</sub>-CO<sub>2</sub>. Add MgCl<sub>2</sub> and CaCl<sub>2</sub> (after a few minutes of oxygenation, to avoid precipitation of the divalents and the bicarbonate) then adjust to the final volume with ultrapure water.
2. Keep the cutting solution on ice (2–4 °C) and gently bubble with 95:5% O<sub>2</sub>-CO<sub>2</sub>.
3. Keep ACSF at room temperature and gently bubble with 95:5% O<sub>2</sub>-CO<sub>2</sub>.
4. Prepare the perfusion and dissection station as well as the slice storage chamber (Fig. 1). Work in clean conditions. Sterilization is not required but use alcohol for cleaning the surgical instruments, and also for the holding chamber. Clean and/or change the tubing regularly.

#### 3.2 Anesthesia

The animal must be deeply anesthetized (*see Note 3*). Inject the mixture of ketamine and xylazine (100/15 mg/kg respectively) intraperitoneally. Then begin the dissection and slicing procedure (Fig. 5).

#### 3.3 Perfusion

1. Place the perfusion syringe 80 cm above the bench and fill it with ice-cold oxygenated cutting solution. Let the solution run through the attached tubing until it flows out of the butterfly needle. Check that there are no air bubbles in the tubing and stop the flow using the roller clamp.

Work flow :

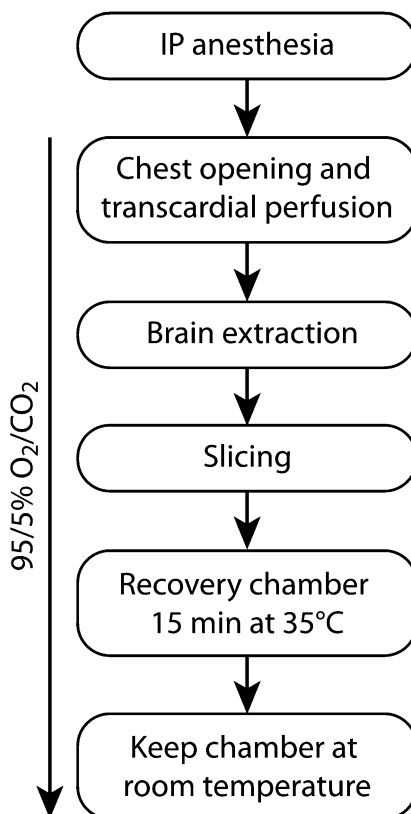


**Fig. 5** Experimental workflow

2. Once the animal is deeply anesthetized, use adhesive tape to maintain the animal stretched out on its back on the bench surgery area. Palpate the sternum, incise the skin immediately above it, and elevate it to expose the abdominal muscles. Incise these muscles to expose the diaphragm and the liver immediately below it on the right side of the abdomen. The sternum is elevated using tweezers. Incise the diaphragm following the ventral lower edge of the rib cage. Care must be taken not to puncture the liver or the heart. Cut open the entire rib cage on both sides from caudal to rostral, using scissors, as dorsal as possible. Use a clamp to hold the sternum bent upward, over the animal's head, exposing the heart.
3. Inject 500 units (100 µl) of heparin (Heparin Choay 5000 U. I./ml) slowly into the left ventricle.
4. Clamp the descending aorta just above the liver. Release the flow of cutting solution and set the perfusion speed to 1–2 ml per minute. Insert the butterfly needle in the left ventricle and cut open the right atrium with small scissors within 1–2 s.

When 30–40 ml of cutting solution have been perfused, the liquid coming out from the atrium should be translucent and the lungs have turned white.

5. Decapitate the animal and place the head in cold cutting solution in a petri dish.
1. Incise the scalp following the midline, from the caudal end to between the eyes, using small scissors. Pull down the skin to either side to expose the skull. Remove vertebrae that may have remained attached to the skull, as well as the conjunctive tissue on the skull and the muscles on the side, to expose lambda. Using the very tip of small scissors, cut the skull following the axis of the sagittal suture, starting caudally, from the foramen magnum, and extending rostrally, toward the orbits.
2. Make a T-shaped incision by adding a small perpendicular cut just caudal to the orbit, on both sides. Make a horizontal cut of the occipital bones from the foramen magnum to the external auditory meatus.
3. Hold the head horizontally, between index and thumb, and pull one side of the cranial bone sideways away from the brain. The movement resembles the turning of the page of a book. Repeat for the other half of the skull. The head should then be held by the sideways bent half skulls on either side of the brain. The ventral part of the skull cavity should be gently separated from the brain by inserting a round spatula under the brain. The brain is then separated from the cranial nerves with the spatula. Extract the brain, and immerse it in fresh and cold cutting solution. Depending on the brain structure of interest the brain may be further dissected to obtain the final area to slice.
4. Identify which side of the block should be glued. For horizontal hippocampal slices, glue the cortex to the vibratome's cutting plate so that the brain sits upside down for slicing. Remove the excess of liquid by gently positioning the block on the filter paper, the side being glued (here the dorsal part) facing down.
5. Spread a thin and homogeneous layer of superglue on the vibratome's cutting plate and transfer the block on top of it. Then submerge the plate and the brain in cutting solution.
6. Cut the brain in 200–400  $\mu\text{m}$ -thick slices (*see Note 4*) at a speed of 0.05–0.07 mm/s and an amplitude of 0.9–1 mm. Additional scalpel cuts may reduce the size of the slices and facilitate their handling and positioning in the resting and recording chambers.
7. Using the slice transfer pipette, place the slices in the recovery chamber filled with ACSF in a 35 °C warm water bath. Let the slices recover for 15 min, then take the chamber out of the warm bath and let it rest at room temperature for about 45 min before use.

### 3.4 Brain Dissection for Hippocampal Slices

### 3.5 Preparing the Recording Session

1. Pull pipettes to obtain a resistance of 3–8 MΩ once filled with internal solution. You may wish to check the tip shape under the microscope (*see Note 5*). Keep pipettes in a box until use. Handle carefully, do not touch the tip, and protect from dust.
2. Prepare the custom pipette filling system with the internal solution. Aspirate the internal solution in the syringe and position, sequentially, the filter, the 200 µl pipette tip and the microloader (Fig. 4). Chase any bubbles. Test eject 100 µl of solution. The filling pipette system is now ready and should be kept at 4 °C.
3. Turn on the rig and set up the acquisition system. The recording software should be ready to play a pipette resistance test in voltage clamp, that is, short (5–20 ms) voltage steps (−2 to −10 mV) repeated at high frequency (~20 Hz).
4. Set the perfusion and temperature of the recording chamber: continuously perfuse ACSF warmed at 35–37 °C and bubbled with 95:5% O<sub>2</sub>-CO<sub>2</sub> through to the recording chamber (2–5 ml/min). The output flow from the chamber can be directed to the same container to recycle the ACSF. Turn on the closed-loop heating unit to maintain the ACSF in the chamber at the desired temperature (35 °C, *see Note 6*).
5. Place a slice in the recording chamber.
6. Place the slice holding harp over the slice to maintain it. The ACSF perfusion (and the closed loop heating unit) can be shortly paused during this manipulation (but *see Note 6*).

### 3.6 Patching—Step-by-Step

1. Identify a cell to patch under the 60× objective (*see Note 7*).
2. Fill approximately 3/4 of a patch pipette with the internal solution, using the syringe with the microloader (Fig. 4). Place the pipette in the pipette holder, secure the micromanipulator to an appropriate starting position and apply positive pressure using a syringe or your mouth.
3. Move up the objective to make some space between the slice and the objective until a column of liquid starts forming under the lens. Use the micromanipulator to position the pipette tip in the center of the column of liquid under the lens. If well aligned at the beginning, the pipette should be well under the lens, maybe unfocused at first.
4. The positive pressure exerted to the pipette results in an outflow of internal solution from the pipette and should be visible while focusing on the pipette tip. The pipette tip should be clean. If necessary, you may increase the pressure transiently to get rid of any dust particles, or change the pipette.
5. Start the pipette resistance test on the software (−2 mV at 20 Hz, 50 ms ON—50 ms OFF). The response to the voltage step, a current jump, should be visible and proportionate to the

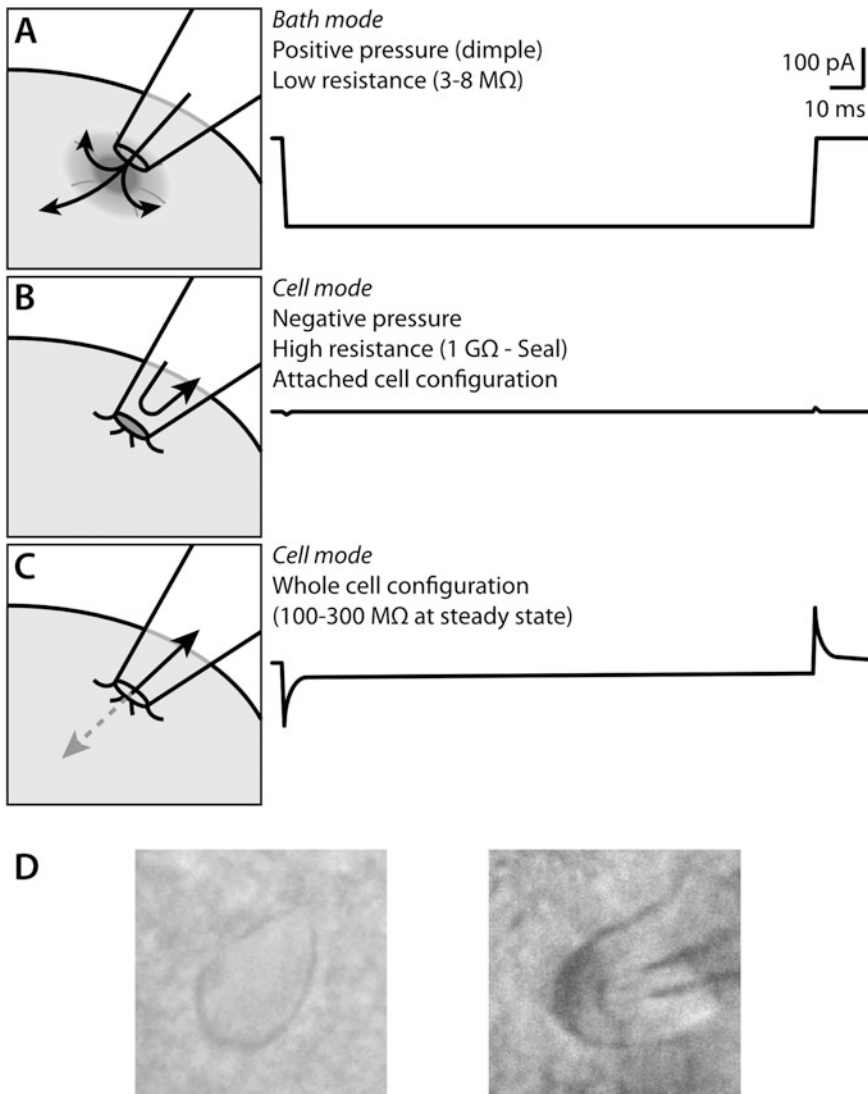


**Fig. 6** Step-by-step schematic of patch-clamp. Left, illustration, (right) corresponding traces in voltage-clamp mode. (a) Pipette approaching a neuron and forming a “dimple.” Applying  $-2$  mV voltage. Current jump between pipette and bath indicates pipette resistance. (b) Positive pressure is released, and negative pressure applied, resulting in seal formation between pipette tip and neuronal membrane. Continue to monitor resistance, until formation of a high resistance giga-seal between pipette and cell. (c) Quick negative pressure is used to rupture the membrane patch under the pipette and break into the cell. Direct electrical access to the cell’s interior, and dialysis via the membrane opening between cell and pipette. (d) Examples of cells to patch. A smooth, homogenous aspect of the cell surface, with low contrast, ideal for patching (left). Positive pressure producing a “dimple” at the surface of a cell (right)

pipette resistance (Fig. 6a, right). Check that the resistance is appropriate ( $3-8$  MΩ) and adjust the pipette offset to 0 pA. Lower the objective and then the pipette in small steps, until the slice surface is in focus.

6. Approach the cell in a movement that follows as much as possible the axis of the pipette, limiting lateral movements and resulting lesions of the tissue. The positive pressure should be sufficient to push aside the brain slice tissue in front of the pipette tip and ‘clean’ the cell surface.
7. When pushing the pipette tip against the cell body, a “dimple” appears on the membrane (Fig. 6a and 6d).
8. Form a giga-ohm seal by releasing the pressure and apply gentle and transient negative pressure (Fig. 6b). The steady state current response to the pulse should decrease rapidly and now be close to 0 pA, indicating a cell-attached configuration and a seal resistance of 1 GΩ or higher.
9. Release any pressure to the pipette.
10. Apply a -65 mV holding potential. Set the test pulse amplitude to -10 mV and its frequency to 100 Hz (10 ms ON—10 ms OFF).
11. Compensate for fast and slow pipette capacitance transients [17].
12. “Break-in” by exerting a quick negative pressure (“kissing” the syringe, gently at first, then vigorously if needed) to establish whole cell configuration (Fig. 6c).

### **3.7 Recording Two Cells**

1. If two cells need to be recorded, approach the cells with two patch pipettes, one coming from the left, the other from the right side (*see Note 8*).
2. Approach each pipette tip close to its target neuron (less than 100 μm distance), before establishing a seal onto one neuron and then onto the other neuron. Once good quality giga-seals have been established, break in one cell, then followed by the other.

### **3.8 Artefact Compensation**

Single pipette patch clamp generates aberrations that should be corrected in order to read proper signals and minimize the effect of the recording on the cell activity [18, 19]. Instructions for pipette capacitance compensation and neutralization of artefacts are given in the Multiclamp 700B manual ([https://mdc.custhelp.com/euf/assets/content/MultiClamp\\_700B\\_Manual2.pdf](https://mdc.custhelp.com/euf/assets/content/MultiClamp_700B_Manual2.pdf)).

We routinely use the bridge balance compensation in current clamp recordings. This can be achieved by using the “auto” bridge balance. For manually adjusting bridge balance, bypass filtering, and repeatedly inject a high amplitude negative current of brief duration (e.g., -2 nA during 0.5 ms at 30 Hz). Increase bridge balance compensation to roughly 2.5-fold the pipette resistance. Increase the capacitance compensation as needed; in presubicular neurons the final values are typically around 7–9 pF. Bridge balance and capacitance compensation need to be increased alternately and

iteratively, under visual control of the voltage response. Stop increasing further just before oscillations become apparent. Enable the functionality “disable if oscillation detected” check box from the Multiclamp 700B panel to protect against unwarranted changes of recording quality during the recording that may lead to oscillations and cell loss.

### **3.9 Resting Membrane Potential**

1. Once the recording mode has been switched to current clamp, make sure that the current command is set to zero and record the membrane potential for a few minutes.
2. At the beginning of the recording, the membrane potential may gradually drift before stabilizing after several minutes of whole cell recording. Membrane potential should be determined when the potential is stable (*see Note 9*).

### **3.10 Intrinsic Electrophysiological Properties**

1. Use hyperpolarizing and depolarizing step current injections to determine intrinsic properties.
2. The cell can be either held at its resting potential ( $V_{rest}$ , more physiological) or at a standardized potential (easier for comparison between cells, standardize to the population average of  $V_{rest}$ ), and apply current steps of 0.8 s every 5 s (Fig. 7; *see Note 10*).
3. Start with a negative step current injection allowing a steady state hyperpolarization to around  $-105$  mV (if the cell can handle it) and increase incrementally during the successive steps toward positive values leading to action potential firing, and until depolarization block.
4. The incremental current steps should be small, so as to cover the range of potentials with a precise resolution. Especially, the first current triggering an action potential should be subtly approached (*see Note 10*)—this will indicate the rheobase. The final level of injected current should lead to a total or partial depolarization block, to make sure that most of the cell’s response range has been explored, until the maximum firing rate and beyond.
5. Some of the intrinsic neuronal properties such as the resistance and capacitance, as well as the firing pattern or action potential waveforms can be easily determined from these kind of all-in-one protocols (cf. [12, 13], for more details about the analyses).

### **3.11 Dual Recordings: Synaptic Connectivity and Dynamics**

1. Testing the connectivity of cell pairs can be done either in current clamp or in voltage clamp (*see Note 11*). Choose the recording configuration according to your experimental question, the context of the experiments and the subsequent analyses [14].

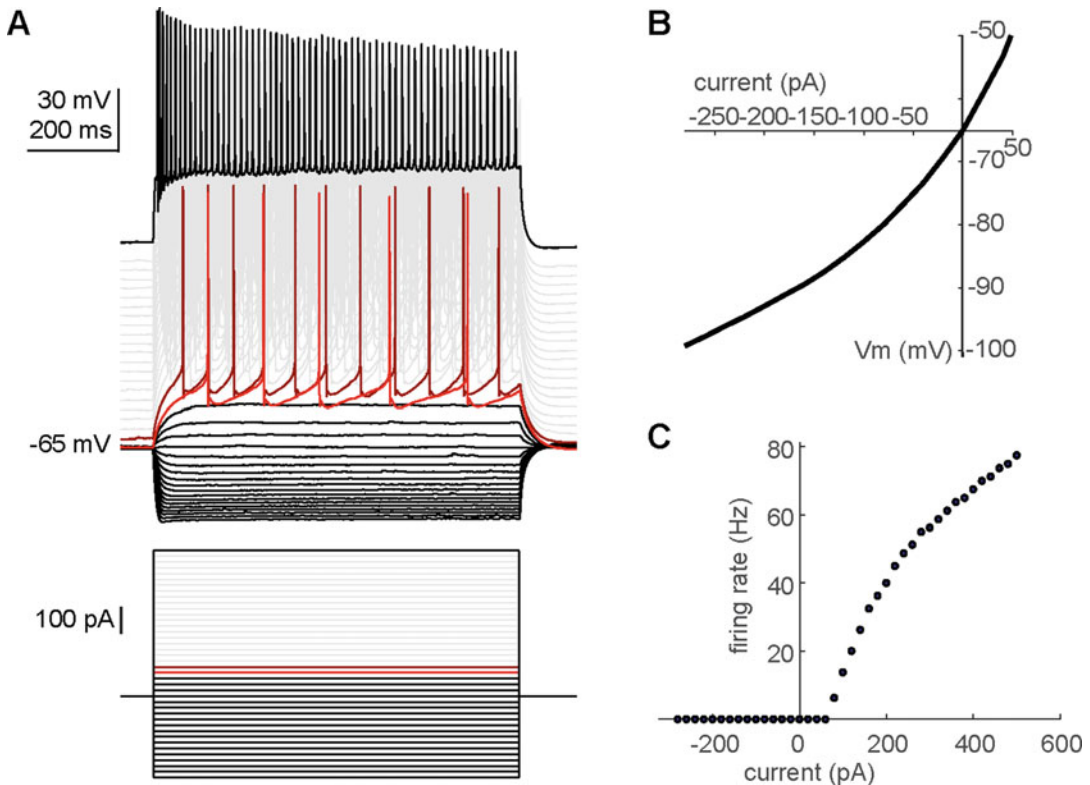


**Fig. 7** Current step protocols reveal neuronal intrinsic properties. **(a)** A presubiculum cell recorded in whole-cell configuration, from an acute adult mouse slice, using a potassium gluconate based internal solution. The cell was recorded in current clamp mode and maintained near its resting membrane potential at  $-65\text{ mV}$ . Current steps of 800 ms duration were applied every 4 s (bottom), the first current step was  $-280\text{ pA}$ , with an increment of 20 pA at each iteration, to reach  $+500\text{ pA}$ . The membrane potential hyperpolarized as a response to negative current steps, and then depolarized for positive current steps. The first step triggering action potentials (rheobase) is in light red, the second in dark red. Subsequent steps are shown in light gray and the last step in black. (Steps with action potentials are displayed with an incremental offset for clarity.) **(b)** Corresponding  $I/V$ -curve (Current–Voltage), plotting voltage as a function of injected current, up to  $+50\text{ pA}$ . **(c)** Corresponding input/output curve of the spike frequency (number of evoked action potentials per second) as a function of injected current. Rheobase is  $+80\text{ pA}$

2. Trigger individual action potentials/currents by injecting a brief high amplitude current (depending on the input resistance of the cell, about 1–2 nA during 1 ms), or by holding the potential around 0–20 mV for 0.5 ms (Fig. 8). Action potentials/currents may be initiated alternately in the two cells and the responses should be observed in the putative postsynaptic cell held at the appropriate voltage/potential. Repeat this protocol ideally at least 100 times in order to determine the probability of neurotransmitter release versus failure rate, and the average amplitude and variability of the postsynaptic events.

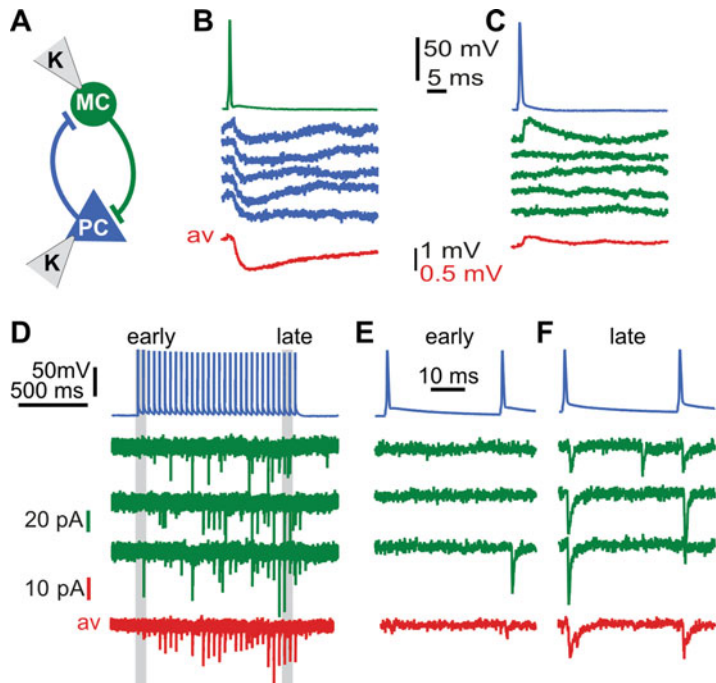


**Fig. 8** Testing connectivity and synaptic dynamics using dual patch clamp recordings. (a) An excitatory pyramidal cell (PC) and an inhibitory Martinotti cell (MC) from the presubiculum were recorded simultaneously in the acute slice preparation of an adult mouse, using the potassium gluconate based solution with low chloride (5.2 mM; cf. Table 2). (b) The connectivity from the Martinotti cell to the pyramidal cell was tested triggering a single action potential in Martinotti cell (Top, green trace) while recording the pyramidal cell in current clamp, maintaining its potential around  $-50$  mV (bottom, 5 different trials (blue) and the average response (amplitude,  $-0.7$  mV; red)). The Martinotti cell action potential reliably elicited inhibitory postsynaptic potentials in the pyramidal cell with short monosynaptic latencies (1–2 ms). (c) The connectivity from the pyramidal cell to the Martinotti cell was tested triggering single action potentials in the pyramidal cell (top, blue) while recording the Martinotti cell in current clamp, holding its potential around  $-65$  mV (bottom, 5 different trials (green) and the average response (amplitude,  $0.2$  mV; red)). The pyramidal cell action potential did not reliably elicit excitatory postsynaptic potentials in the Martinotti cell initially. When a response was detected, it had a short monosynaptic latency (1–2 ms). (d) The dynamics of the synaptic connection was tested using repeated stimulations of the pyramidal cell, with 30 spikes fired at 30 Hz. This stimulus train was repeated every 30 s (Top, blue). The postsynaptic Martinotti cell was recorded in voltage clamp holding its potential at  $-65$  mV (bottom, 3 different trials (green) and the average response (red)). (e) Spikes initiated early in the train only rarely evoked any postsynaptic response in the Martinotti cell. (f) In contrast, the late spikes showed an increased efficacy in transmitting information. These protocols revealed the slow facilitating dynamics at the pyramidal cell to Martinotti cell synapse in the mouse presubiculum, a phenomenon that classic paired pulse stimulation would not have fully captured. (Figure adapted from Simonnet et al. (2017) *Nature Comms.*, with permission)

3. Determine the paired pulse ratio with successive stimulations (paired pulse stimulation) repeated at 20 or 50 Hz, or other frequencies that may be relevant for short term plasticity.
4. There may be a need to probe synaptic transmission using trains of 10 or 30 repeated stimulations at moderate to high frequency. Some central synapses are rather inefficient in releasing neurotransmitter—in this case, strong repeated stimulation is the most appropriate way to detect the functional connectivity between two cells [14].

**3.12 Afferent Connectivity: Optogenetics Combined with Patch Clamp Recording**

1. Use virus-mediated channelrhodopsin expression in upstream areas of the brain to study long-range afferent innervation with photostimulation in brain slices. We have obtained reliable results with a AAV2/5 serotype expressing Chronos, a fast channelrhodopsin-2 variant, fused to green fluorescent protein (GFP) under the control of the Synapsin promoter: AAV5.Syn. Chronos-GFP.WPRE.bGH (*see Note 12*).
2. To investigate projection neuron circuits, prepare brain slices for patch clamp recording of the postsynaptically connected neurons, after a suitable time for transgene expression. Choose a slice that contains Chronos expressing axon terminals by visualizing the fluorescent reporter GFP, using a hand-held flashlight and appropriate glasses (Nightsea DFP-1; *see Note 12*).
3. Transfer the slice into the recording chamber. Briefly illuminate the slice with the blue LED via the objective to identify a zone with GFP expressing fibers. Choose a principal neuron in that zone for patch clamp recording.
4. Establish a whole cell recording as described above in Subheading 3.10, using a K-gluconate based internal solution.
5. Record in current clamp configuration, holding the neuron at its resting membrane potential, usually close to  $-65$  mV. Stimulate afferent fibers with brief pulses of blue light whole field illumination (470 nm LED). Start using 0.5 ms duration and 0.1 mW light intensity. If no responses are observed, the light intensity may be increased as needed up to 2 mW [15]. Duration may be increased to 2 ms (*see Note 13*). For strong synaptic connections and strong illumination, postsynaptic action potentials will be initiated (Fig. 9).
6. Postsynaptic responses may also be recorded in voltage clamp configuration, with a holding potential of  $-65$  mV. Figure 9c shows the response of a presubiculum neuron to activation of thalamic fibers with a 2 ms light pulse, and Fig. 9d shows depressing response dynamics for a train of 5 pulses.
7. Record from two putative postsynaptic neuron types at the same time to compare the strength (amplitudes) and dynamics of afferent inputs to different cell types in the same brain area.

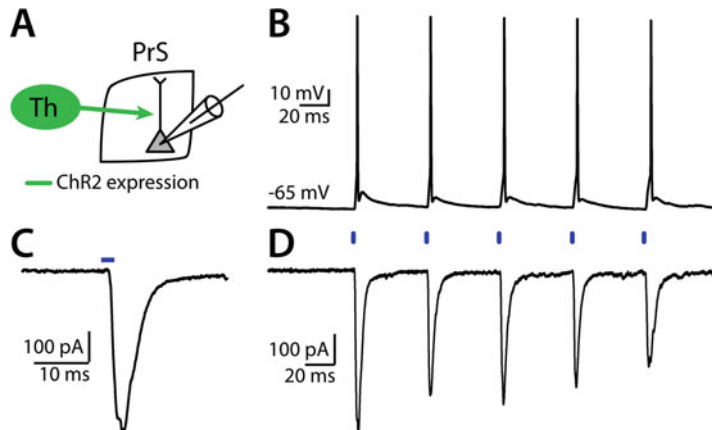


**Fig. 9** Photostimulation. (a) Schematic of ChR2 expressing thalamic (Th) afferents projecting to a presubicular (PrS) pyramidal cell recorded in whole-cell patch clamp. (b) 20 Hz optogenetic activation (blue light) of thalamic afferents leads to action potential firing in the presubicular cell in current clamp mode. (c, d) EPSC are evoked by the activation of thalamic afferents at 20 Hz. (c) first evoked EPSP with a monosynaptic latency (<2 ms) shown at a shorter time scale

Double recordings allow standardization across animals and across slices, for varying levels of channelrhodopsin expression [15].

8. Use pharmacology to identify the neurotransmitter that is being released (i.e., APV + NBQX should block responses of glutamatergic synapses. Cf. Table 3).
9. Determine response latencies during offline analysis. Response latencies for monosynaptic connections are typically between 0.5 and 4 ms. Longer latency responses may be due to indirect activation of the recorded neuron via the local microcircuit (*see Note 14*).

### 3.13 Anatomy

For recovering cellular anatomy, the pipette must be retracted carefully from the recorded cells and the slice should be processed according to standard protocols described previously ([13]; *see Note 15*).

---

## 4 Notes

1. The choice of the cutting solution (external solution) might depend on the animal's age (NaCl/Sucrose, ACSF, choline Chloride, NMDG). Additional recipes are available on <https://www.brainslicemethods.com/> and in [20].

We obtained similar results with Choline-chloride based or NaCl/Sucrose based cutting solution for adult animals (from p35 to p60). Replacing sodium ions, increasing Mg<sup>2+</sup> and decreasing Ca<sup>2+</sup> during the cutting procedure protects the brain tissue from excitotoxicity. In addition, low temperature is critical.

ACSF is designed to mimic the composition of the cerebrospinal fluid. The amount of divalent cations (Ca<sup>2+</sup> and Mg<sup>2+</sup>) may be adjusted to modify excitability of neurons, that is, by lowering MgCl<sub>2</sub> to 1.8 or increasing CaCl<sub>2</sub> to 2.2 or up to 4 mM. This will also affect firing threshold and neurotransmitter release. Increasing K<sup>+</sup> will lead to a more depolarized resting potential [5].

2. The K-Gluc internal solution is close to the composition of the cell's interior and is useful to study neuronal active and passive properties or responses to synaptic input. Low chloride in the internal solutions keeps the equilibrium potential of chloride low (around—75 mV). The reversal potential can be calculated using the Nernst equation, and measured experimentally by varying the holding potential while activating GABA<sub>A</sub> receptors. Excitatory postsynaptic potentials can be recorded at around —65 mV (Fig. 8c–f; [14]). Note that EGTA, a slow calcium chelator, may be increased up to 10 mM, to help prevent excitotoxicity due to increase in intracellular calcium. However, EGTA influences calcium dynamics and intracellular calcium signaling, and therefore we prefer low EGTA in our experiments. Mg-ATP, Tris-ATP and Na<sub>2</sub>-phosphocreatine provide sources of energy and second messengers, while they are not critical for successful patching.

The Cs-Gluc internal solution contains cesium as the main cation. Therefore it cannot be used to study action potentials in current clamp, because cesium blocks potassium currents necessary for membrane repolarization. In voltage clamp configuration, Cs-gluconate improves space clamp issues, by reducing leak K<sup>+</sup> conductances. However only the perisomatic area can be controlled [21], while currents generated very distally are clamped after passive or active integration by the dendritic tree. Outward inhibitory postsynaptic currents can be recorded by clamping the membrane potential at +40 mV (Fig. 8b; [14]).

3. Make sure to obtain the necessary permissions for animal experimentation and follow local guidelines. Anesthesia will slow down the breathing of the animal. The breathing frequency of a mouse normally ranges from 80 to more than 200 breaths per minute. Anesthesia should slow it down to 20–40 breaths per minute. Test pain reflexes (hind paw pinch) to determine whether the anesthesia is sufficiently deep.

4. Slice thickness depends on several factors, including the area of interest, age of animals, the scientific question, and the exact configuration of the setup. We preferred 300  $\mu\text{m}$  slices (as thick as possible while still assuring good oxygenation), to largely preserve local connections and neuron integrity. For presubiculum slices, it is preferable that the blade runs from the caudal to the rostral part of the cerebrum, attacking the cut at the level of the entorhinal cortex.
5. Glass capillaries with a filament are recommended for easy filling of the pipette tip. Thick walled glass (1.5 mm O.D. and 0.86 mm I.D.) allows for low noise recordings. The pipette shape and resistance depends on the targeted cells (soma size, elasticity of the membrane) but also on the space constraints of the recording setup. For instance, choose long tapers if the lens should be moved after patching (e.g., to adjust the light stimulation location) to minimize the risk of possible collision of the lens with the pipette.
6. Temperature control is important for slice quality, and also for ion channel biophysics. Channel kinetics and thus action potentials are slowed at room temperature. Any change in the flow speed might result in a transient change in the chamber temperature, rapidly compensated by the closed loop heating device. We recommend turning off the heating system if the ACSF perfusion is transiently interrupted to avoid a transient overheating of the chamber when the perfusion is turned back on.
7. Choose a cell for patching that is as deep below the slice surface as the optics allow. Patching very superficial cells is easier, but the chance to record from neurons with cut neurites is higher, and might result in recording intrinsic properties or synaptic connectivity from damaged neurons with incomplete morphology. Transgenic mouse lines may be useful to target genetically defined subpopulations of neurons with a somatically expressed fluorescent reporter protein.
8. Coarse movements of the micromanipulators may give rise to vibrations and are more safely carried out before establishing a recording. This is recommended to avoid movements of a pipette in the slice while a seal has already been established, and to reduce the risk of losing a cell due to movement of the brain tissue. Sometimes a second attempt becomes necessary while one neuron is already in cell-attached or whole-cell recording configuration. It's always worth a try!
9. It is surprisingly tricky to measure the true membrane potential due to various junction potentials. A noninvasive study of membrane potential using the K<sup>+</sup> current reversal potential in cell attached configuration gave values 13 mV more negative compared to membrane potential measures from the same

neurons in whole cell recordings [5, 22]. This is probably due to a Donnan equilibrium potential between pipette and cytoplasm (reviewed in [23]; *see also* [17]).

10. Use current step injections in current clamp mode to assess the intrinsic properties. The duration of the current steps can be adjusted, depending on the cells or on the experimental question. To study firing adaptation over long time periods it may be useful to apply current steps for 2 s or more [12]. The time interval between step current injections is chosen depending on the time that the membrane potential needs to stabilize to the baseline value. Injecting negative current may result in a depolarizing rebound and vice versa. The longer the interval the better, but of course long intervals increase the experiment duration.

If the aim of the current injection protocol is to define the input/output or frequency/intensity function of the neurons, the resolution of the current step protocol (i.e., the amplitude difference between successive current steps) should be set optimally to avoid inaccuracy. The number of action potentials fired is plotted against the injected current to determine the threshold current and the neuronal gain [12, 13]. If the difference between the incremental current steps is too high, the experimentally determined threshold current may be overestimated. Alternatively, the rheobase can be estimated by linear extrapolation [24].

11. Choose your experimental condition for paired recordings appropriately. For example, studying the dynamic properties of GABAergic synapses (GABA-A) might require a different internal solution and holding potential than focusing on glutamatergic synapses [14]. On the other hand, a Cs-based solution for paired recordings precludes studying intrinsic properties.

The whole cell current clamp or voltage clamp configuration may be used. Voltage clamp is fraught with error in central neurons because of the complexity and length of their dendritic trees preventing a proper clamp of the voltage (i.e., inadequate space clamp, *see* [21]). Somatic voltage clamp can still be useful to detect postsynaptic currents even though current kinetics from distant inputs may be distorted. Current clamp recordings of postsynaptic potentials will reveal somatic excitatory postsynaptic potential (EPSP) shape. EPSP duration is longer than that of postsynaptic currents, and EPSPs may sum depending on the stimulation frequency. Current clamp recording will allow to detect amplifying currents of the peri-somatic region, that would otherwise be clamped in voltage clamp configuration [25]. Dual recordings can also be used to study indirect connectivity [26].

12. Viruses can be purchased from Addgene. Methods for intracerebral stereotaxic viral injections have been described in detail [27]. Work in low light during slicing to avoid ChR2 excitotoxicity. Store slices in the dark. When illuminating the slice under the microscope, use infrared light as much as possible. Illumination with blue LED light will be necessary to localize the zone containing GFP expressing axons, but this will also activate the ChR2 at the same time, consequently the illumination time should be kept to a minimum (no more than a few seconds).
13. To determine the light intensity under the objective, use a power meter (Thorlabs PM100D). Chronos is very light sensitive and should respond to brief and low intensity illumination at 470 nm. Depending on the number of transfected afferent fibers present in the slice, and the strength of the synaptic connection, higher light intensities may be required to give detectable postsynaptic responses. Due to variability of efficiency of viral transfections, the range of useful photostimulation intensities should be carefully determined for each animal and each slice [15]. More fibers will be recruited when using stronger light stimulations.
14. A pharmacological trick to identify monosynaptic responses following light stimulation consists of the application of TTX (1  $\mu$ M)—which should decrease or abolish action potential dependent postsynaptic responses—followed by the addition of 4-AP (100  $\mu$ M; Table 3). 4-AP will enhance channelrhodopsin induced depolarization of presynaptic terminals, and so help neurotransmitter release and reestablish postsynaptic responses. Increasing the light intensity in the TTX/4-AP condition may help. If in the presence of TTX/4-AP photoinduced postsynaptic responses are detected, with latencies  $>0.5$  ms, the connection is monosynaptic.  
Note: If the photostimulation leads to immediate (less than 0.5 ms delay) responses in the recorded neuron, it is likely that the recorded neuron itself expresses channelrhodopsin. In this case, the response will persist in the presence of TTX. For prolonged illumination of 500 ms duration, the response will last as long as the illumination (see [15], Fig. 1f).
15. A few minutes in whole-cell configuration are enough for filling the dendritic tree and the axon. Higher concentrations of biocytin may be used if the complete morphological recovery is critical [28].

## Acknowledgments

This work was supported by the Humboldt Universiteat zu Berlin, Bernstein Center For Computational Neuroscience and Deutsche Forschungsgemeinschaft BR 3479/12-1 (J.S.), the French Ministry for Education and Research (L.R.) and Agence Nationale de la Recherche Grant ANR-18-CE92-0051-01 (D.F.). We thank François Simon and Brandon Stell for critically reading the manuscript. *Disclosures:* The authors declare no competing financial interests.

## References

1. Neher E, Sakmann B (1976) Single-channel currents recorded from membrane of denervated frog muscle fibres. *Nature* 260:799–802. <https://doi.org/10.1038/260799a0>
2. Hamill OP, Marty A, Neher E et al (1981) Improved patch-clamp techniques for high-resolution current recording from cells and cell-free membrane patches. *Pflugers Arch* 391:85–100
3. Ogden DD, Stanfield PR (1999) Chapter 4 Patch clamp techniques for single channel and whole-cell recording
4. Llinás RR (1988) The intrinsic electrophysiological properties of mammalian neurons: insights into central nervous system function. *Science* 242:1654–1664. <https://doi.org/10.1126/science.3059497>
5. Fricker D, Verheugen JAH, Miles R (1999) Cell-attached measurements of the firing threshold of rat hippocampal neurons. *J Physiol* 517:791–804. <https://doi.org/10.1111/j.1469-7793.1999.0791s.x>
6. Pastoll H, Ramsden HL, Nolan MF (2012) Intrinsic electrophysiological properties of entorhinal cortex stellate cells and their contribution to grid cell firing fields. *Front Neural Circuits* 6:17. <https://doi.org/10.3389/fncir.2012.00017>
7. Alonso A, Klink R (1993) Differential electroresponsiveness of stellate and pyramidal-like cells of medial entorhinal cortex layer II. *J Neurophysiol* 70:128–143. <https://doi.org/10.1152/jn.1993.70.1.128>
8. Stell BM, Rostaing P, Triller A, Marty A (2007) Activation of presynaptic GABA<sub>A</sub> receptors induces glutamate release from parallel fiber synapses. *J Neurosci* 27:9022. <https://doi.org/10.1523/JNEUROSCI.1954-07.2007>
9. Epsztain J, Brecht M, Lee AK (2011) Intracellular determinants of hippocampal CA1 place and silent cell activity in a novel environment. *Neuron* 70:109–120. <https://doi.org/10.1016/j.neuron.2011.03.006>
10. Fricker D, Dinocourt C, Eugène E et al (2009) Pyramidal cells of rodent presubiculum express a tetrodotoxin-insensitive Na<sup>+</sup> current. *J Physiol Lond* 587:4249–4264. <https://doi.org/10.1113/jphysiol.2009.175349>
11. Huang L-W, Simonnet J, Nassar M et al (2017) Laminar localization and projection-specific properties of presubicular neurons targeting the lateral mammillary nucleus, thalamus, or medial entorhinal cortex. *eNeuro* 4(2):ENEURO.0370-16.2017. <https://doi.org/10.1523/ENEURO.0370-16.2017>
12. Simonnet J, Eugène E, Cohen I et al (2013) Cellular neuroanatomy of rat presubiculum. *Eur J Neurosci* 37:583–597. <https://doi.org/10.1111/ejn.12065>
13. Nassar M, Simonnet J, Lofredi R et al (2015) Diversity and overlap of parvalbumin and somatostatin expressing interneurons in mouse presubiculum. *Front Neural Circuits* 9:20. <https://doi.org/10.3389/fncir.2015.00020>
14. Simonnet J, Nassar M, Stella F et al (2017) Activity dependent feedback inhibition may maintain head direction signals in mouse presubiculum. *Nat Commun* 8:16032. <https://doi.org/10.1038/ncomms16032>
15. Nassar M, Simonnet J, Huang L-W et al (2018) Anterior thalamic excitation and feedforward inhibition of Presubicular neurons projecting to medial entorhinal cortex. *J Neurosci* 38:6411–6425. <https://doi.org/10.1523/JNEUROSCI.0014-18.2018>
16. Penner R (1995) A practical guide to patch clamping. In: Sakmann B, Neher E (eds) *Single-Channel recording*. Springer US, Boston, MA, pp 3–30
17. Marty A, Neher E (1995) Tight-seal whole-cell recording. In: Sakmann B, Neher E (eds) *Single channel recording*. Plenum Press, New York, pp 31–52

18. Molecular Devices (2012) The Axon Guide, Electrophysiology and Biophysics Laboratory Techniques Third Edition 1-2500-0102 D
19. Barbour B (2014) Electronics for electrophysiologists. Available online. [https://www.biologie.ens.fr/~barbour/electronics\\_for\\_electrophysiologists.pdf](https://www.biologie.ens.fr/~barbour/electronics_for_electrophysiologists.pdf)
20. Ting JT, Daigle TL, Chen Q, Feng G (2014) Acute brain slice methods for adult and aging animals: application of targeted patch clamp analysis and Optogenetics. In: Martina M, Taverna S (eds) Patch-clamp methods and protocols. Springer New York, New York, NY, pp 221–242
21. Williams SR, Mitchell SJ (2008) Direct measurement of somatic voltage clamp errors in central neurons. *Nat Neurosci* 11:790–798. <https://doi.org/10.1038/nn.2137>
22. Verheugen JA, Fricker D, Miles R (1999) Non-invasive measurements of the membrane potential and GABAergic action in hippocampal interneurons. *J Neurosci* 19:2546–2555
23. Barry PH, Lynch JW (1991) Liquid junction potentials and small cell effects in patch-clamp analysis. *J Membr Biol* 121:101–117
24. Altwegg-Boussac T, Chavez M, Mahon S, Charpier S (2014) Excitability and responsiveness of rat barrel cortex neurons in the presence and absence of spontaneous synaptic activity in vivo. *J Physiol Lond* 592:3577–3595. <https://doi.org/10.1113/jphysiol.2013.270561>
25. Fricker D, Miles R (2000) EPSP amplification and the precision of spike timing in hippocampal neurons. *Neuron* 28:559–569
26. Silberberg G, Markram H (2007) Disynaptic inhibition between neocortical pyramidal cells mediated by Martinotti cells. *Neuron* 53:735–746. <https://doi.org/10.1016/j.neuron.2007.02.012>
27. Richevaux L, Schenker L, Beraneck M, Fricker D (2019) In Vivo Intracerebral Stereotaxic Injections for Optogenetic Stimulation of Long-Range Inputs in Mouse Brain Slices. *J. Vis. Exp.* (151), e59534, <https://doi.org/10.3791/59534>
28. Jiang X, Wang G, Lee AJ et al (2013) The organization of two new cortical interneuronal circuits. *Nat Neurosci* 16:210–218. <https://doi.org/10.1038/nn.3305>



# Chapter 16

## Optogenetics and Optical Tools in Automated Patch Clamping

**Kim Boddum, Peder Skafte-Pedersen, Jean-Francois Rolland, and Sandra Wilson**

### Abstract

Automated patch clamping (APC) has been used for almost two decades to increase the throughput of electrophysiological measurements, especially in preclinical safety screening of drug compounds. Typically, cells are suctioned onto holes in planar surfaces and a stronger subsequent suction allows access to a whole cell configuration for electrical measurement of ion channel activity. The development of optogenetic tools over a wide range of wavelengths (UV to IR) provides powerful tools for improving spatiotemporal control of *in vivo* and *in vitro* experiments and is emerging as a powerful means of investigating cell networks (neuronal), single cell transduction, and subcellular pathways.

Combining APC and optogenetic tools paves the way for improved investigation and control of cell kinetics and provides the opportunity for collecting robust data for new and exciting applications and therapeutic areas. Here, we present an APC optogenetics capability on the Qube Opto 384 system including experiments on light activated ion channels and photoactivated ligands.

**Key words** Automated patch clamp, APC, Optogenetics, Caged compounds, Fast ligand gated channels, ChR2, Channelrhodopsin, Rubi-GABA, bPAC, cAMP, HCN phosphorylation, Spatiotemporal kinetics, Qube Opto 384

---

### 1 Introduction

Nature has a wide range of light sensitive proteins that, over the last 20 years, have become increasingly popular for studying the kinetics of biology. Optogenetics makes use of these tools for studying protein function, membrane currents, and signaling pathway modulation.

Automated patch clamping (APC) is used to increase data throughput of electrophysiological experiments in research and preclinical drug discovery. It generates data in conventional or perforated and whole cell patch clamp configurations and is a powerful tool for the study of voltage gated, current clamped and ligand gated ion channels.

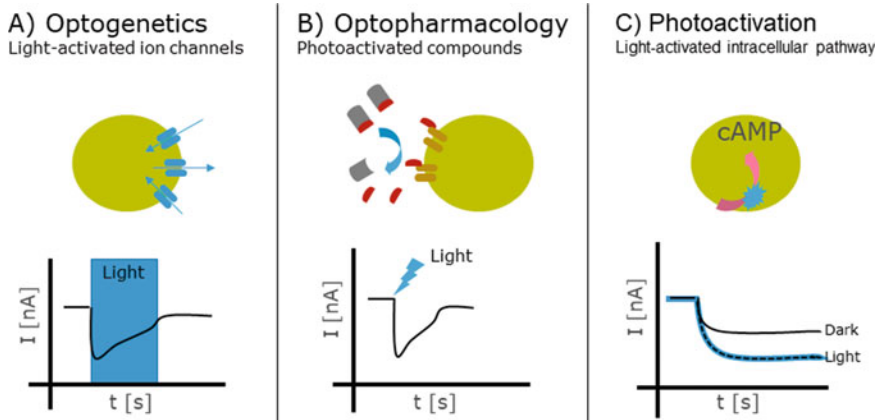


**Fig. 1** An overview of applications for APC optogenetics. Cross section of light access to the cell in the Qube opto setup, showing light ( $h\nu$ ) and voltage ( $U$ ) or current ( $I$ ) control modes, with a current ( $I$ ) or voltage ( $U$ ) readout (left). On the right three application areas (a) Optogenetics, (b) Optopharmacology, and (c) Photoactivation of actuators

This chapter details three different applications (optogenetics, optopharmacology, and photoactivation of actuators) that have been investigated by combining optical stimulation and APC. They are outlined in Fig. 1.

### 1.1 Optogenetics

The first area investigated uses genetically engineered light-sensitive ion channels and receptors that are expressed in mammalian cells, a technique often referred to as optogenetics (Fig. 1a). Since the recent employment and further development of channelrhodopsins (ChRs), a photoreceptor type found in green algae [1], there has been an explosion in the development of new light activated proteins, to now include a broad selection of receptors, enzymes and ion channels [2].

Optogenetics combines genetic manipulation and optics offering unprecedented and reversible opportunities for control of cells by light and provides millisecond-scale temporal resolution that allows the experimenter to keep up with fast biological information processing. ChRs are extensively used for controlling cells by light. They are typically blue light-sensitive and are relatively nonselective cation channels, permeable to  $\text{Na}^+$ ,  $\text{K}^+$ , and  $\text{Ca}^{2+}$ , that depolarize the membrane, when opened upon illumination [3]. Light-driven, hyperpolarizing ion pumps have also been described, for example, halorhodopsins, which pumps  $\text{Cl}^-$  ions across the cell membrane. Novel ChR mutants continue to be developed, with increased sensitivity, selectivity, speed, and therapeutic functions [4–7]. Here we demonstrate a range of experiments that show activation of channelrhodopsin-2 (ChR2) mediated by both light and voltage, demonstrating activation times as short as 4 ms.

## 1.2 Optopharmacology

Very fast ligand-gated channels are traditionally difficult to address in automated patch clamping due to a comparatively slow solution exchange speed relative to extremely fast channel desensitization, which makes electrophysiological results challenging to evaluate and requires more complex assay development. Photochemistry for pharmacology (optopharmacology, Fig. 1b) has been used to develop light modulated chemical structures that can be attached to standard drugs. One example is to attach a light-sensitive chemical tag to ligands that prevents receptor binding until a flash of light releases the chemical bond making the ligand immediately available to bind the target channel. This dramatically increases the temporal precision of experiments.

A chemically modified drug (e.g., a caged compound) enables the pharmacological manipulation of receptors, ion channels and other proteins [8]. The caged compound can either be cleaved by light to, for example, release an active ligand, or be photoswitchable which means photons induce a conformational change of the photoswitchable component freeing up a binding site on the active drug. The photoactive component is activated and passivated either by light/dark or different switch on/switch off wavelengths.

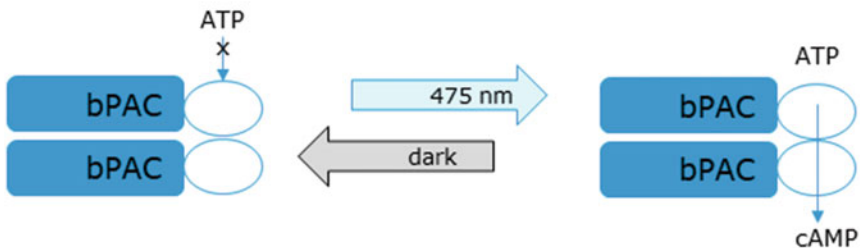
Here we present the use of caged (light activated ruthenium based)  $\gamma$ -aminobutyric acid (Rubi-GABA) for recordings of light-induced GABA<sub>A</sub> receptor (GABA<sub>AR</sub>) mediated current. Rubi-GABA chemistry was developed to uncage at visible light (blue) which presents a more stable chemistry for uncaging compared to UV caged GABA compounds. In our experiments, the GABA<sub>AR</sub> response was both concentration and light intensity dependent.

## 1.3 Optical Modulators/Actuators of Cellular Pathways

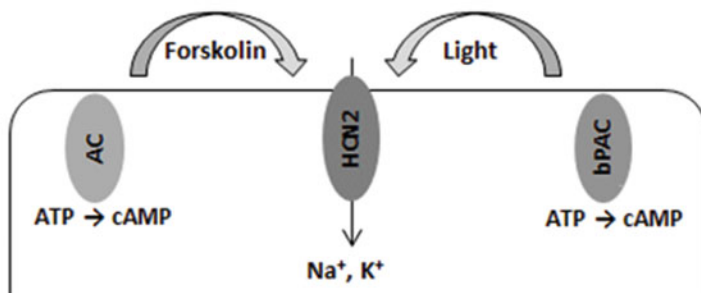
Further development of photochemistry now supports the interrogation of intracellular events (Fig. 1c, photoactivation), their kinetics and mechanisms as they relate to ion channel function as an output. As a natural extension of optopharmacology, light activated chemical tags have been attached to proteins that can be used for precise temporal interrogation of intracellular pathways that was previously not possible directly by APC. The following paragraph of this chapter describes one option of many. bPAC is a bacterial photoactivated adenylyl cyclase from *Beggiatoa*, a sulfide-oxidizing bacterium [9, 10]. bPAC was used to modulate protein phosphorylation through cAMP production (see Fig. 2) and thereby activate the hyperpolarization-activated cyclic nucleotide modulated ion channel 2 (HCN2) channel, dramatically changing its kinetics.

bPAC has a maximum absorption at a wavelength of 441 nm and when activated by light, the enzyme converts ATP into cyclic AMP, thereby increasing the intracellular cAMP level (Fig. 2) [9, 11]. This leads to activation of a myriad of cellular reactions and intracellular signaling pathways [11, 12]. Protein kinase A (PKA) is

## Bacterial photoactivated adenylate cyclase



### HCN2 activation by Forskolin or bPAC



Agus et al., 2015

**Fig. 2** bPAC activation and cAMP production modulates HCN2 channel kinetics, similar in method to Forskolin-mediated HCN2 modulation

one of the cellular proteins that is regulated by cAMP levels. When cAMP binds to PKA, it becomes enzymatically active and phosphorylates target proteins.

HCNs are, to a high degree, regulated by PKA [13, 14]. It is a family of ion channels, with HCN4 being the best described family member, playing a fundamental pacemaking role in the heart. Modulation of cardiac activity by cAMP is attributed mainly to HCN4, the principle subtype expressed in the SA node, whereas HCN2 has a supporting role [15, 16]. HCN2 channels are also present in neuronal tissues and are potential targets for therapeutic intervention in neuropathic pain [13, 17].

In summary, optogenetics applied in APC (opto APC) is a powerful combination of technologies that support an increased mechanistic understanding of ion channel functions, complex intracellular actions related to ion channels and to study and develop therapeutic interventions.

## 2 Materials

### 2.1 Cell Culture

#### 2.1.1 Cells

HEK293 cells transiently expressing ChR2—Neo Scientific, lentivirus transfection of ChR2-GFP into 293T cells. NCBI ref.: gi|189314003|gb|EU714030.1| Synthetic construct channel rhodopsin-2-GFP (ChR2-GFP) gene.

HEK293 cells stably expressing GABA<sub>A</sub>R ( $\alpha_5\beta_3\gamma_2$ ), provided by ChanTest.

HEK293 cells stably expressing HCN2/bPAC, provided by Axxam

#### 2.1.2 Solutions and Reagents

Phosphate buffered saline (PBS) without Ca<sup>2+</sup> and Mg<sup>2+</sup>.

TRYPSIN solution containing 180 µg ethylenediaminetetraacetic acid (EDTA) per mL (cell splitting).

Detachin solution (Genlantis) 1.0 mL per 75 cm<sup>2</sup> surface area (experimental prep.)

Trypan blue

#### 2.1.3 Culture Media

Dulbecco's Modified Eagle's Medium (DMEM)/Nutrient mixture F-12, 500 mL.

Fetal bovine serum (FBS), 10% (see Note 1).

Penicillin/Streptomycin (P/S) 100 µg/mL

#### 2.1.4 Serum-Free Media (SFM)

CHO cell culture media (C5467, Sigma) 25 mL.

4-(2-hydroxyethyl)-1-piperazineethanesulfonic acid (HEPES) solution (1 M), 25 mL.

Penicillin/Streptomycin (P/S) 100 µg/mL.

Soybean trypsin inhibitor (SBTI) 0.04 mg/mL

#### 2.1.5 Selection Factors

For GABA<sub>A</sub>R ( $\alpha_5\beta_3\gamma_2$ ), the culture medium was supplemented with the selection factors: 0.1 mg/mL hygromycin B, 0.5 mg/mL G418, and 0.1 mg/mL Zeocin.

For HCN2/bPAC, the culture medium was supplemented with 0.2 µg/mL puromycin and 0.4 mg/mL G418.

### 2.2 Solutions

#### 2.2.1 Intra and Extracellular Solutions

Prepare all solutions using ultrapure water (prepared by purifying deionized water to achieve a sensitivity of 18 MΩ·cm at 25 °C) and analytical grade reagents. Prepare and store all reagents at room temperature. Diligently follow all applicable waste disposal regulations when disposing of waste materials.

ChR2	<i>Extracellular solution</i> (in mM): 2 CaCl <sub>2</sub> , 1 MgCl <sub>2</sub> , 10 HEPES, 4 KCl, 145 NaCl. pH = 7.4 with NaOH, Osmolarity = 305 mOsm with sucrose (before adjustment 285–295 mOsm).  <i>Intracellular solution</i> (in mM): 149 CsF, 1/5 EGTA/CsOH, 10 HEPES, 10 NaCl. pH = 7.3 with CsOH, Osmolarity = 320 mOsm with sucrose (before adjustment 280–290 mOsm).
GABA <sub>A</sub> R ( $\alpha_5\beta_3\gamma_2$ )	<i>Extracellular solution</i> (in mM): extracellular ringer (in mM): 2 CaCl <sub>2</sub> , 1 MgCl <sub>2</sub> , 10 HEPES, 4 KCl, 145 NaCl. pH = 7.4 with NaOH, Osmolarity = 305 mOsm with sucrose (before adjustment 285–295 mOsm).  <i>Intracellular solution</i> (in mM): intracellular ringer (in mM): 90 KCl, 50 KF, 1 MgCl <sub>2</sub> , 11 EGTA, 10 HEPES. pH = 7.3 with KOH, Osmolarity = 300 mOsm with sucrose (before adjustment 280—290 mOsm).
HCN2/bPAC	<i>Extracellular solution</i> (in mM): 2 CaCl <sub>2</sub> , 1 MgCl <sub>2</sub> , 10 HEPES, 4 KCl, 145 NaCl, 2 or 10 BaCl (see Note 2). pH = 7.0 with KOH, Osmolarity = 320 mOsm with sucrose (before adjustment 285–295 mOsm).  <i>Intracellular solution</i> (in mM): 70 KCl, 50 KSO <sub>4</sub> , 10 HEPES, 25 KOH, 5 EGTA, 5 HEDTA 3.83 MgCl <sub>2</sub> , 3.83 CaCl <sub>2</sub> . pH = 7.4 with NaOH, adjust osmolarity according to your IC with sucrose.

### 2.3 Optical Electrophysiology

A Qube Opto 384 system with an installed light wavelength of 475 nm (blue) with light intensity set at any percentage between 10 and 100% (Cree XLamp series), using Sophion ViewPoint and Sophion Analyzer.

Qube Opto 384 is a fully integrated high-throughput screening (HTS) system that combines optical stimulation with automated patch clamping (APC). Light control is fully integrated into Qube software and addresses 384 patch wells simultaneously where it is possible to have individual light control of 24 columns. Users can control light timing, duration, intensity, and program light ramps and other optical waveforms freely. The dark cabinet allows for automated handling of light sensitive compounds and cells. The system is compatible with other Qube features such as temperature control.

T175 cell culture flasks.

Microtiter plates (MTPs) 1 × 1 (Sophion SB2260), 1 × 24 (Sophion SB2262), 384 well plates (Greiner Bio-One 781280).

QChip 384X Multi-hole (10 holes per well, Sophion SB2115).

Cell transfer plate (CTP) (Sophion, SB 3301).  
 Magnet for QStirrer (Sophion, SB3070).  
 QStirrer cup (Sophion, SB2050).  
 QFuge tube (Sophion, SB2251).  
 Cell preparation unit (SCP) tip (Sophion, SB2210).  
 Cell preparation unit (ACP) reservoir for EC solution (Sophion, SB2255).  
 Cell waste bottle (Sophion, SB2253).  
 Liquid management system (LMS) supply containers (Sophion, SB3331).  
 Liquid management system (LMS) waste containers (Sophion, SB 3332).  
 Pipette tips for 384-robot (Sophion, SB2200).

### 3 Methods

#### 3.1 Compound Preparation

RuBi-GABA (Tocris, UK): Prepare 6 mL, 1 mM RuBi-GABA in GABA<sub>AR</sub> ( $\alpha_5\beta_3\gamma_2$ ) extracellular solution. From that, make a three-fold dilution with 11 concentrations. Fill a 24 × 1 compound tray: two compartments per concentration + two compartments with extracellular solution only.

GABA reference: Prepare 50 mL 1 mM GABA in GABA<sub>AR</sub> ( $\alpha_5\beta_3\gamma_2$ ) extracellular solution and fill into a 1 × 1 compound tray.

#### 3.2 Cell Culture

##### 3.2.1 Culturing of Cells from Frozen Vials

1. Thaw the vial quickly in a 37 °C water bath.
2. Transfer the contents of the vial to a T75 flask containing prewarmed culture media.
3. Change the culture media the next day.
4. Allow the cells to reach 70–80% confluence before subculturing. We recommend passaging cells every 2–3 days using trypsin or Detachin™.

##### 3.2.2 Sub-Culturing (T175 Flask)

1. Remove old culture media and wash with 7 mL PBS.
2. Add Trypsin, gently swirl the flask and aspirate (leave approx. 1 mL).
3. Place the culture flask in an incubator at 37 °C for ~2 min. (Ensure the cells have a round shape before doing the next step).
4. Gently tap on the side of the flask and add 5–7 mL culture media and resuspend the cells by working the cell suspension up and down using a pipette, 5–10 times.

5. Determine the cell density and viability by counting the cells in a hemocytometer by diluting an aliquot in a 1:2 ratio of Trypan Blue.
6. Add the appropriate number of cells to the mother flask and the experiment flasks (*see Note 3*).
7. Culture the cells at 37 °C, 5% CO<sub>2</sub> to maximum 80% confluence.
8. After 1–2 weeks of subculturing the cells have reached a stable growth pattern that is suitable for Qube experiments.

### **3.2.3 Cell Preparation for Experiments**

1. Remove the culture media and wash with 7 mL PBS.
2. Add 3 mL Detachin™, gently swirl the flask and aspirate (leave about 1 mL) (*see Note 4*).
3. Place the culture flask in a 37 °C incubator for ~5 min (ensure that the cells have reached a round shape before doing the next step).
4. Add 5 mL serum-free media and resuspend the cells by working the cell suspension up and down using a pipette, 5–10 times.
5. Determine the cell density and viability by diluting an aliquot 1:2 in Trypan Blue and counting the cells in a hemocytometer.
6. Ensure there are 2–6 million cells/mL added to the QStirrer.

## **3.3 Qube Opto 384 Experiments**

ViewPoint is the software used to set up and execute experiments on Qube Opto 384 and it allows the user to specify and choose the following five protocols: Worktable, Cell preparation, Whole-cell, Experiment, and Cleanup. All protocols are built by inserting one or more blocks based on predefined block templates. When a block is selected, a parameter field block can be opened to make changes to the block.

### **3.3.1 Optogenetics**

1. *Worktable:* Choose the block template: “2 compound worktable.” Ensure the barcode reader is disabled (*see Note 5*) and automatic delidding is enabled.
2. *Cell preparation:* Choose the block template “Cell preparation: Standard.” Set the following parameters:  
*Centrifuge g-force:* 80 × g.  
*No. of cell washes:* 2.  
*Centrifuge time:* 220 s.
3. *Whole-cell protocol.* Choose the block template “Whole-cell block: Standard” and change the whole-cell pressure to:

Start time (ms)	0	10,000	11,000	21,000
Duration (ms)	10,000	1000	10,000	1000
Start/End pressure (mbar)	−10	−250	−10	−350

Set the following parameters:

*Pressure during positioning:*  $-50$  mbar before positioning and  $-10$  mbar after positioning-.

**Holding potential:**  $-110$  mV during seal formation, whole cell suction and after whole-cell ( $V_{\text{hold}}$ ).

*Seal formation duration:*  $300$  s before whole cell suction.

### 3.3.2 Optopharmacology

1. *Worktable:* Choose the block template: “*2 compound worktable*.” Ensure the barcode reader is disabled (see Note 5) and automatic delidding is enabled.
2. *Cell preparation:* Choose the block template “*Cell preparation: Standard*.” Set the following parameters:  
*Centrifuge g-force:*  $80 \times g$ .  
*No. of cell washes:*  $2$ .  
*Centrifuge time:*  $220$  s.
3. *Whole-cell protocol.* Choose the block template “*Whole-cell block: Standard*” and change the whole-cell pressure to:

Start time (ms)	0	10,000	11,000	21,000
Duration (ms)	10,000	1000	10,000	1000
Start/End pressure (mbar)	$-10$	$-100$	$-10$	$-150$

Set the following parameters:

*Pressure during positioning:*  $-50$  mbar before positioning and  $-10$  mbar after positioning.

**Holding potential:**  $-90$  mV during seal formation, whole cell suction and after whole-cell ( $V_{\text{hold}}$ ).

*Seal formation duration:*  $300$  s before whole cell suction.

### 3.3.3 Optical Modulation of Actuators

1. *Whole-cell protocol.* Choose the block template “*Whole-cell block: Standard*” and change the whole-cell pressure to:

Start time (ms)	0	10,000	11,000	21,000
Duration (ms)	10,000	1000	10,000	1000
Start/End pressure (mbar)	$-10$	$-250$	$-10$	$-350$

Set the following parameters:

*Pressure during positioning:*  $-50$  mbar before positioning and  $-10$  mbar after positioning-.

**Holding potential:**  $-30$  mV during seal formation, whole cell suction and after whole-cell ( $V_{\text{hold}}$ ).

*Seal formation duration:*  $300$  s before whole cell suction.

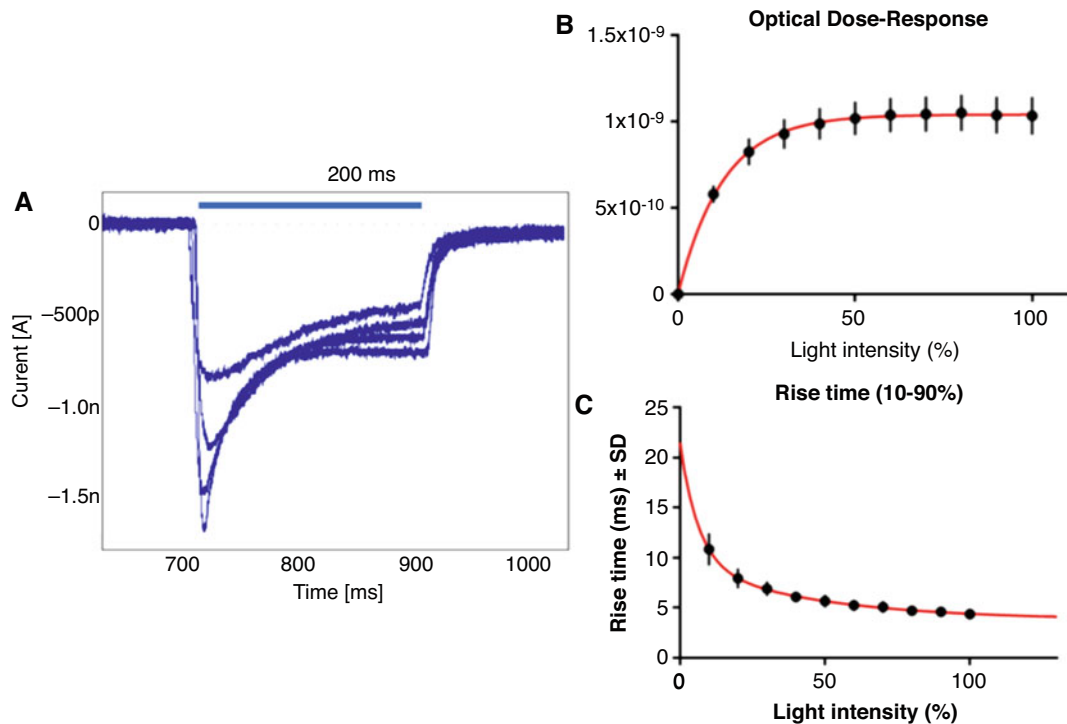


**Fig. 3** Light intensity dependent activation of ChR2. **(a)** Typical light evoked current at LED output intensity 10, 20, 40, and 100% and a holding potential of  $-90$  mV. **(b)** Dose–response relationship for light from 0% to 100%. **(c)** Fast activation kinetics: rise time calculated as time from 10% to 90% of maximum current amplitude. Data is represented as mean  $\pm$  standard deviation of  $n = 12$

### 3.4 Optogenetics

#### Evaluating the Light Intensity Dependency of ChR2 Activation

1. Select a voltage gated liquid period protocol with one liquid addition (extracellular ringer) and set recording to start after liquid addition. The protocol should contain 10 voltage segments, each of 1 s duration, voltage clamped at  $-90$  mV.
2. Within each voltage segment, set a 200 ms light pulse to start after 200 ms. The light pulse intensity starts at 10% and increases each time by 10% reaching 100% in the 10th voltage segment (*see Fig. 3*).
3. Additional parameters are set as follows: Parameter estimation before first sweep. Leak subtraction enabled. Sample rate: 25000 Hz, cut-off frequency: 5000 Hz, filter: Bessel.

#### Evaluating the Current–Voltage Relationship of ChR2

1. Select a voltage gated liquid period protocol with one liquid addition (extracellular solution) and start recording after liquid addition. The protocol should start with 500 ms segments voltage clamped at  $-100$  mV.

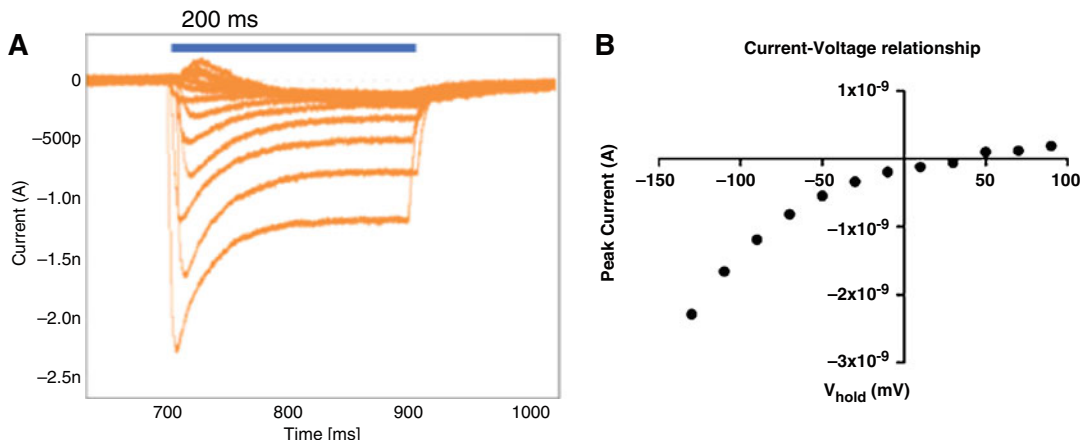


**Fig. 4** ChR2 current–voltage relationship. (a) Typical light-evoked current at varying holding potentials. The stimulation pulse was 200 ms and the intensity 100%. The holding potential was depolarized with +20 mV between sweeps, starting at -130 mV and stepwise reaching 90 mV. (b) IV plot: The maximum current amplitude plotted against holding potential. Note that the ChR2 mediated current showed an inward rectification

2. After 500 ms, insert a step protocol consisting of 1 s steps starting at -130 mV, with 20 mV steps and 12 steps in total (see Fig. 4). A light pulse of 200 ms duration, starting at 700 ms and 100% intensity is introduced into each of these steps.
  3. The protocol should end with a 500 ms voltage segment, clamped at -110 mV.
  4. Additional parameters are set as follows: Parameter estimation before first sweep. Leak subtraction enabled. Sample rate: 25,000 Hz, cut-off frequency 5000 Hz, filter: Bessel.
- #### 3.4.1 Optogenetics Data Analysis
1. Set up quality control filters: Create an experiment filter on “Whole cell resistance” to filter out sites with a low seal resistance (see Note 6). Set the filter to 20 MΩ. Since the experiment is performed on a multihole plate, with 10 patch holes per site, a 20 MΩ cutoff will filter out sites with an average resistance less than 200 MΩ per cell).
 

Create an additional experimental filter on “Whole cell capacitance” and set the cutoff to 50 pF (average capacitance greater than 5 pF/cell).
  2. To evaluate the light intensity dependent activation of ChR2, place a cursor interval, covering the 200 ms period of light activation. Set the cursors to find the peak current (see Note 7) and rise time, from 10% to 90% of the max. Current amplitude.
  3. Export the data and import it to a third party software; we use GraphPad Prism, CA, USA.

4. Plot average peak current  $\pm$  standard deviation as a function of light intensity and fit a monoexponential curve to the data. See Fig. 3 for example traces and data.
5. To evaluate the current–voltage relationship of ChR2, place a cursor interval in the voltage step protocol, covering the 200 ms period of light activation. Set the cursor to find peak current (see Note 7).
6. Plot peak current as a function of voltage to access the current–voltage relationship. See Figs. 3 and 4 for example traces and data.

### 3.5 Optopharmacology

Evaluating the Concentration Response for RuBi-GABA on GABA<sub>AR</sub> ( $\alpha_5\beta_3\gamma_2$ )

1. Add RuBi-GABA: select a ligand gated liquid period protocol with one liquid addition. Add solution from compound tray 1 (see Note 8) in order to expose the cell to varying concentrations of caged GABA. Make the protocol 10 s long and clamp the voltage to  $-90$  mV. No GABA receptor mediated current should be elicited here (see Note 9).
2. Uncage GABA: select a liquid period without liquid addition. 1 s into the voltage protocol, start a 200 ms light pulse with an intensity at 100. Protocol length: 10 s.  $V_{hold}$ :  $-90$  mV.
3. Wash twice with extracellular ringer: use a ligand gated liquid period protocol with one liquid addition and clamp the voltage to  $-90$  mV.
4. Add GABA reference for normalization: select a ligand gated liquid period protocol with one liquid addition. Add the GABA reference solution (1 mM). Protocol length: 10 s.  $V_{hold}$ :  $-90$  mV.
5. Parameter estimation before first sweep. Leak subtraction enabled. Sample rate: 10,000 Hz, Cutoff frequency: 3000 Hz, Filter: Bessel.

#### 3.5.1

##### Optopharmacology—Data Analysis

1. Set up quality control filters: create an experiment filter on “Whole-cell resistance” to filter out sites with low seal resistance (see Note 6). Set the filter to  $20\text{ M}\Omega$  to filter out sites with an average resistance less than  $200\text{ M}\Omega$  per cell.  
Create an additional experiment filter on “Whole-cell capacitance” and set the cutoff to 50 pF (average capacitance larger than 5 pF/cell).
2. To evaluate the concentration response for RuBi-GABA on GABA<sub>AR</sub> ( $\alpha_5\beta_3\gamma_2$ ), place a cursor interval that covers the first 500 ms after light activation onset. Set the cursor to find the peak current (see Note 7).

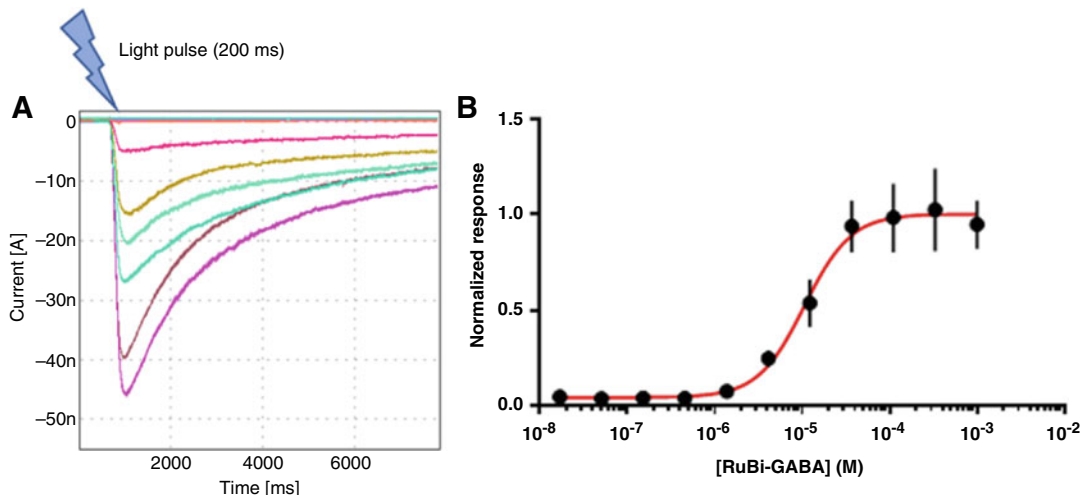


**Fig. 5** RuBi-GABA concentration–response relationship. **(a)** HEK 293 cells expressing GABA<sub>A</sub> ( $\alpha_5\beta_3\gamma_2$ ) were exposed to varying concentrations of RuBi-GABA (Tocris). GABA was photoreleased upon a 200 ms light pulse (475 nm) at 100%. **(b)** Noncumulative concentration–response curve for RuBi-GABA of a threefold dilution series. A Hill equation was fitted to the data and the calculated EC<sub>50</sub> was  $11 \mu\text{M} \pm 0.5 \mu\text{M}$ ,  $n = 32$

3. A similar cursor interval should be used to find the GABA reference peak values for normalization.
4. Normalize each single peak current value, evoked by uncaging of RuBi-GABA, to the GABA reference peak value, measured within the same QChip site (same ten cells).
5. Export the data and import them to third party software. We use GraphPad Prism, CA, USA.
6. Plot the average normalized peak current  $\pm$  standard deviation as a function of RuBi-GABA concentration and fit a Boltzmann equation to the data.
7. Use the estimated minimum and maximum values for renormalization of the data in order to scale the y-range to a 0 to 1 span.
8. Now, plot the average, renormalized peak current  $\pm$  standard deviation as a function of RuBi-GABA concentration and fit a Boltzmann equation to the data. See Fig. 5 for example traces and data.

### 3.6 Photoactivation of Actuators

#### Evaluating the Effect of bPAC Photoactivation on HCN2 Activation Kinetics

1. Improve seal resistance by increasing the Barium concentration: If priming was executed in a 2 mM Barium extracellular buffer, the Barium concentration should be increased to 10 mM. Select a voltage gated liquid period protocol with one liquid addition and add extracellular ringer with 10 mM Barium. The data is unimportant so restrict the voltage

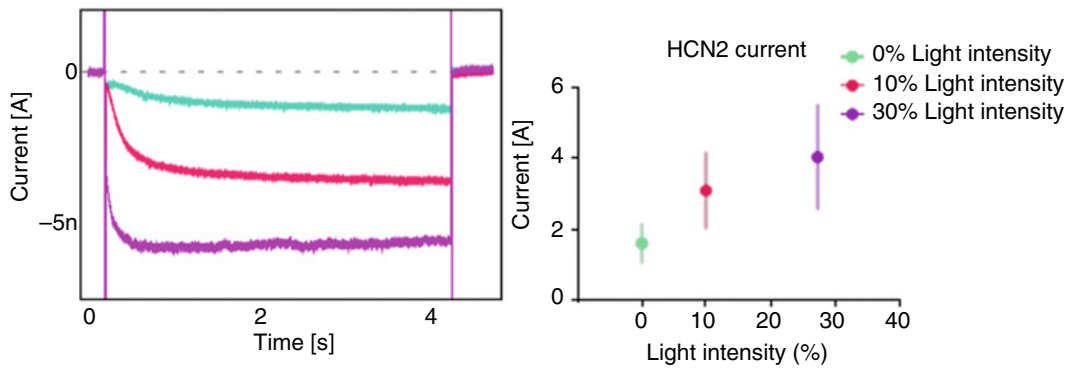


**Fig. 6** An example of typical hyperpolarization evoked HCN2 current traces upon increasing light intensities, 0% (cyan), 10% (red) or 30% (purple), after at least 5 min of optical stimulation (left). Average stable current from a 200 ms interval at the end of the voltage step, showing the effect of optical stimulation on current size (right). Data points are average  $\pm$  standard deviation,  $n = 348$  experiments

protocol to 100 ms, clamped at  $-30$  mV. Enable leak subtraction (*see Note 10*).

2. *For evaluation of the HCN2 response to increasing light intensities (see Fig. 6):* Select a voltage gated liquid period protocol with one liquid addition (extracellular ringer with 10 mM barium) and with the recording starting after liquid addition. The protocol should contain 10 voltage segments, each 4-s-long, clamped at  $-90$  mV. Parameter estimation before first sweep. Leak subtraction disabled. Sample rate: 25,000 Hz, Cutoff frequency: 5000 Hz, Filter: Bessel.
3. Optical stimulation: 500 ms of stimulation every 2 s. Excitation wavelength of 475 nm.
4. Using this voltage protocol and optical stimulation, record the HCN2 mediated current after 5 min of optical stimulation at the following intensities 0%, 10%, 30% and 100% (*see Note 14*).
5. *To evaluate the effect of photoactivation of bPAC on HCN2 current amplitude (see Figs. 7 and 8), activation kinetics and shift in voltage dependence of activation:* Select a voltage gated liquid period protocol with one liquid addition (extracellular ringer with 10 mM Ba<sup>2+</sup>).
6. The voltage protocol (*see Fig. 9* for a graphic representation) should contain 11 voltage segments, each starting with 100 ms at  $-30$  mV, followed by a hyperpolarizing step, varying in both duration and voltage (*see Note 11*): The first voltage segment of the 11 segments is 12 s long, clamped at  $-30$  mV. For each segment, the voltage should be stepped  $-10$  mV and the duration shortened by 1 s. The 11th segment will hence be clamped at  $-130$  mV and last 1 s. The voltage steps are followed by a 1.5-s-long segment, clamped at  $-140$  mV for

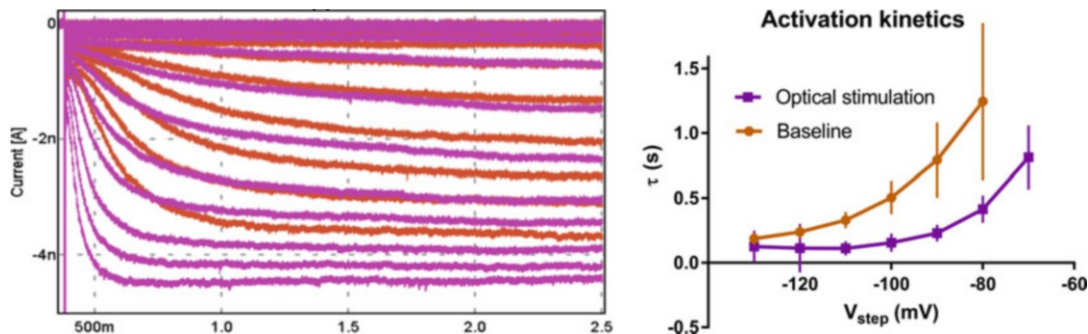


**Fig. 7** An example of a typical HCN2 response to increasing hyperpolarizing voltage steps before (red) and after (purple) 5 min of optical stimulation (left). The effect of optical stimulation on the activation kinetics (right). Only time constants with an average lower than 2 s were included in the analysis. Data points are average  $\pm$  standard deviation,  $n = 219$  experiments

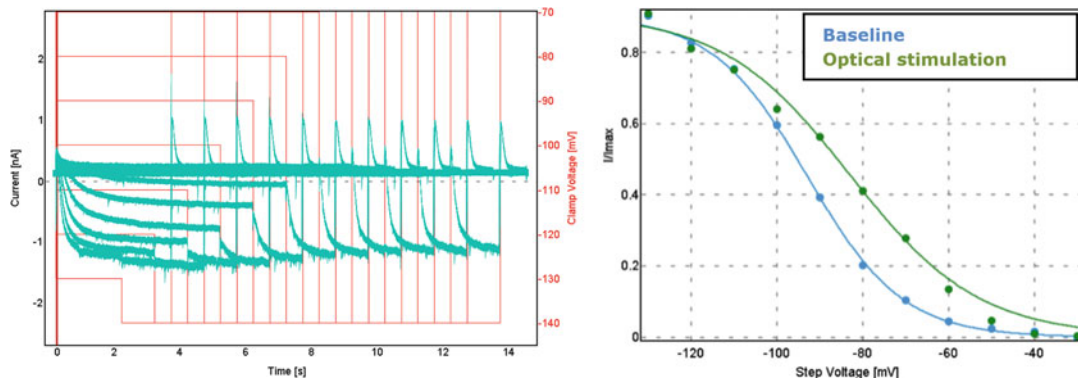


**Fig. 8** An example of typical HCN2 current traces, optically unstimulated but in response to an IV-protocol, where the hyperpolarization duration decreases while hyperpolarization amplitude increases (left) (see Subheading 3 for details). A Boltzmann fit to the normalized current recorded before and after optical stimulation (right). The Boltzmann fit to the  $I/I_{max}$  values revealed an  $8.7 \pm 3.1$  mV depolarized shift in  $V_{1/2}$  upon optical stimulation, ( $n = 324$ , average  $\pm$  standard deviation)

normalization ( $I/I_{max}$ ) and an 800 ms step to 10 mV (see Note 12) before returning to  $V_{hold}$  ( $-30$  mV).

7. For this protocol, choose parameter estimation before first sweep. Leak subtraction disabled (see Note 10). Sample rate: 25,000 Hz, Cutoff frequency: 5000 Hz, Filter: Bessel.
8. Optical stimulation: With an excitation wavelength of 475 nm, optical stimulation is on for 500 ms every 2 s (see Note 13).
9. After 5 min of optical stimulation, the aforementioned step protocol can be repeated, this time under optical stimulation.
10. For reversion of the bPAC activation and cAMP clearance, let the cells rest for 5 min (see Note 13).

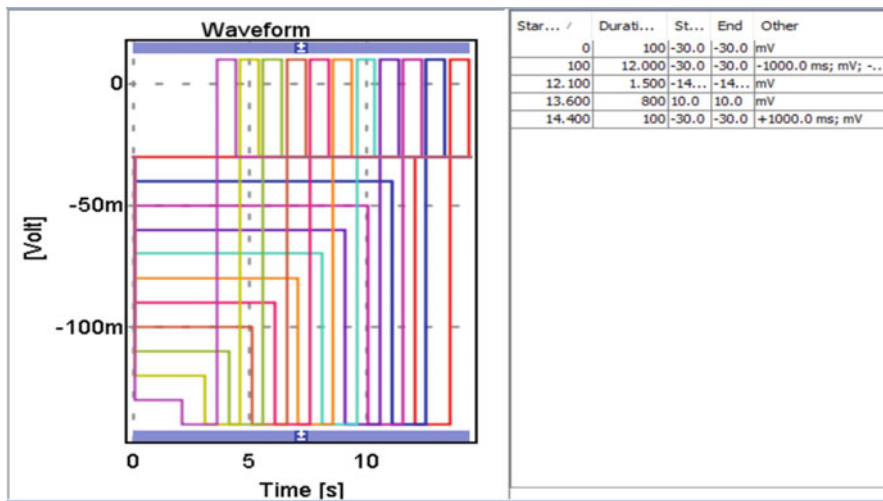


**Fig. 9** The step protocol employed to investigate the impact of optical stimulation on HCN2 activation. The HCN2 current is elicited by decreasing membrane voltages (from  $-30$  mV to  $-130$  mV) in steps. The larger the hyperpolarizing step, the shorter the time to activate; therefore, the length of the hyperpolarizing step is inversely proportional to the hyperpolarization amplitude (spanning from  $12$  s at  $-30$  mV to  $2$  s at  $-130$  mV). Following the voltage step, a  $1.5$  s step to  $-140$  mV was used to find the max. current

### 3.6.1 Photoactivation of Actuators—Data Analysis

1. Set up quality control filters: Create an experiment filter on “Whole-cell resistance” to filter out sites with low seal resistance (*see Note 6*). Set the filter to  $40\text{ M}\Omega$  to filter out sites with an average resistance less than  $400\text{ M}\Omega$  per cell.  
Create an additional experiment filter on “Whole-cell capacitance” and set the cutoff to  $50\text{ pF}$  (average capacitance larger than  $5\text{ pF}/\text{cell}$ ).
2. To evaluate the HCN2 max current in response to increasing bPAC activating by different optical stimulation intensities (0%, 10%, 30% and 100%), place a cursor interval, covering the last  $200$  ms of the  $4$ -s-long,  $-90$  mV voltage step. Set the cursor to find the average current (Fig. 6).
3. Calculate mean  $\pm$  standard deviation current at each light intensity.
4. Export the data and import them to third party software. We use GraphPad Prism, CA, USA.
5. Plot average current  $\pm$  standard deviation as a function of light. *See Fig. 6* for example traces and data.
6. *For evaluation of optical stimulation on the HCN2 activation kinetics*, place a cursor interval covering the first  $2$  s of the step voltage protocol (Fig. 9). Set the cursor to find rise time.
7. Calculate average risetime  $\pm$  standard deviation for each step voltage, both before and during optical stimulation (*see Note 15*).

8. Export the data and import them to third party software. We use GraphPad Prism, CA, USA.
9. Plot average rise  $\pm$  standard deviation as a function of voltage. See Fig. 7 for example trace and example data and see Note 15, that explains the reason for excluding datapoints in Fig. 7.
10. Lastly, to quantify the optical induced shift in the voltage dependence of activation place a cursor interval, covering the last 200 ms of the hyperpolarizing voltage step (Fig. 9). Set to cursor to find the average current.
11. Then place a similar cursor interval to find max current ( $I_{\max}$ ), covering the last 200 ms of the  $-140$  mV hyperpolarizing voltage step (Fig. 9). Again, set the cursor to find the average current.
12. Normalize the measured current to the max current within the same trace to find  $I/I_{\max}$ . See Figs. 7 and 10 for cursor settings.
13. Make a Boltzmann fit to the  $I/I_{\max}$  values both before and after optical stimulation and find  $V_{1/2}$ . See Fig. 8 for example traces and data.
14. Subtract the  $V_{1/2}$  values, before and after optical stimulation, to find the shift in voltage dependence of activation.

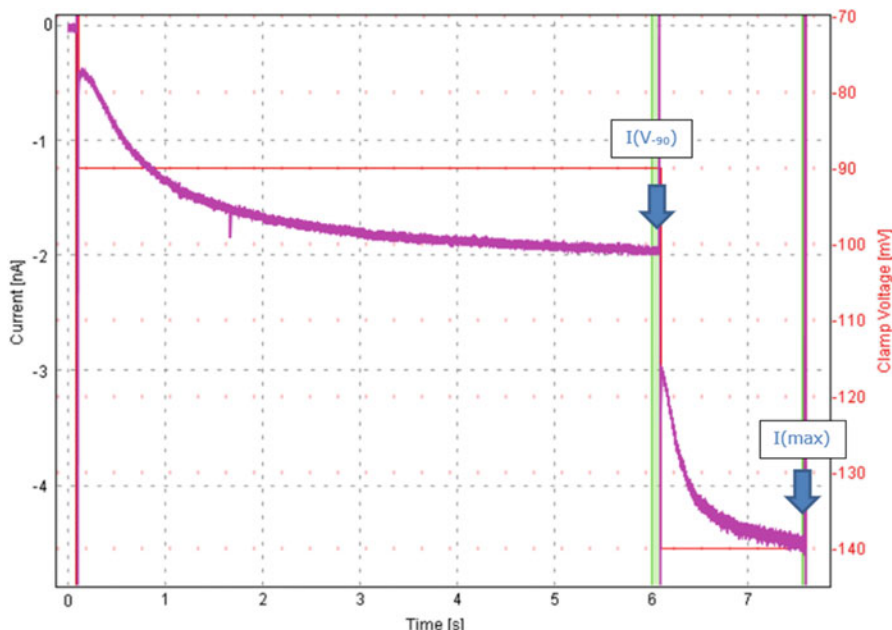


**Fig. 10** A typical HCN2 current trace upon plasma membrane hyperpolarization (from  $-30$  to  $-90$  mV) (left) to demonstrate how  $I/I_{\max}$  is determined. Two cursor intervals (200 ms, green) are inserted for measuring the average current at the individual voltage steps (here  $I(V_{-90})$ ) and from a  $-140$  mV hyperpolarizing step ( $I(\max)$ )

15. Find the average  $V_{1/2}$  shift  $\pm$  standard deviation for all experiments to get an estimate of the optically induced shift in the voltage dependence of activation of HCN2.
- 

## 4 Notes

1. FBS varies from company to company and even using the same FBS, but from a different lot might affect your cell growth. If you are changing your FBS supplier, you must perform batch testing. You need to keep the cells growing for at least 2 weeks (with splitting) in the different FBS to make sure the new FBS is not having an effect. We usually reserve a whole batch, and when the Lot is finished, we perform quality tests on the new batch. We use FBS (F6178) from Sigma, USA.

2. High concentrations of  $Ba^{2+}$  (10 mM) might precipitate in the patch hole and clog the holes before the cells attach. This can be avoided by using reducing the barium concentration to 2 mM during priming and use the first liquid addition to increase the concentration to 10 mM  $Ba^{2+}$ . The addition of 10 mM  $Ba^{2+}$  should then be followed by 5 min incubation time to increase the seal resistance.

3. Subculturing plan for making mother flasks and experiment flasks:

Add  $6 \times 10^4$  cells/cm<sup>2</sup> for subculturing/experiments after 24 h.

Add  $3 \times 10^4$  cells/cm<sup>2</sup> for subculturing/experiments after 48 h\*.

Add  $2 \times 10^4$  cells/cm<sup>2</sup> for subculturing/experiments after 72 h\*.

Add  $1 \times 10^4$  cells/cm<sup>2</sup> for subculturing/experiments after 96 h.

For passage of HEK293 cells we recommend to Sub-Culture cells every Monday and Friday.

\*We recommend 48, 72 or 96 h of sub-culturing for best results.

4. Many ion channels are affected by trypsin; therefore, we only use it for splitting cells and prefer to use Detachin™ for cell recording experiments.

5. The light of the barcode scanner is sufficiently powerful that it might interfere with light sensitive proteins.

6. When one of two electrodes immersed in an electrolyte is illuminated, a potential difference arises between the electrodes, an effect known as the Becquerel effect [18]. This gives a

very characteristic curve that may seem like a cell response. Data should be carefully screened to rule this out.

7. When ChR2 opens, primarily  $\text{Na}^+$  ions will enter the cell and the channels will conduct an inward current. In the recordings, this current will appear as a downward deflection of the current trace. Hence, to find the peak current, the settings should be set to find “min. Current”.
8. Automatic delidding will allow you to prepare your compounds in a dark space and cover the compound tray with a black lid. However, if automatic delidding is activated, you must place a tray with a lid as compound 1. If not, the entire tray will be removed by the gripper.
9. When cells are exposed to the caged form of GABA, the compound should inactivate and hence there should not be a GABA response. This is first expected when GABA is released upon light exposure. If, however, a fraction of the RuBi-GABA should be prematurely uncaged during synthesis or handling, a GABA evoked response will appear with this liquid addition.
10. Since HCN2 is hyperpolarization-activated, care must be taken to design leak subtraction protocols that do not activate the channel (i.e., at voltages above  $-80$  mV).
11. At low hyperpolarization steps, up to 12 s was needed for full HCN2 opening. However, HCN2 mediated currents can be cytotoxic over a longer period, for example, at  $-130$  mV, and the duration of the voltage steps must therefore decrease in duration with increasing hyperpolarization (for protocol *see* Fig. 9).
12. A depolarizing step to 10 mV will ensure a fast transition of open HCN2 channels to a closed conformation.
13. A simple voltage protocol with repetitive 1 s voltage step to  $-90$  mV every 20 s running during the 5 min. Optical stimulation will allow you to monitor the onset and saturation of bPAC activation. The same is the case in the 5 min reversion period.
14. This protocol should be at the end of the experiment, as the cells are not expected to survive. With the described optical protocol, the cells are expected to die due to phototoxicity. In our hands, most cells survive optical stimulation with a light intensity of 30%, but with a reduced data quality. Only a few sites are successful at a light intensity of 100% for 5 min.

## References

1. Nagel G et al (2002) Channelrhodopsin-1: a light-gated proton channel in green algae,” Science, p. 2395–2398.
2. Jiang J et al (2017) Optogenetics and pharmacogenetics: principles and applications. Am J Physiol Regul Integr Comp Physiol., vol. 6, no. 313, pp. 633–645.

3. Volkov O et al (2017) Structural insights into ion conduction by channelrhodopsin 2 Science, vol. 24, no. 358, p. 6336.
4. Cho Y et al (2019) Multidimensional screening yields channelrhodopsin variants having improved photocurrent and order-of-magnitude reductions in calcium and proton currents, *Journal of Biological Chemistry*, vol. 294, pp. 3806–3821.
5. Duan X et al (2019) Mutated Channelrhodopsins with Increased Sodium and Calcium Permeability,” *Appl. Sci.*, vol. 9, no. 664.
6. Stahlberg M et al (2019) Investigating the feasibility of channelrhodopsin variants for nanoscale optogenetics, *Neurophotonics*, vol. 6, no. 1.
7. Gefvert B (2016) Optogenetics: Ten years after - Optogenetics progresses in clinical trials, BioOptics World.
8. Zayat L (2003) A new strategy for neurochemical photodelivery: Metal-ligand heterolytic cleavage. *J.Am.Chem.Soc.*
9. Stierl M et al (2011) Light modulation of cellular cAMP by a small bacterial photoactivated adenylyl cyclase, bPAC, of the soil bacterium Beggiatoa, *J. Biol. Chem.*, no. 286, p. 1181–1188.
10. Hinck S et al (2007) Physiological adaptation of a nitrate-storing Beggiatoa sp. to diel cycling in a phototrophic hypersaline mat., *Appl. Environ. Microbiol.*, vol. 73, no. 21, pp. 7013–7022.
11. Efetova M et al (2015) Photoactivatable Adenylyl Cyclases (PACs) as a Tool to Study cAMP Signaling In Vivo: An Overview,” *Methods in molecular biology*, no. 1294, pp. 131–135.
12. Paramonov V et al (2015) Genetically-encoded tools for cAMP probing and modulation in living systems. *Front. Pharmacol.*, vol. 6, no. 196.
13. Tsantoulas C et al (2016) HCN2 ion channels: basic science opens up possibilities for therapeutic intervention in neuropathic pain. *Biochem. J.*, vol. 473, pp. 2717–2736.
14. Spinelli S et al (2018) Hyperpolarization-activated cyclic-nucleotide-gated channels: pathophysiological, developmental, and pharmacological insights into their function in cellular excitability. *Canadian Journal of Physiology and Pharmacology* 96 (10):977–984.
15. Ludwig A et al (1999) Two pacemaker channels from human heart with profoundly different activation kinetics. *The EMBO Journal* 18 (9):2323–2329.
16. Shi W et al (1999) Distribution and Prevalence of Hyperpolarization-Activated cation Channel (HCN) mRNA Expression in Cardiac Tissues. *Circulation Research* 85 (1).
17. Wickenden A (2009) HCN Pacemaker Channels and Pain: A Drug Discovery Perspective., *Curr. Pharm. Des.*, vol. 15, pp. 2149–2168.
18. Korlyakov E.D (1969) The becquerel effect. *Soviet Physics Journal* 12, 1054–1056.

# INDEX

## A

Action potential.....1, 5, 13, 16, 26, 27, 30, 44, 45, 68, 94, 110, 128, 129, 135, 145, 158, 160, 165, 167, 191, 230, 232, 240, 266, 285, 299–301, 303–307

Acute brain slice .....182

Acute tissue slice .....112, 113, 122–125

Amphotericin B .....9, 94, 97, 98, 104

Artificial cerebrospinal fluid (aCSF).....15, 16, 112, 115, 123–125, 232–235, 237, 241, 246, 248–250, 252–255, 261, 262, 266, 286, 287, 289, 290, 292–294, 296, 303–305

Artificial lipid bilayer .....67–90

Automated patch clamp (APC) .....93, 94, 96–99, 311–329

Axon instruments, *see* Molecular Devices

## B

Bacterial photoactivated adenylyl cyclase (bPAC) .....313–316, 323–326, 329

Behaviors .....264, 265, 285, 286

Beta ( $\beta$ )-escin .....94, 95, 97, 98, 105, 106

Biophysics .....305

Black lipid membranes (BLMs) .....67, 68

## C

Caged compounds .....313

Calcium channels (Cav) .....12, 151, 152, 230, 312

Calcium phosphate .....54, 58–60, 63

Capacitance .....3, 4, 9, 10, 13, 22, 27–30, 32, 36, 42, 69, 74, 75, 86, 87, 101, 104, 144, 151, 152, 159, 162, 165, 167, 219, 231, 232, 238, 297–299, 321, 322, 326

Cell culture .....52, 61, 78, 96–98, 109, 111, 113, 116–120, 126, 127, 137, 138, 140, 142, 195, 197, 207, 244, 247, 251, 286, 315–318

Channelrhodopsin (ChR) .....302, 303, 307, 312

Chinese hamster ovary (CHO) .....12, 96, 97, 151, 315

Chloride channels (ClC) .....230

Confocal .....234

Current clamp .....3, 6, 8, 9, 13, 15, 17, 23, 24, 26–27, 30, 32, 44, 145, 147, 152, 159, 162, 181, 189, 260, 297, 299–301, 303, 304, 306

Current density .....9, 12, 63, 64, 231, 232, 240

Current-voltage (I-V) relationship .....13, 36, 61, 145–147, 180, 320–322

## D

Data acquisition .....22, 33–34, 36, 37, 40–43, 85, 86, 130, 131, 136, 138, 144, 158–160, 165, 169, 236, 289

Dopamine .....274

dPatch .....23, 26, 32, 34–36, 43

Dulbecco's Modified Eagles Media (DMEM) .....52–55, 60, 61, 96, 315

Dynamic clamp .....34, 43–44, 157–162, 164, 165, 167, 169, 170

## E

Electrode .....1, 3, 8, 10, 11, 14, 16, 17, 24, 28–31, 40, 72, 74, 75, 87, 88, 96, 109, 110, 112–117, 119–122, 124, 125, 128–131, 136–138, 142, 147, 152, 160, 183, 220, 226, 230, 231, 236, 238, 264, 289, 327

Electrophysiology .....1, 21–23, 34, 40, 41, 52, 60, 67, 68, 93–108, 110–113, 117, 122, 135, 157, 160, 179, 182, 192, 196, 219, 221, 226, 236, 237, 241, 244, 245, 252, 291, 293, 316

European Collection of Authenticated Cell Cultures (ECACC) .....52

Excitability .....6, 68, 134, 135, 191, 245, 304

Excitatory postsynaptic potential (EPSP) .....303, 306

Expression .....12, 13, 16, 51–64, 69, 70, 77–80, 88, 89, 150, 165, 179, 180, 185, 193, 194, 201, 207, 274, 280, 283, 300, 303

Extracellular (EC) .....97, 101, 317

Ex vivo .....6, 15, 109, 244, 285–307

## F

Fiber optics .....274, 279, 280

Fiber photometry .....273–276, 281

Fluorescence .....41, 206, 215–217, 219, 225, 252, 275

## G

Genetically-encoded calcium indicator .....283

Gramicidin .....68, 80, 82, 94, 97, 98, 104, 106

Green fluorescent protein (GFP) .....58, 59, 63, 64, 300, 307

## H

- Halorhodopsin ..... 312
- Headstage ..... 4, 11, 23–26, 28, 34, 36, 43, 116, 122, 124, 125, 131, 136, 138, 146, 147, 158, 160, 162, 235, 236, 261, 266, 289
- HEK293 ..... 52, 145, 151, 192, 193, 197, 201, 203–205, 218, 219, 222, 225, 315, 327
- HEKA Elektronik Dr. Schulze GmbH ..... 22, 34, 47
- Heterologous ..... 51, 79
- Hippocampus ..... 16, 17, 117, 118, 124, 237, 245, 250, 259
- Holding potential ..... 8, 27, 38, 85, 145, 219, 230, 298, 300, 304, 306, 319–321
- Human embryonic kidney (HEK) ..... 12, 51, 52, 135, 138, 140, 143, 145, 323
- Hybrid system ..... 157

## I

- Imaging ..... 14, 18, 34, 52, 60, 63, 183, 200, 203, 211, 214, 244, 274, 289
- Inhibition ..... 77, 225, 273, 275
- Intracellular (IC) ..... 93, 94, 97–99, 101–104, 106, 316
- In vitro ..... 69, 79, 80, 88, 111, 116, 121, 135, 142, 179, 251, 254
- In vivo ..... 17, 19, 44, 110, 111, 116, 179, 244, 245, 259–263, 265, 266, 268, 274

## L

- LabView ..... 22
- Ligand gated channels ..... 147
- Light emitting diode (LED) ..... 42, 281, 291, 300, 307, 320
- Light sensitive ion channels ..... 312
- Lipids ..... 4, 5, 8, 17, 67–70, 72–80, 82, 84, 87–89, 101

## M

- Macropatch ..... 7, 13, 229–242
- MatLab ..... 22, 138, 147, 149, 276
- Micelles ..... 69, 72, 80, 82, 84, 89
- Microelectrode ..... 3, 32, 69, 88, 109, 116, 122, 289
- Microelectrode-cavity array (MECA) ..... 69, 70, 73, 75, 89, 90
- Microfluidics ..... 69, 144
- Micromanipulator ..... 11, 15, 23, 235, 236, 238, 291, 296, 305
- Molecular Devices ..... 22, 26, 34, 47, 69, 85, 86, 138, 159, 169, 236, 291
- Multi-electrode array (MEA) ..... 109–111, 113–117, 119, 122, 124, 125, 127, 128, 130, 131, 135, 136, 141, 142, 146–150

## N

- Nanodiscs ..... 80
- Neuronal network ..... 6, 109, 136, 148, 245
- Noise ..... 5, 7, 10–12, 23–26, 30, 69, 85, 86, 115, 116, 122, 130, 219, 236, 305
- Nystatin ..... 9, 84, 90, 94, 97, 98, 104

## O

- Optogenetics ..... 18, 273–283, 285–307, 311–329
- Optopharmacology ..... 312, 313, 319, 322, 323
- Orbit 16 ..... 70, 75, 82
- Orbit mini ..... 70, 74, 75
- Organotypic slice ..... 110, 113, 123–128, 243–245, 247

## P

- Patch clamp amplifier ..... 5, 11, 17, 22–24, 27, 28, 30, 34, 94, 138, 158–161, 165, 167, 169, 236, 265
- Perforated patch clamp ..... 9, 93, 94
- Perforating agent ..... 94, 96–99, 101, 102, 104, 106–108
- Phosphate buffered saline (PBS) ..... 54, 60, 78, 96, 98, 197–199, 203, 204, 207, 219, 220, 315, 317, 318
- Photodetector ..... 281
- Photostimulation ..... 292, 300, 303, 307
- Pipette ..... 2–17, 23, 24, 27–32, 52–57, 60, 63, 74, 75, 80, 86–88, 96, 97, 101, 112, 113, 119, 124, 126, 127, 129, 134, 135, 137, 141–145, 150, 152, 159, 162, 167, 183–185, 188, 189, 204, 207, 220, 222, 226, 233, 236, 238, 239, 247, 250, 251, 260, 263, 266, 267, 269, 278, 279, 286, 289–291, 293, 294, 296–298, 303, 305, 306, 317, 318
- Pore-forming agent ..... 94
- Potassium channels (K<sub>v</sub>) ..... 52, 60, 152, 165, 170, 230, 289, 312
- Protein purification ..... 79
- Proteoliposome ..... 69, 80, 84, 88–90

## Q

- Qube 384 ..... 94, 97, 99–101
- Qube 384 Opto ..... 316, 318–319

## R

- Reconstituted ion channels ..... 68, 84
- RNA ..... 179–189, 208
- Rodent ..... 117, 126, 136, 232, 245
- Rubi-GABA ..... 313, 317, 322, 323, 329
- Run-down ..... 7, 9, 94

**S**

- Seal ..... 2–4, 6–9, 11, 12, 14, 19, 28, 29, 73, 74, 94, 106, 108, 120, 139, 142–144, 150–152, 199, 220, 225, 226, 233, 235, 238, 239, 260, 297, 298, 305, 319, 321–323, 326, 327  
Series resistance ... 5, 27, 30–32, 40, 104, 144, 159, 162, 167, 238  
Single-channel recording ..... 8–10, 12, 15, 24  
Sodium channels (Nav) ..... 16, 152, 169, 170, 199, 230, 232, 289, 312, 329  
Stimulus calibration ..... 273–283  
Surgery ..... 264, 265, 269, 277, 279, 280, 283, 294  
Sutter Instrument Company ..... 22, 47  
SutterPatch ..... 26, 34–37, 39–42, 44, 45  
Synaptic transmission ..... 302

**T**

- Transfection ..... 51, 52, 54, 58–60, 63, 139, 140, 145, 150, 192–194, 196, 197, 200, 201, 203–205, 222, 244, 307, 315

- Transgenic ..... 110, 136, 147–149, 180, 274, 286, 305  
tsA201 cells ..... 51–53, 58, 60, 64  
TurboFect ..... 60, 63

**V**

- Vesicles ..... 8, 31, 69, 72, 80, 84, 88  
Voltage clamp ..... 3, 4, 6–8, 10–19, 23, 24, 27–30, 36, 42, 51, 67, 72, 85, 145, 147, 152, 162, 184, 189, 230–232, 238, 260, 296, 297, 299–301, 304, 306

**W**

- Whole-cell ..... 3–12, 16, 17, 19, 24, 25, 28, 30–32, 34, 40, 93–108, 144, 150–152, 159, 162, 165, 179–188, 230–232, 238, 239, 260, 262, 263, 266, 286, 298–300, 303, 305, 306, 311, 318, 319, 321, 322, 326  
Whole-cell patch-clamp recording ..... 184